THE UNIVERSITY of ADELAIDE

Hydrologic and Isotopic Lake Modelling for Palaeoclimate Research

Martin James Ankor

Department of Earth Sciences

School of Physical Sciences

The University of Adelaide

This thesis is submitted in fulfilment of the requirements for the degree of Doctor of Philosophy

January 2020

Table of Contents

Abstract

Numerical lake hydrological and geochemical models are valuable tools for interpreting and quantifying palaeoclimate reconstructions derived from lake sediment archives, and the sensitivity of lakes under future climate scenarios. This study details the development and calibration of a holistic lake model, alongside related projects focussed on the development of tools and datasets associated with lake modelling.

Lake monitoring was conducted over three years at twelve sites in the Newer Volcanic Province, south-eastern Australia on a bi-monthly basis, collecting water levels, and water samples for analysis of oxygen and hydrogen isotopes and major/minor ions. A correlation was identified between the lake morphology and the ^{18}O and ^{2}H isotopic enrichment of lake water, visible as variations in the regression slopes of $\delta^{18}O$ and $\delta^{2}H$ (local evaporation lines). Cl^-/Br^- and HCO_3^-/Cl^- ratios were used to partition the source of water for each lake between groundwater and direct precipitation. Lakes high in the landscape, above the regional aquifers, were found to have lower Cl^-/Br^- ratios, suggesting they are predominantly rainfall fed, whereas the other lakes have Cl^-/Br^- ratios similar to groundwater. HCO_3^-/Cl^- ratios were ambiguous, likely due to the variability of HCO_3^-/Cl^- in groundwater. Deuterium excess (d-excess) data were used to assess the degree to which lakes exhibited through-flow or terminal hydrology. The d-excess results showed strong seasonal variability as a function of lake depth, suggesting that a more conservative solute may be better suited to determine the groundwater regime for these lakes.

One challenge encountered throughout this research was the need to monitor the isotopic composition of daily precipitation feeding into lake systems. To address this challenge in future research, an autonomous rainfall sampler was developed. A computational method using hydrologic-isotopic modelling to estimate the original isotopic composition and volume of evaporated samples was also described.

An important yet poorly constrained component of lake hydrological models is the interaction between lakes and their surrounding groundwater. A single layer, finite difference groundwater model was developed to simulate and investigate this interaction. The model was designed to operate using spreadsheet software, and is able to model transient groundwater flows, confined and unconfined aquifers incorporating recharge, abstraction and injection, no-flow, fixed-head and head-dependent boundary conditions. The model was validated using nine groundwater

scenarios and applied to demonstrate that the use of a specified saturated thickness for unconfined aquifers beneath lakes may give more realistic results.

A holistic lake hydrological and geochemical model was developed, coupling mass and energy balances, hydrology, groundwater, catchment processes, geochemistry and water isotopes. The model was applied to Lake Bullen Merri and Lake Gnotuk, neighbouring maar crater lakes in Victoria, Australia. The model was able to simulate lake hydrology from 1889–2018, water temperatures and chemistry from ~1965–2018, and water isotopes from 2015–2018. The simulations suggest that both lakes experienced through-flow hydrology at high water levels, transitioning to terminal lakes at lower water levels. The potential for the isotopic composition of the lake water to become disconnected from the hydrological balance of the lake was also identified. The newly developed model offers significant potential to constrain past climates and to forecast the trajectory of lake hydrological and geochemical change under future climate scenarios.

Thesis Declaration

I certify that this work contains no material which has been accepted for the award of any other degree or diploma in my name in any university or other tertiary institution and, to the best of my knowledge and belief, contains no material previously published or written by another person, except where due reference has been made in the text. In addition, I certify that no part of this work will, in the future, be used in a submission in my name for any other degree or diploma in any university or other tertiary institution without the prior approval of the University of Adelaide.

I acknowledge that copyright of published works contained within this thesis resides with the copyright holders of those works.

I give permission for the digital version of my thesis to be made available on the web, via the University's digital research repository, the Library Search and also through web search engines, unless permission has been granted by the University to restrict access for a period of time.

I acknowledge the support I have received for my research through the provision of an Australian Government Research Training Program Scholarship.

Martin Ankor Date 03/01/2019

Publications arising from this thesis

Journal articles

Ankor, M.J., Tyler, J.J., Hughes, C.E., 2019. Development of an autonomous, monthly and daily, rainfall sampler for isotope research. Journal of Hydrology, 575: 31-41.

Ankor, M.J., Tyler, J.J., 2019. Development of a spreadsheet-based model for transient groundwater modelling. Hydrogeology Journal: 1-14.

Acknowledgements

I would like to acknowledge and thank AINSE limited for their financial support, provided through a Post Graduate Research Award, giving me the opportunity to spend time at ANSTO collaborating with many knowledgeable people, and running analyses for lake samples. I would also like to thank the Environmental Institute of the University of Adelaide, and INQUA, for grants assisting the funding of trips to the INQUA 2019 and AQUA 2018 conferences, and the INQUA 2016 ECR workshop.

Many sincere thanks go to my supervisors and co-authors, Jonathan Tyler, Cath Hughes, Juraj Farkas and Derrick Hasterok, for their advice and guidance, and for supporting me with their confidence in my work – especially when I was not feeling so optimistic. Working with them has broadened my perspective and helped me understand how my research fits into the broader jigsaw of climate research. I would also like to thank some colleagues whose names do not appear in this thesis as co-authors or supervisors, but have provided much valued advice – Dioni Cendon, Mark Peterson and Bernd Zolitschka.

My time spent in the lab was greatly assisted by the expertise and assistance of David Bruce, Tony Hall, and the staff at Flinders Analytical and ANSTO. I greatly appreciate the time they spent training me, and the skills I have picked up from working with them. I'd also like to acknowledge Fab Lab Adelaide, for providing a space and equipment that allowed me to transform some of my ideas from imagination to the real world.

Thanks to John Tibby for graciously providing data and background for many of the lakes investigated during this thesis. Many thanks also to Jessica Reeves, Peter Dahlhaus, Matthew Currell and Darrell Kaufman for their assistance in collecting samples and field data, as well as many useful discussions drawing on their extensive knowledges of the lakes studied. I would like to express my gratitude to Leon and Judy Sjolund for providing access to the Basin lakes.

I would like to thank my PhD colleagues for their friendship, support and advice. While we may have all been working on different projects, it was an absolute pleasure working with you.

Most importantly, I would like to thank my partner, Karen, for her boundless support and assistance, and my family for their interest, support and humorous commentary on my PhD progress.

Chapter 1

Introduction, thesis aims and background

1 Introduction

To predict future climate change requires a conceptual understanding of the mechanisms that influence climate, and the capability to numerically model them (Skinner, 2008). Direct meteorological observations only cover a few decades to centuries of a period of relatively stable climate. To comprehend and assess the potential range of climatic conditions beyond the observational record requires data over longer timeframes. Studies of palaeoclimate conditions are therefore essential to inform our understanding of the climate system, as well as provide data to validate climate models (Skinner, 2008). Lakes are sensitive to climate variability and their sediments are a key source of terrestrial palaeoclimate archives, with many providing continuous high resolution records spanning tens, to hundreds of thousands of years (Cohen, 2003). In addition, lakes are rare, but important features in the Australian landscape supporting aquatic ecosystems, drinking water, cultural significance, recreation, and tourism (Brookes and Hamilton, 2009). Given projected climate changes, there is a need to understand how lakes respond to external climatic changes, both to predict the behaviour of lakes under future climatic conditions, and to improve our interpretation of palaeoclimate lake sediment records.

Lake water balance varies in response to changes in climate, driving changes in lake chemistry and the isotopic composition of lake waters (Battarbee, 2000; Cohen, 2003; Leng and Marshall, 2004). Such changes in the lake system have a direct impact upon the ecological functioning and taxonomic composition of the lake (e.g., Barr et al., 2014; Fritz et al., 1991; Rudd et al., 2016), and the isotopic and chemical composition of inorganic minerals, organic matter, and microfossils, such as carbonates, cellulose, and biogenic silica (e.g., Leng and Marshall, 2004; Ricketts and Johnson, 1996; Sachse et al., 2004; Steinman et al., 2012; Tibby and Tiller, 2007; Tyler et al., 2008; Wolfe et al., 2002).

An important challenge for palaeoclimatology is to obtain quantitative estimates of past climate conditions, such as temperature, precipitation and wind speed/direction. Whilst some lake-based proxies are nominally quantitative, e.g. the inference of lake water balance via salinity reconstructions (e.g., Barr et al., 2014; Chivas et al., 1985; Fritz et al., 1991; Gasse et al., 1997; Tibby and Tiller, 2007) or $\delta^{18}O$ (e.g., Leng and Marshall, 2004; Steinman et al., 2012), translation of lake geochemical and stable isotopic signatures to quantifiable palaeoclimate values remains problematic. Lakes are complex and dynamic systems and often respond to climatic forcing in a non-linear manner (Battarbee, 2000; Wigdahl et al., 2014). Individual lakes respond to climatic forcing differently due to differences in morphology, groundwater interaction, catchment processes, and past and current lake conditions. Consequently, lakes will rarely exhibit the same

response to changes in climate, or produce identical palaeoclimate records to other lakes in close geographic proximity (Tierney et al., 2013; Tyler et al., 2015). This variability undermines confidence in lake based palaeoclimate records and efforts to combine those records with other archives to form regional composites (Emile-Geay et al., 2017).

In parallel to the need to both conceptualise and model climate systems, and recognising the complexities of lake systems, numerical modelling can be applied to model lake responses to climate projections, as well as resolve some of the uncertainties encountered in lake based palaeoclimate studies. Specifically, by quantifying the hydrological, isotopic and geochemical balances and fluxes within a lake system, numerical modelling may enable or improve quantitative inferences from numerous proxies. Several numerical lake models have been developed – a full review is included in section 1.5. However, most lake models are developed for specific lakes, and often lack modelling routines required for different lakes. There is a need for a general lake model, able to simulate lake water balance, water chemistry, $\delta^{18}O$, and $\delta^{2}H$ for all hypothesised palaeoclimate conditions and future climate projections.

2 Thesis aims and objectives

The primary aim of this project is to develop a holistic lake model focussed on meeting the needs for palaeoclimate research, and to collect sufficient data to test and validate the model. In parallel to model development this thesis aims to contribute to related fields that develop techniques and input data that may be relevant or required for the development of lake models.

Specifically, the objectives of the research underpinning this thesis are:

- Establish a lake monitoring program to collect input and calibration data that can be applied to the lake model.
- Investigate numerous geochemical and isotopic indicators of lakes in the Newer Volcanic Province, Victoria, Australia to better identify how they interact with the surrounding landscape, and what physical processes are potentially under-represented in conceptual and numerical lake models.
- Develop new techniques for the sampling of rainfall from remote regions, specifically for $\delta^{18}O$ and $\delta^{2}H$ analysis.
- To develop a holistic lake model that is versatile enough to be applied to almost any lake, coupling mass and energy balances, groundwater, isotopes, chemistry, and catchment processes.

3 Background

3.1 Lake modelling concepts and terminology

Most numerical lake models can be separated into two categories – mass balance or energy balance models (Fig. 1.1). Many lake models incorporate additional modelling processes, but the mass balance or energy balance routine typically represents the core model upon which other modelling routines are constructed. Mass balance models are based on the conservation of mass – by quantifying and balancing all known fluxes and reservoirs, unknown quantities can be derived. Energy balance models apply a similar concept – a balance of fluxes and reservoirs – except that the quantities are based on energy, not mass (Henderson-Sellers, 1986).

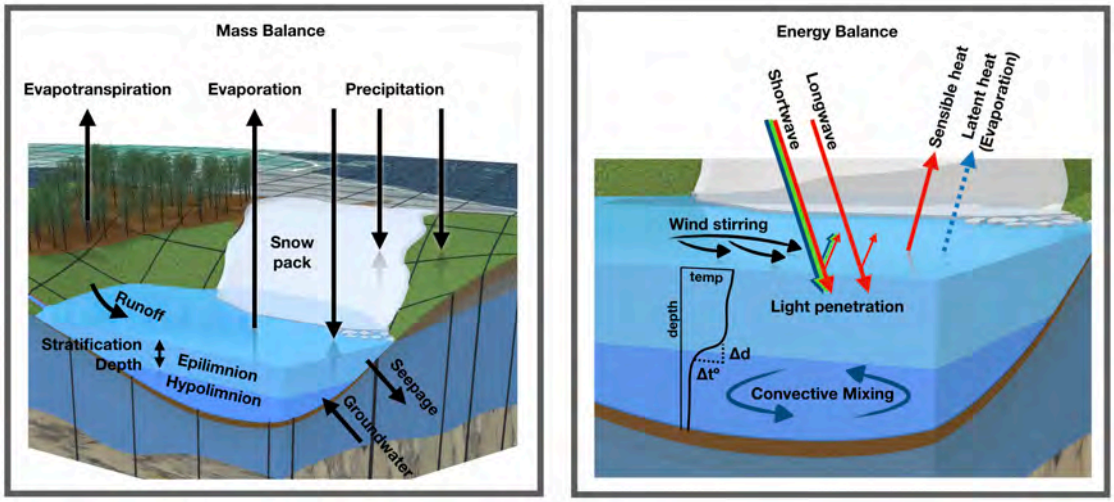

Figure 1.1: Schematic showing example mass and energy balance models for lakes. Fluxes and reservoirs will vary depending on model designs. Only a portion of possible fluxes and reservoirs are shown.

A mass balance is therefore useful for modelling the hydrological change in a lake system, while an energy balance model is well suited for modelling the energy change of a lake, identifiable as variations in evaporation rate, stratification depth and water temperature. Many lake energy balance models incorporate some mass balance functionality, whereas few mass balance models include a complete energy balance functionality. The basic functionality of a mass balance or energy balance model can be extended via additional modelling of physical processes. For example, a mass balance lake model may include equations to estimate evaporation, or functions to estimate hydrological fluxes in the lake catchment by modelling canopy interception and soil infiltration (e.g., Steinman et al., 2010; Van Boxel et al., 2013). Lake mass balance models can be further enhanced by coupling the hydrological mass balance routines to equations describing isotopic and geochemical fractionation and mixing. The isotopic and geochemical equations are then calculated in parallel with the water mass balance to determine the isotopic and chemical composition for each hydrological flux and reservoir.

3.2 Model design: considerations for palaeoclimate research

Lake based palaeoclimate research imposes several requirements on model design. While lake models that are designed to investigate short term, current, or steady state phenomena can often rely on input data and parameterisations derived from observations, such as evaporation rates, lake stratification depth, and water temperatures, such data is unlikely to be valid for all past lake and climate conditions. Most meteorological and lake observations only extend across a few decades to centuries, whereas lake based palaeoclimate reconstructions may span over tens, to hundreds of thousands of years. Additionally, many lake derived palaeoclimate reconstructions infer climatic and hydrological conditions that extend well outside the range of observations (Fig. 1.2). The problem of data scarcity and the associated difficulty of defining valid model parameters presents a major challenge for palaeoclimate model-based research.

One potential solution is to incorporate additional modelling routines to estimate the missing data. For example, an energy balance model may be applied to estimate stratification depth, water temperature and evaporative flux of the lake (Henderson-Sellers, 1986), using only the model state and meteorological input data. Likewise, lake-groundwater fluxes vary based on the lake water level and surrounding aquifer hydraulic head heights. Defining these fluxes via direct observation is challenging even for current lake conditions. Coupling a groundwater and soil percolation model to the lake model can provide estimates of groundwater flux, while only requiring meteorological data and hydrogeological parameters. In contrast to the lake-groundwater fluxes, hydrogeological parameters represent the material properties of the surrounding geology (Anderson et al., 2015), and are unlikely to vary significantly over the timeframe of most lake model simulations.

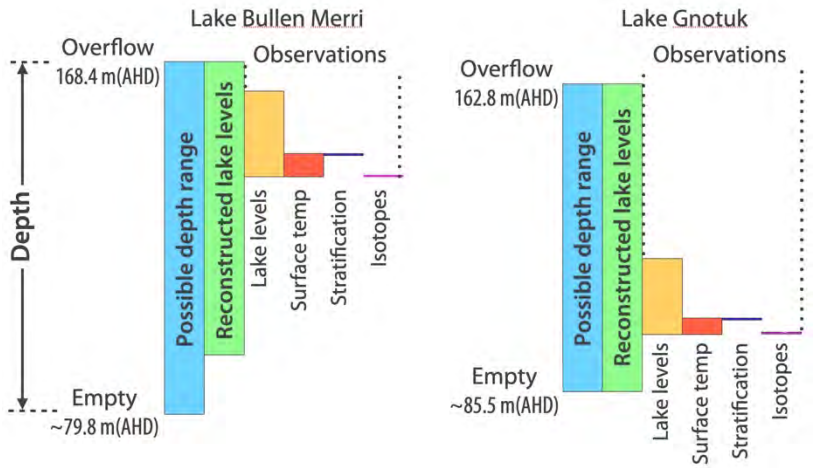

Figure 1.2: An example of the mismatch between hypothesised lake level reconstructions (green) and observational data (between the dotted lines, in orange, red, dark blue, magenta) for two lakes. The observational data for surface water temperature, stratification and isotopes is displayed as the range of lake levels for which observations have been recorded (Jones, 1995; Tibby and Tiller, 2007; Timms, 1976). Heights shown are relative to the Australian Height Datum (AHD).

3.3 Model design: matching the model to the proxy

Proxies commonly used for palaeoclimate studies also impose requirements on model development. Some proxies are linked directly to the lake water level and can be used to infer past hydroclimate conditions. E.g. inference of lake water level based on sediment texture (Wilkins et al., 2013). However, most proxies are used to infer lake salinity or isotopic composition, providing an indirect route to reconstructions of a lake's hydrological balance and hydroclimate. Changes in salinity may be reflected both ecologically, through changes in populations of diatoms (e.g., Barr et al., 2014; Fritz et al., 1991; Rudd et al., 2016), or through geochemical indicators, such as the Sr/Ca and Mg/Ca ratios found within ostracod valves (e.g., Chivas et al., 1985; De Deckker et al., 1999). Variations in the isotopes of water – $\delta^{18}O$ and $\delta^{2}H$ – may also be identified in proxies derived from carbonates, organic components of lacustrine sediment, and biogenic silica (e.g., Leng and Marshall, 2004; Ricketts and Johnson, 1996; Sachse et al., 2004; Steinman et al., 2012; Tyler et al., 2008; Wolfe et al., 2002). To facilitate comparisons between model results and proxy derived values, palaeoclimate lake models should incorporate equations describing water chemistry and isotopic mixing and fractionation, to provide quantitative values of lake water chemistry, $\delta^{18}O$, and $\delta^{2}H$. Such models can be further extended through the development of transfer functions that estimate the transport and incorporation of isotopes and chemistry from the lake water into the proxy material, sometimes described as a proxy system model (Dee et al., 2018).

3.4 Model design: physical processes

A lake model designed for palaeoclimate research may require numerous modelling routines to account for data scarcity, and to facilitate model-proxy comparisons. While it is tempting (and would greatly simplify model development) to think of a lake model as a hierarchy, with a main program – perhaps a mass balance model – used to determine hydrological behaviour, which is then used as the basis of calculations by coupled model routines, this is rarely the case. Whilst in a few cases, model routines may exist in comparative isolation from the rest of the model, many modelling routines describe physical processes that interact with many other aspects of the lake system. For example, changes to lake hydrology may alter the concentrations of lake water chemistry, resulting in a feedback process as lake chemistry, in turn, modulates evaporation rates (Harbeck Jr, 1955). Water chemistry and lake surface temperature influence the evaporative fractionation of $\delta^{18}O$ and $\delta^{2}H$ (Gat, 2010). Likewise lake water depth can affect the lake temperature profile, which in turn influences evaporation (Henderson-Sellers, 1986; Stepanenko et al., 2013). Wind speed has an effect on evaporation, which can drive changes in

the hydrological balance, potentially changing the degree of sheltering and influencing the wind speed at the lake surface (McNaughton, 1988; Penman, 1948).

One interaction that may be of significant concern for palaeoclimate lake studies is the lake-groundwater interaction and the potential flow-on effects to lake geochemistry. A through-flow lake, where groundwater flows into a lake, while the lake simultaneously loses water as out-seepage, may prevent salts from accumulating in the lake waters, as they are removed by the outgoing seepage. A recharge lake has negligible groundwater influx, but may have substantial out-seepage to groundwater (Winter, 1999). In contrast, a terminal (or discharge) lake has negligible out-seepage, resulting in high salinity as salts can accumulate. Terminal lakes are ideal for palaeoclimate research as they are often considered as palaeo-rain gauges, and water chemistry is assumed to be closely correlated with lake water level (Gell et al., 1994). Unfortunately, some lakes can transition from through-flow at high lake levels to terminal lakes at lower lake levels (Winter, 1976). This means that the chemical mass balance of a lake may change during periods of high lake levels, and care must be taken in comparing geochemistry derived proxy results separated by periods of inferred high lake levels.

These examples represent only a few of the potential interactions within and around a lake . The relationship between the various modelling routines can be better described as a network, with the calculated values from each modelling routine shared amongst other routines, to use as required. Therefore, in addition to the inclusion of modelling routines designed to circumvent the issues of data scarcity and problematic parameters, or designed to facilitate model-proxy comparisons, model development must also account for interactions between the numerous physical processes within a lake and surrounding environment.

3.5 Lake modelling: a review

Several researchers have developed lake models (Table 1.1) capable of modelling various aspects of lake systems ranging from relatively simple spreadsheet mass balance models (Becht and Harper, 2002; Ohlendorf et al., 2013; Yihdego and Webb, 2012) to more complex models featuring some combination of energy balance modelling, coupled isotope modelling, coupled chemistry or groundwater modelling (Crowe, 1993; Jones et al., 2001; Kirono et al., 2009; Kirono et al., 2012; Van Boxel et al., 2013; Vassiljev et al., 1995). Examples of hydrological mass balance models include the model developed by Jones et al. (2001) and used by Kirono et al. (2009), incorporating lake salinity and its influence on evaporation, and a soil component that modelled evapotranspiration and the percolation of water through the soil to the lake. Becht

and Harper (2002) incorporated a hypothetical unconfined aquifer in their mass balance model, modelling the interaction between the lake and groundwater and the buffering of lake level change in response to changes in hydroclimate. This method may be suitable for short term projections, but is untested over longer model runs, and over significant changes in hydrological conditions. The model introduced by Van Boxel et al. (2013) is of interest as it incorporates a 2D grid design allowing for varying ratios of vegetation surfaces in the catchment as the lake rises and falls.

Combining the hydrological flux calculations with calculations for mixing and fractionation of isotopes results in a coupled hydrologic-isotopic model (Gibson et al., 2002; Hostetler and Benson, 1994; Jones et al., 2005; Ricketts and Johnson, 1996; Shapley et al., 2008; Steinman et al., 2012; Steinman et al., 2010; Stets et al., 2010). A common inclusion to these models is the modelling of the stratification of the lake, as the isotopic composition of lake waters varies vertically due to seasonal and diurnal stratification (Kumar et al., 2001; Sánchez-España et al., 2014; Steinman et al., 2010). Most of these models model $\delta^{18}O$ and $\delta^{2}H$, though there are examples that incorporate tritium isotopes (Kumar et al., 2001; Michel and Kraemer, 1995).

The incorporation of stratification into a mass balance model also requires a method of determining the level of stratification. Some mass balance models use empirical data from lake surveys (Steinman et al., 2010). However, as palaeoclimate conditions often differ from current conditions, with a corresponding change in lake surface area, depth and wind protection, these empirical values are not necessarily valid (Imberger, 2001). Inclusion of a lake energy balance model can resolve this problem. The need for an understanding of water quality in reservoirs has produced many models able to model the stratification behavior of a lake. These models are typically one dimensional, with multiple layers able to vary in thickness and properties depending on the thermal profile of the lake (Henderson-Sellers, 1984; Hipsey et al., 2013; Hondzo, 1993; Hostetler and Bartlein, 1990; Imberger et al., 1978; Riley and Stefan, 1988). The model of Hostetler and Bartlein (1990) has been applied recently to form the basis of a proxy system model, coupling mass and energy balances, isotopes and salinity (Dee et al., 2018).

Not all lake models have been considered in the summary table. In particular, models that focus on just a single aspect of a lake have not been not been included – e.g. models that only model the energy balance (Henderson-Sellers, 1984), or the fractionation of the stable isotopes of water (Craig and Gordon, 1965).

Table 1.1: Lake models that have been applied, or may potentially be applied, to palaeoclimate research. Cells marked in green denote features that may enable the use of the model in data-sparse scenarios, such as outside the range of meteorological records. Cells marked in yellow indicate partial support for features, e.g. models that include support for salinity may need further work to incorporate individual ions used as palaeoclimate proxies.

Model	Purpose	Language	Mass balance	Energy balance	Isotope enabled	Chemistry enabled	Catchment & surface inflow	Soils & evapo-transpiration	Groundwater	Ice and Snow	Evaporation	Lake stratification	Lake temperatures	Other Notes
Imberger, et al. (1978)	Water quality, temperature profiles	Fortran 95	Yes	Yes	No	No	Parameterised flows	Parameterised flows	Parameterised flows	Yes	Energy balance	Energy balance	Energy balance	
Riley and Stefan (1988)	Water quality	Unknown	Yes	Yes	No	Bio-chemical	Parameterised flows	No	Parameterised flows	Yes	Energy balance	Energy balance	Energy balance	Assessed by Yao, et al. (2014)
Hostetler and Bartlein (1990)	Climate	Fortran	Yes	Yes	No	No	Parameterised flows	No	No	Yes	Energy balance	Energy balance	Energy balance	Applied to Pyramid & Harney-Malheur lakes, USA. Assessed by Yao, et al. (2014)
Crowe (1993)	Groundwater flux estimation	Unknown	Yes	No	No	Salinity	Runoff and percolation to subsurface drainage	Single layer	Mass balance	Yes	Meteorological records	No	No	Applied to Wabamun Lake, Alberta, Canada
Hostetler and Benson (1994)	Climate	Fortran	Yes	Yes	Yes	No	Parameterised flows	No	No	Yes	Energy balance	Energy balance	Energy balance	Extention of Hostetler and Bartlein (1990)
Michel and Kraemer (1995), Kumar et al. (2001).	Residence time, Groundwater flux estimation	Unknown	Yes	No	Yes	No	Parameterised flows	Parameterised flows	Parameterised flows	No	Meteorological records	No	No	Applied to Finger Lakes in NY, USA, and Lake Naini , India
Vassiljev, et al. (1995)	Climate	Unknown	Yes	Yes	No	No	Runoff and percolation to subsurface drainage	Two layer,	Parameterised flows	Partial	Meteorological records	No	No	Applied to Lake Viljandi, Estonia
Kirono, et al. (2009) Jones, et al. (2001)	Climate	Fortran	Yes	No	No	Salinity	Percolation through soil to subsurface drainage (baseflow)	Single layer. CRAE (Morton 1983)	Baseflow derived from soil percolation	No	CRLE (Morton 1983)	No	No	Applied to maar lakes in Victoria, Australia
Becht and Harper (2002)	Safe yield/ abstraction	Spread-sheet	Yes	No	No	No	Parameterised flows	No	Hypothetical aquifer used as lake buffer (Darcy 1856)	No	Meteorological records	No	No	Lake Naivasha, Kenya.
Gibson, et al. (2002)	Throughflow, residence time and catchment runoff.	Unknown	Yes	No	Yes	No	Model result	No	No	Yes	Meteorological records	No	No	Uses ^{18}O and ^{2}H observations to estimate difficult to measure water fluxes.
Benson and Paillet (2002)	Climate	Fortran	Yes	No	Yes	No	Parameterised flows	No	Parameterised flows	No	Meteorological records	Parameterised	No	Applied to Pyramid lake, Nevada

Table 1.1: continued.

Model	Purpose	Language	Mass balance	Energy balance	Isotope enabled	Chemistry enabled	Catchment & surface inflow	Soils & evapo-transpiration	Groundwater	Ice and Snow	Evaporation	Lake stratification	Lake temperatures	Other Notes
Jones, et al. (2005)	Climate	Spread-sheet	Yes	No	Yes	No	Runoff coefficient	No	Parameterised flows	No	Penman, 1948. (Simplified, Linacre 1992)	No	No	Applied to Nar Golu, Turkey
Shapley, et al. (2008)	Climate	Visual Basic	Yes	No	Yes	No	Parameterised flows	No	Percentage of lake volume outflow	Partial	Regional Penman equations	Parameterised	No	Applied to Evans Lake and Jones Lake, Montana, USA.
Jones and Imbers (2010)	Climate	Spread-sheet	Yes	No	Yes	No	Unknown	No	Parameterised flows	No	Penman, 1948. (Simplified, Linacre 1992)	No	No	Based on Jones 2005
Steinman, et al. (2010)	Climate	Stella	Yes	No	Yes	No	Runoff and percolation to subsurface drainage	2 layers. Penman, (1948) / Valiantzas, 2006).	Percentage of lake volume outflow	Partial	Penman (1948) / Valiantzas (2006)	Parameterised	Observed	Applied to Castor and Scanlon Lakes, Washington State.
Yihdego and Webb (2012) Yihdego, et al. (2015) Yihdego and Webb (2015)	Hydrological and salinity budgeting	Spread-sheet	Yes	No	No	Salinity	Tanh method (Grayson et al, 1996)	No	Darcy (1856)	No	Meteorological records	No	No	Applied to lakes in Victoria, Australia.
Van Boxel, et al. (2013)	Climate	Unknown	Yes	No	No	No	Runoff & delayed percolation to subsurface drainage	Single layer. Penman (1948) + crop coefficient + linear relation to soil moisture	No	No	Penman (1948)	No	No	Gridded lake model. Applied to Lake La Cocha, Colombia.
Ohlendorf, et al. (2013)	Climate	Unknown	Yes	No	No	No	Runoff	Penman (1948) / Brutsaert (1982)	Parameterised flows	No	Penman (1948) / Brutsaert (1982)	No	No	Applied to Laguna Potrok Aike (Argentina)
Hipsey, et al. (2013)	General lake model	C / Fortran	Yes	Yes	No	Salinity	Parameterised flows	Parameterised flows	Parameterised flows	Yes	Energy balance	Energy balance	Energy balance	Assessed by Yao, et al. (2014)
Dee, et al. (2018)	Climate	Fortran / Python	Yes	Yes	Yes	Salinity	Parameterised flows	No	No	Yes	Energy balance	Energy balance	Energy balance	Based on Hostetler and Bartlein, 1990. Includes transfer functions for full proxy system modelling.
CHIMBLE (Chemistry, Hydrology, Isotope, Mass Balance for Lake Environs)	Climate	R / C++	Yes	Yes	Yes	Yes	Runoff and percolation to groundwater or subsurface drainage	Yes	Finite difference model (MODFLOW subset)	Partial	Energy balance	Energy balance	Energy balance	Model developed for this thesis

There are no lake models identified that can be described as holistic lake models, capable of modelling all the major physical, hydrological, isotopic and geochemical processes within a lake system. Typically, lake models are developed for specific lakes, and lack the capacity to model processes associated with different lakes. There is a need for a holistic lake model, coupling lake hydrology, catchment processes, groundwater, energy balance, isotopes, water chemistry, and other relevant physical processes. Chapter Five of this thesis describes the development and calibration of a holistic lake model called CHIMBLE (Chemistry, Hydrology, Isotopes, Mass-Balance for Lake Environs).

3.6 Data requirements for modelling of lakes

A key requirement of numerical lake models developed for palaeoclimate research is that model input data should be available for the entire time period studied. The input data required for lake modelling varies depending on model complexity. Meteorological data is almost always a necessary input, and may be derived from climate model simulations or synthesised by applying suitable shifts and transformations to existing time series of meteorological observations, e.g. Yihdego et al. (2015). Lake hypsographic data (relating lake surface depth to surface area and volume) may be compiled from topographic and bathymetric sources, or estimated using mathematical models, e.g. Jones et al. (2005). In many cases, additional modelling routines may be applied as a substitute for input data.

However, some input data cannot be estimated with a modelling approach. A particular challenge relates to isotope enabled models as they require the isotopic composition of all source waters, specifically, the isotopic composition of precipitation. Isotope enabled climate models, or models describing the spatial and temporal distribution of isotopes in precipitation, may be a source for such data, e.g. Bowen and Revenaugh (2003); Brady et al. (2019); Hollins et al. (2018). The isotopic data used to develop and validate these models is typically based on the Global Network of Isotopes in Precipitation (GNIP) database, a spatially diverse, but sparse, dataset of monthly $\delta^{18}O$ and $\delta^{2}H$ in precipitation collected since 1961 (Rozanski et al., 1993). Unfortunately, the temporal resolution and spatial distribution of GNIP stations – there are only 15 in Australia (Hollins et al., 2018) – present a degree of uncertainty regarding the isotopic composition of rainfall remote from the stations. This introduces a level of uncertainty in isotope enabled lake models, and also limits the potential to correlate the isotopic composition of rainfall to synoptic weather patterns and topographic factors.

The need for additional modelling, and the uncertainties regarding some input data, demonstrate that modelling requirements may therefore extend well beyond the shoreline of the lake or the catchment boundary. Development of a general lake model for palaeoclimate research requires the inclusion of research and understanding from many related fields, such as meteorology, groundwater, and lake dynamics, as well as long term monitoring to provide observational data that may be used as input data and to validate lake models.

3.7 Site selection and regional background.

Development and calibration of a useful holistic lake model requires study sites with long term lake observations that cover a large range of lake conditions – water levels, water chemistry, $\delta^{18}O$ and $\delta^{2}H$ values, water temperatures, stratification depth, and groundwater head heights. Lake Bullen Merri and Lake Gnotuk in the Newer Volcanic Province – a region of monogenetic basalt plains in the south east of Australia – were chosen for model development. Lake Bullen Merri and Lake Gnotuk are maar crater lakes in neighbouring craters. Lake Bullen Merri and Lake Gnotuk are ideal candidates for model development as they share the same climate, yet have significant hydrological and chemical differences. They also have long records documenting a wide range of lake conditions. Lake Bullen Merri is brackish, and ~60 m deep, whereas Lake Gnotuk is 15 m deep and hypersaline. The water level of lake Gnotuk is 40m lower than that of Lake Bullen Merri, and water levels for both lakes have dropped ~30 m since 1841 (Jones et al., 2001). Both lakes are positioned within an unconfined aquifer of sandstones and overlying basalt, and separated from deeper groundwater aquifers by the Gellibrand Marl (SKM, 2009; Victorian Department of Sustainability and Environment, 2012).

Several other lakes in the Newer Volcanic Province were also considered as candidates for model development. There are over 400 volcanic eruption points in the region (Boyce, 2013), resulting in many permanent lakes. The frequency and variety of these lakes, combined with their location in between the Pacific, Indian and Southern Oceans and associated climate systems, make many of them important palaeoclimate study sites (Gouramanis et al., 2013; Neukom and Gergis, 2012). Therefore, in addition to the model development, and in recognition of the need for a broad understanding of the interactions between lakes and the surrounding landscape, an additional ten lakes were monitored over the course of this PhD.

4 Thesis outline

4.1 Chapter Two: Lake water ionic and isotopic signatures in relation to lake morphology and hydrogeology: a case study of twelve lakes in south-eastern Australia

This chapter describes monitoring data on twelve lakes of the Newer Volcanic Province in Western Victoria. Lake water levels, and water samples for major and minor ions, $\delta^{18}O$, and $\delta^{2}H$ analysis were collected every two months for ~three years. A full description of each lake is included in this chapter. These data were used to investigate several aspects of lake behaviour. $\delta^{18}O$ and $\delta^{2}H$ data were applied to investigate differences in evaporation and isotopic fractionation between lakes. Oxygen and hydrogen isotopes fractionate during evaporation, enriching the lake water in ^{18}O and ^{2}H along a trend line known as a local evaporation line. A 'Lake Sheltering Index', describing the degree of wind sheltering for each lake was correlated to the slopes of the isotopic enrichment of lake water, relating the isotopic behaviour of a lake to basin morphology and lake water level. Cl^-/Br^- and HCO_3^-/Cl^- geochemical indicators were applied to investigate the source of waters that contribute to the lakes, and d-excess (an isotopic metric that indicates the degree of evaporation) was applied to investigate the groundwater regime for each lake following Barton et al. (2013). Based on Cl^-/Br^- results, nine of the twelve lakes studied interact with the shallow groundwater aquifer across the region, but three lakes are situated above the aquifer, and have Cl^-/Br^- ratios that may reflect rainfall ratios. HCO_3^-/Cl^- and d-excess values for each lake showed significant seasonal variation. It is proposed that increased spatial resolution of groundwater sampling may be required to refine the results from the HCO_3^-/Cl^- indicator, and the use of a conservative ion such as Cl^- is likely to be more effective than d-excess to determine the groundwater regime as d-excess is related to the residence time of water, whereas a conservative ion is related to the solute residence time within a lake.

4.2 Chapter Three: Development of an autonomous, monthly and daily, rainfall sampler for isotope research

This chapter describes the development of an autonomous rainfall sampler, designed to collect daily and integrated monthly rainfall samples to facilitate isotopic rainfall sampling in remote locations. $\delta^{18}O$ and $\delta^{2}H$ of precipitation is a necessary input dataset for isotope enabled lake models. Sampling of rainfall for isotopes is problematic as evaporation must be minimised to avoid isotopic enrichment of samples. This chapter describes the design of the rainfall sampler, and two methods of preventing evaporation – paraffin oil and inlet tubes (where the sample bottle is sealed, and water enters via a small tube. Once water enters the sample bottle, the tube

is sealed, and evaporation is limited to the tiny water surface area in the tube). The inlet tube method requires bespoke bottle caps, which were fabricated using a 3D printer. The effectiveness of four different types of plastics at preventing water and isotopic transfer through the bottle caps was also assessed. Of the four plastics tested – PLA, ABS, PETG and ABS treated with acetone – acetone treated ABS was most effective at minimising evaporation, closely followed by PETG. A coupled hydrologic-isotopic model was applied to the results, successfully modelling the fractionation process for all methods and closure types. A closure modelling technique that takes advantage of the different evaporation rates between monthly and daily samples was then developed to back-calculate the initial sample volume and isotopic composition.

This chapter is published as:

ANKOR M. J., TYLER J. J. & HUGHES C. E. 2019. Development of an autonomous, monthly and daily, rainfall sampler for isotope research. *Journal of Hydrology*. 575, 31-41.

4.3 Chapter Four: Development of a spreadsheet-based model for transient groundwater modelling

Groundwater is rarely implemented in lake models developed for palaeoclimate research, yet is often a key component in a lake's hydrological balance (Winter, 1999). More importantly, the lake-groundwater interaction varies depending on hydroclimate and lake water level. A spreadsheet groundwater model (A2016) designed for transient groundwater modelling was developed, based on the mathematics of MODFLOW (McDonald and Harbaugh, 1988), with support for confined and unconfined aquifers, recharge, evapotranspiration, injection and abstraction pumping, heterogeneous hydraulic conductivity and storativity, fixed head, no flow and head dependent boundary conditions. A2016 was developed as a prototype to the finite difference groundwater module incorporated in the lake model developed for this thesis (Chapter Five). A2016 is also relevant for pedagogical purposes, as it runs in the Excel spreadsheet program and this chapter includes a full theoretical background. A2016 is compared with MODFLOW and the spreadsheet model of Karahan and Ayvaz (2005) for nine different scenarios. In all scenarios, A2016 and MODFLOW gave identical results, demonstrating that the mathematical basis of A2016 is correct. The spreadsheet model was also applied to demonstrate that using a specified saturated thickness approximation for the groundwater region beneath a lake may result in more realistic representation of lake-groundwater interaction.

This chapter is published as:

ANKOR M. J. & TYLER J. J. 2019. Development of a spreadsheet-based model for transient groundwater modelling. *Hydrogeology Journal*. 1-14.

4.4 Chapter Five: A holistic lake model for palaeoclimate research

This chapter describes the design, calibration, and model simulations of a holistic lake model called CHIMBLE (Chemistry, Hydrology, Isotopes, Mass Balance for Lake Environs). CHIMBLE couples a hydrological mass balance to a lake energy balance, a finite difference groundwater model, a dual layer soil catchment model, water chemistry, and an $\delta^{18}O$ and $\delta^{2}H$ isotope model. CHIMBLE was calibrated for Lake Bullen Merri and Lake Gnotuk. Since 1849 the water levels have dropped by almost 30m at a similar rate for both lakes. This substantial lake level change is beneficial from a model development and calibration perspective as it provides a way to test the lake-groundwater-catchment interaction across a large range. Though numerous aspects of the lake and groundwater system are under-determined, CHIMBLE was able to simulate lake level change and salinity change in both lakes to a high degree of accuracy over the entire historical range. More importantly, the parameters established by calibration were within likely estimates and parsimonious with the condition of both lakes. The modelling was able to demonstrate that both lakes are through-flow lakes at high lake levels, becoming terminal lakes as lake levels fall. In more recent decades, the seasonal cycle of salinity and $\delta^{18}O$ and $\delta^{2}H$ was well represented but only when lake stratification depths were decreased relative to the initial simulation. The parameters for the energy balance model were initially based on data from 1969–1972 (Timms, 1976). This need to alter the parameters for the stratification model suggests a recent increase in water turbidity - and hence light absorbance - which is consistent with the trajectory towards eutrophication in these lakes (Timms, 2005). The simulations of Lake Bullen Merri and Lake Gnotuk suggest that complex lake models like CHIMBLE can give excellent results, even in poorly defined and under-determined lake systems.

4.5 Chapter Six: Discussion and future directions

This chapter reviews and summarise the combined findings of chapters two to five. The results are discussed with respect to the overall field of palaeoclimate research, as well as potential implications to other areas of research. The need for ongoing development in both lake model design, and in associated research fields such as microclimate, wind sheltering, isotopic sampling and modelling and lake monitoring is also discussed with a focus on future research requirements.

5 References

Anderson, M.P., Woessner, W.W., Hunt, R.J., 2015. Applied groundwater modeling: simulation of flow and advective transport. Academic press.

Barr, C., Tibby, J., Gell, P., Tyler, J., Zawadzki, A., Jacobsen, G.E., 2014. Climate variability in south-eastern Australia over the last 1500 years inferred from the high-resolution diatom records of two crater lakes. Quaternary Science Reviews, 95: 115-131. DOI:https://doi.org/10.1016/j.quascirev.2014.05.001

Barton, A., Herczeg, A., Dahlhaus, P., Cox, J., 2013. A geochemical approach to determining the hydrological regime of wetlands in a volcanic plain, south-eastern Australia (Chapter 7) In: Ribeiro L, Stigter TY, Chambel A et al.(eds) Groundwater and Ecosystems. IAH Selected Papers on Hydrogeology Series 18. CRC Press (Taylor and Francis). p.

Battarbee, R.W., 2000. Palaeolimnological approaches to climate change, with special regard to the biological record. Quaternary Science Reviews, 19(1–5): 107-124. DOI:http://dx.doi.org/10.1016/S0277-3791(99)00057-8

Becht, R., Harper, D., 2002. Towards an understanding of human impact upon the hydrology of Lake Naivasha, Kenya. The International Journal of Aquatic Sciences, 488(1): 1-11.

Benson, L., Paillet, F., 2002. HIBAL: a hydrologic-isotopic-balance model for application to paleolake systems. Quaternary Science Reviews(12): 1521-1539.

Bowen, G.J., Revenaugh, J., 2003. Interpolating the isotopic composition of modern meteoric precipitation. Water Resources Research, 39(10): 1-13. DOI:10.1029/2003WR002086

Boyce, J., 2013. The Newer Volcanics Province of southeastern Australia: a new classification scheme and distribution map for eruption centres. Australian Journal of Earth Sciences, 60(4): 449-462.

Brady, E., Stevenson, S., Bailey, D., Liu, Z., Noone, D., Nusbaumer, J., Otto-Bliesner, B.L., Tabor, C., Tomas, R., Wong, T., Zhang, J., Zhu, J., 2019. The Connected Isotopic Water Cycle in the Community Earth System Model Version 1. Journal of Advances in Modeling Earth Systems, 11(8): 2547-2566. DOI:10.1029/2019ms001663

Brookes, J.D., Hamilton, D.P., 2009. Lakes and Reservoirs of Australia and New Zealand. In: Likens, G.E. (Ed.), Encyclopedia of Inland Waters. Academic Press, Oxford, pp. 513-523. DOI:https://doi.org/10.1016/B978-012370626-3.00037-5

Chivas, A.R., De Deckker, P., Shelley, J.M.G., 1985. Strontium content of ostracods indicates lacustrine palaeosalinity. Nature, 316(6025): 251-253. DOI:10.1038/316251a0

Cohen, A.S., 2003. Paleolimnology: the history and evolution of lake systems. Oxford University Press, USA.

Craig, H., Gordon, L.I., 1965. Deuterium and oxygen 18 variations in the ocean and the marine atmosphere. In: Schink, D.R., Corless, J.T. (Eds.), Marine Geochemistry. University, Rhode Island, University, Rhode Island, pp. 277-374.

Crowe, a.S., 1993. The application of a coupled water-balance-salinity model to evaluate the sensitivity of a lake dominated by groundwater to climatic variability. Journal of Hydrology, 141(1-4): 33-73. DOI:10.1016/0022-1694(93)90044-A

De Deckker, P., Chivas, A.R., Shelley, J.M.G., 1999. Uptake of Mg and Sr in the euryhaline ostracod Cyprideis determined from in vitro experiments. Palaeogeography, Palaeoclimatology, Palaeoecology, 148(1): 105-116. DOI:https://doi.org/10.1016/S0031-0182(98)00178-3

Dee, S.G., Russell, J.M., Morrill, C., Chen, Z., Neary, A., 2018. PRYSM v2.0: A Proxy System Model for Lacustrine Archives. Paleoceanography and Paleoclimatology, 33(11): 1250-1269. DOI:10.1029/2018PA003413

Emile-Geay, J., McKay, N.P., Kaufman, D.S., von Gunten, L., Wang, J., Anchukaitis, K.J., Abram, N.J., Addison, J.A., Curran, M.A.J., Evans, M.N., Henley, B.J., Hao, Z., Martrat, B., McGregor, H.V., Neukom, R., Pederson, G.T., Stenni, B., Thirumalai, K., Werner, J.P., Xu, C., Divine, D.V., Dixon, B.C., Gergis, J., Mundo, I.A., Nakatsuka, T., Phipps, S.J., Routson, C.C., Steig, E.J., Tierney, J.E., Tyler, J.J., Allen, K.J., Bertler, N.A.N., Björklund, J., Chase, B.M., Chen, M.-T., Cook, E., de Jong, R., DeLong, K.L., Dixon, D.A., Ekaykin, A.A., Ersek, V., Filipsson, H.L., Francus, P., Freund, M.B., Frezzotti, M., Gaire, N.P., Gajewski, K., Ge, Q., Goosse, H., Gornostaeva, A., Grosjean, M., Horiuchi, K., Hormes, A., Husum, K., Isaksson, E., Kandasamy, S., Kawamura, K., Kilbourne, K.H., Koç, N., Leduc, G., Linderholm, H.W., Lorrey, A.M., Mikhalenko, V., Mortyn, P.G., Motoyama, H., Moy, A.D., Mulvaney, R., Munz, P.M., Nash, D.J., Oerter, H., Opel, T., Orsi, A.J., Ovchinnikov, D.V., Porter, T.J., Roop, H.A., Saenger, C., Sano, M., Sauchyn, D., Saunders, K.M., Seidenkrantz, M.-S., Severi, M., Shao, X., Sicre, M.-A., Sigl, M., Sinclair, K., St. George, S., St. Jacques, J.-M., Thamban, M., Kuwar Thapa, U., Thomas, E.R., Turney, C., Uemura, R., Viau, A.E., Vladimirova, D.O., Wahl, E.R., White, J.W.C., Yu, Z., Zinke, J., Consortium, P.A.k., 2017. A global multiproxy database for temperature reconstructions of the Common Era. Scientific Data, 4(1): 170088. DOI:10.1038/sdata.2017.88

Fritz, S.C., Juggins, S., Battarbee, R.W., Engstrom, D.R., 1991. Reconstruction of past changes in salinity and climate using a diatom-based transfer function. Nature, 352(6337): 706.

Gasse, F., Barker, P., Gell, P.A., Fritz, S.C., Chalie, F., 1997. Diatom-inferred salinity in palaeolakes: an indirect tracer of climate change. Quaternary Science Reviews, 16(6): 547-563.

Gat, J., 2010. Isotope hydrology a study of the water cycle. London: Imperial College Press, London.

Gell, P.A., Barker, P.A., De Deckker, P., Last, W.M., Jelicic, L., 1994. The Holocene history of West Basin Lake, Victoria, Australia; chemical changes based on fossil biota and sediment mineralogy. Journal of Paleolimnology, 12(3): 235-258.

Gibson, J.J., Prepas, E.E., McEachern, P., 2002. Quantitative comparison of lake throughflow, residency, and catchment runoff using stable isotopes: modelling and results from a regional survey of Boreal lakes. Journal of Hydrology, 262(1): 128-144.

Gouramanis, C., De Deckker, P., Switzer, A.D., Wilkins, D., 2013. Cross-continent comparison of high-resolution Holocene climate records from southern Australia—Deciphering the impacts of far-field teleconnections. Earth-Science Reviews, 121: 55-72.

Harbeck Jr, G.E., 1955. The effect of salinity on evaporation. 272A.

Henderson-Sellers, B., 1984. Development and application of "U.S.E.D.": A hydroclimate lake stratification model. Ecological Modelling, 21(4): 233-246. DOI:10.1016/0304-3800(84)90061-9

Henderson-Sellers, B., 1986. Calculating the surface energy balance for lake and reservoir modeling: A review. Reviews of Geophysics, 24(3): 625-649. DOI:10.1029/RG024i003p00625

Hipsey, M., Bruce, L., Hamilton, D., 2013. GLM General Lake Model. Model overview and user information. The University of Western Australia Technical Manual, Perth, Australia.

Hollins, S.E., Hughes, C.E., Crawford, J., Cendón, D.I., Meredith, K.M., 2018. Rainfall isotope variations over the Australian continent–Implications for hydrology and isoscape applications. Science of the Total Environment, 645: 630-645.

Hondzo, M., 1993. Lake water temperature simulation model. Journal of Hydraulic Engineering, 119(11): 1251-1251.

Hostetler, S.W., Bartlein, P.J., 1990. Simulation of lake evaporation with application to modeling lake level variations of Harney-Malheur Lake, Oregon. Water Resources Research, 26(10): 2603-2612.

Hostetler, S.W., Benson, L.V., 1994. Stable isotopes of oxygen and hydrogen in the Truckee River–Pyramid Lake surface-water system. 2. A predictive model of δ18O and 182H in Pyramid Lake. Limnology and Oceanography, 39(2): 356-364. DOI:10.4319/lo.1994.39.2.0356

Imberger, J., 2001. Characterizing the dynamical regimes of a lake. Physical processes in natural waters. Univ. de Girona, Spain: Servei de Publicacions: 77-92.

Imberger, J., Loh, I., Hebbert, B., Patterson, J., 1978. Dynamics of reservoir of medium size. Journal of the Hydraulics Division, 104(5): 725-743.

Jones, M.D., Imbers, J., 2010. Modeling Mediterranean lake isotope variability. Global and Planetary Change, 71(3): 193-200. DOI:https://doi.org/10.1016/j.gloplacha.2009.10.001

Jones, M.D., Leng, M.J., Roberts, C.N., Türkeş, M., Moyeed, R., 2005. A Coupled Calibration and Modelling Approach to the Understanding of Dry-Land Lake Oxygen Isotope Records. Journal of Paleolimnology, 34(3): 391-411. DOI:10.1007/s10933-005-6743-0

Jones, R.N., 1995. Modelling hydrologic and climatic controls of closed lakes, western Victoria. Ph. D. Thesis, University of Melbourne.

Jones, R.N., McMahon, T.A., Bowler, J.M., 2001. Modelling historical lake levels and recent climate change at three closed lakes, Western Victoria, Australia (c.1840–1990). Journal of Hydrology, 246(1): 159-180.

Karahan, H., Ayvaz, M.T., 2005. Time-dependent groundwater modeling using spreadsheet. Computer applications in engineering education, 13(3): 192-199.

Kirono, D.G., Jones, R.N., Kent, D.M., 2009. Modelling future lake levels and salinity at three lakes, Western Victoria. National Research Flagships, Climate Adaptation CSIRO—A report prepared for the Environment Protection Authority (EPA) Victoria.

Kirono, D.G.C., Kent, D.M., Jones, R.N., Leahy, P.J., 2012. Assessing Climate Change Impacts and Risks on Three Salt Lakes in Western Victoria, Australia. Human and Ecological Risk Assessment: An International Journal, 18(1): 152-167. DOI:10.1080/10807039.2012.632291

Kumar, U.S., Jacob, N., Navada, S.V., Rao, S.M., Nachiappan, R.P., Kumar, B., Murthy, J.S.R., 2001. Environmental isotope study on hydrodynamics of Lake Naini, Uttar Pradesh, India. Hydrological Processes, 15(3): 425-439. DOI:10.1002/hyp.158

Leng, M.J., Marshall, J.D., 2004. Palaeoclimate interpretation of stable isotope data from lake sediment archives. Quaternary Science Reviews, 23(7): 811-831.

McDonald, M.G., Harbaugh, A.W., 1988. A modular three-dimensional finite-difference ground-water flow model.

McNaughton, K., 1988. 1. Effects of windbreaks on turbulent transport and microclimate. Agriculture, Ecosystems & Environment, 22: 17-39.

Michel, R.L., Kraemer, T.F., 1995. Use of isotopic data to estimate water residence times of the Finger Lakes, New York. Journal of Hydrology, 164(1): 1-18. DOI:https://doi.org/10.1016/0022-1694(94)02586-Z

Neukom, R., Gergis, J., 2012. Southern Hemisphere high-resolution palaeoclimate records of the last 2000 years. The Holocene, 22(5): 501-524. DOI:10.1177/0959683611427335

Ohlendorf, C., Fey, M., Gebhardt, C., Haberzettl, T., Lücke, A., Mayr, C., Schäbitz, F., Wille, M., Zolitschka, B., 2013. Mechanisms of lake-level change at Laguna Potrok Aike (Argentina) - insights from hydrological balance calculations. Quaternary Science Reviews, 71: 27-45. DOI:10.1016/j.quascirev.2012.10.040

Penman, H.L., 1948. Natural Evaporation from Open Water, Bare Soil and Grass. Proceedings of the Royal Society of London. Series A, Mathematical and Physical Sciences, 193(1032): 120-145.

Ricketts, R.D., Johnson, T.C., 1996. Climate change in the Turkana basin as deduced from a 4000 year long δO 18 record. Earth and Planetary Science Letters, 142(1): 7-17.

Riley, M.J., Stefan, H.G., 1988. Minlake: A dynamic lake water quality simulation model. Ecological Modelling, 43(3-4): 155-182. DOI:10.1016/0304-3800(88)90002-6

Rozanski, K., Araguás-Araguás, L., Gonfiantini, R., 1993. Isotopic patterns in modern global precipitation. Climate change in continental isotopic records: 1-36.

Rudd, R.C., Tyler, J.J., Tibby, J., Yokoyama, Y., Tavernier, I., Verleyen, E., Fukui, M., Takano, Y., 2016. A diatom-inferred record of lake variability during the last 900 years in

Lützow–Holm Bay, East Antarctica. Journal of Quaternary Science, 31(2): 114-125. DOI:10.1002/jqs.2845

Sachse, D., Radke, J., Gleixner, G., 2004. Hydrogen isotope ratios of recent lacustrine sedimentary n-alkanes record modern climate variability. Geochimica et Cosmochimica Acta, 68(23): 4877-4889.

Sánchez-España, J., Diez Ercilla, M., Pérez Cerdán, F., Yusta, I., Boyce, A.J., 2014. Hydrological investigation of a multi-stratified pit lake using radioactive and stable isotopes combined with hydrometric monitoring. Journal of Hydrology, 511: 494-508. DOI:10.1016/j.jhydrol.2014.02.003

Shapley, M.D., Ito, E., Donovan, J.J., 2008. Isotopic evolution and climate paleorecords: modeling boundary effects in groundwater-dominated lakes. Journal of Paleolimnology, 39(1): 17-33.

Skinner, L., 2008. Facing future climate change: is the past relevant? Philosophical Transactions of the Royal Society A: Mathematical, Physical and Engineering Sciences, 366(1885): 4627-4645. DOI:doi:10.1098/rsta.2008.0228

SKM, 2009. The Victorian Aquifer Framework – Summary report submitted to DSE, Melbourne.

Steinman, B.A., Abbott, M.B., Mann, M.E., Stansell, N.D., Finney, B.P., 2012. 1,500 year quantitative reconstruction of winter precipitation in the Pacific Northwest. Proceedings of the National Academy of Sciences, 109(29): 11619-11623. DOI:10.1073/pnas.1201083109

Steinman, B.A., Rosenmeier, M.F., Abbott, M.B., Bain, D.J., 2010. The isotopic and hydrologic response of small, closed-basin lakes to climate forcing from predictive models: Application to paleoclimate studies in the upper Columbia River basin. Limnology and Oceanography, 55(6): 2231–2245.

Stepanenko, V.M., Martynov, A., Jöhnk, K.D., Subin, Z.M., Perroud, M., Fang, X., Beyrich, F., Mironov, D., Goyette, S., 2013. A one-dimensional model intercomparison study of thermal regime of a shallow, turbid midlatitude lake. Geoscientific Model Development, 6(4): 1337-1352. DOI:10.5194/gmd-6-1337-2013

Stets, E.G., Winter, T.C., Rosenberry, D.O., Striegl, R.G., 2010. Quantification of surface water and groundwater flows to open- and closed-basin lakes in a headwaters watershed using a descriptive oxygen stable isotope model. Water Resources Research, 46(3). DOI:10.1029/2009WR007793

Tibby, J., Tiller, D., 2007. Climate–water quality relationships in three Western Victorian (Australia) lakes 1984–2000. Hydrobiologia, 591(1): 219-234. DOI:10.1007/s10750-007-0804-5

Tierney, J.E., Smerdon, J.E., Anchukaitis, K.J., Seager, R., 2013. Multidecadal variability in East African hydroclimate controlled by the Indian Ocean. Nature, 493(7432): 389.

Timms, B.V., 1976. A Comparative study of the limnology of three maar lakes in western Victoria. I. Physiography and physicochemical features. Marine and Freshwater Research, 27(1): 35-60.

Timms, B.V., 2005. Salt Lakes in Australia: Present Problems and Prognosis for the Future. Hydrobiologia, 552(1): 1-15. DOI:10.1007/s10750-005-1501-x

Tyler, J., Leng, M., Sloane, H., Sachse, D., Gleixner, G., 2008. Oxygen isotope ratios of sedimentary biogenic silica reflect the European transcontinental climate gradient. Journal of Quaternary Science, 23(4): 341-350.

Tyler, J.J., Mills, K., Barr, C., Sniderman, J.M.K., Gell, P.A., Karoly, D.J., 2015. Identifying coherent patterns of environmental change between multiple, multivariate records: an application to four 1000-year diatom records from Victoria, Australia. Quaternary Science Reviews, 119(October): 94-105. DOI:10.1016/j.quascirev.2015.04.010

Van Boxel, J.H., González-Carranza, Z., Hooghiemstra, H., Bierkens, M., Vélez, M.I., 2013. Reconstructing past precipitation from lake levels and inverse modelling for Andean Lake La Cocha. Journal of Paleolimnology, 51(1): 63-77. DOI:10.1007/s10933-013-9755-1

Vassiljev, J., Harrison, S.P., Haxeltine, A., 1995. Recent Lake-Level and Outflow Variations at Lake Viljandi, Estonia - Validation of a Coupled Lake Catchment Modeling Scheme for Climate-Change Studies. Journal of Hydrology, 170(1-4): 63-77. DOI:Doi 10.1016/0022-1694(95)02691-H

Victorian Department of Sustainability and Environment, 2012. Victorian Aquifer Framework: updates for seamless mapping of aquifer surfaces. Produced by GHD for the Victorian Department of Sustainability and Environment.

Wigdahl, C.R., Saros, J.E., Fritz, S.C., Stone, J.R., Engstrom, D.R., 2014. The influence of basin morphometry on the regional coherence of patterns of diatom-inferred salinity in lakes of the northern Great Plains (USA). The Holocene, 24(5): 603-613. DOI:10.1177/0959683614523154

Wilkins, D., Gouramanis, C., De Deckker, P., Fifield, L.K., Olley, J., 2013. Holocene lake-level fluctuations in Lakes Keilambete and Gnotuk, southwestern Victoria, Australia. The Holocene, 23(6): 784-795. DOI:10.1177/0959683612471983

Winter, T.C., 1976. Numerical simulation analysis of the interaction of lakes and ground water. USGS Professional Paper 1001.

Winter, T.C., 1999. Relation of streams, lakes, and wetlands to groundwater flow systems. Hydrogeology Journal, 7(1): 28-45. DOI:10.1007/s100400050178

Wolfe, B.B., Edwards, T.W., Elgood, R.J., Beuning, K.R., 2002. Carbon and oxygen isotope analysis of lake sediment cellulose: methods and applications, Tracking environmental change using lake sediments. Springer, pp. 373-400.

Yihdego, Y., Webb, J., 2012. Modelling of seasonal and long-term trends in lake salinity in southwestern Victoria, Australia. Journal of environmental management, 112: 149-159.

Yihdego, Y., Webb, J., 2015. Use of a conceptual hydrogeological model and a time variant water budget analysis to determine controls on salinity in Lake Burrumbeet in southeast Australia. Environmental Earth Sciences, 73(4): 1587-1600. DOI:10.1007/s12665-014-3509-x

Yihdego, Y., Webb, J.A., Leahy, P., 2015. Modelling of lake level under climate change conditions: Lake Purrumbete in southeastern Australia. Environmental Earth Sciences, 73(7): 3855-3872. DOI:10.1007/s12665-014-3669-8

Chapter 2

Lake water ionic and isotopic signatures in relation to lake morphology and hydrogeology: a case study of twelve lakes in south-eastern Australia

Notes: This chapter has been formatted to match the rest of this thesis. Figure and table numbers have been prefixed with the chapter number (e.g. Fig. 1 has been changed to Fig. 2.1).

Statement of Authorship

Title of Paper	Lake water ionic and isotopic signatures in relation to lake morphology and hydrogeology: a case study of twelve lakes in south-eastern Australia
Publication Status	☐ Published ☐ Accepted for Publication ☐ Submitted for Publication ☒ Unpublished and Unsubmitted w ork w ritten in manuscript style
Publication Details	

Principal Author

Name of Principal Author (Candidate)	Martin Ankor
Contribution to the Paper	Corresponding Author. Devised initial concept, model design, experimental design. Analysis of results. Wrote manuscript.
Overall percentage (%)	90%
Certification:	This paper reports on original research I conducted during the period of my Higher Degree by Research candidature and is not subject to any obligations or contractual agreements with a third party that would constrain its inclusion in this thesis. I am the primary author of this paper.
Signature	Date: 19 Dec 2019

Co-Author Contributions

By signing the Statement of Authorship, each author certifies that:

i. the candidate's stated contribution to the publication is accurate (as detailed above);

ii. permission is granted for the candidate in include the publication in the thesis; and

iii. the sum of all co-author contributions is equal to 100% less the candidate's stated contribution.

Name of Co-Author	Jonathan T. Tyler
Contribution to the Paper	Evaluated and edited manuscript.
Signature	Date: 19 Dec 2019

Please cut and paste additional co-author panels here as required.

Abstract

Understanding how lakes interact with their surrounding landscape is a crucial aspect for many lake-based studies, particularly lake modelling projects. The influence of a lake's position in the landscape on the evaporative isotopic fractionation of oxygen and hydrogen, sources of lake water, and groundwater interaction was investigated via ionic and isotopic indicators collected during three years of bi-monthly monitoring at 12 lakes in the Newer Volcanic Field, south-eastern Australia. $\delta^{18}O$ and $\delta^{2}H$ values correlated in all lakes, with regression slopes typical of water evaporation, albeit subject to differences in slope between lakes. For some lakes, hypersaline waters are known to be an important driver of surface water isotopic fractionation, and the effect of this process was modelled using a hydrologic-isotopic mass balance model. Combining data from all sites - including the salinity corrected evaporation slopes for hypersaline lakes - indicated that the slopes of those regression lines (known as local evaporation lines, or LELs) correlate (r^2=0.89) with the degree to which each lake was sheltered. Cl^-/Br^- and HCO_3^-/Cl^- geochemical ratios were used to identify likely source water for each lake. Cl^-/Br^- ratios for nine of the lakes are similar to the local groundwater. However, three of the lakes had Cl^-/Br^- ratios well below the ratio of seawater and groundwater. As these lakes are also situated high in the topography above the regional aquifers these observations are interpreted as indicating that the lakes are predominantly fed by rain water. HCO_3^-/Cl^- ratios were used to infer whether the source water to each lake was surface fed (high HCO_3^-/Cl^-) or from deeper aquifers. The HCO_3^-/Cl^- results were less clear, with several lakes that are likely groundwater fed being classified as surface fed. It is proposed that an increased spatial density of groundwater sampling is required, especially in regions of younger volcanic ejecta (stony rises) where a high HCO_3^-/Cl^- ratio is commonplace due to rapid water infiltration and associated mineral weathering. Lake water deuterium excess (d-excess) has been proposed as a tracer of lake-groundwater interaction in this region, however the data presented here indicates that seasonal variability obscures any trace of a groundwater signature. It is suggested that a conservative ion may be more likely to indicate the lake-groundwater regime (through-flow or terminal), as d-excess reflects the water residence time, rather than the solute residence time. Overall, the studied lakes in the Newer Volcanic Province are marked by a preponderance of groundwater dependency, in addition to significant evaporative enrichment of major ions and isotopes. These observations lay the foundation, both for palaeoclimatic research using lake sediment geochemistry in the region, as well as for better understanding the response of these lakes to future climate change.

1 Introduction

Lakes are important landscape features, often with high social, cultural and ecological value (Ramsar Convention Secretariat, 2013). Lake sediments also provide insight into past climates, using a variety of geochemical and palaeoecological tracers (Cohen, 2003). However, lakes are also complex, non-linear systems, and a single climatic trend may result in very different hydrological, isotopic and geochemical responses in lakes across a region. (Battarbee, 2000; Rueda et al., 2005; Wigdahl et al., 2014). There is therefore a need for detailed information on the behaviour of lakes across a range of hydroclimate conditions, both to predict how lakes will behave under future climate scenarios, and for improved quantification of past climatic estimates derived from lake sedimentary archives.

A lake's hydrological, isotopic and geochemical balance is primarily determined by incoming and outgoing fluxes (Benson and Paillet, 2002; Crowe, 1993). Defining how lakes interact with the surrounding landscape is a crucial step in the development of conceptual and numerical lake models. Here, we describe a ~3 year dataset of lake water major/minor ionic composition, $\delta^{18}O$, and $\delta^{2}H$ for twelve lakes in south-eastern Australia. These data are used to investigate how differing lake and catchment morphologies are represented in the $\delta^{18}O$ and $\delta^{2}H$ composition of lake waters. In addition, the ratio of Cl^-/Br^- is used to investigate the source of lake water, namely groundwater vs precipitation. Previous research has suggested that HCO_3^-/Cl^- is also indicative of the source water, while d-excess is a tracer of groundwater influence in the region, specifically whether a lake is a through-flow lake with short residence time, or a terminal lake with long residence time (Barton et al., 2013). HCO_3^-/Cl^- and d-excess indicators are assessed to determine their effectiveness over a full seasonal range of lake conditions.

2 Background

2.1 Oxygen and hydrogen isotopes in lake water

The stable isotopes of water – $\delta^{18}O$ and $\delta^{2}H$ – are important tracers of fluxes through the hydrological cycle, commonly used in groundwater studies, ecological and forensic source identification, palaeoclimate research, climate and meteorological studies and water resource management (Bowen and Revenaugh, 2003; Gibson and Reid, 2014; Mattey et al., 2008; Treble et al., 2005; Tyler et al., 2007; Tyler et al., 2015). An important trait of the stable isotopes of water is the preferential evaporation of lighter isotopes (^{16}O, ^{1}H) resulting in an enrichment of heavier isotopes (^{18}O, ^{2}H) in surface waters (Gat, 2010). The isotopic composition of a water

body is a convolution of the fluxes that have contributed to its hydrologic budget and its evaporative history. Isotopic values are commonly reported in delta notation as per mil (‰) deviations from Vienna Standard Mean Ocean Water (VSMOW2), which is related to the isotopic ratio by:

$$\delta_x = 1000\left(\frac{R_x}{R_{VSMOW2}} - 1\right) \quad (1)$$

Where R is $^{18}O/^{16}O$, or $^{2}H/^{1}H$ and x is the hydrological component in question. Fractionation of water isotopes during evaporation is described by the model of Craig and Gordon (1965). This model describes a two stage fractionation process, with equilibrium fractionation occurring at the phase change at the water surface, and then a second transport fractionation (sometimes called kinetic fractionation) process from the water surface, through a diffusion layer into the turbulent atmosphere (Fig. 2.1, Eq. 2).

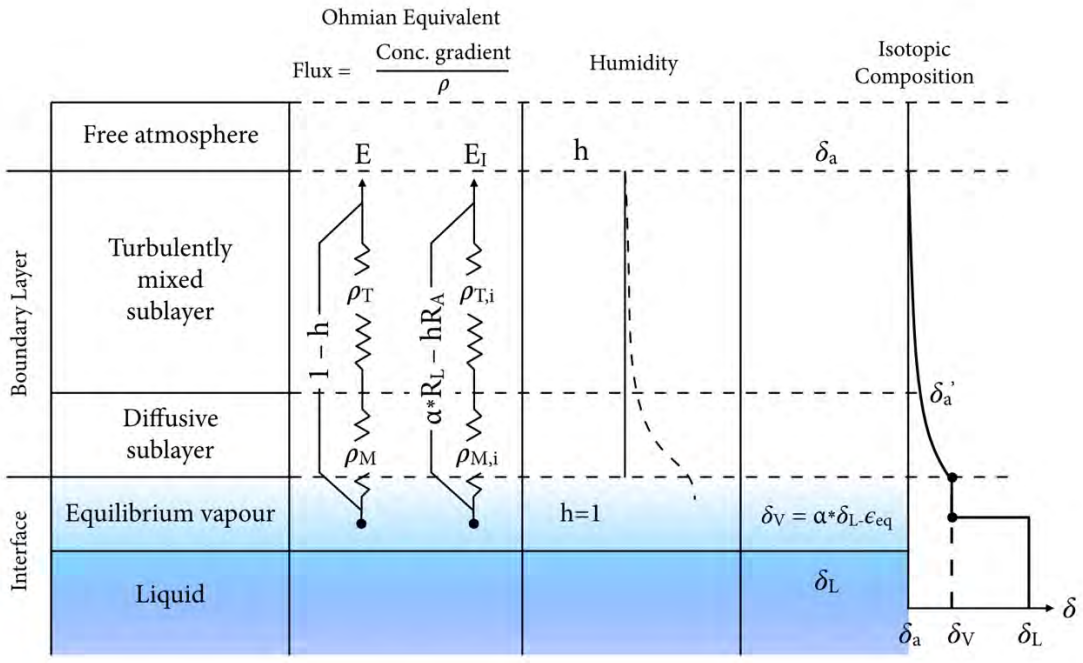

Figure 2.1: The Craig–Gordon model of fractionation of water isotopes during evaporation from a free water surface, adapted from (Gat, 2010).

$$\delta_E = \frac{\alpha^*\delta_w - h_n\delta_A - \varepsilon_{eq} - \varepsilon_{kin}}{1 - h_n + 0.001\varepsilon_{kin}} \quad (2)$$

Where α^* is the reciprocal of the equilibrium fractionation factor, calculated using the equations of Horita and Wesolowski (1994). δ_W and δ_A represent the isotopic composition of the water and atmosphere, and h_n refers to the relative humidity normalised to the water temperature.

The equilibrium separation is calculated by:

$$\varepsilon_{eq} = 1000(1 - \alpha^*) \quad (3)$$

While the transport isotopic separation is calculated by:

$$\varepsilon_{kin} = (1 - h_n)\theta n C_k \quad (4)$$

C_k is an experimentally derived constant determined by Merlivat (1978) as 28.5‰ for $\delta^{18}O$, and 25.1‰ for δ^2H. θ is a parameter describing the transport resistance of the diffusion layer, while n is a turbulence factor that relates isotopic separation to wind conditions. The θ and n terms both have a range of 0 to 1 and define the behaviour of the transport separation. Many authors use alternative values of C_k for lake studies – 14.2‰ for $\delta^{18}O$, and 12.5‰ for δ^2H – assuming an n value of 0.5 (Gibson et al., 2015; Horita et al., 2008). θ is often assumed to be 1 for lakes (Gibson et al., 2015; Gibson et al., 2002; Jones et al., 2005; Shapley et al., 2008; Steinman et al., 2010), however, lower values of θ (e.g. θ = 0.5) have been used to match observations for some lakes (Kebede et al., 2009). While not commonly used for lake research, an alternative formulation for transport fractionation (Merlivat and Jouzel, 1979) is widely used in global climate models (Gibson et al., 2015).

Evaporative fractionation of a body of water follows a generally linear trend in the relationship between $\delta^{18}O$ and δ^2H, known as a local evaporation line (LEL). The slope of LELs is dependent upon the degree of equilibrium and transport fractionation. Soil water samples that evaporate through a non-turbulent, fully formed diffusion layer typically have a value of 1 for both θ and n terms, defining an LEL with a slope of ~2.5 (Gat, 2010). Conversely, a value of 0 for θn will completely remove the transport separation and yield a local evaporation line of ~8. This is similar to the slope of $\delta^{18}O$ vs. δ^2H in global precipitation, known as the global meteoric water line (GMWL). Craig and Gordon (1965) defined the slope of the GMWL as $\delta^2H = 8\delta^{18}O + 10$. Differences in the slopes of LELs have often been assumed to be primarily influenced by near surface humidity (Holland and Turekian, 2010; Mackay et al., 2003; Mook and Rozanski, 2000; Shapley et al., 2008). However, Gat (2010) demonstrated that in scenarios where δ_A is in equilibrium with the isotopic composition of precipitation (δ_P) the slope is not affected by humidity. δ_A is often assumed to be in equilibrium with local δ_P, however recent studies have suggested that this assumption may only be valid around the time that the rainfall is sampled (Crawford et al., 2019). One aspect that is rarely considered in assessing lake LELs is the lake morphology. It is commonly accepted that the n turbulence parameter is set to 1 for soil

evaporation, and 0.5 for lakes. However turbulence varies along this continuum as a function of the interaction between wind speed and the degree of sheltering afforded by the topography and vegetation. There has been limited work exploring how *n* varies between these two end-members.

2.2 Cl^-/Br^- and HCO_3^-/Cl^-: determination of lake source water

Determination of the sources of lake water is a key criterion for understanding and modelling lake hydrological variability. The ratio between chloride and bromide ions (Cl^-/Br^-) may be applied as a tracer to identify the sources that contribute to a body of water (Alcalá and Custodio, 2008; Cartwright et al., 2013; Cartwright et al., 2006; Davis et al., 1998). While Cl^- and Br^- are both conservative halogen ions with broadly similar geochemical characteristics (Behne, 1953), there are differences in both natural variation, as well as solubility, with bromine compounds being more soluble than chlorine, leading to Br^- being concentrated in brines while halite precipitates out (Davis et al., 1998). The Cl^-/Br^- mass ratio of seawater is 288-292 (650–660 molar ratio) and Cl^-/Br^- ratios in precipitation generally decrease with distance from the coastline (Cartwright et al., 2006; Davis et al., 1998). Davis et al. (1998) speculated that the Cl^-/Br^- of precipitation ranged from 130 to 180 (293–406 molar ratio) near the coast, decreasing to 50 (112 molar ratio) several hundred kilometers inland, based on a compilation of seven studies, with data from Alaska, Hawaii, Antarctica, Massachusetts, Ontario, Nevada, California, and Arizona. The studied lakes in south-eastern Australia extend from 25 to 76 km from the coastline and may potentially display a gradient in Cl^-/Br^- ratios. In contrast, Cl^-/Br^- ratios of groundwater within the study area are similar to those of seawater (Barton et al., 2013; Cartwright et al., 2013), likely due to halite precipitation and redissolution (eg: evapotranspiration, salt lakes), or windblown halite from the interior of the continent (Cartwright et al., 2006).

An alternative indicator of lake source water is the HCO_3^-/Cl^- ratio (Barton et al., 2013). The HCO_3^-/Cl^- ratio may be applied to determine whether the lake is predominantly fed by surface waters or groundwater. High HCO_3^- and low Cl^- is attributed to mineral weathering by surface water and interflow that produces HCO_3^- as a by-product, whereas groundwater is assumed to be higher salinity and lower HCO_3^- due to carbonate precipitation and evapotranspiration in the soil zone (Barton et al., 2013). Previous research in western Victoria used HCO_3^-/Cl^- ratios to infer the dominant source of water at 24 sites, including rivers, estuaries and lakes (Barton et al., 2013). However, that study was conducted over a limited temporal range, with only one or

two samples per site over a three month period. There are therefore uncertainties regarding the degree to which HCO_3^-/Cl^- ratios reflect lake-groundwater interaction over the seasonal cycle.

2.3 Deuterium excess: determination of lake-groundwater regime

An important aspect of lake hydrology is the interaction between surface waters and surrounding groundwater (Winter, 1999). A method for determining the groundwater regime of lake systems – applied specifically to lakes in the Newer Volcanic Province, south-eastern Australia, is to use the deuterium excess (a measure of deviation from the GMWL: d-excess = $\delta^2H - 8\delta^{18}O$) of a lake to define the flow regime (Barton et al., 2013). Low d-excess values are considered indicative of a terminal lake (also described as discharge lake), with long residence times and negligible flux from the lake to groundwater, reflecting a high contribution of evaporation to outgoing hydrological fluxes. Conversely, high d-excess has been interpreted to reflect a through-flow lake–groundwater system with short residence times, where evaporation contributes only a relatively small fraction of the outgoing fluxes (Barton et al., 2013).

2.4 Site selection

The Newer Volcanic Province in western Victoria and south-eastern South Australia is a unique region in Australia, with a multitude of lakes featuring different origins, morphologies, and hydrological and chemical behaviour, all sharing a similar climate (Figure 2.2).

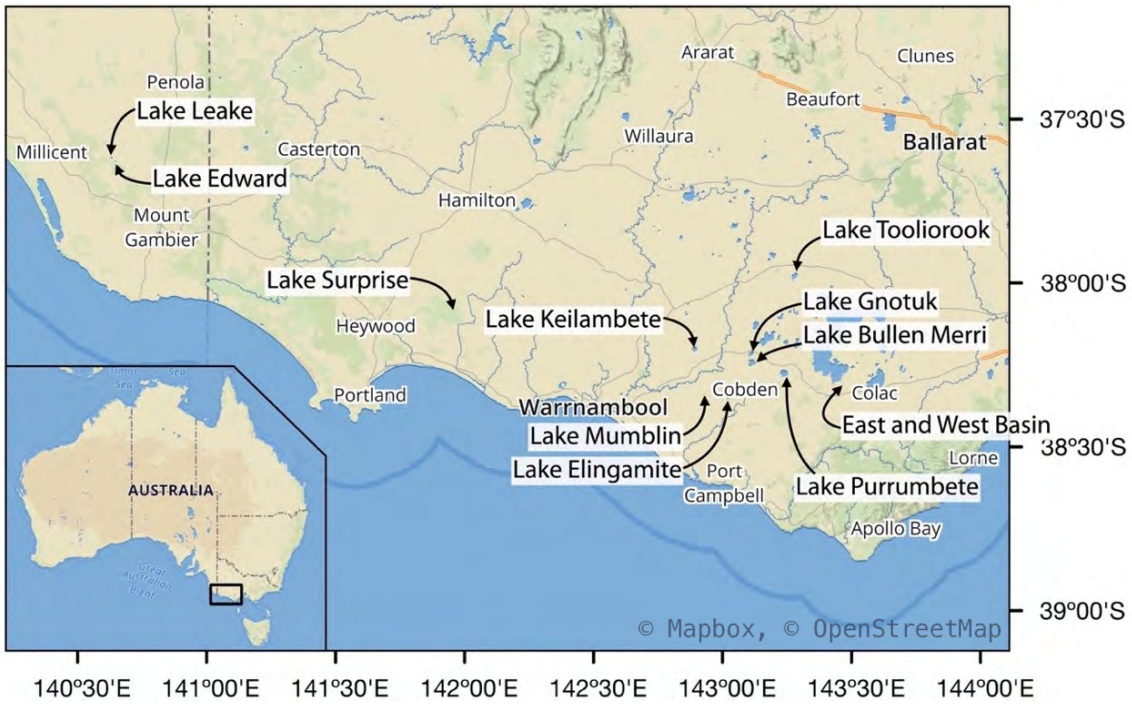

Figure 2.2: Regional setting, showing lakes of the Newer Volcanic Province monitored during this study.

The lakes sampled for this study (Table 2.1) were chosen mostly for their relevance to palaeoclimate research, combined with their potential for lake modelling. Desirable attributes were that the lake had to be permanent in nature – as it can be problematic to model through a dry lake scenario – with the potential to develop datasets required for model calibration, such as: lake and catchment bathymetry and topography; lake water level records; water temperature and/or stratification; and the isotopic and geochemical composition of lake waters. In addition, lakes with simple morphology and catchments were preferred to avoid obfuscation of lake responses with signals from well outside the lake. An extended background for each lake is included in the supplementary data, detailing lake conditions, morphology, and the lake's position in relation to the surrounding geological formations and aquifers.

	(Sep 2018)		Aug 2016 – Sep 2018						
	Depth (m)	Water level (mAHD)	Average surface water temp °C	Average pH	Average TDS (mg/L)	Average $\delta^{18}O$	Average $\delta^{2}H$	Local evaporation line slope	Lake sheltering index
Lake Leake	2	90.4	17.6 ± 5.3	8.7 ± 0.4	3790 ± 910	1.9 ± 2.9	10.3 ± 13.7	4.6	14
Lake Edward	6	104.1	16.8 ± 4.9	6.3 ± 0.9	4280 ± 340	2.6 ± 0.8	13.8 ± 3.5	4.6	17
Lake Surprise	11.5	78.5	17.1 ± 5.6	8.9 ± 0.5	452 ± 27	2.5 ± 0.6	9.7 ± 2.2	4.2	5
Lake Keilambete	~9 *	103.02 (Aug 2016)	18 ± 6.9	8.8 ± 0.1	101600 ± 4100	2.7 ± 0.5	12.0 ± 2.7	4.6	27
Lake Mumblin	~8	90.4	17.2 ± 6.3	7.8 ± 0.7	788 ± 69	2.8 ± 1.9	11.3 ± 7.8	4.2	7
Lake Elingamite	3.2 *	125.8	17.2 ± 6.8	8.0 ± 0.5	3600 ± 800	1.1 ± 2.7	7.4 ± 13.8	5.0	67
Lake Bullen Merri	60	139.5	16.1 ± 4.8	9.3 ± 0.1	9260 ± 190	3.1 ± 0.2	16.0 ± 1.4	5.5	19
Lake Gnotuk	15	100.2	17.8 ± 5.6	8.6 ± 0.1	69700 ± 2200	3.4 ± 0.3	15.7 ± 2.5	4.7	12
Lake Purrumbete	45	135.0	15.6 ± 4.5	8.7 ± 0.3	525 ± 27	2.0 ± 0.5	12.6 ± 3.0	5.5	100
Lake Tooliorook	~2 *	-	16.4 ± 5.6	8.0 ± 0.5	3930 ± 850	1.0 ± 1.7	6.5 ± 8.7	5.4	100
West Basin	12.5 *	111.5	16.5 ± 5.3	8.8 ± 0.1	107000 ± 9400	3.4 ± 0.9	12.2 ± 4.3	4.1	14
East Basin	12.1 *	113.6	16.5 ± 5.2	9.0 ± 0.1	82500 ± 4700	2.3 ± 0.8	14.9 ± 4.1	4.4	18

Table 2.1: Summary table of lakes studied. Average values shown are from Aug 2016 to Sep 2018 and are shown to one standard deviation. Lake sheltering index is defined as the ratio of horizontal to vertical distance from the highest windbreak (typically crater rim) to lake centre.
** Lake level data is from earlier studies. See the supporting information for specific lake details.*

2.5 Regional setting

The Newer Volcanic Province is a region of Pliocene to Holocene monogenetic basalt plains extending from Melbourne, Victoria to Millicent, South Australia. There are over 416 eruption centres within the province, including numerous maars and scoria cones (Boyce, 2013). The Newer Volcanic Province is divided into 3 sub-provinces: The Central Highlands, the Western Plains, and the Mt Gambier sub-province (Cas et al., 1993; Nicholls and Joyce, 1989). The Central Highlands lie in the north east of the province with the basalt flows directly overlying the Palaeozoic basement (Lesti et al., 2008). The Western Plains sub-province contains all the Victorian lakes studied, and overlies the Cretaceous–Tertiary sediments of the Otway Basin. The Mt Gambier sub-province is a small region of volcanic plains overlying the limestones of

the Gambier Embayment of the Otway Basin and includes the youngest eruption centre of Mt Gambier with an age of ~5 ka (van Otterloo and Cas, 2013) as well as Lakes Leake and Edward. Almost all the maar or maar-cone complexes are in the south of the Newer Volcanic Province (Fig. 2.2) where the basalts overlie the sediments and associated aquifers of the Otway Basin (Boyce, 2013). This provides somewhat of a constraint on lake locations. Of the twelve lakes that fitted the selection criteria, specifically that they form permanent water bodies, only three, Lake Surprise, Lake Mumblin and Lake Tooliorook, are not maar or maar-cone lakes, likely due to the tendency for maar eruptions to form deep craters below the natural topography.

Underlying the Western Plains sub-province are several sedimentary formations of the Otway Basin, the configuration of which varies across the province. In the north-eastern part of the basin lies the Sandringham Sands formation (previously defined as the Moorabool Viaduct formation), consisting of shallow marine and fluvial sands and sandstones, lying unconformably above sediments from a marine transgression and late Miocene regression. The underlying units are either the Gellibrand Marl or the Port Campbell limestone. The Port Campbell Limestone extends inland tapering out ~50 km from the current coastline. Below the limestone lies the Gellibrand Marl, an aquitard of clay and marl, which extends beneath all the lakes. The Gellibrand Marl near the lakes is typically several hundred metres thick and separates the aquifers contained within the overlying limestone, sands and basalt from deeper underlying aquifers and formations (Victorian Department of Sustainability and Environment, 2014).

Hydrogeologically, the basalt and sands have similar hydraulic properties, with hydraulic conductivities of 10^{-2} to 10^{1} and 10^{-3} to 10^{2} m/day respectively. They are hydraulically connected and are often treated as a single unconfined aquifer (Dahlhaus et al., 2002b; Yihdego et al., 2014). The Port Campbell Limestone has a variable hydraulic conductivity typically <1 m/day, increasing in the upper parts due to karst formation (Nicolaides, 1997). The Gellibrand Marl has a likely hydraulic conductivity of 10^{-6} to 10^{-2} m/day (Dahlhaus et al., 2002a).

The Mt Gambier sub-province overlies the limestones of the Mt Gambier Embayment. The craters of Lake Leake and Edward extrude through the late Pleistocene calcarenite of the Bridgewater Formation and overlying aeolian sands. On the plains surrounding the craters, the volcanic ejecta is covered by the Bridgewater formation, and overlies the Oligo-Miocene Gambier Limestone (Boult and Hibburt, 2002; Forestry SA, 2010). The Gambier Limestone is an important unconfined aquifer in the region, with very high hydraulic transmissivities, from 20 to above 25000 m^2/day in karstic regions (Mustafa and Lawson, 2002), and numerous karst features such as cenotes, dolines, and caves.

2.6 Regional climate

The Newer Volcanic province lies within a temperate climate. Average daily temperatures are around 13 °C with an average daily temperature of 18.9 °C in summer to 8.4 °C in winter. Average humidity is ~75 %. Yearly average rainfall varies across the province from ~1100mm in the most southern regions by the coast, to ~600 mm along the northern edges. Most of the lakes lie within the middle of the province, from 25 to 50km from the ocean, with a rainfall of around 700 to 800 mm/year. Rainfall is brought to the region predominantly by mid-latitude storms and fronts during winter, and via tropical-extratropical driven cloud bands from the north-west during autumn and early winter (Murphy and Timbal, 2008). Yearly rainfall amounts are fairly homogeneous across the lakes, but there is variation in seasonality. The long term (1961-1990) monthly average rainfall from Bureau of Meteorology (BOM) stations near each lake shows that the westernmost lakes – Leake and Edward in South Australia – receive a higher portion of winter rainfall (~41 % of yearly total) than the Victorian lakes, which receive ~33 % of their yearly total rainfall during the winter months. The Victorian lakes, however, receive more rainfall in spring and summer (43 % of yearly total) than Leake and Edward (34 % of yearly total).

3 Methods

3.1 Lake water levels

Lake water levels and benchmarks were initially established using a CORS network (Leica Smartnet) enabled 1200GG GPS in April 2016. Existing benchmarks based on survey marks near lakes (Purrumbete, Gnotuk, Bullen Merri, Leake) were checked against current survey mark values. On subsequent sampling trips, a Leica 1200 TCRP R300 total station was used to locate the current lake water levels relative to the benchmarks. Levels were recorded for all lakes except Tooliorook and Keilambete. All heights are measured to the Australian Height Datum (AHD) and GPS derived heights have had geoid corrections applied.

3.2 Lake sheltering index

A metric of lake morphology was determined by assessing the most common wind direction (south-westerly) for the lakes during the months of greatest evaporation (from October to May). For each catchment, the most significant windbreak on the upwind side of the lake was determined (typically the crater rim), with a lake sheltering index (*LSI*) determined as distance from the windbreak to the lake centre, divided by the height of the windbreak from the lake

surface. This is similar to the windbreak assessment methods used in agriculture and microclimate studies (McNaughton, 1988).

3.3 Water sampling

Lakes were sampled near the shorelines. Samples for stable isotopes were collected in 15–30 ml HDPE bottles. Samples for chemistry were collected in acid washed 500 ml sample bottles. All bottles were rinsed 3 times in lake water with the samples collected from undisturbed water slightly away from the rinsing location. All samples were refrigerated when possible during each trip and immediately upon return. Conductivity, pH and water temperature were recorded with a Hanna 98194 water quality meter, calibrated in the lab prior to each field trip with a single point conductivity calibration using 5000 µs/cm standard, and a two point pH calibration using 9.18 and 4.01 pH standards. Weather conditions for each day were documented, recording air temperature, humidity, cloud conditions, water clarity, water surface conditions (small waves, calm), and wind speed and direction. Air temperature and humidity data were collected from the nearest BOM weather station, whereas the remainder were on site observations. Photos and GPS coordinates of each sampling site were recorded. Due to time constraints for each field trip, alkalinity determinations were done in the laboratory shortly after each trip using a Hach digital titrator to pH 4.5. Each 500 ml sample was split in the laboratory with ~100 ml used for alkalinity testing, two sets of 0.45 µm filtered 50 ml samples in acid washed centrifuge tubes for cations and anions analysis, with the remainder kept as an archive sample in an acid washed bottle. The cation sample was treated with two drops of analytical grade HNO_3 to drop the pH of the sample to <2 and prevent cation adsorption and precipitation.

3.4 Major/minor ions, $\delta^{18}O$, and $\delta^{2}H$

Samples were analysed at the Australian Nuclear Science and Technology Organisation (ANSTO) for major and minor ions and trace elements. Anions were analysed using ion chromatography (Dionex ICS-2100 Ion Chromatograph) with samples diluted 10–100x with high purity (18 MΩ) water if necessary. Each sample was analysed using external calibration from 0.01 to 100 ppm, combined with a check for instrument drift against a standard every 20 samples. Cations were determined using Inductively Coupled Plasma Atomic Emission Spectrometry (ICP-AES; Thermo Fisher iCAP 7600). Electroneutrality charge balance checks for most samples were within 10 %, with 90 % of samples within 5 %. Three freshwater samples (TDS <1000 mg/L) had a charge balance difference just outside 10 % up to 13.5 %. $\delta^{18}O$ and $\delta^{2}H$ were analysed at ANSTO and Flinders Analytical using a Picarro Cavity Ring-Down

Spectrometer (Picarro, Inc., Santa Clara, CA, USA), or by continuous flow isotope ratio mass spectrometry (IRMS) (Delta V Advantage) at ANSTO for some high salinity samples. CO_2 equilibrium was used for $\delta^{18}O$ IRMS analysis, and platinum reduction for $\delta^{2}H$. IRMS results were converted from activity to concentration scale using the technique of Gat (2010). Samples run at ANSTO were calibrated against 2 in-house standards (AILS-006 and AILS 008), with a QC check against 4 additional in-house standards (AILS-005, AILS-007, AILS-009, AILS-012). Picarro calibration at Flinders was performed using 2 in-house standards (DESAL and EVIAN), with a QC check against a third in-house standard (RAIN). Samples processed at ANSTO on the Picarro were injected 7 times, with the first two samples not included in the analysis to minimise memory effects. Results are reported as accurate to ± 0.15 ‰ for $\delta^{18}O$, and ±1 ‰ for $\delta^{2}H$. Flinders Analytical samples were injected 7 times with the first 3 injections discarded. A precision (1σ) was reported against an in-house QC standard (RAIN) of ±0.1 ‰ for $\delta^{18}O$, and ±0.5 ‰ for $\delta^{2}H$. ANSTO in-house standards were run alongside the samples processed at Flinders Analytical to ensure consistent results between both labs. All isotopic results are reported using the delta notation as per mil (‰) deviations from Vienna Standard Mean Ocean Water (VSMOW2). The results from these analyses are included in Appendix One of this thesis.

3.5 Isotopic modelling to account for salinity effects

In order to tease out the effects of salinity upon isotopic fractionation during evaporation for the four hypersaline lakes (Lakes Keilambete, Gnotuk, East Basin and West Basin), a numerical model (described in detail in Chapter 5 this thesis) was used to simulate $\delta^{18}O$ and $\delta^{2}H$ evolution, both with observed salinity and assuming salinity of zero. This provided an estimated slope for each local evaporation line with and without the influence of salinity.

3.6 Isotopic modelling for sensitivity analysis

A model was applied to examine how evaporative fractionation of $\delta^{18}O$ and $\delta^{2}H$ is influenced by humidity, evaporative feedback (where some portion of the air at the lake surface is derived from evaporated flux from the lake), and scenarios where δ_A is not in equilibrium with δ_P. A simple numeric model of a desiccating pond was applied, using eq. 2, and the C_k values of Merlivat (1978) as 28.5 ‰ for $\delta^{18}O$, and 25.1 ‰ for $\delta^{2}H$, with θ and n both set to 0.5. Three scenarios were simulated. One, with atmospheric feedback of 10 %, and two with δ_A shifted from δ_P by ±10 %. Each of these scenarios was run with humidity set to 65 %, 75 % and 85 % for a total of 9 simulations. 85 % was used as an upper limit due to the increase in error propagation in the Craig and Gordon model at high humidity values (Kumar and Nachiappan, 1999).

4 Results

4.1 Lake levels

At the start of the monitoring in 2016, most lakes had quite low water levels, with no access to the water at Lake Leake and Lake Elingamite, and areas of lake bed mud exposed at Lake Mumblin. Lakes Leake and Edward generally had similar level responses, with a large seasonal cycle and a rapid recovery from the low lake levels (Fig. 2.4). Likewise, Lakes Surprise and Purrumbete had a very rapid recovery with lake levels rising ~1 m by late 2016. Lake Mumblin also had a rapid recovery, increasing nearly as much as Surprise and Purrumbete by 2018, with Elingamite slightly lower. Unfortunately, both Lakes Mumblin and Elingamite were unable to be surveyed in April 2016. East and West Basin had very sluggish or minimal recovery, with lake levels only rising slightly during the course of the monitoring. Lakes Bullen Merri and Gnotuk continued their long term decline with lake levels slightly lower in 2018 compared to 2016.

4.2 General lake water chemistry

Most of the studied lakes are Na/Cl type, with an increased dominance of Na/Cl ions at higher salinities (Fig. 2.3). The typically acidic Lake Edward has a higher ratio of sulphate ions compared to the other lakes of similar salinity. The freshwater Lake Purrumbete and Lake Surprise showed increased dominance of bicarbonate ions (Fig. 2.3). Average pH for all lakes except Lake Edward was 8.7 ±0.6, whereas Lake Edward had an average pH of 6.5 ±1.1 (Fig. 2.4). pH generally does not correlate with lake water level, with the exception of Lake Edward, which showed a clear negative correlation. Most of the lakes showed a negative correlation between water level and TDS values, though a few lakes – Bullen Merri, Purrumbete, Surprise – showed occasional deviations where TDS values varied separately to water level (Fig. 2.4). Generally, TDS and $\delta^{18}O$ and $\delta^{2}H$ composition of the lakes tracked together through the seasonal cycle.

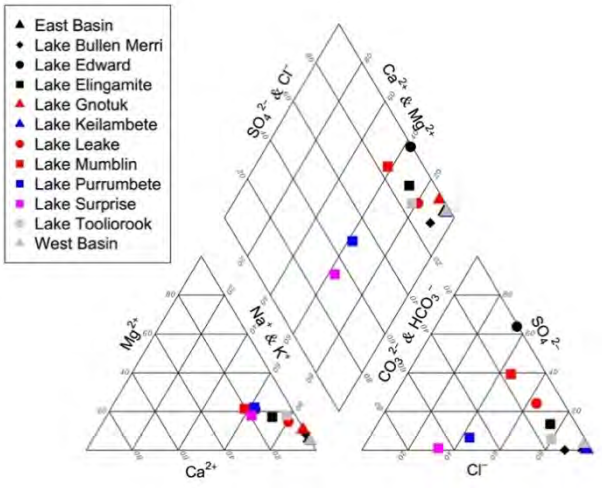

Figure 2.3: Piper diagram showing average chemical composition for each lake. Triangles represent hypersaline lakes. Diamonds represent brackish lakes (Lake Bullen Merri). Squares represent the fresher lakes with a TDS < 4000 mg/L. Circles represent the two South Australian lakes, Lake Leake and Lake Edward.

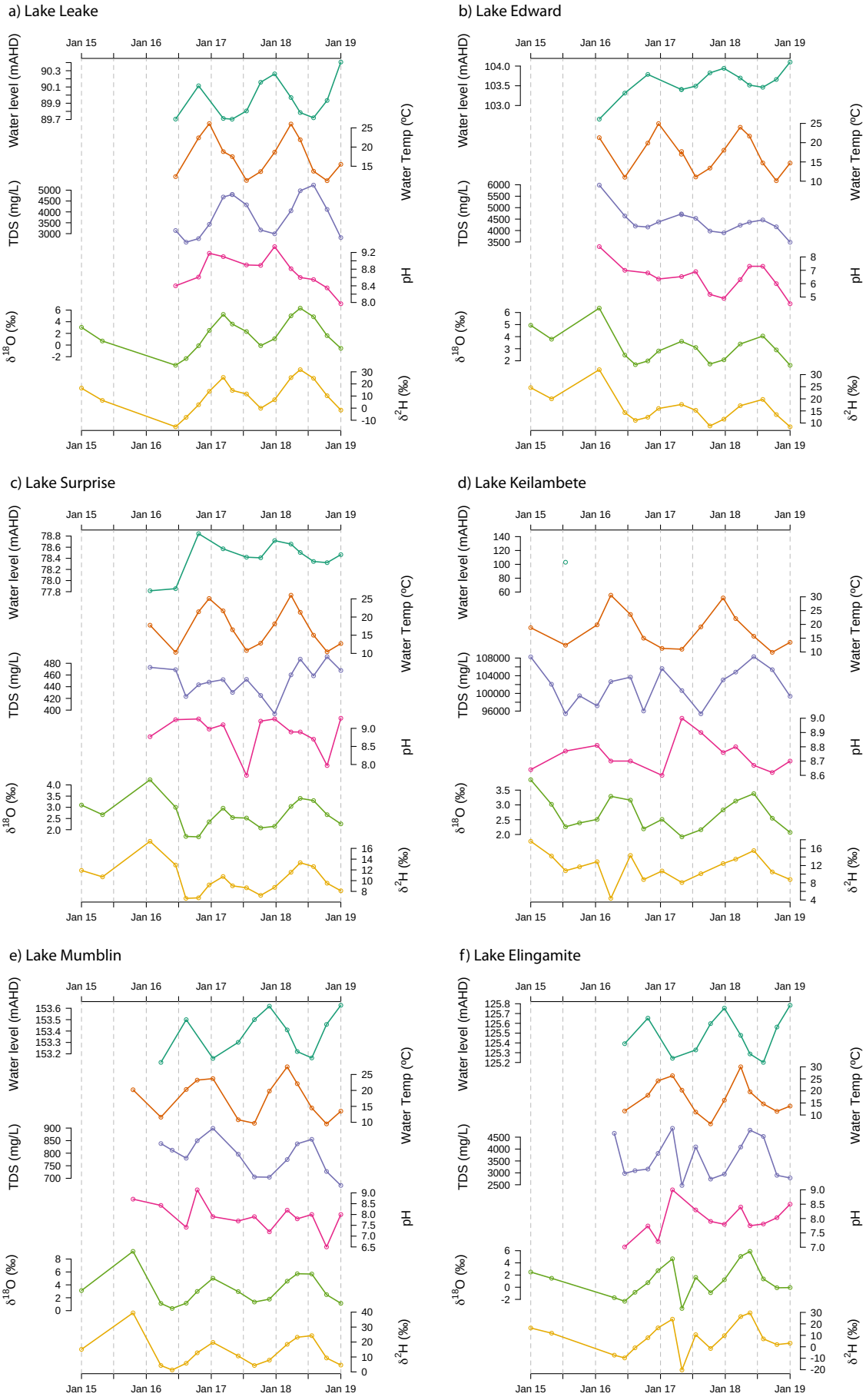

Figure 2.4: Monitoring results. Time series of lake levels, water temperature, TDS, pH, $\delta^{18}O$ and $\delta^{2}H$ for the 12 lakes.

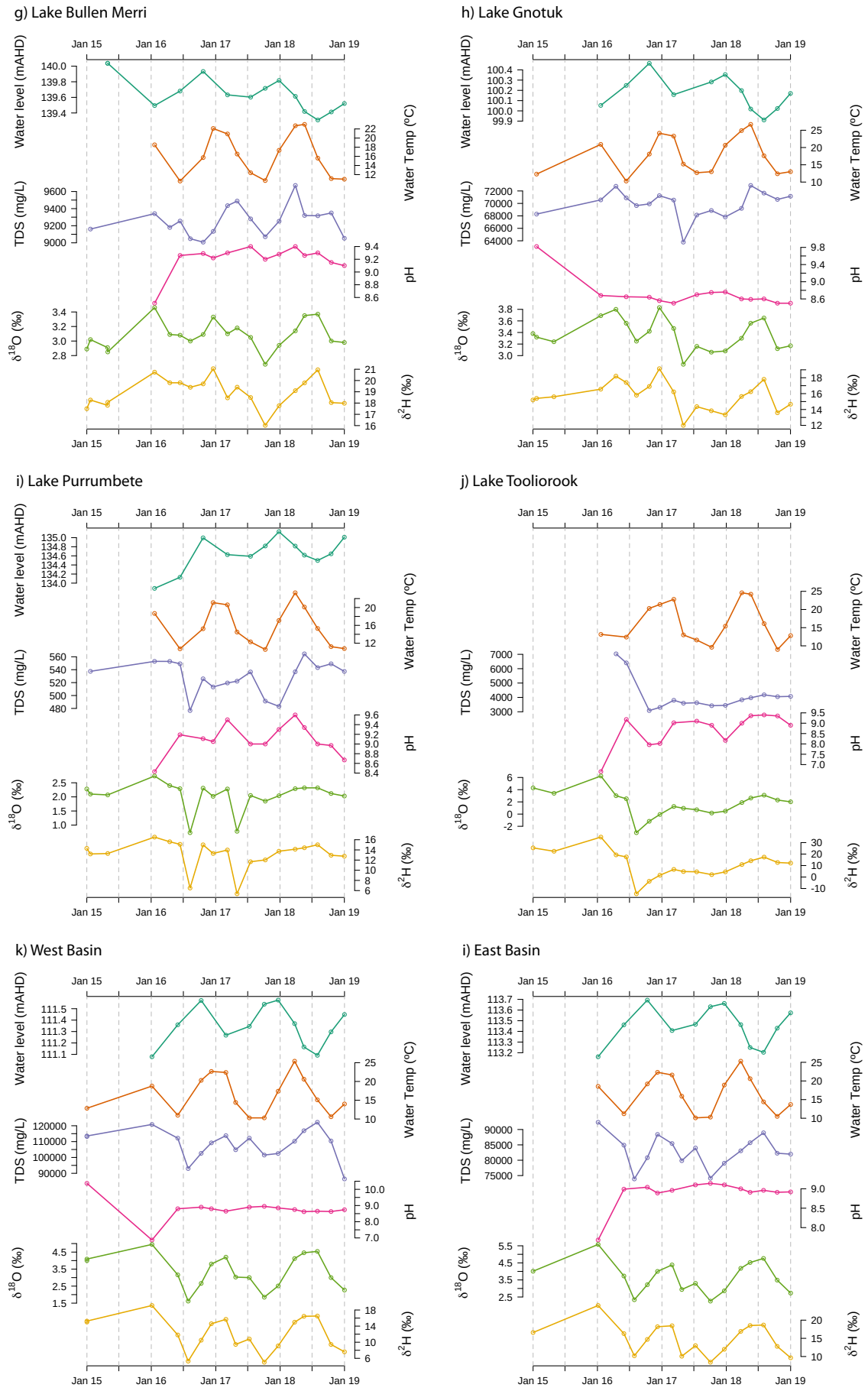

Figure 2.4: Continued

4.3 Between site differences in $\delta^{18}O$ and $\delta^{2}H$

As salinity can affect $\delta^{18}O$ and $\delta^{2}H$ evaporative fractionation (Gat, 2010), the lakes were divided into two categories based on whether they were hypersaline or fresh/brackish. The eight lakes with lower salinity exhibited three distinct local evaporation lines (Fig. 2.5a). Of these, the South Australian lakes, Leake and Edward, at the extreme western margin of the studied region, formed a well-defined evaporation line with a slope of 4.6 (r^2 = 0.99, n = 32) (Fig. 2.5a). The intersect between the South Australian lakes and the global meteoric water line (GMWL, slope of $\delta^{2}H = 8\delta^{18}O + 10$) (Craig, 1961), lies slightly higher than the Victorian lakes, intersecting at -2.5 ‰ for $\delta^{18}O$ and -10 ‰ for $\delta^{2}H$. The lake sheltering index value for these lakes is 14 for Leake, and 17 for Edward.

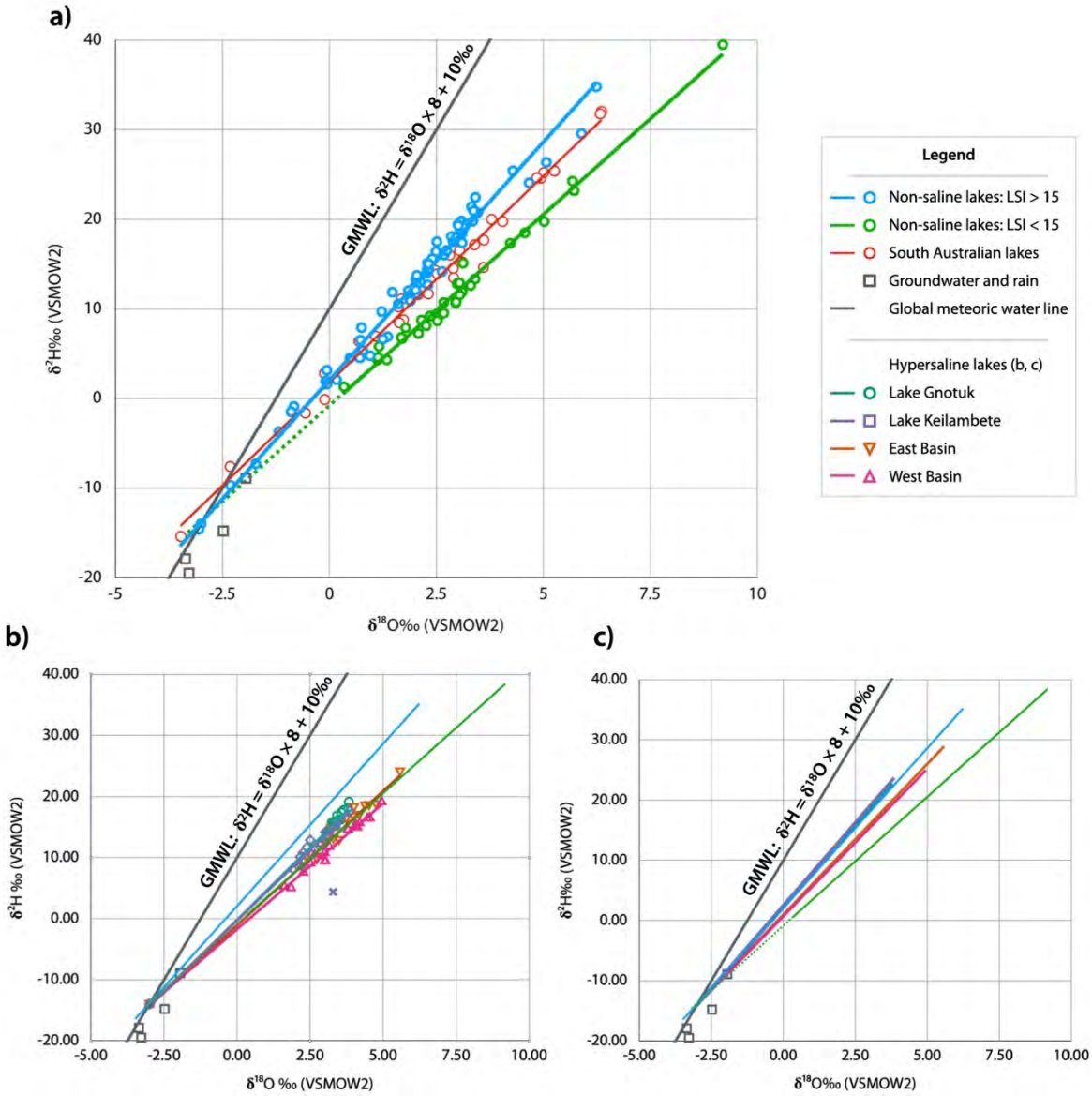

Figure 2.5: a) Average local evaporation lines for fresh–brackish lakes. b) Local evaporation lines for hypersaline lakes. c) Modelled local evaporation lines for hypersaline lakes, corrected for salinity effects. Also shown in (c) and (b) are the fresh-brackish local evaporation lines (light blue, green) for Victorian lakes from (a) for comparison. The outlier from Lake Keilambete, marked with an x symbol in (b) was not used in the determination of the Lake Keilambete LEL slope.

The Victorian fresh–brackish lakes formed two distinct local evaporation lines. The isotopic data for Lakes Bullen Merri, Elingamite, Purrumbete and Tooliorook exhibited steeper evaporation lines, with an average slope of 5.3 (r^2 = 0.98, n = 76). The two remaining lakes - Surprise and Mumblin, defined LELs with an average slope of 4.3 (r^2 = 0.98, n = 33). The differences in slope of the LELs appears to correspond with the degree of sheltering between different lakes, with *LSI* values of 100 for Toliorook and Purrumbete, 67 for Elingamite, and 19 for Bullen Merri. Lake Surprise and Lake Mumblin, being the smallest lakes lying within steep craters, are well sheltered, with *LSI* values of 5 and 7 respectively. Both LELs defined by sheltered and unsheltered lakes intersect with the GMWL at -3 ‰, -14 ‰ for $\delta^{18}O$ and $\delta^{2}H$.

The hyper-saline lakes defined 4 evaporation lines, with slopes of 4.6 for Keilambete, 4.7 for Gnotuk, 4.1 for West Basin and 4.4 for East Basin (Fig. 2.5b, Table 1). One outlier was noted for the Lake Keilambete data as it had very low $\delta^{2}H$ values relative to $\delta^{18}O$, approximately 10 ‰ lower than suggested by the evaporation line. The reason for this outlier was uncertain, however as the $\delta^{18}O$ and $\delta^{2}H$ values for that datapoint are not compatible with hydrological mixing and evaporative isotopic fractionation processes, that datapoint was not used in the determination of the LEL slope. The isotopic values for the hyper-saline lakes did not extend close to the GMWL, remaining relatively enriched during the entire monitoring timeframe. These slopes are therefore derived assuming an intersection point of -3.0 ‰ for $\delta^{18}O$, and -14 ‰ for $\delta^{2}H$ at the GMWL, as per the other lakes in the study. Model derived local evaporation line slopes, assuming a freshwater system for each lake, resulted in slopes of 5.4 for Gnotuk, 5.5 for Keilambete, and 5.0 and 4.9 for East and West Basin respectively (Fig. 2.5c). Lake Gnotuk has an *LSI* value of 12, Lake Keilambete is 27, and East and West Basin are 18 and 14 respectively. A θn value of 0.2 was required for the modelling of Keilambete, 0.21 for Gnotuk, 0.25 for East Basin and 0.27 for West Basin. To achieve an LEL of 4.2 as observed at Lake Surprise and Lake Mumblin, required a θn *of ~0.43.*

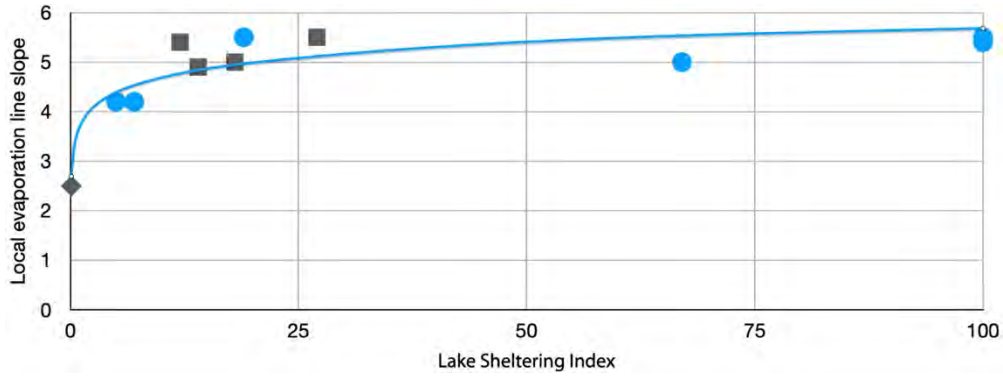

Figure 2.6: Log-regression for slope of the local evaporation line against the lake sheltering index for the Victorian lakes. R^2 = 0.83. Fresh-brackish lakes shown in blue, while hypersaline lakes are shown in grey. Soil water, representing the condition of maximum isotopic transport fractionation through a fully formed diffusion layer, is shown as a grey diamond. Regression equation is: LEL slope = 0.4327 ln(LSI) + 3.6896.

The slope of local evaporation lines for all ten Victorian lakes appears to correspond to the lake sheltering index. To test for correlation, a log-regression model was applied to the lake data, combined with the local evaporation line typically defined by soil water, with a slope of 2.5 and an *LSI* of 0, representing one end of the turbulence continuum, with a fully formed diffusion layer and minimal turbulence (Fig. 2.6). The regression model between log transformed *LSI* values and LEL slopes yielded an r^2 of 0.83, with a p value of < 0.001 (Fig. 2.6).

4.4 Isotopic modelling for sensitivity analysis

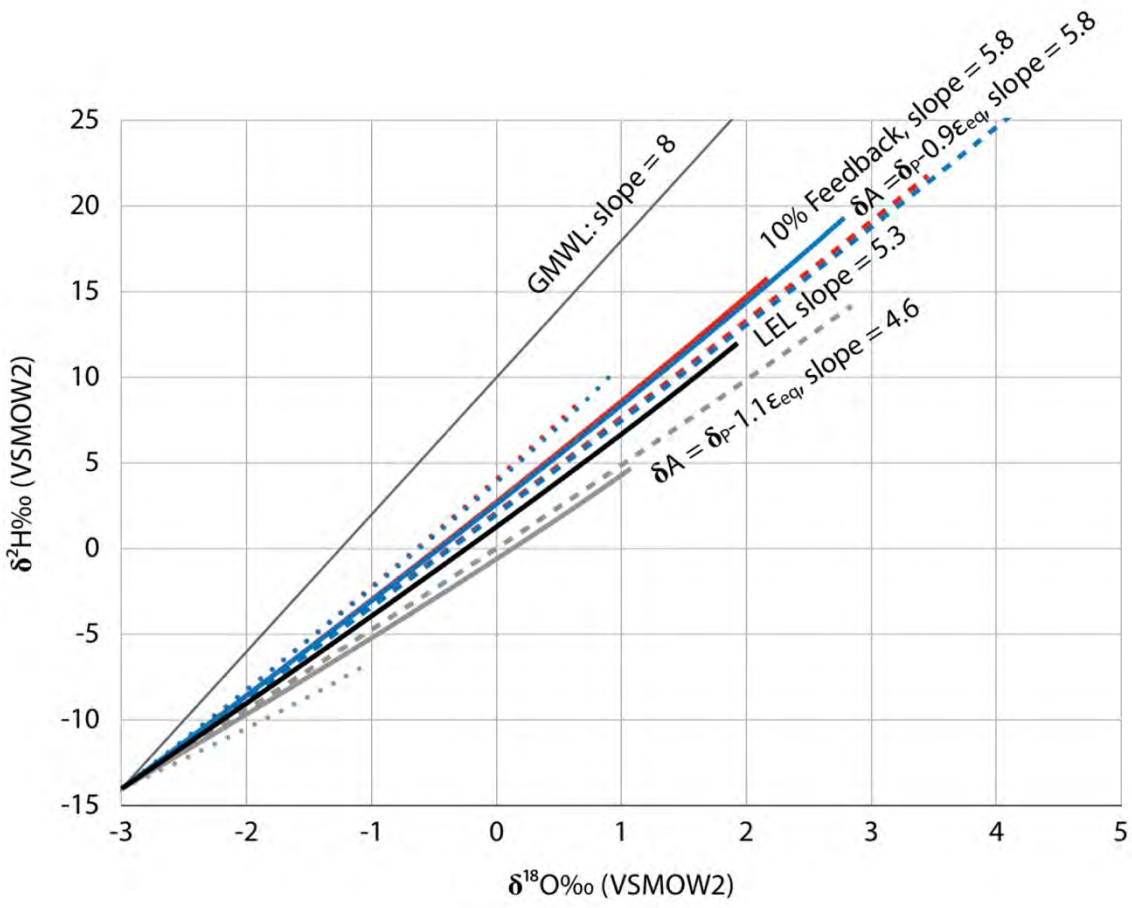

Figure 2.7: Modelled isotopic enrichment of a desiccating pond for 4 scenarios. 75 % humidity values shown as solid line. 65 % humidity values shown as a dashed line. 85 % humidity scenarios shown with a dotted line. Default scenario shown in black. 10 % evaporative feedback scenario shown in red. $\delta_A = \delta_P - 0.9\varepsilon_{eq}$ scenario shown in blue. $\delta_A = \delta_P - 1.1\varepsilon_{eq}$ shown in grey.

A numerical model of a desiccating pond with δ_A in equilibrium with δ_P, and θ and n both set to 0.5, produced an enrichment of lake water $\delta^{18}O$ and δ^2H along a local evaporation line with a slope of 5.3 (Fig. 2.7). Increasing humidity did not change the slope, but did decrease the extent of lake water $\delta^{18}O$ and δ^2H evolution (Fig. 2.7). An increase of 10 % humidity lowered the maximum enrichment of lake water from 1.9 ‰ to 0.1 ‰ for $\delta^{18}O$ and from 12.0 ‰ to 1.7 ‰ for δ^2H. Introducing 10 % of evaporative feedback – where some of the evaporated flux is mixed back into the atmosphere – increased the slope of the local evaporation line defined by the $\delta^{18}O$

and δ^2H evolution of lake waters to 5.8 (Fig. 2.7). Under these conditions, humidity had an effect, with an increase in humidity steepening the slope of the local evaporation line, while lowering the extent of isotopic enrichment of the lake waters, with the opposite effect for a decrease in humidity. Shifting δ_A from equilibrium with δ_P ($\delta_A = \delta_P - 0.9\varepsilon_{eq}$) had a similar effect on the local evaporation line slope, increasing it to 5.8, but also increased the extent of δ^{18}O and δ^2H enrichment of lake water. Defining δ_A as $\delta_P - 1.1\varepsilon_{eq}$ decreased the slope and extent of enrichment. Under this scenario, the effect of humidity on the slope of the local evaporation line was reversed, and an increase in humidity decreased the modelled local evaporation line slope to 4.6.

4.5 Cl^-/Br^- source water investigation

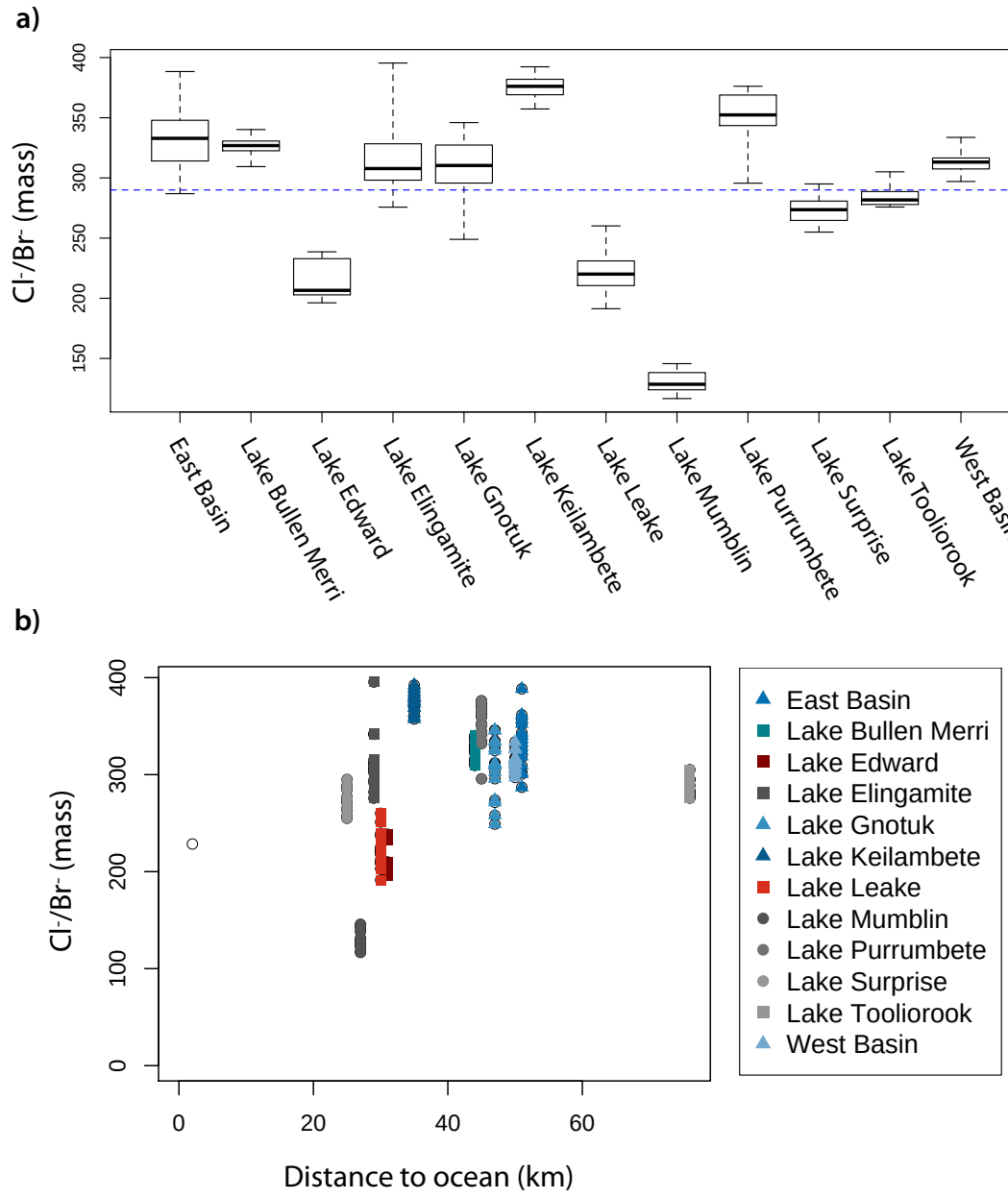

Figure 2.8: a) Box plot showing the Cl^-/Br^- ratios for each lake. b) Scatterplot of Cl^-/Br^- vs distance from the ocean.

Most of the lakes have Cl^-/Br^- ratios close to or above seawater (290 Cl^-/Br^- mass ratio). However, Lakes Mumblin, Edward and Leake all have Cl^-/Br^- ratios substantially lower, with ~130 for Mumblin to ~220 for Leake and Edward. Cl/Br ratios for the monitored lakes show no statistically significant relationship with distance from coast. Furthermore, the weak trend that they do suggest is counter to that proposed by Davis et al. (1998), with increased Cl^-/Br^- ratio for lakes further inland.

4.6 HCO_3^-/Cl^- and d-excess lake assessment

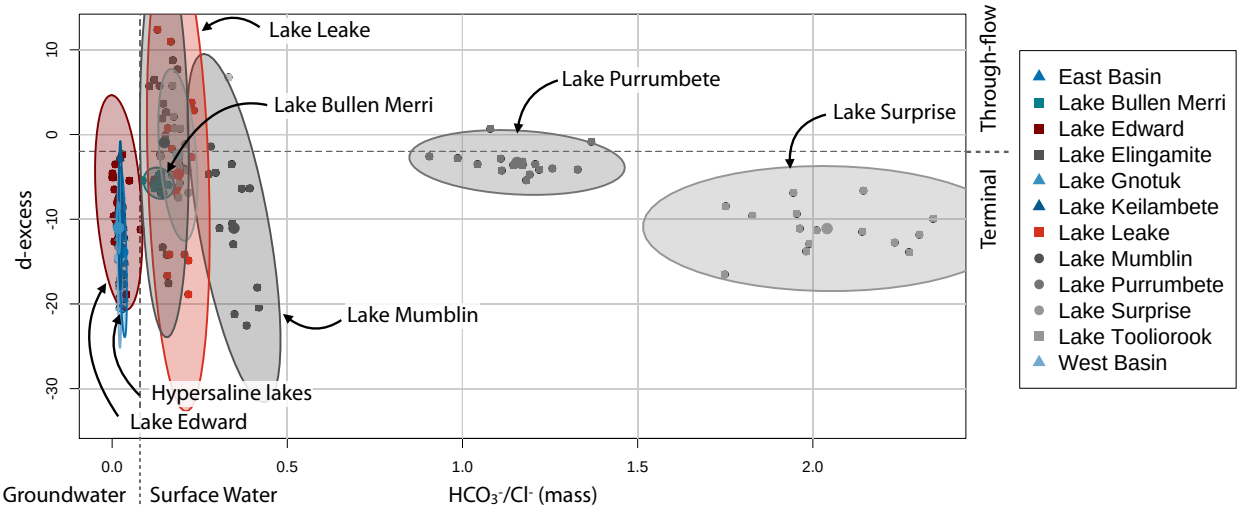

Figure 2.9: HCO_3^-/Cl^- and d-excess plot for all 12 lakes. Ellipses show observed range for some lakes. Dotted lines represent the proposed category boundaries of Barton et al. (2013).

HCO_3^-/Cl^- can potentially define whether a lake is groundwater fed or surface water fed, with surface water fed lakes having a higher HCO_3^-/Cl^- (Barton et al., 2013). Applying the methodology proposed by Barton et al. (2013) placed all the hyper-saline lakes in the "groundwater dominated" category, with HCO_3^-/Cl^- ratios from 0.018 to 0.03, below the category boundary of ~0.08 proposed by Barton et al. (2013) (Fig 2.9). Lake Edward also fell within that category, likely due to the acidic nature of the lake preventing any concentration of HCO_3^-. Lakes Leake, Elingamite, Bullen Merri, Tooliorook and Mumblin fell within the "surface water dominated" category with HCO_3^-/Cl^- ratios from ~0.13 to ~0.35. Lake Surprise and Lake Purrumbete also fell within the "surface water dominated" category with very high HCO_3^-/Cl^- ratios of ~1.2 and ~2 respectively. Deuterium excess was applied to determine the residence time of the lake. According to Barton et al. (2013) low d-excess is interpreted to infer that a lake has a long residence time and is a terminal lake, whereas high d-excess suggests that a lake is predominantly through-flow, with a short residence time. Using the average d-excess for each lake, and the proposed boundary between long residence, terminal lakes and short residence

time, through-flow lakes of -2 ‰ (Barton et al., 2013), defined all of the lakes except Lake Elingamite and Lake Toolirook as terminal lakes, with an average d-excess of -9.1 ‰, ranging from -3.3 ‰ for Lake Purrumbete to -14.5 ‰ for West Basin. Many of the lakes had a significant seasonal variation in d-excess, ranging from 2.4 ‰ for Lake Bullen Merri to 32.6 ‰ for Lake Mumblin, with an average range of 16.5 ‰ for all lakes over the three years of monitoring.

5 Discussion

5.1 General lake chemistry and lake water levels

All lakes share a similar climate, so it could be expected that lake levels would behave similarly across all lakes, however, this was not the case. The monitoring program began at the end of a dry spell, with several of the lakes inaccessible during early visits due to exposed mud. The lakes responded in four different ways. The South Australian lakes recovered very quickly. Lake Edward and Lake Leake rose very quickly during 2016, with average yearly levels continuing to rise over the following 2 years. This rapid recovery can be attributed to high rainfall, with yearly rainfall amounts of 1097 mm, 886 mm and 863 mm (BOM station at Lake Leake) for 2016–2018. Over that timeframe the Victorian lakes only received ~841 mm, ~813 mm and ~641 mm (Average of BOM stations at Macarthur, Terang and Camperdown). Besides explaining the rapid recovery of Lake Leake and Lake Edward, this observation further emphasises that the South Australian lakes are exposed to a different seasonal rainfall pattern than the Victorian lakes. The Victorian lakes responded in 3 different ways. The hypersaline East and West Basin rose very slightly over 2016–2018, essentially being near steady state. Lake Bullen Merri and Lake Gnotuk continued the pattern of long-term decline as manifest since the 1850s (Currey, 1970; Jones et al., 2001), while less saline lakes all increased lake levels significantly over the monitoring timeframe. It appears that, with the exception of Lake Bullen Merri and Lake Gnotuk, the lakes' response to hydroclimate is correlated to their salinity, which is likely related to the groundwater regime – through-flow, terminal or intermediate. The freshest lakes – Purrumbete and Surprise, followed by Lake Mumblin – responded rapidly and achieved the highest September 2018 levels relative to Aug 2016. The intermediate Lake Elingamite increased its water levels, expressing an intermediate magnitude of change between that of the fresh lakes and that of East and West Basin.

Differences in the groundwater regime, in combination with the differing response times of lakes and groundwater to changes in hydroclimate may influence lake water level behaviour.

Whilst a lake will respond rapidly to changes in hydroclimate, groundwater systems may have a delayed response (Urbano et al., 2004). As lake levels drop in response to a period of dry hydroclimate, groundwater gradients towards a through-flow lake may increase, while the downward gradient will decrease, or possibly even reverse, resulting in an increased flux into the lake (Tweed et al., 2009; Webster et al., 2006). Following the return of wetter conditions, the lake may recover water levels quickly, before slowing as the groundwater system catches up . A similar lagged response to lake-groundwater interaction was observed from 1997–2006 at the nearby through-flow Lake Colac, where the water level increased during a drought, due to increased groundwater input, before dropping rapidly from 2006 as the groundwater system eventually responded to the drought (Tweed et al., 2009). In contrast the groundwater gradients for a terminal lake all fall towards the lake. As such a terminal lake may see an increase in flow due to steepening groundwater gradients but will not simultaneously undergo a decrease in outgoing flows, likely leading to a more subdued response than through-flow lakes. This hypothesis may explain why the through-flow lakes responded very quickly in 2016, but then did not undergo much change in 2017–2018. Unfortunately, this does not explain the behaviour of Lake Bullen Merri and Lake Gnotuk. Further modelling is required to test these hypotheses.

Some of the lakes had a very clear inverse relationship between lake level and TDS, $\delta^{18}O$, and $\delta^{2}H$, in particular, Lake Leake and Lake Edward in South Australia. Deeper lakes such as Lake Bullen Merri, Lake Purrumbete, Lake Gnotuk, did not show such a clear relationship, with the seasonal maxima and minima for TDS, $\delta^{18}O$, and $\delta^{2}H$ often slightly out of sync with the maximum and minimum lake levels. This behaviour is suspected to be due to the onset and breakdown of seasonal stratification. E.g., as thermocline depth increases, the volume of water transferred from the hypolimnion to the epilimnion may be greater than the evaporative flux.

All of the lakes in the study are alkaline, with the exception of Lake Edward. The acidity of Lake Edward has been observed since 1966 (Bayly and Williams, 1966), with high sulphate levels noted since 1918 (Ward (1918), in Bayly and Williams (1964)). The acidity has been attributed to the plantations of conifers in the Lake Edward catchment (Bayly and Williams, 1966), with the mechanism suspected to be increased capture of atmospheric pollutants, such as sulphur, by canopy interception (Bayly and Williams, 1966; Drinan et al., 2013; Nisbet, 2001; Parfitt and Ross, 2011). However the high sulphate ions observed by Ward (1918) (in Bayly and Williams (1964)) also suggest an alternative source of sulphur may be present as Forestry SA only began purchasing land for forestry in 1929 (Forestry SA, 2010). Further work is needed to assess whether the high sulphate levels, and corresponding low pH in Lake Edward, are solely due to the catchment land use, or whether there is a secondary sulphur source.

5.2 Morphological influence on $\delta^{18}O$ and $\delta^{2}H$ lake water enrichment

Understanding how isotopic fractionation is influenced by lake morphology and water level is an essential aspect for lake modelling based palaeoclimate research. There is an apparent correlation ($r^2 = 0.85$, $p < 0.001$) between the log of the lake sheltering index and the slope of the local evaporation lines. However, the two lakes that are most sheltered are also the smallest lakes, meaning there is also a potential correlation with lake size. As the fetch of a lake increases, there is increased opportunity for atmospheric feedback to occur – as air moves across the water surface it is mixed with evaporative flux, modifying the atmospheric isotopic composition and the humidity for a portion of the lake's surface. Humidity alone should also be considered as a factor. Several authors have attributed humidity as a primary influence on the slope of local evaporation lines (Holland and Turekian, 2010; Mackay et al., 2003; Mook and Rozanski, 2000; Shapley et al., 2008). In addition δ_A is not necessarily in equilibrium with δ_P (Crawford et al., 2019). Therefore, the effect of varying δ_A on the slope of local evaporation lines must also be quantified. Applying a numerical model of a desiccating pond to test the sensitivity of isotopic enrichment of surface waters demonstrated that these factors – humidity, atmospheric feedback, and δ_A – were unlikely to be the main cause of variation in the observed slopes of the local evaporation lines. The model results (Fig. 2.7) demonstrate that modifications to humidity alone, with δ_A in equilibrium with δ_P, do not influence the slope of the local evaporation line, in agreement with Gat (2010). Instead, humidity primarily influences the range of isotopic enrichment, with lower humidity resulting in increased enrichment (and vice versa). Shifting δ_A below equilibrium with δ_P (e.g: $\delta_A = \delta_P - 1.1\varepsilon_{eq}$) will both decrease the slope of the LEL, and the extent of fractionation (and vice versa). If δ_A is not in equilibrium with δ_P then humidity is able to influence the slope of the LEL to a small degree. Atmospheric feedback typically increases the slope of the local evaporation line and extent of isotopic fractionation (Fig. 2.7). If we assume the null hypothesis – that windspeed has little effect on isotopic fractionation – then either δ_A must not be in equilibrium with δ_P, or atmospheric feedback must influence the isotopic enrichment of each lake. Under both these scenarios, humidity can influence the slope of the local evaporation lines. However, the sensitivity modelling demonstrates that even significant changes in humidity have only a limited influence on the slope of local evaporation lines, while having a major effect on the extent of enrichment along the local evaporation lines. Therefore, while variations in δ_A and atmospheric feedback may have some minor effects on isotopic enrichment of lakes, and the resultant local evaporation line slopes, these factors are insufficient to explain the observed data.

Lake sheltering provides a straightforward mechanism to explain the observed LEL slopes. A decrease in wind at the lake surface, results in less wave formation and surface roughness, leading to an increased opportunity for a diffusion layer to form between the water surface and the turbulent atmosphere, leading to an increase in transport fractionation of $\delta^{18}O$ and $\delta^{2}H$. If this proposition is correct, then we would expect that LEL slopes would increase from ~2.5 in perfectly sheltered conditions (soil, rainfall samplers (e.g: Chapter Three, this thesis)), up to around ~5.5 or so at an *LSI* of around 15, beyond which sheltering is far less effective and the LEL slope is determined predominantly by other processes such as atmospheric feedback. This is based on the same mechanism, and is broadly analogous to, windspeed behaviour downwind from a windbreak described by McNaughton (1988), consisting of a 'quiet zone' up to around 8 *h* (*h* = horizontal/vertical ratio) and a 'wake zone' beyond that distance. As there are significant morphological differences between a lake catchment and a windbreak – wind has to go up and over a windbreak – then it is not expected that *h* and *LSI* will be directly comparable between windbreaks and lake catchments. The lake monitoring results suggest that θ and *n* values, when combined into a single term (θn) range along a continuum from 1 for soils, through ~0.5 for very well sheltered lakes, up to ~0.2 for large lakes with fully turbulent conditions with an *LSI* greater than ~15. E.g. Lake Surprise and Lake Mumblin have a θn *of* ~0.43, while Lake Keilambete and Lake Gnotuk required a θn *of* 0.20 and 0.21 respectively. Larger lakes, such as Lake Bullen Merri (*LSI* = 12, slope = 5.5), Lake Keilambete (LSI = 27, slope = 5.5) and particularly Lake Gnotuk (*LSI* = 12, slope = 5.4) tend to have steeper LELs than the regression line would suggest. This is likely due to atmospheric feedback due to the larger lake surface area. The effect of atmospheric feedback was not modelled for each lake in this study, but as noted in the sensitivity test, an increase in atmospheric feedback will result in steeper LELs. This study only has a small data set, but the sheltering effect can also be identified in other studies. Gat (1970) observed the isotopic change in evaporative flux during pan experiments as a response to wind at Lake Tiberius, Israel. Sveinbjörnsdóttir and Johnsen (1992) documented LELs for many surface water bodies, ranging from 3.4 to 5.5, that appear to correspond to the degree of lake sheltering across the Thingvallavatn region in Iceland. A similar conclusion was also reached by Gonfiantini et al. (2018). Probably the most exciting prospect of this study is the potential to define a function that links surface windspeed to degree of sheltering to isotopic fractionation and evaporation. Without isotopes, defining how windspeed changes due to sheltering is a problematic exercise requiring extensive windspeed measurements. By isotopic sampling of waters across a morphologically diverse region it may be possible to define a robust empirical function relevant to many fields such as lake modelling, microclimate studies and agriculture.

5.3 Cl^-/Br^- source water investigation

While differences in evaporative conditions between lakes may be reflected in the slope of local evaporation lines and the extent of lake water isotopic enrichment, different sources of lake water may be reflected by a lake's geochemical composition, specifically Cl^-/Br^- and HCO_3^-/Cl^- ratios. Cl^-/Br^- ratios for most of the lakes lie within a range of 270 to 375, with an average of 320, approximately similar to seawater (~290 Cl^-/Br). However, Lake Mumblin, Lake Leake and Lake Edward have much lower Cl^-/Br^- ratios of 130–220. For most lakes, Cl^-/Br^- ratios do not seem to be related to the surrounding geology, specifically, whether the lakes are predominantly surrounded by the Port Campbell Limestone or the Sandringham Sands. However, the three lakes that lie entirely within the basalt – Mumblin, Leake and Edward – do show clear differences to the rest of the lakes, with ratios much closer to those proposed for precipitation (Davis et al., 1998). An important characteristic of these three lakes is that they sit above the regional aquifers and can potentially flush any additional Cl^- or Br^- sources downwards, whereas the other lakes all sit at similar, or lower, levels than the regional aquifers. A preliminary interpretation is that lakes that sit above the regional aquifers reflect the lower Cl^-/Br^- ratio of rainfall as suggested by Davis et al. (1998), whereas lakes lower in the landscape interact with the larger unconfined aquifer of the Newer Volcanic Province or the Port Campbell aquifer and have an Cl^-/Br^- ratio more reflective of the groundwater. A similar interpretation has been applied to studies in north-western Victoria (Cartwright et al., 2006). These results suggest that it may be possible to distinguish between lakes that interact with water derived predominantly from rainfall, and those that interact with the regional aquifers. However, it seems unlikely that the Cl^-/Br^- ratios can be used to differentiate between limestone and sandstone based lithologies. While there may be a trend of decreasing Cl^-/Br^- ratios in rainfall as a function of distance from the coast as suggested by (Davis et al., 1998), our dataset is unable to show it, likely due to the presence of large regional aquifers with a Cl-/Br- ratio similar to that of seawater. One surprising feature of the dataset is that the lakes sit within a wide range of land use types: farming, forestry, and one – East Basin – was used as a dairy waste dump for 60 years, yet there is no indication of any significant additional Cl^- or Br^-.

5.4 HCO_3^-/Cl^- and d-excess lake assessment

HCO_3^-/Cl^- ratio and d-excess indicators provide an alternative method to determine source water, and may differentiate between lake-groundwater interactions for each lake (Barton et al., 2013). The dataset presented here provides a unique opportunity to assess the effectiveness of the HCO_3^-/Cl^- ratio and d-excess indicators proposed by (Barton et al., 2013), as it presents

several full seasonal cycles of a wide range of lakes. To assess the effectiveness of the HCO_3^-/Cl^- and d-excess indicators as a tool to define lake regimes in the region, we must first categorise the lakes. Most of the studied lakes are permanent water bodies, that sit in relatively simple basins, with no surficial inflow or outflow. Tooliorook is the exception with a large catchment and surface drainage to and from the lake. The groundwater across the region has a low range of salinity, with a TDS ranging from <500 mg/L to 3500 mg/L (FedUni, 2015). This simplicity makes it feasible to define the lake-groundwater regime for each lake. A lakes solute load is a result of the relative proportion of evaporation against other outgoing fluxes. Evaporation removes water from the lake, without significantly modifying the volume of solutes in the lake, whereas hydrological fluxes that flow to groundwater or outlet streams remove both solutes and water from the lake. Terminal lakes sit at the end-point of water flow paths, with evaporation dominating the water loss from the lake, leading to a build-up of salinity, whereas through-flow lakes both gain and lose water from and to the groundwater system. If flux to the groundwater makes up a significant proportion relative to evaporation, then salts cannot build-up in the lake. Of the lakes studied, Keilambete, East and West Basin and Lake Gnotuk, being hyper-saline, are clearly terminal lakes. Lakes Surprise and Lake Mumblin are likely through-flow lakes, as they are very fresh, and salts are clearly unable to accumulate. Lake Purrumbete has undergone hydrologic modelling demonstrating that it is a through-flow lake system(Yihdego et al., 2015). The remaining lakes likely have an intermediate flow regime, building up a small amount of salts, but also flushing many away. These lakes are difficult to categorise as lake levels have been falling through most of the last 150 years, and as such the lakes represent transient systems. Lakes can be both through-flow lakes at higher water levels, and terminal lakes at lower water levels (Winter, 1976), therefore these intermediate lakes require significant work to determine their current flow regime. With the exception of Tooliorook the lakes in our study could at first glance be classified as groundwater fed lakes, as they have negligible surficial run-off and inflow. Toolirook has a large surface catchment to the north. However, consideration must be made that some lakes, while groundwater fed, may be fed from shallow groundwater and interflow that has not had sufficient interaction with the underlying geology to precipitate carbonates and decrease the HCO_3^-/Cl^- ratio. The differentiation within the Cl^-/Br^- results may be applicable, suggesting that lakes Mumblin, Leake and Edward may qualify as surface water fed, in keeping with their position sited above the regional aquifers.

The hyper-saline terminal lakes of our study appear to be well described by the HCO_3^-/Cl^- and d-excess method, with all four lakes falling in the "Groundwater dominated, long residence time" quadrant (Fig. 2.9). Lake Edward also falls within this category as a result of its low pH,

and hence low HCO_3^-. This qualifies as an external factor, likely due to the pine plantations surrounding the lake, and should not be considered as part of any assessment of the HCO_3^-/Cl^- method. Most of the intermediate lakes fall within the surface water category, close to the delineation between surface and groundwater dominated (Fig. 2.9). Unfortunately, the range of HCO_3^-/Cl^- ratios covered by Lakes Bullen Merri and Elingamite (both likely groundwater fed lakes), and Leake and Tooliorook (both surface fed lakes), overlap, making it difficult to differentiate between them. Lake Surprise and Purrumbete present a unique challenge, with high HCO_3^-/Cl^- ratios representing the extreme extent of surface water dominated lakes, however, these two lakes are most likely examples of groundwater fed through-flow lakes. One possible reason for such high ratios are the presence of "stony rises" – regions of recent, blocky and stony basalt rises – at both Lake Surprise (the Mt Eccles lava flow) and Purrumbete. Groundwater recharge is variable across the Newer Volcanic Province, with high recharge noted in areas of stony rises (Nolan et al., 1990). High recharge combined with recently formed basalt makes it likely that those regions are undergoing greater weathering – with an increased formation of HCO_3^- as a byproduct (Dessert et al., 2003) – resulting in higher levels of HCO_3^- in the local groundwater. Future work may focus on improving the spatial resolution of groundwater sampling and identifying regions that differ from the average HCO_3^-/Cl^- ratios.

Deuterium excess is applied to determine whether a lake is through-flow or terminal in nature (Barton et al., 2013). Unfortunately, the range of d-excess for many of the lakes fluctuates from terminal to through-flow throughout the year, mostly as a function of lake depth. Deeper lakes with longer residence times typically had less variation (Bullen Merri, Purrumbete, Surprise, and the four hyper-saline lakes). However, lakes shallower than ~10 m regularly varied across the category delineation between "through-flow" and "long residence time". The tendency for more sheltered lakes to have more shallow evaporation lines, as noted in this study, can also skew results derived from d-excess values. A problematic aspect with using d-excess to determine groundwater regime is that it assumes residence time for lake water is comparable to the lake-groundwater flow-regime. For studies based on the isotopic composition of water, residence time for a lake should be defined as volume/total output rate (including evaporation), approximating the time a molecule of water spends in the lake. As evaporation is ~1000 mm/year for most lakes in the region, residence time can be very loosely approximated as the lake depth in metres. However, the lake-groundwater flow regime is better represented by the average time a solute spends in the lake. In the case of conservative ions, the ion residence time can be approximated as volume/outflow rate (without including evaporation) (Brezonik, 2018). For other ions such as Ca^{2+}, the ion residence time may be further modified by precipitation of

minerals in saturated lakes. The hyper-saline lakes represent the best examples of this difference, with a maximum water residence time of ~10-20 years, but with ion residence times on the order of centuries. This would suggest that using a conservative ion, such as Cl^- may be a more effective way to rapidly determine whether a lake is through-flow, terminal or intermediate.

6 Conclusion

This study aimed to explore the isotopic and geochemical signatures related to evaporation, groundwater interaction and the source lake water for twelve lakes across the Newer Volcanic Province in south east Australia (Fig. 2.1). It was found that:

1 Lake water levels responded to a change in hydroclimate (dry prior to 2016, then wetter over 2016–2018) in order of their salinity values, with the exception of Bullen Merri and Gnotuk. The freshest lakes increased water levels the most, with a rapid water level increase, while the hyper-saline lakes responded poorly. This is attributed to the suspected groundwater regime for the lakes, with through-flow lakes responding strongly to changes in hydroclimate, while terminal lakes had a more subdued response.

2 Lake local evaporation lines showed a link to lake morphology. A metric – the Lake Sheltering Index – has been defined. Lakes with a low Lake Sheltering Index, indicating a higher degree of sheltering, have local evaporation lines with lower slopes, likely as the reduced windspeed and surface roughness allows a more robust diffusion layer to form, and increased transport fractionation.

3 Cl^-/Br^- ratios for the studied lakes that sit high in the topography, above the main aquifers of the region, had lower Cl^-/Br^- ratios, and may record the Cl^-/Br^- ratio of rainfall. The Cl^-/Br^- of the main aquifers in the region, and the lakes that are sited at or below the regional water table surface had Cl^-/Br^- ratios close to seawater.

4 HCO_3^-/Cl^- and d-excess are only partially effective at categorising lakes based on hydrological regime. HCO_3^-/Cl^- ratios overlap for several lakes, and the groundwater HCO_3^-/Cl^- values across the region may require a higher spatial resolution, particularly in the region of stony rises, which may have elevated HCO_3^-/Cl^- ratios and likely provide the source of water to Lake Surprise and Lake Purrumbete. D-excess is likely not a useful indicator of lake groundwater regime (through-flow, terminal or intermediate) as the residence time of the lake water is not necessarily related to the residence time for ions in the lake.

7 References

Alcalá, F.J., Custodio, E., 2008. Using the Cl/Br ratio as a tracer to identify the origin of salinity in aquifers in Spain and Portugal. Journal of Hydrology, 359(1): 189-207. DOI:https://doi.org/10.1016/j.jhydrol.2008.06.028

Barr, C., Tibby, J., Gell, P., Tyler, J., Zawadzki, A., Jacobsen, G.E., 2014. Climate variability in south-eastern Australia over the last 1500 years inferred from the high-resolution diatom records of two crater lakes. Quaternary Science Reviews, 95: 115-131. DOI:https://doi.org/10.1016/j.quascirev.2014.05.001

Barton, A., Herczeg, A., Dahlhaus, P., Cox, J., 2013. A geochemical approach to determining the hydrological regime of wetlands in a volcanic plain, south-eastern Australia (Chapter 7) In: Ribeiro L, Stigter TY, Chambel A et al.(eds) Groundwater and Ecosystems. IAH Selected Papers on Hydrogeology Series 18. CRC Press (Taylor and Francis). p.

Barton, C.E., Barbetti, M., 1982. Geomagnetic secular variation from recent lake sediments, ancient fireplaces and historical measurements in southeastern Australia. Earth and Planetary Science Letters, 59(2): 375-387. DOI:https://doi.org/10.1016/0012-821X(82)90139-X

Barton, C.E., McElhinny, M.W., 1981. A 10 000 yr geomagnetic secular variation record from three Australian maars. Geophysical Journal of the Royal Astronomical Society, 67(2): 465-485. DOI:10.1111/j.1365-246X.1981.tb02761.x

Barton, C.E., Polach, H.A., 1980. 14 C ages and magnetic stratigraphy in three Australian maars. Radiocarbon, 22(3): 728-739.

Battarbee, R.W., 2000. Palaeolimnological approaches to climate change, with special regard to the biological record. Quaternary Science Reviews, 19(1–5): 107-124. DOI:http://dx.doi.org/10.1016/S0277-3791(99)00057-8

Bayly, I., Williams, W., 1964. Chemical and biological observations on some volcanic lakes in the south-east of South Australia. Marine and Freshwater Research, 15(2): 123-132.

Bayly, I.A.E., Williams, W.D., 1966. Further chemical observations on some volcanic lakes of south-east Australia of South Australia. Marine and Freshwater Research, 17(2): 229-238.

Behne, W., 1953. Untersuchungen zur Geochemie des Chlor und Brom. Geochimica et Cosmochimica Acta, 3(4): 186-215.

Benson, L., Paillet, F., 2002. HIBAL: a hydrologic-isotopic-balance model for application to paleolake systems. Quaternary Science Reviews(12): 1521-1539.

Boult, P., Hibburt, J., 2002. The Petroleum Geology of South Australia. Vol. 1, The Otway Basin. South Australia, Department of Primary Industries and Resources, Petroleum ….

Bowen, G.J., Revenaugh, J., 2003. Interpolating the isotopic composition of modern meteoric precipitation. Water Resources Research, 39(10): 1-13. DOI:10.1029/2003WR002086

Bowler, J.M., 1970. Late quaternary environments : a study of lakes and associated sediments in south-eastern Australia. DOI:10.25911/5d6c3cba91a43

Boyce, J., 2013. The Newer Volcanics Province of southeastern Australia: a new classification scheme and distribution map for eruption centres. Australian Journal of Earth Sciences, 60(4): 449-462.

Brezonik, P., 2018. Chemical kinetics and process dynamics in aquatic systems. Routledge.

Builth, H., Kershaw, A.P., White, C., Roach, A., Hartney, L., McKenzie, M., Lewis, T., Jacobsen, G., 2008. Environmental and cultural change on the Mt Eccles lava-flow landscapes of southwest Victoria, Australia. The Holocene, 18(3): 413-424. DOI:10.1177/0959683607087931

Camperdown Chronicle, 1896. THE OUTLET AT LAKE ELINGAMITE, Camperdown Chronicle (Vic. : 1877 - 1954), Vic., pp. 2.

Cartwright, I., Gilfedder, B., Hofmann, H., 2013. Transient hydrological conditions implied by chloride mass balance in southeast Australian rivers. Chemical Geology, 357: 29-40. DOI:http://dx.doi.org/10.1016/j.chemgeo.2013.08.028

Cartwright, I., Weaver, T.R., Fifield, L.K., 2006. Cl/Br ratios and environmental isotopes as indicators of recharge variability and groundwater flow: an example from the southeast Murray Basin, Australia. Chemical geology, 231(1): 38-56.

Cas, R., Satō, H., Simpson, C.J., 1993. Newer Volcanics Province-Processes and Products of Phreatomagmatic Activity: IAVCEI, Canberra 1993: Excursion Guide. Australian Geological Survey Organisation.

Chivas, A.R., De Deckker, P., Cali, J.A., Chapman, A., Kiss, E., Shelley, G., Michael, J., 1993. Coupled Stable-Isotope and Trace-Element Measurements of Lacustrine Carbonates as Paleoclimatic Indicators. Climate change in continental isotopic records: 113-121.

Chivas, A.R., De Deckker, P., Shelley, J.M.G., 1985. Strontium content of ostracods indicates lacustrine palaeosalinity. Nature, 316(6025): 251-253. DOI:10.1038/316251a0

Cohen, A.S., 2003. Paleolimnology: the history and evolution of lake systems. Oxford University Press, USA.

Craig, H., 1961. Isotopic variations in meteoric waters. Science, 133(3465): 1702-1703.

Craig, H., Gordon, L.I., 1965. Deuterium and oxygen 18 variations in the ocean and the marine atmosphere. In: Schink, D.R., Corless, J.T. (Eds.), Marine Geochemistry. University, Rhode Island, University, Rhode Island, pp. 277-374.

Crawford, J., Azcurra, C.S., Hughes, C.E., Gibson, J.J., Parkes, S.D., 2019. Comparison of atmospheric water vapour δ18O and δ2H estimated using evaporation pan, rainfall equilibrium and continuous measurements. Journal of Hydrology, 576: 551-560. DOI:https://doi.org/10.1016/j.jhydrol.2019.06.056

Crowe, a.S., 1993. The application of a coupled water-balance-salinity model to evaluate the sensitivity of a lake dominated by groundwater to climatic variability. Journal of Hydrology, 141(1-4): 33-73. DOI:10.1016/0022-1694(93)90044-A

Currey, D.T., 1970. Lake systems, Western Victoria. Australian Society for Limnology Bulletin, 3: 1-13.

Dahlhaus, P., Heislers, D., Dyson, P., 2002a. Corangamite Catchment Management Authority Groundwater Flow Systems. Report No. CCMA, 2(02).

Dahlhaus, P., Heislers, D., Dyson, P., 2002b. Glenelg Hopkins Catchment Management Authority, Groundwater Flow Systems. Consultancy report no. GHCMA, 2(02).

Davis, S.N., Whittemore, D.O., Fabryka-Martin, J., 1998. Uses of Chloride/Bromide Ratios in Studies of Potable Water. Groundwater, 36(2): 338-350. DOI:10.1111/j.1745-6584.1998.tb01099.x

De Deckker, P., 1982. Holocene ostracods, other invertebrates and fish remains from cores of four maar lakes in southeastern Australia. Proceedings of the Royal Society of Victoria, 94(4): 183-220.

Dessert, C., Dupré, B., Gaillardet, J., François, L.M., Allègre, C.J., 2003. Basalt weathering laws and the impact of basalt weathering on the global carbon cycle. Chemical Geology, 202(3): 257-273. DOI:https://doi.org/10.1016/j.chemgeo.2002.10.001

Dodson, J., 1974a. Vegetation and climatic history near Lake Keilambete, western Victoria. Australian Journal of Botany, 22(4): 709-717.

Dodson, J., 1975. Vegetation History and Water Fluctuations at Lake Leake, South-Eastern South Australia. II. 50 000 B.P. To 10 000 B.P. Australian Journal of Botany, 23(5): 815-831. DOI:https://doi.org/10.1071/BT9750815

Dodson, J.R., 1974b. Vegetation history and water fluctuations at Lake Leake, south-eastern South Australia. 1. 10,000 B.P. to present. Australian Journal of Botany, 22(4): 719-741.

Dodson, J.R., 1979. Late Pleistocene vegetation and environments near Lake Bullenmerri, Western Victoria. Australian Journal of Ecology, 4(4): 419-427. DOI:10.1111/j.1442-9993.1979.tb01570.x

Drinan, T., Graham, C., O'Halloran, J., Harrison, S., 2013. The impact of catchment conifer plantation forestry on the hydrochemistry of peatland lakes. Science of the Total Environment, 443: 608-620.

Falster, G., Tyler, J., Grant, K., Tibby, J., Turney, C., Löhr, S., Jacobsen, G., Kershaw, A.P., 2018. Millennial-scale variability in south-east Australian hydroclimate between 30,000 and 10,000 years ago. Quaternary Science Reviews, 192: 106-122.

FedUni, 2015. Visualising Victoria's Groundwater. Centre for eResearch and Digital Innovation, Federation University Australia, Mt Helen, Ballarat, Victoria, FedUni.

Forestry SA, 2010. The Mount Lyon Native Forest Reserves Resource Document. ForestrySA, Mount Gambier.

García, A., 1999. Charophyte flora of south-eastern South Australia and south-western Victoria, Australia: systematics, distribution and ecology. Australian Journal of Botany, 47(3): 407-426.

Gat, J., 1970. Environmental isotope balance of Lake Tiberias. Isotope hydrology, 109.

Gat, J., 2010. Isotope hydrology a study of the water cycle. London: Imperial College Press, London.

Gell, P.A., Barker, P.A., De Deckker, P., Last, W.M., Jelicic, L., 1994. The Holocene history of West Basin Lake, Victoria, Australia; chemical changes based on fossil biota and sediment mineralogy. Journal of Paleolimnology, 12(3): 235-258.

Gibson, J., Reid, R., 2014. Water balance along a chain of tundra lakes: A 20-year isotopic perspective. Journal of Hydrology, 519: 2148-2164.

Gibson, J.J., Birks, S.J., Yi, Y., 2015. Stable isotope mass balance of lakes: a contemporary perspective. Quaternary Science Reviews, 131: 316-328.

Gibson, J.J., Prepas, E.E., McEachern, P., 2002. Quantitative comparison of lake throughflow, residency, and catchment runoff using stable isotopes: modelling and results from a regional survey of Boreal lakes. Journal of Hydrology, 262(1): 128-144.

Gonfiantini, R., Wassenaar, L.I., Araguas-Araguas, L., Aggarwal, P.K., 2018. A unified Craig-Gordon isotope model of stable hydrogen and oxygen isotope fractionation during fresh or saltwater evaporation. Geochimica et Cosmochimica Acta, 235: 224-236. DOI:https://doi.org/10.1016/j.gca.2018.05.020

Green, J., 1981. Associations of rotifers in Australian crater lakes. Journal of Zoology, 193(4): 469-486.

Holland, H.D., Turekian, K.K., 2010. Isotope Geochemistry: A derivative of the Treatise on Geochemistry. Academic Press.

Horita, J., Rozanski, K., Cohen, S., 2008. Isotope effects in the evaporation of water: a status report of the Craig–Gordon model. Isotopes in Environmental and Health Studies, 44(1): 23-49.

Horita, J., Wesolowski, D.J., 1994. Liquid-vapor fractionation of oxygen and hydrogen isotopes of water from the freezing to the critical temperature. Geochimica et Cosmochimica Acta, 58(16): 3425-3437.

Jones, M.D., Leng, M.J., Roberts, C.N., Türkeş, M., Moyeed, R., 2005. A Coupled Calibration and Modelling Approach to the Understanding of Dry-Land Lake Oxygen Isotope Records. Journal of Paleolimnology, 34(3): 391-411. DOI:10.1007/s10933-005-6743-0

Jones, R., Bowler, J., McMahon, T., 1998. A high resolution Holocene record of P/E ratio from closed lakes in Western Victoria. Palaeoclimates, 3(1-3): 51-82.

Jones, R.N., 1995. Modelling hydrologic and climatic controls of closed lakes, western Victoria. Ph. D. Thesis, University of Melbourne.

Jones, R.N., McMahon, T.A., Bowler, J.M., 2001. Modelling historical lake levels and recent climate change at three closed lakes, Western Victoria, Australia (c.1840–1990). Journal of Hydrology, 246(1): 159-180.

Kebede, S., Travi, Y., Rozanski, K., 2009. The δ18O and δ2H enrichment of Ethiopian lakes. Journal of Hydrology, 365(3): 173-182. DOI:https://doi.org/10.1016/j.jhydrol.2008.11.027

Khan, T.A., 2003. Limnology of four saline lakes in western Victoria, Australia: I. Physico-chemical parameters. Limnologica, 33(4): 316-326. DOI:https://doi.org/10.1016/S0075-9511(03)80026-9

Kumar, B., Nachiappan, R.P., 1999. On the sensitivity of Craig and Gordon Model for the estimation of the isotopic composition of lake evaporates. Water Resources Research, 35(5): 1689-1691. DOI:10.1029/1999wr900011

Last, W.M., 1992. Petrology of modern carbonate hardgrounds from East Basin lake, a saline maar lake, southern Australia. Sedimentary Geology, 81(3): 215-229. DOI:https://doi.org/10.1016/0037-0738(92)90071-X

Last, W.M., Deckker, P., 1990. Modern and Holocene carbonate sedimentology of two saline volcanic maar lakes, southern Australia. Sedimentology, 37(6): 967-981.

Lennard, R.P., 1983. The Hydrological Setting and Limnology of Lakes Edward and Leake, South Australia, Flinders University of South Australia, School of Earth Sciences.

Lesti, C., Giordano, G., Salvini, F., Cas, R., 2008. Volcano tectonic setting of the intraplate, Pliocene-Holocene, Newer Volcanic Province (southeast Australia): Role of crustal fracture zones. Journal of Geophysical Research: Solid Earth, 113(B7). DOI:10.1029/2007jb005110

Mackay, A., Battarbee, R., Birks, J., Oldfield, F., 2003. Global change in the Holocene. Arnold, Hodder Headline Group.

Mattey, D., Lowry, D., Duffet, J., Fisher, R., Hodge, E., Frisia, S., 2008. A 53 year seasonally resolved oxygen and carbon isotope record from a modern Gibraltar speleothem: Reconstructed drip water and relationship to local precipitation. Earth and Planetary Science Letters, 269(1): 80-95. DOI:10.1016/j.epsl.2008.01.051

McGimsey, R.G., Maharrey, J.Z., Neal, C.A., 2014. 2011 Volcanic activity in Alaska: Summary of events and response of the Alaska Volcano Observatory: U.S. Geological Survey Scientific Investigations Report 2014-5159. DOI:http://dx.doi.org/10.3133/sir20145159.

McNaughton, K., 1988. 1. Effects of windbreaks on turbulent transport and microclimate. Agriculture, Ecosystems & Environment, 22: 17-39.

Merlivat, L., Jouzel, J., 1979. Global climatic interpretation of the deuterium-oxygen 18 relationship for precipitation. Journal of Geophysical Research: Oceans, 84(C8): 5029-5033. DOI:10.1029/JC084iC08p05029

Mook, W., Rozanski, K., 2000. Environmental isotopes in the hydrological cycle. IAEA Publish, 39.

Mooney, S., 1997. A fine-resolution palaeoclimatic reconstruction of the last 2000 years, from Lake Keilambete, southeastern Australia. The Holocene, 7(2): 139-149.

Murphy, B.F., Timbal, B., 2008. A review of recent climate variability and climate change in southeastern Australia. International journal of Climatology, 28(7): 859-879.

Mustafa, S., Lawson, J.S., 2002. Review of Tertiary Gambier Limestone aquifer properties, lower south-east, South Australia. Department of Water, Land and Biodiversity Conservation Naracoorte, SA ….

Nicholls, I., Joyce, E., 1989. Newer volcanics. Cambridge University Press, pp. 137-143.

Nicolaides, S., 1997. Marine-derived dolomite in the shallowly buried temperate Port Campbell Limestone (Miocene), Otway Basin, Australia. Sedimentology, 44(1): 143-157. DOI:10.1111/j.1365-3091.1997.tb00429.x

Nisbet, T., 2001. The role of forest management in controlling diffuse pollution in UK forestry. Forest Ecology and Management, 143(1-3): 215-226.

Nolan, J., Stanley, D., Wijesekera, N., Mann, B., 1990. Basalt plains hydrogeological investigation progress report No. 1. Rural Water Commission, Victoria, Investigation Branch Report, 1.

Ollier, C.D., 1967. Maars their characteristics, varieties and definition. Bulletin Volcanologique, 31(1): 45-73. DOI:10.1007/BF02597005

Parfitt, R.L., Ross, D.J., 2011. Long-term effects of afforestation with Pinus radiata on soil carbon, nitrogen, and pH: a case study. Soil Research, 49(6): 494-503. DOI:https://doi.org/10.1071/SR11106

Ramsar Convention Secretariat, 2013. The Ramsar Convention Manual: a Guide to the Convention on Wetlands (Ramsar, Iran, 1971). 6th edn, Ramsar Convention Secretariat: Gland, Switzerland.

Rueda, F.J., Schladow, S.G., Monismith, S.G., Stacey, M.T., 2005. On the effects of topography on wind and the generation of currents in a large multi-basin lake. Hydrobiologia, 532: 139-151. DOI:10.1007/s10750-004-9522-4

SA, F., 2010. The Mount Lyon Native Forest Reserves Resource Document. ForestrySA, Mount Gambier.

Shapley, M.D., Ito, E., Donovan, J.J., 2008. Isotopic evolution and climate paleorecords: modeling boundary effects in groundwater-dominated lakes. Journal of Paleolimnology, 39(1): 17-33.

Smith, R.E., Tyler, J.J., Reeves, J., Blockley, S., Jacobsen, G.E., 2017. First Holocene cryptotephras in mainland Australia reported from sediments at Lake Keilambete,

Victoria, Australia. Quaternary Geochronology, 40: 82-91. DOI:https://doi.org/10.1016/j.quageo.2016.08.007

Steinman, B.A., Rosenmeier, M.F., Abbott, M.B., Bain, D.J., 2010. The isotopic and hydrologic response of small, closed-basin lakes to climate forcing from predictive models: Application to paleoclimate studies in the upper Columbia River basin. Limnology and Oceanography, 55(6): 2231–2245.

Sveinbjörnsdóttir, Á.E., Johnsen, S.J., 1992. Stable isotope study of the Thingvallavatn area. Groundwater origin, age and evaporation models. Oikos: 136-150.

Tibby, J., Kershaw, A.P., Builth, H., Philibert, A., White, C., 2006. Environmental change and variability in southwestern Victoria: changing constraints and opportunities for occupation and land use. The social archaeology of Australian indigenous societies: 254-269.

Tibby, J., Penny, D., Leahy, P., Kershaw, A.P., 2012. Vegetation and water quality responses to Holocene climate variability in Lake Purrumbete, western Victoria. Peopled Landscapes: Archaelogical and Bogeographic Approaches to Landscapes (Eds SG Haberle & B. David): 359-373.

Timms, B., 1974. Morphology and benthos of three volcanic lakes in the Mt. Gambier district, South Australia. Marine and Freshwater Research, 25(3): 287-297. DOI:http://dx.doi.org/10.1071/MF9740287

Timms, B., 1975. Basic limnology of two crater lakes in western Victoria, Proc. R. Soc. Victoria, pp. 159-165.

Timms, B., 1977. Morphometry of Lake Elingamite, western Victoria. Victorian Naturalist, 94: 242-243.

Timms, B., Brand, G., 1973. A limnological survey of the Basin Lakes, Nalangil, western Victoria, Australia. Aust. Soc. Limnol. Bull, 5: 32-40.

Timms, B.V., 1976. A Comparative study of the limnology of three maar lakes in western Victoria. I. Physiography and physicochemical features. Marine and Freshwater Research, 27(1): 35-60.

Treble, P.C., Chappell, J., Gagan, M.K., McKeegan, K.D., Harrison, T.M., 2005. In situ measurement of seasonal δ18O variations and analysis of isotopic trends in a modern speleothem from southwest Australia. Earth and Planetary Science Letters, 233(1): 17-32. DOI:10.1016/j.epsl.2005.02.013

Tweed, S., Leblanc, M., Cartwright, I., 2009. Groundwater–surface water interaction and the impact of a multi-year drought on lakes conditions in South-East Australia. Journal of Hydrology, 379(1–2): 41-53. DOI:http://dx.doi.org/10.1016/j.jhydrol.2009.09.043

Tyler, J.J., Leng, M.J., Arrowsmith, C., 2007. Seasonality and the isotope hydrology of Lochnagar, a Scottish mountain lake: implications for palaeoclimate research. The Holocene, 17(6): 717-727. DOI:10.1177/0959683607080513

Tyler, J.J., Mills, K., Barr, C., Sniderman, J.M.K., Gell, P.A., Karoly, D.J., 2015. Identifying coherent patterns of environmental change between multiple, multivariate records: an application to four 1000-year diatom records from Victoria, Australia. Quaternary Science Reviews, 119(October): 94-105. DOI:10.1016/j.quascirev.2015.04.010

Urbano, L.D., Person, M., Kelts, K., Hanor, J.S., 2004. Transient groundwater impacts on the development of paleoclimatic lake records in semi-arid environments. Geofluids, 4(3): 187-196. DOI:10.1111/j.1468-8123.2004.00081.x

van den Hove, J.C., Ailleres, L., Betts, P.G., Cas, R.A.F., 2015. Subsurface structure of a large basaltic maar volcano examined using geologically constrained potential field modelling, Lake Purrumbete Maar, Newer Volcanics Province, southeastern Australia. Journal of Volcanology and Geothermal Research, 304: 142-159. DOI:https://doi.org/10.1016/j.jvolgeores.2015.08.020

van Otterloo, J., Cas, R.A., 2013. Reconstructing the eruption magnitude and energy budgets for the pre-historic eruption of the monogenetic~ 5 ka Mt. Gambier Volcanic Complex, south-eastern Australia. Bulletin of volcanology, 75(12): 769.

Victorian Department of Sustainability and Environment, 2014. Victorian Aquifer Framework - Grids, Bioregional Assessment Source Dataset. Victorian Department of Sustainability and Environment.

Webster, K.E., Bowser, C., Anderson, M., Lenters, J., 2006. Understanding the lake-groundwater system: just follow the water. Long-term dynamics of lakes in the landscape: Long-term ecological research on north temperate lakes: 19-48.

Wigdahl, C.R., Saros, J.E., Fritz, S.C., Stone, J.R., Engstrom, D.R., 2014. The influence of basin morphometry on the regional coherence of patterns of diatom-inferred salinity in lakes of the northern Great Plains (USA). The Holocene, 24(5): 603-613. DOI:10.1177/0959683614523154

Wilkins, D., De Deckker, P., Fifield, L.K., Gouramanis, C., Olley, J., 2012. Comparative optical and radiocarbon dating of laminated Holocene sediments in two maar lakes: Lake Keilambete and Lake Gnotuk, south-western Victoria, Australia. Quaternary Geochronology, 9: 3-15. DOI:https://doi.org/10.1016/j.quageo.2012.01.008

Wilkins, D., Gouramanis, C., De Deckker, P., Fifield, L.K., Olley, J., 2013. Holocene lake-level fluctuations in Lakes Keilambete and Gnotuk, southwestern Victoria, Australia. The Holocene, 23(6): 784-795. DOI:10.1177/0959683612471983

Winter, T.C., 1976. Numerical simulation analysis of the interaction of lakes and ground water. USGS Professional Paper 1001.

Winter, T.C., 1999. Relation of streams, lakes, and wetlands to groundwater flow systems. Hydrogeology Journal, 7(1): 28-45. DOI:10.1007/s100400050178

Yezdani, G.H., 1970. A study of the Quaternary vegetation in the volcanic lakes region of western Victoria [Ph. D. thesis]. [Melbourne (Victoria)]: Monash University.

Yihdego, Y., Webb, J.A., Leahy, P., 2014. Modelling of lake level under climate change conditions: Lake Purrumbete in southeastern Australia. Environmental Earth Sciences, 73(7): 3855-3872. DOI:10.1007/s12665-014-3669-8

Yihdego, Y., Webb, J.A., Leahy, P., 2015. Modelling of lake level under climate change conditions: Lake Purrumbete in southeastern Australia. Environmental Earth Sciences, 73(7): 3855-3872. DOI:10.1007/s12665-014-3669-8

Supporting information: details of lakes studied

Lake Leake and Lake Edward

Lake Leake and Lake Edward are adjacent maar crater lakes at the western end of the Newer Volcanic Province about 40km north west of Mt Gambier. Lake Leake is around 2 km north west of Lake Edward. Lake Leake is a shallow crater lake with a current maximum depth of ~2 m, and a nearly circular shape ~800 m diameter and surface area of 60 ha (Appendix 2 of this thesis). The lake water level has dropped over the last few decades as Dodson (1974b) noted a depth of 6 m, while Timms (1974) measured a depth of 4.5. Lake Edward is smaller with a current maximum depth of around ~6 m (compared to 7 m (Timms, 1974)), a diameter of ~500m and a surface area of 25 ha. In September 2018, the surface level of Lake Leake was 90.4 mAHD (Australian Height Datum), while Lake Edward had a water level of 104.1 mAHD. Lake Edward lies within a poorly defined and shallow maar with a diameter of ~2000 m. A dry lagoon with a diameter of ~500 m is connected to the north west side of Lake Leake with a sill level of ~92.7 mAHD. The craters for Leake and the adjacent lagoon are much more defined with distinct, often steep crater walls with a rim diameter of ~ 1500 m for the main Lake Leake crater. Between 2016–2018, Lake Leake had an average TDS of ~3800 mg/L, while Lake Edward had an average TDS of ~4400 mg/L. An interesting peculiarity is that while all the other lakes in the study are alkaline, with a pH around 7.5–9, Lake Edward has consistently returned a pH of < 7 (García, 1999; Lennard, 1983; Timms, 1974). This may be related to the large pine plantations (Drinan et al., 2013; Parfitt and Ross, 2011) that now cover 60 % of the catchment up from 38 % in the 1960's (Bayly and Williams, 1966).

Unlike many permanent lakes in the Newer Volcanic Province, Lake Leake and Lake Edward sit quite high within their catchments with a lake level above the Gambier Limestone. The crater rims sit above the surrounding plains, but the volcanic ash on the plains below the craters is covered by the Bridgewater calcarenite and aeolian sands, giving hint to the significant age of the eruptions (Boult and Hibburt, 2002; SA, 2010). Lake Edward is surrounded by peat, drying recently to form cracks and potholes near the lake shore. Likewise, the lagoon to the northwest

of Lake Leake is filled with peat and clay layers. A core taken from centre of the lagoon has a basal age of ~ 50 ka (Dodson, 1975).

There have been numerous studies of lake morphology, chemistry and benthos (Bayly and Williams, 1964; Bayly and Williams, 1966; Timms, 1974). In terms of palaeoclimate research, (Dodson, 1975; Dodson, 1974b) studied the vegetation history covering the last 50 ka.

Lake Surprise

Lake Surprise is part of the Budj Bim cultural landscape. A UNESCO world heritage site encompassing the Budj Bim (Mt Eccles) lava flow and Tae Rak (Lake Condah) wetland ecosystem. Lake Surprise is a deep sheltered lake approximately midway between the South Australian lakes and the main cluster of Victorian lakes. Lake Surprise sits within a deep elongated crater with a crater rim ~50m above the lake water level. The crater appears to form part of a fissure system, with a large eruption site in the centre and a smaller eruption site at each end, resulting in an elongate lake with small 'lagoons' at each end and a total length of ~600 m long, a width of ~200 m and an area of ~6.3 ha (Appendix 2 of this thesis). To the south, in line with the long axis of the lake, lie several smaller eruption features. In September 2019, the depth of Lake Surprise was ~11.5m with a lake level of 77.9 mAHD. The crater walls are very steep with a regular "stepped" appearance caused by alternating layers of ash and lava. The catchment area is very small, with an area of ~23 ha and no inflow or outflow streams. Based on the Victorian Aquifer Framework data, the base of the lake sits ~15 m lower than the top surface of the Port Campbell Limestone, and ~60 m above the Gellibrand Marl. The lake is freshwater, and between 2016–2018 had an average TDS of ~450 mg/L.

Lake Surprise has been the focus of numerous palaeoclimate studies: pollen and charcoal to determine palaeo-ecology (Builth et al., 2008; Tibby et al., 2006); XRF and carbon isotopes to investigate the hydrological cycle (Falster et al., 2018); and palaeo-conductivity reconstructions based on diatoms (Barr et al., 2014). Timms (1975) recorded bathymetry, limnological characteristics and morphology for the lake. Cores from Lake Surprise have a basal age of ~30 ka, with a sedimentation rate of ~1 mm/year (Builth et al., 2008).

Lake Keilambete

Lake Keilambete is a large, hypersaline maar lake near Terang. It has a near circular catchment area of ~410 ha, with a lake surface area of ~250 ha. The catchment is mostly pasture farmland, along with several quarries extracting limestone and tuff from the eastern crater wall and rim. In

August 2016, the lake water level was ~103 mAHD, ~37m below the crater rim. Lake depth was ~11 m in 1968 (Bowler, 1970), dropping to ~9 in 1990 (Jones et al., 2001). Current lake depth is uncertain. There are numerous ridges, likely representing palaeo-shorelines, visible on the crater walls, primarily along the northern half of the crater, including a significant 2-3m high cliff interpreted by Jones et al. (2001) as wave-cut and marking a long term lake level. Lake Keilambete is hypersaline with TDS values of ~102000 mg/L. There is little shoreline vegetation, with the northern near shore environment transitioning from grass to muds to thin carbonate layers at the water's edge forming a hardened surface or, more commonly broken up into many plates 5-30 cm across.

Lake Keilambete sits within all four of the upper Western Plains geological formations, with the Newer Volcanic Basalt overlying the Sandringham Sands, the Port Campbell Limestone and Gellibrand Marl in sequence. The Victorian Aquifer Framework dataset suggests that the lake level is near the marl/limestone transition at around 104m AHD, with the Port Campbell limestone forming a 10–20 m thick layer beneath a thin layer of sands from the Sandringham Sands and a 5 to 20 m thick deposit of basalt and tuffs. This is similar to boreholes described in Jones (1995). According to Jones et al. (2001) the Port Campbell Limestone is confined beyond the crater rim, separated from an overlying, perched, unconfined aquifer within the tuff by a layer of calcareous clay. Hydraulic heads for the Port Campbell aquifer under the eastern crater rim were ~19 m above the 1990 water level, and 14 m above under the western rim, with the water table in the tuffs from 1 to 7 m higher still. Near the lake both aquifers merge together to form springs that flow from the crater walls (Jones et al., 2001). Springs are often visible on the northern side of the crater, especially in the north east at the base of the wave cut slope.

Lake Keilambete is an important site for palaeoclimate research, with studies applying tephrochronology, sedimentology, ostracod valve chemistry, secular magnetic variations, hydrological modelling, palynology and microfossil analysis (Barton and Barbetti, 1982; Barton and McElhinny, 1981; Barton and Polach, 1980; Chivas et al., 1993; Chivas et al., 1985; De Deckker, 1982; Dodson, 1974a; Jones et al., 1998; Mooney, 1997; Smith et al., 2017; Wilkins et al., 2012; Wilkins et al., 2013). Lake Keilambete cores gave basal dates of ~9.5 ka at a depth of 4 m, usually terminating in a dense clay formed during a dry lake period (Barton and Polach, 1980; Wilkins et al., 2013). Sedimentation rates in the past (between 500 to 2000 yr B.P.) were around 0.31 mm/year (Barton and Barbetti, 1982).

Lake Mumblin

Lake Mumblin has unusual morphology, sitting within a small, sheltered, spatter rim crater at the top of Staughton Hill, one of several volcanic features forming the Staughton Hill complex, alongside, but separate from a maar, a scoria cone and a small lava pit (Ollier, 1967). Lake Mumblin has a small, circular catchment approximately 11 ha in size. In September 2018, the lake had a surface area of ~2 ha, with a lake water level of ~153.6 mAHD, approximately 30 m below the crater rim. Timms (1975) described the lake as 12m deep with a surface area of 3.8 ha. A surface area of such an extent would place the shoreline back into the existing tree-line surrounding the lake, and the retreat of the shoreline to its current position would suggest the current lake depth is ~8 m. Peat surrounds the lake (Timms, 1975), forming a quaking bog near the waters edges, then sloping gently upward to the steeper banks of the crater. Some abstraction from the lake has occurred, as evidenced by the presence of a pump shed and piping. However, the volume of abstraction is uncertain. The lake and catchment is surrounded by farmland, but the catchment itself is well vegetated with trees and dense scrub. Lake Mumblin is situated entirely within the Newer Volcanic basalts, with current water level ~20 m above the Sandringham Sands and Port Campbell Limestone (Victorian Department of Sustainability and Environment, 2014). As of September 2018, the lake was freshwater, with a TDS value of ~800 mg/L.

There has been limited research at Lake Mumblin. Timms (1975) described the limnological and morphological characteristics of the lake. Green (1981) examined rotifer associations of several lakes, including Mumblin and Surprise.

Lake Elingamite

Lake Elingamite lies within a sub-circular maar crater of low relief with an average diameter of ~2200 m and an area of ~390 ha. The crater is asymmetric, deeper on the eastern side than the west, with the deepest point around 700m from the eastern crater rim. A similar asymmetry is seen in the Cobrico Swamp maar, ~5 km to the north. The current lake surface area is ~215 ha, surrounded by peat and reed beds. The lake water level has been falling over the years from a 9.2 m lake depth recorded by Timms (1977), to 3.2 m depth in 2003 (Barr et al., 2014). In September 2018, the lake water level was 125.8 mAHD. The lake is limited in height by the crater walls with an overflow level of ~135 mAHD. A small outlet runs from the north west rim through the pastures to the north west, though it should not be assumed that the current outlet level represents the past conditions as there was a debate about the outlet being blocked in 1896 (Camperdown Chronicle, 1896).

The Lake Elingamite crater sits within the Port Campbell Limestone aquifer, with the top of the Port Campbell Limestone intersecting the crater at ~120 mAHD. Above the Port Campbell Limestone lies a 5–15m layer of Sandringham Sands, overlain by the surface basalt and tuffs. The Port Campbell Limestone achieves a significant thickness in the region of ~130 m, before the underlying Gellibrand Marl is encountered near 0 mAHD.

The Lake Elingamite catchment was part of the region burnt during the Cobden-Camperdown fires of March 2018. The entire catchment, with the exception of a few small areas such as the picnic shelter, burnt during the blaze, with peat fires burning underground for ~50 days following the surface fire event.

In spite of the size, permanence and ease of access, there has been limited palaeoclimate research at Lake Elingamite. Barr et al. (2014) retrieved a 178 cm core from Lake Elingamite, with a basal age of AD 480. The core was used to develop a diatom-transfer function based on diatom populations to reconstruct lake conductivity.

Lake Bullen Merri and Lake Gnotuk

Lake Bullen Merri and Lake Gnotuk are described in further detail in Chapter 5 of this thesis. The two lakes are adjacent maars, yet feature very different salinity and hydrological behaviour in spite of their close proximity. Lake Gnotuk is a hypersaline lake, with a TDS value of ~70,000 mg/L. In September 2018 the lake depth was ~15 m, with a water level of 100.2 mAHD, a surface area of ~208 ha and a catchment area of ~617 ha. Lake Bullen Merri is brackish, with a TDS value of ~9300 mg/L. In September 2018, Bullen Merri was ~60 m deep, with a water level of 139.5 mAHD, and a lake surface area of ~435 ha. The catchment area is ~886 ha. The crater of Lake Bullen Merri is cloverleaf in shape, suggesting three eruption points, but the lake itself is conical in shape, deepest in the centre (Timms, 1976). Lake Bullen Merri overflows into Lake Gnotuk at a saddle between the two craters, with a height of ~168.4 mAHD. At very high levels, Lake Gnotuk overflows at ~163.8 m AHD. An overflow event from Lake Bullen Merri to Lake Gnotuk occurred in 1849 (Sutcliffe in Currey (1970)) with lake levels then falling at a similar rate in both lakes to their current levels. However, it seems unlikely that much overflow has occurred from either lake, as there is little sign of scouring or channel formation. The soils, tuffs and sands encountered around each lake seem unlikely to prevent channel cutting and any significant overflow, particularly over the steep gradient from Lake Bullen Merri to Lake Gnotuk would result in major scouring, similar to that seen at a smaller maar in Alaska (McGimsey, 2014). There are visible past shorelines on the crater walls of both lakes. Springs are

seen occasionally on the southern side of Lake Gnotuk. There is a small basin between the two lakes, forming a small swamp.

Lake Bullen Merri and Lake Gnotuk have similar heights (~80–85.5 mAHD) for the bottom of each lake (Timms, 1976), however, the geological formations surrounding each lake differ. The lakes lie at the approximate extent of the Port Campbell Limestone (Victorian Department of Sustainability and Environment, 2014). The base of Lake Gnotuk lies near the top of the Gellibrand Marl, with possibly some minor traces of Port Campbell Limestone, overlain by a ~60–80 m thick layer of Sandringham Sands, and then the basalt and tuff thinning towards the north. The marl slopes away towards the south west, and the base of Lake Bullen Merri sits just above the level of the marl and possibly a thin layer of Port Campbell Limestone thinning to the north east. Above the marl and limestone is a ~100m thickness of Sandringham Sands, overlain by the basalt and tuff.

There is considerable overlap in research between Lake Keilambete and Lake Gnotuk. Many of the studies referenced in the Lake Keilambete section also studied Lake Gnotuk. Lake Bullen Merri has not undergone as much research as Lake Gnotuk, possibly due to its unique water chemistry, being the only brackish lake in the series, and its significant depth. Jones et al. (1998) applied a hydrological mass balance modelling approach to both lakes to estimate P/E ratios through the Holocene. Dodson (1979) applied palynology to reconstruct the surrounding vegetation from ~8–16 ka. Secular magnetic variation was studied by Barton and Barbetti (1982). An age of ~10 ka was obtained at a gap corrected depth of 7 m from an 11.73 m core from Bullen Merri (Barton and Polach, 1980). A ~4 m Core from Lake Gnotuk gave a basal age of 11.5 ± 0.3 ka (Wilkins et al., 2013) terminating in a dense grey clay.

Lake Purrumbete

Lake Purrumbete is the largest lake in the group, approximately circular, with an average diameter of 2500 m and a surface area of 520 ha. The lake lies in an maar crater of low relief, and unlike most of the lakes in the study, where the crater rim usually approximates the topographic catchment, the lake's catchment is substantially larger than the maar crater alone, with a catchment area of ~30 km^2 (Yihdego et al., 2015). Lake Purrumbete's depth was reported as ~45 m (Timms, 1976), and had a September 2018 water level of 135 mAHD. There are two bays in the lake: a small one on the north side, and a larger one with a boat ramp and caravan park on the southern side. The southern bay at least does not appear to be volcanic in origin as it is shallow and flat bottomed. Lake Purrumbete has a man-made outlet that drains to the

Curdies River at high lake levels. The outlet has been lowered over the years from 134.99 mAHD prior to 1981, to 134.79 in 1981, to 134.6 mAHD in 1992 (Yihdego et al., 2015). The discrepancy between the outlet height and the current lake level may mean that there has been some sediment buildup in the outlet over the last few decades. Lake Purrumbete is a freshwater lake, with a TDS of ~530 mg/L. The catchment has been modified over the years, with several minor drainage schemes added to drain swampy farmland to the south of the lake.

The base of the lake sits slightly higher than the Gellibrand marl, which has a top surface ~70-90 mAHD around the lake. The Port Campbell Limestone tapers out a few kilometres to the west, leaving a ~50 m thickness of the Sandringham Sands, and the overlying basalt. Yihdego et al. (2015) estimated hydraulic conductivities of 3.6 m/day, and a specific yield of 0.13. Lake Purrumbete is one of the few lakes in this study which has undergone research into the diatreme structure beneath the lake. Van den Hove et al. (2015) applied magnetic and gravimetric potential field modelling to establish possible diatreme structures > 250 m deep.

Cores have been taken from Lake Purrumbete by Yezdani (1970), investigating lake pollen and algae, and De Deckker (1982), to infer lake levels and salinity based on ostracods and fossil remains. Tibby et al. (2012) retrieved cores for palynology and diatom based proxy reconstructions of vegetation and water quality, with a basal core age of ~8000 BP.

Lake Tooliorook

Lake Tooliorook is a permanent, shallow lake likely formed by lava from Mount Elephant blocking a creek to the south of the lake. Tooliorook has a large catchment with the lake filling mostly from two inlets, a minor one flowing from Lake Koonangurt, in the northwest of the lake, and a major stream collecting water from a large region to the north of the lake. At high levels the lake overflows through a channel to the south east. It had a depth of ~2 m and a surface area of 322 ha (Khan, 2003). As of this study, Lake Tooliorook had a TDS of ~4200 mg/L. The lake sits within a ~10 m thickness of the Sandringham Sands, overlying the palaeozoic basement, and with a small thickness of basalt over the top. There has been no palaeoclimate research at Tooliorook, but there has been significant sampling over the years as part of an investigation into salinity across the region (Barton et al., 2013).

Nalangil Basins

The Basin Lakes at Nalangil are the easternmost lakes in the study. These hypersaline lakes lie within adjacent maar craters surrounded by pasture farmland. As of September 2018, East Basin

is elongate in shape trending northwest–southeast, with a catchment area of 69 ha and a water surface area of 20 ha. West Basin is sub-circular, with a catchment area of 47 ha, and a water surface area of 13.6 ha. The water levels were 111.4 mAHD for West Basin, and 113.6 for East Basin, placing the water levels around ~20–25m below the crater rims. Max water depths were 12.5 m for West Basin and 12.1 m for East Basin in 1986 (Gell et al., 1994; Last, 1992). Both lakes are surrounded by thick layers of dolomite carbonate hard-grounds (Last, 1992; Last and Deckker, 1990). Liquid waste from the nearby dairy was deposited in East Basin between 1900 and 1960 resulting in high recent organic productivity and an additional flux to the hydrological budget of the lake (Timms and Brand, 1973).

The Basins surrounding geology is fairly similar to that found at Purrumbete. The base of the lakes lies just below the top surface of the Gellibrand Marl, which has a height of ~105 mAHD. Uncomformably overlying the marl is ~20m thickness of the Sandringham Sands, followed by the overlying basalts.

Some palaeoclimate work has been undertaken at the Basins, including a multiproxy study at West Basin (Gell et al., 1994), and a study of the carbonate composition of Holocene sediment cores from both lakes, which date to ~10 ka at West Basin and ~6 ka at East Basin (Last and Deckker, 1990).

Chapter 3

Development of an autonomous, monthly and daily,

rainfall sampler for isotope research

This chapter is published as:

Ankor, M. J., Tyler, J. J., & Hughes, C. E. (2019). Development of an autonomous, monthly and daily, rainfall sampler for isotope research. *Journal of Hydrology, 575*, 31-41.

Notes: This chapter has been reformatted to match the rest of this thesis. Figure and table numbers have been prefixed with the chapter number (e.g. Fig. 1 has been changed to Fig. 3.1). The published version of this paper has been included in Appendix 3.

Statement of Authorship

Title of Paper	Development of an autonomous, monthly and daily, rainfall sampler for isotope research
Publication Status	☒ Published ☐ Accepted for Publication ☐ Submitted for Publication ☐ Unpublished and Unsubmitted w ork w ritten in manuscript style
Publication Details	ANKOR M. J., TYLER J. J. & HUGHES C. E. 2019. Development of an autonomous, monthly and daily, rainfall sampler for isotope research. *Journal of Hydrology*. 575, 31-41.

Principal Author

Name of Principal Author (Candidate)	Martin Ankor		
Contribution to the Paper	Corresponding Author. Devised initial concept, sampler design, experimental design. Analysis of results. Wrote manuscript.		
Overall percentage (%)	90%		
Certification:	This paper reports on original research I conducted during the period of my Higher Degree by Research candidature and is not subject to any obligations or contractual agreements with a third party that would constrain its inclusion in this thesis. I am the primary author of this paper.		
Signature		Date	19 Dec 2019

Co-Author Contributions

By signing the Statement of Authorship, each author certifies that:

i. the candidate's stated contribution to the publication is accurate (as detailed above);

ii. permission is granted for the candidate in include the publication in the thesis; and

iii. the sum of all co-author contributions is equal to 100% less the candidate's stated contribution.

Name of Co-Author	Jonathan T. Tyler		
Contribution to the Paper	Evaluated and edited manuscript. Provided guidance for aspects of experimental design and sampler design.		
Signature		Date	19 Dec 2019

Name of Co-Author	Catherine E. Hughes		
Contribution to the Paper	Evaluated and edited manuscript. Provided guidance for aspects of experimental design and sampler design.		
Signature		Date	20/12/19

Please cut and paste additional co-author p

Abstract

An autonomous, low cost (< US$750), and open source rainfall sampler has been developed for hydrogen and oxygen isotope research, able to sample daily and monthly for up to 60 days of rainfall, over a three month period. The sampler is designed to use modern fabrication methods such as 3D printing and laser cutting to minimise the need for machined and injection molded components. The sampler can use either paraffin oil or a submerged inlet tube (also known as tube-dip-in samplers) to prevent evaporation, with the use of the inlet tube method facilitated by 3D printed bottle caps. An experiment was performed to identify the most suitable plastic for these caps, with acetone treated ABS (Acrylonitrile Butadiene Styrene) being most suitable, followed by PETG (Polyethylene Terephthalate Glycol), untreated ABS, and PLA (Polylactic acid). In addition, the effectiveness of both paraffin oil and the inlet tube method for preventing evaporation was quantified, with paraffin identified as being the most effective at present. During a 90 day outdoor experiment, the $^{18}O/^{16}O$ vs. $^{2}H/^{1}H$ ratios of some water samples evolved along a local evaporation line, with increased isotopic enrichment of samples correlating to water loss. A coupled hydrologic-isotopic model was applied to these data, and successfully predicted the change in isotope ratios based on the amount of water lost from each sample. This modelling approach, combined with daily and monthly sample collection and quantification of evaporation rates within the sheltered environment of the sampler allows for back calculation of the original volume and isotopic composition of daily and monthly rainfall samples. The rainfall sampler thus facilitates cost -and time- effective remote monitoring of the isotopic composition of precipitation to support an array of Earth system research.

1 Introduction

The natural variation of the oxygen and hydrogen isotopes of water in the hydrological cycle is tied to numerous climatic and meteorological variables (Craig, 1961; Craig and Gordon, 1965; Dansgaard, 1954; Gat, 2010; Gibson et al., 2016; Gibson et al., 2008). This variation forms a key dataset for many branches of research, including climate and meteorological research, water resource management, forensic and ecological source identification and spatial and temporal mapping of changes and fluxes in meteoric water (Bowen and Revenaugh, 2003; Bowen et al., 2005; Gibson and Reid, 2014; Mattey et al., 2008; Steinman et al., 2010; Treble et al., 2005; Tyler et al., 2015; Tyler et al., 2007).

At the centre of the water cycle is precipitation. The Global Network of Isotopes in Precipitation (GNIP) has underpinned knowledge on monthly and annual scale variability in the isotopic composition of precipitation since 1961 (Rozanski et al., 1993), however, several applications demand rainfall sampling at higher spatial and temporal resolution, often from remote locations, placing significant demand upon time and financial resources. In addition, the isotopes of water – $^{3}H/^{2}H/^{1}H$ and $^{18}O/^{17}O/^{16}O$ – fractionate as water molecules undergo phase change and diffusion. In response to evaporation, residual liquid water becomes relatively enriched in the heavy isotopes as a function of both the climate and the evaporative history of the water. Evaporation of collected samples presents a challenge to sampling rainfall, requiring dedicated systems that minimise evaporation and accompanying isotopic alteration. Therefore, there is a need for an adaptable precipitation sampler which preserves the integrity of oxygen and hydrogen isotope ratios ($^{3}H/^{1}H$, $^{2}H/^{1}H$, $^{18}O/^{16}O$ and $^{17}O/^{16}O$).

1.1 Previous designs

There has been no shortage of rainfall sampler designs over the last few decades, with many designs developed for acid rain research in the 1970s (Raynor and McNeil, 1978). Laquer (1990) identified over 70 reports of sequential rainfall samplers, focused on recording variations of rainfall over the course of a rainfall event, using a variety of techniques. While some aspects of a sequential rainfall sampler may form a useful design basis for a daily/monthly sampler, many rely on mains power, require manual preparation, are not suited to long term on/off operation, and often segment rainfall by volume rather than time. Few of these older samplers feature designs that are well suited to modern, low cost fabrication techniques. There are, however, some novel innovations as well as commonalities amongst many of these samplers. One of the most robust and simplest sequential sampler designs is the sampler of Kennedy et al. (1979) consisting of a series of interlinked bottles. As each bottle is filled, the overflow is diverted to the next sample bottle. Mixing of samples is prevented by the use of a narrow inlet tube to the base of each sample bottle. Ronneau et al. (1978) developed an entirely mechanical sampler for remote areas driven solely by gravity and using tipping, latching sample containers on a circular platter. A resistance based rainfall detector was used by Asman (1980), whereas Gray et al. (1974) used a loud speaker, which, when struck by a raindrop, would generate an electronic pulse that would trigger the sampler's mechanism. Gatz et al. (1971) developed a sampler able to collect up to 70 samples (500-1000 ml) from 70 mm of rainfall. At 1 x 1 x 2 m and 91 kg, this probably represents the heavyweight class of sequential samplers, closely challenged by the Raynor and McNeil (1978) sampler at 1.5 x 1.5 x 0.64 m, both of which were designed as permanent installations. A more recent sequential sampler design is the 96 vial sampler of

Coplen (2010); (2015), that incorporates a novel teflon coated cover to prevent evaporation from inactive sample vials. In terms of commonality between existing sampler designs, many make use of a tipping bucket system to quantify the rainfall amount. As many of these samplers segment rainfall by volume, a tipping bucket sensor provides an effective way to prevent overflows. Circular, rotating platters are also very common, taking advantage of mechanical and electronic simplicity and robustness.

Two more recent designs break with these common design elements. Akkoyunlu et al. (2013) developed a sampler that quantifies rainfall using MATLAB controlled solenoids, located beneath the collector funnel, separated by a tube with a volume of 5 ml. Rainfall was then gravimetrically segmented to 21 individual sample bottles. However, unlike some older systems that rely on sample bottles filling to enable the next bottle in the sequence, the sample bottles were instead capped with solenoids. As each solenoid closed, water was diverted down the inlet tube to the next bottle until all bottles were filled. Hartmann et al. (2018) developed an Arduino based, battery powered field auto-sampler that uses a Cartesian based control system to fill a grid of gas-tight sample vials. Like the design of Akkoyunlu et al. (2013), an inlet tube with a known volume (12 ml) holds the sample prior to storage. A peristaltic pump then transfers the sample via piston flow to the sample vials. A pair of cannulas pierce the vial cap for sample injection and pressure equalisation, and the sealing nature of the rubber vial cap prevents exchange with the atmosphere. This device has been used for sampling of cave waters. The evaporation prevention mechanism is of significant interest to rainfall sampling, however, it is unclear at this stage how this system could be adapted to rainfall collection, as the thin diameters of the auto-sampler cannula will likely face problems with the detritus usually collected in rainfall sampler funnels. In addition to the above, the 3700C Compact and 6712 Fullsize samplers (Teledyne ISCO, USA) represent commercial sampler designs that have been adapted for sequential rainfall sampling (Rücker et al., 2019). These samplers utilise the common design element of a circular array with up to 24 sample bottles, combined with a peristaltic pump for filling samples. There is also ongoing development focused on in-field analysis where mobile labs are established at the site of interest, with analyses of samples undertaken in near real time (Berman et al., 2009; von Freyberg et al., 2017). These systems are typically expensive, require on-site power and regular attendance, making them unsuitable at this stage for use in remote locations with limited infrastructure.

While there are many examples of sequential rainfall samplers in the literature, there are relatively few that are designed for discrete daily/monthly sampling, possibly due to the added complexity required. Unlike sequential samplers, daily/monthly samplers have to prevent

evaporation of samples for long time periods, require accurate timekeeping, must be sufficiently robust, and must store sufficient samples to operate for months in the field. Samplers designed for remote sites also need to be small enough to be transported and installed, as well as having the means to maintain power supply for the period of deployment. Of the samplers mentioned above, only the auto-sampler of Hartmann et al. (2018) and the sequential sampler of Coplen (2010) have most of the components required for daily/monthly sampling of rainfall in remote sites. However, in the case of Hartmann et al. (2018), there would be significant modifications required to adapt it for rainfall sampling including attachment of a catchment funnel, rainfall sensor, a water reservoir that the auto-sampler can sample and that can be emptied when rainfall has occurred, and a filter system to deal with the detritus collected in rainfall catchment funnels. The design of Coplen (2010) would require less modification, with the main changes being to the control software, and the inclusion of an evaporation prevention system for the main reservoir, where water is stored prior to being transferred to the sample vials. The design of Akkoyunlu et al. (2013) has potential as a monthly sampling system, as control of ~14 solenoids is manageable with low power electronics such as the open source Arduino platform.

1.2 Fabrication methods and materials

Design and construction of bespoke equipment such as precipitation samplers can be challenging due to the absence of off-the-shelf components that can be easily incorporated. Even parts as simple as a UV stabilised funnel of a suitable size can prove difficult, for example Asman (1980) made use of a square funnel, due to the difficulty of fabricating a large cylindrical funnel. Injection moulding, complex machining and custom electronics are not feasible manufacturing techniques for low volume production as they typically have high initial costs. Fortunately, in the last decade, several developments in manufacturing have emerged that enable low volume, complex designs to be manufactured at low cost (Berman, 2012; Rayna and Striukova, 2016). Two in particular are heavily used in our sampler. 3D Printing, or fused filament fabrication, enables the fabrication of complicated plastic components, though typically of fairly small size. When combined with computer numerical control (CNC) laser cutting, larger designs of considerable complexity can be manufactured. More importantly, once a design is complete, it can easily be fabricated by anyone else with a 3D printer, laser cutting or CNC milling capability. Low cost, extensible, microprocessor based electronics such as the Arduino system provide accurate timing, motor control, data logging and support for multiple sensors, e.g., Hund et al. (2016). In the same way that the manufacturing designs can be published and fabricated, the program that controls the Arduino can be shared.

1.3 Methods of preventing evaporation

With respect to evaporation prevention, two methods have demonstrated effectiveness: paraffin oil, or the submerged inlet tube system of Gröning et al. (2012) (Michelsen et al., 2018; Terzer et al., 2016). The oil method prevents evaporation by the addition of a ~5 mm layer of paraffin oil to the sample, which forms a barrier between the sample and the air. The inlet tube system uses a narrow (typically ~4 mm diameter) inlet tube that passes to the bottom of the sample container. Once the first portion of rainfall enters the sample container, the base of the inlet tube is submerged, and evaporation can only occur through the small surface area exposed in the inlet tube. Pressure is equalised through a second tube that vents the container, but is sufficiently long and thin to minimise diffusion with the exterior atmosphere. The sample container and vent tube are then protected from sunlight to minimise heating and corresponding pressure changes within the sample container. Given the simplicity and effectiveness of the paraffin oil technique, it might be expected to be the preferred collection method. However, as analysis of the samples is often complicated by the presence of oil in the sample (IAEA, 2014), in many situations the inlet tube method is preferred.

The choice of sampling bottle must also be considered as isotopes may exchange or permeate through the sample bottle material. Spangenberg (2012) investigated multiple plastics for their suitability for storing waters for stable isotope analysis, namely: High and low density polyethylene (HDPE, LDPE), polypropylene, polycarbonate, polyethylene terephthalate (PET), perfluoroalkoxy-Teflon and glass over a timeframe of 659 days. Significant variations of +5 ‰ for $\delta^{2}H$ and +2 ‰ for $\delta^{18}O$ were observed for polycarbonate and PET. The recommended materials for use in sample bottles used for stable isotope investigations are glass, HDPE or teflon, with a preference for thicker walled containers. Unfortunately, there is little overlap between the common laboratory plastics tested by (Spangenberg, 2012) and the plastics commonly used in 3D printing: acrylonitrile butadiene styrene (ABS), polylactic acid (PLA) and polyethylene terephthalate-glycol modified (PETG).

1.4 Objectives

There is a clear need for an autonomous rainfall isotope sampler that can be deployed for long time periods in remote locations. Given that no design has thus far been able to prevent losses and fractionation due to evaporation, there is also need to be able to evaluate, and potentially correct for the effects of evaporation on samples. This paper presents the development of a low cost (< US$750), autonomous, battery powered sampler using novel construction methods and

open source electronics. Design files are available from https://github.com/Mjankor/MARS-Rainfall-Sampler. Aspects of the design of the sampler are considered, with tests quantifying the amount of water lost due to surface wetting along the flow-path, and the ability of the sampler to divide the flow accurately between daily and monthly samples. In addition to discussing the design of the rainfall sampler, we also present results investigating the effectiveness of 3D printing bottle caps using ABS (Acrylonitrile Butadiene Styrene), PETG (Polyethylene Terephthalate Glycol), PLA (Polylactic acid), and acetone treated ABS, for preserving the integrity of stable isotope ratios in water samples. A coupled hydrologic-isotopic model was applied to the bottle caps experiment data, to predict the change in the isotopic composition of the water based on the water lost from each sample. Based on the results from the isotopic modelling, we describe how a hydrologic-isotopic model, taking advantage of the differing rates of evaporation from daily and monthly samples, can be used to back calculate the original volume and isotopic composition of rainfall samples.

2 Design principles

The many varied designs of rainfall sampler from the last few decades show a few commonalities, but no de facto design standard. Therefore, rather than rework an existing design, we established several design principles that were used as the basis for development.

Usage: The sampler should be easily deployed in remote environments. As major cities often have GNIP stations, and generally have personnel available for event or daily sampling, there is little benefit in designing a sampler that is reliant upon significant infrastructure.

Cost: Samplers will be deployed in remote or uncontrolled environments where there is potential for vandalism, weather damage, and other mishaps. Minimising costs means that the loss of a sampler is less of a burden on research budgets, or that more samplers can be deployed for better spatial resolution and redundancy.

Outer casing: Needs to be weatherproof and robust over the timeframe of years. It should also prevent wildlife from occupying the sampler, and should protect the electronics and interior components from sunlight and excessive heat. In addition, the sampler should be entirely self-contained without any external components such as batteries or cables which can be easily damaged.

Battery powered: The sampler must operate without an external power source for a long period of time. When combined with solar panels, a sampler should be able to operate indefinitely.

Easy to construct: As the intent is to provide a design for others to replicate, it is beneficial that the construction of the sampler is straightforward. This is also an important feature for a field sampler, where repairs and maintenance may need to be carried out at remote locations with minimal equipment.

Sampling capabilities: Capturing both daily and monthly precipitation provides some redundancy in case of failure of some components, and allows for quality control by comparing the mass balance of daily and monthly samples.

Flexibility: The sampler must be suitable for differing rainfall conditions. This is rarely a challenging problem with rainfall samplers as the collection funnel can be changed to increase or reduce the amount of rainfall collected. However, funnels with specific diameters are sometimes difficult to purchase. Therefore the design process included the development of multiple funnel options. In addition, regions with very variable rainfall should be considered, requiring a method to prevent overflow from large events

The ability to quantify rainfall: Quantifying the amount of rain is important, partly, as an explanatory variable for the isotopic composition of rainfall, and more importantly, to prevent overflows during heavy events and to avoid changing sample bottles on days of no rain.

Preservation of isotope ratios: The rainfall sampler is designed to accommodate both the paraffin oil and inlet tube methods to prevent evaporation, though it is noted that the inlet tube method has analytical and operational benefits. Oil is an option regardless of the sampler design, however the inlet tube method requires significant space to store the vent tubes, and attaching both the inlet tube and vent tube to sample bottles can be complicated or expensive.

2.1 Design

Based on the above criteria, a low cost, automated rainfall sampler was designed for remote field deployment, which for simplicity is named MARS. The choice of outer casing was an early priority in the design process. The sampler needed to be large enough to contain multiple sample bottles, as well as the sampling mechanism, electronics, battery, and a rainfall collection funnel. Fortunately, a cheap, common, off the shelf solution was identified; 200 litre plastic drums, typically used for transporting food and chemicals are extremely common, and recycled ones can be purchased for very low cost. These drums are typically blue HDPE plastic around 4 mm thick and are UV resistant. They have a diameter of ~58 cm and a height of ~93 cm, and are typically completely sealed with just two inlet ports for filling and emptying. The entire

drum is not used for the sampler. The top half of the drum is used as a lid that can be easily removed to provide access to the daily sample bottle area. The lower third of the drum is used to provide a protected enclosure below the main sampler where monthly sample bottles are placed. It should be noted that the lower shell is not designed to be water proof and it is expected that some water will make its way into that space as the seal between upper and lower shells is not watertight. There is a drain in the lower shell to prevent water building up in that space. The outer shell has had its height reduced as much as possible to minimise the wind effect on rainfall sampling (Bureau of Meteorology, 2007), to reduce the chance of it being blown over, and to make it easy to transport.

At the centre of the MARS sampler, forming the top of the lower shell, is a 12 mm plywood baseplate. This baseplate holds the electronics, battery and provides a firm fixing point for the mechanical system (Fig. 3.1). Positioned about 6 cm above the main baseplate is a rotating platter of 12 mm plywood, sitting on a 30 cm turntable bearing. This platter has a support frame on it designed to hold 60 x 225 ml HDPE bottles (48.4 mm diameter x 161 mm) in two rings of 33 and 27 bottles. A central plastic tower sits at the centre of the baseplate, and holds the tipping bucket mechanism, and a 'water switch' that can divert water from the tipping bucket outflows to either the inner or outer ring of daily sample bottles, and between first, second or third of the monthly samples. One benefit to using a rotating platter is that there is a 'dead spot' in the centre, which provides an ideal location to place the vent tubes used for the inlet tube evaporation prevention method. The platter's rotation is controlled by a ring gear driven by a stepper motor.

Three 8 mm silicone tubes run from the water switch, down the central tower and through the baseplate to 3 monthly sampling bottles (2 L, HDPE). These bottles also use the inlet tube method, with the vent tubes stored inside the lower compartment.

On the baseplate are a cabinet for the electronics, the motor for rotating the main platter, a small 12 V, 2.1 Ah sealed lead acid battery and the support for the platter bearing. In addition are two drains in case of overflow of the daily bottles, and guides with encapsulated nuts around the outer rim, used to guide and secure both top and bottom shells in place. The drains are a holdover from an earlier design and should rarely be needed in the current design.

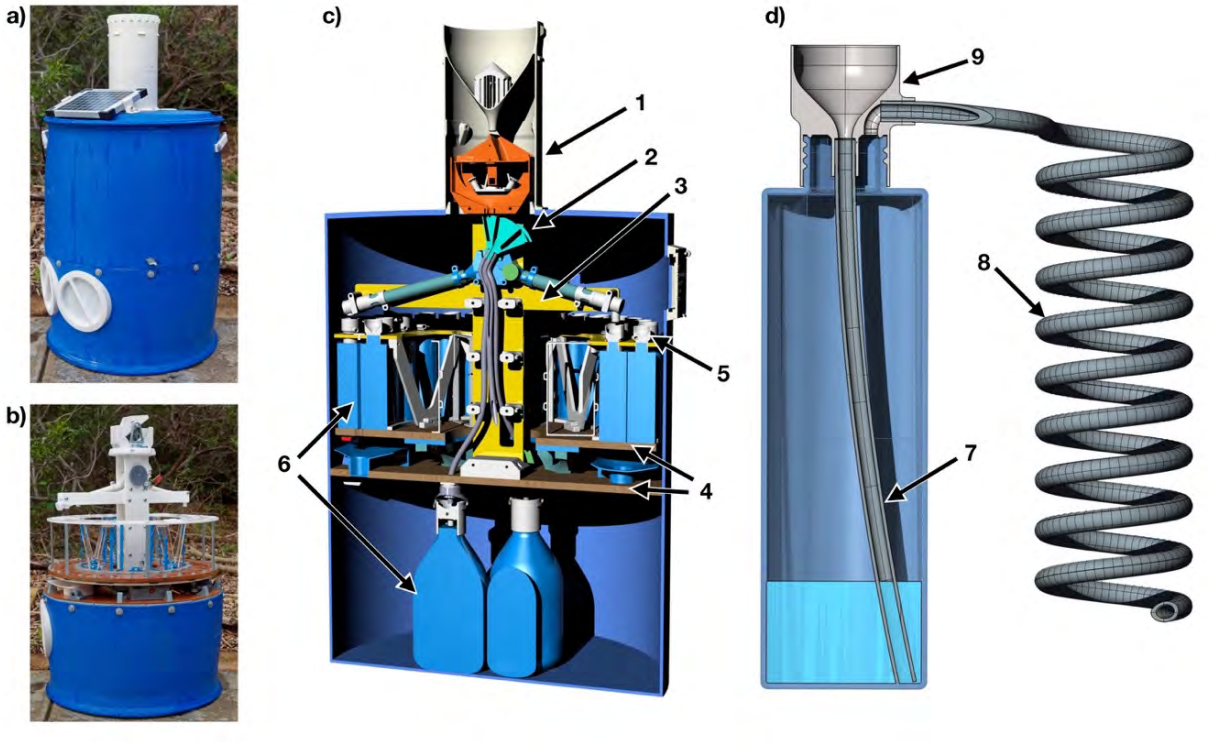

Figure 3.1: (a) Photo of sampler, with lid in place. (b) Photo of the sampler with the lid removed. (c) Cutaway view of the MARS rainfall sampler showing tipping bucket (1, orange), water switch (2, cyan), laser cut platter and tower components (3, yellow), baseplate and platter (4, wood texture), bottlecaps (5, grey) and bottles (6, blue). (d) Cutaway view of the inlet tube method, showing inlet tube (7), vent tube (8) and 3D printed bottle cap (9). (For interpretation of the references to colour in this figure legend, the reader is referred to the web version of this article.)

The electronics are controlled by an Arduino Nano 3.x (Duinotech Nano V3.0) on a breakout board. The breakout board keeps the need for soldering to a minimum, with jumper cables used to connect most of the components. Two stepping motors are used, one driving the platter, and the other controlling the water switch on the tower. A reed sensor determines when the tipping bucket is activated and a microswitch on the tower is used to reset the water switch. The position of the main platter is not reset electronically as it is much quicker to disengage the motor and rotate the platter by hand to the starting position. A real time clock and an SD Card reader keep time and a log for each sample changeover date. The Arduino platform also means that MARS can be easily reprogrammed for different roles, such as time or volume based sequential sampling of rainfall events.

Attached to the outer shell is a 3D printed funnel positioned ~30 cm above the top of the sampler. While it could be positioned closer to the outer shell, 30 cm was chosen to prevent splashes from the casing bouncing into the funnel. The top half of this funnel is designed to be easily replaced so that different sized funnels can be used. There are vents situated around the exterior of the funnel. When combined with the drains in the lower shell, these vent warm air

from the sampler, replenished with cooler air from near ground level, thus preventing greenhouse style warming in the sampler. All vents and drains are designed so that mesh can be applied to exclude insects.

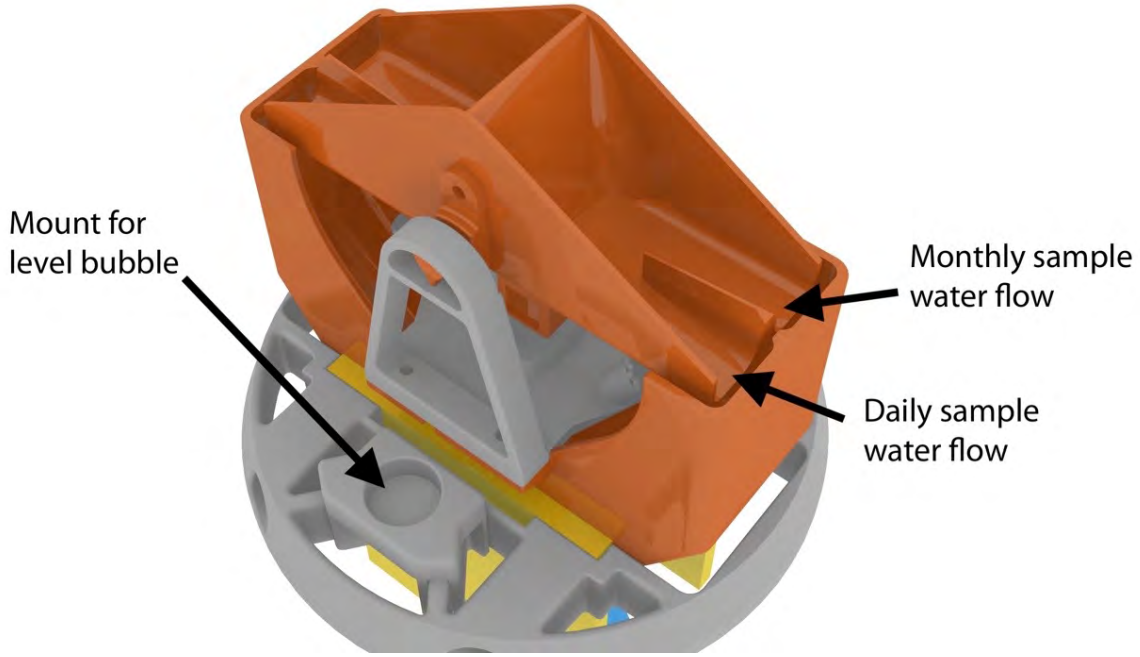

Figure 3.2: The tipping bucket, showing the flow splitting divider. A level bubble is incorporated into the design to ensure that the tipping bucket is vertically aligned

The tipping bucket design is unique due to the way that it separates the flow-path for monthly and daily sample collection (Fig 3.2). Tipping buckets have been used before to divide rainfall into multiple samples, with alternating tips of the bucket passing water through different flow-paths e.g. Gatz et al. (1971). While such a design is ideal for volumetric based segmentation in a rainfall event, it introduces potential systematic uncertainties. Any difference in tipping volume between the buckets would result in a bias towards either daily or monthly samples. In addition, most tipping buckets are designed to tip for each 0.2 mm of rainfall. If a series of small rainfall events occurs, then on a day with rainfall of 0.2 mm all of the rain may go into the daily sample, and none into the monthly. On a day of 1.4 mm of rainfall, 0.8 mm may go to daily, and 0.6 mm into the monthly. To avoid this issue, and taking advantage of the ability to fabricate complex structures with 3D printing, our tipping bucket splits the flow for each bucket, with half the water from each bucket tip going to daily, and half going to monthly samples. The tipping bucket is designed to tip with a volume of 4 ml, resulting in a tip every 0.2 mm of rainfall with a 159.6 mm diameter funnel. The success of this mechanism to divide water equally is dependent on the rainfall sampler being vertically aligned, thus a level bubble is built into the design of the tipping bucket.

Fabrication is achieved predominantly using 3D printed components, while some of the bottle support structure, ring gear and central tower uses laser cut 6 mm acrylic plastic. To build the design requires a few basic tools (jigsaw, drill, screwdriver, soldering iron) as well as a 3D printer able to print ABS with a build volume of 200 x 200 x 180. All 3D printed parts were printed using a Wanhao i3 Plus 3D printer. Components that form the water flowpath were printed with 0.2 mm layer thickness, and sanded with 1500 grit sandpaper to smooth the layered structure of the printed surface.

3D printing was able to resolve a significant problem in the design of the bottle caps. Modifying existing bottle caps to include an inlet tube and a vent tube is complicated, and space on and above a platter of daily sample bottles is limited. Using 3D printing we were able to fabricate lids featuring a small funnel to capture incoming water, an inlet tube holder that clamped the outside of the inlet tube and a curved vent pipe attachment so that vent tube could be routed horizontally towards the centre of the platter (Fig. 3.3). By clamping the outside of the inlet tube, the smallest diameter along the water flow-path was the 4 mm diameter of the inlet tube thereby minimising the chance of blockages.

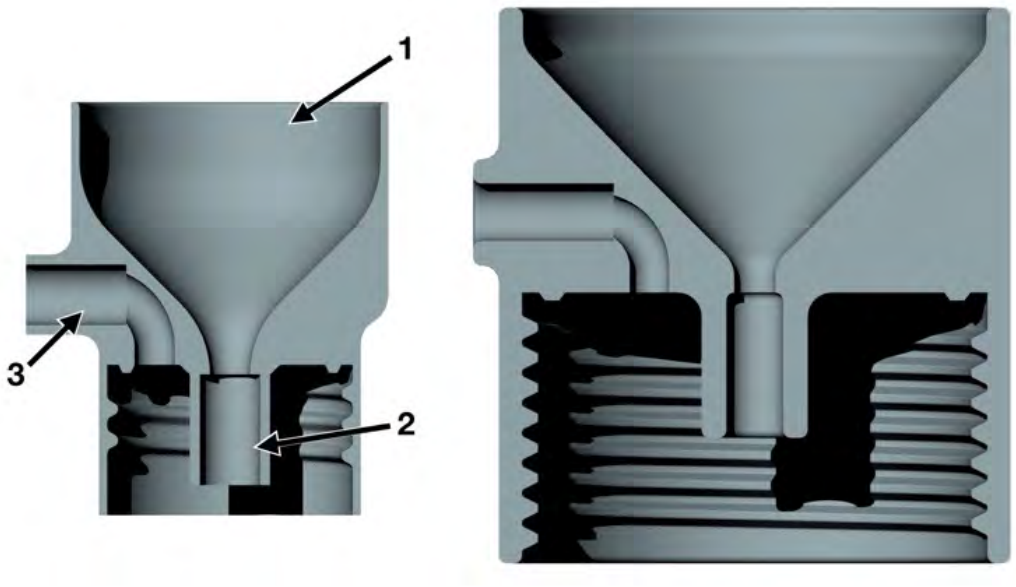

Figure 3.3: Cutaway view of the 3D printed bottle caps, with funnel (1), offset formed vent tube holder (2) and central inlet tube holder (3) (Left, cap for 225 ml bottles, right, cap for 2 L bottle).

3 Design and material tests: experimental methods

3.1 Quantification of water loss from surface wetting

In order to quantify the amount of water lost through wetting of surfaces along the flow-path, various quantities (12, 20, 40, 60, 100 ml) of water were dripped into the sampler at a rate of ~ 1 ml/s wetting the entire funnel and top surface of the filter, representing rainfall events from 0.6 to 5 mm of rainfall. The amount of water collected in the bottles were subsequently weighed. This experiment was repeated 3 times.

3.2 Quantification of water loss through bottle caps

The use of 3D printed plastics along the water flow-path was not considered problematic with regard to preservation of water isotope ratio integrity, as water would only be in contact with those plastics briefly. However, the use of 3D printed plastics for bottle closures was a concern. To test which plastics were most effective at preserving the initial water isotope ratio, bottle caps were fabricated using three different types of plastic. The plastics used were blue PLA, grey ABS and white PETG from 3DFillies (https://3dfillies.com/). In addition, grey ABS modified with acetone treatment was also tested, where acetone is used to partially dissolve and smooth the ABS plastic surface, potentially improving the sealing between printed layers (Garg et al., 2016; Singh et al., 2017). Acetone treated parts were placed in a 4 L tin lined with acetone soaked paper towels for 30 minutes at 20 °C, then allowed to dry overnight.

In order to test the effectiveness of different plastic caps, and to validate the use of the inlet tube system, an experiment was conducted using 33 x 225 ml HDPE bottles, each with ~40 ml of recent rainfall (equivalent to 4 mm of rain, using a 159.6 mm diameter funnel divided between monthly and daily samples). For each plastic, sealed bottle caps were fabricated using the same design as used in the sampler, but with the inlet and outlet holes sealed. Unsealed bottle caps of the same design were also fabricated in all 4 plastics and combined with the inlet tube and vent tube to replicate the system used in the sampler. The inlet and vent tube consisted of ~4 mm Ø (internal) LDPE tubing with a ~ 1 mm wall thickness. Triplicates of each design were fabricated for each plastic giving a total of 24 bottle-caps (Table 3.1). Triplicate bottles using the oil method of evaporation prevention were also prepared, with 5 mm of paraffin oil sealing each ~40 ml water sample. As a control, 6 bottles were prepared, sealed with wadded polypropylene caps.

Sample Description		Mass Change					Observed δ				Modelled δ	
Sample ID/Plastic type	Seal type	Lid weight (or paraffin oil weight) (g)	Initial water weight (g)	Final water weight (g)	Water loss (g)	Water loss (%)	$\delta^{18}O$ (‰)	$\delta^{2}H$ (‰)	$\delta^{18}O$ σ (‰)	$\delta^{2}H$ σ (‰)	$\delta^{18}O$ (‰)	$\delta^{2}H$ (‰)
HPDE01	Wadded PP cap	2.16	39.32	39.32	0	0	-4.6	-18.1	0.02	0.32	-4.57	-18
HPDE02	Wadded PP cap	2.15	39.5	39.5	0	0	-4.55	-17.7	0.01	0.11	-4.57	-18
HPDE03	Wadded PP cap	2.15	38.2	38.2	0	0	-4.56	-17.6	0.02	0.15	-4.57	-18
HPDE04	Wadded PP cap	2.14	39.42	39.3	0.11	0.3	-4.56	-18.1	0.05	0.23	-4.46	-17.7
HPDE05	Wadded PP cap	2.16	39.53	39.44	0.09	0.2	-4.52	-18	0.03	0.29	-4.5	-17.8
HPDE06	Wadded PP cap	2.15	39.36	39.25	0.1	0.3	-4.62	-19.1	0.01	0.11	-4.46	-17.7
PLA01	Inlet Tube	9.23	38.37	35.05	3.33	8.7	-1.45	-10.2	0.06	0.33	-1.43	-10.3
PLA02	Inlet Tube	9.27	39.02	36.22	2.8	7.2	-2.14	-12	0.09	0.25	-1.98	-11.7
PLA03	Inlet Tube	9.28	39.49	36.83	2.67	6.7	-2.23	-12.2	0.04	0.21	-2.16	-12.1
PLA04	Sealed inlet/outlet ports	9.88	39.32	38.66	0.66	1.7	-4.03	-16.7	0.04	0.21	-3.96	-16.5
PLA05	Sealed inlet/outlet ports	9.9	39.89	38.01	1.88	4.7	-2.92	-14.1	0.06	0.41	-2.89	-13.9
PLA06	Sealed inlet/outlet ports	9.87	39.99	38.06	1.94	4.8	-2.76	-13.6	0.06	0.25	-2.85	-13.8
PETG01	Inlet Tube	9.47	39.05	37.72	1.33	3.4	-3.43	-15.3	0.01	0.21	-3.35	-15
PETG02	Inlet Tube	9.49	39.51	38.03	1.48	3.7	-3.29	-14.9	0.03	0.31	-3.25	-14.8
PETG03	Inlet Tube	9.36	40.1	38.72	1.38	3.5	-3.37	-15.1	0.04	0.21	-3.32	-15
PETG04	Sealed inlet/outlet ports	10.01	39.24	38.52	0.72	1.8	-4.02	-17.5	0.08	0.36	-3.93	-16.4
PETG05	Sealed inlet/outlet ports	10.01	39.63	39.01	0.62	1.6	-4.19	-17.3	0.16	0.44	-4	-16.6
PETG06	Sealed inlet/outlet ports	10.03	39.59	39.08	0.51	1.3	-4.12	-16.7	0.06	0.44	-4.11	-16.9
ABS01	Inlet Tube	7.84	39.65	38.05	1.6	4	-3.27	-14.8	0.11	0.59	-3.14	-14.5
ABS02	Inlet Tube	7.84	39.26	37.78	1.49	3.8	-3.29	-14.7	0.06	0.39	-3.21	-14.7
ABS03	Inlet Tube	7.83	39.28	37.69	1.59	4.1	-3.24	-14.8	0.01	0.32	-3.1	-14.4
ABS04	Sealed inlet/outlet ports	8.29	39.59	38.4	1.19	3	-3.5	-15.3	0.03	0.17	-3.5	-15.4
ABS05	Sealed inlet/outlet ports	8.28	38.86	37.65	1.22	3.1	-3.4	-15.1	0.03	0.41	-3.46	-15.3
ABS06	Sealed inlet/outlet ports	8.29	39.27	37.51	1.76	4.5	-3.05	-14.1	0.04	0.48	-2.96	-14.1
ACET01	Inlet Tube	7.95	39.18	37.89	1.29	3.3	-3.49	-15.4	0.04	0.19	-3.39	-15.1
ACET02	Inlet Tube	7.97	38.29	37.25	1.04	2.7	-3.67	-16.6	0.05	0.4	-3.61	-15.7
ACET03	Inlet Tube	7.96	39.76	38.43	1.34	3.4	-3.46	-15.7	0.03	0.14	-3.35	-15
ACET04	Sealed inlet/outlet ports	8.41	40.08	39.7	0.38	1	-4.26	-17.4	0.02	0.11	-4.21	-17.1
ACET05	Sealed inlet/outlet ports	8.41	39.46	39.02	0.45	1.1	-4.22	-17.2	0.05	0.31	-4.18	-17
ACET06	Sealed inlet/outlet ports	8.36	39.18	38.76	0.42	1.1	-4.23	-17.4	0.04	0.37	-4.18	-17
PARA01	Light paraffin oil	12.15	39.26	38.9	0.37	0.9	-4.4	-17.4	0.03	0.18	-4.25	-17.2
PARA02	Light paraffin oil	11.8	39.56	39.2	0.36	0.9	-4.43	-17.6	0.04	0.24	-4.25	-17.2
PARA03	Light paraffin oil	13.56	38.97	38.66	0.31	0.8	-4.46	-17.5	0.04	0.22	-4.29	-17.3

Table 3.1: Data for each bottle cap showing plastic and evaporation prevention method, water loss and observed and modelled isotopic results. PLA, PETG, ABS in sample names refer to plastic type. ACET refers to acetone treated ABS. PARA refers to paraffin oil samples, and HDPE (highlighted in grey) are the control samples with wadded caps. Columns $\delta^{18}O$ σ and $\delta^{2}H$ σ are the reported instrumental precision.

Each bottle was weighed when empty, then again once the ~40 ml of sample was added, using an Ohaus Adventurer AR3130, three decimal point balance. Each lid was also weighed to assess whether any water had been absorbed or condensed onto the lid over the course of the experiment. For the oil bottles each empty bottle was weighed, then weighed again with oil, and then again once the sample was added. Each bottle and lid was then weighed again at the end of the 3 months to determine any loss of water.

Each water sample was filtered through a 0.2 µm polyethersulfone syinge filter directly into 2 ml vials for analysis. Paraffin oil samples were left undisturbed for several hours, then a syringe needle was pushed through the side of the bottle well below the paraffin/water interface to extract the sample. Oxygen and hydrogen isotope analyses were conducted with an L2130-i Picarro Cavity Ring-Down Spectrometer (Picarro, Inc., Santa Clara, CA, USA) with a precision against an in-house QA standard of ±0.05 ‰ for $\delta^{18}O$, and ±0.4 ‰ for $\delta^{2}H$. Each batch of 10 samples was preceded by calibration with 2 in-house standards, and a quality check against a 3rd in-house standard, with a final quality check at the end of the sample run. Each sample and standard were injected 7 times, with the first 3 injections discarded to prevent memory effects, and the remaining 4 injection results assessed for any residual trend. Chemcorrect (Picarro Inc.) was used to validate that samples had not been contaminated. Isotopic results are reported using the delta notation as per mil (‰) deviations from Vienna Standard Mean Ocean Water (VSMOW2) where:

$$\delta_x = 1000\left(\frac{R_x}{R_{VSMOW2}} - 1\right)$$

R is $^{18}O/^{16}O$, or $^{2}H/^{1}H$ and x is the sample in question.

Water from 3 of the control bottles (HDPE01, HDPE02 & HDPE 03) were analysed for $^{18}O/^{16}O$ and $^{2}H/^{1}H$ at the start of the experiment, with average values of -4.57 ‰ $\delta^{18}O$ (σ of 0.03 ‰), and δ -17.8 ‰ $\delta^{2}H$ (σ of 0.2 ‰). The remaining 30 bottles – 12 sealed plastics, 12 inlet tube plastics, 3 paraffin oil, and 3 sealed control bottles – were stored in a box outside, under shelter, for ~ 3 months (from 31/10/17 to 28/1/18), approximating conditions found in the sampler. Humidity and temperature were monitored with an Arduino data logger, measured every 15 minutes with an Aosong DHT22 sensor (factory calibrated, accuracy RH ±2 %, Temperature ±0.5 °C). Sporadic problems with the SD card of the logger resulted in some gaps in the data. However, sufficient data (38 complete days) was collected to correlate local conditions with temperature and humidity data from two nearby weather stations (Australian Bureau of Meteorology site 023090 - Kent Town, Adelaide and site 023000 - West Terrace, Adelaide), using 'Patched Point' data from the SILO database (Jeffrey et al., 2001).

3.3 Isotopic Modelling

Each sample can be modelled as a slowly desiccating pond, with a slow loss of water from the initial sample volume. A numerical simulation using the Craig & Gordon (1965) model of isotope fractionation (Eq. 1) during evaporation was applied to the data to investigate whether a

modelling approach could predict the change in $\delta^{18}O$ and $\delta^{2}H$ for a particular amount of evaporative water loss.

$$\delta_E = \frac{\alpha^* \delta_W - h_n \delta_A - \varepsilon_{eq} - \varepsilon_{kin}}{1 - h_n + 0.001\varepsilon_{kin}} \quad (1)$$

Where α^* is the reciprocal of the equilibrium fractionation factor, calculated using the equations derived by Horita and Wesolowski (1994). δ_W and δ_A are the isotopic composition of the water and atmosphere respectively. h_n refers to the relative humidity (RH). In studies of natural waters, this value is usually normalized to the temperature of the water. However, in our modelling, due to the small sample size it was assumed that air and sample water had a similar temperature, and the atmospheric RH was used. The per mil equilibrium isotopic separation (ε_{eq}) is calculated by:

$$\varepsilon_{eq} = 1000(1 - \alpha^*) \quad (2)$$

and the kinetic isotopic separation (ε_{kin}) by:

$$\varepsilon_{kin} = (1 - h_n)\theta n C_k \quad (3)$$

C_k is an experimentally derived constant determined by Merlivat (1978) as 28.5 ‰ for $\delta^{18}O$, and 25.1 ‰ for $\delta^{2}H$. θ is a parameter describing the transport resistance of the diffusion layer, typically assumed to be 1 for small water bodies, and n is a value relating isotopic separation to wind conditions, ranging from 0.5 for fully turbulent condition, to 1 for stagnant conditions (Gat, 2010). Alternative values of ~14.2 ‰ for $\delta^{18}O$ and ~12.5 ‰ for $\delta^{2}H$ are often used for studies of natural waters, combined with a similar equation to eq. 3 without the n term (e.g., Araguás-Araguás et al., 2000; Gibson et al., 2015; Skrzypek et al., 2015; Steinman et al., 2010). δ_E is the isotopic composition of evaporated flux, and is combined with a simple numerical model to predict the isotopic composition of the remaining sample water (Eq. 4 & 5).

$$V^t = V^{t-1} - E^{t-1} \quad (4)$$

$$\delta_W^t = \frac{\delta_W^{t-1} V^{t-1} - \delta_E^{t-1} E^{t-1}}{V^t} \quad (5)$$

Where t is the timestep (daily). V is the volume of the sample, E is the volume of evaporative flux, and the subscript denotes sample water (W) or evaporative flux (E). Average meteorological conditions and a θ value of 1 (for a fully developed diffusion layer) were applied as model parameters. δ_A was initially assumed to be in equilibrium with precipitation (δ_P) and

the original sample. The model was then calibrated to the observed local evaporation line using the technique of Bennett et al. (2008) by shifting δ_A by 14 % from equilibrium with (δ_P) (Eq. 6).

$$\delta_A = \alpha^* \delta_P - 1.14\varepsilon_{eq} \quad (6)$$

4 Results

4.1 Meteorology

Local meteorological conditions correlated well with the observations from both Kent Town and West Terrace weather stations. To fill in the missing data, a linear regression was derived for average daily temperature (N = 38, R2 = 0.94) and relative humidity (N = 37, R2 = 0.88) based on the correlation with Kent Town (being nearest) (Fig. 3.4). One outlier was removed from the correlation (Ave RH, 21/11/2017) as it seemed to be a local effect at the Kent Town station, and was not representative of local conditions or those at the West Terrace station. The daily average temperature over the course of the experiment was 25.3 °C, with a range from 16.0 °C to 37 °C. Relative humidity ranged from 15 % to 81 % with an average of 41.7 %. Interpolated pan evaporation estimates for both weather stations were an average of 7.7 mm/day for a total of 695 mm over the timeframe of the experiment (Fig. 3.4).

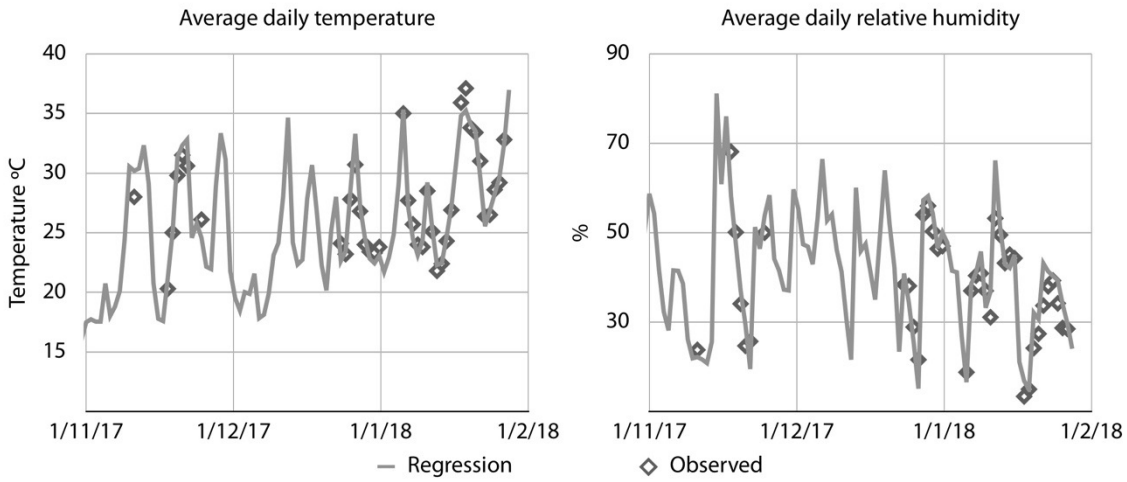

Figure 3.4: Predicted vs observed daily average temperature (N = 38, R^2 = 0.94) and relative humidity (N = 37, R^2 = 0.88) based on linear regressions.

4.2. Quantification of water loss from surface wetting

The average loss of water due to surface wetting was 1.9 ml ±0.53 σ, split fairly evenly between the 159.6 mm diameter funnel (~0.6 ml), tipping bucket and chute (~0.6 ml), and the water switch and pipework (~0.7 ml). This means that for a single event, assuming no re-evaporation of raindrops from the sampler surfaces during the event, ~90 % of rainfall for a 1 mm event is

collected, rising to ~98 % for a 5 mm event. There is also the potential for up to ~4 ml of rainfall (0.2 mm of rainfall with a 159.6 mm diameter funnel) to sit within the tipping bucket if insufficient rain falls to tip the bucket. The ratio for daily vs monthly rainfall captured was evenly split (336.3 ml for daily, 338.1 ml for monthly), demonstrating that the tipping bucket is able to divide the flow accurately with < 1 % variation.

4.3 Volumetric variation in samples

Significant differences in water loss were observed between the different techniques and plastics (Fig. 3.5, Table 3.1). The HDPE control bottles with wadded caps only lost 0.3 % (0.1 ml) of their water over the three months, followed by the paraffin oil bottles with a loss of 0.9 % (0.35 ml). With the exception of the sealed ABS and PLA capped bottles, both sealed and unsealed bottles demonstrated consistent differences between plastic types, with the inlet tube bottles typically losing ~ 2 % (0.8 ml) of mass relative to the sealed plastics. Sealed PETG and acetone treated ABS lost 1.6 % (0.6 ml) and 1.1 % (0.4 ml) respectively, while their corresponding inlet tube variants lost 3.5 % (1.4 ml) and 3.1 % (1.2 ml). The sealed ABS exhibited an average water loss of 3.5 % while the ABS inlet tube bottles lost 4 % (1.6 ml) of water. The PLA sealed bottles lost 3.7 % (1.5 ml) via the sealed lids, and 7.5 % (2.9 ml) for the inlet tube lids. Compared to most of the alternative plastics, the paraffin oil and the control, all of which had a standard deviation of < 0.35 %, the sealed ABS lids exhibited a standard deviation of 0.8 % and PLA had standard deviations of 1.8 % for the sealed and 1 % for the inlet tube lids. These results suggest that either the fabrication method did not produce PLA or ABS caps of consistent quality, or the caps did not seal the bottles adequately. As the inlet tube method is identical for all samples, then it would be expected to contribute a similar amount to the water loss for each sample. For both triplicates of PLA, two samples were similar, with the third varying by a significant amount. Assessing just the two similar samples for each set gives a 7 % (2.73 ml) loss for the inlet tube method and 4.8 % (1.9 ml) loss for the sealed cap, approximately matching the 2 % difference between inlet tube and sealed caps observed in the other plastics. Likewise, the sealed ABS appears to be indicative of variation in bottle cap fabrication, or the sealing between the caps and the bottles.

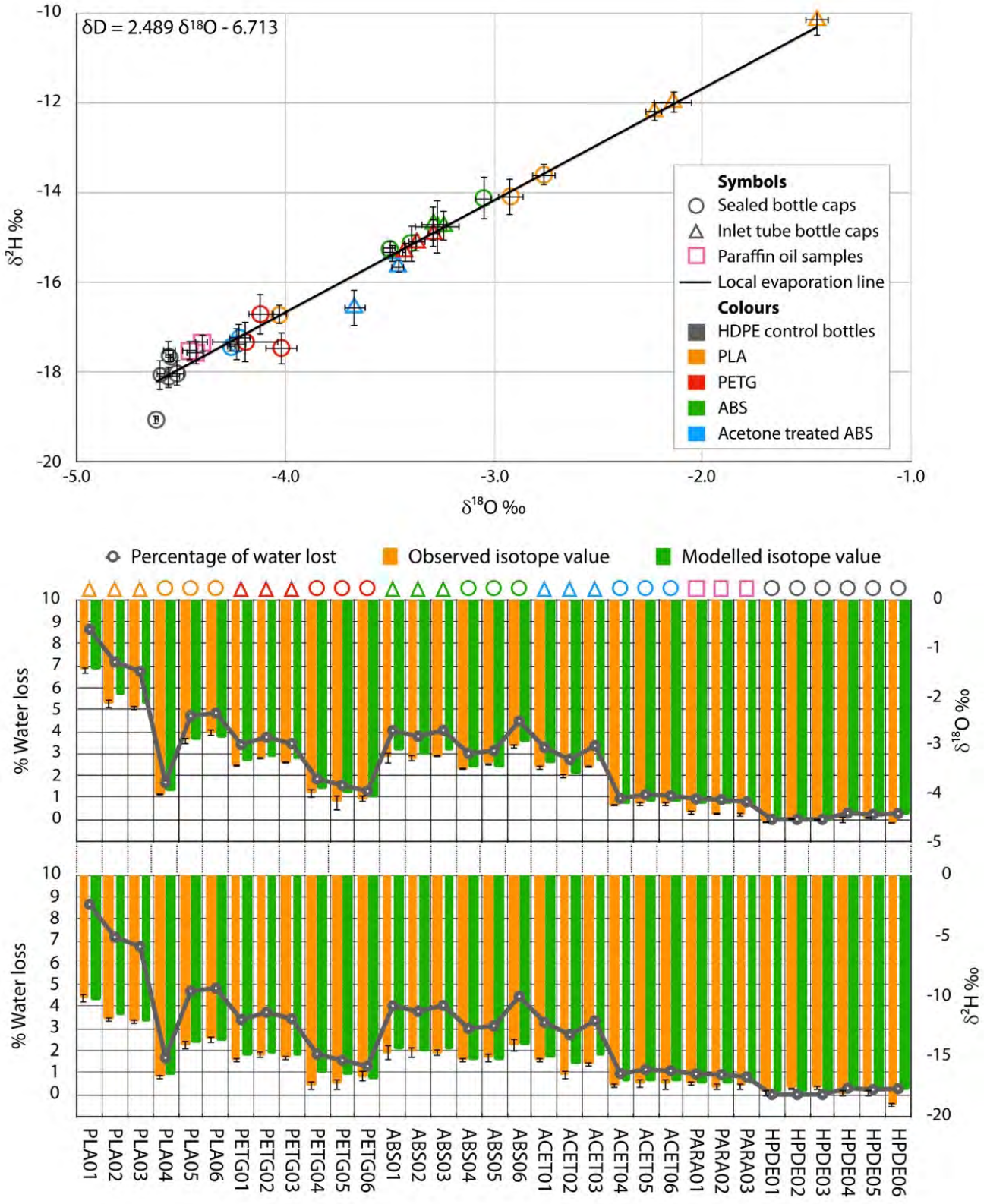

Figure 3.5: (a) Graph showing the sample evaporation line derived from the isotopic values for each sample after ~3 months storage. (b) Observed and modelled $\delta^{18}O$ results (right axis) and percentage of water loss (left axis) for each sample. (c) As per b, but for $\delta^{2}H$. Error bars show the reported instrumental precision.

4.4 Isotopic variation in samples

Changes in the $\delta^{18}O$ and $\delta^{2}H$ of the water samples correlated strongly with the water loss for each sample and a linear regression between $\delta^{18}O$ vs $\delta^{2}H$ exhibited a local evaporation line with a slope of 2.5 (Fig. 3.5). Three potential outliers were noted (PETG04, ACET02 and HDPE06) with $\delta^{2}H$ values falling approximately –0.75 ‰ below the evaporation line. These outliers are suspected to have occurred due to an analytical error and are excluded from subsequent modelling and analysis. Unfortunately, these samples were not able to be re-analysed. Excluding these outliers, enrichment relative to the average original water composition ranged from an average of 0.14 ‰ $\delta^{18}O$, and 0.3 ‰ $\delta^{2}H$ for the paraffin oil samples, up to 2.63 ‰ $\delta^{18}O$, and 6.3 ‰ $\delta^{2}H$ for the PLA inlet tube bottles. Of the three remaining plastics, the inlet tube samples were enriched by an average of 1.21 ‰ $\delta^{18}O$ and 2.7 ‰ $\delta^{2}H$ for PETG, 1.30 ‰ $\delta^{18}O$ and 3.1 ‰ $\delta^{2}H$ for ABS, and 1.10 ‰ $\delta^{18}O$ and 2.3 ‰ $\delta^{2}H$ for acetone treated ABS. Sealed caps underwent less enrichment, ranging from an average of 0.33 ‰ $\delta^{18}O$ and 0.44 ‰ $\delta^{2}H$ for the acetone treated lids to 0.41 ‰ $\delta^{18}O$ and 0.8 ‰ $\delta^{2}H$ for PETG. The sealed, untreated ABS lids suffered greater enrichment in line with their large and variable water loss.

4.5 Isotope modelling

Calibration of the modelled to observed isotope values was achieved through adjustment of the δ_A value as described in section 3.3. The modelled evaporation line was aligned to the observed evaporation line by applying a 14 % increase in equilibrium isotopic separation (ε_{eq}) between δ_A and δ_P. Differences between modelled and observed $\delta^{18}O$ for all samples except the three potential outliers ranged from 0.19 to -0.09 ‰ $\delta^{18}O$ with an average of 0.06 and a σ of 0.07 ‰ $\delta^{18}O$. Differences between modelled and observed $\delta^{2}H$ ranged from 0.7 to -0.5 ‰ $\delta^{2}H$ with an average of 0.12 and a σ of 0.27 ‰ $\delta^{2}H$. For the 3 outliers the differences in $\delta^{18}O$ ranged from 0.06 to 0.16 ‰ $\delta^{18}O$, and 0.9 to 1.3 ‰ $\delta^{2}H$ (Fig. 3.5).

5 Discussion

5.1 General usage notes

Experiments designed to test the validity of the MARS rainfall sampler indicate that the device has the potential to perform remote, automated sampling of rainfall with retention of the primary isotope signature of daily and monthly rainfall. As is the case for manually operated rainfall samplers, the MARS sampler has limits with respect to the minimum amount of rainfall that can be reliably collected, both due to water loss due to wetting of surfaces along the flow-

path and due to evaporative loss through the bottle lids. As a result, we recommend that the sampler is suitable for daily rainfall collections greater than 10 ml (equivalent to 1 mm of rainfall with a 159.6 mm funnel diameter, or 0.25 mm of rainfall with a 319.2 mm wide funnel).

5.2 Evaporation and isotope fractionation

The oxygen and hydrogen isotope enrichment along a well-defined local evaporation line (Fig. 3.5) suggests that the primary method of water loss is evaporation, with a small amount occurring through the paraffin oil, a larger amount through the plastic lids (dependent upon plastic type, degree of sealing, and fabrication consistency), and an additional ~2 % through the tubing (most likely through the inlet tube, with its ~14 cm distance from water surface to atmosphere, instead of the 150 cm long vent tube). A very small amount of water is also lost either across the plastic walls, or through the wadded caps in the control bottles. An important result is that there appears to be no fractionation effect that is unique to only one of the isotopologues. With the use of untested plastics, there was a concern that one of the plastics could preferentially exchange with either deuterium or oxygen (e.g. Spangenberg (2012)) however our results suggest that this is not the case. Modelling of the isotopic fractionation of the samples based on the amount of water loss can simulate this evaporative isotopic enrichment in $\delta^{18}O$ and $\delta^{2}H$ to a precision of 0.07 ‰ $\delta^{18}O$ and 0.27 ‰ $\delta^{2}H$ (σ^{1}).

Both the inlet tube and paraffin oil method of preventing evaporation were able to significantly decrease evaporation. For the 40 ml samples used in the experiment, average evaporation occurred at approximately 0.02 % of the pan evaporation rate. However, both methods still result in some water loss and isotopic enrichment of samples. This is especially true for small sample volumes. All plastics were substantially less effective than the paraffin oil method at preventing water loss. The inlet tube method, subtracting estimated losses through the plastics, typically resulted in ~0.8 ml loss over the 3 months, compared to 0.35 ml for the paraffin oil samples. This is in contrast to the results from Gröning et al. (2012) who observed that their sampler outperformed a paraffin oil based sampler over the course of a year. The differences between our observations and those of Gröning et al. (2012) likely arise predominantly as a result of differences in the size and shape of the sampling bottles used. The effectiveness of paraffin oil to prevent evaporation depends on the ratio of surface area to volume of the sample and quantification of the rate of water loss through paraffin oil requires consideration of the bottle shape. In contrast, the primary water loss from the inlet tube method is determined by the diameter and length of the inlet and vent tubes. Therefore, under conditions where the paraffin oil surface area is small, then paraffin may outperform the inlet tube method. However,

if the bottle diameter was doubled, the surface area of the paraffin oil would be increased fourfold and paraffin may then be outperformed by the inlet tube method. As noted in section 1.3, the method of sample analysis must be considered before deployment as paraffin oil contamination can compromise laser spectroscopy based stable isotope analysis (IAEA, 2014).

Acetone treated ABS was the most effective plastic at preventing evaporation, followed closely by PETG. Three of the plastics used (inlet tube and sealed PLA and sealed ABS) had greater variation of water loss than the other plastics, raising concerns about the degree of sealing and the fabrication consistency. All the lids had very consistent weights, with a typical range of < 0.05 g. A visual inspection also revealed no significant defects, such as delaminated layers or holes, in any of the lids. However, the nature of 3D printed components – many layers of plastic fused together – means that there is potential for tortuous pathways through the plastic layers, resulting in incomplete sealing (McCullough and Yadavalli, 2013). Leakage through 3D printed components can be prevented through configuration of printer settings, or through post processing of prints. Applying a slight over-extrusion during printing can fill any minor voids and pathways, while decreasing dimensional accuracy. Post processing with acetone treatment to the prints can dissolve filament across and between the layers and improve sealing (McCullough and Yadavalli, 2013). Another potential source of leakage is the seal of the lid against the bottle. The lids do not include a rubber washer or similar seal, instead relying on compression and deformation of the rim of the bottle against the plastic cap to seal. One option is to include a sealing washer or wadding in each cap. Washer seals were not tested here as the sampler requires perfectly fitted washers to be effective. Placing delicate seals may be an option for a single experiment, but is not practical when changing out 60 sample bottles in the field. A potentially better solution, that will be tested in the future, is the printing of seals using TPU (thermoplastic polyurethane) or a similar flexible filament. Using this technique means that the seals can be designed specifically for the caps, with suitable cutouts for the inlet tube and vent tube. With the ongoing development of multi-material 3D printers, the entire cap could be printed in a single process. In the short term, our results indicate that acetone treated ABS is the most appropriate material for bottle lids. More importantly, as there is a lot of variability in 3D printers and the software used to prepare prints, we recommend that each lid be tested to ensure consistent evaporation. A variation of the methodology employed in this paper – mass loss over time – can be used to ensure lid fabrication consistency.

5.3 Potential of mass balance closure modelling

A distinct advantage of the MARS sampler is that both daily and monthly rainfall are captured at the same time. This potentially allows for the calculation of the original isotopic composition using a modelling approach based on the difference in evaporation rates of monthly and daily rainfall. Assuming the volume of rainfall collected by the sampler is split evenly between daily and monthly samples (Eq. 7).

$$V_i^{Monthly} = \sum_{n=1}^{m} V_{i,n}^{Daily} \tag{7}$$

Where V is the volume of the sample. The superscript represents the sample type – either a daily or monthly sample, m is the total number of daily samples collected. The subscript describes initial (i) or final (f) volume, and sample number (n). Each sample may then undergo some minor evaporation while awaiting collection from the sampler. The initial sample volume for a daily sample (S) is therefore related to the final volume by Eq. 8.

$$V_{i,n}^{Daily} = V_{f,n}^{Daily} + \sum_{d=1}^{t} E_{d,n}^{Daily} \tag{8}$$

E is the daily volumetric loss from evaporation for each sample type, d is the day, and t is the total number of days a sample is exposed to evaporation. The combined volume of all daily samples (n) is therefore:

$$\sum_{n=1}^{m} V_{i,n}^{Daily} = \sum_{n=1}^{m}\left(V_{f,n}^{Daily} + \sum_{d=1}^{t} E_{d,n}^{Daily}\right) = \sum_{n=1}^{m} V_{f,n}^{Daily} + \sum_{n=1}^{m}\sum_{d=1}^{t} E_{d,n}^{Daily} \tag{9}$$

And the integrated monthly sample is related to the initial monthly sample by Eq. 10.

$$V_i^{Monthly} = V_f^{Monthly} + \sum_{d=1}^{t} E_d^{Monthly} \tag{10}$$

From Eq. 7 to 10, it can be seen that:

$$V_f^{Monthly} + \sum_{d=1}^{t} E_d^{Monthly} = \sum_{n=1}^{m} V_{f,n}^{Daily} + \sum_{n=1}^{m}\sum_{d=1}^{t} E_{d,n}^{Daily} \tag{11}$$

We relate daily evaporation rates outside the sampler to evaporation rates within the sampler using a coefficient (similar to relating PET to class-A pan evaporation) such that:

$$E_{d,n}^{Daily} = E_{d,n}^{external} k^{daily} \tag{12}$$

$$E_d^{Monthly} = E_d^{external} k^{monthly} \quad (13)$$

Where $E^{external}$ is an evaporative measure (either from meteorological records or calculated using the Penman equation (Penman, 1948) or similar) and k is a coefficient defining a proportional evaporation rate for each sample type. There should be two values of k, one representing the evaporation rate of the daily bottles (k^{daily}), and a second for the monthly bottles ($k^{monthly}$). These coefficients are expected to be similar, but not necessarily identical due to the differences between monthly and daily sample bottles. Rearranging Eq. 11 and substituting Eq. 12 and 13 gives Eq. 14.

$$V_f^{Monthly} - \sum_{n=1}^{m} V_{f,n}^{Daily} = \sum_{n=1}^{m} \sum_{d=1}^{t} E_{d,n}^{external} k^{daily} - \sum_{d=1}^{t} E_d^{external} k^{monthly} \quad (14)$$

For each of Eq. 7 to 14, a parallel series of equations can be written for the isotopic mass balance, resulting in Eq. 15.

$$\delta_f^{Monthly} V_f^{Monthly} - \sum_{n=1}^{m} \delta_{f,n}^{Daily} V_{f,n}^{Daily} = \sum_{n=1}^{m} \sum_{d=1}^{t} \delta_{e,d,n}^{Daily} E_{d,n}^{external} k^{daily}$$

$$- \sum_{d=1}^{t} \delta_{e,d}^{Monthly} E_d^{external} k^{monthly} \quad (15)$$

Where δ describes the isotopic composition of the sample or evaporative flux. The isotopic composition of evaporative fluxes are defined by the '*e*' subscript and are calculated using the model of Craig and Gordon (1965). From Equations 14 and 15, k^{daily} and $k^{monthly}$ can be solved. As the isotopic fractionation of evaporation is partly determined by the isotopic composition of the sample, a numerical solution should be used with isotopic fractionation calculated at daily (or shorter) timesteps. The original volume and isotopic composition for the integrated monthly sample can then be derived from the initial volume and isotopic composition of the daily samples.

One benefit of applying this modelling technique is that it lowers the ideal sampling requirement from "elimination of evaporation from the sample bottle", to "minimisation and quantification of evaporation from the sample bottle". This latter objective is substantially easier to achieve, with both paraffin oil and inlet tube methods fulfilling that requirement. Even under relatively intense evaporation conditions during an Australian summer, with water losses of up to 9 %, modelling of the isotopic change due to evaporation was able to achieve a precision of 0.07 ‰ $\delta^{18}O$ and 0.27 ‰ $\delta^{2}H$ (σ^{1}).

6 Conclusion

We have developed an autonomous, daily and monthly rainfall sampler (MARS), able to be deployed and left unattended for up to 3 months between visits, capable of collecting and storing up to 60 daily rainfall samples as well as integrated monthly samples. The sampler can also be reprogrammed for sequential sampling of rainfall events, either on a time or amount basis. This sampler makes significant use of modern fabrication techniques and open source technology to minimise costs and complexity. We have quantified the effectiveness of various plastics commonly used in 3D printing (PETG, PLA, ABS and acetone treated ABS) at preventing evaporation, with acetone treated ABS being most suitable, and PLA being least suitable. The inlet tube method of preventing evaporation from the sample bottles was compared with the use of paraffin oil, and it was noted that the type of sampling bottle, the amount of water and environmental conditions are significant factors in the relative effectiveness of these methods. In our experiments, paraffin oil outperformed the inlet tube method, in contrast to previous research (Gröning et al., 2012). As neither technique can fully prevent evaporation, a modeling approach was developed which takes advantage of the combined monthly and daily sample collection. Our automated rainfall sampler, augmented by a mass balance modeling approach to quantify minor evaporation effects, provides a low cost (< US$750) and effective means of sampling precipitation for isotope analysis with potential applications that span a range of Earth system sciences.

7 References

Akkoyunlu, B.O., Dogruel, M., Tayanc, M., Oruc, I., 2013. Design and Construction of a Computer Controlled Automatic Sequential Rain Sampler. Biotechnology & Biotechnological Equipment, 27(3): 3890-3895.

Araguás-Araguás, L., Froehlich, K., Rozanski, K., 2000. Deuterium and oxygen-18 isotope composition of precipitation and atmospheric moisture. Hydrological processes, 14(8): 1341-1355.

Asman, W.A.H., 1980. Draft, construction and operation of a sequential rain sampler. Water, Air, and Soil Pollution, 13(2): 235-245. DOI:10.1007/bf02279550

Bennett, K., Gibson, J., McEachern, P., 2008. Water-yield estimates for critical loadings assessment: comparisons of gauging methods versus an isotopic approach. Canadian Journal of Fisheries and Aquatic Sciences, 65(1): 83-99.

Berman, B., 2012. 3-D printing: The new industrial revolution. Business Horizons, 55(2): 155-162. DOI:10.1016/j.bushor.2011.11.003

Berman, E.S., Gupta, M., Gabrielli, C., Garland, T., McDonnell, J.J., 2009. High-frequency field-deployable isotope analyzer for hydrological applications. Water Resources Research, 45(10).

Bowen, G.J., Revenaugh, J., 2003. Interpolating the isotopic composition of modern meteoric precipitation. Water Resources Research, 39(10): 1-13. DOI:10.1029/2003WR002086

Bowen, G.J., Wassenaar, L.I., Hobson, K.A., 2005. Global application of stable hydrogen and oxygen isotopes to wildlife forensics. Oecologia, 143(3): 337-348. DOI:10.1007/s00442-004-1813-y

Bureau of Meteorology, A.G., 2007. Observation of rainfall. Commonwealth of Australia, Bureau of Meteorology.

Coplen, T.B., 2010. Sequential, time-integrated collector of precipitation, ground water, and surface water for analysis of isotopes: US Patent No. 7,687,028.

Coplen, T.B., Neiman, P.J., White, A.B., Ralph, F.M., 2015. Categorisation of northern California rainfall for periods with and without a radar brightband using stable isotopes and a novel automated precipitation collector. Tellus B: Chemical and Physical Meteorology, 67(1): 28574. DOI:10.3402/tellusb.v67.28574

Craig, H., 1961. Isotopic variations in meteoric waters. Science, 133(3465): 1702-1703.

Craig, H., Gordon, L.I., 1965. Deuterium and oxygen 18 variations in the ocean and the marine atmosphere. In: Schink, D.R., Corless, J.T. (Eds.), Marine Geochemistry. University, Rhode Island, University, Rhode Island, pp. 277-374.

Dansgaard, W., 1954. The O18-abundance in fresh water. Geochimica et Cosmochimica Acta, 6(5-6): 241-260.

Garg, A., Bhattacharya, A., Batish, A., 2016. On Surface Finish and Dimensional Accuracy of FDM Parts after Cold Vapor Treatment. Materials and Manufacturing Processes, 31(4): 522-529. DOI:10.1080/10426914.2015.1070425

Gat, J., 2010. Isotope hydrology a study of the water cycle. London: Imperial College Press, London.

Gatz, D.F., Selman, R.F., Langs, R.K., Holtzman, R.B., 1971. An automatic sequential rain sampler. Journal of Applied Meteorology, 10(2): 341-344.

Gibson, J., Birks, S., Yi, Y., 2016. Stable isotope mass balance of lakes: a contemporary perspective. Quaternary Science Reviews, 131: 316-328.

Gibson, J., Reid, R., 2014. Water balance along a chain of tundra lakes: A 20-year isotopic perspective. Journal of hydrology, 519: 2148-2164.

Gibson, J.J., Birks, S.J., Edwards, T.W.D., 2008. Global prediction of δA and δ2H- δ18O evaporation slopes for lakes and soil water accounting for seasonality. Global Biogeochemical Cycles, 22(2): 1-12. DOI:10.1029/2007GB002997

Gray, J., Hage, K.D., Mary, H.W., 1974. An automatic sequential rainfall sampler. Review of Scientific Instruments, 45(12): 1517-1519. DOI:10.1063/1.1686550

Gröning, M., Lutz, H., Roller-Lutz, Z., Kralik, M., Gourcy, L., Pöltenstein, L., 2012. A simple rain collector preventing water re-evaporation dedicated for δ 18 O and δ 2 H analysis of cumulative precipitation samples. Journal of hydrology, 448: 195-200. DOI:10.1016/j.jhydrol.2012.04.041

Hartmann, A., Luetscher, M., Wachter, R., Holz, P., Eiche, E., Neumann, T., 2018. Technical note: GUARD - An automated fluid sampler preventing sample alteration by contamination, evaporation and gas exchange, suitable for remote areas and harsh conditions. Hydrol. Earth Syst. Sci. Discuss., 2018: 1-19. DOI:10.5194/hess-2017-697

Horita, J., Wesolowski, D.J., 1994. Liquid-vapor fractionation of oxygen and hydrogen isotopes of water from the freezing to the critical temperature. Geochimica et Cosmochimica Acta, 58(16): 3425-3437.

Hund, S.V., Johnson, M.S., Keddie, T., 2016. Developing a hydrologic monitoring network in data-scarce regions using open-source arduino dataloggers. Agricultural & Environmental Letters, 1(1).

IAEA, 2014. IAEA/GNIP precipitation sampling guide. International Atomic Energy Agency.

Jeffrey, S.J., Carter, J.O., Moodie, K.B., Beswick, A.R., 2001. Using spatial interpolation to construct a comprehensive archive of Australian climate data. Environmental Modelling and Software, 16(4): 309-330.

Kennedy, V.C., Zellweger, G.W., Avanzino, R.J., 1979. Variation of rain chemistry during storms at two sites in northern California. Water Resources Research, 15(3): 687-702.

Laquer, F.C., 1990. Sequential precipitation samplers: a literature review. Atmospheric Environment. Part A. General Topics, 24(9): 2289-2297.

Mattey, D., Lowry, D., Duffet, J., Fisher, R., Hodge, E., Frisia, S., 2008. A 53 year seasonally resolved oxygen and carbon isotope record from a modern Gibraltar speleothem: Reconstructed drip water and relationship to local precipitation. Earth and Planetary Science Letters, 269(1): 80-95. DOI:10.1016/j.epsl.2008.01.051

McCullough, E.J., Yadavalli, V.K., 2013. Surface modification of fused deposition modeling ABS to enable rapid prototyping of biomedical microdevices. Journal of Materials Processing Technology, 213(6): 947-954. DOI:10.1016/j.jmatprotec.2012.12.015

Merlivat, L., 1978. Molecular diffusivities of H 2 16 O, HD 16 O, and H 2 18 O in gases. The Journal of Chemical Physics, 69(6): 2864-2871.

Michelsen, N., van Geldern, R., Roßmann, Y., Bauer, I., Schulz, S., Barth, J.A.C., Schüth, C., 2018. Comparison of precipitation collectors used in isotope hydrology. Chemical Geology, 488: 171-179. DOI:10.1016/j.chemgeo.2018.04.032

Penman, H.L., 1948. Natural Evaporation from Open Water, Bare Soil and Grass. Proceedings of the Royal Society of London. Series A, Mathematical and Physical Sciences, 193(1032): 120-145.

Rayna, T., Striukova, L., 2016. From rapid prototyping to home fabrication: How 3D printing is changing business model innovation. Technological Forecasting and Social Change, 102: 214-224. DOI:10.1016/j.techfore.2015.07.023

Raynor, G.S., McNeil, J.P., 1978. Brookhaven Automatic Sequential Precipitation Sampler. BNL-50818 United States 10.2172/7090407 Dep. NTIS, PC A03/MF A01. BNL English, ; Brookhaven National Lab., Upton, NY (USA).

Ronneau, C., Cara, J., Navarre, J., Priest, P., 1978. An automatic sequential rain sampler. Water, Air, & Soil Pollution, 9(2): 171-176.

Rozanski, K., Araguás-Araguás, L., Gonfiantini, R., 1993. Isotopic patterns in modern global precipitation. Climate change in continental isotopic records: 1-36.

Rücker, A., Zappa, M., Boss, S., von Freyberg, J., 2019. An optimized snowmelt lysimeter system for monitoring melt rates and collecting samples for stable water isotope analysis. Journal of Hydrology and Hydromechanics, 67(1): 20-31.

Singh, J., Singh, R., Singh, H., 2017. Investigations for improving the surface finish of FDM based ABS replicas by chemical vapor smoothing process: a case study. Assembly Automation, 37(1): 13-21.

Spangenberg, J.E., 2012. Caution on the storage of waters and aqueous solutions in plastic containers for hydrogen and oxygen stable isotope analysis. Rapid Communications in Mass Spectrometry, 26(22): 2627-2636.

Steinman, B.A., Rosenmeier, M.F., Abbott, M.B., Bain, D.J., 2010. The isotopic and hydrologic response of small, closed-basin lakes to climate forcing from predictive models: Application to paleoclimate studies in the upper Columbia River basin. Limnology and Oceanography, 55(6): 2231–2245.

Terzer, S., Wassenaar, L.I., Douence, C., Araguas-Araguas, L., 2016. An assessment of the isotopic (2H/18O) integrity of water samples collected and stored by unattended precipitation totalizers, EGU General Assembly Conference Abstracts, pp. 15992.

Treble, P.C., Chappell, J., Gagan, M.K., McKeegan, K.D., Harrison, T.M., 2005. In situ measurement of seasonal δ18O variations and analysis of isotopic trends in a modern speleothem from southwest Australia. Earth and Planetary Science Letters, 233(1): 17-32. DOI:10.1016/j.epsl.2005.02.013

Tyler, J.J., Jones, M., Arrowsmith, C., Allott, T., Leng, M.J., 2015. Spatial patterns in the oxygen isotope composition of daily rainfall in the British Isles. Climate Dynamics(January 2016). DOI:10.1007/s00382-015-2945-y

Tyler, J.J., Leng, M.J., Arrowsmith, C., 2007. Seasonality and the isotope hydrology of Lochnagar, a Scottish mountain lake: implications for palaeoclimate research. The Holocene, 17(6): 717-727. DOI:10.1177/0959683607080513

von Freyberg, J., Studer, B., Kirchner, J.W., 2017. A lab in the field: high-frequency analysis of water quality and stable isotopes in stream water and precipitation. Hydrology and Earth System Sciences, 21: 1721-1739.

Chapter 4

Development of a spreadsheet-based model for transient groundwater modelling

This chapter is published as:

Ankor, M. J., & Tyler, J. J. (2019). Development of a spreadsheet-based model for transient groundwater modelling. *Hydrogeology Journal*, 1-14.

Notes: The models developed for this project run in either Microsoft Excel (v15.27), or MODFLOW 2005 (https://water.usgs.gov/ogw/MODFLOW/index.html). MODFLOW models were developed and run using Modelmuse, (https://water.usgs.gov/nrp/gwsoftware/ModelMuse/ModelMuse.html). All Excel model files are available from http://dx.doi.org/10.17632/r6hcbkp53n.5

This chapter has been reformatted to match the rest of this thesis. Figure and table numbers have been prefixed with the chapter number (e.g. Fig. 1 has been changed to Fig. 4.1). The published version of this paper has been included in Appendix 4.

Statement of Authorship

Title of Paper	Development of a spreadsheet-based model for transient groundwater modelling
Publication Status	☒ Published ☐ Accepted for Publication ☐ Submitted for Publication ☐ Unpublished and Unsubmitted work written in manuscript style
Publication Details	ANKOR M. J. & TYLER J. J. 2019. Development of a spreadsheet-based model for transient groundwater modelling. *Hydrogeology Journal*. 1-14.

Principal Author

Name of Principal Author (Candidate)	Martin Ankor
Contribution to the Paper	Corresponding Author. Devised initial concept, model design, experimental design. Analysis of results. Wrote manuscript.
Overall percentage (%)	90%
Certification:	This paper reports on original research I conducted during the period of my Higher Degree by Research candidature and is not subject to any obligations or contractual agreements with a third party that would constrain its inclusion in this thesis. I am the primary author of this paper.
Signature	Date: 19 Dec 2019

Co-Author Contributions

By signing the Statement of Authorship, each author certifies that:

i. the candidate's stated contribution to the publication is accurate (as detailed above);

ii. permission is granted for the candidate in include the publication in the thesis; and

iii. the sum of all co-author contributions is equal to 100% less the candidate's stated contribution.

Name of Co-Author	Jonathan T. Tyler
Contribution to the Paper	Evaluated and edited manuscript.
Signature	Date: 19 Dec 2019

Please cut and paste additional co-author panels here as required.

Abstract

Understanding and modelling the passage of groundwater is important to a wide range of environmental and earth scientific disciplines. The science of groundwater modelling is mature, and advanced modelling algorithms are routinely implemented, for example via the widely used MODFLOW software. However, for the non-specialist scientist or student, the fundamentals of such software can be difficult to comprehend, whilst the algorithms are arguably too complex to be easily applied for many applications which require integration of a groundwater model with climate, surface-water, soil or ecological data. In this context, a spreadsheet-based groundwater model (A2016), capable of solving transient groundwater behaviour in multiple spatial dimensions, was developed. Inter-comparison tests investigating nine transient groundwater scenarios were performed between MODFLOW, A2016 and the Time-dependent Groundwater Modeling using Spreadsheet Simulation (TGMSS) model. Results demonstrated that A2016 is directly comparable to MODFLOW with identical hydraulic heads in all model experiments. TGMSS was not able to accurately simulate hydraulic heads for any of the model experiments. A groundwater–lake interaction scenario was identified for which MODFLOW will produce unrealistic results, due to the way conductance beneath lakes is determined. Applying a specified saturated thickness approximation for the region beneath the lake resulted in improved lake–groundwater interactions. A2016 is potentially useful for educational purposes, and as a tool for groundwater experiments by non-specialists, as it is modular in nature and incorporates MODFLOW terminology and techniques.

1 Introduction

Ongoing development of groundwater modelling software relies upon an understanding of the underlying theory and mathematics describing groundwater behaviour. Of the many groundwater modelling codes available, MODFLOW is considered the de facto standard (Neville and Tonkin 2001, McDonald and Harbaugh 2003, Elemer et al. 2010). Spreadsheet programs provide an excellent introduction to the finite difference technique used in MODFLOW and similar groundwater modelling programs (Olsthoorn 1985, Ousey 1986, Mahmud 1996, Anderson and Bair 2001, Akhter et al. 2006, Anderson et al. 2015). Spreadsheets are commonly used to demonstrate steady-state, two-dimensional, finite difference techniques and the accompanying groundwater flow behaviour described by the Laplace and Poisson equations (Anderson and Bair 2001, Bair and Lahm 2006, Anderson et al. 2015). However, there

are few examples in the literature of more complex spreadsheet models, able to model multi-dimensional, transient behaviour (Olsthoorn 1985, Karahan and Ayvaz 2005a). The most recent published spreadsheet model identified that meets these criteria is the TGMSS model of Karahan and Ayvaz (2005a), Karahan and Ayvaz (2005b). This gap between simple spreadsheet models and more complex groundwater modelling software is understandable given the maturity and capabilities of software such as MODFLOW. The existence of capable groundwater software could imply that the development of spreadsheet solutions is no longer relevant. However, ongoing development serves two purposes. From a pedagogical perspective, a spreadsheet model capable of demonstrating the transient and three-dimensional behaviour of groundwater and explaining the theoretical basis of MODFLOW may be a valuable educational tool. In addition, increased reliance on modelling in other scientific fields means there is still a need for new groundwater modelling code, e.g. coupling optimised groundwater models to spatial data systems (Almeida et al. 2014), to isotopic, limnological and palaeoclimate models (Jones et al. 2001, Smerdon et al. 2007, Stets et al. 2010, Ohlendorf et al. 2013), or to resolve engineering problems, such as encountered in tunnel construction (Huang et al. 2013). Developing such models in spreadsheets is an effective way to prototype and to test the model's structure prior to developing dedicated software.

This paper introduces a new spreadsheet based technique (A2016) able to solve two-dimensional (i.e. 1-layer) transient groundwater problems for both confined and unconfined aquifers. A2016 was developed as a precursor to coupling a groundwater model to a hydrologic-isotopic lake model for palaeoclimate applications. A2016 is then compared with MODFLOW and the equivalent spreadsheet model (TGMSS) developed by Karahan and Ayvaz (2005a). Model experiments incorporating external sources and sinks, Cauchy (head dependent), Dirichlet (fixed head) and Neumann (no flow) boundary conditions, and heterogeneous hydraulic conductivity and storage were performed for both unconfined and confined aquifers. All models are available in the electronic supplementary material (ESM) datasets.

As A2016 is based on the governing groundwater equation and block-centred flow structure used by MODFLOW, it is also ideal for pedagogical purposes. The groundwater equation is simplified into components and uses the same terminology as MODFLOW, thus linking the underlying mathematics to MODFLOW's structure and to groundwater behaviour.

2 Background

Derived from the principles of conservation of mass and Darcy's law, the general governing equation for groundwater flow through a representative elementary volume of heterogeneous and anisotropic material is:

$$\frac{\partial}{\partial x}\left(K_x \frac{\partial h}{\partial x}\right) + \frac{\partial}{\partial y}\left(K_y \frac{\partial h}{\partial y}\right) + \frac{\partial}{\partial z}\left(K_z \frac{\partial h}{\partial z}\right) = S_s \frac{\partial h}{\partial t} - W^* \quad (1)$$

This represents flow in a confined aquifer, where h is the potentiometric hydraulic head and K defines hydraulic conductivity, with the subscripts allowing for anisotropic conditions in the x, y and z directions. S_s refers to the specific storage of the aquifer, and W^* represents sources or sinks, such as wells, recharge and seepage. For a full derivation of this equation, see Anderson et al. (2015).

Numerical models are widely used in groundwater modelling research. By using an approximate form of the groundwater equation, calculated at numerous locations across the region of interest, a numerical model can resolve groundwater flow behaviour in multiple spatial dimensions and time. Numerical models are ideal for solving scenarios with anisotropic and heterogeneous hydraulic properties, and complex initial and boundary conditions (Anderson et al. 2015).

The majority of numerical groundwater models use either the grid based finite difference technique or the more complex finite element technique, which can solve irregularly shaped, triangular networks (Holzbecher and Sorek 2005, Anderson et al. 2015). The finite difference technique is most well-known, due to its simplicity and ease of implementation. Finite difference models are further divided into two categories, mesh-centred and block-centred models, based on where the flux boundaries are located. In a mesh-centred model, the flux boundaries are located at each node, whereas in a block-centred model they are located at the edge of each block (Anderson et al. 2015). This means the two model types treat boundaries differently but nevertheless share many similarities in model structure. Block-centred models are slightly easier to implement and are more commonplace. MODFLOW uses the block-centred, finite difference technique.

Anderson and Bair (2001) note that the lack of a common programming language taught in science courses today presents a challenge to teaching students numerical modelling methods. In the past, Fortran was used to demonstrate such techniques. Spreadsheet software has been

used to fill this gap and provides an ideal environment for demonstrating the finite difference technique, as the gridded nature of the finite difference model is easily recreated in the grid of spreadsheet cells. Unfortunately, without macros or scripts – aspects not regularly taught in classes – spreadsheets lack the looping function found in general programming languages. Loops are essential for modelling multi-dimensional, transient, groundwater behaviour, where the solution for the current time-step is used as the starting point for the next calculation. The result is that while students are introduced to two dimensional, steady state models, or one dimensional, transient models, they rarely get to experiment with the full two or three dimensional, transient, finite difference technique that is used in MODFLOW. A spreadsheet model that is able to model multi-dimensional, transient conditions would be a useful educational tool, able to provide insight into how programs such as MODFLOW are structured.

There have been several efforts to develop spreadsheet models able to perform multi-dimensional transient modelling. For example, Olsthoorn (1985) developed a robust set of examples, demonstrating methods to solve the Laplace equation, sinks and sources (Poisson equation), heterogeneous aquifers, linked aquifers, unconfined aquifers, three dimensional flow, transient flow, and refinement of the gridded network. Also included was a discussion on the use of over-relaxation as a method to speed up the iteration process. While terminology in the paper reflects earlier practices the techniques are still applicable today. The lack of macro and scripting capabilities in spreadsheet software of the time posed difficulties for transient modelling, resolved through manual copying and pasting of the model cells from the current to previous time-steps. This requirement for manual data manipulation limits the use of this spreadsheet model for more complex scenarios.

With respect to the requirement for macros in transient modelling, advances were made by the TGMSS models of Karahan and Ayvaz (2005a, 2005b). These two papers present very similar models, with the main difference being the use of the arithmetic mean for determining hydraulic conductivity (K) between cells in Karahan and Ayvaz (2005b) and the harmonic mean in Karahan and Ayvaz (2005a). These papers introduced a single-stage solution algorithm that links the time-stepping process to the iteration process for solving transient problems. However, these models exhibit inconsistencies with MODFLOW, which, as will be described below, is due to the way they handle iteration and the characterization of the aquifer.

Anderson and Bair (2001) demonstrated spreadsheet models to solve the Laplace and Poisson equations, with examples of both mesh and block-centred models, implicit and explicit one dimensional transient models and two dimensional, steady state models. In addition, mass

balance techniques were introduced along with some of the terminology used in MODFLOW, e.g. conductance. Anderson and Bair (2001) also suggested that the block-centred flow structure of MODFLOW could be replicated through linked spreadsheets.

Of the models reviewed here, those described in Olsthoorn (1985) are the most complete from a mathematical perspective, but lack the programming required for automated transient modelling. Karahan and Ayvaz (2005A and 2005B) describe a novel technique for transient modelling, however results from these models are inconsistent with MODFLOW. There is a need for an up to date spreadsheet-based groundwater model, based on current terminology, and capable of transient modelling in multiple spatial dimensions.

3 Theoretical Basis

The governing equation for groundwater (Eq. 1) is applicable to a representative elementary volume (REV), a cube of material representing a portion of the aquifer. By integrating over the thickness (b) of the aquifer, transmissivity (T) and storativity (S) are defined and the source term, W^* is converted to a flux (R) representing flow from external sources.

$$T = Kb \tag{2}$$

$$S = S_s b \tag{3}$$

$$R = W^* b \tag{4}$$

When further simplified to 2D horizontal flow as per the Dupuit-Forchheimer approximation, Eq. 1 becomes:

$$\frac{\partial}{\partial x}\left(T_x \frac{\partial h}{\partial x}\right) + \frac{\partial}{\partial y}\left(T_y \frac{\partial h}{\partial y}\right) = S \frac{\partial h}{\partial t} - R \tag{5}$$

The simplification to 2D is applicable to 3D groundwater modelling, as the determination of vertical conductance between layers requires a slightly different method than that used for horizontal transmissivity (Harbaugh 2005). MODFLOW can be considered a series of 2D layers, linked via vertical flow terms. The 2D structure is also easily represented in a spreadsheet.

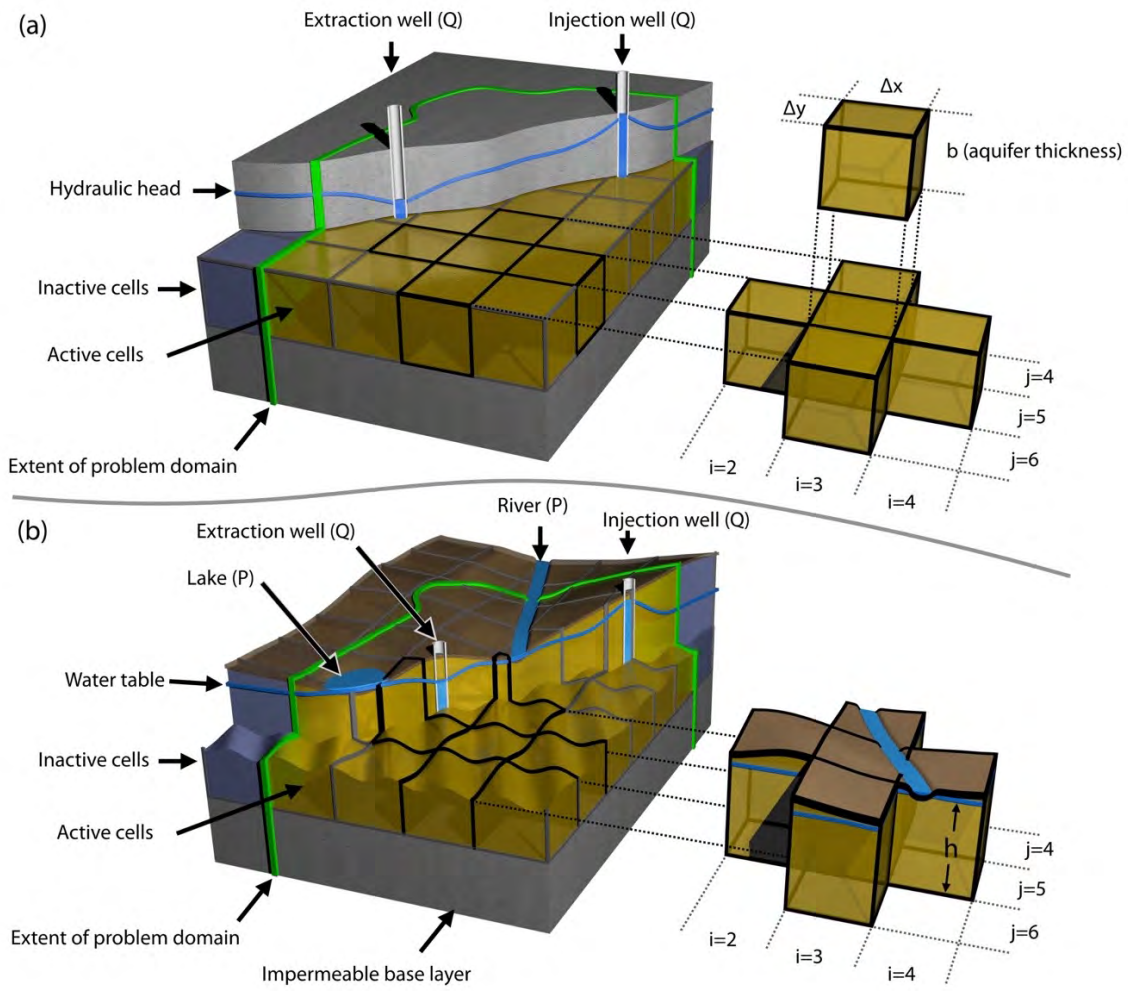

Figure 4.1: Cutaway view of a single-layer (2D) finite-difference model for (a) a confined aquifer and (b) an unconfined aquifer. Shown are the various external sources, both head dependent flows (P) which vary depending upon groundwater condition (Cauchy boundary condition), and flows that are independent of the groundwater condition (Q). Inactive cells lie outside the problem domain and play no part in the finite difference model. Active cells along the edge of the problem domain are typically defined with a no-flow (Neumann) boundary condition.

Equation 5 determines the behaviour of a singular point location in the aquifer. To adapt this equation to a finite difference model requires an approximation by converting derivatives to differences, defined by the *x* and *y* dimensions of each cell (Fig. 4.1). Therefore, for a model with regular cell dimensions, the equation for a cell with coordinates *i,j* in the grid becomes:

$$T_{i,j-\frac{1}{2}}\left(\frac{h_{i,j-1}-h_{i,j}}{\Delta x^2}\right)+T_{i,j+\frac{1}{2}}\left(\frac{h_{i,j+1}-h_{i,j}}{\Delta x^2}\right)+T_{i-\frac{1}{2},j}\left(\frac{h_{i-1,j}-h_{i,j}}{\Delta y^2}\right)+T_{i+\frac{1}{2},j}\left(\frac{h_{i+1,j}-h_{i,j}}{\Delta y^2}\right)+R_{i,j}=S_{i,j}\frac{dh}{dt} \quad (6)$$

In the models described in this paper, transmissivity is the harmonic mean (MODFLOW default) between cells (defined by subscripts), taken at the block face between each node.

Integrating from the approximated point equation to the full cell dimensions through multiplying both sides of the equation by the *x* and *y* dimensions of each cell results in:

$$T_{i,j-\frac{1}{2}}\Delta y\left(\frac{h_{i,j-1}-h_{i,j}}{\Delta x}\right)+T_{i,j+\frac{1}{2}}\Delta y\left(\frac{h_{i,j+1}-h_{i,j}}{\Delta x}\right)+T_{i-\frac{1}{2},j,}\Delta x\left(\frac{h_{i-1,j}-h_{i,j}}{\Delta y}\right)$$

$$+T_{i+\frac{1}{2},j,}\Delta x\left(\frac{h_{i+1,j}-h_{i,j}}{\Delta y}\right)+Q_{\mathrm{S},i,j}=S_{i,j}\Delta x\Delta y\frac{dh}{dt} \quad (7)$$

Q_S is now the volumetric flow into or out of the cell from external sources, and each portion of the left-hand side of the equation represents the volumetric flow from the neighbouring cells, recognisable as Darcy's Law. This is the basis of the governing equation behind MODFLOW, where the change in hydraulic head of a cell is a result of the specific storage and cell volume and the sum of all flows into and out of the cell over a period of time. Flow rate to the cell consists of flows to and from the four surrounding cells and external flows (Q_S) such as recharge or wells.

External flows (Q_S) can be further divided into two categories: Fluxes that occur independently of the groundwater condition, such as wells and recharge, and head dependent fluxes that vary depending on the groundwater head, such as evapotranspiration and river/lake seepage. Both types of flows can be represented by the expression:

$$Q_{S,i,j}=P_{i,j}h_{i,j}+Q_{i,j} \quad (8)$$

Where Q_S is the total external flow to the cell, *P* represents head-dependent flows, and *Q* represents fluxes that are independent of the groundwater head (Fig. 4.1). For a full derivation of the external flows term, please see Harbaugh (2005).

MODFLOW simplifies equation 7 through the introduction of a conductance term (*C*), that combines transmissivity and the cell dimensions into a single value.

$$T_{i,j+\frac{1}{2}}\Delta y\frac{1}{\Delta x}=C_{i,j+\frac{1}{2}} \quad (9)$$

$$T_{i,j-\frac{1}{2}}\Delta y\frac{1}{\Delta x}=C_{i,j-\frac{1}{2}} \quad (10)$$

$$T_{i+\frac{1}{2},j}\Delta x\frac{1}{\Delta y}=C_{i+\frac{1}{2},j} \quad (11)$$

$$T_{i-\frac{1}{2},j}\Delta x\frac{1}{\Delta y}=C_{i-\frac{1}{2},j} \quad (12)$$

This results in the simplified form of equation 7:

$$C_{i,j+\frac{1}{2}}\left(h_{i,j+1}-h_{i,j}\right)+C_{i,j-\frac{1}{2}}\left(h_{i,j-1}-h_{i,j}\right)+C_{i+\frac{1}{2},j}\left(h_{i+1,j}-h_{i,j}\right)$$

$$+C_{i-\frac{1}{2},j}\left(h_{i-1,j}-h_{i,j}\right)+P_{i,j}h_{i,j}+Q_{i,j}=\ S_{i,j}\Delta x\Delta y\frac{dh}{dt} \qquad (13)$$

To account for transient behaviour, the time differential is also approximated with a backward difference from current time (t^m) to the previous time (t^{m-1}), using the hydraulic head for the current time-step (h^m), for which the spatial differences are being determined, and the previous time-step (h^{m-1}), thereby giving a fully implicit numerical solution.

$$C_{i,j+\frac{1}{2}}\left(h_{i,j+1}^{m}-h_{h_{i,j}}^{m}\right)+C_{i,j-\frac{1}{2}}\left(h_{i,j-1}^{m}-h_{h_{i,j}}^{m}\right)+C_{i+\frac{1}{2},j}\left(h_{i+1,j}^{m}-h_{h_{i,j}}^{m}\right)$$

$$+C_{i-\frac{1}{2},j}\left(h_{i-1,j}^{m}-h_{h_{i,j}}^{m}\right)+P_{i,j}^{m}h_{i,j}^{m}+\ Q_{i,j}^{m}=S_{i,j}\Delta x\Delta y\frac{h_{h_{i,j}}^{m}-h_{h_{i,j}}^{m-1}}{t^{m}-t^{m-1}} \qquad (14)$$

Expanding and rearranging equation 13 forms a 2D finite difference equation (Eq. 14), similar to that of MODFLOW, and suitable to be rewritten in matrix form for use with matrix solution methods.

$$C_{i,j+\frac{1}{2}}h_{i,j+1}^{m}+C_{i,j-\frac{1}{2}}h_{i,j-1}^{m}+C_{i+\frac{1}{2},j}h_{i+1,j}^{m}+C_{i-\frac{1}{2},j}h_{i-1,j}^{m}$$

$$+h^{m}\left(-C_{i,j+\frac{1}{2}}-C_{i,j-\frac{1}{2}}-C_{i+\frac{1}{2},j}-C_{i-\frac{1}{2},j}+\mathrm{HCOF}_{i,j}\right)=\ \mathrm{RHS}_{i,j} \qquad (15)$$

Where HCOF represents all the coefficients of h^m that do not include conductance or storage, and RHS represents the remaining right hand side components.:

$$HCOF_{i,j}=\ P_{i,j}^{m}-S_{i,j}\Delta x\Delta y\frac{1}{t^{m}-t^{m-1}} \qquad (16)$$

$$RHS_{i,j}=\ -S_{i,j}\Delta x\Delta y\frac{h^{m-1}}{t^{m}-t^{m-1}}-Q_{i,j}^{m} \qquad (17)$$

Equation 15 has one major difference compared to the complete MODFLOW equation as the vertical flow terms are not included (Harbaugh 2005). These are straightforward to add if required, but were not considered necessary for the purpose of this project.

A spreadsheet often cannot use matrix solvers, instead relying on Gauss-Seidel iteration at each point of the grid until a convergence value has been achieved (Wang and Anderson 1982, Ousey 1986). Rewriting equation 15 gives the equation (Eq. 18) for use where point by point iteration is required.

$$h_{i,j} = \frac{RHS_{i,j} - \left(C_{i,j+\frac{1}{2}} h^m_{i,j+1} + C_{i,j-\frac{1}{2}} h^m_{i,j-1} + C_{i+\frac{1}{2},j} h^m_{i+1,j} + C_{i-\frac{1}{2},j} h^m_{i-1,j}\right)}{\left(-C_{i,j+\frac{1}{2}} - C_{i,j-\frac{1}{2}} - C_{i+\frac{1}{2},j} - C_{i-\frac{1}{2},j} + HCOF_{i,j}\right)} \tag{18}$$

The above equations define groundwater behaviour for a confined aquifer. For an unconfined aquifer modifications are required. Storativity must be changed from $S_S b$ (specific storage integrated over the aquifer thickness) to S_Y (specific yield), as the water released from storage is no longer predominantly determined by rearrangement of the solid matrix, and, to a lesser degree, the expansion of water, but instead by the drainable porosity of the cell (Anderson et al. 2015). The RHS and HCOF terms then become:

$$RHS_{i,j} = -S_{Y\,i,j} \Delta x \Delta y \frac{h^{m-1}}{t^m - t^{m-1}} - Q^m_{i,j} \tag{19}$$

$$HCOF_{i,j} = P^m_{i,j} - S_{Y\,i,j} \Delta x \Delta y \frac{1}{t^m - t^{m-1}} \tag{20}$$

In addition, references in the equations (2, 3, 4) to aquifer thickness (b) must be modified to incorporate the hydraulic head (h), as the thickness of the aquifer is now defined by the modelled water table (Fig. 4.1). The equation for an unconfined aquifer spreadsheet is therefore:

$$h_{i,j} = \frac{RHS_{i,j} - \left(h^m_{i,j+\frac{1}{2}} K^m_{i,j+\frac{1}{2}} \Delta y \frac{1}{\Delta x} h^m_{i,j+1} + h^m_{i,j-\frac{1}{2}} K^m_{i,j-\frac{1}{2}} \Delta y \frac{1}{\Delta x} h^m_{i,j-1} + h^m_{i+\frac{1}{2},j} K^m_{i+\frac{1}{2},j} \Delta x \frac{1}{\Delta y} h^m_{i+1,j} + h^m_{i-\frac{1}{2},j} K^m_{i-\frac{1}{2},j} \Delta x \frac{1}{\Delta y} h^m_{i-1,j}\right)}{\left(-h^m_{i,j+\frac{1}{2}} K^m_{i,j+\frac{1}{2}} \Delta y \frac{1}{\Delta x} - h^m_{i,j-\frac{1}{2}} K^m_{i,j-\frac{1}{2}} \Delta y \frac{1}{\Delta x} - h^m_{i+\frac{1}{2},j} K^m_{i+\frac{1}{2},j} \Delta x \frac{1}{\Delta y} - h^m_{i-\frac{1}{2},j} K^m_{i-\frac{1}{2},j} \Delta x \frac{1}{\Delta y} + HCOF_{i,j}\right)} \tag{21}$$

While Eq. 21 appears longwinded, the structure and simplified conductance terms applied in the confined aquifer equation can still be used within an unconfined aquifer spreadsheet model by linking the aquifer thickness value to the current hydraulic head for each cell.

4 Methodology

4.1 Model Structure

The spreadsheet model (A2016) separates equations 18 and 21 into components, with RHS, HCOF, conductance, and the $C_{i,j+\frac{1}{2}}h^m_{i,j+1} + C_{i,j-\frac{1}{2}}h^m_{i,j-1} + C_{i+\frac{1}{2},j}h^m_{i+1,j} + C_{i-\frac{1}{2},j}h^m_{i-1,j}$ section computed in separate sheets. This reduces the likelihood of errors in the spreadsheet formulas, and makes it straightforward to update and replace components, for example, replacing the averaging method used to determine inter-cell conductance. Additional sheets were used to define hydrogeological parameters such as specific storage, conductivity, wells, recharge, and aquifer thickness, as well as the head values (h^{m-1}) for the previous time-step.

Transient modelling requires the head values from the end of the previous time-step as initial values for the current time-step. A macro was developed that manages the time-step loop, and transfers the calculated head values to the previous values sheet at the beginning of each iteration cycle. Additional macros were developed to allow the user to step through individual time-steps or reset the model.

Conductance was determined in separate sheets for each cardinal direction. Instead of starting the model in the first row and column of the spreadsheet, a border of blank cells was left, surrounding the grid representing the model region. This border then forms part of the conductance calculations and means that conductance along the edge of each model boundary is 0, thereby representing the commonly used no-flow boundary condition. It should be noted that this technique is only suitable for the spreadsheet model. Developing a similar model in other software or programming language would typically require the use of edge and corner nodes that do not rely on data from outside the FDM grid. A useful benefit to structuring the spreadsheet in this fashion is that it removes the need for different equations at the edge of the model. The same formula is used throughout the spreadsheet without the need to mirror or remove nodes outside the model boundary, thus simplifying the rebuilding of the model for different shaped regions.

A mass balance was run in parallel with the model, quantifying flows to each cell for each time-step, as well as cumulative flows for the simulation run. These values were then compared to the combined inflow and outflow to the model from external sources.

4.2 K2005M

K2005M is a modified version of Karahan and Ayvaz's (2005a) TGMSS model. K2005M was developed to investigate the cause of the discrepancies observed between MODFLOW and TGMSS. In K2005M an aquifer thickness variable has been included and used in place of hydraulic heads in the source term (W) and an initial head value has been defined for the storage term ($CC(H_{i,j})$) (Karahan and Ayvaz 2005a).

4.3 Experiments

Nine model experiments were run (Table 4.1), loosely based on the first example of Karahan and Ayvaz (2005a). Four experiments (#1-4) compared MODFLOW 2005 and the spreadsheet models of A2016, TGMSS and the modified version of TGMSS (K2005M). The model runs simulated the transient behaviour of groundwater in a confined aquifer, consisting of homogenous or heterogeneous hydraulic conductivity and storage conditions, with one central pumping well, two nearby injection wells and areal recharge over the modelled region. Aquifer thickness was set to 20 m.

Four further experiments (#5-8) compared MODFLOW with the unconfined aquifer variant of A2016, simulating the transient behaviour of groundwater in an unconfined aquifer under conditions similar to the confined aquifer experiments.

Experiment 9a compared the unconfined aquifer variant of A2016 with MODFLOW in a simulation incorporating topography, two head dependent boundary conditions, no-flow and fixed head perimeter boundaries and recharge. The two head dependent boundaries consisted of evapotranspiration of 0.002 mm/day over the whole model, with a 0.1 m extinction depth, linked to the topographic surface, and a lake covering the central 49 cells of the model. Parameters for the lake are similar to those required for the RES (reservoir) package in MODFLOW, with a specified lake stage (20 m), bottom sediment thickness (0.5 – 2.0 m), and sediment hydraulic conductivity (0.01 m/day). Recharge was set at 0.001 mm/day. For complete parameters and topography please see the electronic supplementary material (ESM).

Exp. #	Model name	Hydraulic conductivity	Specific storage	Simulation time (days)	Boundaries	Grid dimensions
Confined aquifer: wells						
1	TGMSS	Homogeneous	Homogeneous	1, 30, 360, 3600	Specified head, specified flow.	23x23 rows and columns. 100-m grid spacing.
	K2005M					
	A2016 Confined					
	MODFLOW					
Confined aquifer: wells + recharge						
2	TGMSS	Homogeneous	Homogenous	1, 30, 360, 3600	Specified head, specified flow.	23x23 rows and columns. 100-m grid spacing.
	K2005M					
	A2016 Confined					
	MODFLOW Confined					
3	TGMSS	Heterogeneous	Homogeneous			
	K2005M					
	A2016 Confined					
	MODFLOW Confined					
4	TGMSS	Homogeneous	Heterogeneous			
	K2005M					
	A2016 Confined					
	MODFLOW Confined					
Unconfined aquifer: wells						
5	A2016 Unconfined	Homogeneous	Homogeneous	1, 30, 360, 3600	Specified head, specified	23x23 rows and columns. 100-m grid
	MODFLOW Unconfined					
Unconfined aquifer: wells + recharge						
6	A2016 Unconfined	Homogeneous	Homogeneous	1, 30, 360, 3600	Specified head, specified flow.	23x23 rows and columns. 100-m grid spacing.
	MODFLOW Unconfined					
7	A2016 Unconfined	Heterogeneous	Homogeneous			
	MODFLOW Unconfined					
8	A2016 Unconfined	Homogeneous	Heterogeneous			
	MODFLOW Unconfined					
Lake, recharge, evapotranspiration & head dependent boundaries.						
9a	A2016 Unconfined	Homogeneous	Homogeneous	1, 30, 360, 3600	Specified head, specified flow, no flow, head dependent.	23x23 rows and columns. 100-m grid spacing.
	MODFLOW Unconfined					
9b	A2016 / MODFLOW			3600		
	$A2016_{STA}$					

Table 4.1: Table defining hydrogeological conditions and model parameters for each set of model experiments.

Experiment 9b expanded upon 9a by testing an alternative method of calculating conductance for the cells beneath the lake, using the specified saturated thickness approximation (Sheets et al. 2015). In Experiment 9a, A2016 featured cell to cell conductance for the full model region, determined by the aquifer thickness from base of aquifer to the water table as per an unconfined aquifer (Fig. 4.2). This represents the standard MODFLOW + RES package and is similar to the scenario demonstrated in the RES package documentation (Fenske et al. 1996) where a reservoir is situated within, and interacting with an unconfined aquifer. Experiment 9b used a variant of A2016 ($A2016_{STA}$), where cell to cell conductance beneath the lake was derived from the specified saturated aquifer thickness between the base of the aquifer and the base of the lake sediments (Fig. 4.2). Two lake depths were modelled to identify how the different transmissivities might affect the interaction between the lake and groundwater. Parameters were chosen to approximate the water table configuration from Winter (1976; Fig. 12), with a flow through lake and a steady state hydraulic head just above lake level, leading to seepage into the lake across the lake floor. As a groundwater model using the Dupuit-Forchheimer cannot simulate three-dimensional flow, a fixed flux across the model was included to approximate seepage from the layer to deeper flowpaths.

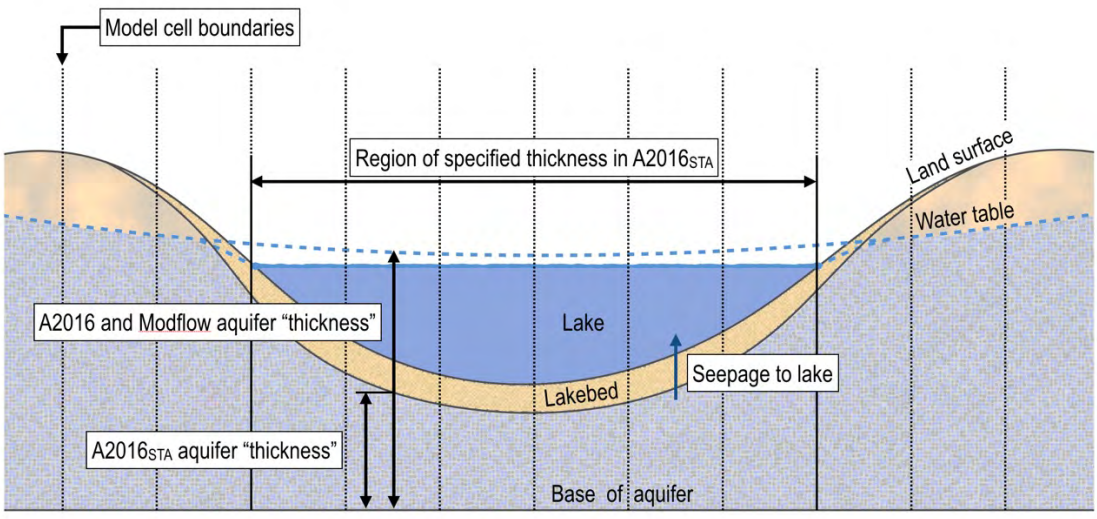

Figure 4.2: Differences in aquifer thickness for A2016 & MODFLOW (experiment 9a), and $A2016_{STA}$, which uses a specified thickness approximation for the region beneath the lake (experiment 9b).

It should be noted that parameters for these model experiments were not intended to represent real world conditions. Instead parameters that result in significant variation in modelled hydraulic heads were selected to emphasise differences between the models.

5 Results

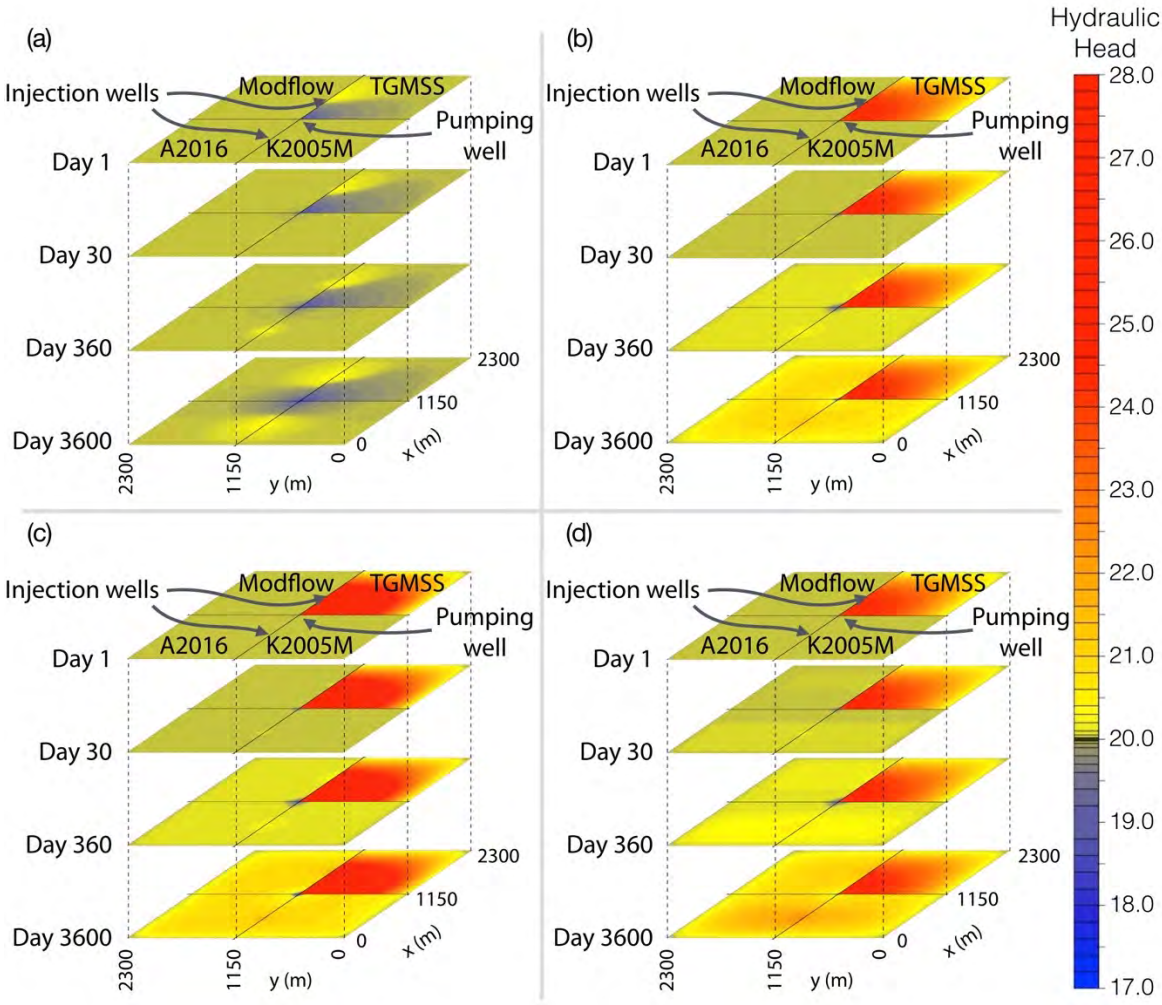

Figure 4.3: Hydraulic head (m) maps showing modelled transient groundwater behaviour for model experiments 1-4, for days 1, 30, 360 and 3600. Each quadrant shows results for one of the models examined (MODFLOW, A2016, TGMSS, K2005M). Model experiments shown are: (a) Confined aquifer with pumping and injection wells. (b) Confined aquifer with wells and recharge. (c) Confined aquifer with wells, recharge and heterogeneous conductivity. (d) Confined aquifer with wells, recharge and heterogeneous storage.

MODFLOW, A2016 and K2005M showed good agreement in all confined aquifer experiments. In experiment 1, for a confined aquifer with injection and pumping wells, MODFLOW and A2016 showed identical results (Fig. 4.3a). Differences for calculated hydraulic heads between the two models were less than 1 mm in all grid cells for all time-steps. In contrast, hydraulic head values of Model K2005M differed from MODFLOW and A2016 as the timeframe for the model simulation increased. At the central pumping well, K2005M and MODFLOW had identical hydraulic heads for day 1. By day 30, K2005M was 0.008 m higher than MODFLOW, 0.14 m higher at day 360 and 0.16 m higher at day 3600 (Table 4.2). TGMSS displayed very different results to the other models. For day 1 and day 30 at the central well, TGMSS's surface

was ~1.6 m lower than the other models, 1.05 m lower at day 360, and 0.16 m lower at day 3600 (Table 4.2, Fig. 4.4). MODFLOW, A2016 and K2005M did not achieve steady state within 3600 days. Additional model runs suggest that steady state groundwater flow for the first simulation would be achieved after ~100,000 days. TGMSS achieved steady state after ~10 days (Fig. 4.4).

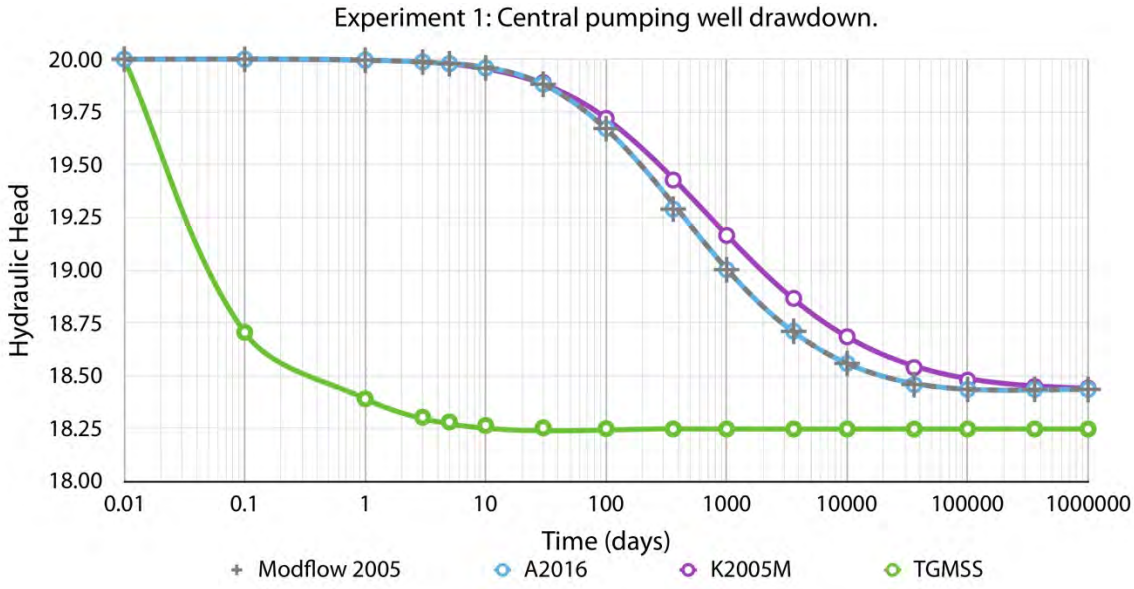

Figure 4.4: Modelled hydraulic heads (m) at the central pumping well for each model for model experiment 1, with injection and pumping wells, and homogenous conductivity and storage.

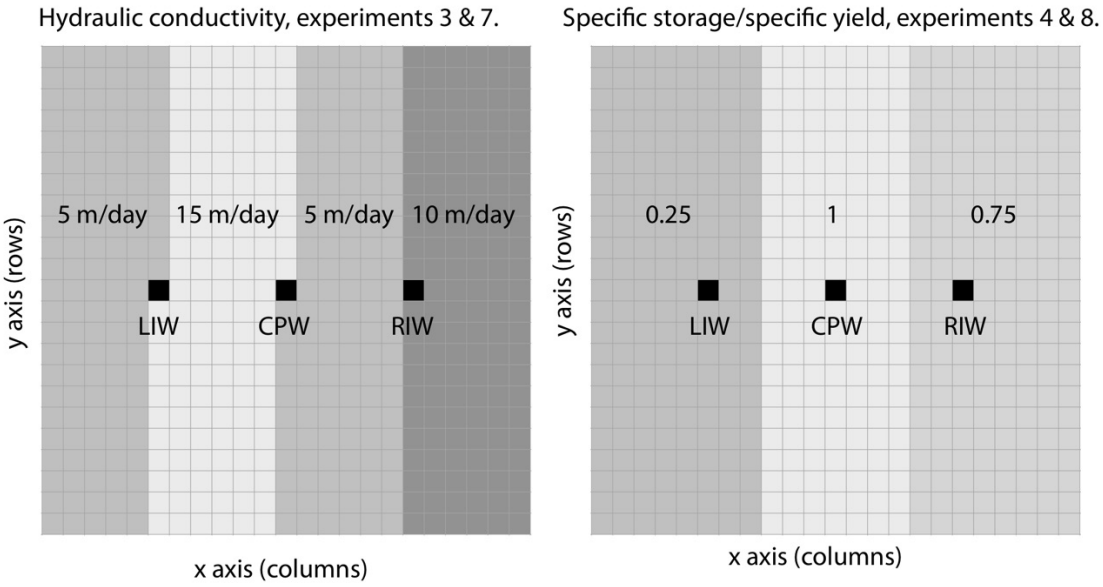

Figure 4.5: Map showing left and right injection wells (LIW & RIW) and the central pumping well (CPW). Greyscale is indicative of regions with different hydraulic conductivities and specific storage or specific yield within the model space.

MODFLOW, A2016 and K2005M also produced similar results for experiments 2-4, incorporating recharge and heterogeneous conductivities and specific storage (Fig. 4.3b, c and d, Fig. 4.5). At all time-steps, MODFLOW and A2016 gave identical results with hydraulic head differences of less than 1 mm. K2005M diverged from MODFLOW and A2016 as simulation time increased, with a maximum difference observed in the heterogeneous storage experiment, where one of the injection wells had a surface 0.36 m lower than the MODFLOW hydraulic head on day 3600 (Fig. 4.3d, Table 4.2). This well was in a region of low specific storage. TGMSS showed significant differences from the other models, at all time-steps. The maximum difference was on day 30 in the heterogeneous conductivity experiment (experiment 3) where TGMSS simulated a hydraulic head ~7.4 m above the MODFLOW value for one of the injection wells (Table 4.2).

Exp.#	Timestep	MODFLOW			A2016			K2005M			TGMSS		
		LIW	CPW	RIW	LIW	CPW	RIW	LIW	CPW	RIW	LIW	CPW	RIW
1	1	20.002	19.996	20.002	20.002	19.996	20.002	20.002	19.996	20.002	20.621	18.391	20.621
	30	20.059	19.882	20.059	20.059	19.882	20.059	20.055	19.890	20.055	20.549	18.254	20.549
	360	20.355	19.290	20.355	20.355	19.290	20.355	20.286	19.428	20.286	20.546	18.248	20.546
	3600	20.635	18.711	20.635	20.635	18.711	20.635	20.552	18.867	20.552	20.546	18.248	20.546
2	1	20.002	19.996	20.002	20.002	19.996	20.002	20.002	19.996	20.002	24.126	23.560	24.126
	30	20.067	19.889	20.067	20.067	19.889	20.067	20.063	19.897	20.063	24.210	23.700	24.211
	360	20.445	19.380	20.445	20.445	19.380	20.445	20.376	19.518	20.376	24.213	23.704	24.213
	3600	21.493	19.610	21.493	21.493	19.610	21.493	21.335	19.736	21.335	24.213	23.705	24.213
3	1	20.002	19.996	20.002	20.002	19.996	20.002	20.002	19.996	20.002	27.275	25.943	26.184
	30	20.068	19.886	20.069	20.068	19.886	20.069	20.065	19.893	20.066	27.454	26.180	26.298
	360	20.506	19.259	20.545	20.505	19.259	20.545	20.427	19.417	20.460	27.460	26.187	26.302
	3600	21.735	19.188	21.882	21.735	19.188	21.882	21.588	19.403	21.689	27.460	26.188	26.302
4	1	20.009	19.996	20.003	20.009	19.996	20.003	20.009	19.996	20.003	24.162	23.585	24.142
	30	20.217	19.889	20.087	20.217	19.889	20.087	20.188	19.897	20.080	24.212	23.701	24.211
	360	20.887	19.380	20.518	20.887	19.380	20.518	20.780	19.519	20.442	24.213	23.704	24.213
	3600	22.522	19.743	21.723	22.522	19.743	21.723	22.158	19.864	21.523	24.213	23.705	24.213

Table 4.2: Hydraulic heads for each cell containing an injection or pumping well. Central pumping well highlighted in blue. Offset injection wells shown unshaded. Locations of wells are shown in figure 4.5.

A2016 was also compared against MODFLOW in a series of unconfined aquifer experiments (Fig. 4.6). TGMSS and K2005M were not included in this comparison, as they are not designed to model unconfined aquifers. Identical results were achieved in all simulations, for all time-steps, with a maximum difference in hydraulic head of less than 1 mm.

Performance in A2016 is slower than MODFLOW with a time of around 10-15 minutes for 3600 time-steps. In comparison, MODFLOW takes around 1 to 3 minutes using the preconditioned conjugate gradient solver. These values are from model runs on different systems (A2016 was run on the Mac version of Excel 2015, whereas MODFLOW was run with the Model Muse GUI on a Windows 7 virtual machine, both on a Macbook Pro 2.8 Ghz i7).

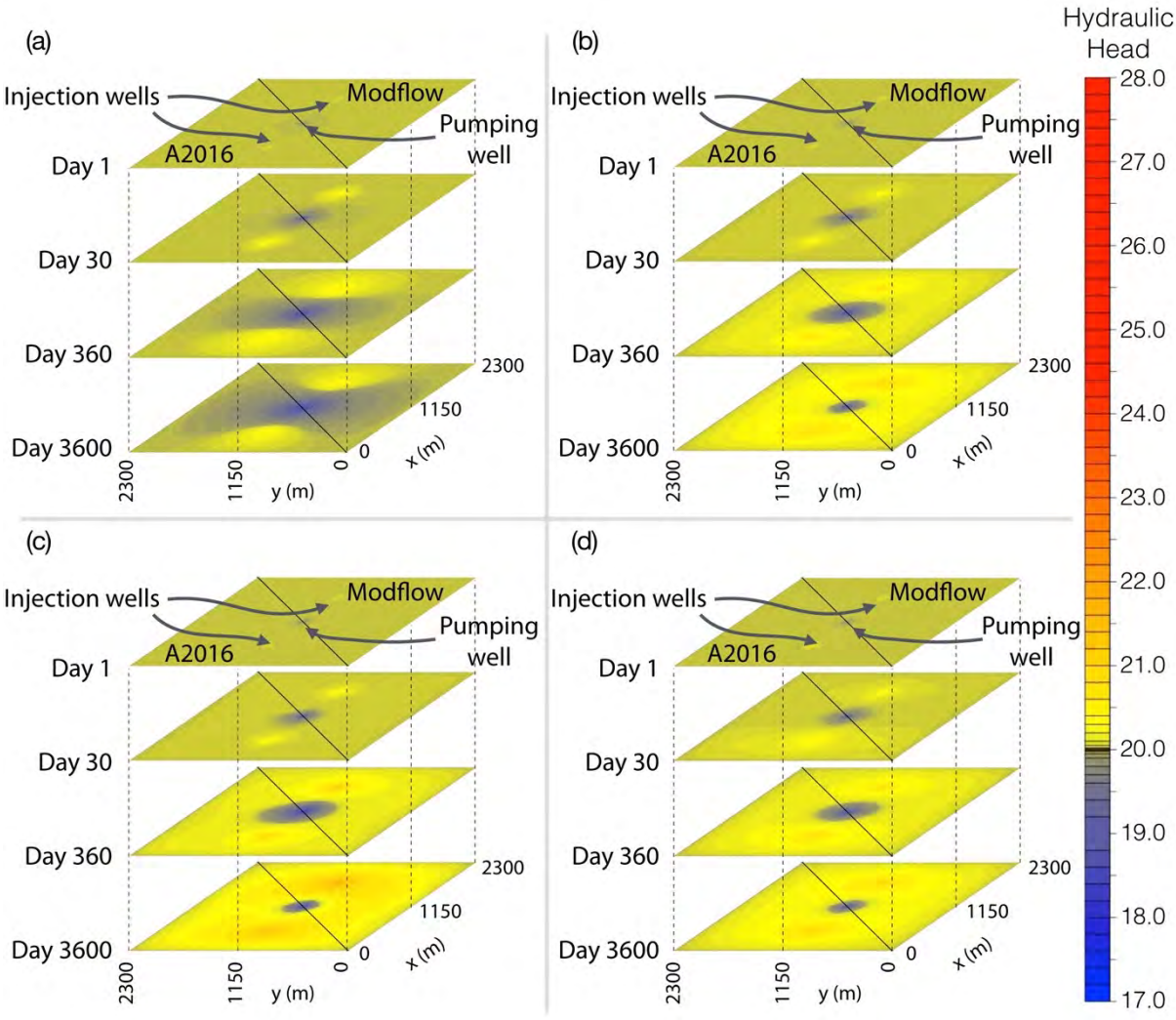

Figure 4.6: Hydraulic head (m) maps showing modelled transient groundwater behavior for experiments 5-8, for days 1, 30, 360 and 3600. Each half shows results for one of the models examined (MODFLOW and A2016). Model experiments shown are: (a) Unconfined aquifer with pumping and injection wells. (b) Unconfined aquifer with wells and recharge. (c) Unconfined aquifer with wells, recharge and heterogeneous conductivity. (d) Unconfined aquifer with wells, recharge and heterogeneous storage.

Model experiment 9a incorporates specified head, specified flux, no flow and head dependent boundaries. In the initial experiment, cell to cell conductance for all cells was determined by the aquifer "thickness" between the base of the aquifer and the water table. MODFLOW and A2016 produced identical results (Fig. 7), for all cells and time-steps. Initial seepage to the lake occurred as inflow across the entire lake floor, with the majority of seepage, combined with rapid drawdown of the groundwater head, occurring near the thinner sediments along the lake shore (average 910 m^3/day per cell). At day 30, inflow to the lake occurred at a consistent rate (average 120 m^3/day per cell) across the whole lake floor, with the increased flow through the thicker central sediments occurring due to a high remnant water table hydraulic head in the centre of the lake. By day 360, the water table mound in the centre of the lake had become a depression with a hydraulic head of ~19.8 m and lake seepage occurred as inflow along the lake edges (average 48 m^3/day per cell) and outflow in the lake centre (average 8 m^3/day per cell). By day 3600, the overall pattern was similar, with an increase in inflow along the lake edges (average 78 m^3/day per cell). Away from the lake, the water table height increased due to recharge until near day 3600 when the water table height intersected the evapotranspiration boundary in areas of lower topography. Once this occurs, the water table followed the topography as seen in the region around x: 2100, y: 20 (Fig. 7).

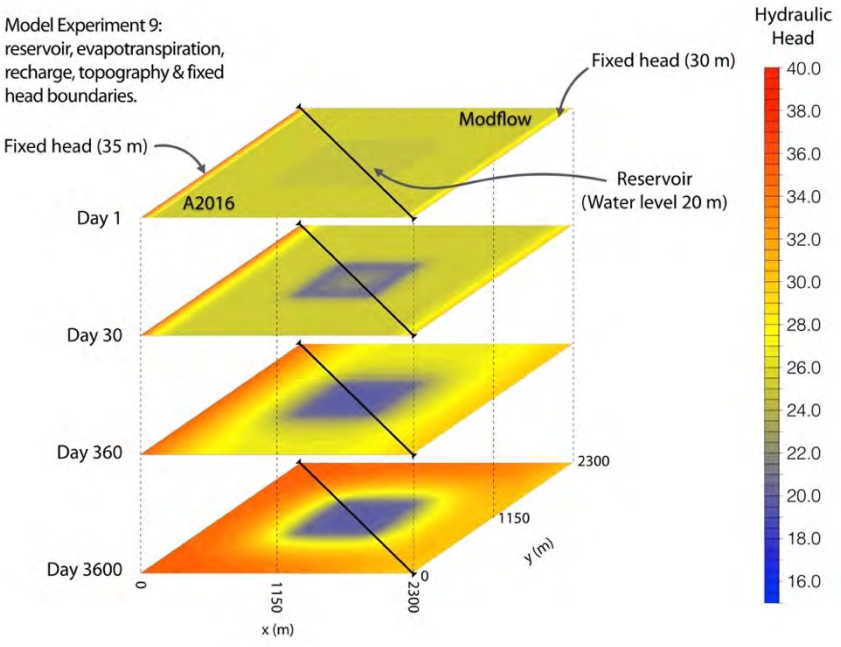

Figure 4.7: Hydraulic head (m) map showing modelled transient groundwater behaviour for model experiment 9, for days 1, 30, 360 and 3600. Each half shows results for one of the models examined (MODFLOW and A2016). Model experiment conditions consist of a central reservoir with head dependent boundaries determining seepage through the lake floor, recharge and evapotranspiration over the model, and no-flow and fixed head perimeter boundaries. Initial hydraulic heads were 25 m and the reservoir hydraulic head was set at 20 m. Evapotranspiration is linked to the topographic surface with an extinction depth of 0.1m. The water table in the region centred around x=2100, y = 200 is constrained by the evapotranspiration boundary.

In the second series of simulations (9b), conductance in $A2016_{STA}$ was calculated differently for cells that lay beneath the lake. The thickness of the aquifer in this region was specified as the distance between the base of the aquifer and the base of the lake sediments (Fig. 4.2), using the specified thickness approximation (Sheets et al. 2015). Initial comparisons between MODFLOW/A2016 and $A2016_{STA}$ using a shallow lake (5.5 m depth) showed small differences (Fig. 4.8). Hydraulic heads for $A2016_{STA}$ were slightly higher (~25 mm) than MODFLOW/A2016 for the water table mounds, and slightly lower (~ 70 mm) across the lake, resulting in slightly less seepage into the lake. Seepage into the lake occurred across the entire lake floor in both models, with the largest seepage occurring on the "downstream" side of the lake (Columns 13 & 14; Fig. 4.8).

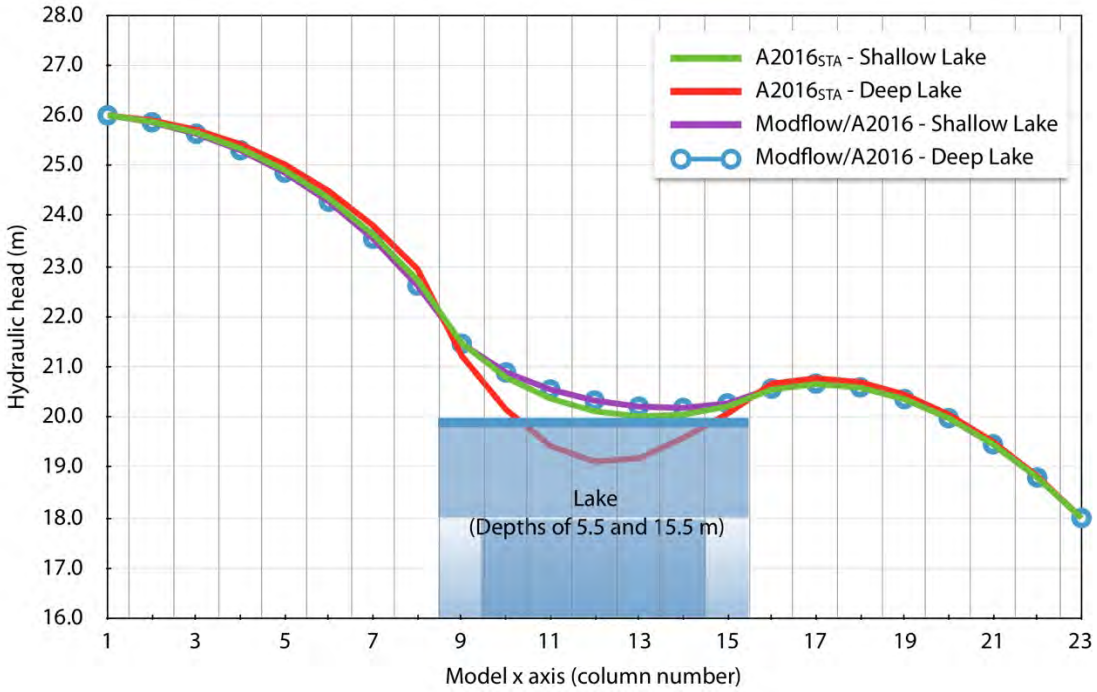

Figure 4.8: Hydraulic heads for day 3600 along the middle row of the model, for MODFLOW/A2016 and $A2016_{STA}$. $A2016_{STA}$ calculates conductance for the region beneath the lake using a specified thickness as described in figure 4.1.

In contrast, simulations with the deep lake showed no change in the MODFLOW/A2016 simulations, but significant change in the $A2016_{STA}$ simulation (Fig. 4.8). Hydraulic heads away from the lake were an average of ~170 mm higher, and lake cells were ~440 mm lower, than the MODFLOW/A2016 simulations. In addition, the lake changed from gaining water, to losing water across ~1/3 of the lake floor (Fig. 4.8).

6 Discussion

MODFLOW is the *de facto* standard for groundwater modelling software. The primary objective of this paper was to investigate the development of a comparable spreadsheet model, for simple experiments, prototyping and teaching purposes. From the model inter-comparison, it is clear that A2016 is a simple and suitable alternative to MODFLOW for the scenarios investigated in this paper (Table 4.1). A2016 gave identical results to MODFLOW in all simulations. However, there are two caveats that must be considered: MODFLOW and A2016 differ in the method of iteration, and A2016 does not include the full and extensive range of features of MODFLOW. The difference in iteration method, with A2016 using Gauss-Seidel point based iteration, compared to MODFLOW's matrix solver, is unlikely to lead to significant disparities, though it may occasionally result in situations where the contours do not align perfectly between models; while the difference in hydraulic heads between models may be sub-millimetre, even minuscule variations between models may define a contour. Of the numerous MODFLOW features not included in A2016, two notable omissions include the 3D layer structure, and anisotropy of hydraulic conductivity. The relative simplicity of A2016 compared to MODFLOW should not pose significant problems as long as usage is appropriate, and the limitations of the single-layer, Dupuit-Forchheimer approximation are considered. The structured nature of A2016, with separate, clearly named sheets for the hydrogeological features and model layers, should minimise the use of inappropriate data.

The tendency of K2005M to deviate from MODFLOW and A2016 as simulation time increases, before returning to a similar steady flow condition (Fig. 4.4) is understandable once the model structure for K2005M is examined. The model structure of K2005M is that of a single layer groundwater model (as per A2016), able to do a single time-step. The initial head value is parametrized, and there is no mechanism to update it for incrementing timesteps. Therefore, a simulation over 3600 days using K2005M is identical to a simulation in MODFLOW or A2016 over 3600 days, using a single timestep of 3600 days. There are no stability concerns in using long timestep lengths in these models as they all use implicit calculation techniques. However, longer timesteps can result in a decrease of accuracy (Table 4.2, Fig. 4.4).

TGMSS was able to approximate the MODFLOW steady state solution in only one experiment (Fig. 4.3a), and was unable to model the transient behaviour of groundwater in any of the simulations. This is primarily due to linking the hydraulic head in the storage term to the iteration process (Eq. 22), instead of using the hydraulic head from the previous time-step (Eq. 23). In TGMSS the hydraulic head value is calculated during each iteration. With each iteration

a new "initial" hydraulic head is introduced to the FDM, which is not likely to be correct (as the iteration cycle is not complete) and which has little relationship to the actual initial head value from the start of the time-step. In essence, this makes the model "chase its own tail" during each iteration cycle and gives spurious results.

$$\frac{S_{i,j}\left(h^{m}-h^{\text{iteration}}\right)}{t_m-t_{m-1}} \tag{22}$$

$$\frac{S_{i,j}\left(h^{m}-h^{m-1}\right)}{t_m-t_{m-1}} \tag{23}$$

A further difference between the models that must be considered during usage, is that the spreadsheet equations used for TGMSS and K2005M do not define the volumetric flows to and from each cell. Instead these are based on the equation for a representative elementary volume (REV). Therefore, care must be taken to ensure that appropriate integration is carried out to determine actual flow rates. This is not a concern with A2016 as the integration to account for cell size is incorporated into the spreadsheet equations (Eq. 7).

While MODFLOW and the unmodified version of A2016 had identical results in all experiments, the results from experiment 9a and 9b suggest that care must be taken with MODFLOW when used with the RES (reservoir) package. In MODFLOW, by default, conductance between cells beneath the reservoir is calculated without taking into account any confinement of the aquifer, or change in aquifer thickness caused by the placement of the reservoir (Fig. 4.2). As the reservoir takes up a greater proportion of the layer thickness, the discrepancy between MODFLOW's calculated conductance, and the actual conductance of groundwater beneath the reservoir increases. In these situations, MODFLOW will calculate greater horizontal flow through the cells beneath the reservoir, potentially resulting in lower hydraulic heads and less groundwater mounding. This is particularly relevant in situations where a lake provides a natural barrier to groundwater flow. Winter (1976; Figures 12 & 18) demonstrated that for many groundwater systems, such as those approximated in experiment 9b, shallow lakes may gain water from surrounding local groundwater systems, whereas deeper lakes in the same setting are likely to lose water. This behaviour is observed in $A2016_{STA}$, where the combination of seepage through the base of the layer, recharge, and cell to cell conductance combine to form a water table and lake behaviour, that is qualitatively similar to the simulations of Winter (1976). In contrast, MODFLOW and A2016 were unaffected by changes in the lake depth, and penetration of the aquifer.

The approach taken in $A2016_{STA}$ is based on the specified saturated thickness approximation (Sheets et al. 2015). The specified thickness approximation is commonly used to simplify and linearize the determination of transmissivity through an unconfined aquifer. Specifying the aquifer thickness disconnects the non-linear derivation of transmissivity from saturated thickness. The commonly cited benefit of this approximation is that model run times may be much faster, and stability improved (Sheets et al. 2015). In addition, the specified thickness approximation is also an ideal method to limit the transmissivity of an aquifer that is limited in thickness by an overlying lake.

The RES package and its precursor, the RIV (river) package (Fenske et al. 1996), share similar designs, and both may see some benefit from the application of the specified thickness approximation to define conductance beneath reservoirs, lakes and rivers. However, the approximation is most relevant to the RES package as reservoirs and lakes are more likely to take up a significant proportion of a layer's thickness, resulting in a much greater difference between the default MODFLOW calculation for conductance and the lower conductance derived from the specified thickness approximation.

Applying the specific thickness approximation to just the region beneath lakes presents a difficulty, as MODFLOW does not allow for specification of the thickness of an unconfined layer. For many groundwater scenarios, the specified thickness approximation is commonly implemented using a confined layer (Sheets et al. 2015). This method is not suitable for limiting conductance beneath lakes unless the specified thickness approximation is applied across the whole model. The use of a convertible layer, with a top surface mirroring the land surface may be applicable, assuming that the water table never rises above the land surface. The modular nature of MODFLOW allows packages to append the HCOF and RHS matrices, but does not include a way for packages to modify layer thickness or type. To make use of the specified thickness approximation on an ad-hoc basis, over small regions of cells, implementation could be achieved by adding a "layer surface" matrix alongside the HCOF and RHS matrices. Components of the groundwater model would be able to append the HCOF and RHS matrix, as occurs currently in MODFLOW, as well as modify the "layer surface" matrix, to account for regions where the user may want to specify the saturated thickness. In the lake scenario, the layer surface matrix would simply mirror the water table (for unconfined) or top of aquifer (for confined) matrices. In regions where a lake penetrates the aquifer, then the layer surface values for cells beneath the lake would be defined by the bottom of the lake sediments, rather than the water table/top of layer.

7 Conclusion

Groundwater modelling is a complex science, for which comprehensive models such as MODFLOW are required. However, despite the existence of such advanced modelling software, development of simple spreadsheet-based groundwater models is important for both teaching purposes and prototyping new modelling code. A prototype model – A2016 – was developed in preparation for linking a groundwater model to a coupled hydrologic-isotopic mass balance lake model. Nine experimental simulations were carried out to test numerous hydrogeological conditions, such as sources and sinks, heterogeneous storage and hydraulic conductivity, and specified head, specified flux, head dependent and no-flow boundary conditions.

In all simulations A2016 produced identical results to MODFLOW 2005 for both transient and steady state groundwater conditions, in both confined and unconfined aquifers. In addition, the model inter-comparison from this study demonstrates that modelling transient behaviour of groundwater still requires the use of macros or similar programmatic constructs to control the time-stepping. Previous efforts to develop a spreadsheet that is not reliant on macros (TGMSS; Karahan and Ayvaz 2005b, Karahan and Ayvaz 2005a) have been shown to be unable to simulate transient groundwater behaviour. In this respect, A2016 provides a clear advance on existing spreadsheet based models.

Spreadsheet models also provide the means to examine functions within more complex groundwater models. Experiment 9b highlighted a scenario in which MODFLOW may derive incorrect conductance values for cells beneath a lake in an unconfined aquifer when using the RES package. This is attributed to the use of an aquifer thickness calculated from the water table to the base of the aquifer. A modified version of A2016 was developed that uses the specified thickness approximation (Sheets et al. 2015) and calculates aquifer thickness from the base of the lake sediments, to the base of the aquifer.

A2016 provides an excellent framework for teaching by linking the underlying mathematics, MODFLOW concepts and modelled groundwater behaviour in a structured environment, using spreadsheet software that all students are familiar with. While only features deemed necessary to the ongoing project were included and tested in A2016, adding features, such as anisotropy or 3D flow modelling should be straightforward and may provide an excellent educational opportunity. Most additions to the model can be achieved through standard spreadsheet manipulation thereby providing a simple and flexible tool of value to both research and teaching.

8 References

Akhter, M.G., Ahmad, Z., Khan, K.A., 2006. Excel based finite difference modeling of ground water flow. Journal of Himalayan Earth Sciences, 39: 49-53.

Almeida, C.N., Roehrig, J., Wendland, E., 2014. Development and Integration of a Groundwater Simulation Model to an Open Geographic Information System. JAWRA Journal of the American Water Resources Association, 50(1): 101-110. DOI:10.1111/jawr.12119

Anderson, M., Bair, E., 2001. The power of spreadsheet models, Proceedings, MODFLOW 2001 and Other Modeling Odysseys Conference, pp. 815-822.

Anderson, M.P., Woessner, W.W., Hunt, R.J., 2015. Applied groundwater modeling: simulation of flow and advective transport. Academic press.

Ankor, M.J., 2018. Transient groundwater modelling using spreadsheets for education and model prototyping. https://doi.org/10.17632/ r6hcbkp53n.4; https://data.mendeley.com/datasets/r6hcbkp53n/4. Accessed 8 Aug 2018

Bair, E.S., Lahm, T.D., 2006. Practical problems in groundwater hydrology, 1. Prentice Hall.

Elemer, B., Sz, P., Aniko, T., Attila, K., 2010. Complex Scientific Analysis in Geothermal Exploration in the Pannonian Basin. Proceedings World Geothermal Congress 2010, Bali, Indonesia, 25-29 April 2010.

Fenske, J.P., Leake, S., Prudic, D.E., 1996. Documentation of a computer program (RES1) to simulate leakage from reservoirs using the modular finite-difference ground-water flow model (MODFLOW). 2331-1258, US Geological Survey; Branch of Information Services [distributor].

Harbaugh, A.W., 2005. MODFLOW-2005, the US Geological Survey modular ground-water model: the ground-water flow process. US Department of the Interior, US Geological Survey Reston, VA, USA.

Holzbecher, E., Sorek, S., 2005. Numerical models of groundwater flow and transport. Encyclopedia of Hydrological Sciences.

Huang, Y., Yu, Z., Zhou, Z., 2013. Simulating Groundwater Inflow in the Underground Tunnel with a Coupled Fracture-Matrix Model. Journal of Hydrologic Engineering, 18(11): 1557-1561. DOI:10.1061/(ASCE)HE.1943-5584.0000455

Jones, R.N., McMahon, T.A., Bowler, J.M., 2001. Modelling historical lake levels and recent climate change at three closed lakes, Western Victoria, Australia (c.1840–1990). Journal of Hydrology, 246(1): 159-180.

Karahan, H., Ayvaz, M.T., 2005a. Time-dependent groundwater modeling using spreadsheet. Computer applications in engineering education, 13(3): 192-199.

Karahan, H., Ayvaz, M.T., 2005b. Transient groundwater modeling using spreadsheets. Advances in Engineering Software, 36(6): 374-384.

Mahmud, M., 1996. Spreadsheet Solutions To Laplace's Equation: Seepage And Flow Net. Jurnal Teknologi, 25: 53-67.

McDonald, M.G., Harbaugh, A.W., 2003. The history of MODFLOW. Groundwater, 41(2): 280-283.

Neville, C.J., Tonkin, M.J., 2001. Representation of multiaquifer wells in MODFLOW, Proceedings of Modflow 2001 Conference at the International Ground Water Modeling Center, Golden, Colorado, pp. 51-59.

Ohlendorf, C., Fey, M., Gebhardt, C., Haberzettl, T., Lücke, A., Mayr, C., Schäbitz, F., Wille, M., Zolitschka, B., 2013. Mechanisms of lake-level change at Laguna Potrok Aike (Argentina) - insights from hydrological balance calculations. Quaternary Science Reviews, 71: 27-45. DOI:10.1016/j.quascirev.2012.10.040

Olsthoorn, T.N., 1985. The power of the electronic worksheet: modeling without special programs. Groundwater, 23(3): 381-390.

Ousey, J.R., 1986. Modeling Steady-State Groundwater Flow Using Microcomputer Spreadsheets. Journal of Geological Education, 35(5): 305-11.

Sheets, R.A., Hill, M.C., Haitjema, H.M., Provost, A.M., Masterson, J.P., 2015. Simulation of Water-Table Aquifers Using Specified Saturated Thickness. Groundwater, 53(1): 151-157.

Smerdon, B.D., Mendoza, C.A., Devito, K.J., 2007. Simulations of fully coupled lake-groundwater exchange in a subhumid climate with an integrated hydrologic model. Water Resources Research, 43(1): 1-13. DOI:10.1029/2006WR005137

Stets, E.G., Winter, T.C., Rosenberry, D.O., Striegl, R.G., 2010. Quantification of surface water and groundwater flows to open- and closed-basin lakes in a headwaters watershed using a descriptive oxygen stable isotope model. Water Resources Research, 46(3). DOI:10.1029/2009WR007793

Wang, H.F., Anderson, M.P., 1982. Introduction to groundwater modeling : finite difference and finite element methods. Academic Press, San Francisco.

Winston, R.B., 2009. ModelMuse: a graphical user interface for MODFLOW-2005 and PHAST. US Geological Survey Reston, VA.

Winter, T.C., 1976. Numerical simulation analysis of the interaction of lakes and ground water. USGS Professional Paper 1001.

Chapter 5

A holistic lake model for palaeoclimate research

Notes: The code for CHIMBLE is available from: https://github.com/Mjankor/CHIMBLE

This chapter has been formatted to match the rest of this thesis. Figure and table numbers have been prefixed with the chapter number (e.g. Fig. 1 has been changed to Fig. 5.1).

Statement of Authorship

Title of Paper	A holistic lake model for palaeoclimate research
Publication Status	☐ Published ☐ Accepted for Publication ☐ Submitted for Publication ☒ Unpublished and Unsubmitted w ork w ritten in manuscript style
Publication Details	

Principal Author

Name of Principal Author (Candidate)	Martin Ankor		
Contribution to the Paper	Corresponding Author. Devised initial concept, model design, experimental design. Analysis of results. Wrote manuscript.		
Overall percentage (%)	90%		
Certification:	This paper reports on original research I conducted during the period of my Higher Degree by Research candidature and is not subject to any obligations or contractual agreements with a third party that would constrain its inclusion in this thesis. I am the primary author of this paper.		
Signature		Date	19 Dec 2019

Co-Author Contributions

By signing the Statement of Authorship, each author certifies that:

i. the candidate's stated contribution to the publication is accurate (as detailed above);

ii. permission is granted for the candidate in include the publication in the thesis; and

iii. the sum of all co-author contributions is equal to 100% less the candidate's stated contribution.

Name of Co-Author	Jonathan T. Tyler		
Contribution to the Paper	Evaluated and edited manuscript.		
Signature		Date	19 Dec 2019

Please cut and paste additional co-author panels here as required.

Abstract

Lake hydrological, physical and geochemical models are valuable tools for interpreting past climate variability recorded within lake sediments, and the sensitivity of lakes under future climate conditions. A holistic lake model was developed and applied to two maar crater lakes – Lake Bullen Merri and Lake Gnotuk – in the Newer Volcanic Province, Victoria, Australia. The lake model incorporates mass and energy balances, a finite difference groundwater model, a dual layer soil model, water chemistry, and mass balance mixing and fractionation of oxygen and hydrogen stable isotopes. Parameters derived from the calibration process were parsimonious for both lakes. Estimated groundwater hydraulic conductivities and storativity were comparable to other studies in the region, and the same groundwater parameters were applicable to both lakes. The model was able to simulate lake behaviour for both lakes for the entire observational record – historical lake level change from 1889 to 2019, lake chemistry and lake surface temperature from ~1960 to 2019, and surface water oxygen and hydrogen isotopes between 2015-2019, albeit subject to some uncertainties. Differences between modelled and observed seasonal isotopic and chemical variability are best explained by changes in lake stratification depth, suggesting that in recent decades the depth to thermocline at Lake Bullen Merri has declined. Model simulations were also validated against a previously published model by Steinman et al. (2010) [Limnology and Oceanography, 55(6), 2231–2245]. The model experiments indicate that both Lake Bullen Merri and Lake Gnotuk are through-flow lakes at higher lake levels, and transition to terminal lakes at lower lake levels. These observations have significance for interpreting past hydrological change using lake sediments and stable isotopes.

1 Introduction

Lake sediments are important archives of past climate, able to provide continuous, high resolution records across a broad geographical and temporal range (Cohen, 2003). Variations in the characteristics of lake sediments offer direct insights into past hydroclimate, both within the catchment and on a regional scale, by recording changes in lake water volume, chemistry, biology, aeolian influx, and catchment erosion (e.g., Barr et al., 2014; Battarbee, 2000; Cadd et al., 2018; Donders et al., 2007; Jones et al., 2005; Jones et al., 1998; Jones et al., 2001; Leng and Marshall, 2004; Steinman et al., 2012; Talbot, 1990; Van Boxel et al., 2013; Wilkins et al., 2013). Hydroclimate variability is often inferred from estimates of lake water salinity, as inferred from microfossil assemblages (e.g., Barr et al., 2014; Fritz et al., 1991; Rudd et al., 2016) the elemental

composition of microfossils (e.g., Chivas et al., 1985), or from lake water isotope ratios ($^{18}O/^{16}O$, $^{2}H/^{1}H$), reflected in the isotopic composition of carbonate, biogenic silica and organic components of lacustrine sediment (e.g., Leng and Marshall, 2004; Ricketts and Johnson, 1996; Sachse et al., 2004; Steinman et al., 2012; Tyler et al., 2008; Wolfe et al., 2002). However, quantitative inferences of past hydrological balance, and thus climate, are hindered by the non-linear response of lake hydrology, chemistry, and isotope ratios to climatic forcing as well as differences between the responses of sites to a common forcing (Battarbee, 2000; Wigdahl et al., 2014). Consequently, lakes within close geographic proximity, perhaps even sharing the same climate, will rarely produce identical palaeoclimate records, undermining both the confidence in those records and efforts to produce regional palaeoclimate syntheses (e.g., Tierney et al., 2013; Tyler et al., 2015). Understanding and quantifying lake hydrological, chemical and isotopic responses to climate is therefore a crucial step towards developing accurate records of past climate change.

Numerical modelling of lakes, their catchments and surroundings can be applied to investigate how lakes respond to climate change. Numerous lake models have been developed, both specifically for, or adaptable to, palaeoclimate research (Table 1.1). Lake models for palaeoclimate research are commonly based on either mass balance or energy balance equations. Hydrological mass balance modelling aims to quantify the various hydrologic fluxes through a system, a common technique used in fields ranging from lake studies (e.g., Jones et al., 2001; Yihdego et al., 2015), catchments (e.g., Boughton, 2005), agriculture (e.g., Panigrahi and Panda, 2003) and global climate simulations (e.g., Neilson, 1995). Lake energy balance models balance incoming and outgoing energy, and temperature mixing through the lake to estimate evaporation, thermal stratification, and water heat storage (e.g., Dee et al., 2015; Hipsey et al., 2013; Hostetler and Bartlein, 1990; Hostetler et al., 1993). Few mass balance models incorporate energy balance equations, while most energy balance models used for lake research include some mass balance functionality.

As many lake-based climate reconstructions rely on interpretation of isotopic signatures, these models can be extended further by coupling of the hydrological mass balance equations to equations describing oxygen and hydrogen isotopic mixing and fractionation within water (e.g., Dinçer, 1968; Gat, 2010; Gibson et al., 2015; Gonfiantini, 1986). Coupled hydrologic-isotopic mass balance models provide a method to resolve some of the uncertainties related to a lake's hydrological and isotopic responses to climate by quantifying the various hydrologic fluxes through the lake and catchment as well as their isotopic composition. As the hydrological mass

balance is a result of the sum of the inflows and outflows of a system, so too must the isotopic values balance (Jones et al., 2005).

Modelling of lakes for palaeoclimate research presents several challenges related to defining model parameters. Fundamentally, the purpose of palaeoclimate research is to understand and quantify climatic conditions outside the range of instrumental records. Most instrumental meteorological and lake hydrological records only cover a relatively short time period (typically 0 - 200 years), whereas lake based palaeoclimate records often span timescales ranging from centuries through to millions of years. As a consequence, palaeoclimate records often demonstrate a far greater range of lake and climatic conditions than found in the instrumental records (e.g: glacial/interglacial cycles). Fossil lake shorelines demonstrate this clearly, with numerous examples of fossil shorelines either well above or below documented lake levels, particularly in the currently semi-arid climates of Australia (Jones et al., 2001; Last and Deckker, 1990; Wilkins et al., 2013). From a modelling perspective, this variation in lake and climate conditions presents several significant problems. Changes in lake depth alters both the degree of sheltering and the length of fetch across a lake, both of which influence evaporation, heat storage, and degree of stratification (Imberger, 2001). Degree of stratification in particular is an important consideration for interpretation of lake records, affecting both the chemistry and isotopic composition of the productive surface waters, and the likelihood of anoxic deeper waters (Hambright et al., 1994). Likewise, changes in climate and lake level can affect the groundwater-lake dynamics. Lakes may shift between through-flow groundwater behaviour, where groundwater seeps both in and out of the lake, terminal behaviour with groundwater only seeping into the lake, or outseepage lakes, where the lakes are perched above a regional water table and water is lost to the underlying systems (Tweed et al., 2009; Winter, 1978; Winter et al., 2003). This groundwater-lake interaction may vary according to climatic state, with some lakes switching between through-flow, terminal and outseepage behaviour depending on lake level (Ankor and Tyler, 2019; Winter, 1976). Both groundwater-lake interactions and lake stratification are complex, non-linear systems that are difficult to parameterise, particularly for the long timescales commonly encountered in palaeoclimate research. A further challenge encountered when studying lake records spanning thousands of years is incorporating known or hypothesised changes in the lake's physical environment. For example, land use changes, such as the clearing of land following European settlement of Australia (e.g., Jones, 1999), the filling of lakes with sediment (e.g., Cadd et al., 2018), or more dramatic changes, such as volcanic and tectonic activity which can divide or constrict lake basins (e.g., Obrochta et al., 2018).

One potential solution to these problems is to extend existing lake models by modelling all interconnected physical processes and hydrological systems that influence lake behaviour, such as groundwater modelling and energy balance modelling. The goal behind developing a 'holistic' lake model of this nature is to minimise the reliance upon parameterisations that are only valid for a small range of lake conditions, instead incorporating modelling methods that rely on parameterisations that can be assumed not to change significantly over the duration of the lake record. Modelling groundwater using methodologies such as finite difference or finite element modelling (FDM/FEM) requires determination of hydrogeological parameters such as the hydraulic conductivity and storativity (Anderson et al., 2015). The assumption that hydrogeological parameters are consistent for the duration of the lake sediment record is not unreasonable, whereas it is difficult to justify the assumption that groundwater fluxes estimated from observations covering only a small range of lake conditions are applicable outside those conditions. Likewise, estimation of the degree of stratification for a lake under past climates cannot necessarily rely on a small set of observations recorded under current climate conditions. Instead, energy balance modelling can be applied to estimate evaporation, water heat storage and lake stratification directly from the hypothesised climatic and lake conditions by estimating and balancing the incoming and outgoing energy sources and the mixing of temperature through the lake (Henderson-Sellers, 1986; Hostetler and Bartlein, 1990).

Based on the above, an ideal lake model for palaeoclimate research should be capable of modelling the lake and all interconnected systems. The model should avoid parameterisations that are only valid over a small range of lake conditions. A lake model for palaeoclimate research should have a method to include changes in the lake system, such as lake sediment filling and land use changes. An ideal lake model should also include lake water elemental and isotope geochemistry, partly to account for the effect of water chemistry on evaporation and stratification, and because geochemical tracers are often central to the interpretation of past climates from lake sediments.

Numerous researchers have developed hydrologic-isotopic mass balance models for palaeoclimate studies, e.g. (e.g., Jones and Imbers, 2010; Jones et al., 2005; Steinman et al., 2012) or for determining source water contributions and tracing fluxes through a lake system (e.g., Gibson and Reid, 2014; Gibson et al., 2002; Shapley et al., 2008; Stets et al., 2010). However, none of these models include the full suite of components required for a general palaeoclimate lake model. Generally speaking, lake models are developed for specific lakes, and often lack coupled components necessary for other lakes. This specificity contrasts with the ever expanding suite of lake derived palaeoclimate reconstructions and associated efforts to use lake

models as components of 'proxy system models' – combination models that simulate the processes by which climate signals are transferred and encapsulated within proxy materials (Dee et al., 2015). There is therefore a need for a general model adaptable to different lakes and able to utilise datasets of varying completeness, without extensive recoding and with an open, extensible framework that can be expanded upon in future studies. In this paper we introduce a new model which aims to address this demand – the Chemical, Hydrological, Isotopic Mass Balance for Lake Environments (CHIMBLE), which we apply to two crater lakes, Lake Bullen Merri and Lake Gnotuk, in Victoria, Australia.

2 Model structure

CHIMBLE (https://github.com/Mjankor/CHIMBLE) is an adaptable lake model, designed to model many different lake scenarios using various levels of input data (Fig. 5.1). CHIMBLE's interface is written in R (Ihaka and Gentleman, 1996), with the main program loop written in C++ using the Rcpp library (Eddelbuettel, 2013; Eddelbuettel and Francois, 2011).

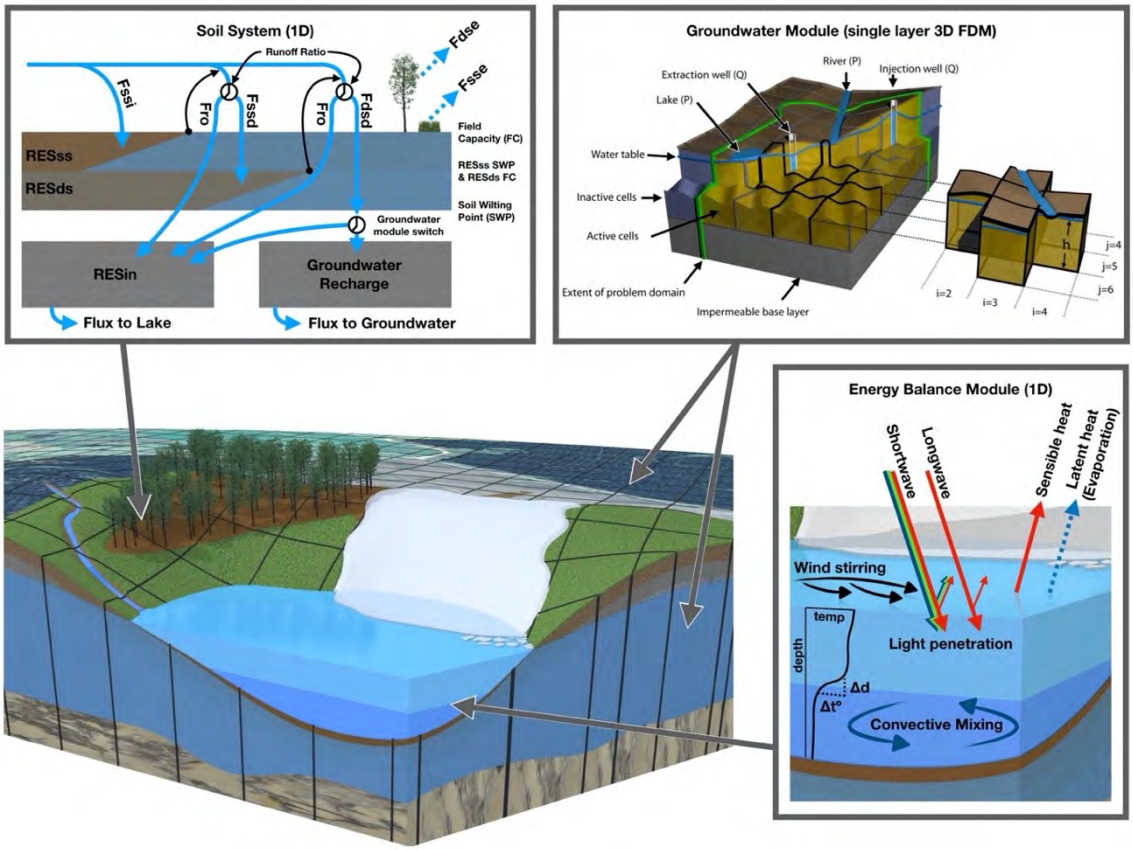

Figure 5.1: A schematic of CHIMBLE showing how the one dimensional mass balance model encompassing the lake and catchment, couples to the lake energy balance module and single layer groundwater finite difference model.

At its simplest level CHIMBLE is a mass balance model coupling hydrology, isotopes and chemistry. CHIMBLE is loosely based on the model developed by Steinman et al. (2010) (hereafter referred to as S2010), using the principle that any change in the hydrologic and

isotopic mass balance of a lake is the sum of the input and output fluxes, as described in equations 1 and 2 (Dinçer, 1968; Gat, 2010; Gibson et al., 2015; Gonfiantini, 1986).

$$\frac{\Delta V_L}{\Delta t} = \sum I - \sum O \tag{1}$$

$$\frac{\Delta V_L \delta_L}{\Delta t} = \sum I\delta_I - \sum O\delta_O \tag{2}$$

ΔV_L represents a change in lake volume, and $\sum I$ and $\sum O$ are the total inflow and outflow of the lake over a period of time. δ is the hydrogen or oxygen isotopic composition of a hydrological component as denoted by subscripts (eg: δ_L is isotopic composition of the lake). Isotopic results are reported using the delta notation as per mil (‰) deviations from Vienna Standard Mean Ocean Water (VSMOW2) where:

$$\delta_x = 1000\left(\frac{R_x}{R_{VSMOW2}} - 1\right) \tag{3}$$

R represents $^{18}O/^{16}O$, or $^{2}H/^{1}H$ and x is the reservoir in question.

The mass balance consists of six reservoirs representing the lake, divided into an epilimnion and hypolimnion (depending on the degree of stratification), a two layer soil model, snow pack, and an 'inflow' reservoir. These reservoirs are comparable to the reservoirs in S2010 as described by Steinman et al. (2010), and generally have similar parameters. E.g. the soil layers don't model soil thickness, but instead model the available water capacity (AWC) of each soil layer. In addition, a groundwater reservoir is active if the groundwater module is enabled. The inflow reservoir can act as either a delay mechanism for catchment runoff, or as base-flow mechanism for subsurface drainage if the groundwater module is disabled. Evaporation and evapotranspiration are estimated using a simplified Penman equation (Valiantzas, 2006).

Coupled to the mass balance are groundwater and energy balance modules. If enabled, the groundwater module replaces all parameterised subsurface flows of the mass balance with a single layer finite difference model based on MODFLOW (McDonald and Harbaugh, 1988) and A2016 (Ankor and Tyler, 2019). The groundwater module uses a specified aquifer thickness for the cells beneath the lake, as described in Ankor and Tyler (2019), and an unconfined aquifer for the surrounding region. The groundwater model can model recharge (drainage through the catchment soil layers), evapotranspiration, injection and abstraction, and other defined Cauchy,

Neumann and Dirichlet boundary conditions. The groundwater model can model up to nine lakes at once, with additional lake levels defined in relation to the primary lake being modelled. Nine hydrogeological regions can be modelled with differing values for hydraulic conductivity and storativity.

The energy balance module is based on the model of Hostetler and Bartlein (1990), recently updated by Dee et al. (2018) as a component of the PRYSM 2 model. The energy balance module replaces parameterised stratification depth and lake surface temperature time-series with values derived from the meteorological conditions and lake temperature state. Evaporation from the lake is calculated via the energy balance model, rather than the simplified Penman equation (Valiantzas, 2006) used by the mass balance. In the current version of CHIMBLE a stratification depth is extracted from the energy balance derived lake temperature profile, based on the change in temperature over depth – a necessary conceit to couple the multiple layers of the energy balance to the two reservoirs of the lake mass balance.

Chemistry is incorporated into the mass balance model. The chemical composition through all fluxes and reservoirs is treated conservatively, with no gain or loss of chemical components due to precipitation of salts, outgassing or other processes, though CHIMBLE is designed so that functions that model such processes may be easily added. The mass balance chemistry can model TDS (total dissolved solids), salinity, and/or any number of ions. The chemistry of lake water is applied to both lake evaporation and associated isotopic fractionation. The activity of the lake water is estimated based on its chemical composition using either salinity or major ions. In the case of major ions, the salt content for five common salts (NaCl, $MgCl_2$, $CaCl_2$, KCl, and NaBr) is estimated based on stoichiometric matchups of ions. An approximate density and salinity of the water is calculated assuming full disassociation. The approximate salinity is then compared and corrected against a known salinity-density curve (typically seawater). Once the density and salinity values correspond, salt molalities are determined, and the activity of the water is calculated using the additive method of Robinson and Bower (1965). The major ions are used directly in the isotopic fractionation equation to account for the influence of salinity, using the equations described in Gat (2010).

Isotopic fractionation of evaporative flux is calculated using the Craig and Gordon (1965) equation as described in (Steinman et al., 2010). However, the fractionation equations have been developed further in CHIMBLE to account for water chemistry, atmospheric feedback (a buildup of humidity over lake water due to evaporative flux), and the situation where atmospheric isotopic composition is not in equilibrium with rainfall (equilibrium between

atmospheric and rainfall isotopic composition is a common assumption in isotopic modelling) (Bennett et al., 2008; Gat, 2010; Gibson et al., 2015).

Some features are common across all levels of modelling, regardless of whether the groundwater and energy balance modules are enabled. Hypsographic curves, linking a lake's surface area, volume and depth can be defined using either LOESS smoothing (Cleveland, 1981) or linear interpolation. CHIMBLE can sample isotopic and chemical values from any specific depth, taking into account the thermocline depth of the lake at the time. Daily and monthly input data are supported, along with fractional time-steps. CHIMBLE also models catchment processes such as evapotranspiration, runoff ratio (amount of runoff vs percolation into the deeper soil) and whether rainfall infiltration and percolation through the soil occurs via a piston flow mechanism, or with mixing of isotopes and chemistry.

A requirement for model based palaeoclimate research is the need to update and modify datasets and variables used by the model during the simulation. This may be for exploratory research (e.g. testing how sensitive the lake system is under various climate regimes) but more essential is the need to account for changes over the timeframe of a palaeoclimate record (e.g. change in sediment depth over time). CHIMBLE uses an "Event Manager" to manage changes to datasets and variables during a simulation, and "Scenario" files to store any changes specific to a simulation. Event and scenario data are stored in separate files to the main model data so that individual simulations can be run or archived, while the default model parameters are unmodified.

3 Regional setting

Australian lake sediment records have global significance due to their location between the Pacific, Indian and Southern Oceans and accompanying climate systems (Gouramanis et al., 2013; Neukom and Gergis, 2012). South-eastern Australian palaeoclimate records also hold regional significance, due to the need to quantify climate and anthropogenic impacts on water resources in a largely evaporation dominated landscape which supports intensive agriculture (Ho et al., 2015; Kiem et al., 2017). Several studies have attempted to reconstruct past changes in lake water balance in the region, using oxygen isotope analyses of lake carbonates (specifically ostracods), plus sedimentological and palaeoecological data (Barr et al., 2014; Chivas et al., 1993; Chivas et al., 1985; Gouramanis et al., 2010; Wilkins et al., 2013).

For some of these records, hydrological balance models have been used to estimate palaeoclimate variables (Jones et al., 1998) or to forecast future lake volume change (Yihdego et al., 2015), however, there are few examples of coupled hydrologic isotopic models applied to Australian lakes.

The Newer Volcanic Province is a region of Pliocene to Holocene basaltic plains, unconformably overlying older igneous, metamorphic and sedimentary formations in the south east of South Australia and western Victoria (Dahlhaus et al. 2003). The basalt forms a 10-130 m thick unconfined aquifer, dotted with over 416 eruption centres, consisting of lava shields, scoria cones, tuff rings and maars (Boyce, 2013). Some of these eruptive centres have since formed significant lakes (Fig. 5.2).

Figure 5.2: Regional setting, showing some key lakes of the Newer Volcanic Province. The two lakes chosen for model development – Lake Bullen Merri and Lake Gnotuk – are shown in bold.

The crater lakes of the Newer Volcanic Province in western Victoria and South Australia (Fig. 5.2) are ideal for model development due to the frequency and variety of lakes, many of which have relatively simple basin morphologies and water chemistries which fall along a hydrology-driven salinity mixing line between hypersaline and fresh (Chang et al., 2014; Maddocks, 1967; Williams, 1981). Of 32 lakes in the Newer Volcanic Province considered for their potential to develop a hydrologic-isotopic model, Lake Bullen Merri and Lake Gnotuk, hereafter referred to as Bullen Merri and Gnotuk respectively, were selected as the focus of this research (Fig. 5.3).

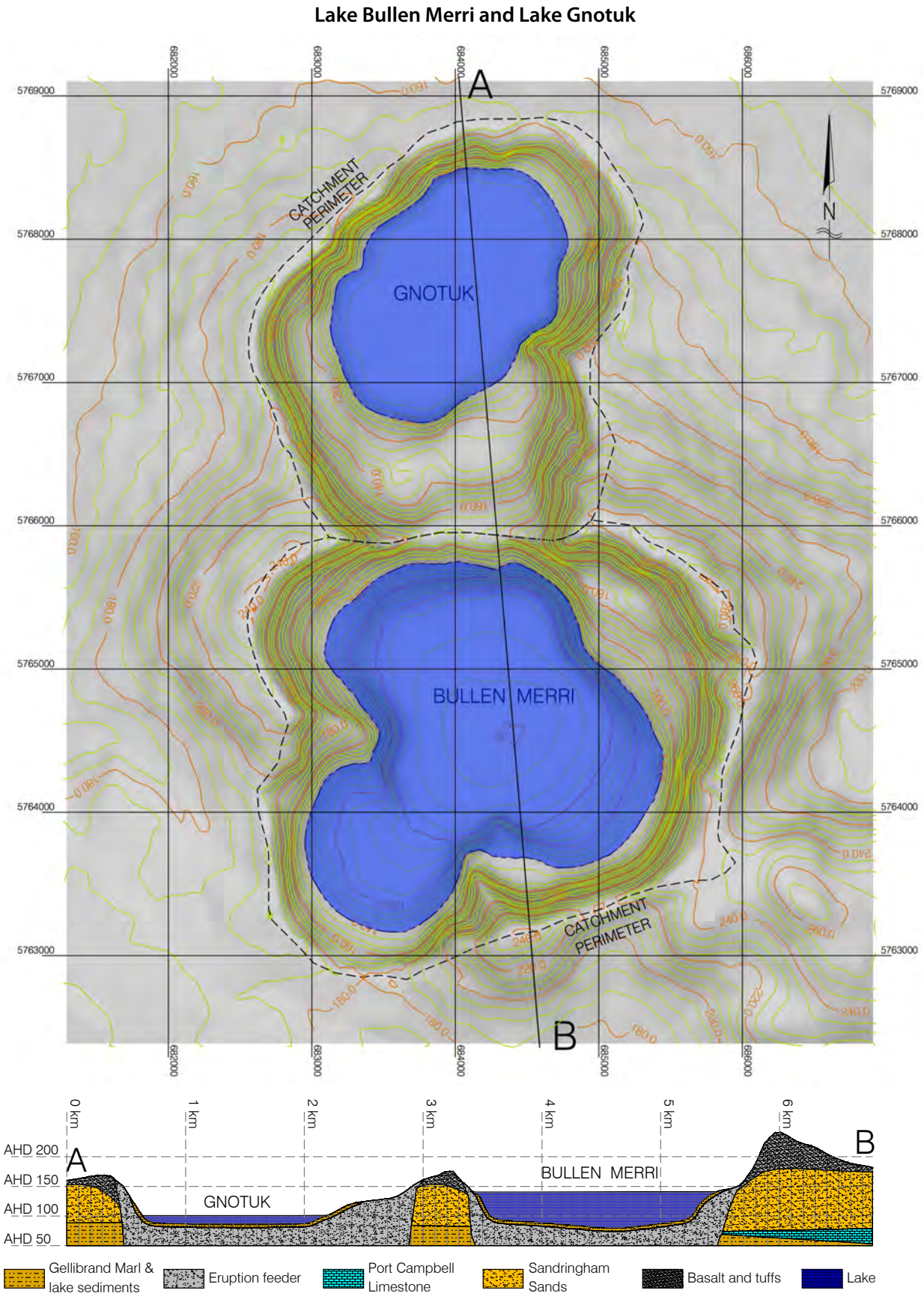

Figure 5.3: Map of Lake Bullen Merri and Lake Gnotuk, showing catchment area, topography and current water levels. Geological formations are derived from the Victorian Aquifer Framework (Victorian Department of Sustainability and Environment, 2012). Coordinates are in MGA94 (Map grid of Australia), zone 54, Heights are shown in AHD (Australian Height Datum).

Long instrumental records of lake water depth are available for both lakes, and neither are thought to have dried out completely within the last ~10 ka. The lakes also have differing but relatively simple catchment morphology (Fig. 5.3) and, being located in neighbouring craters, the two lakes provide an excellent testing ground for examining the differing hydrological and isotopic response of lakes driven by a common climate forcing.

Both Lake Bullen Merri and Lake Gnotuk have been previously modelled. A hydrological mass balance lake model was developed that couples the evaporation model of Morton (1983), to a lake water balance and a catchment soil model (Jones et al., 2001). The catchment soil model accounts for evapotranspiration, with percolation through the soil layer draining to the subsurface to form a baseflow to the lakes. A percolation coefficient, *KQ*, defined through model calibration, determines the rate of percolation. Model calibrations starting from an earlier date (1881) required a lower KQ value than equivalent calibrations using only the more recent data (1964), suggesting an increase in percolation as the lake levels dropped. Several hypotheses were suggested to explain this phenomenon – that percolation rate is increasing over time, a bias in early evaporation or precipitation observations, or a fall in lake levels creates a positive feedback in groundwater input (Jones et al., 2001). This model has also been used to develop projections for lake level and salinity up to the year 2100 (Kirono et al., 2009).

Gnotuk is a flat bottomed, hypersaline (~ 70 g/L) lake, currently around 15 m deep (100.2 m AHD (Australian Height Datum), September 2018), with a surface area of approx. 208 ha, and a catchment area of approx. 617 ha (Fig. 5.3). In contrast, Bullen Merri is a conical, brackish (~ 9 g/L), lake, with a current depth of around 60 m (139.5 m AHD, September 2018), a surface area of approx. 435 ha, and a catchment of approx. 886 ha. At both lakes water levels have dropped by approx. 20 m since 1881 CE (Jones et al. 2001). The maars are of uncertain age, but Timms (1976) suggested an age of between 30000 to 7000 years old. More recent cores from Gnotuk give a minimum age of at least 11.5 ± 0.3 ka (Wilkins et al., 2013), and an 11.73 m core from Bullen Merri had an age of ~10 ka at a depth of 7 m (Barton and Polach, 1980).

Inflow to the lakes is predominantly derived from subsurface flows, with the exception of overflow from Bullen Merri to Gnotuk that occurs when Bullen Merri reaches a height of ~168.4 mAHD, last observed in 1841 CE (Currey, 1970). Surface runoff is uncommon, with even extreme rainfall events (e.g 125 mm in 24 h in Feb 1992 producing no observable runoff (Jones et al., 2001)).

Both lakes lie within maar craters surrounded by, in sequence: the younger tuffs and basalt volcanic sequence at the surface; the Sandringham Sands Formation (also known as the Moorabool Viaduct Formation) of fluvial and marine deposits; and the Gellibrand Marl (Fig. 5.3). Several authors also suggest that the Port Campbell Limestone lies between the Gellibrand Marl and Sandringham Sands Formation beneath both lakes (e.g., Jones et al., 2001; Leahy et al., 2010; Yihdego et al., 2015). However, the Victorian Aquifer Framework (SKM, 2009; Victorian Department of Sustainability and Environment, 2012), suggests that the Port Campbell Limestone lies to the south west, and tapers out beneath Lake Bullen Merri. This is also supported by an assessment of drill logs from 37 wells in the ~80 km^2 region surrounding the lakes. Hydrogeologically the upper stratigraphic units – tuffs/basalt and the Sandringham Sands Formation – are often treated as a single unit. They share similar hydraulic conductivity (10^{-2} to 10^{1} and 10^{-3} to 10^{2} m/day respectively) and are hydraulically connected (Dahlhaus et al., 2002; Yihdego et al., 2015). The Port Campbell Limestone is a regional aquifer, thought to have limited influence on the lakes, due to its low yield and slope away from the lakes (Jones et al., 1998; Jones et al., 2001; Yihdego et al., 2015). The bases of Gnotuk and Bullen Merri lie at the same depth as the Gellibrand Marl, an aquiclude preventing interaction with deeper groundwater systems (Leahy et al., 2010; Tweed et al., 2009). Some seepage is expected through the volcanic necks to lower aquifers beneath the marl (Raiber et al., 2008).

Bullen Merri and Gnotuk are in a temperate climate, with a mean annual temperature of around 13 °C, ranging from an average daily temperature of 18.0 °C in summer to 8.2 °C in winter. Annual rainfall is around 775 mm/year, predominantly from May to November, and yearly class A pan evaporation is around 1250 mm/year based on interpolated daily data from SILO database from 1970 to 2017 (Jeffrey et al., 2001).

4 Methods and calibration

4.1 Input datasets

CHIMBLE requires numerous input datasets, depending on what model options are set. If CHIMBLE is used for a simple hydrological mass balance then only hypsographic, meteorological, morphological, lake temperature, and lake level datasets may be required. However, for a full isotope and chemistry enabled model, using groundwater and energy balance modules, then CHIMBLE also requires chemistry, isotope and stratification data for calibration, and multiple grids defining hydrogeological parameters for the groundwater module.

CHIMBLE requires meteorological time series for precipitation, average temperature, relative humidity, solar radiation, windspeed (at 2 m above surface), and mean sea level pressure. External flows (e.g. pumping to or from the lake, rivers, etc.) are defined within the meteorological input file, as are $\delta^{18}O$ and $\delta^{2}H$ values for precipitation and external flows if the stable isotopes of water are being modelled. Both daily and monthly data are supported by CHIMBLE. SILO data-drill time-series (Jeffrey et al., 2001) were used for the Bullen Merri and Gnotuk simulations, providing daily data from 1889 to present. Daily average temperature was calculated as the mean of the maximum and minimum daily temperature. The average relative humidity was derived by determining the daily dewpoint temperature using the August-Roche-Magnus Approximation (Alduchov and Eskridge, 1996; Magnus, 1844) from the daily minimum and maximum humidity, then calculating the average humidity based on the average daily temperature. Wind data were extracted from 2 m wind run grids developed by McVicar et al. (2008) covering the time period from 1975 to current. For data prior to 1975, average windspeeds for each month were estimated from the ~40 year dataset. Monthly average meteorological data were derived from the daily timeseries for model input.

There is very limited information about the stratification behaviour of the studied lakes, with only 3 years of stratification data collected by Timms (1976). Water surface temperatures were collated from Timms (1976) for the years 1969–1972, from Tibby and Tiller (2007) (Bullen Merri only, 1984 to 2000), and the Victorian Department of Environment, Land, Water and Planning (Bullen Merri and Gnotuk, 2005 to 2019) and from the monitoring collected as part of this research (2015-2018). Lake level data for both lakes extends from 1965 to 2006, and from 2015 to 2018, with some historical levels for 1881 and 1949 documented by Jones et al. (2001).

Major ion compositions, conductivity, and $\delta^{18}O$ and $\delta^{2}H$ values for the lakes were collected from 2015 to 2018 (Chapter 2, this thesis). Additional TDS data came from Timms (1976) who documented TDS values for Bullen Merri from 1953–1968 and Gnotuk from 1964–1968 from a range of sources (Bayly and Williams, 1966; Currey, 1970; Hussainy, 1969; Williams, 1966). Conductivity values for Bullen Merri from 1984 to 2019 and for Gnotuk from 1993 to 2019 came from the Department of Environment and Tibby and Tiller (2007) and were converted to TDS values (EC@25 x 0.565). Major ion concentrations were used for the model simulations, with TDS values maintained in parallel for comparison with observations. Major ion values for groundwater used in the modelling were the average of the major ion concentrations of 15 groundwater wells with records within the region, with an average TDS of 2042 mg/L, ranging from 550 to 4000 mg/L. $\delta^{18}O$ and $\delta^{2}H$ groundwater values used in the model were the average value of samples collected from springs on the shores of Lake Gnotuk, Lake Keilambete and West Basin during the 2015 to 2018 sampling program. Seven spring samples were collected, but only five were used for the average as two appeared to have undergone evaporation. The isotopic composition of precipitation was based on the monthly averaged GNIP (Global Network of isotopes in Precipitation (Schotterer et al. 1996)) data for Melbourne. The monthly averages were flux-weighted and integrated into a yearly average. The difference between the yearly average and the intersection of the observed local evaporation line and the meteoric water line was then applied to the monthly isotope estimates to provide a seasonal isotopic signal aligned to local conditions (Gibson et al., 1993).

Groundwater grids were established to cover the lakes, catchments and surrounding region with an extent from 680500, 5770700 in the north west, to 687700, 5761500 in the south east (Map Grid of Australia 94) with a grid cell size of 50x50 m, for a total areal coverage of 66.24 km^2. Catchment topography was digitised from 1:30K Vicmap (2014) topographic maps inside the catchments, and SRTM DEM-H DEMs (Gallant et al. 2011) outside the catchment perimeter. Bathymetry was digitised from surveys by Timms (1976), then scaled and aligned to best fit the topography. Bathymetry and topography were combined using 12D Model (12D Solutions) to form a topographic surface. Volumes, surface areas and heights defining the hypsographic curves were then calculated from lake floor to the overflow height at 0.2 m intervals. Catchment areas were defined by the direction of surficial flow, typically the crater rim.

Hydrogeological information was extracted from the Victorian Aquifer Framework dataset (Victorian Department of Sustainability and Environment, 2014). The top surface of the Gellibrand Marl aquitard (Aquifer ID 108), was used to define the base surface grid. Within the crater the base of the diatreme was estimated based on models and observations of diatreme

structure (Blaikie et al., 2014; Lorenz, 2003), defining a bowl shaped depression of varying depth. Two different base surface grids were investigated during the modelling process, with differing diatreme depths. The shallow aquifer base was set only ~20 m below the deepest part of each lake, to test the assumption that the fine, post-eruptive sedimentary layers common to the upper levels of diatremes (White and Ross, 2011) would isolate the upper aquifer from water lower in the diatreme. The deeper aquifer base formed a bowl structure ~200 m below the lake in Gnotuk and ~600 m below Bullen Merri. To define the hydrogeology for the region surrounding the lake catchments the surfaces for both the basalt and Sandringham Sands formation were assessed. Each cell was assigned to one of four hydrogeological zones by binning, based on the relative contribution of each type of geology, to investigate any major differences in conductivity between the two formations (Fig. 5.4). As the Port Campbell Limestone likely tapers out beneath the lakes and has a similar hydrological conductivity to the Sandringham Sands formation (Nicolaides, 1997), it was included within the Sandringham Sands formation. Within the catchments there is little geological information about the diatreme and crater sediments, so two hydrogeological zones were defined, one from the base of the crater to a few metres above the current lake depth, and a second zone extending further up the crater walls. These two zones were used to investigate the possibility of changing hydrogeological conditions towards the centre of the diatreme, similar to the hypothesis of Jones et al. (2001).

The lake sediment grid defines lake sediment thickness for each lake, with lake seepage treated as a head dependent boundary condition. As there is little information on lake sediment thickness depth, sediment depths were estimated with a depth of 0 at the estimated maximum lake height, increasing to a maximum thickness of 10 m for Gnotuk and 15.5 m for Bullen Merri, based on age-depth models of lake cores for both lakes (Barton and Polach, 1980; Wilkins et al., 2013) and an assumed eruption date ~ 25 ka. An exponential function was used, combined with a weighting function based on the topographic slope to bias sediment thickness towards the deeper and flatter parts of the basin.

Initial water table heights were not able to be determined from observation. While 74 groundwater wells were identified within the model extents, none had a record of water table values. More importantly, as the lakes were around 20m higher in 1889, at the start of the meteorological record, any current values for the water table are unlikely to be valid. The initial water table values were established by spinning up the model for 200 to 400 years before the model run.

The targets for the spin up cycle were to achieve a near steady state condition for the lake based on the average climate, followed by modification to the precipitation/evaporation (P/E) ratio to raise Bullen Merri to overflow in 1841, before falling to the observed level in 1881, with continuation until 1889 to provide an initial water table surface and lake level for the observation driven model runs.

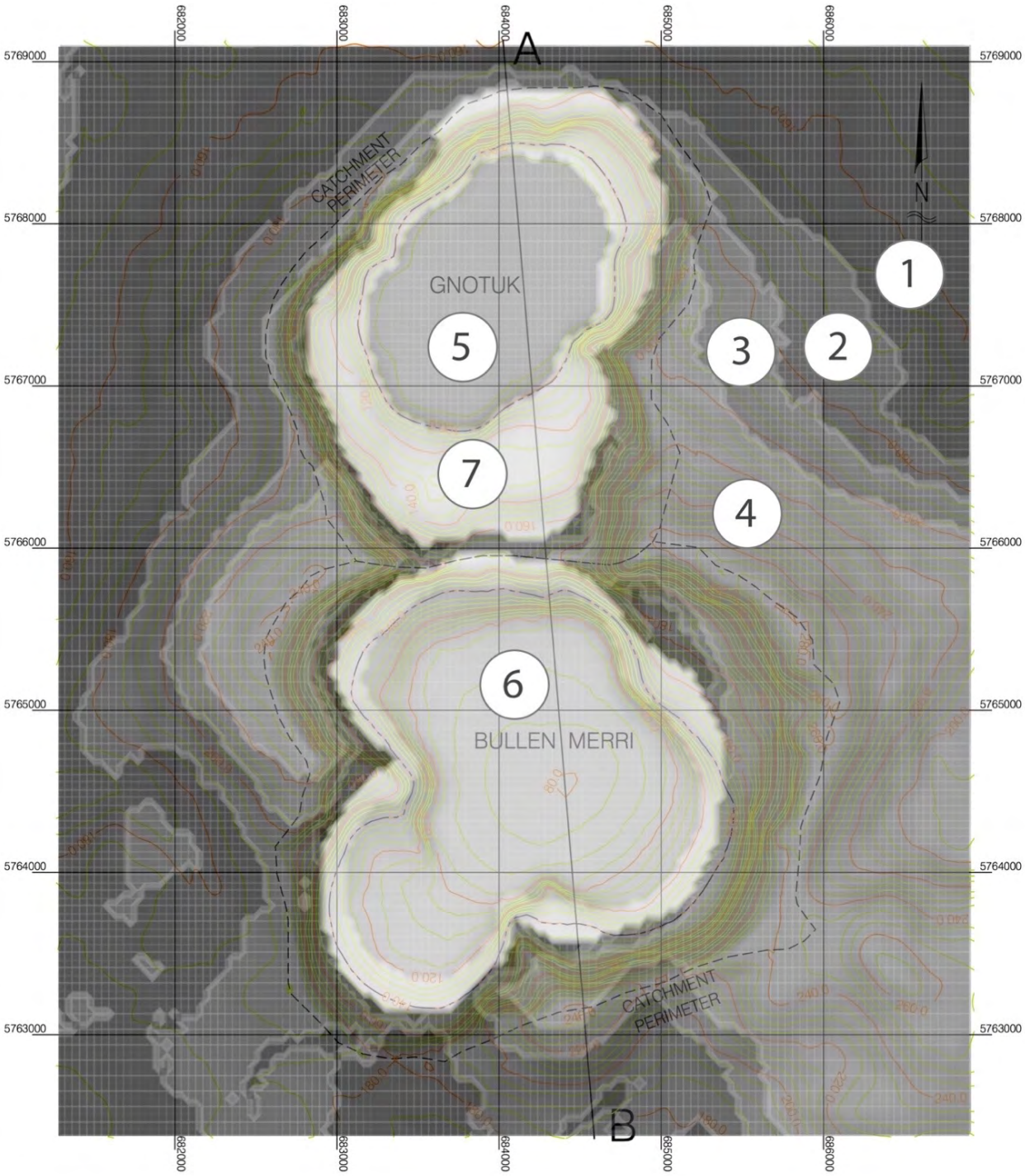

Figure 5.4: Geological zones defined for the groundwater model. Zones external to the craters (1 to 4) are based on the contribution of sandstones and tuffs/basalt within each cell. Zones 5,6 and 7 represent the diatreme zones used to investigate hydrogeologic properties within the craters.

While conditions prior to 1841 are unknown, it is very unlikely that the lake spent any length of time at overflow height, as there is no evidence of significant scouring or channels on the slopes of Gnotuk below the overflow point. A long term meteorological dataset, required for the spin up cycle, was established by randomising the existing 130 year dataset on a year by year basis. Randomising the data in this nature averages out any long term trends in the data, while preserving month by month variation in meteorology. As recharge rate to the groundwater is determined by the amount and frequency of rainfall, some variation of rainfall through the meteorological record is necessary. If a long term monthly average was used instead, then the recharge rate during model spin-up would be significantly lower.

The P/E ratio was modified using two methods. The first method applied a modifier to increase precipitation from ~1790 until 1849, trending back to the unmodified precipitation values to lower the lake level by ~6 m by 1881. This method increased recharge significantly over the period of increased precipitation. The concern with this approach is that the increased recharge may lead to increased groundwater mounding which may not be compatible with the rapid fall of the lakes. Based on this concern, this method was used only for preliminary investigations. The second method was to decrease evaporation so that the groundwater recharge rate was less affected, with the majority of the lake level rise being driven by a shift in the P/E ratio, rather than a massive increase in rainfall. This was achieved by increasing relative humidity by 20 %, increasing precipitation by 20 %, and decreasing windspeed by 10 % over the 1790 to 1849 time period. Hydraulic head heights for the aquifers beneath the Gellibrand Marl were interpolated at the lakes location and compared to the lake levels. These deeper aquifers (Victorian Aquifer Framework: Aquifer ID 111 and 113) had hydraulic heads well below the existing lake levels and are unlikely to contribute to the lake water balance. The groundwater model was constrained with fixed head boundaries on the northern edges, and at a topographic low point in the centre of the southern extents of the grid. The fixed head for these boundaries was set 5m below the topographic surface – a typical depth to groundwater for those areas (FedUni, 2015).

4.2 Calibration methods

Lakes Bullen Merri and Gnotuk were chosen for model development because they represent a challenging and unusual hydrological scenario. Like many sites valued for palaeoclimate research they are underdetermined systems. The goal during model calibration was to identify a parsimonious set of parameters that were able to match observed lake levels, stratification, surface temps, isotopes and chemistry for both lakes, while simultaneously being within the likely and reasonable range of values for variables like hydraulic conductivity and storativity.

The calibration process was broken up into several steps, based on which aspect of the model was likely to have the greatest effect on the simulation. As a first step, the groundwater module was disabled and inflow to the lake directly specified to achieve the observed lake level change. Initial chemistry was estimated as a percentage of the 2016–2018 average values, based on the mass balance change. The stratification module was enabled, and the neutral drag coefficient (primarily controlling surface temperature) and short wave extinction coefficient (primarily controlling stratification depth) were adjusted to match the observed lake temperatures and stratification as described in Dee et al. (2018). Following the preliminary estimation of chemistry and energy balance variables, thus providing a close approximation of lake evaporation, calibration of the groundwater module was performed. Calibration may not be the best description as the process was more an exploration of a multi-variable space with a transient, non-linear, hydrological response. Over 1560 groundwater module experiments were performed to investigate what parameter values were required to match the lake level change of both lakes, and to establish which parameters were most useful for future lake modelling at different sites. Each experiment varied hydraulic conductivity, storativity (specific yield), recharge (through modifying the available water capacity parameter for each soil layer), lake sediment thickness and geologic boundaries. Hydraulic conductivity was varied across a range of 20 – 1 x 10^{-5} m/d and specific yield from 2 to 25 %. These values extend outside the expected ranges for conductivity and specific yield, with the more extreme values typically used to examine hydrological behaviour, or limit the influence of a particular hydrological component (e.g., a value of 1x10^{-5} m/day may be applied to lake sediments to limit seepage to and from the lake so as to examine the surrounding groundwater behavior). A further complication is that while Bullen Merri forms only a slight depression in the water table, based on both modelling results, and from the Visualising Victoria Groundwater dataset (FedUni, 2015), the water level of Gnotuk is ~40 m lower, forming a very significant depression in the water table. Considering Gnotuk has a surface area less than half that of Bullen Merri, and is hypersaline (further decreasing evaporative flux), this suggests that there may be a significant sink of groundwater within the Gnotuk crater. An obvious candidate is seepage through the volcanic neck to lower aquifers, e.g. Raiber et al. (2008). To examine this behaviour, the pumping grid (responsible for injection and abstraction processes) was used to define drainage to lower aquifers for numerous scenarios.

Once parameters for the groundwater module were defined, then the initial chemistry and parameters for the stratification module were reassessed, followed by isotopic calibration. The isotope fractionation equations used by CHIMBLE are based on the Craig and Gordon (1965)

model (eq. 4), describing a two part fractionation process with both equilibrium fractionation associated with the phase change, and an additional transport fractionation process through a diffusive layer between the water and the turbulent atmosphere.

$$\delta_E = \frac{\alpha^* \delta_w - h_n \delta_A - \varepsilon_{eq} - \varepsilon_{kin}}{1 - h_n + 0.001\varepsilon_{kin}} \tag{4}$$

Where α^* is the reciprocal of the equilibrium fractionation factor, calculated using the equations of (Horita and Wesolowski, 1994). Equilibrium and transport separation factors are defined by ε_{eq} and ε_{kin}. h_n refers to the relative humidity normalised to the water temperature. δ_W and δ_A represent the isotopic composition of the water and atmosphere respectively. The equilibrium separation (ε_{eq}) is calculated by:

$$\varepsilon_{eq} = 1000(1 - \alpha^*) \tag{5}$$

While the transport isotopic separation (ε_{kin}) is calculated by:

$$\varepsilon_{kin} = (1 - h_n)\theta n C_k \tag{6}$$

C_k is an experimentally derived constant of 28.5 ‰ for $\delta^{18}O$, and 25.1 ‰ for $\delta^{2}H$ (Merlivat 1978). θ describes the transport resistance of the diffusion layer, while n relates isotopic separation to wind conditions. θ and n range from 0 to 1. A combined value for θn of 0 defines a local evaporation line (LEL) with a slope of ~8. A combined value of 1 typically results in a LEL slope of around 2.5, and describes evaporation through a fully formed diffusive layer such as soil (Ankor et al., 2019; Gat, 2010).

δ_A is often assumed to be in isotopic equilibrium with rainfall, but recent research suggests this may only be valid when estimated in close temporal proximity to rainfall events (Crawford et al., 2019). The technique of Bennett et al. (2008) was used to calibrate the local evaporation line, achieved by shifting δ_A from equilibrium with δ_P by 14 ‰ (Eq. 7).

$$\delta_A = \alpha^* \delta_P - 1.14\varepsilon_{eq} \tag{7}$$

Atmospheric feedback has also been included in the isotope equations, and further modifies the atmospheric isotopic composition through mixing of evaporated flux into the air above the lake. This is done as a two stage process, with an initial estimation of the unaltered isotopic fractionation using equations 5 to 7. Using this estimate, a new δ_A and h_n is calculated based on the proportion of feedback, followed by a second fractionation calculation using the mixed values. The feedback parameter is also applied in the calculations of evaporative flux through the humidity variable.

To calibrate the isotopes, θn, feedback and the atmospheric shift were adjusted. Numerical experiments demonstrated that changes to the atmospheric isotopic composition influenced both the slope of the local evaporation line, and the extent of fractionation (Chapter 2, this thesis). Changes to θn predominantly affected the LEL slope, and the degree of atmospheric feedback predominantly influenced the extent of fractionation. Feedback, θn and the atmospheric shift were adjusted until a similar atmospheric shift was required for both lakes, and with θn and feedback values commensurate with their lake conditions. As atmospheric feedback affects evaporation, this process: groundwater → stratification → chemistry → isotopes; was repeated until a parsimonious result was achieved.

The observational record of lake water $\delta^{18}O$ and $\delta^{2}H$ spans only ~three years. When combined with the lack of stratification data over that time period, this data scarcity presented a challenge for calibration of the isotopic component of CHIMBLE. Variations in stratification depth alter the volume of water in the epilimnion, which can significantly affect the range of surface water $\delta^{18}O$ and $\delta^{2}H$ values through the year. To further validate the isotopic component of CHIMBLE, a model comparison was run between CHIMBLE and S2010 using input data for Castor Lake (Steinman et al., 2010) until both models achieved a steady seasonal cycle for lake levels and $\delta^{18}O$. There are significant differences in the modelling of catchment hydrology between CHIMBLE and S2010. For example, CHIMBLE partitions all infiltration into the soil layers during the timestep in which the infiltration occurs, whereas S2010 partitions infiltration across multiple timesteps. In addition, S2010 limits the ability for soil layers to dry out when the soil layers contain less water than the monthly potential evapotranspiration. CHIMBLE includes the option to apply crop coefficients (*Kc*) to account for differing levels of evapotranspiration due to differing soil and vegetation types (Allen et al., 1998). To account for the differences in soil modelling between CHIMBLE and S2010, the crop coefficients in CHIMBLE were adjusted in a stepwise fashion until the average lake levels of CHIMBLE matched the results of S2010.

5 Results

5.1 Hydrology

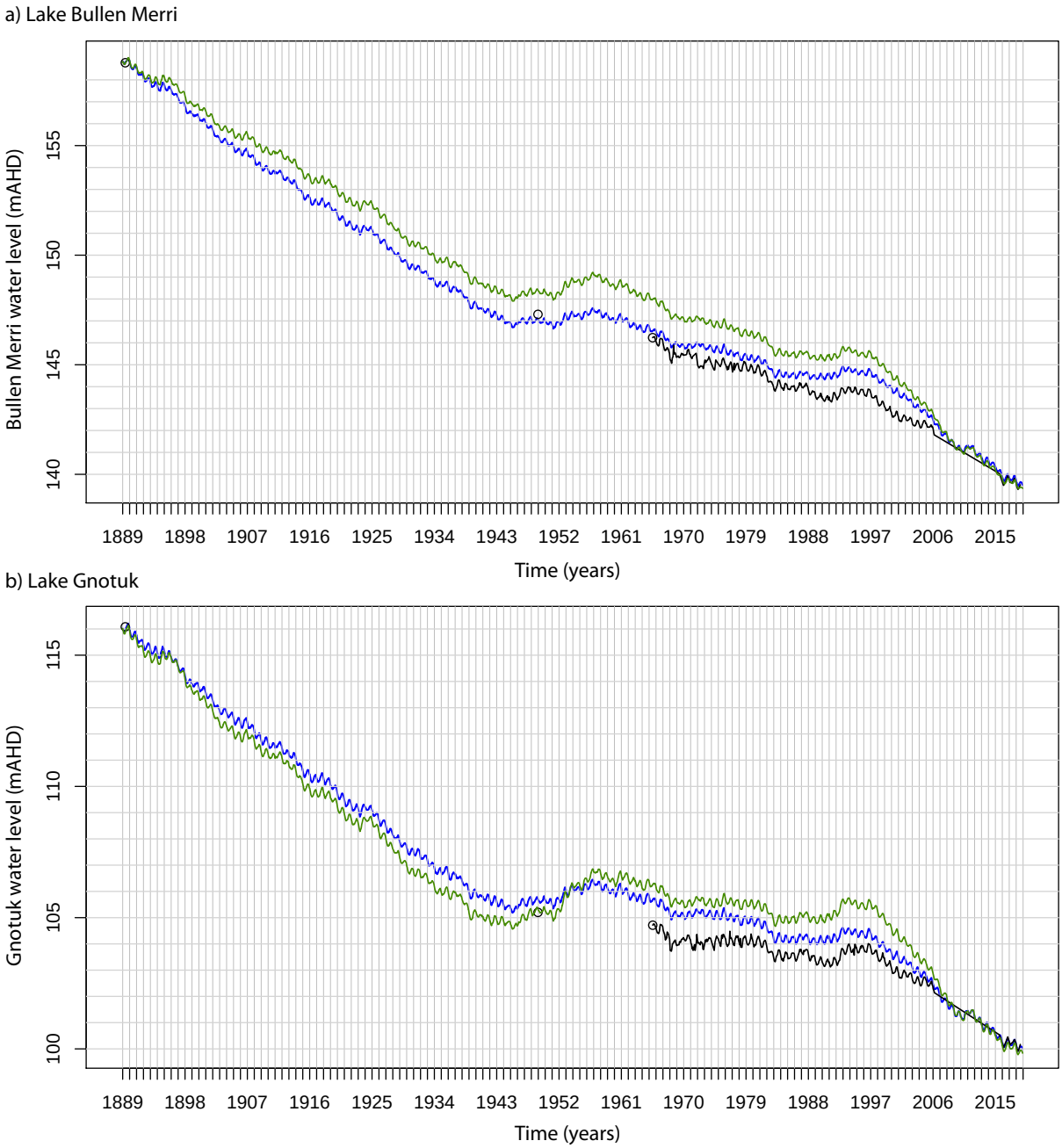

Figure 5.5: Modelled (blue and green) and observed lake levels (black lines and open circles) for Lake Bullen Merri (a) and Lake Gnotuk (b). Modelled lake levels in green are simulations with the groundwater module disabled, whereas blue lines represent the modelled lake levels with the groundwater module enabled.

Modelled lake levels matched observed lake levels with an RMSE (root mean squared error) of 0.75 m for Lake Gnotuk, and 0.74 m for Bullen Merri (Fig. 5.5). The modelled results were generally higher than observed levels throughout the model run, with a maximum difference of

1.48 m in 1972 for Lake Gnotuk, and a maximum difference of 1.18 m in 2000 for Bullen Merri. To achieve these results, the available water capacity (*AWC*) parameters for the two soil layers were set to 0.1 m. A value of 0 allows all rainfall to drain to the groundwater system. A value of around 0.2 m prevents almost all recharge to groundwater, except during occasional months featuring extremely high rainfall amounts. With a value of 0.1 m, recharge is around 0.07 m per year. In comparison, (Raiber et al., 2008) estimated a value of 0.05 m for third phase basalts near Mt Fyans, around 50 km to the north. Storativity was set to 0.13 and hydraulic conductivity for the surrounding basalts and Sandringham Sands Formation (and Port Campbell Limestone) was estimated at 1.2 m/day, with a hydraulic conductivity of 0.02 m/day for the sediments within the lake crater (Fig. 5.4). The lower conductivity sediments within the crater did not extend to the top of the crater wall, with an upper limit derived from the model experiments of ~170 mAHD in the Bullen Merri crater, and ~165 mAHD in the Gnotuk crater. Lake sediment conductivity was set to 0.001 m/day, similar to the 9×10^{-4} of Yihdego et al. (2015), with lake sediment thickness decreasing with height up the crater walls until tapering out at 130 mAHD in the Gnotuk crater and 168 mAHD in the Bullen Merri crater. Experiments were carried out with both a shallow and deep aquifer base. There was very little difference between the two base grids, with the shallow aquifer requiring a slight increase in recharge (*AWC* = 0.09) to give an RMSE for Bullen Merri of 0.8 m. This is likely because hydraulic head gradients in the centre of the crater are typically low, reducing any effect of increased transmissivity due to a deeper diatreme.

In the early stages of the simulation when the lake was at quite high level, the net flux to and from Lake Bullen Merri to the groundwater system had to be around zero, rising over time to around 27,000 m^3 per month. This is quite straightforward to achieve for Bullen Merri as Gnotuk can act as a groundwater sink. However, Gnotuk also requires a net groundwater flux of around zero at the start of the simulation, rising to around 5600 m^3 per month. Calculated evaporation was much lower at Gnotuk since the lake is hypersaline, more sheltered, and has less than half the surface area of Bullen Merri.

Even at the start of the simulation, Gnotuk sits within a groundwater depression, and as Bullen Merri is ~40 m higher than Gnotuk, there is a significant groundwater gradient towards Gnotuk from Bullen Merri of around 7 %. Several scenarios to explain this phenomenon were tested during the groundwater experiments. One scenario tested for decreased flows into Gnotuk was the presence of zones of low hydraulic conductivity within and around the crater. However, unlike a groundwater well, where flows to the cell typically increase as the hydraulic head in the cell is lowered, as the lake level dropped, flows to the lake typically decreased. This is counter

intuitive but can be observed in a simple groundwater model. A large abstraction of groundwater spread over a large area (evaporation of a full lake) may only lower hydraulic heads slightly, whereas a small amount of localised abstraction (evaporation of a lake at low level) can result in a much deeper cone of depression combined with much lower flows. While the cone of depression may be much deeper in the latter example, the radius of influence is also much smaller, so water is drawn in from a smaller region, and flows are lower. It follows that simply surrounding Gnotuk with a zone of low hydraulic conductivity may decrease flows to the lake but will also lead to flows decreasing as the lake level falls – the opposite of what is observed. The second scenario investigated was the presence of seepage across the entire crater floor to deeper aquifers. This method provided a sink allowing Gnotuk to achieve negative flows at the start of the run. However, as the seepage was always present beneath the lake, and flows to the lake decreased over the model run, then the issue of decreasing flows over the model run remained. In addition, the lake remained in a permanent through-flow state, with groundwater entering the lake along the shoreline, then seeping out through the lake floor, preventing the high salinity buildup that is observed in Gnotuk today. The third scenario investigated was the presence of seepage, predominantly between the shoreline of Gnotuk, and the crater wall, representing either a perched lake system, or seepage down ring-faults that commonly occur along the edge of diatremes (Fig. 5.6).

The presence of seepage, some distance from the lake shoreline, enabled Gnotuk to mirror the behaviour of Bullen Merri. In both cases, the lakes had significant water flux to groundwater when the lakes were at high level, compensating for flux to the lakes (eg: flux from Bullen Merri to Gnotuk). As lake levels fell, the distance to the seepage zone from the Gnotuk shoreline, or from Bullen Merri to Gnotuk increased, decreasing the hydraulic gradient and outgoing flows. While flows to the lakes did not increase significantly as lake levels fell, seepage out of the lakes did decrease resulting in a net flux increase to the lakes over the course of the simulation.

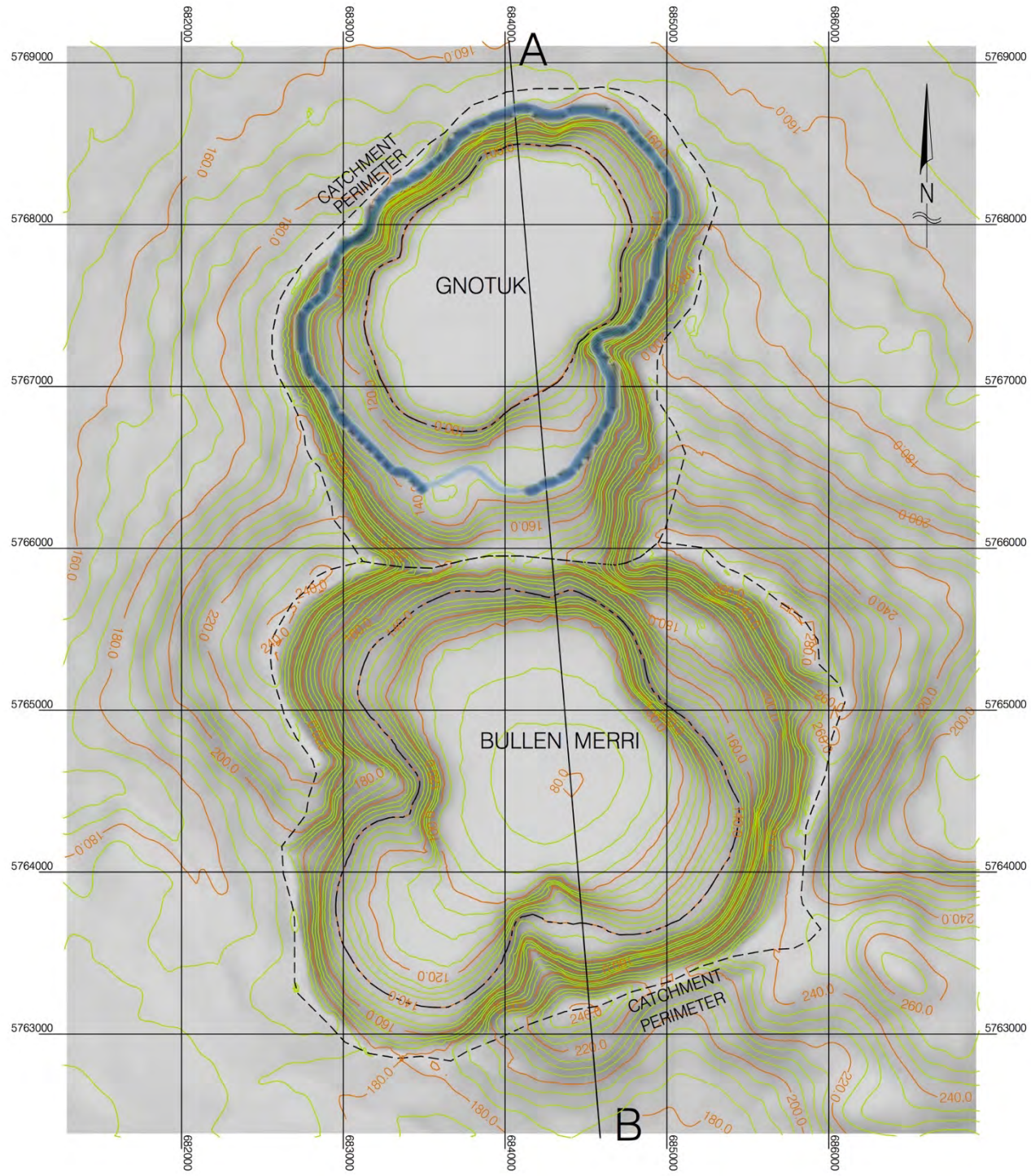

Figure 5.6: Hypothesized seepage zone (shown in blue) around lake Gnotuk

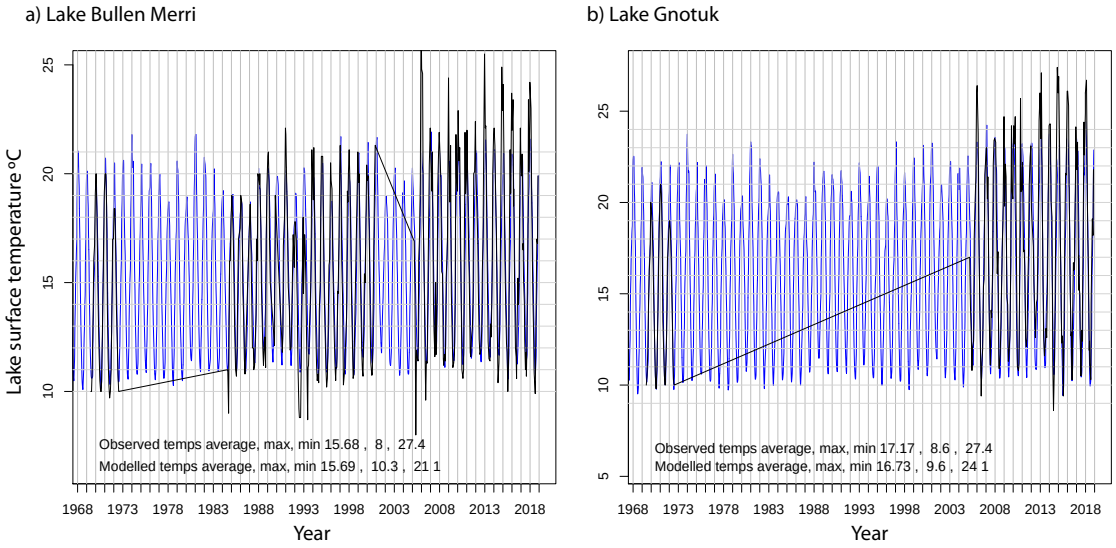

Figure 5.7: Modelled lake surface temperatures shown in blue, and observations in black for Bullen Merri (a) and Gnotuk (b).

5.2 Energy balance calibration

To calibrate the energy balance module, the initial determinations of the neutral drag coefficient were 0.003 and 0.0025, while the short wave extinction coefficients were 0.07 and 0.2 for Bullen Merri and Gnotuk respectively. CHIMBLE successfully modelled the stratification observed by Timms (1976) between 1969 and 1972, with a thermocline developing ~20 m deep in Bullen Merri in October/November, deepening over summer to ~40 m before the onset of mixing in May/June. In Gnotuk, the modelled and observed stratification began in September/October with a thermocline depth of ~6 m, increasing to ~13 m before mixing in March/April. A good average match was achieved between observed and modelled surface temperatures; however it was noted that the model temperatures were less than observed temperatures towards the end of the model run. This was expected, as modelled surface temperatures are related to the friction of the water surface, which is correlated to wind speed through wave formation. It is expected that as the water levels fall the lakes become more sheltered within their craters, with a corresponding decrease in wind speed and surface roughness. The neutral drag coefficient was estimated to be 0.0035, decreasing with lake levels to 0.0029 for Bullen Merri and 0.003, decreasing to 0.0021 for Gnotuk. Modelled lake surface temperatures then matched observed temperatures from 1970 to 2019 well, with an RMSE of 1.7 °C for Bullen Merri and 1.8 °C for Gnotuk (Fig. 5.7).

5.3 Lake water chemistry

There is little calibration required for the modelling of lake water chemistry, requiring just an initial concentration specified for each chemical component. A single factor was used for TDS and all modelled ions. Bullen Merri required an initial ion and TDS concentration of 67 % of the 2018 values resulting in an initial TDS value of 6064 mg/L, whereas Gnotuk required 44 % giving an initial TDS value of 31280 mg/L. Comparisons between modelled TDS values and observed values between years 2005 and 2019 had an RMSE of 1954 mg/L for Gnotuk, and 149 mg/L for Bullen Merri (Fig. 5.8). While there are observed TDS values from 1953 to 2000 for Bullen Merri and from 1964 to 1996 for Gnotuk (Fig. 5.8), these observations were not used in the error assessment as the degree of variation within the observations, which by far exceeded the range of those measured between 2001-2018, raised concerns about the quality of the older data and/or their representativeness of the entire lake water column. Modelled TDS values for Gnotuk were slightly lower than the observations documented by Timms (1976), with an average TDS of 49400 mg/L, compared to ~56000 mg/L between the years of 1964 and 1968. Bullen Merri's modelled TDS values are a very close match to the observations from 1953 to 1969, with an average TDS of 7800 mg/L, compared to an observational average of ~7900 mg/L.

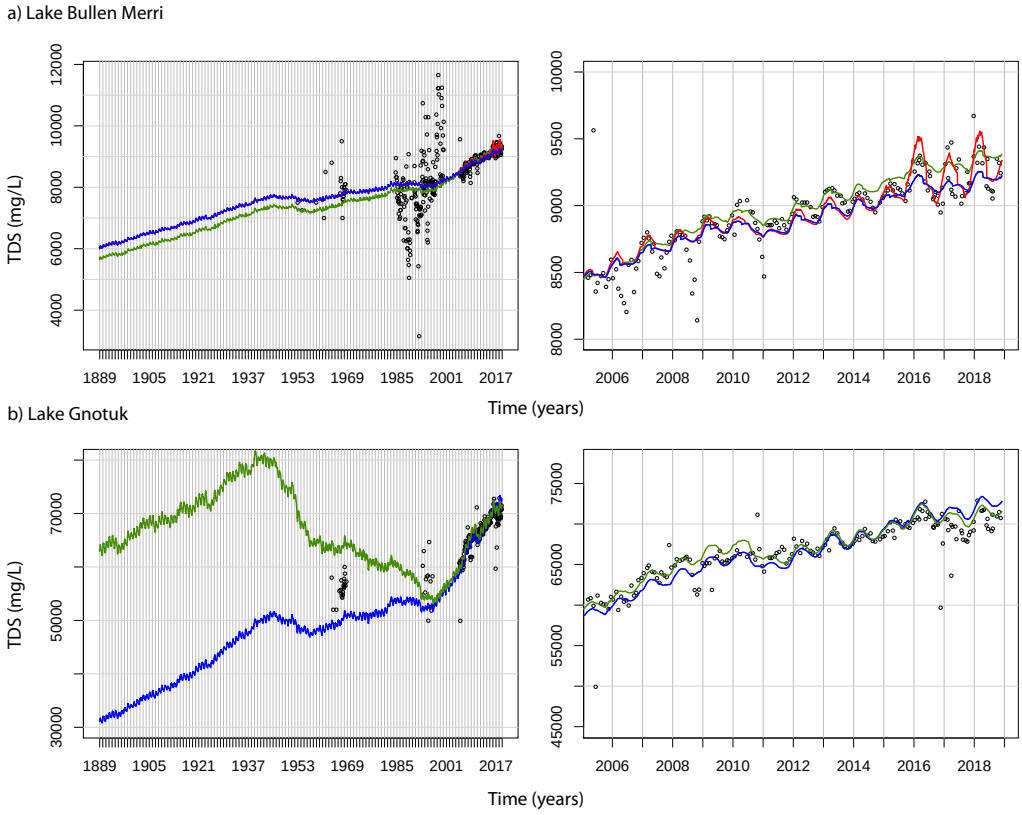

Figure 5.8: Modelled and observed TDS values for Bullen Merri (a) and Gnotuk (b). Default model run shown in blue. Groundwater disabled model run shown in green. Modelled results using a shallow stratification depth for Lake Bullen Merri are shown in red. Historical TDS values shown as black circles.

The long term modelled lake water TDS values for Bullen Merri from 1988 to 2015 matched observations well, however for many years the seasonal cycle is not well represented. To assess whether a change in lake stratification was the cause of the increased variation, the short wave extinction coefficient was modified, changing from the default value of 0.07, based on Timms (1976) observations, to 0.1 in 2005, and then to 0.3 in 2015. This decreased the initial stratification depth to ~10 m increasing throughout summer to 30 m, and then from ~5 m increasing to 15 m. With these values, the RMSE decreased to 146 mg/L and the simulated seasonal TDS cycle was much closer to observations.

5.4 Isotopes

There is only a short observational record for $\delta^{18}O$ and $\delta^{2}H$, from 2015 to 2018 (Chapter Two, this thesis). Isotopic calibration required modification of the atmospheric isotopic composition from equilibrium with precipitation (predominantly influences LEL slope and degree of fractionation), θn (predominantly affects LEL slope) and atmospheric feedback (predominantly affects the degree of fractionation). The goal was to identify values for these three parameters that were parsimonious with both lakes. It was expected that any shifts in the isotopic composition of the atmosphere would be identical for both lakes, whereas θn and atmospheric feedback would likely be greater at Bullen Merri than Gnotuk for any given LEL slope due to the increased fetch and lesser degree of sheltering. Shifting the isotopic composition of the atmosphere by 14 %, combined with a θn value of 0.25 for Bullen Merri and Gnotuk, and an atmospheric feedback percentage of 7.5 % for Bullen Merri resulted in LEL slopes of 4.7 for Gnotuk, and 5.5 for Bullen Merri, compared with observed LELs of around 4.8 and 5.5. In the initial simulation, seasonal variation in the isotope observations was significantly greater than simulations predicted, particularly for Lake Bullen Merri (Fig. 5.9). Between 2015 to 2018, modelled $\delta^{18}O$ values for Gnotuk ranged from 3.13 ‰ to 3.62 ‰, compared to an observed ranged of 2.85 ‰ to 3.8 ‰. Modelled $\delta^{18}O$ values for Bullen Merri ranged from 3.07 ‰ to 3.22 ‰, in contrast to the observations of 2.68 ‰ to 3.46 ‰ (Fig. 5.9).

The initial isotopic composition of the lake had little influence on the simulated isotopic composition of the lake waters in 2015–2018. Specifying a starting isotopic composition equal to average precipitation resulted in Bullen Merri rapidly reaching near the enrichment limit around 1940, with a $\delta^{18}O$ of around 2.3 ‰ and $\delta^{2}H$ value of 14 ‰. Gnotuk neared the enrichment limit faster, reaching similar values in 1920 (Fig. 5.9c & d). Beginning the model runs with initial isotope values near the enrichment limits had no effect on the simulated isotopic values from 2015 to 2018 (Fig. 5.9a).

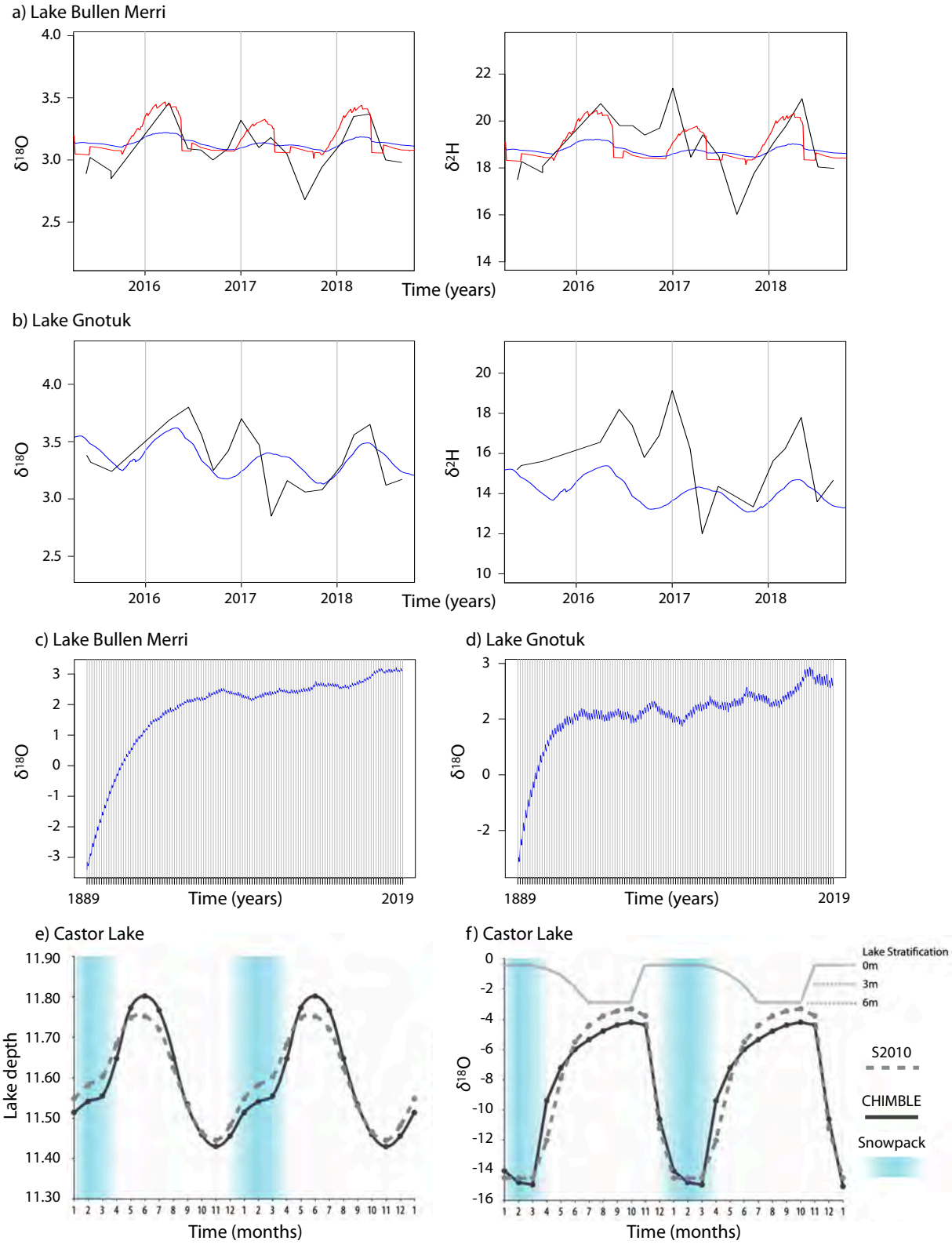

Figure 5.9: Isotopic response in Lake Bullen Merri (a) and Lake Gnotuk (b). Default modelled results are in blue, with observations shown in black. Modelled results using a shallow stratification depth for Lake Bullen Merri are shown in red. (c) $\delta^{18}O$ evolution for Lake Bullen Merri. (d) $\delta^{18}O$ evolution for Lake Gnotuk. Years on the x-axis reflect the beginning of each year.(e) Lake levels for Castor Lake for both CHIMBLE (dark grey) and S2010 (grey dashed). (f) Modelled $\delta^{18}O$ for Castor lake for CHIMBLE (dark grey) and S2010 (grey dashed).

As was the case for simulated TDS values, the altered lake stratification depth for Lake Bullen Merri resulted in a better approximation of lake water $\delta^{18}O$ and $\delta^{2}H$, and the spread of modelled seasonal $\delta^{18}O$ values for Bullen Merri increased to 3.0–3.45 ‰ (Fig 5.9). The sporadic sawtooth pattern in the modelled data is an artifact of the modelling process, caused by the use of averaged monthly data, resulting in a stepped, rather than smooth input time-series, in combination with sub-monthly timesteps.

Both CHIMBLE and S2010 were able to achieve a broadly similar seasonal cycle around an equilibrium lake level for Castor Lake (Fig. 5.9e & f). A *Kc* value of 0.365 for both soil layers in CHIMBLE was used to account for the differences in the soil layer modelling, resulting in similar average lake levels for both S2010 and CHIMBLE. The amplitude of the seasonal lake cycle was greater in the CHIMBLE simulation with a maximum lake level 0.05 m higher in June, and a low lake level 0.02 m lower in November, than the S2010 modelled lake levels. $\delta^{18}O$ values for CHIMBLE were typically around 1 ‰ lower than the S2010 modelled $\delta^{18}O$ values. However, under conditions where CHIMBLE simulated a lower lake level than S2010 (e.g. April and May),the $\delta^{18}O$ values simulated by CHIMBLE were higher than those modelled by S2010. The upper soil layers modelled by CHIMBLE and S2010 exhibited very different behavior, with those modelled by CHIMBLE drying out substantially to around 20% of saturated capacity during the warmer months, while the upper soil layer in S2010 rarely dropped below 60 % of saturated capacity.

5.5 Comparison with a non-groundwater enabled lake model

To test the significance of coupling the groundwater model to the lakes, both Bullen Merri and Gnotuk simulations were run without the groundwater module enabled. Instead, catchment runoff was directed to the lakes, and seepage from the lakes used to calibrate lake levels similar to Steinman et al. (2010). After an iterative selection process, an available water capacity value for each soil layer of 0.09 m was found to best achieve sufficient inflow. A seepage rate (seepage leaving the lakes as a proportion of lake volume) of 0 was applied at Bullen Merri, and 0.00055 at Gnotuk. Under these conditions, simulated lake levels were a poorer fit than groundwater enabled simulations with RMSE of 1.45 m for Gnotuk and 1.61 m for Bullen Merri (Fig. 5.5). $\delta^{18}O$, $\delta^{2}H$ and surface temperature values were not significantly different. Modelled TDS values for Bullen Merri were similar to the groundwater enabled model, requiring just a slightly lower starting value of 63 % of the 2018 values and yielding an RMSE of 193 mg/L. However, Gnotuk required initial chemistry values of 89 % of the 2018 values with an initial TDS of 63272 mg/L.

The TDS of Gnotuk then rose above 80000 mg/L in 1939, then fell to 53300 mg/L in 1996, before rising to the 2018 values of ~71000 mg/L.

6 Discussion

6.1 Calibration and simulation assessment

The primary purpose of this research was to develop and validate a holistic lake model – CHIMBLE – suitable to be applied to palaeoclimate research problems. Such applications require an efficient model able to simulate thousands of years at daily to monthly timesteps, , yet which includes sufficient functionality to resolve processes such as lake-groundwater interaction, lake water stratification, and geochemical feedbacks that are difficult to parameterize beyond the short observational timescale. CHIMBLE successfully meets these criteria. Applying CHIMBLE to Lake Bullen Merri and Lake Gnotuk demonstrated that even in poorly defined and under-determined systems, the model can give excellent results across a broad range of hydrologic change. Bullen Merri and Gnotuk have been a challenge to model in the past. Jones et al. (2001) applied a mass-balance technique but noted that the model under-estimated the lake level fall, and modelled results were 3 and 2 m higher than the 1949 observations for Bullen Merri and Gnotuk respectively. In comparison, the lake depths modelled using CHIMBLE were 0.23 m below the 1949 level for Bullen Merri, and 0.5 m above for Gnotuk, with the groundwater module enabled. More importantly, there is a high level of parsimony in the model parameters as well as the results for hydrology, chemistry and $\delta^{18}O$ and $\delta^{2}H$, across two very different lakes sharing the same climate system. Modelled hydrology and lake water chemistry in particular match observations for both craters, using the same underlying groundwater model and catchment parameters, with meteorological and energy balance parameters that correspond to each lake's morphological state and degree of sheltering. The energy balance module provides a partial test for the quality of the groundwater calibration. If the stratification module required parameters that were not compatible with observed lake surface temperatures to achieve the required amount of evaporation, then that would indicate that flows to or from the lakes were not correct.

Modelling of lake water chemistry provides an additional test of the hydrological modelling. A terminal lake, with negligible outflow will accumulate salts over time, whereas a lake with significant through-flow will flush salts with the outgoing flows, limiting the maximum salt content of the lake as a function of the solute residence time. The hydrological modelling of Bullen Merri and Gnotuk suggests that both lakes feature through-flow behaviour at high lake

levels, with Bullen Merri losing water down to Gnotuk, and Gnotuk losing water to the hypothesised seepage, then switching towards more terminal type lake behaviour at lower lake levels. The degree of groundwater through-flow and associated changes in lake water chemistry for Bullen Merri seem to be well represented, with a good match between modelled and observed salinity over several decades.

Simulated TDS values at Gnotuk were lower than the observations between 1964–1968, recorded by Timms (1976), but given the relatively small volume of Lake Gnotuk, this is most likely due to the simulated lake levels being slightly higher than observed over that timeframe. Recalculating salinity balance based on the observed lake level gives a TDS value of 53000 mg/L, within 5–10 % of the average data documented by Timms (1976). The amount of variation seen in TDS observations from 1953–2000 is a concern. In particular in Bullen Merri, a TDS range from 3000–12000 suggests that a portion of the lake water was either evaporated to 25 %, or diluted to 4x, its original volume. This may be possible under some circumstances where a very shallow stratification layer forms. Based on the annual precipitation and evaporation fluxes, the stratification depth would likely have to be somewhere less than 1 m. As Bullen Merri has a fetch of over 2 km, the chance of such a shallow stratification depth remaining stable is considered very unlikely (Imberger, 1985). While the data has been kept in the historical comparison to provide context, it has not been used for error assessment of the model runs.

The modelled isotope and lake water chemistry often shows less variability than observations, especially for Bullen Merri, when using parameters derived from the 1969–1972 observations of stratification. There are several possible explanations for this behaviour, but the most likely cause is that a smaller portion of the lake water is affected by evaporation and rainfall input, than the fully mixed lake or the deep thermocline with a large volume epilimnion estimated by CHIMBLE's energy balance module. Lake Gnotuk has a much smaller volume than Bullen Merri, even when fully mixed, and shows an isotopic and chemical response more representative of observations. In addition, the Castor Lake comparison between CHIMBLE and S2010 demonstrated that CHIMBLE can effectively model quite large seasonal isotopic variations. The minor differences in modelled lake levels and $\delta^{18}O$ values between CHIMBLE and S2010 are predominantly due to the differences in soil layer modelling. Specifically, S2010 captures more of the snowmelt in the soil layers by spreading the partitioning of infiltration through each soil layer across multiple timesteps, while at the same time maintaining a higher level of soil moisture in the upper soil throughout the year. This model design leads to a decrease of flow to the lake during very wet periods, such as during snowmelt and increased run-off to the lake during dryer months, rather than infiltration and evapotranspiration of the

upper soil layer, thus explaining the lower amplitude seasonal cycle in S2010 relative to CHIMBLE. In addition, as the $\delta^{18}O$ composition of rainfall for Castor Lake increases from March through to June, (-15.2 ‰ to -10.2 ‰), the higher amount of run-off inflow to the lake results in an increase in the modelled $\delta^{18}O$ composition of the lake waters. In contrast, inflow to lake in CHIMBLE simulations is dominated by snowmelt with a much lower $\delta^{18}O$ value (-15.2 ‰). This is the cause of the lower $\delta^{18}O$ values in the CHIMBLE simulation, compared to the S2010 simulation. Given the observations from Gnotuk and Castor Lake, it seems likely that the differences between modelled and observed $\delta^{18}O$ and $\delta^{2}H$ values at Bullen Merri are more likely due to data scarcity, particularly with regard to the stratification of the lake, rather than the capabilities of the isotopic modelling component of CHIMBLE.

If uncertainty in the depth of lake stratification is the primary cause of the difference between modelled and observed $\delta^{18}O$ and $\delta^{2}H$ variability, then that would suggest two possibilities. The first is that the stratification regime for Bullen Merri may be quite variable, with the seasonal thermocline depth changing significantly over the years. The second possibility is that the thermocline formation may be more complex than allowed for with the two reservoir system of CHIMBLE. For example, Imberger (1985) describes the seasonal thermocline as an accumulation of past diurnal stratification and mixing. The first of these possibilities was assessed during the modelling process. Stratification depth in CHIMBLE is primarily defined by the shortwave extinction coefficient. In clear water conditions shortwave radiation can penetrate to greater depth, resulting in formation of a deep thermocline. However, if water turbidity is high, for example due to algal blooms, then a shallow thermocline may form, which can isolate the deeper lake and effectively limit the volume of lake water subjected to changes in influx and evaporation. This scenario was tested by modifying the shortwave extinction coefficient over the course of the model run, with a decrease in stratification depth from ~20 m, to ~15 m from 2005 to ~5 m in 2015 sufficient to match most of the observed seasonal variability for lake water TDS and isotopes (Fig. 5.8). This suggests a decrease in visibility through the water column, and an associated rise in the depth of thermocline formation for Lake Bullen Merri, possibly indicating increased eutrophication, as has been observed at other lakes in the region (Timms, 2005). It also raises the prospect that modelling combined with near shore grab samples may be a useful method to assess stratification processes in water bodies where taking depth profiles is not feasible. There is a possibility that CHIMBLE may be able to model more complex stratification processes such as diurnal stratification as described in Imberger (1985) using daily data, and future research should explore modifying the simple twin lake reservoir model to incorporate multiple layers, as used in the energy balance module. A

third possible explanation for the data-model mismatch is that samples taken at the lake edge may not be representative of the entire epilimnion, with the shallow water along the shoreline being influenced to a greater extent by evaporation and inflow than the central lake waters. This third possibility requires significant further research to determine feasibility, assessing shoreline morphology and the meteorological conditions leading up to sample collection. Complex stratification processes, and the representativeness of near shore grab samples are of concern, especially if applying CHIMBLE to investigate phenomena occurring at a high temporal frequency (e.g. stratification formation on a daily scale). However, as CHIMBLE is predominantly focussed on research over long time scales, using monthly averaged timeseries, then the need for simulating all observational variability is reduced, and focus should be on acquiring sufficient monitoring data for calibration so that an average seasonal cycle can be determined.

6.2 Implications for lake-based palaeoclimatology/palaeohydrology

A common interpretation in lake based palaeoclimate studies is that higher $\delta^{18}O$ and $\delta^{2}H$ values reflect a dryer hydroclimate and accompanying changes in the P/E ratio and lake water balance (Leng and Marshall, 2004). The simulations of Lake Bullen Merri and Lake Gnotuk demonstrate a scenario where $\delta^{18}O$ and $\delta^{2}H$ become disconnected from lake water level, with very little isotopic change for the last 7–8 decades (Fig. 5.9c & d), despite a lake level fall of 6-10 m. The modelled $\delta^{18}O$ and $\delta^{2}H$ late in the model run are not very sensitive to initial isotopic values. As the lake levels fall the $\delta^{18}O$ and $\delta^{2}H$ values initially increase. However, as the lake water becomes more enriched in $\delta^{18}O$ and $\delta^{2}H$, the vapour at the lake surface also becomes more enriched until the isotopic composition of the evaporating flux is similar to the lake water, and the enrichment process of the lake ceases. This is well recognised in the literature, as the limit of isotopic enrichment (e.g., Gat, 2010; Gibson et al., 2015). Once a lake nears its isotopic enrichment limit, then the change in $\delta^{18}O$ and $\delta^{2}H$ of the lake no longer reflects the change in lake level, but instead typically oscillates around a seasonal cycle, with wet season rainfall driving the lake to more negative $\delta^{18}O$ and $\delta^{2}H$, before returning to near the limit of isotopic enrichment during periods of evaporation. This behaviour presents a challenge for interpretation of palaeoclimate proxies based on $\delta^{18}O$ and $\delta^{2}H$. Testing hypothesized past climates using a modelling technique may inform researchers about scenarios in which lake water isotopes are likely to become disconnected from lake water level (and therefore no longer represent changes in P/E ratio), and may also resolve disparities with other proxies such as those based on salinity. Perhaps more importantly, modelling may be able to identify periods within proxy archives that show isotopic shifts when $\delta^{18}O$ and $\delta^{2}H$ are likely to be disconnected from lake level change. If the $\delta^{18}O$ and

δ^2H of the lake can be separated from the lake water balance, then δ^{18}O and δ^2H within lake sediments reflecting those time periods are predominantly controlled by water temperature and the isotopic composition of source water, typically precipitation (Leng and Marshall, 2004).

6.3 Implications for calibrating CHIMBLE for other lake systems

Calibration of CHIMBLE to a lake system is subject to a complex array of parameters, such as the initial volume and geochemical composition of reservoirs, and isotope fractionation and energy balance parameters. However, the most challenging parameters to resolve for the Lake Bullen Merri and Lake Gnotuk simulations were related to the lake-groundwater interaction. While many parameters had a relatively direct affect upon model behaviour, the lake-groundwater interaction was very non-linear in nature, presenting challenges to relating parameters to model behaviour. In spite of this, some tentative relationships were identified. The conductivity of the surrounding geology and the extent of low conductivity zones within the crater had an apparent effect on the modelled hydrological behavior of both lakes. Both lakes require groundwater low flows at high lake levels, with groundwater flows increasing as lake levels fall. A larger zone of low hydraulic conductivity within the crater decreased the sensitivity of the lake level to precipitation change at high levels, making Bullen Merri less likely to undergo a sufficiently rapid fall from 1889 to 1940. A larger low conductive zone also made the lake more sensitive at lower levels as the distance from the lake shoreline to the more highly conductive surrounding geology was greater, resulting in lower groundwater gradients and lower flows to the lake. The hydraulic conductivity of the zone outside the craters is very strongly linked to the rate of lake level fall from 1889 to 1940. High rates of hydraulic conductivity result in a very rapid lake level drop, as groundwater is able to rapidly flow to Gnotuk or to the fixed head boundaries on the extent of the groundwater model. The hypothesised seepage through the diatreme and eruption feeder within the Gnotuk crater to lower aquifers is very uncertain. It is apparent that Gnotuk requires a significant secondary sink nearby, to account for the low lake levels and low inflow (that increases with lake level fall). Raiber et al. (2008) determined that eruption sites are often zones of preferential recharge to lower aquifers. We have not attempted to quantify the amount of water lost via seepage. If the seepage occurs at the ring faults commonly found around the perimeter of diatreme structures (White and Ross, 2011), and abutting the highly permeable surrounding geology, that would suggest a seepage loss to lower aquifers of around 600000 m^3 per month, which seems highly unlikely. However, if the seepage zone were within the low conductivity sediments within the upper diatreme, essentially representing a perched lake, then seepage could be quite low. Although the spatial relationship between Lake Gnotuk and the seepage zone is well defined,

with variations to that relationship heavily influencing the lake water level and through-flow behaviour, the relationship between the proposed seepage and surrounding geology is very uncertain. Further work incorporating information from the deeper aquifers and their potential recharge rates may help define the groundwater system beneath the lakes.

The challenge of modelling the groundwater around Gnotuk does emphasise a very important advantage CHIMBLE has compared with lake models that are not groundwater enabled. The groundwater in the region is not well defined and the modelling in this research had to rely on an exploration of multiple parameters, with the goal of achieving a modelling "best fit" between observations while maintaining parameter values within their likely range. While it would always be preferable to have a full suite of information available to calibrate models, such data is not commonly available for many palaeoclimate sites. However, if future groundwater studies in the region provide information on seepage, hydraulic conductivity, and water table levels then that data can be incorporated directly within CHIMBLE as the groundwater component uses common groundwater modelling techniques. CHIMBLE in this way enables and emphasises the value of cross-disciplinary research.

6.4 Future model development

The CHIMBLE model presented here includes novel functionality for modelling lake-climate interactions over decades to centennial timescales, including modelling of groundwater, energy balance, and lake water geochemistry. However, there are still many aspects to be considered for future development. The snow/ice aspect of CHIMBLE is currently quite rudimentary, with limited support for freezing of the lake surface water. Future developments will focus on incorporating ice formation on the lake, and snowfall on the catchment and lake ice, and the accompanying effect on isotopic fractionation and lake energy balance. While such functionality is not exactly a high priority for lakes in Australia it is relevant to studies in other regions. The groundwater is currently treated as a single reservoir, with single $\delta^{18}O$, $\delta^{2}H$ and major anion/cation values shared across all cells. Future CHIMBLE development aims to support per-cell values for isotopes and chemistry, to account for situations such as lakes that seep out to groundwater at high levels, before reversing flows as lake levels fall. In such scenarios, the groundwater in the seepage zone will partially consist of lake outseepage, with a $\delta^{18}O$, $\delta^{2}H$ and salinity composition that likely differs from the regional groundwater. Upon flow reversal this water may return to the lake representing an input to the lake that differs (temporarily) from the regional groundwater.

The energy balance module matches observations for Bullen Merri and Gnotuk, but some lakes used for palaeoclimate research are quite shallow (< 20 m), or become shallow over their lifespans. The energy balance module does not yet model sediment warming, which may be necessary for modelling of shallow water bodies. An important future goal in model development is to couple an ecology module, partly for the value of linking ecology to lake conditions and proxies, and more importantly, to provide an estimate for the short wave extinction coefficient, based on lake conditions, removing the requirement for an observation based parameter. Finally, there is a need to link lake morphology and water level to atmospheric feedback, lake water surface roughness, isotopic fractionation and windspeed to account for changes in sheltering.

Ongoing data collection is also necessary. Lake Bullen Merri and Lake Gnotuk have some of the longest records in the Newer Volcanic Province for historical lake water levels, water chemistry and water temperature, recording significant changes in lake conditions over decadal timeframes. Such long timeseries of lake hydrology provide a degree of confidence in the parameters determined for the model simulations. However, there are still issues of data scarcity, presenting a challenge to define and validate parameters for lake conditions outside of the observational record. For example, there is only a short isotopic record which does not match up temporally with records of lake stratification, thereby removing the opportunity to validate the hypothesized parameters for stratification derived from the isotopic calibration against observations. An important consideration is that the calibration of a lake model does not necessarily benefit most from observations over long time frames, but instead from observations that document significant changes in lake conditions.

7 Conclusion

Lake process modelling is an important tool for lake palaeoclimate research, with potential to improve interpretations of lake sediments, quantify the relationships between climate and lake behaviour, and identify common climate trends from lakes exhibiting different hydroclimate responses. In this paper we present a new model – CHIMBLE – coupling groundwater, catchment processes, lake energy balance, water chemistry and water stable isotopes. CHIMBLE was applied to the neighbouring maar lakes Bullen Merri and Gnotuk in Victoria, Australia. Simulations for both lakes, using the same underlying groundwater system and parameters parsimonious with the lakes' morphological and hydrological states produced results that aligned well with each lake's hydrological behaviour over 130 years, including a 20 m change in lake water level. Modelled surface temperatures matched observations within 1.8 °C RMSE,

whereas lake water chemistry and stable isotope ratios exhibited inter- and intra-annual patterns which captured many of the features of the observed patterns, with differences accredited to the possibility of a poorly mixed epilimnion, particularly at Lake Bullen Merri. The isotopic calibration of $\delta^{18}O$ and $\delta^{2}H$ demonstrated a situation where isotopes become disconnected from lake level, with both lakes reaching an isotopic enrichment limit after a lake level fall of ~10 m, with a further lake level fall of ~8 m resulting in very little isotopic change. This tendency for isotopes of water to become disconnected from lake water balance emphasises the need for holistic models such as CHIMBLE, where model simulations may explain disparate results from different proxies.

8 References

Alduchov, O.A., Eskridge, R.E., 1996. Improved Magnus Form Approximation of Saturation Vapor Pressure. Journal of Applied Meteorology, 35(4): 601-609. DOI:10.1175/1520-0450(1996)035<0601:IMFAOS>2.0.CO;2

Allen, R.G., Pereira, L.S., Raes, D., Smith, M., 1998. Crop evapotranspiration-Guidelines for computing crop water requirements-FAO Irrigation and drainage paper 56. FAO, Rome, 300(9): D05109.

Anderson, M.P., Woessner, W.W., Hunt, R.J., 2015. Applied groundwater modeling: simulation of flow and advective transport. Academic press.

Ankor, M.J., Tyler, J.J., 2019. Development of a spreadsheet-based model for transient groundwater modelling. Hydrogeology Journal: 1-14.

Ankor, M.J., Tyler, J.J., Hughes, C.E., 2019. Development of an autonomous, monthly and daily, rainfall sampler for isotope research. Journal of Hydrology, 575: 31-41. DOI:https://doi.org/10.1016/j.jhydrol.2019.04.074

Barr, C., Tibby, J., Gell, P., Tyler, J., Zawadzki, A., Jacobsen, G.E., 2014. Climate variability in south-eastern Australia over the last 1500 years inferred from the high-resolution diatom records of two crater lakes. Quaternary Science Reviews, 95: 115-131. DOI:https://doi.org/10.1016/j.quascirev.2014.05.001

Barton, C.E., Polach, H.A., 1980. 14 C ages and magnetic stratigraphy in three Australian maars. Radiocarbon, 22(3): 728-739.

Battarbee, R.W., 2000. Palaeolimnological approaches to climate change, with special regard to the biological record. Quaternary Science Reviews, 19(1–5): 107-124. DOI:http://dx.doi.org/10.1016/S0277-3791(99)00057-8

Bayly, I.A.E., Williams, W.D., 1966. Further chemical observations on some volcanic lakes of south-east Australia of South Australia. Marine and Freshwater Research, 17(2): 229-238.

Bennett, K., Gibson, J., McEachern, P., 2008. Water-yield estimates for critical loadings assessment: comparisons of gauging methods versus an isotopic approach. Canadian Journal of Fisheries and Aquatic Sciences, 65(1): 83-99.

Blaikie, T.N., Ailleres, L., Betts, P.G., Cas, R.A.F., 2014. A geophysical comparison of the diatremes of simple and complex maar volcanoes, Newer Volcanics Province, south-eastern Australia. Journal of Volcanology and Geothermal Research, 276: 64-81.

Boughton, W., 2005. Catchment water balance modelling in Australia 1960–2004. Agricultural Water Management, 71(2): 91-116.

Boyce, J., 2013. The Newer Volcanics Province of southeastern Australia: a new classification scheme and distribution map for eruption centres. Australian Journal of Earth Sciences, 60(4): 449-462.

Cadd, H.R., Tibby, J., Barr, C., Tyler, J., Unger, L., Leng, M.J., Marshall, J.C., McGregor, G., Lewis, R., Arnold, L.J., Lewis, T., Baldock, J., 2018. Development of a southern hemisphere subtropical wetland (Welsby Lagoon, south-east Queensland, Australia) through the last glacial cycle. Quaternary Science Reviews, 202: 53-65. DOI:https://doi.org/10.1016/j.quascirev.2018.09.010

Chang, J.C., Woodward, C., Shulmeister, J., 2014. A snapshot of the limnology of eastern Australian water bodies spanning the tropics to Tasmania: the land-use, climate, limnology nexus. Marine and Freshwater Research, 65(10): 872-883.

Chivas, A.R., De Deckker, P., Cali, J.A., Chapman, A., Kiss, E., Shelley, G., Michael, J., 1993. Coupled Stable-Isotope and Trace-Element Measurements of Lacustrine Carbonates as Paleoclimatic Indicators. Climate change in continental isotopic records: 113-121.

Chivas, A.R., De Deckker, P., Shelley, J.M.G., 1985. Strontium content of ostracods indicates lacustrine palaeosalinity. Nature, 316(6025): 251-253. DOI:10.1038/316251a0

Cleveland, W.S., 1981. LOWESS: A program for smoothing scatterplots by robust locally weighted regression. American Statistician: 54-54.

Cohen, A.S., 2003. Paleolimnology: the history and evolution of lake systems. Oxford University Press, USA.

Craig, H., Gordon, L.I., 1965. Deuterium and oxygen 18 variations in the ocean and the marine atmosphere. In: Schink, D.R., Corless, J.T. (Eds.), Marine Geochemistry. University, Rhode Island, University, Rhode Island, pp. 277-374.

Crawford, J., Azcurra, C.S., Hughes, C.E., Gibson, J.J., Parkes, S.D., 2019. Comparison of atmospheric water vapour δ18O and δ2H estimated using evaporation pan, rainfall equilibrium and continuous measurements. Journal of Hydrology, 576: 551-560. DOI:https://doi.org/10.1016/j.jhydrol.2019.06.056

Currey, D.T., 1970. Lake systems, Western Victoria. Australian Society for Limnology Bulletin, 3: 1-13.

Dahlhaus, P., Heislers, D., Dyson, P., 2002. Corangamite Catchment Management Authority Groundwater Flow Systems. Report No. CCMA, 2(02).

Dee, S., Emile-Geay, J., Evans, M., Allam, A., Steig, E., Thompson, D., 2015. PRYSM: An open-source framework for PRoxY System Modeling, with applications to oxygen-isotope systems. Journal of Advances in Modeling Earth Systems, 7(3): 1220-1247.

Dee, S.G., Russell, J.M., Morrill, C., Chen, Z., Neary, A., 2018. PRYSM v2.0: A Proxy System Model for Lacustrine Archives. Paleoceanography and Paleoclimatology, 33(11): 1250-1269. DOI:10.1029/2018PA003413

Department of Environment Land Water and Planning Victoria Australia, Victorian Water Measurement Information System. Department of Environment, Land, Water and Planning, Victoria, Australia.

Dinçer, T., 1968. The Use of Oxygen 18 and Deuterium Concentrations in the Water Balance of Lakes. Water Resources Research, 4(6): 1289-1306.

Donders, T.H., Haberle, S.G., Hope, G., Wagner, F., Visscher, H., 2007. Pollen evidence for the transition of the Eastern Australian climate system from the post-glacial to the present-day ENSO mode. Quaternary Science Reviews, 26(11): 1621-1637.

Eddelbuettel, D., 2013. Seamless R and C++ integration with Rcpp. Springer.

Eddelbuettel, D., Francois, R., 2011. Rcpp: Seamless R and C++ Integration. 2011, 40(8): 18. DOI:10.18637/jss.v040.i08

FedUni, 2015. Visualising Victoria's Groundwater. Centre for eResearch and Digital Innovation, Federation University Australia, Mt Helen, Ballarat, Victoria, FedUni.

Fritz, S.C., Juggins, S., Battarbee, R.W., Engstrom, D.R., 1991. Reconstruction of past changes in salinity and climate using a diatom-based transfer function. Nature, 352(6337): 706.

Gat, J., 2010. Isotope hydrology a study of the water cycle. London: Imperial College Press, London.

Gibson, J., Edwards, T., Bursey, G., Prowse, T., 1993. Estimating evaporation using stable isotopes: quantitative results and sensitivity analysis for. Nordic Hydrology, 24: 79-94.

Gibson, J., Reid, R., 2014. Water balance along a chain of tundra lakes: A 20-year isotopic perspective. Journal of Hydrology, 519: 2148-2164.

Gibson, J.J., Birks, S.J., Yi, Y., 2015. Stable isotope mass balance of lakes: a contemporary perspective. Quaternary Science Reviews, 131: 316-328.

Gibson, J.J., Prepas, E.E., McEachern, P., 2002. Quantitative comparison of lake throughflow, residency, and catchment runoff using stable isotopes: modelling and results from a regional survey of Boreal lakes. Journal of Hydrology, 262(1): 128-144.

Gonfiantini, R., 1986. Environmental isotopes in lake studies. Handbook of environmental isotope geochemistry, 2: 113-168.

Gouramanis, C., De Deckker, P., Switzer, A.D., Wilkins, D., 2013. Cross-continent comparison of high-resolution Holocene climate records from southern Australia—Deciphering the impacts of far-field teleconnections. Earth-Science Reviews, 121: 55-72.

Gouramanis, C., Wilkins, D., De Deckker, P., 2010. 6000 years of environmental changes recorded in Blue Lake, South Australia, based on ostracod ecology and valve chemistry. Palaeogeography, Palaeoclimatology, Palaeoecology, 297(1): 223-237.

Hambright, K.D., Gophen, M., Serruya, S., 1994. Influence of long-term climatic changes on the stratification of a subtropical, warm monomictic lake. Limnology and Oceanography, 39(5): 1233-1242. DOI:10.4319/lo.1994.39.5.1233

Henderson-Sellers, B., 1986. Calculating the surface energy balance for lake and reservoir modeling: A review. Reviews of Geophysics, 24(3): 625-649. DOI:10.1029/RG024i003p00625

Hipsey, M., Bruce, L., Hamilton, D., 2013. GLM General Lake Model. Model overview and user information. The University of Western Australia Technical Manual, Perth, Australia.

Ho, M., Kiem, A.S., Verdon-Kidd, D.C., 2015. A paleoclimate rainfall reconstruction in the Murray-Darling Basin (MDB), Australia: 1. Evaluation of different paleoclimate archives, rainfall networks, and reconstruction techniques. Water Resources Research, 51(10): 8362-8379.

Horita, J., Wesolowski, D.J., 1994. Liquid-vapor fractionation of oxygen and hydrogen isotopes of water from the freezing to the critical temperature. Geochimica et Cosmochimica Acta, 58(16): 3425-3437.

Hostetler, S.W., Bartlein, P.J., 1990. Simulation of lake evaporation with application to modeling lake level variations of Harney-Malheur Lake, Oregon. Water Resources Research, 26(10): 2603-2612.

Hostetler, S.W., Bates, G.T., Giorgi, F., 1993. Interactive coupling of a lake thermal model with a regional climate model. Journal of Geophysical Research: Atmospheres, 98(D3): 5045-5057.

Hussainy, S.U., 1969. Ecological studies on some microbiota of lakes in western Victoria. Department of Zoology, Monash University.

Ihaka, R., Gentleman, R., 1996. R: a language for data analysis and graphics. Journal of computational and graphical statistics, 5(3): 299-314.

Imberger, J., 1985. The diurnal mixed layer. Limnology and Oceanography, 30(4): 737-770. DOI:10.4319/lo.1985.30.4.0737

Imberger, J., 2001. Characterizing the dynamical regimes of a lake. Physical processes in natural waters. Univ. de Girona, Spain: Servei de Publicacions: 77-92.

Jeffrey, S.J., Carter, J.O., Moodie, K.B., Beswick, A.R., 2001. Using spatial interpolation to construct a comprehensive archive of Australian climate data. Environmental Modelling and Software, 16(4): 309-330.

Jones, M.D., Imbers, J., 2010. Modeling Mediterranean lake isotope variability. Global and Planetary Change, 71(3): 193-200. DOI:https://doi.org/10.1016/j.gloplacha.2009.10.001

Jones, M.D., Leng, M.J., Roberts, C.N., Türkeş, M., Moyeed, R., 2005. A Coupled Calibration and Modelling Approach to the Understanding of Dry-Land Lake Oxygen Isotope Records. Journal of Paleolimnology, 34(3): 391-411. DOI:10.1007/s10933-005-6743-0

Jones, R., Bowler, J., McMahon, T., 1998. A high resolution Holocene record of P/E ratio from closed lakes in Western Victoria. Palaeoclimates, 3(1-3): 51-82.

Jones, R.N., 1999. Natural and human influences on the distribution and extent of Victorian lowland grasslands. Adv Nat Conserv, 2: 19-39.

Jones, R.N., McMahon, T.A., Bowler, J.M., 2001. Modelling historical lake levels and recent climate change at three closed lakes, Western Victoria, Australia (c.1840–1990). Journal of Hydrology, 246(1): 159-180.

Kiem, A., Vance, T., Tozer, C., Roberts, J., 2017. Incorporating palaeoclimate data into water security planning and decision making-a case study from southeast Queensland, Australia, EGU General Assembly Conference Abstracts, pp. 2021.

Kirono, D.G., Jones, R.N., Kent, D.M., 2009. Modelling future lake levels and salinity at three lakes, Western Victoria. National Research Flagships, Climate Adaptation CSIRO—A report prepared for the Environment Protection Authority (EPA) Victoria.

Last, W.M., Deckker, P., 1990. Modern and Holocene carbonate sedimentology of two saline volcanic maar lakes, southern Australia. Sedimentology, 37(6): 967-981.

Leahy, P., Robinson, D., Patten, R., Kramer, A., 2010. Lakes in the Western District of Victoria and climate change. EPA Victoria.

Leng, M.J., Marshall, J.D., 2004. Palaeoclimate interpretation of stable isotope data from lake sediment archives. Quaternary Science Reviews, 23(7): 811-831.

Lorenz, V., 2003. Maar-diatreme volcanoes, their formation, and their setting in hard-rock or soft-rock environments. Geolines, 15: 72-83.

Maddocks, G.E., 1967. The geochemistry of surface waters of the Western District of Victoria. Marine and Freshwater Research, 18(1): 35-52.

Magnus, G., 1844. Versuche über die Spannkräfte des Wasserdampfs. Annalen der Physik, 137(2): 225-247. DOI:10.1002/andp.18441370202

McDonald, M.G., Harbaugh, A.W., 1988. A modular three-dimensional finite-difference ground-water flow model.

McVicar, T.R., Van Niel, T.G., Li, L.T., Roderick, M.L., Rayner, D.P., Ricciardulli, L., Donohue, R.J.C.L., 2008. Wind speed climatology and trends for Australia, 1975,Äì2006: Capturing the stilling phenomenon and comparison with near-surface reanalysis output. 35(20).

Morton, F.I., 1983. Operational estimates of areal evapotranspiration and their significance to the science and practice of hydrology. Journal of Hydrology, 66(1–4): 1-76. DOI:http://dx.doi.org/10.1016/0022-1694(83)90177-4

Neilson, R.P., 1995. A model for predicting continental-scale vegetation distribution and water balance. Ecological Applications, 5(2): 362-385.

Neukom, R., Gergis, J., 2012. Southern Hemisphere high-resolution palaeoclimate records of the last 2000 years. The Holocene, 22(5): 501-524. DOI:10.1177/0959683611427335

Nicolaides, S., 1997. Marine-derived dolomite in the shallowly buried temperate Port Campbell Limestone (Miocene), Otway Basin, Australia. Sedimentology, 44(1): 143-157. DOI:10.1111/j.1365-3091.1997.tb00429.x

Obrochta, S., Yokoyama, Y., Yoshimoto, M., Yamamoto, S., Miyairi, Y., Nagano, G., Nakamura, A., Tsunematsu, K., Lamair, L., Hubert-Ferrari, A., 2018. Mt. Fuji Holocene eruption history reconstructed from proximal lake sediments and high-density radiocarbon dating. Quaternary Science Reviews, 200: 395-405.

Panigrahi, B., Panda, S.N., 2003. Field test of a soil water balance simulation model. Agricultural Water Management, 58(3): 223-240.

Raiber, M., Webb, J.A., Jacobsen, G.E., Chisari, R., Williams, A.A., 2008. Geological Controls on the Spatial Variability of Groundwater Recharge and Salinity in a Regional-scale Basalt Aquifer in Western Victoria. Modbury, SA: Engineers Australia

Causal Productions, pp. 1279-1283.

Ricketts, R.D., Johnson, T.C., 1996. Climate change in the Turkana basin as deduced from a 4000 year long δO 18 record. Earth and Planetary Science Letters, 142(1): 7-17.

Robinson, R., Bower, V., 1965. An additivity rule for the vapor pressure lowering of aqueous solutions. J. Res. Nat. Bur. Stand. A, 69: 365-367.

Rudd, R.C., Tyler, J.J., Tibby, J., Yokoyama, Y., Tavernier, I., Verleyen, E., Fukui, M., Takano, Y., 2016. A diatom-inferred record of lake variability during the last 900 years in Lützow–Holm Bay, East Antarctica. Journal of Quaternary Science, 31(2): 114-125. DOI:10.1002/jqs.2845

Sachse, D., Radke, J., Gleixner, G., 2004. Hydrogen isotope ratios of recent lacustrine sedimentary n-alkanes record modern climate variability. Geochimica et Cosmochimica Acta, 68(23): 4877-4889.

Shapley, M.D., Ito, E., Donovan, J.J., 2008. Isotopic evolution and climate paleorecords: modeling boundary effects in groundwater-dominated lakes. Journal of Paleolimnology, 39(1): 17-33.

SKM, 2009. The Victorian Aquifer Framework – Summary report submitted to DSE, Melbourne.

Steinman, B.A., Abbott, M.B., Mann, M.E., Stansell, N.D., Finney, B.P., 2012. 1,500 year quantitative reconstruction of winter precipitation in the Pacific Northwest. Proceedings of the National Academy of Sciences, 109(29): 11619-11623. DOI:10.1073/pnas.1201083109

Steinman, B.A., Rosenmeier, M.F., Abbott, M.B., Bain, D.J., 2010. The isotopic and hydrologic response of small, closed-basin lakes to climate forcing from predictive models: Application to paleoclimate studies in the upper Columbia River basin. Limnology and Oceanography, 55(6): 2231–2245.

Stets, E.G., Winter, T.C., Rosenberry, D.O., Striegl, R.G., 2010. Quantification of surface water and groundwater flows to open- and closed-basin lakes in a headwaters watershed using a descriptive oxygen stable isotope model. Water Resources Research, 46(3). DOI:10.1029/2009WR007793

Talbot, M.R., 1990. A review of the palaeohydrological interpretation of carbon and oxygen isotopic ratios in primary lacustrine carbonates. Chemical Geology: Isotope Geoscience section, 80(4): 261-279. DOI:https://doi.org/10.1016/0168-9622(90)90009-2

Tibby, J., Tiller, D., 2007. Climate–water quality relationships in three Western Victorian (Australia) lakes 1984–2000. Hydrobiologia, 591(1): 219-234. DOI:10.1007/s10750-007-0804-5

Tierney, J.E., Smerdon, J.E., Anchukaitis, K.J., Seager, R., 2013. Multidecadal variability in East African hydroclimate controlled by the Indian Ocean. Nature, 493(7432): 389.

Timms, B.V., 1976. A Comparative study of the limnology of three maar lakes in western Victoria. I. Physiography and physicochemical features. Marine and Freshwater Research, 27(1): 35-60.

Timms, B.V., 2005. Salt Lakes in Australia: Present Problems and Prognosis for the Future. Hydrobiologia, 552(1): 1-15. DOI:10.1007/s10750-005-1501-x

Tweed, S., Leblanc, M., Cartwright, I., 2009. Groundwater–surface water interaction and the impact of a multi-year drought on lakes conditions in South-East Australia. Journal of Hydrology, 379(1–2): 41-53. DOI:http://dx.doi.org/10.1016/j.jhydrol.2009.09.043

Tyler, J., Leng, M., Sloane, H., Sachse, D., Gleixner, G., 2008. Oxygen isotope ratios of sedimentary biogenic silica reflect the European transcontinental climate gradient. Journal of Quaternary Science, 23(4): 341-350.

Tyler, J.J., Jones, M., Arrowsmith, C., Allott, T., Leng, M.J., 2015. Spatial patterns in the oxygen isotope composition of daily rainfall in the British Isles. Climate Dynamics(January 2016). DOI:10.1007/s00382-015-2945-y

Valiantzas, J.D., 2006. Simplified versions for the Penman evaporation equation using routine weather data. Journal of Hydrology, 331(3): 690-702.

Van Boxel, J.H., González-Carranza, Z., Hooghiemstra, H., Bierkens, M., Vélez, M.I., 2013. Reconstructing past precipitation from lake levels and inverse modelling for Andean Lake La Cocha. Journal of Paleolimnology, 51(1): 63-77. DOI:10.1007/s10933-013-9755-1

Victorian Department of Sustainability and Environment, 2012. Victorian Aquifer Framework: updates for seamless mapping of aquifer surfaces. Produced by GHD for the Victorian Department of Sustainability and Environment.

Victorian Department of Sustainability and Environment, 2014. Victorian Aquifer Framework - Grids, Bioregional Assessment Source Dataset. Victorian Department of Sustainability and Environment.

White, J.D.L., Ross, P.S., 2011. Maar-diatreme volcanoes: A review. Journal of Volcanology and Geothermal Research, 201(1): 1-29.

Wigdahl, C.R., Saros, J.E., Fritz, S.C., Stone, J.R., Engstrom, D.R., 2014. The influence of basin morphometry on the regional coherence of patterns of diatom-inferred salinity in lakes

of the northern Great Plains (USA). The Holocene, 24(5): 603-613. DOI:10.1177/0959683614523154

Wilkins, D., Gouramanis, C., De Deckker, P., Fifield, L.K., Olley, J., 2013. Holocene lake-level fluctuations in Lakes Keilambete and Gnotuk, southwestern Victoria, Australia. The Holocene, 23(6): 784-795. DOI:10.1177/0959683612471983

Williams, W., 1966. Conductivity and the concentration of total dissolved soilds in Australian lakes. Marine and Freshwater Research, 17(2): 169-176.

Williams, W.D., 1981. 19. The limnology of saline lakes in Western Victoria. Hydrobiologia, 81-82(1): 233-259. DOI:10.1007/BF00048719

Winter, T.C., 1976. Numerical simulation analysis of the interaction of lakes and ground water. USGS Professional Paper 1001.

Winter, T.C., 1978. Numerical simulation of steady state three-dimensional groundwater flow near lakes. Water Resources Research, 14(2): 245-254. DOI:10.1029/WR014i002p00245

Winter, T.C., Rosenberry, D.O., LaBaugh, J.W., 2003. Where does the ground water in small catchment come from? Groundwater, 41(7): 989-1000. DOI:10.1111/j.1745-6584.2003.tb02440.x

Wolfe, B.B., Edwards, T.W., Elgood, R.J., Beuning, K.R., 2002. Carbon and oxygen isotope analysis of lake sediment cellulose: methods and applications, Tracking environmental change using lake sediments. Springer, pp. 373-400.

Yihdego, Y., Webb, J.A., Leahy, P., 2015. Modelling of lake level under climate change conditions: Lake Purrumbete in southeastern Australia. Environmental Earth Sciences, 73(7): 3855-3872. DOI:10.1007/s12665-014-3669-8

Chapter 6

Discussion and future directions

Summary

The primary aim of this thesis was to develop a lake model for palaeoclimate research, expanding upon previous models to improve the state of the art. This was achieved with the development of CHIMBLE, a holistic lake model incorporating many key features from previous models, and addressing key uncertainties with previous models through inclusion of complex groundwater modelling and full water chemistry. However, when reflecting back over the model development, the calibration process, and other related lake physical processes, such as the link between basin morphology and evaporation and isotopic fractionation, it may be possible to chart out a course for future lake modelling developments. This chapter summarises the outcomes of this thesis against the original objectives, and how the models, methods and collected data may be applied within the greater field of palaeoclimate research. In conclusion, some suggestions are made regarding directions for future model developments and research projects focussed on lake physical processes.

1 Objectives

1.1 Objective 1: Establish a lake monitoring program to collect input and calibration data that can be applied to the model.

Chapter Two describes the results from a lake monitoring program, with data from twelve lakes, collected bi-monthly over ~3 years. Samples for major and minor ion, $\delta^{18}O$, and $\delta^{2}H$ analysis, as well as water temperature, pH, and conductivity were collected for all lakes, and water levels for most lakes. The hydrogeology surrounding each lake was identified and described. In addition to the data described in Chapter Two, Lake Leake, Lake Edward and Lake Surprise were also surveyed for bathymetry, and aerial photos were used to reconstruct historical lake water levels for Lake Leake and Lake Edward (Appendix 2). Lake levels were not recorded for Lake Tooliorook and Lake Keilambete, but both lakes are ideally suited to aerial imagery based lake level reconstructions. These data, combined with the data described in Chapter Two, are intended as an initial data set to enable CHIMBLE to model lakes across the region. There is ongoing palaeoclimate research at many of the lakes monitored (Barr et al., 2014; Falster et al., 2018; Wilkins et al., 2013), and it is anticipated that CHIMBLE model simulations and the data collected will be a valuable resource for interpretation of palaeoclimate archives, and to refine conceptual models for how each lake behaves under different hydroclimate conditions.

1.2 Objective 2: Investigate numerous geochemical and isotopic indicators of lakes to better identify how lakes interact with the surrounding landscape, and what physical processes are under-represented in conceptual and numerical lake models.

A key process in lake modelling is the conceptualisation of how a lake interacts with the surrounding landscape. The surrounding topography and hydrogeology of a lake influence the isotopic and geochemical signatures of lake water. In Chapter Two, several isotopic and geochemical indicators were applied to investigate these interactions. One aspect that is rarely considered during lake isotope studies, but is potentially an important factor in lake isotopic modelling is how the degree of wind sheltering affects isotopic fractionation. Water enrichment of $\delta^{18}O$ and $\delta^{2}H$ due to evaporation varies along a linear trend due to differences in the relative degree of transport fractionation, with the data plotting along local evaporation lines in $\delta^{18}O$ and $\delta^{2}H$ space. Water evaporating from soil, through a complete diffusion layer, forms local evaporation lines with a slope of 2.5, whereas open water evaporation from lakes has a much steeper local evaporation slope, typically from 4 to 6. $\delta^{18}O$ and $\delta^{2}H$ data for the monitored lakes suggests that the transition from fully sheltered to unsheltered is identifiable within the local evaporation lines slopes for each lake. The slopes of the local evaporation lines were correlated to the degree of sheltering of each lake, with the well sheltered lakes having a lower slope of around 4.3, while the unsheltered lakes have slopes of around 5.3.

Cl^-/Br^- and HCO_3^-/Cl^- ratios were used to investigate source water contributions to each lake. Cl^-/Br^- ratios recorded in groundwater across the region have a mass ratio of ~290, similar to sea water (Barton et al., 2013; Cartwright et al., 2006), while observations of Cl^-/Br^- in rainfall suggest a ratio ranging from 130–180 near the coast, decreasing further inland (Davis et al., 1998). An expected trend relating Cl^-/Br^- ratio to distance from the coast was not observed in the monitoring data, but the Cl^-/Br^- ratios were able to identify which lakes are likely to interact with the regional aquifers, and which lakes are likely to be rainfall fed. Lake Leake, Lake Edward and Lake Mumblin all sit high in the basalt above the regional aquifers, and have low Cl^-/Br^- ratios. These results are interpreted to reflect that these lakes are predominantly fed with rainfall, with any influxes of halite or other sources that may influence the Cl^-/Br^- ratio being flushed downward to the regional aquifer.

HCO_3^-/Cl^- is suggested as an indicator to identify whether source water is predominantly derived from surface and interflow sources or groundwater (Barton et al., 2013). High HCO_3^-

/Cl^- ratios are interpreted as surface water sources as HCO_3^- is thought to concentrate in the upper soil due to evapotranspiration and carbonate precipitation (Barton et al., 2013). A possible complexity in the application of HCO_3^-/Cl^- ratios to determine source water was noticed, with the freshwater Lakes Purrumbete and Surprise reporting extremely high HCO_3^-/Cl^- ratios, while likely being predominantly groundwater fed through-flow lakes. Lake Purrumbete has been successfully modelled as a through-flow lake (Yihdego et al., 2015). It is suspected that this mismatch is due to the presence of fresh volcanic ejecta near the lakes (often referred to as stony rises). These are regions of high recharge and may result in groundwater in those regions having high HCO_3^-/Cl^- ratios. It is suggested that a higher spatial resolution of sampling, and assessing each lake against the surrounding groundwater may improve the results from the indicator.

The lake-groundwater interaction of each lake was assessed using d-excess, following Barton et al. (2013). This indicator is based on the concept that lakes with high residence times are likely to be terminal lakes, and undergo a greater degree of evaporation, whereas through-flow lakes are likely to have shorter residence times (Barton et al., 2013). Unfortunately, the seasonal variation of d-excess was significant for many lakes, especially for lakes that are shallow. Two issues were identified with the use of d-excess to differentiate lake-groundwater interactions. The first is that d-excess is determined partly by the degree of evaporation, but also by the local evaporation line slope. More sheltered lakes are likely to report higher values of d-excess, compared to unsheltered lakes with similar lake-groundwater regimes. The second is that d-excess is a measure of the residence time of lake water – which, as most of the lakes in the region have ~1000 mm of evaporation per year, can be loosely approximated as the lake depth in metres. It is proposed that a more appropriate indicator of the type of groundwater regime is the solute residence time, which is a measure of how long a solute, such as Cl- remains in the lake (Brezonik, 2018).

From a model development perspective, refining the influence of lake morphology on isotopic fractionation is the most important outcome from Chapter Two. The isotopic fractionation equations within CHIMBLE (also used in many other lake-isotope models) have a parameter to account for turbulence effects (n). Likewise, most equations that are used to estimate evaporation include a wind parameter, e.g., the neutral drag coefficient in the case of the energy balance model in CHIMBLE. Currently the two parameters are uncoupled, but both describe a very similar process. A potential future research project is to either couple the isotopic fractionation equations directly to the evaporation equations, or, at the very least, to identify a method to allow both sets of equations to share a single wind/turbulence parameter. Coupling

these parameters would exemplify the ongoing goal to simplify and refine model parameters and would be beneficial to both CHIMBLE and other isotope enabled model development.

1.3 Objective 3: Develop new techniques for the sampling of rainfall, specifically for $\delta^{18}O$ and $\delta^{2}H$ analysis.

Chapter Three describes the development of an autonomous rainfall sampler. The development of a rainfall sampler may not seem directly related to lake model development. It is, however, intended to resolve a problem related to lake modelling that cannot easily be solved through lake model development alone. The $\delta^{18}O$ and $\delta^{2}H$ composition of rainfall is an important input dataset for many lake models. Currently the $\delta^{18}O$ and $\delta^{2}H$ composition of rainfall can be estimated through interpolation of existing datasets, e.g., the GNIP dataset (Bowen and Revenaugh, 2003; Rozanski et al., 1993), or through isotope enabled climate models (e.g.,Brady et al., 2019). However, the GNIP dataset has a limited spatial and temporal resolution, with only 15 stations across Australia. The rainfall sampler described in Chapter Three is a low cost, autonomous daily and monthly sampler. Many lakes used for palaeoclimate research are in remote areas with minimal infrastructure. The sampler is intended to be deployed in such environments to provide direct observations of the $\delta^{18}O$ and $\delta^{2}H$ of rainfall near study sites, allowing researchers to confirm the validity of modelled or interpolated $\delta^{18}O$ and $\delta^{2}H$ values. Collecting daily, in addition to monthly, rainfall may facilitate further investigation of the synoptic climatology behind daily variability in rainfall $\delta^{18}O$ and $\delta^{2}H$, for example, via synoptic back tracing (Tyler et al., 2015).

1.4 Objective 4: To develop a holistic lake model that is versatile enough to be applied to almost any lake, coupling mass and energy balances, groundwater, isotopes, chemistry, and catchment processes.

Chapters Four and Five detail model development. Chapter Four describes a spreadsheet-based finite difference groundwater model (A2016), based on the mathematics of MODFLOW. Chapter Five describes the development of a lake model that includes many features desirable for model-based palaeoclimate research, including the groundwater functionality of A2016.

The functionality and theoretical background of A2016 is fully described within this thesis, but one aspect that has not been discussed, beyond noting that it is potentially useful for prototyping and pedagogy, is how it may be useful in practice. As A2016 is a spreadsheet model, running in Excel, it is a very quick and efficient way to test hypotheses about the behaviour of

groundwater. A specific example is found in the investigation of the observation that as a lake level falls, the influx from groundwater may decrease. This is surprising and unintuitive behaviour; however, testing through A2016 demonstrated that it is compatible with existing groundwater theory. This behaviour is explained by a phenomenon whereby the lake's shoreline moves horizontally away from the groundwater source as the lake level falls, potentially resulting in a decrease of the groundwater gradient. It is hoped that A2016 is useful to other researchers, both to explore lake-groundwater interactions, and to provide a template for others to include groundwater modelling within their own lake models.

CHIMBLE, described in Chapter Five, is designed to facilitate lake-modelling based palaeoclimate research. To accommodate common proxies used in palaleoclimate research, CHIMBLE includes a full chemical mass balance, with support for individual ions, TDS, and salinity, as well as a complete $\delta^{18}O$ and $\delta^{2}H$ mixing and fractionation model. The chemical mass balance is also applied to model the effect of salinity on evaporation, which may be significant in hypersaline lakes, with potential to lower evaporation rates by several percent (~5 % in Lake Gnotuk currently), and influence the relative fractionation of $\delta^{18}O$ and $\delta^{2}H$ (Gat, 2010). Groundwater is incorporated into CHIMBLE through a single layer finite difference model based on A2016 (documented in Chapter Four). An energy balance model based on the model of Hostetler and Bartlein (1990), and updated by Dee et al. (2018) is used to estimate evaporation, lake water temperatures and thermal stratification.

Simulations for Lake Bullen Merri and Lake Gnotuk in the Newer Volcanic Province, Victoria, Australia, were undertaken, with modelled hydrological behaviour matching observations closely over a 130 year timeframe. Salinity and water temperature simulations likewise aligned closely with observations over a ~50 year timeframe. Modelled salinity since 2005, and $\delta^{18}O$ and $\delta^{2}H$ from 2015–2019 (the timeframe for which observations exist), required a decrease in stratification depth (facilitated through adjustment to the shortwave extinction coefficient in the energy balance module), to accurately match the observed seasonal cycle of Bullen Merri, suggesting an increase in water turbidity over recent years resulting from eutrophication. The isotopic modelling results may be important to palaeoclimate interpretations due to the tendency for $\delta^{18}O$ and $\delta^{2}H$ to become disconnected from lake water levels once the $\delta^{18}O$ and $\delta^{2}H$ composition of lake waters approaches the isotopic enrichment limit (Gat, 2010). This is a potential concern for any studies that interpret proxy estimates of lake water $\delta^{18}O$ and $\delta^{2}H$ as a precipitation/evaporation indicator.

To achieve a degree of confidence in the modelling results, it was required that the groundwater model parameters be identical for both lakes, as the hydrogeology for the surrounding aquifers is not influenced by the lake condition. Multiple lake-groundwater scenarios were tested, with the final simulations suggesting that there is a significant flux through the volcanic neck and diatreme of Lake Gnotuk to lower aquifers. At high lake levels, the thickness of lake sediment near the shoreline is assumed to be fairly thin, permitting a greater degree of outseepage with a through-flow style lake-groundwater regime. As the lake level falls, the relative thickness of lake sediment increases, outseepage decreases, and Lake Gnotuk transitions to a terminal lake system. A similar result is observed for Lake Bullen Merri, though with most of the outseepage from Lake Bullen Merri contributing to Lake Gnotuk's water balance, rather than seeping to lower aquifers. Further research is required to verify and quantify this lake-groundwater behaviour. The energy balance module required lake specific parameters, as the lakes have different degrees of sheltering and fetch. The effects of sheltering and fetch were identifiable in the calibrated energy balance parameters as a decrease in the neutral drag coefficients (representing wind influence) as lake levels fell, which resulted in improved simulations of water surface temperatures for both lakes.

The simulation results and calibrated parameters are important results, but a particularly important observation from the modelling process was how each component included in CHIMBLE was able to complement and interact with other modelling routines. It was uncertain at the beginning of the model development process whether the increased complexity of CHIMBLE relative to many other models would also increase the difficulty and potential ambiguity of the calibration process. However, this was not the case, and once the groundwater module was calibrated, the rest of the calibrations were rapidly resolved. The model development of CHIMBLE was focussed on avoiding arbitrary and difficult to define parameters and input data, instead opting to use additional modelling routines, and associated parameters, that describe physical processes. Therefore, the majority of parameters used within CHIMBLE arise from real world conditions such as wind sheltering, water clarity, aquifer hydraulic conductivity, and porosity, and it is little surprise that the calibrated parameters are consistent with conditions for both lakes, and that results for each aspect of the model are consistent with results from other model components. In contrast, simulations with CHIMBLE for Lake Gnotuk with the groundwater module disabled demonstrated how an approximation that is not particularly representative of real world processes – outseepage as a function of lake volume – could result in a clear disparity between the results from the water chemistry and hydrological modelling components (Chapter Five, this thesis, Fig. 5.8). By maintaining a full

chemical mass balance in parallel with the hydrological balance, it was clear that while lake level simulation was possible (though with less accuracy than with the groundwater module enabled), the fluxes entering and exiting the lake were quite unrealistic, with very high salinity at a time of high lake levels. Such a scenario is quite unlikely as groundwater salinity around Lake Gnotuk showed no indication of hypersaline outseepage (FedUni, 2015). Likewise, Jones et al. (2001) noted the need for very different percolation constants (defining baseflow from the catchment), both for each lake, and for different simulation time frames for their model-based study of Lake Bullen Merri and Lake Gnotuk. While the percolation constant may approximate a real world process of percolation through soil layers, the assumption that all percolation flowed to the lake as baseflow, as a function of catchment area, is not likely to be correct. The combination of modelling components within CHIMBLE provides a degree of confidence in the modelling results as each component may support results from other components, and many model parameters are constrained by real world conditions and observations. Such a capability is not necessarily available for less complex lake models, and suggests that great care must be taken to ensure that the conceptual model of a lake, upon which numerical models are based, is accurate.

CHIMBLE was designed for palaeoclimate research, but it is also an ideal tool to test and develop the conceptual understanding of in-lake physical processes and interactions between lakes and the surrounding landscape. The ability to assess multiple aspects of lake behaviour with each simulation, combined with the capacity to model complex effects such as lake-groundwater interaction make CHIMBLE well suited to such investigations. In particular, the potential for there to be a degree of consilience across the multiple physical processes modelled within CHIMBLE may be an important indicator as to whether the conceptual model of a lake is valid.

2 Proposed future research

The CHIMBLE model described in this thesis includes novel functionality which is largely absent from previously published models. However, there is still potential for future improvements to CHIMBLE. Considering the process of model development, future work may focus on:

- The groundwater module currently treats the groundwater system as a single reservoir, with singular values for $\delta^{18}O$ and $\delta^{2}H$, and for the ions, TDS and salinity values in the chemical mass balance. Future versions of the groundwater module should incorporate cell

by cell values, so that localised effects such as outseepage into a small region of the groundwater model are simulated.

- A primary focus of model development was the modelling of physical processes to mitigate the need for parameters that are dependent upon the lake condition. Several parameters are still defined manually, in particular, the neutral drag coefficient that relates wind to evaporation (and *n*, the similar turbulence parameter from the isotopic fractionation equations), and the short wave extinction coefficient, that represents water turbidity. One option to avoid the requirement to manually specify these parameters is to implement further modelling. Water quality modelling is a common process in reservoir studies, due to the need to predict algal blooms and other events that may impact water supply (Davis and Koop, 2006; Hamilton and Schladow, 1997). CHIMBLE already has a full chemical mass balance and full water column temperature profile modelling. It is anticipated that these capabilities facilitate inclusion of a water quality module to avoid the need to manually specify the short wave extinction coefficient. The effect of wind sheltering is potentially easier to incorporate, as CHIMBLE already includes programming hooks in anticipation of such functions, as well as a full topographical grid, for estimating lake fetch and the degree of sheltering, as part of the groundwater module.

- While lakes used for palaeoclimate research are often quite deep, the hypothesised past lake conditions often infer time periods where those lakes are shallow. In shallow lakes, solar radiation can pass through the shallow water and directly warm the lake sediments, or the sediments may be warmed from the lake water (Hondzo, 1993). Such processes are not yet modelled in the CHIMBLE energy balance, but may be necessary for accurate modelling of such conditions.

- Similarly, the support for the freezing of lake water and snow formation in CHIMBLE is currently rudimentary. While not much of a concern for current lake conditions in Australia, CHIMBLE is intended to be applied to all lakes across all time periods, including during periods of glaciation. The inclusion of full support for snow and ice is a necessary future development.

Most projects considered for future development are focused on improving model features and capabilities. However, there is also need for ongoing work investigating the interaction between lakes and the surrounding landscape. The correlation between lake morphometry and isotopic fractionation is well defined by the lakes studied, and has also been observed in other studies

(e.g., Sveinbjörnsdóttir and Johnsen, 1992). However, the results are not sufficient to build a rigorous model linking the degree of wind sheltering to isotopic fractionation. There is a need for future studies to further define and clarify this relationship.

In parallel with the need for ongoing research into lake physical processes, there is need for ongoing lake monitoring. Lake models applied for palaeoclimate research are typically required to simulate lake conditions outside the range of observational data. Therefore, monitoring of lakes should aim to capture as large a range of lake conditions as possible to provide confidence in the validity of parameters derived for use within lake models.

The next step is to apply CHIMBLE to investigate and interpret hypothesized past climate signals within lake sedimentary archives. The main focus of this thesis was on model development, and establishing the many interlinked components necessary for a robust lake model for palaeoclimate lake research. While there is much scope for future model development, CHIMBLE is now sufficiently advanced to be applied to data beyond the observational record.

3 References

Barr, C., Tibby, J., Gell, P., Tyler, J., Zawadzki, A., Jacobsen, G.E., 2014. Climate variability in south-eastern Australia over the last 1500 years inferred from the high-resolution diatom records of two crater lakes. Quaternary Science Reviews, 95: 115-131. DOI:https://doi.org/10.1016/j.quascirev.2014.05.001

Barton, A., Herczeg, A., Dahlhaus, P., Cox, J., 2013. A geochemical approach to determining the hydrological regime of wetlands in a volcanic plain, south-eastern Australia (Chapter 7) In: Ribeiro L, Stigter TY, Chambel A et al.(eds) Groundwater and Ecosystems. IAH Selected Papers on Hydrogeology Series 18. CRC Press (Taylor and Francis). p.

Bowen, G.J., Revenaugh, J., 2003. Interpolating the isotopic composition of modern meteoric precipitation. Water Resources Research, 39(10): 1-13. DOI:10.1029/2003WR002086

Brady, E., Stevenson, S., Bailey, D., Liu, Z., Noone, D., Nusbaumer, J., Otto-Bliesner, B.L., Tabor, C., Tomas, R., Wong, T., Zhang, J., Zhu, J., 2019. The Connected Isotopic Water Cycle in the Community Earth System Model Version 1. Journal of Advances in Modeling Earth Systems, 11(8): 2547-2566. DOI:10.1029/2019ms001663

Brezonik, P., 2018. Chemical kinetics and process dynamics in aquatic systems. Routledge.

Cartwright, I., Weaver, T.R., Fifield, L.K., 2006. Cl/Br ratios and environmental isotopes as indicators of recharge variability and groundwater flow: an example from the southeast Murray Basin, Australia. Chemical geology, 231(1): 38-56.

Davis, J.R., Koop, K., 2006. Eutrophication in Australian Rivers, Reservoirs and Estuaries – A Southern Hemisphere Perspective on the Science and its Implications. Hydrobiologia, 559(1): 23-76. DOI:10.1007/s10750-005-4429-2

Davis, S.N., Whittemore, D.O., Fabryka-Martin, J., 1998. Uses of Chloride/Bromide Ratios in Studies of Potable Water. Groundwater, 36(2): 338-350. DOI:10.1111/j.1745-6584.1998.tb01099.x

Dee, S.G., Russell, J.M., Morrill, C., Chen, Z., Neary, A., 2018. PRYSM v2.0: A Proxy System Model for Lacustrine Archives. Paleoceanography and Paleoclimatology, 33(11): 1250-1269. DOI:10.1029/2018PA003413

Falster, G., Tyler, J., Grant, K., Tibby, J., Turney, C., Löhr, S., Jacobsen, G., Kershaw, A.P., 2018. Millennial-scale variability in south-east Australian hydroclimate between 30,000 and 10,000 years ago. Quaternary Science Reviews, 192: 106-122.

FedUni, 2015. Visualising Victoria's Groundwater. Centre for eResearch and Digital Innovation, Federation University Australia, Mt Helen, Ballarat, Victoria, FedUni.

Gat, J., 2010. Isotope hydrology a study of the water cycle. London: Imperial College Press, London.

Hamilton, D.P., Schladow, S.G., 1997. Prediction of water quality in lakes and reservoirs. Part I — Model description. Ecological Modelling, 96(1-3): 91-110. DOI:10.1016/S0304-3800(96)00062-2

Hondzo, M., 1993. Lake water temperature simulation model. Journal of Hydraulic Engineering, 119(11): 1251-1251.

Hostetler, S.W., Bartlein, P.J., 1990. Simulation of lake evaporation with application to modeling lake level variations of Harney-Malheur Lake, Oregon. Water Resources Research, 26(10): 2603-2612.

Jones, R.N., McMahon, T.A., Bowler, J.M., 2001. Modelling historical lake levels and recent climate change at three closed lakes, Western Victoria, Australia (c.1840–1990). Journal of Hydrology, 246(1): 159-180.

Rozanski, K., Araguás-Araguás, L., Gonfiantini, R., 1993. Isotopic patterns in modern global precipitation. Climate change in continental isotopic records: 1-36.

Sveinbjörnsdóttir, Á.E., Johnsen, S.J., 1992. Stable isotope study of the Thingvallavatn area. Groundwater origin, age and evaporation models. Oikos: 136-150.

Tyler, J.J., Jones, M., Arrowsmith, C., Allott, T., Leng, M.J., 2015. Spatial patterns in the oxygen isotope composition of daily rainfall in the British Isles. Climate Dynamics(January 2016). DOI:10.1007/s00382-015-2945-y

Wilkins, D., Gouramanis, C., De Deckker, P., Fifield, L.K., Olley, J., 2013. Holocene lake-level fluctuations in Lakes Keilambete and Gnotuk, southwestern Victoria, Australia. The Holocene, 23(6): 784-795. DOI:10.1177/0959683612471983

Yihdego, Y., Webb, J.A., Leahy, P., 2015. Modelling of lake level under climate change conditions: Lake Purrumbete in southeastern Australia. Environmental Earth Sciences, 73(7): 3855-3872. DOI:10.1007/s12665-014-3669-8

Appendix 1

This appendix contains a table of the data resulting from the lake monitoring and sampling program, described in Chapter 2, as well as field reports from most of the lake sampling trips.

Date	Sample#	Lake name	Lake Water Level	$\delta^{18}O$	$\delta^{2}H$	Temp	pH	EC (us/cm)	F^-	Cl^-	NO_2^-	SO_4^{2-}	Br^-	NO_3^-	I	PO_4^{3-}	Alk
			m(AHD)			°C			mg/L	mg/L	mg/L	mg/L	mg/L	mg/L		mg/L	mg/L
10/06/2015	MA0021	East Basin		4.01	16.60					50			1				
05/04/2016	MA0054	East Basin	113.162	5.58	24.03	18.5	7.7	128500	<0.1	55968	<0.1	651	163	<5	<0.5	<50	1625
02/08/2016	MA0111	East Basin	113.461	3.73	16.3	11.2	9.0	120600	<0.1	51105	<0.1	592	145	<5	<0.5	<50	1600
19/09/2016	MA0152	East Basin		2.34	10.2				<0.1	44837	<0.1	528	124	<5	<0.5	<50	1335
18/11/2016	MA0173	East Basin	113.693	3.22	14.7	19.2	9.0	97360	<0.1	49275	<0.1	578	138	<5	<0.5	<50	1560
04/01/2017	JT0193	East Basin		4.00	18.19	22.3	8.9	117300	<0.1	55155	<0.1	662	142	<5	<0.5	<50	1400
12/03/2017	MA0224	East Basin	113.408	4.38	18.45	21.6	9.0	104800	<0.1	48600	<0.1	629	157	<5	-	<10	1565
26/04/2017	JR0260	East Basin		2.94	10.08	15.9			<0.1	45800	<0.1	595	136	<5	-	<10	1200
28/06/2017	MA0264	East Basin	113.466	3.30	12.99	10.1	9.1	102500	<0.1	49000	<0.1	636	151	<5	-	<10	1445
05/09/2017	MA0289	East Basin	113.631	2.26	8.44	10.3	9.1	103200	<0.1	42700	<0.1	559	134	<5	-	<10	785
08/11/2017	MA0296	East Basin	113.662	2.86	11.99	18.9	9.1	104800	<0.1	46200	<0.1	606	161	<5	-	<10	1375
23/01/2018	MA0307	East Basin	113.463	4.18	16.92	25.3	9.0	105200	<0.1	47500	<0.1	621	158	<5	-	<10	1545
07/03/2018	MA0320	East Basin	113.249	4.52	18.52	20.6	8.9	125600	<1	50600	<5	644	152	<10		<100	1685
08/05/2018	MA0342	East Basin	113.204	4.76	18.66	14.4	9.0	119200	<1	52300	<5	663	173	<10		<100	1800
10/07/2018	MA0365	East Basin	113.430	3.49	12.79	10.5	8.9	113800	<1	48300	<5	594	147	<10		<100	1695
10/09/2018	MA0379	East Basin	113.574	2.73	9.65	13.7	8.9	115300	<1	48700	<5	602	143	<10		<100	1655
24/05/2015	MA0012	Lake Bullen Merri		2.89	17.50												
10/06/2015	MA0023	Lake Bullen Merri		3.02	18.27				0.36	5200	<0.01	1.93	15.4	1.51	<0.05	<5	690.5
29/08/2015	MA0031	Lake Bullen Merri	140.037	2.91	17.80												
30/08/2015	MA0032	Lake Bullen Merri	140.037	2.85	18.07												
05/04/2016	MA0062	Lake Bullen Merri	139.495	3.46	20.74	18.5	8.5	16660	<0.01	5268	<0.01	1.71	16.3	<0.5	<0.05	<5	735
15/06/2016	MA0135	Lake Bullen Merri		3.09	19.8				<0.01	5205	<0.01	1.99	15.3	<0.5	<0.05	<5	710
02/08/2016	MA0106	Lake Bullen Merri	139.681	3.08	19.8	10.6	9.3	16270	<0.01	5239	<0.01	1.94	15.5	<0.5	<0.05	<5	700
19/09/2016	MA0148	Lake Bullen Merri		3.00	19.4				0.38	5128	<0.01	2.11	15.7	<0.5	<0.05	<5	715
18/11/2016	MA0180	Lake Bullen Merri	139.932	3.09	19.7	15.7	9.3	13930	0.37	5087	<0.01	1.9	15.5	<0.5	<0.05	<5	715
04/01/2017	JT0201	Lake Bullen Merri		3.33	21.05	22.1	9.2	16320	<0.01	5210	<0.01	1.82	15.6	<0.5	<0.05	<5	675
12/03/2017	MA0233	Lake Bullen Merri	139.632	3.10	18.46	20.9	9.3	14230	0.73	5390	<0.1	2.05	16.3	<5	-	<10	655
26/04/2017	JR0256	Lake Bullen Merri		3.18	19.41	16.5			0.73	5310	<0.1	2.68	16.1	<5	-	<10	700
28/06/2017	MA0268	Lake Bullen Merri	139.603	3.05	18.49	12.4	9.4	14090	0.71	5300	<0.1	2.48	16.1	<5	-	<10	630
04/09/2017	MA0282	Lake Bullen Merri	139.716	2.68	16.02	10.7	9.2	15190	0.76	5230	<0.1	2.21	16.0	<5	-	<10	455
08/11/2017	MA0302	Lake Bullen Merri	139.817	2.94	17.76	17.3	9.3	15190	0.81	5290	<0.1	1.74	16.4	<5	-	<10	620
23/01/2018	MA0314	Lake Bullen Merri	139.613	3.14	19.10	22.7	9.4	14520	0.70	5350	<0.1	1.77	16.4	<5	-	<10	730
07/03/2018	MA0327	Lake Bullen Merri	139.419	3.35	19.79	23.0	9.3	16800	0.18	5260	<0.5	1.52	17.0	<1		<10	770
08/05/2018	MA0352	Lake Bullen Merri	139.310	3.37	20.95	15.6	9.3	15670	0.31	5190	<0.5	1.66	16.5	<1		<10	735
10/07/2018	MA0369	Lake Bullen Merri	139.413	3.00	18.04	11.1	9.2	15400	<0.1	5120	<0.5	1.79	16.2	<1		<10	825
09/09/2018	MA0375	Lake Bullen Merri	139.521	2.98	17.98	11.0	9.1	16110	0.12	5060	<0.5	1.82	16.2	<1		<10	760
23/05/2015	MA0005	Lake Edward		4.94	24.60												
28/08/2015	MA0025	Lake Edward		3.79	20.00												

Date	Sample#	Lake name	Lake Water Level	$\delta^{18}O$	$\delta^{2}H$	Temp	pH	EC (us/cm)	F^-	Cl^-	NO_2^-	SO_4^{2-}	Br^-	NO_3^-	I	PO_4^{3-}	Alk
			m(AHD)			°C			mg/L	mg/L	mg/L	mg/L	mg/L	mg/L		mg/L	mg/L
06/04/2016	MA0087	Lake Edward	102.653	6.36	32.04	21.3	8.8	7445	0.16	1395	<0.01	2241	5.87	<0.5	<0.05	<5	55.6
03/08/2016	MA0126	Lake Edward	103.315	2.47	14.3	11.0	7.0	5900	0.13	1023	<0.01	1777	4.39	1.64	<0.05	<5	50
21/09/2016	MA0143	Lake Edward		1.68	11.1				0.11	908	<0.01	1630	3.9	1.28	<0.05	<5	26
18/11/2016	MA0191	Lake Edward	103.788	1.99	12.4	19.9	6.8	4477	0.11	909	<0.01	1652	3.81	1	<0.05	<5	8
07/01/2017	JT0214	Lake Edward		2.81	16	25.0	6.4	5479	0.12	961	<0.01	1740	4.06	0.73	<0.05	<5	6
23/04/2017	MA0246	Lake Edward	103.405			17.0			0.17	986	<0.01	1810	4.89	0.80	-	<1	9.2
24/04/2017	JR0251	Lake Edward	103.405	3.61	17.67	17.7	6.5	5842	0.17	963	0.14	1770	4.84	0.87	-	<1	78
29/06/2017	MA0274	Lake Edward	103.492	3.10	15.25	11.1	6.9	4898	0.16	950	<0.01	1740	4.61	1.54	-	<1	8
03/09/2017	MA0277	Lake Edward	103.827	1.73	8.78	13.4	5.2	4686	0.15	824	<0.01	1530	4.16	2.02	-	<1	2.8
07/11/2017	MA0292	Lake Edward	103.943	2.08	11.60	18.1	4.9	4582	0.17	802	<0.01	1500	3.93	1.25	-	<1	0
22/01/2018	MA0304	Lake Edward	103.697	3.39	17.14	24.0	6.3	4626	0.21	881	<0.01	1620	4.49	<0.5	-	<1	7.3
06/03/2018	MA0317	Lake Edward	103.517			21.7	7.3	5585	0.21	924	<0.5	1650	4.40	<1		<10	11
07/05/2018	MA0339	Lake Edward	103.462	4.05	19.75	14.7	7.3	5248	0.22	947	<0.5	1700	4.59	<1		<10	6.1
09/07/2018	MA0358	Lake Edward	103.661	2.90	13.47	10.1	6.0	5000	0.21	876	<0.5	1590	4.24	<1		<10	3.6
11/09/2018	MA0381	Lake Edward	104.101	1.63	8.45	14.7	4.5	4495	0.22	737	<0.5	1370	3.54	<1		<10	0.7
24/05/2015	MA0010	Lake Elingamite		2.49	16.40												
29/08/2015	MA0030	Lake Elingamite		1.47	11.86												
15/06/2016	MA0131	Lake Elingamite		-1.72	-7.3				0.05	1222	0.26	1543	3.09	44.41	<0.05	<5	146
02/08/2016	MA0117	Lake Elingamite	125.392	-2.31	-9.7	11.7	7.0	4660	0.09	968	<0.01	658	3.18	86.66	<0.05	<5	168
19/09/2016	MA0145	Lake Elingamite		-0.83	-0.9				0.09	1479	<0.01	308	4.33	3.92	<0.05	<5	200
18/11/2016	MA0182	Lake Elingamite	125.653	0.75	7.9	18.2	7.7	4724	0.08	1539	<0.01	284	4.5	<0.5	<0.05	<5	220
04/01/2017	JT0203	Lake Elingamite		2.73	16.5	24.2	7.2	6649	0.09	1897	<0.01	329	5.55	<0.5	<0.05	<5	228
12/03/2017	MA0235	Lake Elingamite	125.243	4.67	24.06	26.3	9.0	7059	0.18	2410	<0.1	333	7.83	<5	-	<10	348
25/04/2017	JR0253	Lake Elingamite		-3.49	-20.22	20.3			0.05	1160	<0.01	155	3.68	9.11	-	<1	216
28/06/2017	MA0269	Lake Elingamite	125.328	1.61	10.54	11.2	8.3	6000	0.14	1970	<0.1	348	6.32	7.63	-	<10	270
05/09/2017	MA0286	Lake Elingamite	125.597	-0.90	-1.49	6.3	7.9	4592	0.1	1270	<0.1	291	4.08	<5	-	<10	134
08/11/2017	MA0298	Lake Elingamite	125.755	1.22	9.70	16.1	7.8	4739	0.13	1380	<0.1	250	4.51	<5	-	<10	210
23/01/2018	MA0312	Lake Elingamite	125.477	5.07	26.35	30.0	8.4	6210	0.20	1990	<0.1	273	6.59	<5	-	<10	310
07/03/2018	MA0322	Lake Elingamite	125.287	5.89	29.56	19.6	7.8	8154	0.17	2390	<0.5	316	8.12	<1		<10	384
08/05/2018	MA0344	Lake Elingamite	125.201	1.36	6.89	14.6	7.8	7081	0.14	2130	<0.5	367	7.30	<1		<10	432
10/07/2018	MA0367	Lake Elingamite	125.562	-0.09	1.93	11.5	8.0	4683	0.19	1340	<0.5	284	4.86	<1		<10	206
09/09/2018	MA0373	Lake Elingamite	125.784	-0.06	3.15	13.7	8.5	4790	0.17	1320	<0.5	255	4.68	<1		<10	192
24/05/2015	MA0013	Lake Gnotuk		3.38	15.20												
10/06/2015	MA0016	Lake Gnotuk		3.32	15.40	12.3	9.8	104800	<0.1	41658	<0.1	89.3	134	<5	<0.5	<50	840
30/08/2015	MA0033	Lake Gnotuk		3.24	15.60												
05/04/2016	MA0066	Lake Gnotuk	100.053	3.69	16.56	20.9	8.7	105700	<0.1	43530	<0.1	94.4	134	<5	<0.5	<50	820
15/06/2016	MA0130	Lake Gnotuk		3.80	18.2				<0.1	45954	<0.1	100	133	<5	<0.5	<50	795
02/08/2016	MA0103	Lake Gnotuk	100.248	3.56	17.4	10.3	8.7	103900	<0.1	44189	<0.1	96.8	135	<5	<0.5	<50	775

Date	Sample#	Lake name	Lake Water Level	$\delta^{18}O$	$\delta^{2}H$	Temp	pH	EC (us/cm)	F^-	Cl^-	NO_2^-	SO_4^{2-}	Br^-	NO_3^-	I	PO_4^{3-}	Alk
			m(AHD)			°C			mg/L	mg/L	mg/L	mg/L	mg/L	mg/L		mg/L	mg/L
19/09/2016	MA0149	Lake Gnotuk		3.25	15.8				<0.1	43409	<0.1	98.1	130	<5	<0.5	<50	795
18/11/2016	MA0177	Lake Gnotuk	100.464	3.42	16.9	18.1	8.6	88140	<0.1	43182	<0.1	95.6	129	<5	<0.5	<50	790
04/01/2017	JT0199	Lake Gnotuk		3.83	19.14	24.1	8.6	101600	<0.1	44634	<0.1	98.6	129	<5	<0.5	<50	780
12/03/2017	MA0231	Lake Gnotuk	100.158	3.47	16.22	23.3	8.5	89700	<0.1	42100	<0.1	99.2	139	<5	-	<10	785
26/04/2017	JR0257	Lake Gnotuk		2.85	12.00	15.2			<0.1	36600	<0.1	89.8	147	<5	-	<10	600
28/06/2017	MA0266	Lake Gnotuk		3.16	14.36	12.7	8.7	87980	<0.1	40500	<0.1	98.1	157	<5	-	<10	775
04/09/2017	MA0280	Lake Gnotuk	100.282	3.06	13.84	13.0	8.8	95680	<0.1	41700	<0.1	102	141	<5	-	<10	555
08/11/2017	MA0301	Lake Gnotuk	100.354	3.08	13.34	20.7	8.8	96280	<0.1	39900	<0.1	94.6	147	<5	-	<10	740
23/01/2018	MA0313	Lake Gnotuk	100.198	3.30	15.64	24.9	8.6	91500	<0.1	40800	<0.1	96.2	149	<5	-	<10	815
07/03/2018	MA0326	Lake Gnotuk	100.018	3.56	16.24	26.7	8.6	106500	<1	45000	<5	94.5	145	<10		<100	845
08/05/2018	MA0351	Lake Gnotuk	99.911	3.65	17.80	17.6	8.6	99930	<1	44000	<5	92.5	142	<10		<100	895
10/07/2018	MA0368	Lake Gnotuk	100.023	3.12	13.59	12.4	8.5	98580	<1	43600	<5	95.7	141	<10		<100	910
09/09/2018	MA0374	Lake Gnotuk	100.170	3.17	14.66	13.0	8.5	102900	<1	44000	<5	94.2	141	<10		<100	840
05/04/2016	MA0074	Lake Keilambete		3.85	17.64	18.8	8.6	148300	<0.1	66338	<0.1	144	172	<5	<0.5	<50	1600
15/06/2016	MA0132	Lake Keilambete		3.02	14.2				<0.1	61751	<0.1	135	164	<5	<0.5	<50	1520
02/08/2016	MA0121	Lake Keilambete	103.018	2.26	10.8	12.5	8.8	134100	<0.1	57878	<0.1	137	151	<5	<0.5	<50	1470
19/09/2016	MA0147	Lake Keilambete		2.39	11.7				<0.1	61023	<0.1	134	157	<5	<0.5	<50	1420
18/11/2016	MA0186	Lake Keilambete		2.51	12.89	19.8	8.8	119100	<0.1	59271	<0.1	131	156	<5	<0.5	<50	1355
04/01/2017	JT0207	Lake Keilambete		3.29	4.37	30.6	8.7	141000	<0.1	63561	<0.1	140	162	<5	<0.5	<50	1350
12/03/2017	MA0239	Lake Keilambete		3.16	14.35	23.6	8.7	124500	<1	60900	<1	141	165	<50	-	<100	1455
26/04/2017	JR0258	Lake Keilambete		2.19	8.74	15.0			<1	55700	<1	137	149	<50	-	<100	1065
28/06/2017	MA0271	Lake keilambete		2.51	10.73	11.3	8.6	123800	<1	62800	<1	146	165	<50	-	<100	1550
04/09/2017	MA0284	Lake Keilambete		1.92	8.05	11.0	9.0	129100	<1	60500	<1	141	162	<50	-	<100	1215
08/11/2017	MA0300	Lake Keilambete		2.16	10.10	19.1	8.9	130000	<1	54100	<1	126	144	<50	-	<100	1235
23/01/2018	MA0310	Lake Keilambete		2.83	12.46	29.6	8.8	125300	<1	60600	<1	140	160	<50	-	<100	1490
07/03/2018	MA0324	Lake Keilambete		3.13	13.50	22.1	8.8	147000	<1	63500	<5	137	172	<10		<100	1515
08/05/2018	MA0347	Lake Keilambete		3.38	15.47	15.7	8.7	140400	<1	66100	<5	142	185	<10		<100	1600
10/07/2018	MA0361	Lake Keilambete		2.55	10.51	9.9	8.6	137770	<1	64000	<5	137	176	<10		<100	1535
09/09/2018	MA0371	Lake Keilambete		2.07	8.75	13.5	8.7	139500	<1	60400	<5	133	168	<10		<100	1510
23/05/2015	MA0004	Lake Leake		3.04	16.50												
28/08/2015	MA0024	Lake Leake		0.69	6.39												
03/08/2016	MA0128	Lake Leake	89.705	-3.47	-15.40	12.3	8.4	5132	0.07	1285	0.8	498	4.94	18.69	<0.05	<5	166
21/09/2016	MA0142	Lake Leake		-2.32	-7.60				0.17	989	0.7	453	3.94	9.73	<0.05	<5	166
18/11/2016	MA0193	Lake Leake	90.114	-0.12	2.80	22.4	8.6	3908	0.08	1023	0.28	484	4.32	1.23	<0.05	<5	232
07/01/2017	JT0216	Lake Leake		2.52	13.90	26.1	9.2	5565	0.11	1362	<0.01	513	5.7	<0.5	<0.05	<5	254
13/03/2017	MA0243	Lake Leake	89.713	5.26	25.39	18.8	9.1	6323	0.36	1870	<0.1	723	8.30	<5	-	<10	294
23/04/2017	MA0248	Lake Leake	89.704						0.35	1910	1.27	720	8.57	<5	-	<10	320
24/04/2017	JR0250	Lake Leake		3.60	14.63	17.5			0.14	1900	<0.01	731	9.93	2.75	-	<1	310

Date	Sample#	Lake name	Lake Water Level	$\delta^{18}O$	$\delta^{2}H$	Temp	pH	EC (us/cm)	F^-	Cl^-	NO_2^-	SO_4^{2-}	Br^-	NO_3^-	I	PO_4^{3-}	Alk
			m(AHD)			°C			mg/L	mg/L	mg/L	mg/L	mg/L	mg/L		mg/L	mg/L
29/06/2017	MA0275	Lake Leake	89.805	2.31	11.67	11.3	8.9	5865	0.31	1720	0.22	632	7.75	<5	-	<10	314
03/09/2017	MA0276	Lake Leake	90.158	-0.11	-0.12	13.6	8.9	4753	0.25	1240	0.32	489	5.66	6.54	-	<10	197
07/11/2017	MA0291	Lake Leake	90.261	1.08	6.94	18.7	9.3	4478	0.27	1160	0.1	463	5.33	<5	-	<10	198
22/01/2018	MA0303	Lake Leake	89.970	5.01	25.21	26.0	8.8	5612	0.33	1600	<0.1	582	7.27	<5	-	<10	348
06/03/2018	MA0316	Lake Leake	89.785	6.33	31.77	21.9	8.6	7774	0.47	1990	<0.5	687	9.39	<1		<10	432
07/05/2018	MA0329	Lake Leake	89.721	4.85	24.63	13.7	8.6	7832	<0.01	2130	<0.05	723	10.2	<0.1		<1	440
09/07/2018	MA0357	Lake Leake	89.934	1.61	10.22	11.2	8.4	6087	0.34	1640	<0.5	564	7.84	1.48		<10	372
11/09/2018	MA0382	Lake Leake	90.406	-0.56	-1.63	15.5	8.0	4473	0.26	1080	0.55	417	5.32	5.32		<10	252
29/08/2015	MA0029	Lake Mumblin		3.12	15.10												
05/04/2016	MA0070	Lake Mumblin		9.19	39.50	20.2	8.7	1603.00									
02/08/2016	MA0119	Lake Mumblin	153.125	1.12	4.30	11.6	8.4	1206	0.02	246	0.1	214	1.72	8.27	<0.05	<5	68
19/09/2016	MA0150	Lake Mumblin		0.34	1.30				0.02	220	0.22	227	1.51	12.07	<0.05	<5	62
18/11/2016	MA0184	Lake Mumblin	153.500	1.16	5.80	20.3	7.4	957	0.01	199	0.05	222	1.39	<0.5	<0.05	<5	68
04/01/2017	JT0205	Lake Mumblin		2.98	12.8	23.2	9.1	1184	0.02	235	<0.01	235	1.7	<0.5	<0.05	<5	72
12/03/2017	MA0237	Lake Mumblin	153.160	5.02	19.74	23.7	7.9	1146	0.02	241	<0.01	210	1.89	<0.5	-	<1	101
28/06/2017	MA0270	Lake Mumblin	153.301	2.95	10.66	10.8	7.7	1014	0.02	220	<0.01	188	1.71	<0.5	-	<1	76
05/09/2017	MA0285	Lake Mumblin	153.500	1.34	4.31	9.7	7.9	974	0.01	189	<0.01	171	1.44	0.70	-	<1	70
08/11/2017	MA0299	Lake Mumblin	153.618	1.78	7.89	19.8	7.2	979	0.01	180	0.01	177	1.40	2.31	-	<1	70.8
23/01/2018	MA0311	Lake Mumblin	153.410	4.57	18.49	27.4	8.2	1024	0.02	214	0.01	169	1.74	<0.5	-	<1	88.6
07/03/2018	MA0323	Lake Mumblin	153.220	5.72	23.20	22.1	7.8	1268	0.07	250	<0.05	178	2.12	<0.1		<1	96
08/05/2018	MA0346	Lake Mumblin	153.164	5.68	24.25	14.5	8.0	1200	0.1	259	<0.05	182	2.22	0.32		<1	90.5
10/07/2018	MA0360	Lake Mumblin	153.458	2.48	9.33	9.5	6.5	1016	0.06	212	0.06	165	1.71	0.74		<1	72.6
09/09/2018	MA0372	Lake Mumblin	153.626	1.14	4.59	13.5	8.0	1000	0.07	196	<0.05	157	1.57	<0.1		<1	58
24/05/2015	MA0011	Lake Purrumbete		2.28	14.30												
10/06/2015	MA0022	Lake Purrumbete		2.10	13.20				0.22	158	0.06	21.9	0.42	<0.5	<0.05	<5	185
30/08/2015	MA0035	Lake Purrumbete		2.07	13.29												
05/04/2016	MA0058	Lake Purrumbete	133.884	2.74	16.52	18.7	8.4	849	0.22	161	<0.01	22.2	0.43	<0.5	<0.05	<5	190.2
15/06/2016	MA0133	Lake Purrumbete		2.40	15.60				0.23	166	<0.01	23	0.45	<0.5	<0.05	<5	190
02/08/2016	MA0113	Lake Purrumbete	134.128	2.29	15.10	10.7	9.2	848	0.22	164	<0.01	22.7	0.45	<0.5	<0.05	<5	192
18/09/2016	MA0153	Lake Purrumbete		0.73	6.50				0.22	139	<0.01	30.5	0.37	1	<0.05	<5	150
18/11/2016	MA0175	Lake Purrumbete	134.996	2.31	15.00	15.2	9.1	706	0.23	163	<0.01	23.8	0.44	<0.5	<0.05	<5	170
04/01/2017	JT0197	Lake Purrumbete		2.02	13.30	21.1	9.1	815	0.21	155	<0.01	20.8	0.43	<0.5	<0.05	<5	172
12/03/2017	MA0226	Lake Purrumbete	134.626	2.28	13.98	20.6	9.5	720	0.21	151	<0.01	24.2	0.42	<0.5	-	<1	168
26/04/2017	JR0255	Lake Purrumbete		0.78	5.37	14.5			0.20	136	1.26	20.0	0.46	0.90	-	<1	186
28/06/2017	MA0265	Lake Purrumbete	134.590	2.05	11.67	12.3	9.0	723	0.20	151	<0.01	23.4	0.43	<0.5	-	<1	180
05/09/2017	MA0290	Lake Purrumbete	134.817	1.85	12.03	10.6	9.0	767	0.20	148	0.03	23.5	0.42	<0.5	-	<1	146
08/11/2017	MA0297	Lake Purrumbete	135.131	2.04	13.74	17.1	9.3	776	0.20	148	<0.01	23.6	0.43	<0.5	-	<1	134
23/01/2018	MA0308	Lake Purrumbete	134.815	2.29	14.14	23.3	9.6	732	0.22	151	<0.01	23.7	0.43	<0.5	-	<1	184

Date	Sample#	Lake name	Lake Water Level	$\delta^{18}O$	$\delta^{2}H$	Temp	pH	EC (us/cm)	F^-	Cl^-	NO_2^-	SO_4^{2-}	Br^-	NO_3^-	I	PO_4^{3-}	Alk
			m(AHD)			°C			mg/L	mg/L	mg/L	mg/L	mg/L	mg/L		mg/L	mg/L
07/03/2018	MA0321	Lake Purrumbete	134.615	2.32	14.42	20.1	9.3	844	0.20	158	<0.05	23.9	0.46	<0.1		<1	210
08/05/2018	MA0343	Lake Purrumbete	134.498	2.32	15.01	15.3	9.0	811	0.21	157	<0.05	23.9	0.46	0.23		<1	184
10/07/2018	MA0366	Lake Purrumbete	134.644	2.12	12.95	11.2	9.0	784	0.20	156	<0.05	23.6	0.47	0.71		<1	196
10/09/2018	MA0377	Lake Purrumbete	135.010	2.03	12.76	10.8	8.7	816	0.21	154	<0.05	24.0	0.46	<0.1		<1	186
23/05/2015	MA0006	Lake Surprise		3.10	11.90												
29/08/2015	MA0026	Lake Surprise		2.67	10.70												
06/04/2016	MA0081	Lake Surprise	77.816	4.23	17.32	17.8	8.8	680	0.32	118	<0.01	1.24	0.4	<0.5	<0.05	<5	206.4
03/08/2016	MA0124	Lake Surprise	77.854	3.0	12.9	10.3	9.2	666	0.3	109	<0.01	1.6	0.38	<0.5	<0.05	<5	214
20/09/2016	MA0144	Lake Surprise		1.70	6.70				0.29	96.7	0.06	3.64	0.34	2.32	<0.05	<5	188
18/11/2016	MA0189	Lake Surprise	78.843	1.68	6.80	21.5	9.3	553	0.28	94.2	0.09	4.77	0.34	0.99	<0.05	<5	202
06/01/2017	JT0212	Lake Surprise		2.35	9.20	25.1	9.0	676	0.31	104	<0.01	4.64	0.36	<0.5	<0.05	<5	190
12/03/2017	MA0241	Lake Surprise	78.571	2.96	10.76	21.7	9.1	587	0.28	98.5	<0.01	4.10	0.36	<0.5	-	<1	196
25/04/2017	JR0252	Lake Surprise		2.54	9.03	16.5			0.28	93.5	<0.01	3.25	0.34	<0.5	-	<1	188
29/06/2017	MA0273	Lake Surprise	78.420	2.52	8.67	10.8	7.7	597	0.29	95.3	0.01	2.31	0.37	0.52	-	<1	204
03/09/2017	MA0278	Lake Surprise	78.409	2.08	7.26	12.8	9.2	604	0.27	92.1	0.01	2.24	0.34	0.66	-	<1	180
07/11/2017	MA0293	Lake Surprise	78.718	2.15	8.75	18.1	9.3	584	0.27	90.2	<0.01	2.82	0.34	<0.5	-	<1	158
22/01/2018	MA0305	Lake Surprise	78.656	3.04	11.56	26.0	8.9	588	0.30	94.9	<0.01	2.66	0.36	<0.5	-	<1	212
06/03/2018	MA0318	Lake Surprise	78.505	3.40	13.33	21.3	8.9	686	0.31	102	<0.05	2.55	0.37	<0.1		<1	232
07/05/2018	MA0340	Lake Surprise	78.343	3.30	12.61	15.0	8.7	647	0.29	103	<0.05	2.25	0.39	0.17		<1	204
09/07/2018	MA0359	Lake Surprise	78.322	2.67	9.52	10.4	8.0	639	0.39	102	<0.05	2.26	0.40	0.37		<1	235
11/09/2018	MA0380	Lake Surprise	78.466	2.26	8.11	12.7	9.3	661	0.35	95.6	<0.05	2.41	0.35	0.29		<1	224
24/05/2015	MA0014	Lake Tooliorook		4.29	25.40												
30/08/2015	MA0036	Lake Tooliorook		3.41	22.45												
05/04/2016	MA0044	Lake Tooliorook		6.24	34.80	13.2	6.7	12890									
15/06/2016	MA0134	Lake Tooliorook		3.01	19.30				0.25	3742	<0.01	212	12.7	<0.5	<0.05	<5	640
02/08/2016	MA0115	Lake Tooliorook		2.51	17.50	12.4	9.2	11580	0.22	3351	<0.01	253	12.1	<0.5	<0.05	<5	465
18/09/2016	MA0167	Lake Tooliorook		-3.05	-14.60												
17/11/2016	MA0169	Lake Tooliorook		-1.18	-3.70	20.3	8.0	4762	0.11	1620	0.1	133	5.31	<0.5	<0.05	<5	278
06/01/2017	JT0209	Lake Tooliorook		-0.06	1.60	21.4	8.0	5990	0.15	1701	<0.01	134	5.76	<0.5	<0.05	<5	300
12/03/2017	MA0228	Lake Tooliorook		1.25	6.63	22.8	9.0	5691	0.40	1920	<0.1	141	6.65	<5	-	<10	366
26/04/2017	JR0254	Lake Tooliorook		0.95	4.77	13.0			0.39	1800	0.16	131	6.42	<5	-	<10	342
27/06/2017	MA0262	Lake Tooliorook		0.71	4.54	11.6	9.1	5406	0.39	1820	<0.1	134	6.47	<5	-	<10	380
05/09/2017	MA0287	Lake Tooliorook		0.17	2.10	9.6	8.9	5682	0.39	1740	<0.1	133	6.16	<5	-	<10	310
08/11/2017	MA0294	Lake Tooliorook		0.48	4.51	15.4	8.2	5660	0.41	1730	0.14	138	6.16	<5	-	<10	336
24/01/2018	MA0315	Lake Tooliorook		1.89	10.89	24.6	9.0	5775	0.41	1890	<0.1	147	6.70	<5	-	<10	406
07/03/2018	MA0325	Lake Tooliorook		2.63	14.17	24.2	9.4	7000	<0.01	2030	<0.05	119	7.17	0.16		<1	442
08/05/2018	MA0349	Lake Tooliorook		3.10	17.37	16.1	9.4	6870	0.43	2150	<0.5	146	7.74	<1		<10	405
10/07/2018	MA0363	Lake Tooliorook		2.30	12.67	9.0	9.4	6701	0.46	2110	<0.5	144	7.65	<1		<10	408

Date	Sample#	Lake name	Lake Water Level	$\delta^{18}O$	$\delta^{2}H$	Temp	pH	EC (us/cm)	F^-	Cl^-	NO_2^-	SO_4^{2-}	Br^-	NO_3^-	I	PO_4^{3-}	Alk
			m(AHD)			°C			mg/L	mg/L	mg/L	mg/L	mg/L	mg/L		mg/L	mg/L
09/09/2018	MA0370	Lake Tooliorook		2.01	12.12	12.8	8.9	6851	0.59	2090	<0.5	142	7.52	<1		<10	404
23/05/2015	MA0008	Tower Hill		0.74	6.10												
29/08/2015	MA0027	Tower Hill		-0.25	2.29												
20/09/2016	MA0158	Tower Hill		-1.42	-4.60				0.19	2125	0.14	319	9.3	<0.5	<0.05	<5	706
06/01/2017	JT0211	Tower Hill		5.69	25.90												
10/06/2015	MA0018	West Basin		4.00	15.00				<0.1	66897	<0.1	2055	215	<5	<0.5	<50	1580
10/06/2015	MA0019	West Basin		4.09	15.25	12.9	10.4	163400	<0.1	66738	<0.1	2047	200	<5	<0.5	<50	1425
05/04/2016	MA0050	West Basin	111.079	4.95	19.12	18.8	6.9	159100	<0.1	72346	<0.1	2243	229	<5	<0.5	<50	1540
02/08/2016	MA0109	West Basin	111.359	3.16	11.8	11.0	8.8	150300	<0.1	67113	<0.1	2075	206	<5	<0.5	<50	1530
19/09/2016	MA0151	West Basin		1.62	5.3				<0.1	54975	<0.1	1701	168	<5	<0.5	<50	1280
18/11/2016	MA0171	West Basin	111.572	2.66	10.5	20.3	8.9	119800	<0.1	61234	<0.1	1902	193	<5	<0.5	<50	1320
04/01/2017	JT0195	West Basin		3.80	14.59	22.7	8.8	145600	<0.1	65320	<0.1	2038	207	<5	<0.5	<50	1405
12/03/2017	MA0222	West Basin	111.268	4.20	15.68	22.4	8.7	131500	<1	64200	<1	2100	205	<50	-	<100	1365
26/04/2017	JR0259	West Basin		3.03	9.45	14.4			<1	58800	<1	1940	187	<50	-	<100	1025
28/06/2017	MA0263	West Basin	111.345	3.00	10.79	10.3	8.9	128000	<1	65200	<1	2140	209	<50	-	<100	1195
05/09/2017	MA0288	West Basin	111.539	1.85	5.04	10.3	9.0	129800	<1	59200	<1	1930	187	<50	-	<100	965
08/11/2017	MA0295	West Basin	111.575	2.51	9.08	17.4	8.9	129900	<1	59700	<1	1970	192	<50	-	<100	1145
23/01/2018	MA0306	West Basin	111.369	4.12	14.97	25.4	8.8	132500	<1	61500	<1	2040	200	<50	-	<100	1420
07/03/2018	MA0319	West Basin	111.165	4.46	16.44	20.6	8.6	157200	<1	69700	<5	2250	231	<10		<100	1500
08/05/2018	MA0341	West Basin	111.092	4.54	16.50	15.1	8.7	148600	<1	71600	<5	2310	234	<10		<100	1545
10/07/2018	MA0364	West Basin	111.297	3.00	9.44	10.6	8.6	142100	<1	66100	<5	2160	218	<10		<100	1370
10/09/2018	MA0378	West Basin	111.449	2.27	7.61	14.0	8.7	142300	<1	50200	<5	1570	169	<10		<100	1070

Date	Sample#	Lake name	Al	Ba	Bi	Ca	Co	Cr	Cu	Fe	K	Li	Lu	Mg	Mn	Mo	Na	Ni	P	S	Sc
			mg/L	mg/L	mg/L	mg/L	mg/L	mg/L	mg/L	mg/L	mg/L	mg/L	mg/L	mg/L	mg/L	mg/L	mg/L	mg/L	mg/L	mg/L	mg/L
10/06/2015	MA0021	East Basin																			
05/04/2016	MA0054	East Basin	<0.01	0.26	<0.05	30.978	<0.001	<0.005	<0.005	0.008	1207.732	0.28	<0.001	2129.683	<0.001	<0.005	30344.733	0.003	0.541	230.518	<0.005
02/08/2016	MA0111	East Basin	<0.01	0.239	<0.05	27.838	<0.001	<0.005	0.005	0.019	1114.031	0.257	<0.001	1964.291	<0.001	<0.005	28134.862	0.005	0.715	212.825	<0.005
19/09/2016	MA0152	East Basin	<0.01	0.208	<0.05	24.16	<0.001	<0.005	0.011	0.007	948.369	0.233	<0.001	1659.752	<0.001	<0.005	24250.1	0.003	0.611	187.725	<0.005
18/11/2016	MA0173	East Basin	<0.01	0.223	<0.05	25.344	<0.001	<0.005	0.036	0.006	996.182	0.239	<0.001	1790.476	<0.001	<0.005	26239.823	0.003	0.659	201.222	<0.005
04/01/2017	JT0193	East Basin	<0.01	0.235	<0.05	25.671	<0.001	<0.005	0.016	<0.005	1068.078	0.25	<0.001	1886.525	<0.001	0.005	27836.406	0.004	0.718	212.587	<0.005
12/03/2017	MA0224	East Basin	<0.1	0.217	<0.5	26.1	<0.01	<0.05	<0.05	<0.05	1170	0.447	<0.01	1870	<0.01	<0.05	31100	<0.01	1.01	311	<0.05
26/04/2017	JR0260	East Basin	<0.1	0.204	<0.5	24.8	<0.01	<0.05	<0.05	<0.05	1120	0.417	<0.01	1780	<0.01	<0.05	28900	<0.01	0.98	291	<0.05
28/06/2017	MA0264	East Basin	<0.1	0.204	<0.5	23.9	<0.01	<0.05	<0.05	<0.05	1140	0.429	<0.01	1790	<0.01	<0.05	29500	<0.01	1.03	286	<0.05
05/09/2017	MA0289	East Basin	<0.1	0.187	<0.5	21.0	<0.01	<0.05	<0.05	<0.05	1020	0.400	<0.01	1650	<0.01	<0.05	27000	<0.01	1.12	263	<0.05
08/11/2017	MA0296	East Basin	0.11	0.189	<0.5	21.3	<0.01	<0.05	<0.05	<0.05	1080	0.413	<0.01	1700	<0.01	<0.05	27600	<0.01	1.08	272	<0.05
23/01/2018	MA0307	East Basin	<0.1	0.204	<0.5	22.4	<0.01	<0.05	<0.05	<0.05	1180	0.445	<0.01	1830	<0.01	<0.05	29900	<0.01	1.08	294	<0.05
07/03/2018	MA0320	East Basin	<0.1	0.250	<0.1	22.4	<0.05	<0.01	0.075	<0.05	1150	0.469	<0.01	1980	<0.01	<0.05	29100	<0.05	1.3	346	0.01
08/05/2018	MA0342	East Basin	<0.1	0.252	<0.1	21.8	<0.05	<0.01	0.105	<0.05	1170	0.470	<0.01	2040	<0.01	<0.05	30400	<0.05	1.4	357	0.012
10/07/2018	MA0365	East Basin	<0.1	0.233	<0.1	20.0	<0.05	<0.01	0.271	<0.05	1100	0.441	<0.01	1890	<0.01	<0.05	28200	<0.05	1.6	326	0.01
10/09/2018	MA0379	East Basin	<0.1	0.230	<0.1	19.2	<0.05	<0.01	<0.05	<0.05	1050	0.432	<0.01	1790	<0.01	<0.05	27700	<0.05	1.2	313	0.01
24/05/2015	MA0012	Lake Bullen Merri																			
10/06/2015	MA0023	Lake Bullen Merri	<0.01	0.051	<0.05	16.593	<0.001	<0.005	<0.005	<0.005	107.842	<0.005	<0.001	281.293	<0.001	<0.005	2843.724	0.004	0.038	1.211	<0.005
29/08/2015	MA0031	Lake Bullen Merri																			
30/08/2015	MA0032	Lake Bullen Merri																			
05/04/2016	MA0062	Lake Bullen Merri	<0.01	0.047	<0.05	14.834	<0.001	<0.005	<0.005	<0.005	112.499	<0.005	<0.001	292.425	<0.001	<0.005	2899.193	0.002	0.011	1.103	<0.005
15/06/2016	MA0135	Lake Bullen Merri	<0.01	0.05	<0.05	15.791	<0.001	<0.005	<0.005	<0.005	110.126	<0.005	<0.001	283.789	<0.001	<0.005	2836.513	0.003	0.018	1.129	<0.005
02/08/2016	MA0106	Lake Bullen Merri	<0.01	0.054	<0.05	16.375	0.001	<0.005	<0.005	<0.005	109.82	<0.005	<0.001	286.96	0.013	<0.005	2883.501	0.002	0.042	1.093	<0.005
19/09/2016	MA0148	Lake Bullen Merri	<0.01	0.051	<0.05	16.335	<0.001	<0.005	0.006	<0.005	108.159	<0.005	<0.001	285.837	0.004	0.005	2774.896	0.002	0.025	1.202	<0.005
18/11/2016	MA0180	Lake Bullen Merri	<0.01	0.053	<0.05	16.158	<0.001	<0.005	0.02	<0.005	107.321	<0.005	<0.001	279.604	0.002	0.005	2783.459	0.003	0.015	1.374	<0.005
04/01/2017	JT0201	Lake Bullen Merri	<0.01	0.055	<0.05	16.573	<0.001	<0.005	<0.005	<0.005	107.641	<0.005	<0.001	288.344	<0.001	<0.005	2817.235	0.003	0.013	1.091	<0.005
12/03/2017	MA0233	Lake Bullen Merri	<0.1	0.054	<0.5	17.0	<0.01	<0.05	<0.05	<0.05	107	0.012	<0.01	285	<0.01	<0.05	2960	<0.01	<0.1	1.30	<0.05
26/04/2017	JR0256	Lake Bullen Merri	<0.1	0.054	<0.5	17.8	<0.01	<0.05	<0.05	<0.05	110	0.011	<0.01	299	<0.01	<0.05	3030	<0.01	<0.1	1.70	<0.05
28/06/2017	MA0268	Lake Bullen Merri	<0.1	0.052	<0.5	17.0	<0.01	<0.05	<0.05	<0.05	104	0.011	<0.01	278	<0.01	<0.05	2930	<0.01	<0.1	1.40	<0.05
04/09/2017	MA0282	Lake Bullen Merri	<0.1	0.054	<0.5	17.1	<0.01	<0.05	<0.05	<0.05	107	0.012	<0.01	281	<0.01	<0.05	2960	<0.01	<0.1	1.50	<0.05
08/11/2017	MA0302	Lake Bullen Merri	<0.1	0.052	<0.5	17.1	<0.01	<0.05	<0.05	<0.05	105	0.012	<0.01	280	<0.01	<0.05	2920	<0.01	<0.1	1.30	<0.05
23/01/2018	MA0314	Lake Bullen Merri	<0.1	0.047	<0.5	16.5	<0.01	<0.05	<0.05	<0.05	112	0.012	<0.01	282	<0.01	<0.05	3160	<0.01	<0.1	1.30	<0.05
07/03/2018	MA0327	Lake Bullen Merri	<0.01	0.048	<0.01	15.3	<0.005	<0.001	0.016	<0.005	111	0.002	<0.001	283	<0.001	<0.005	2860	<0.005	0.03	1.50	<0.001
08/05/2018	MA0352	Lake Bullen Merri	<0.01	0.052	<0.01	15.1	<0.005	<0.001	0.015	<0.005	110	0.002	<0.001	276	<0.001	<0.005	2970	<0.005	0.03	1.60	0.001
10/07/2018	MA0369	Lake Bullen Merri	<0.01	0.054	<0.01	16.1	<0.005	<0.001	0.012	<0.005	109	0.002	<0.001	279	0.012	0.007	2980	<0.005	0.07	1.80	0.001
09/09/2018	MA0375	Lake Bullen Merri	<0.01	0.054	<0.01	15.9	<0.005	<0.001	<0.005	<0.005	108	0.002	<0.001	279	0.009	<0.005	2810	<0.005	0.05	1.70	0.001
23/05/2015	MA0005	Lake Edward																			
28/08/2015	MA0025	Lake Edward																			

Date	Sample#	Lake name	Al	Ba	Bi	Ca	Co	Cr	Cu	Fe	K	Li	Lu	Mg	Mn	Mo	Na	Ni	P	S	Sc
			mg/L	mg/L	mg/L	mg/L	mg/L	mg/L	mg/L	mg/L	mg/L	mg/L	mg/L	mg/L	mg/L	mg/L	mg/L	mg/L	mg/L	mg/L	mg/L
06/04/2016	MA0087	Lake Edward	0.01	0.119	<0.05	234.03	<0.001	<0.005	0.009	0.011	116.837	0.024	<0.001	343.578	0.047	<0.005	881.208	0.015	0.01	707.916	<0.005
03/08/2016	MA0126	Lake Edward	0.03	0.084	<0.05	189.783	0.006	<0.005	0.008	0.006	86.69	0.021	<0.001	263.174	0.097	<0.005	661.57	0.048	<0.01	571.233	<0.005
21/09/2016	MA0143	Lake Edward	0.03	0.08	<0.05	174.17	0.005	<0.005	0.01	0.014	76.577	0.021	<0.001	239.149	0.112	<0.005	613.594	0.061	<0.01	515.289	<0.005
18/11/2016	MA0191	Lake Edward	0.04	0.078	<0.05	169.788	0.004	<0.005	0.031	0.022	74.951	0.021	<0.001	233.609	0.128	<0.005	586.932	0.065	<0.01	505.795	<0.005
07/01/2017	JT0214	Lake Edward	0.02	0.083	<0.05	183.091	0.003	<0.005	0.019	0.07	78.777	0.023	<0.001	243.581	0.155	<0.005	618.341	0.053	<0.01	530.973	<0.005
23/04/2017	MA0246	Lake Edward	0.02	0.079	<0.05	205	<0.001	<0.005	0.009	0.007	88.6	0.023	<0.001	251	0.044	<0.005	707	0.03	<0.01	657	<0.005
24/04/2017	JR0251	Lake Edward	0.02	0.077	<0.05	200	<0.001	<0.005	0.006	<0.005	86.5	0.023	<0.001	245	0.032	<0.005	694	0.02	<0.01	648	<0.005
29/06/2017	MA0274	Lake Edward	0.03	0.072	<0.05	190	<0.001	<0.005	0.005	<0.005	82.4	0.021	<0.001	240	0.037	<0.005	681	0.03	<0.01	630	<0.005
03/09/2017	MA0277	Lake Edward	0.68	0.062	<0.05	169	0.004	<0.005	0.015	0.204	72.3	0.020	<0.001	212	0.144	<0.005	602	0.05	<0.01	553	<0.005
07/11/2017	MA0292	Lake Edward	0.65	0.055	<0.05	171	0.009	<0.005	0.019	0.168	73.6	0.021	<0.001	205	0.361	<0.005	589	0.06	<0.01	545	<0.005
22/01/2018	MA0304	Lake Edward	0.02	0.054	<0.05	185	0.006	<0.005	0.007	0.150	81.5	0.023	<0.001	217	0.564	<0.005	632	0.03	<0.01	596	<0.005
06/03/2018	MA0317	Lake Edward	<0.01	0.060	<0.01	192	0.005	<0.001	0.017	<0.005	80.2	0.025	<0.001	252	0.580	<0.005	639	0.02	<0.01	605	<0.001
07/05/2018	MA0339	Lake Edward	0.06	0.060	<0.01	197	0.005	<0.001	0.030	0.008	82.3	0.024	<0.001	252	0.505	<0.005	646	0.04	0.01	624	<0.001
09/07/2018	MA0358	Lake Edward	0.11	0.053	<0.01	183	<0.005	<0.001	0.159	0.011	75.7	0.022	<0.001	237	0.381	<0.005	607	0.04	0.02	581	<0.001
11/09/2018	MA0381	Lake Edward	0.84	0.044	<0.01	148	0.009	<0.001	0.019	0.174	63.5	0.021	<0.001	199	0.419	<0.005	460	0.06	0.01	502	<0.001
24/05/2015	MA0010	Lake Elingamite																			
29/08/2015	MA0030	Lake Elingamite																			
15/06/2016	MA0131	Lake Elingamite	<0.01	0.083	<0.05	346.166	0.001	<0.005	0.02	0.02	22.88	0.014	<0.001	269.381	0.418	<0.005	571.273	0.016	0.718	480.692	<0.005
02/08/2016	MA0117	Lake Elingamite	<0.01	0.083	<0.05	180.366	0.002	<0.005	0.014	0.036	18.33	0.014	<0.001	174.152	0.436	<0.005	484.306	0.018	0.09	221.772	<0.005
19/09/2016	MA0145	Lake Elingamite	<0.01	0.116	<0.05	90.797	<0.001	<0.005	0.01	0.057	30.042	0.009	<0.001	166.59	0.004	<0.005	704.75	0.007	0.022	102.015	<0.005
18/11/2016	MA0182	Lake Elingamite	<0.01	0.128	<0.05	92.417	<0.001	<0.005	0.02	0.036	32.203	0.009	<0.001	169.981	0.018	<0.005	716.364	0.005	0.04	98.25	<0.005
04/01/2017	JT0203	Lake Elingamite	<0.01	0.152	<0.05	102.76	<0.001	<0.005	0.014	0.008	40.987	0.01	<0.001	208.954	<0.001	<0.005	895.826	0.004	0.02	108.481	<0.005
12/03/2017	MA0235	Lake Elingamite	<0.1	0.182	<0.5	121	<0.01	<0.05	<0.05	0.079	54.5	0.018	<0.01	269	0.804	<0.05	1200	<0.01	0.14	124	<0.05
25/04/2017	JR0253	Lake Elingamite	<0.01	0.125	<0.05	79.2	<0.001	<0.005	<0.005	0.373	33.4	0.005	<0.001	125	0.556	<0.005	620	0.005	0.16	66.8	<0.005
28/06/2017	MA0269	Lake Elingamite	<0.1	0.157	<0.5	116	<0.01	<0.05	<0.05	0.050	45.8	0.016	<0.01	221	0.145	<0.05	973	<0.01	<0.1	128	<0.05
05/09/2017	MA0286	Lake Elingamite	0.31	0.097	<0.5	98.2	<0.01	<0.05	<0.05	<0.05	31.1	0.015	<0.01	149	0.015	<0.05	653	<0.01	<0.1	106	<0.05
08/11/2017	MA0298	Lake Elingamite	<0.1	0.056	<0.5	95.1	<0.01	<0.05	<0.05	<0.05	34.9	0.015	<0.01	159	0.062	<0.05	721	<0.01	<0.1	92.5	<0.05
23/01/2018	MA0312	Lake Elingamite	<0.1	0.166	<0.5	111	<0.01	<0.05	<0.05	<0.05	50.4	0.017	<0.01	218	<0.01	<0.05	1020	<0.01	<0.1	104	<0.05
07/03/2018	MA0322	Lake Elingamite	<0.01	0.228	<0.01	118	<0.005	<0.001	0.020	0.023	51.3	0.009	<0.001	266	0.006	<0.005	1130	<0.005	0.3	125	<0.001
08/05/2018	MA0344	Lake Elingamite	<0.01	0.226	<0.01	151	<0.005	<0.001	0.033	0.022	41.2	0.008	<0.001	260	0.009	<0.005	990	0.006	0.4	146	<0.001
10/07/2018	MA0367	Lake Elingamite	<0.01	0.106	<0.01	85.6	<0.005	<0.001	0.037	0.036	28.6	0.01	<0.001	162	0.003	<0.005	675	<0.005	0.04	108	0.001
09/09/2018	MA0373	Lake Elingamite	<0.01	0.109	<0.01	77.9	<0.005	<0.001	0.012	0.013	27.2	0.009	<0.001	149	<0.001	<0.005	660	<0.005	0.03	99.6	<0.001
24/05/2015	MA0013	Lake Gnotuk																			
10/06/2015	MA0016	Lake Gnotuk	<0.01	0.693	<0.05	124.551	<0.001	<0.005	<0.005	0.005	828.453	0.049	<0.001	2823.966	<0.001	0.007	21742.45	0.005	0.578	32.986	<0.005
30/08/2015	MA0033	Lake Gnotuk																			
05/04/2016	MA0066	Lake Gnotuk	<0.01	0.716	<0.05	129.172	<0.001	<0.005	<0.005	0.017	860.116	0.051	<0.001	2929.509	<0.001	0.006	22020.38	0.004	0.564	34.422	<0.005
15/06/2016	MA0130	Lake Gnotuk	<0.01	0.716	<0.05	126.356	<0.001	<0.005	<0.005	0.018	850.151	0.051	<0.001	2827.686	0.003	0.007	21916.065	0.003	0.637	34.447	<0.005
02/08/2016	MA0103	Lake Gnotuk	<0.01	0.706	<0.05	125.288	0.001	<0.005	<0.005	0.025	843.224	0.05	<0.001	2876.782	0.003	0.007	21796.258	0.003	0.659	34.194	<0.005

Date	Sample#	Lake name	Al	Ba	Bi	Ca	Co	Cr	Cu	Fe	K	Li	Lu	Mg	Mn	Mo	Na	Ni	P	S	Sc
			mg/L	mg/L	mg/L	mg/L	mg/L	mg/L	mg/L	mg/L	mg/L	mg/L	mg/L	mg/L	mg/L	mg/L	mg/L	mg/L	mg/L	mg/L	mg/L
19/09/2016	MA0149	Lake Gnotuk	<0.01	0.683	<0.05	121.836	<0.001	<0.005	0.007	0.016	815.218	0.049	<0.001	2824.024	0.003	0.006	21406.59	0.004	0.619	34.29	<0.005
18/11/2016	MA0177	Lake Gnotuk	<0.01	0.687	<0.05	119.121	0.001	<0.005	0.007	0.013	824.845	0.05	<0.001	2800.28	0.002	0.005	21937.565	0.002	0.589	34.315	<0.005
04/01/2017	JT0199	Lake Gnotuk	<0.01	0.701	<0.05	127.371	<0.001	<0.005	0.005	0.014	837.099	0.05	<0.001	2848.357	0.002	0.005	21742.326	0.004	0.626	34.319	<0.005
12/03/2017	MA0231	Lake Gnotuk	<0.1	0.607	<0.5	127	<0.01	<0.05	<0.05	<0.05	885	0.088	<0.01	2640	<0.01	<0.05	23700	<0.01	0.85	46.4	<0.05
26/04/2017	JR0257	Lake Gnotuk	<0.1	0.598	<0.5	119	<0.01	<0.05	<0.05	<0.05	829	0.085	<0.01	2640	<0.01	<0.05	22700	<0.01	0.85	46.3	<0.05
28/06/2017	MA0266	Lake Gnotuk	<0.1	0.590	<0.5	122	<0.01	<0.05	<0.05	<0.05	859	0.088	<0.01	2660	<0.01	<0.05	22900	<0.01	0.82	46.2	<0.05
04/09/2017	MA0280	Lake Gnotuk	<0.1	0.592	<0.5	117	<0.01	<0.05	<0.05	<0.05	828	0.086	<0.01	2660	<0.01	<0.05	22700	<0.01	0.84	46.2	<0.05
08/11/2017	MA0301	Lake Gnotuk	<0.1	0.583	<0.5	123	<0.01	<0.05	<0.05	<0.05	876	0.088	<0.01	2690	<0.01	<0.05	23200	0.01	0.84	45.2	<0.05
23/01/2018	MA0313	Lake Gnotuk	<0.1	0.605	<0.5	124	<0.01	<0.05	<0.05	<0.05	890	0.089	<0.01	2770	<0.01	<0.05	23500	<0.01	0.79	45.3	<0.05
07/03/2018	MA0326	Lake Gnotuk	<0.1	0.681	<0.1	120	<0.05	<0.01	<0.05	<0.05	855	0.083	<0.01	2760	<0.01	<0.05	23000	<0.05	0.9	50.8	<0.01
08/05/2018	MA0351	Lake Gnotuk	<0.1	0.695	<0.1	123	<0.05	<0.01	0.090	<0.05	866	0.084	<0.01	2870	<0.01	<0.05	22600	<0.05	1	52.5	0.01
10/07/2018	MA0368	Lake Gnotuk	<0.1	0.687	<0.1	115	<0.05	<0.01	0.163	<0.05	821	0.087	<0.01	2890	<0.01	<0.05	22000	<0.05	0.9	54.7	0.013
09/09/2018	MA0374	Lake Gnotuk	<0.1	0.671	<0.1	115	<0.05	<0.01	<0.05	<0.05	823	0.082	<0.01	2770	<0.01	<0.05	22300	<0.05	0.9	51.5	<0.01
05/04/2016	MA0074	Lake Keilambete	<0.01	0.537	<0.05	30.841	<0.001	<0.005	<0.005	0.008	1069.108	0.016	<0.001	1991.374	<0.001	0.006	36842.376	0.003	0.275	50.176	<0.005
15/06/2016	MA0132	Lake Keilambete	<0.01	0.499	<0.05	29.502	<0.001	<0.005	<0.005	0.013	1007.431	0.015	<0.001	1843.868	<0.001	0.006	35553.36	0.003	0.302	47.726	<0.005
02/08/2016	MA0121	Lake Keilambete	<0.01	0.472	<0.05	28.719	<0.001	<0.005	<0.005	0.024	933.347	0.014	<0.001	1740.748	0.002	0.007	33010.868	0.003	0.354	48.474	<0.005
19/09/2016	MA0147	Lake Keilambete	<0.01	0.48	<0.05	28.143	<0.001	<0.005	<0.005	0.011	957.753	0.014	<0.001	1793.142	<0.001	0.006	33884.69	0.002	0.283	46.556	<0.005
18/11/2016	MA0186	Lake Keilambete	<0.01	0.479	<0.05	29.039	<0.001	<0.005	<0.005	0.018	941.024	0.014	<0.001	1772.653	0.007	0.006	33470.616	0.003	0.292	45.309	<0.005
04/01/2017	JT0207	Lake Keilambete	<0.01	0.495	<0.05	29.07	<0.001	<0.005	0.009	<0.005	998.23	0.015	<0.001	1830.646	0.001	0.006	34526.358	0.003	0.324	47.428	<0.005
12/03/2017	MA0239	Lake Keilambete	<1	0.439	<5	29.3	<0.1	<0.5	<0.5	<0.5	1010	0.116	<0.1	1900	<0.1	<0.5	38000	<0.1	<1	65.5	<0.5
26/04/2017	JR0258	Lake Keilambete	<1	0.401	<5	28.3	<0.1	<0.5	<0.5	<0.5	957	0.115	<0.1	1720	<0.1	<0.5	36200	<0.1	<1	63.6	<0.5
28/06/2017	MA0271	Lake keilambete	<1	0.433	<5	29.2	<0.1	<0.5	<0.5	<0.5	1000	0.115	<0.1	1850	<0.1	<0.5	38000	<0.1	<1	64.0	<0.5
04/09/2017	MA0284	Lake Keilambete	<1	0.406	<5	28.2	<0.1	<0.5	<0.5	<0.5	943	0.114	<0.1	1780	<0.1	<0.5	35800	<0.1	<1	59.7	<0.5
08/11/2017	MA0300	Lake Keilambete	<1	0.415	<5	29.2	<0.1	<0.5	<0.5	<0.5	976	0.116	<0.1	1800	<0.1	<0.5	36900	<0.1	<1	61.2	<0.5
23/01/2018	MA0310	Lake Keilambete	<1	0.438	<5	29.6	<0.1	<0.5	<0.5	<0.5	1010	0.115	<0.1	1850	<0.1	<0.5	37700	<0.1	<1	63.3	<0.5
07/03/2018	MA0324	Lake Keilambete	<0.1	0.479	<0.1	28.1	<0.05	<0.01	0.056	<0.05	999	0.025	<0.01	1880	<0.01	<0.05	36500	<0.05	0.5	80.4	0.012
08/05/2018	MA0347	Lake Keilambete	<0.1	0.494	<0.1	29.6	<0.05	<0.01	0.060	<0.05	1080	0.026	<0.01	1970	<0.01	<0.05	37100	<0.05	0.6	81.2	0.012
10/07/2018	MA0361	Lake Keilambete	<0.1	0.474	<0.1	29.0	<0.05	<0.01	0.089	<0.05	1030	0.023	<0.01	1870	<0.01	<0.05	36500	<0.05	0.5	78.1	0.013
09/09/2018	MA0371	Lake Keilambete	<0.1	0.462	<0.1	27.4	<0.05	<0.01	0.072	<0.05	946	0.023	<0.01	1790	<0.01	<0.05	34300	<0.05	0.6	75.0	0.011
23/05/2015	MA0004	Lake Leake																			
28/08/2015	MA0024	Lake Leake																			
03/08/2016	MA0128	Lake Leake	0.14	0.069	<0.05	43.962	0.002	<0.005	0.008	0.096	34.423	0.018	<0.001	148.24	0.012	<0.005	764.076	0.016	0.024	175.623	<0.005
21/09/2016	MA0142	Lake Leake	0.13	0.071	<0.05	46.689	0.002	<0.005	0.007	0.136	29.072	0.017	<0.001	127.664	0.008	<0.005	627.505	0.015	0.03	149.371	<0.005
18/11/2016	MA0193	Lake Leake	0.03	0.094	<0.05	54.598	0.002	<0.005	0.026	0.121	30.157	0.019	<0.001	136.107	0.033	<0.005	648.718	0.011	0.028	154.48	<0.005
07/01/2017	JT0216	Lake Leake	0.02	0.108	<0.05	66.099	<0.001	<0.005	0.023	0.011	38.508	0.021	<0.001	177.226	0.005	<0.005	822.237	0.008	0.035	186.911	<0.005
13/03/2017	MA0243	Lake Leake	<0.1	0.099	<0.5	62.6	<0.01	<0.05	<0.05	<0.05	48.4	0.034	<0.01	217	<0.01	<0.05	1190	<0.01	<0.1	269	<0.05
23/04/2017	MA0248	Lake Leake	<0.1	0.106	<0.5	65.3	<0.01	<0.05	<0.05	<0.05	50.0	0.035	<0.01	222	<0.01	<0.05	1230	<0.01	<0.1	269	<0.05
24/04/2017	JR0250	Lake Leake	0.01	0.109	<0.05	68.0	<0.001	<0.005	0.008	0.019	51.5	0.023	<0.001	208	<0.001	<0.005	1240	0.006	0.03	276	<0.005

Date	Sample#	Lake name	Al	Ba	Bi	Ca	Co	Cr	Cu	Fe	K	Li	Lu	Mg	Mn	Mo	Na	Ni	P	S	Sc
			mg/L	mg/L	mg/L	mg/L	mg/L	mg/L	mg/L	mg/L	mg/L	mg/L	mg/L	mg/L	mg/L	mg/L	mg/L	mg/L	mg/L	mg/L	mg/L
29/06/2017	MA0275	Lake Leake	<0.1	0.097	<0.5	59.9	<0.01	<0.05	<0.05	<0.05	51.1	0.031	<0.01	198	<0.01	<0.05	1100	0.01	<0.1	239	<0.05
03/09/2017	MA0276	Lake Leake	<0.1	0.072	<0.5	51.6	<0.01	<0.05	<0.05	<0.05	36.9	0.026	<0.01	150	<0.01	<0.05	812	<0.01	<0.1	178	<0.05
07/11/2017	MA0291	Lake Leake	<0.1	0.076	<0.5	52.9	<0.01	<0.05	<0.05	<0.05	34.2	0.026	<0.01	139	<0.01	<0.05	768	<0.01	<0.1	170	<0.05
22/01/2018	MA0303	Lake Leake	<0.1	0.116	<0.5	64.7	<0.01	<0.05	<0.05	<0.05	48.0	0.032	<0.01	186	<0.01	<0.05	1000	<0.01	<0.1	213	<0.05
06/03/2018	MA0316	Lake Leake	0.01	0.153	<0.01	73.7	<0.005	<0.001	0.019	0.005	52.8	0.027	<0.001	237	<0.001	<0.005	1220	<0.005	0.04	268	<0.001
07/05/2018	MA0329	Lake Leake	<0.01	0.154	<0.01	74.8	<0.005	<0.001	0.023	0.011	56.8	0.026	<0.001	248	<0.001	<0.005	1270	<0.005	0.03	277	<0.001
09/07/2018	MA0357	Lake Leake	0.01	0.114	<0.01	60.6	<0.005	<0.001	0.051	0.009	44.7	0.021	<0.001	195	<0.001	<0.005	1010	0.006	0.03	216	<0.001
11/09/2018	MA0382	Lake Leake	0.05	0.089	<0.01	48.6	<0.005	0.001	0.013	0.126	29.8	0.018	<0.001	136	0.003	<0.005	680	0.009	0.03	161	<0.001
29/08/2015	MA0029	Lake Mumblin																			
05/04/2016	MA0070	Lake Mumblin																			
02/08/2016	MA0119	Lake Mumblin	<0.01	0.05	<0.05	46.434	<0.001	<0.005	0.006	0.014	7.027	<0.005	<0.001	49	0.003	<0.005	126.61	0.002	0.034	69.676	<0.005
19/09/2016	MA0150	Lake Mumblin	0.01	0.051	<0.05	45.829	<0.001	<0.005	0.008	0.019	6.856	0.005	<0.001	48.912	<0.001	<0.005	114.399	0.002	0.04	71.593	<0.005
18/11/2016	MA0184	Lake Mumblin	0.01	0.022	<0.05	46.778	<0.001	<0.005	0.019	0.12	6.739	0.006	<0.001	47.99	0.279	<0.005	111.37	0.001	0.047	74.471	<0.005
04/01/2017	JT0205	Lake Mumblin	<0.01	0.036	<0.05	49.47	<0.001	<0.005	0.016	0.025	7.277	0.006	<0.001	51.645	0.002	<0.005	120.405	0.001	0.165	74.123	<0.005
12/03/2017	MA0237	Lake Mumblin	<0.01	0.036	<0.05	54.3	<0.001	<0.005	0.015	0.038	8.27	0.005	<0.001	55.1	0.378	<0.005	141	0.002	0.31	83.7	<0.005
28/06/2017	MA0270	Lake Mumblin	<0.01	0.048	<0.05	46.4	<0.001	<0.005	0.026	0.012	7.32	0.004	<0.001	50.1	0.016	<0.005	130	<0.001	0.02	73.9	<0.005
05/09/2017	MA0285	Lake Mumblin	0.02	0.043	<0.05	40.9	<0.001	<0.005	0.013	0.055	6.44	0.004	0.002	44.2	0.184	<0.005	114	<0.001	0.13	65.5	<0.005
08/11/2017	MA0299	Lake Mumblin	0.03	0.037	<0.05	43.2	<0.001	<0.005	0.018	0.288	6.47	0.005	0.002	44.6	0.383	<0.005	107	0.002	0.22	68.7	<0.005
23/01/2018	MA0311	Lake Mumblin	0.01	0.059	<0.05	48.0	<0.001	<0.005	<0.005	0.096	8.46	0.005	<0.001	47.9	0.748	<0.005	126	0.003	0.44	67.2	<0.005
07/03/2018	MA0323	Lake Mumblin	<0.01	0.058	<0.01	48.2	<0.005	<0.001	0.009	0.016	8.99	0.005	<0.001	51.1	0.005	<0.005	132	<0.005	0.4	68.8	<0.001
08/05/2018	MA0346	Lake Mumblin	<0.01	0.053	<0.01	44.9	<0.005	<0.001	0.017	0.014	9.17	0.005	<0.001	52.9	<0.001	<0.005	141	<0.005	0.1	71.5	<0.001
10/07/2018	MA0360	Lake Mumblin	<0.01	0.045	<0.01	40.0	<0.005	<0.001	0.044	0.018	7.52	0.004	0.001	45.0	0.004	<0.005	118	<0.005	0.08	63.8	<0.001
09/09/2018	MA0372	Lake Mumblin	0.05	0.015	<0.01	38.1	<0.005	0.001	0.01	0.172	6.65	0.004	<0.001	41.4	<0.001	<0.005	111	<0.005	0.04	60.9	<0.001
24/05/2015	MA0011	Lake Purrumbete																			
10/06/2015	MA0022	Lake Purrumbete	<0.01	0.014	<0.05	25.192	<0.001	<0.005	<0.005	<0.005	6.252	<0.005	<0.001	35.522	<0.001	<0.005	95.526	0.002	0.175	8.233	<0.005
30/08/2015	MA0035	Lake Purrumbete																			
05/04/2016	MA0058	Lake Purrumbete	<0.01	0.015	<0.05	26.502	<0.001	<0.005	<0.005	<0.005	6.427	<0.005	<0.001	36.761	<0.001	<0.005	100.009	<0.001	0.108	8.501	<0.005
15/06/2016	MA0133	Lake Purrumbete	<0.01	0.015	<0.05	25.361	<0.001	<0.005	<0.005	<0.005	6.396	<0.005	<0.001	36.706	<0.001	<0.005	95.432	0.002	0.242	8.398	<0.005
02/08/2016	MA0113	Lake Purrumbete	<0.01	0.016	<0.05	25.194	<0.001	<0.005	<0.005	<0.005	6.156	<0.005	<0.001	35.098	<0.001	<0.005	93.952	<0.001	0.179	8.316	<0.005
18/09/2016	MA0153	Lake Purrumbete	0.02	0.015	<0.05	23.064	<0.001	<0.005	0.007	0.081	6.052	<0.005	<0.001	32.77	<0.001	<0.005	80.175	0.001	0.159	11.341	<0.005
18/11/2016	MA0175	Lake Purrumbete	<0.01	0.014	<0.05	24.816	<0.001	<0.005	0.011	<0.005	6.174	<0.005	<0.001	35.598	<0.001	<0.005	92.461	0.002	0.147	8.561	<0.005
04/01/2017	JT0197	Lake Purrumbete	<0.01	0.018	<0.05	24.027	<0.001	<0.005	0.01	0.007	6.095	<0.005	<0.001	35.549	<0.001	<0.005	90.311	0.002	0.141	7.828	<0.005
12/03/2017	MA0226	Lake Purrumbete	<0.01	0.013	<0.05	25.7	<0.001	<0.005	<0.005	0.009	6.34	0.003	<0.001	36.0	<0.001	<0.005	97.4	<0.001	0.14	9.40	<0.005
26/04/2017	JR0255	Lake Purrumbete	<0.01	0.017	<0.05	29.4	<0.001	<0.005	0.009	0.098	9.13	0.003	<0.001	35.6	0.002	<0.005	91.3	0.002	0.53	8.20	<0.005
28/06/2017	MA0265	Lake Purrumbete	<0.01	0.015	<0.05	26.3	<0.001	<0.005	<0.005	<0.005	6.46	0.003	<0.001	36.3	<0.001	<0.005	102	<0.001	0.18	9.20	<0.005
05/09/2017	MA0290	Lake Purrumbete	<0.01	0.015	<0.05	25.5	<0.001	<0.005	<0.005	<0.005	6.27	0.003	0.003	35.7	0.002	<0.005	95.8	<0.001	0.16	9.20	<0.005
08/11/2017	MA0297	Lake Purrumbete	<0.01	0.012	<0.05	26.2	<0.001	<0.005	0.005	<0.005	6.50	0.003	<0.001	35.8	<0.001	<0.005	98.3	<0.001	0.16	9.30	<0.005
23/01/2018	MA0308	Lake Purrumbete	0.02	0.013	<0.05	25.9	<0.001	<0.005	0.017	0.01	6.49	0.003	0.001	36.2	0.002	<0.005	98.5	0.006	0.14	9.40	<0.005

Date	Sample#	Lake name	Al	Ba	Bi	Ca	Co	Cr	Cu	Fe	K	Li	Lu	Mg	Mn	Mo	Na	Ni	P	S	Sc
			mg/L	mg/L	mg/L	mg/L	mg/L	mg/L	mg/L	mg/L	mg/L	mg/L	mg/L	mg/L	mg/L	mg/L	mg/L	mg/L	mg/L	mg/L	mg/L
07/03/2018	MA0321	Lake Purrumbete	<0.01	0.015	<0.01	25.0	<0.005	0.001	0.009	<0.005	6.31	0.002	0.002	36.6	<0.001	<0.005	93.7	<0.005	0.1	9.60	<0.001
08/05/2018	MA0343	Lake Purrumbete	<0.01	0.015	<0.01	26.2	<0.005	<0.001	0.007	<0.005	6.46	0.002	<0.001	36.6	<0.001	<0.005	97.7	<0.005	0.2	9.60	<0.001
10/07/2018	MA0366	Lake Purrumbete	<0.01	0.016	<0.01	25.3	<0.005	<0.001	0.014	<0.005	6.27	0.002	<0.001	35.7	<0.001	<0.005	94.1	<0.005	0.2	9.50	<0.001
10/09/2018	MA0377	Lake Purrumbete	<0.01	0.016	<0.01	25.2	<0.005	<0.001	<0.005	<0.005	6.22	0.002	<0.001	36.6	<0.001	<0.005	93.7	<0.005	0.2	9.70	<0.001
23/05/2015	MA0006	Lake Surprise																			
29/08/2015	MA0026	Lake Surprise																			
06/04/2016	MA0081	Lake Surprise	<0.01	0.004	<0.05	19.214	<0.001	<0.005	<0.005	<0.005	9.7	<0.005	<0.001	27.093	<0.001	<0.005	88.504	0.001	<0.01	0.75	<0.005
03/08/2016	MA0124	Lake Surprise	<0.01	0.005	<0.05	26.521	<0.001	<0.005	<0.005	<0.005	8.983	<0.005	<0.001	25.333	<0.001	<0.005	80.355	0.001	0.012	0.837	<0.005
20/09/2016	MA0144	Lake Surprise	<0.01	0.004	<0.05	22.495	<0.001	<0.005	0.008	<0.005	8.312	<0.005	<0.001	23.936	<0.001	<0.005	72.763	<0.001	0.013	1.579	<0.005
18/11/2016	MA0189	Lake Surprise	<0.01	0.008	<0.05	27.589	<0.001	<0.005	0.016	<0.005	8.387	<0.005	<0.001	24.394	<0.001	<0.005	72.813	<0.001	<0.01	2.134	<0.005
06/01/2017	JT0212	Lake Surprise	<0.01	0.008	<0.05	28.972	<0.001	<0.005	0.007	0.006	8.779	<0.005	<0.001	25.051	<0.001	<0.005	77.889	<0.001	<0.01	1.991	<0.005
12/03/2017	MA0241	Lake Surprise	0.01	0.007	<0.05	26.6	<0.001	<0.005	<0.005	0.012	9.59	0.004	0.002	26.3	<0.001	<0.005	83.2	<0.001	<0.01	1.90	<0.005
25/04/2017	JR0252	Lake Surprise	<0.01	0.006	<0.05	26.4	<0.001	<0.005	0.005	<0.005	9.20	0.004	<0.001	24.8	<0.001	<0.005	78.7	<0.001	<0.01	1.60	<0.005
29/06/2017	MA0273	Lake Surprise	<0.01	0.005	<0.05	30.8	<0.001	<0.005	0.005	<0.005	9.01	0.004	<0.001	25.3	<0.001	<0.005	79.2	<0.001	<0.01	1.20	<0.005
03/09/2017	MA0278	Lake Surprise	<0.01	0.005	<0.05	31.1	<0.001	<0.005	0.011	<0.005	9.09	0.003	<0.001	24.5	<0.001	<0.005	79.4	<0.001	<0.01	1.20	<0.005
07/11/2017	MA0293	Lake Surprise	<0.01	0.006	<0.05	25.5	<0.001	<0.005	0.011	<0.005	8.64	0.003	<0.001	24.3	<0.001	<0.005	76.6	<0.001	<0.01	1.40	<0.005
22/01/2018	MA0305	Lake Surprise	<0.01	0.005	<0.05	27.4	<0.001	<0.005	0.008	0.006	9.55	0.004	<0.001	24.8	<0.001	<0.005	82.3	<0.001	<0.01	1.40	<0.005
06/03/2018	MA0318	Lake Surprise	<0.01	0.006	<0.01	26.6	<0.005	<0.001	0.01	<0.005	9.43	0.003	<0.001	26.4	<0.001	<0.005	81.8	<0.005	<0.01	1.40	<0.001
07/05/2018	MA0340	Lake Surprise	<0.01	0.006	<0.01	27.0	<0.005	<0.001	0.014	<0.005	9.42	0.003	<0.001	26.3	<0.001	<0.005	80.3	<0.005	0.02	1.20	<0.001
09/07/2018	MA0359	Lake Surprise	<0.01	0.006	<0.01	29.9	<0.005	<0.001	0.037	<0.005	9.16	0.003	<0.001	25.7	<0.001	<0.005	80.2	<0.005	0.01	1.30	<0.001
11/09/2018	MA0380	Lake Surprise	<0.01	0.006	<0.01	29.7	<0.005	<0.001	0.012	<0.005	8.41	0.003	<0.001	24.6	<0.001	<0.005	76.1	<0.005	0.01	1.30	<0.001
24/05/2015	MA0014	Lake Tooliorook																			
30/08/2015	MA0036	Lake Tooliorook																			
05/04/2016	MA0044	Lake Tooliorook																			
15/06/2016	MA0134	Lake Tooliorook	<0.01	0.117	<0.05	55.27	<0.001	<0.005	0.007	0.072	45.418	0.013	<0.001	430.707	0.055	<0.005	1812.535	0.004	0.352	76.043	<0.005
02/08/2016	MA0115	Lake Tooliorook	<0.01	0.099	<0.05	40.023	<0.001	<0.005	0.006	0.014	39.432	0.012	<0.001	410.258	0.009	<0.005	1741.014	0.004	0.105	87.855	<0.005
18/09/2016	MA0167	Lake Tooliorook																			
17/11/2016	MA0169	Lake Tooliorook	<0.01	0.058	<0.05	40.311	<0.001	<0.005	0.02	0.051	20.631	0.009	<0.001	183.059	0.012	<0.005	754.626	0.006	0.286	44.243	<0.005
06/01/2017	JT0209	Lake Tooliorook	<0.01	0.068	<0.05	48.299	<0.001	<0.005	0.011	0.074	23.353	0.009	<0.001	203.916	0.023	<0.005	840.357	0.005	0.418	45.542	<0.005
12/03/2017	MA0228	Lake Tooliorook	<0.1	0.072	<0.5	58.7	<0.01	<0.05	<0.05	<0.05	32.2	0.018	<0.01	236	<0.01	<0.05	987	<0.01	0.47	51.6	<0.05
26/04/2017	JR0254	Lake Tooliorook	<0.1	0.069	<0.5	59.3	<0.01	<0.05	<0.05	<0.05	31.9	0.017	<0.01	223	0.049	<0.05	950	<0.01	0.65	49.7	<0.05
27/06/2017	MA0262	Lake Tooliorook	<0.1	0.064	<0.5	59.5	<0.01	<0.05	<0.05	<0.05	30.5	0.017	<0.01	215	<0.01	<0.05	929	<0.01	0.14	50.0	<0.05
05/09/2017	MA0287	Lake Tooliorook	<0.1	0.063	<0.5	59.7	<0.01	<0.05	<0.05	1.50	29.1	0.016	<0.01	210	<0.01	<0.05	883	<0.01	<0.1	48.4	<0.05
08/11/2017	MA0294	Lake Tooliorook	<0.1	0.074	<0.5	62.9	<0.01	<0.05	<0.05	<0.05	29.9	0.017	<0.01	205	0.017	<0.05	883	<0.01	0.22	51.0	<0.05
24/01/2018	MA0315	Lake Tooliorook	<0.1	0.077	<0.5	70.6	<0.01	<0.05	<0.05	<0.05	32.8	0.017	<0.01	231	<0.01	<0.05	988	<0.01	0.34	55.5	<0.05
07/03/2018	MA0325	Lake Tooliorook	<0.01	0.083	<0.01	65.9	<0.005	<0.001	0.013	<0.005	28.2	0.008	<0.001	243	<0.001	<0.005	971	<0.005	0.2	63.4	<0.001
08/05/2018	MA0349	Lake Tooliorook	<0.01	0.068	<0.01	55.7	<0.005	<0.001	0.028	<0.005	29.3	0.008	<0.001	250	<0.001	<0.005	1070	<0.005	0.2	64.3	<0.001
10/07/2018	MA0363	Lake Tooliorook	0.08	0.063	<0.01	47.7	<0.005	<0.001	0.059	0.075	28.3	0.007	<0.001	251	0.002	<0.005	988	<0.005	0.09	63.1	<0.001

Date	Sample#	Lake name	Al	Ba	Bi	Ca	Co	Cr	Cu	Fe	K	Li	Lu	Mg	Mn	Mo	Na	Ni	P	S	Sc
			mg/L	mg/L	mg/L	mg/L	mg/L	mg/L	mg/L	mg/L	mg/L	mg/L	mg/L	mg/L	mg/L	mg/L	mg/L	mg/L	mg/L	mg/L	mg/L
09/09/2018	MA0370	Lake Tooliorook	<0.01	0.068	<0.01	53.4	<0.005	<0.001	0.021	0.007	28.3	0.007	<0.001	242	<0.001	<0.005	1040	<0.005	0.1	61.9	<0.001
23/05/2015	MA0008	Tower Hill																			
29/08/2015	MA0027	Tower Hill																			
20/09/2016	MA0158	Tower Hill	0.03	0.01	<0.05	28.414	<0.001	<0.005	0.053	0.065	138.556	0.017	<0.001	139.892	0.006	0.007	1409.848	0.003	0.368	115.032	<0.005
06/01/2017	JT0211	Tower Hill																			
10/06/2015	MA0018	West Basin	<0.01	0.263	<0.05	24.709	0.001	<0.005	<0.005	0.027	1169.739	0.231	<0.001	2145.283	0.004	<0.005	38373.843	<0.001	0.275	736.599	<0.005
10/06/2015	MA0019	West Basin	<0.01	0.267	<0.05	25.242	<0.001	<0.005	<0.005	0.024	1182.743	0.235	<0.001	2140.752	0.003	<0.005	39034.207	0.002	0.244	737.25	<0.005
05/04/2016	MA0050	West Basin	<0.01	0.291	<0.05	26.914	<0.001	0.005	<0.005	0.011	1284.654	0.255	<0.001	2325.847	0.002	<0.005	40026.251	0.003	0.238	791.376	<0.005
02/08/2016	MA0109	West Basin	<0.01	0.258	<0.05	24.525	0.001	<0.005	<0.005	0.018	1169.335	0.229	<0.001	2108.069	0.002	<0.005	37193.296	0.002	0.241	730.679	<0.005
19/09/2016	MA0151	West Basin	<0.01	0.215	<0.05	21.413	<0.001	<0.005	<0.005	0.008	973.372	0.199	<0.001	1773.94	<0.001	<0.005	31481.997	0.002	0.196	617.007	<0.005
18/11/2016	MA0171	West Basin	<0.01	0.232	<0.05	23.83	<0.001	0.006	0.021	0.019	1073.319	0.213	<0.001	1895.869	0.003	<0.005	34283.88	0.004	0.196	675.987	<0.005
04/01/2017	JT0195	West Basin	<0.01	0.249	<0.05	24.273	<0.001	0.008	0.022	0.014	1135.335	0.224	<0.001	2036.895	0.003	<0.005	36317.161	0.003	0.205	711.606	<0.005
12/03/2017	MA0222	West Basin	<1	0.216	<5	25.6	<0.1	<0.5	<0.5	<0.5	1240	0.629	<0.1	2150	<0.1	<0.5	41500	<0.1	<1	955	<0.5
26/04/2017	JR0259	West Basin	<1	0.199	<5	23.7	<0.1	<0.5	<0.5	<0.5	1130	0.600	<0.1	1980	<0.1	<0.5	38900	<0.1	<1	874	<0.5
28/06/2017	MA0263	West Basin	<1	0.201	<5	24.6	<0.1	<0.5	<0.5	<0.5	1160	0.605	<0.1	2050	<0.1	<0.5	39300	<0.1	<1	884	<0.5
05/09/2017	MA0288	West Basin	<1	0.182	<5	22.7	<0.1	<0.5	<0.5	<0.5	1030	0.559	<0.1	1870	<0.1	<0.5	35500	<0.1	<1	805	<0.5
08/11/2017	MA0295	West Basin	<1	0.191	<5	23.0	<0.1	<0.5	<0.5	<0.5	1030	0.568	<0.1	1920	<0.1	<0.5	35700	<0.1	<1	822	<0.5
23/01/2018	MA0306	West Basin	<1	0.221	<5	25.5	<0.1	<0.5	<0.5	<0.5	1190	0.629	<0.1	2100	<0.1	<0.5	40800	<0.1	<1	931	<0.5
07/03/2018	MA0319	West Basin	<0.1	0.225	<0.1	24.4	<0.05	<0.01	0.072	<0.05	1190	0.401	<0.01	2190	<0.01	<0.05	38800	<0.05	0.3	970	0.013
08/05/2018	MA0341	West Basin	<0.1	0.232	<0.1	26.3	<0.05	<0.01	0.069	<0.05	1270	0.407	<0.01	2210	<0.01	<0.05	42000	<0.05	0.4	989	0.012
10/07/2018	MA0364	West Basin	<0.1	0.213	<0.1	23.4	<0.05	<0.01	0.064	<0.05	1090	0.373	<0.01	1940	<0.01	<0.05	36600	<0.05	0.3	868	0.012
10/09/2018	MA0378	West Basin	<0.1	0.171	<0.1	18.8	<0.05	<0.01	0.056	<0.05	900	0.314	<0.01	1540	<0.01	<0.05	30200	<0.05	0.3	769	<0.01

Date	Sample#	Lake name	Si	Sr	Ti	Y	Zn	Be	Cd	Cs	La	Pb	Rb	Sb	Sn	Te	Zr	W	Hg	Tl	Th	U
			mg/L	mg/L	mg/L	mg/L	mg/L	µg/L	µg/L	µg/L	µg/L	µg/L	µg/L	µg/L	µg/L	µg/L	µg/L	µg/L	µg/L	µg/L	µg/L	µg/L
10/06/2015	MA0021	East Basin																				
05/04/2016	MA0054	East Basin	1.548	5.006	<0.005	<0.005	<0.005	<1	<1	<5	<5	<5	916	<5	<5	<10	5	<5	<10	<5	<1	18
02/08/2016	MA0111	East Basin	1.51	4.485	<0.005	<0.005	0.011	<1	<1	<5	<5	<5	805	<5	<5	<10	<5	<5	<10	<5	<1	16
19/09/2016	MA0152	East Basin	1.65	3.781	<0.005	<0.005	0.011	<1	<1	<5	<5	<5	714	<5	<5	<10	<5	<5	<10	<5	<1	15
18/11/2016	MA0173	East Basin	1.624	4.116	<0.005	<0.005	0.014	<1	<1	<5	<5	<5	705	<5	<5	<10	<5	<5	<10	<5	<1	24
04/01/2017	JT0193	East Basin	1.611	4.29	<0.005	<0.005	0.006	<1	<1	<5	<5	<5	754	<5	<5	<10	<5	<5	<10	<5	<1	16
12/03/2017	MA0224	East Basin	1.6	3.67	<0.05	<0.01	<0.05	<1	<1	2	<1	2	568	2	2	5	<50	2	<1	2	<1	10
26/04/2017	JR0260	East Basin	1.4	3.40	<0.05	<0.01	<0.05	<1	<1	2	<1	<1	538	2	2	4	<50	266	<1	<1	<1	10
28/06/2017	MA0264	East Basin	1.5	3.42	<0.05	<0.01	<0.05	<1	<1	1	<1	<1	537	2	<1	4	<50	96	<1	<1	<1	10
05/09/2017	MA0289	East Basin	1.6	3.12	<0.05	<0.01	<0.05	<1	<1	<1	<1	<1	502	1	<1	4	<50	223	<1	1	<1	9
08/11/2017	MA0296	East Basin	1.6	3.14	<0.05	<0.01	<0.05	<1	<1	<1	<1	<1	519	2	<1	4	<50	159	<1	2	<1	10
23/01/2018	MA0307	East Basin	1.4	3.37	<0.05	<0.01	<0.05	<1	<1	<1	<1	<1	565	2	<1	4	<50	41	<1	<1	<1	10
07/03/2018	MA0320	East Basin	1.7	3.85	<0.05	<0.01	<0.05	<5	<1	<1	<1	2	544	<5	<5	<10	12	25		<1	<1	10
08/05/2018	MA0342	East Basin	1.7	3.86	<0.05	<0.01	<0.05	<5	<1	<1	<1	2	588	<5	<5	<10	16	426		<1	<1	11
10/07/2018	MA0365	East Basin	1.7	3.51	<0.05	<0.01	<0.05	<5	<1	<1	<1	2	561	<5	<5	<10	12	610		<1	<1	11
10/09/2018	MA0379	East Basin	1.7	3.36	<0.05	<0.01	<0.05	<5	<1	<1	<1	<1	508	<5	<5	<10	12	<10		<1	<1	9
24/05/2015	MA0012	Lake Bullen Merri																				
10/06/2015	MA0023	Lake Bullen Merri	<0.1	0.255	<0.005	<0.005	<0.005	<1	<1	<5	<5	<5	32	<5	<5	<10	5	7	<10	<5	<1	<1
29/08/2015	MA0031	Lake Bullen Merri																				
30/08/2015	MA0032	Lake Bullen Merri																				
05/04/2016	MA0062	Lake Bullen Merri	<0.1	0.222	<0.005	<0.005	<0.005	<1	<1	<5	<5	<5	36	<5	<5	<10	7	<5	<10	<5	<1	<1
15/06/2016	MA0135	Lake Bullen Merri	<0.1	0.238	<0.005	<0.005	<0.005	<1	<1	<5	<5	<5	33	<5	<5	<10	5	<5	<10	<5	<1	<1
02/08/2016	MA0106	Lake Bullen Merri	<0.1	0.25	<0.005	<0.005	<0.005	<1	<1	<5	<5	<5	32	<5	<5	<10	6	<5	<10	<5	<1	<1
19/09/2016	MA0148	Lake Bullen Merri	<0.1	0.25	<0.005	<0.005	<0.005	1	<1	<5	<5	<5	32	<5	<5	<10	6	<5	<10	<5	<1	2
18/11/2016	MA0180	Lake Bullen Merri	<0.1	0.251	<0.005	<0.005	<0.005	1	<1	10	<5	<5	35	<5	<5	<10	6	<5	<10	<5	<1	21
04/01/2017	JT0201	Lake Bullen Merri	<0.1	0.258	<0.005	<0.005	0.006	<1	<1	<5	<5	<5	32	<5	<5	<10	6	<5	<10	<5	<1	<1
12/03/2017	MA0233	Lake Bullen Merri	<1	0.253	<0.05	<0.01	<0.05	<1	<1	<1	<1	<1	22	<1	<1	<1	<50	77	<1	<1	<1	<1
26/04/2017	JR0256	Lake Bullen Merri	<1	0.261	<0.05	<0.01	<0.05	<1	<1	<1	<1	<1	21	<1	<1	<1	2	40	<5	<1	<1	<1
28/06/2017	MA0268	Lake Bullen Merri	<1	0.254	<0.05	<0.01	<0.05	<1	<1	<1	<1	<1	24	<1	<1	2	<50	83	<1	3	<1	<1
04/09/2017	MA0282	Lake Bullen Merri	<1	0.259	<0.05	<0.01	<0.05	<1	<1	<1	<1	<1	23	<1	<1	2	<50	360	<1	4	<1	<1
08/11/2017	MA0302	Lake Bullen Merri	<1	0.253	<0.05	<0.01	<0.05	<1	<1	<1	<1	<1	22	<1	<1	<1	<50	29	<1	<1	<1	<1
23/01/2018	MA0314	Lake Bullen Merri	<1	0.229	<0.05	<0.01	<0.05	<1	<1	<1	<1	<1	24	<1	<1	2	<50	73	<1	1	<1	1
07/03/2018	MA0327	Lake Bullen Merri	<0.1	0.225	<0.005	<0.001	<0.005	<5	<1	<1	<1	3	23	<5	<5	<10	13	32		<1	<1	1
08/05/2018	MA0352	Lake Bullen Merri	<0.1	0.242	<0.005	<0.001	<0.005	<1	<1	<1	<1	<1	22	<1	<1	<1	8	138		<1	<1	<1
10/07/2018	MA0369	Lake Bullen Merri	<0.1	0.264	<0.005	<0.001	<0.005	<1	<1	<1	<1	<1	22	<1	<1	<1	8	188		<1	<1	1
09/09/2018	MA0375	Lake Bullen Merri	<0.1	0.255	<0.005	<0.001	<0.005	<1	<1	<1	<1	<1	22	<1	<1	<1	8	6		<1	<1	<1
23/05/2015	MA0005	Lake Edward																				
28/08/2015	MA0025	Lake Edward																				

Date	Sample#	Lake name	Si	Sr	Ti	Y	Zn	Be	Cd	Cs	La	Pb	Rb	Sb	Sn	Te	Zr	W	Hg	Tl	Th	U
			mg/L	mg/L	mg/L	mg/L	mg/L	µg/L	µg/L	µg/L	µg/L	µg/L	µg/L	µg/L	µg/L	µg/L	µg/L	µg/L	µg/L	µg/L	µg/L	µg/L
06/04/2016	MA0087	Lake Edward	0.269	3.219	<0.005	<0.005	0.012	<1	<1	<1	<1	<1	159	<5	<5	<5	<1	<1	<10	<1	<1	<1
03/08/2016	MA0126	Lake Edward	3.125	2.482	<0.005	<0.005	0.011	<1	<1	<1	<1	<1	125	<5	<5	<5	<1	<1	<10	<1	<1	<1
21/09/2016	MA0143	Lake Edward	4.349	2.283	<0.005	<0.005	0.019	<1	<1	<1	<1	<1	112	<5	<5	<5	<1	<1	<10	<1	<1	<1
18/11/2016	MA0191	Lake Edward	4.709	2.238	<0.005	<0.005	0.024	<1	<1	9	<1	1	108	<5	<5	<5	<1	<1	<10	<1	<1	11
07/01/2017	JT0214	Lake Edward	4.398	2.409	<0.005	<0.005	0.029	<1	<1	<1	<1	<1	112	<5	<5	<5	<1	<1	<10	<1	<1	<1
23/04/2017	MA0246	Lake Edward	2.0	2.66	<0.005	<0.001	0.014	<1	<1	<1	<1	<1	81	<1	<1	<1	<1	575	3	<1	<1	<1
24/04/2017	JR0251	Lake Edward	1.9	2.61	<0.005	<0.001	0.009	<1	<1	<1	<1	<1	85	<1	<1	<1	<1	26	<5	<1	<1	<1
29/06/2017	MA0274	Lake Edward	1.3	2.45	<0.005	<0.001	0.012	<1	<1	<1	<1	<1	81	<1	<1	<1	<1	38	<5	<1	<1	<1
03/09/2017	MA0277	Lake Edward	2.3	2.16	<0.005	<0.001	0.025	<1	<1	<1	<1	<1	70	<1	<1	<1	<1	25	<5	<1	<1	<1
07/11/2017	MA0292	Lake Edward	2.9	2.21	<0.005	<0.001	0.025	<1	<1	<1	<1	<1	72	<1	<1	<1	<1	117	<5	<1	<1	<1
22/01/2018	MA0304	Lake Edward	3.5	2.43	<0.005	0.018	0.016	<1	<1	<1	<1	<1	69	<1	<1	<1	<1	96	<5	<1	<1	15
06/03/2018	MA0317	Lake Edward	3.1	2.54	<0.005	<0.001	0.007	<5	<1	<1	<1	2	92	<5	<5	<10	<10	104		1	<1	<1
07/05/2018	MA0339	Lake Edward	0.1	2.60	<0.005	<0.001	0.015	<1	<1	<1	<1	<1	87	<1	<1	<1	<1	46		<1	<1	<1
09/07/2018	MA0358	Lake Edward	0.2	2.40	<0.005	<0.001	0.031	<1	<1	<1	<1	<1	80	<1	<1	<1	<1	226		<1	<1	<1
11/09/2018	MA0381	Lake Edward	1.8	1.93	<0.005	<0.001	0.024	<1	<1	<1	1	<1	70	<1	<1	<1	1	2		<1	<1	<1
24/05/2015	MA0010	Lake Elingamite																				
29/08/2015	MA0030	Lake Elingamite																				
15/06/2016	MA0131	Lake Elingamite	8.856	2.526	<0.005	<0.005	0.171	<1	<1	<1	<1	<1	13	<5	<5	<5	<1	5	<10	<1	<1	<1
02/08/2016	MA0117	Lake Elingamite	8.962	1.44	<0.005	<0.005	0.172	<1	<1	<1	<1	<1	11	<5	<5	<5	<1	<1	<10	<1	<1	<1
19/09/2016	MA0145	Lake Elingamite	1.265	1.071	<0.005	<0.005	0.009	<1	<1	<1	<1	<1	11	<5	<5	<5	<1	<1	<10	<1	<1	<1
18/11/2016	MA0182	Lake Elingamite	0.142	1.13	<0.005	<0.005	<0.005	<1	<1	4	<1	<1	11	<5	<5	<5	<1	<1	<10	<1	<1	5
04/01/2017	JT0203	Lake Elingamite	0.171	1.319	<0.005	<0.005	0.014	<1	<1	<1	<1	<1	15	<5	<5	<5	<1	<1	<10	<1	<1	<1
12/03/2017	MA0235	Lake Elingamite	1.1	1.48	<0.05	<0.01	<0.05	<1	<1	<1	<1	<1	12	<1	<1	<1	<1	<5	<5	<1	<1	<1
25/04/2017	JR0253	Lake Elingamite	1.4	0.927	0.007	<0.001	0.01	<1	<1	<1	<1	<1	7	<1	<1	<1	<1	233	<1	<1	<1	<1
28/06/2017	MA0269	Lake Elingamite	1.1	1.40	<0.05	<0.01	<0.05	<1	<1	<1	<1	<1	9	<1	<1	<1	<1	83	<5	<1	<1	<1
05/09/2017	MA0286	Lake Elingamite	<1	1.01	<0.05	<0.01	<0.05	<1	<1	<1	<1	<1	7	<1	<1	<1	<1	61	<5	<1	<1	<1
08/11/2017	MA0298	Lake Elingamite	<1	1.06	<0.05	<0.01	<0.05	<1	<1	<1	<1	<1	8	<1	<1	<1	<1	237	5	<1	<1	<1
23/01/2018	MA0312	Lake Elingamite	<1	1.40	<0.05	<0.01	<0.05	<1	<1	<1	<1	<1	11	<1	<1	<1	<1	36	<5	<1	<1	<1
07/03/2018	MA0322	Lake Elingamite	2.5	1.70	<0.005	<0.001	0.006	<1	<1	<1	<1	<1	12	<1	<1	<1	1	19		<1	<1	<1
08/05/2018	MA0344	Lake Elingamite	3.5	1.77	0.005	<0.001	0.006	<1	<1	<1	<1	<1	10	<1	<1	<1	2	44		<1	<1	<1
10/07/2018	MA0367	Lake Elingamite	0.9	1.06	<0.005	<0.001	0.005	<1	<1	<1	<1	<1	7	<1	<1	<1	<1	1060		<1	<1	<1
09/09/2018	MA0373	Lake Elingamite	<0.1	0.983	<0.005	<0.001	<0.005	<1	<1	<1	<1	<1	7	<1	<1	<1	1	29		<1	<1	<1
24/05/2015	MA0013	Lake Gnotuk																				
10/06/2015	MA0016	Lake Gnotuk	2.12	9.356	<0.005	<0.005	0.009	<1	<1	<5	<5	<5	397	<5	<5	<10	<5	14	<10	<5	<1	<1
30/08/2015	MA0033	Lake Gnotuk																				
05/04/2016	MA0066	Lake Gnotuk	2.4	9.669	0.006	<0.005	<0.005	<1	<1	<5	<5	<5	445	<5	<5	<10	<5	6	<10	<5	<1	<1
15/06/2016	MA0130	Lake Gnotuk	2.385	9.647	<0.005	<0.005	<0.005	<1	<1	<5	<5	<5	415	<5	<5	<10	<5	<5	<10	<5	<1	<1
02/08/2016	MA0103	Lake Gnotuk	2.357	9.441	<0.005	<0.005	<0.005	<1	<1	<5	<5	<5	418	<5	<5	<10	<5	<5	<10	<5	<1	<1

Date	Sample#	Lake name	Si	Sr	Ti	Y	Zn	Be	Cd	Cs	La	Pb	Rb	Sb	Sn	Te	Zr	W	Hg	Tl	Th	U
			mg/L	mg/L	mg/L	mg/L	mg/L	µg/L	µg/L	µg/L	µg/L	µg/L	µg/L	µg/L	µg/L	µg/L	µg/L	µg/L	µg/L	µg/L	µg/L	µg/L
19/09/2016	MA0149	Lake Gnotuk	2.23	9.379	<0.005	<0.005	0.007	<1	<1	<5	<5	<5	429	<5	<5	<10	<5	<5	<10	<5	<1	1
18/11/2016	MA0177	Lake Gnotuk	2.126	9.403	0.005	<0.005	<0.005	<1	<1	<5	<5	<5	400	<5	<5	<10	<5	7	<10	<5	<1	2
04/01/2017	JT0199	Lake Gnotuk	2.078	9.674	<0.005	<0.005	0.007	<1	<1	<5	<5	<5	435	<5	<5	<10	<5	<5	<10	<5	<1	<1
12/03/2017	MA0231	Lake Gnotuk	2.0	9.81	<0.05	<0.01	<0.05	<1	<1	1	<1	<1	303	<1	<1	4	<50	154	<1	2	<1	<1
26/04/2017	JR0257	Lake Gnotuk	2.0	9.12	<0.05	<0.01	<0.05	<1	<1	1	<1	21	289	<1	3	1	<50	39	<1	<1	<1	<1
28/06/2017	MA0266	Lake Gnotuk	1.9	9.07	<0.05	<0.01	<0.05	<1	<1	2	<1	<1	294	<1	<1	4	<50	152	<1	<1	<1	<1
04/09/2017	MA0280	Lake Gnotuk	1.9	9.14	<0.05	<0.01	<0.05	<1	<1	<1	<1	<1	315	<1	<1	4	<50	350	<1	1	<1	<1
08/11/2017	MA0301	Lake Gnotuk	1.9	9.10	<0.05	<0.01	<0.05	<1	<1	<1	<1	<1	312	<1	<1	4	<50	5	<1	2	<1	<1
23/01/2018	MA0313	Lake Gnotuk	1.7	9.37	<0.05	<0.01	<0.05	<1	<1	<1	<1	<1	327	<1	<1	4	<50	40	<1	<1	<1	1
07/03/2018	MA0326	Lake Gnotuk	1.7	9.85	<0.05	<0.01	<0.05	<5	<1	<1	<1	<1	303	<5	<5	<10	<10	<10		<1	<1	<1
08/05/2018	MA0351	Lake Gnotuk	1.8	10.0	<0.05	<0.01	<0.05	<5	<1	<1	<1	1	305	<5	<5	<10	11	976		<1	<1	<1
10/07/2018	MA0368	Lake Gnotuk	1.7	9.60	<0.05	<0.01	<0.05	<5	<1	<1	<1	2	307	<5	<5	<10	10	1540		<1	<1	1
09/09/2018	MA0374	Lake Gnotuk	1.3	9.59	<0.05	<0.01	<0.05	<5	<1	<1	<1	<1	305	<5	<5	<10	11	<10		<1	<1	<1
05/04/2016	MA0074	Lake Keilambete	1.764	7.263	0.011	<0.005	<0.005	1	<1	<5	<5	<5	408	<5	<5	<10	15	<5	<10	<5	<1	3
15/06/2016	MA0132	Lake Keilambete	2.13	6.673	0.009	<0.005	<0.005	<1	<1	<5	<5	<5	421	<5	<5	<10	10	29	<10	<5	<1	3
02/08/2016	MA0121	Lake Keilambete	1.939	6.338	0.029	<0.005	<0.005	1	<1	<5	<5	<5	350	<5	<5	<10	14	<5	<10	<5	<1	3
19/09/2016	MA0147	Lake Keilambete	1.757	6.479	0.01	<0.005	0.007	<1	<1	<5	<5	<5	379	<5	<5	<10	12	<5	<10	<5	<1	3
18/11/2016	MA0186	Lake Keilambete	1.944	6.391	0.009	<0.005	<0.005	<1	<1	<5	<5	<5	371	<5	<5	<10	11	12	<10	<5	<1	4
04/01/2017	JT0207	Lake Keilambete	1.828	6.63	0.009	<0.005	0.011	<1	<1	<5	<5	<5	391	<5	<5	<10	12	<5	<10	<5	<1	3
12/03/2017	MA0239	Lake Keilambete	<10	5.97	<0.5	<0.1	<0.5	<1	<1	<1	<1	<1	260	1	1	2	<50	6	<1	<1	<1	2
26/04/2017	JR0258	Lake Keilambete	<10	5.63	<0.5	<0.1	<0.5	<1	<1	2	<1	<1	236	1	2	2	<50	681	1	<1	<1	3
28/06/2017	MA0271	Lake keilambete	<10	5.93	<0.5	<0.1	<0.5	<1	<1	1	<1	<1	266	1	<1	4	<50	82	<1	<1	<1	2
04/09/2017	MA0284	Lake Keilambete	<10	5.58	<0.5	<0.1	<0.5	<1	<1	<1	<1	<1	244	1	<1	3	<50	376	<1	<1	<1	2
08/11/2017	MA0300	Lake Keilambete	<10	5.68	<0.5	<0.1	<0.5	<1	<1	<1	<1	<1	253	1	<1	5	<50	33	<1	1	<1	2
23/01/2018	MA0310	Lake Keilambete	<10	5.92	<0.5	<0.1	<0.5	<1	<1	1	<1	<1	274	1	<1	4	<50	123	<1	<1	<1	3
07/03/2018	MA0324	Lake Keilambete	1.9	6.09	<0.05	<0.01	<0.05	<5	<1	<1	<1	1	254	<5	<5	<10	19	134		<1	<1	2
08/05/2018	MA0347	Lake Keilambete	1.8	6.22	<0.05	<0.01	<0.05	<5	<1	<1	<1	<1	272	<5	<5	<10	23	85		<1	<1	2
10/07/2018	MA0361	Lake Keilambete	1.5	6.01	<0.05	<0.01	<0.05	<5	<1	<1	<1	<1	249	<5	<5	<10	23	159		<1	<1	2
09/09/2018	MA0371	Lake Keilambete	1.6	5.71	<0.05	<0.01	<0.05	<5	<1	<1	<1	<1	247	<5	<5	<10	23	15		<1	<1	1
23/05/2015	MA0004	Lake Leake																				
28/08/2015	MA0024	Lake Leake																				
03/08/2016	MA0128	Lake Leake	2.75	0.725	<0.005	<0.005	<0.005	<1	<1	<1	<1	<1	37	<5	<5	<5	<1	<1	<10	<1	<1	<1
21/09/2016	MA0142	Lake Leake	1.349	0.699	<0.005	<0.005	0.009	<1	<1	4	<1	1	34	<5	<5	<5	<1	<1	<10	<1	<1	4
18/11/2016	MA0193	Lake Leake	0.926	0.841	<0.005	<0.005	<0.005	<1	<1	6	<1	<1	37	<5	<5	<5	<1	<1	<10	<1	<1	12
07/01/2017	JT0216	Lake Leake	0.519	1.031	<0.005	<0.005	0.007	<1	<1	<1	<1	<1	43	<5	<5	<5	<1	<1	<10	<1	<1	<1
13/03/2017	MA0243	Lake Leake	<1	1.13	<0.05	<0.01	<0.05	<1	<1	<1	<1	<1	36	<1	<1	<1	<1	<5	<5	<1	<1	<1
23/04/2017	MA0248	Lake Leake	<1	1.13	<0.05	<0.01	<0.05	<1	<1	<1	<1	<1	36	<1	<1	<1	<1	<5	<5	<1	<1	<1
24/04/2017	JR0250	Lake Leake	0.6	1.22	<0.005	<0.001	<0.005	<1	<1	<1	<1	<1	36	<1	<1	<1	<1	2	<1	<1	<1	<1

Date	Sample#	Lake name	Si	Sr	Ti	Y	Zn	Be	Cd	Cs	La	Pb	Rb	Sb	Sn	Te	Zr	W	Hg	Tl	Th	U
			mg/L	mg/L	mg/L	mg/L	mg/L	µg/L	µg/L	µg/L	µg/L	µg/L	µg/L	µg/L	µg/L	µg/L	µg/L	µg/L	µg/L	µg/L	µg/L	µg/L
29/06/2017	MA0275	Lake Leake	<1	1.05	<0.05	<0.01	<0.05	<1	<1	<1	<1	<1	31	<1	<1	<1	<1	9	<5	<1	<1	<1
03/09/2017	MA0276	Lake Leake	<1	0.791	<0.05	<0.01	<0.05	<1	<1	<1	<1	<1	24	<1	<1	<1	<1	182	<5	<1	<1	<1
07/11/2017	MA0291	Lake Leake	<1	0.803	<0.05	<0.01	<0.05	<1	<1	<1	<1	<1	23	<1	<1	<1	<1	64	<5	<1	<1	<1
22/01/2018	MA0303	Lake Leake	<1	1.08	<0.05	0.012	<0.05	<1	<1	<1	<1	<1	28	<1	<1	<1	<1	98	<5	<1	<1	3
06/03/2018	MA0316	Lake Leake	0.2	1.35	<0.005	<0.001	<0.005	<5	<1	<1	<1	3	41	<5	<5	<10	<10	61		1	<1	<1
07/05/2018	MA0329	Lake Leake	0.2	1.40	<0.005	<0.001	<0.005	<1	<1	<1	<1	<1	41	<1	<1	<1	3	66		<1	<1	<1
09/07/2018	MA0357	Lake Leake	0.3	1.10	<0.005	<0.001	<0.005	<1	<1	<1	<1	<1	33	<1	<1	<1	2	72		<1	<1	<1
11/09/2018	MA0382	Lake Leake	1.2	0.815	<0.005	<0.001	<0.005	<1	<1	<1	<1	<1	24	<1	<1	<1	3	2		<1	<1	<1
29/08/2015	MA0029	Lake Mumblin																				
05/04/2016	MA0070	Lake Mumblin																				
02/08/2016	MA0119	Lake Mumblin	0.844	0.497	<0.005	<0.005	<0.005	<1	<1	<1	<1	<1	10	<1	<1	<1	<1	<1	<1	<1	<1	<1
19/09/2016	MA0150	Lake Mumblin	0.918	0.489	<0.005	<0.005	0.009	<1	<1	<1	<1	<1	10	<1	<1	<1	<1	<1	<1	<1	<1	<1
18/11/2016	MA0184	Lake Mumblin	1.304	0.498	<0.005	<0.005	0.006	<1	<1	1	<1	<1	7	<1	<1	<1	<1	<1	<1	<1	<1	<1
04/01/2017	JT0205	Lake Mumblin	2.359	0.54	<0.005	<0.005	0.006	<1	<1	<1	<1	<1	10	<1	<1	<1	<1	<1	<1	<1	<1	<1
12/03/2017	MA0237	Lake Mumblin	1.3	0.586	<0.005	<0.001	0.020	<1	<1	<1	<1	<1	9	<1	<1	<1	<1	9	<1	<1	<1	<1
28/06/2017	MA0270	Lake Mumblin	1.8	0.487	<0.005	<0.001	0.011	<1	<1	<1	<1	<1	6	<1	<1	<1	<1	399	2	<1	<1	<1
05/09/2017	MA0285	Lake Mumblin	1.3	0.421	<0.005	<0.001	0.009	<1	<1	<1	<1	<1	7	<1	<1	<1	<1	986	8	<1	<1	<1
08/11/2017	MA0299	Lake Mumblin	1.4	0.448	<0.005	<0.001	0.019	<1	<1	<1	<1	<1	7	<1	<1	<1	<1	1380	10	<1	<1	<1
23/01/2018	MA0311	Lake Mumblin	1.8	0.501	<0.005	0.002	<0.005	<1	<1	<1	<1	<1	7	<1	<1	<1	<1	38	<1	<1	<1	2
07/03/2018	MA0323	Lake Mumblin	0.9	0.560	<0.005	<0.001	0.01	<1	<1	<1	<1	<1	10	<1	<1	<1	1	37		<1	<1	<1
08/05/2018	MA0346	Lake Mumblin	0.8	0.520	<0.005	<0.001	<0.005	<1	<1	<1	<1	<1	11	<1	<1	<1	<1	51		<1	<1	<1
10/07/2018	MA0360	Lake Mumblin	<0.1	0.442	<0.005	0.002	<0.005	<1	<1	<1	<1	<1	8	<1	<1	<1	<1	1320		<1	<1	<1
09/09/2018	MA0372	Lake Mumblin	0.2	0.400	<0.005	<0.001	0.012	<1	<1	<1	<1	<1	6	<1	<1	<1	2	3		<1	<1	<1
24/05/2015	MA0011	Lake Purrumbete																				
10/06/2015	MA0022	Lake Purrumbete	0.63	0.308	<0.005	<0.005	0.006	<1	<1	<1	<1	<1	9	<1	<1	<1	<1	<1	<1	<1	<1	<1
30/08/2015	MA0035	Lake Purrumbete																				
05/04/2016	MA0058	Lake Purrumbete	0.207	0.321	<0.005	<0.005	<0.005	<1	<1	<1	<1	<1	12	<1	<1	<1	<1	<1	<1	<1	<1	<1
15/06/2016	MA0133	Lake Purrumbete	0.279	0.32	<0.005	<0.005	<0.005	<1	<1	<1	<1	<1	11	<1	<1	<1	<1	<1	<1	<1	<1	<1
02/08/2016	MA0113	Lake Purrumbete	0.575	0.315	<0.005	<0.005	<0.005	<1	<1	<1	<1	<1	11	<1	<1	<1	<1	<1	<1	<1	<1	<1
18/09/2016	MA0153	Lake Purrumbete	1.674	0.277	<0.005	<0.005	<0.005	<1	<1	<1	<1	<1	11	<1	<1	<1	<1	<1	<1	<1	<1	<1
18/11/2016	MA0175	Lake Purrumbete	0.332	0.306	<0.005	<0.005	<0.005	<1	<1	3	<1	<1	10	<1	<1	<1	<1	<1	<1	<1	<1	3
04/01/2017	JT0197	Lake Purrumbete	0.459	0.302	<0.005	<0.005	0.025	<1	<1	<1	<1	<1	11	<1	<1	<1	<1	<1	<1	<1	<1	<1
12/03/2017	MA0226	Lake Purrumbete	0.3	0.308	<0.005	<0.001	<0.005	<1	<1	<1	<1	<1	9	<1	<1	<1	<1	2	<1	<1	<1	<1
26/04/2017	JR0255	Lake Purrumbete	2.8	0.314	<0.005	<0.001	<0.005	<1	<1	<1	<1	<1	12	<1	<1	<1	<1	11	<1	<1	<1	<1
28/06/2017	MA0265	Lake Purrumbete	0.7	0.306	<0.005	<0.001	<0.005	<1	<1	<1	<1	<1	10	<1	<1	<1	<1	112	2	<1	<1	<1
05/09/2017	MA0290	Lake Purrumbete	0.2	0.307	<0.005	<0.001	<0.005	<1	<1	<1	<1	<1	9	<1	<1	<1	<1	1890	20	<1	<1	<1
08/11/2017	MA0297	Lake Purrumbete	0.4	0.304	<0.005	<0.001	<0.005	<1	<1	<1	<1	<1	8	<1	<1	<1	<1	319	2	<1	<1	<1
23/01/2018	MA0308	Lake Purrumbete	0.2	0.311	<0.005	0.162	0.005	<1	<1	<1	<1	1	<1	<1	<1	<1	<1	709	5	<1	<1	21

Date	Sample#	Lake name	Si	Sr	Ti	Y	Zn	Be	Cd	Cs	La	Pb	Rb	Sb	Sn	Te	Zr	W	Hg	Tl	Th	U
			mg/L	mg/L	mg/L	mg/L	mg/L	µg/L	µg/L	µg/L	µg/L	µg/L	µg/L	µg/L	µg/L	µg/L	µg/L	µg/L	µg/L	µg/L	µg/L	µg/L
07/03/2018	MA0321	Lake Purrumbete	0.3	0.324	<0.005	<0.001	<0.005	<1	<1	<1	<1	<1	9	<1	<1	<1	<1	246		<1	<1	<1
08/05/2018	MA0343	Lake Purrumbete	0.3	0.325	<0.005	<0.001	<0.005	<1	<1	<1	<1	<1	9	<1	<1	<1	<1	65		<1	<1	<1
10/07/2018	MA0366	Lake Purrumbete	0.7	0.315	<0.005	<0.001	<0.005	<1	<1	<1	<1	<1	8	<1	<1	<1	<1	127		<1	<1	<1
10/09/2018	MA0377	Lake Purrumbete	0.7	0.318	<0.005	<0.001	<0.005	<1	<1	<1	<1	<1	9	<1	<1	<1	<1	8		<1	<1	<1
23/05/2015	MA0006	Lake Surprise																				
29/08/2015	MA0026	Lake Surprise																				
06/04/2016	MA0081	Lake Surprise	1.229	0.165	<0.005	<0.005	<0.005	<1	<1	<1	<1	<1	12	<1	<1	<1	<1	<1	<1	<1	<1	<1
03/08/2016	MA0124	Lake Surprise	1.494	0.173	<0.005	<0.005	<0.005	<1	<1	<1	<1	<1	13	<1	<1	<1	<1	<1	<1	<1	<1	<1
20/09/2016	MA0144	Lake Surprise	2.752	0.155	<0.005	<0.005	<0.005	<1	<1	<1	<1	<1	11	<1	<1	<1	<1	<1	<1	<1	<1	2
18/11/2016	MA0189	Lake Surprise	5.08	0.173	<0.005	<0.005	<0.005	<1	<1	1	<1	<1	11	<1	<1	<1	<1	<1	<1	<1	<1	2
06/01/2017	JT0212	Lake Surprise	5.65	0.181	<0.005	<0.005	<0.005	<1	<1	<1	<1	<1	12	<1	<1	<1	<1	<1	<1	<1	<1	<1
12/03/2017	MA0241	Lake Surprise	5.0	0.173	<0.005	<0.001	0.008	<1	<1	<1	<1	<1	9	<1	<1	<1	<1	977	3	<1	<1	<1
25/04/2017	JR0252	Lake Surprise	4.0	0.170	<0.005	<0.001	<0.005	<1	<1	<1	<1	<1	8	<1	<1	<1	<1	5	<1	<1	<1	<1
29/06/2017	MA0273	Lake Surprise	4.0	0.178	<0.005	<0.001	<0.005	<1	<1	<1	<1	<1	9	<1	<1	<1	<1	17	<1	<1	<1	<1
03/09/2017	MA0278	Lake Surprise	3.9	0.170	<0.005	<0.001	<0.005	<1	<1	<1	<1	<1	7	<1	<1	<1	<1	406	2	<1	<1	<1
07/11/2017	MA0293	Lake Surprise	5.4	0.162	<0.005	<0.001	<0.005	<1	<1	<1	<1	<1	9	<1	<1	<1	<1	30	1	<1	<1	<1
22/01/2018	MA0305	Lake Surprise	4.3	0.170	<0.005	0.024	<0.005	<1	<1	<1	<1	<1	10	<1	<1	<1	<1	132	2	<1	<1	4
06/03/2018	MA0318	Lake Surprise	4.0	0.182	<0.005	<0.001	<0.005	<1	<1	<1	<1	<1	10	<1	<1	<1	<1	48		<1	<1	<1
07/05/2018	MA0340	Lake Surprise	4.0	0.180	<0.005	<0.001	<0.005	<1	<1	<1	<1	<1	9	<1	<1	<1	<1	37		<1	<1	<1
09/07/2018	MA0359	Lake Surprise	4.3	0.184	<0.005	<0.001	<0.005	<1	<1	<1	<1	<1	9	<1	<1	<1	<1	896		<1	<1	<1
11/09/2018	MA0380	Lake Surprise	4.4	0.181	<0.005	<0.001	<0.005	<1	<1	<1	<1	<1	9	<1	<1	<1	<1	2		<1	<1	<1
24/05/2015	MA0014	Lake Tooliorook																				
30/08/2015	MA0036	Lake Tooliorook																				
05/04/2016	MA0044	Lake Tooliorook																				
15/06/2016	MA0134	Lake Tooliorook	3.122	1.694	<0.005	<0.005	<0.005	<1	<1	<1	<1	<1	8	<5	<5	<5	<1	<1	<10	<1	<1	2
02/08/2016	MA0115	Lake Tooliorook	1.313	1.495	<0.005	<0.005	<0.005	<1	<1	<1	<1	<1	<5	<5	<5	<5	<1	<1	<10	<1	<1	1
18/09/2016	MA0167	Lake Tooliorook																				
17/11/2016	MA0169	Lake Tooliorook	5.136	0.831	<0.005	<0.005	<0.005	<1	<1	5	<1	<1	<5	<5	<5	<5	<1	<1	<10	<1	<1	14
06/01/2017	JT0209	Lake Tooliorook	1.372	0.954	<0.005	<0.005	0.014	<1	<1	2	<1	<1	<5	<5	<5	<5	<1	<1	<10	<1	<1	2
12/03/2017	MA0228	Lake Tooliorook	<1	1.05	<0.05	<0.01	<0.05	<1	<1	<1	<1	<1	4	<1	<1	<1	1	7	<5	<1	<1	<1
26/04/2017	JR0254	Lake Tooliorook	2.0	1.05	<0.05	<0.01	<0.05	<1	<1	<1	<1	<1	4	<1	<1	<1	<1	180	<5	<1	<1	1
27/06/2017	MA0262	Lake Tooliorook	2.5	1.03	<0.05	<0.01	<0.05	<1	<1	<1	<1	<1	4	<1	<1	<1	<1	13	<5	<1	<1	<1
05/09/2017	MA0287	Lake Tooliorook	<1	1.01	<0.05	<0.01	<0.05	<1	<1	<1	<1	<1	3	<1	<1	<1	<1	135	<5	<1	<1	<1
08/11/2017	MA0294	Lake Tooliorook	3.6	1.05	<0.05	<0.01	<0.05	<1	<1	<1	<1	<1	4	<1	<1	<1	<1	62	<5	<1	<1	1
24/01/2018	MA0315	Lake Tooliorook	3.6	1.15	<0.05	<0.01	<0.05	<1	<1	<1	<1	<1	4	<1	<1	<1	<1	13	<5	<1	<1	1
07/03/2018	MA0325	Lake Tooliorook	1.9	1.22	<0.005	<0.001	<0.005	<1	<1	<1	<1	<1	4	<1	<1	<1	1	9		<1	<1	1
08/05/2018	MA0349	Lake Tooliorook	0.4	1.18	<0.005	<0.001	<0.005	<1	<1	<1	<1	<1	4	<1	<1	<1	<1	34		<1	<1	1
10/07/2018	MA0363	Lake Tooliorook	0.5	1.14	0.006	<0.001	<0.005	<1	<1	<1	<1	<1	4	<1	<1	<1	1	305		<1	<1	<1

Date	Sample#	Lake name	Si	Sr	Ti	Y	Zn	Be	Cd	Cs	La	Pb	Rb	Sb	Sn	Te	Zr	W	Hg	Tl	Th	U
			mg/L	mg/L	mg/L	mg/L	mg/L	µg/L	µg/L	µg/L	µg/L	µg/L	µg/L	µg/L	µg/L	µg/L	µg/L	µg/L	µg/L	µg/L	µg/L	µg/L
09/09/2018	MA0370	Lake Tooliorook	0.9	1.16	<0.005	<0.001	<0.005	<1	<1	<1	<1	<1	4	<1	<1	<1	1	15		<1	<1	<1
23/05/2015	MA0008	Tower Hill																				
29/08/2015	MA0027	Tower Hill																				
20/09/2016	MA0158	Tower Hill	7.283	0.759	0.009	<0.005	0.03	<1	<1	76	<1	3	157	<5	<5	<5	<1	3	<10	<1	<1	218
06/01/2017	JT0211	Tower Hill																				
10/06/2015	MA0018	West Basin	2.102	4.875	<0.005	<0.005	0.009	<1	<1	<5	<5	<5	377	<5	<5	<10	<5	<5	<10	<5	<1	48
10/06/2015	MA0019	West Basin	2.087	5.002	<0.005	<0.005	<0.005	<1	<1	<5	<5	<5	430	5	<5	<10	<5	<5	<10	<5	<1	56
05/04/2016	MA0050	West Basin	1.882	5.435	<0.005	<0.005	0.007	<1	<1	<5	<5	<5	415	<5	<5	<10	<5	<5	<10	<5	<1	54
02/08/2016	MA0109	West Basin	1.746	4.859	<0.005	<0.005	0.005	<1	<1	<5	<5	<5	461	6	<5	<10	<5	<5	<10	<5	<1	60
19/09/2016	MA0151	West Basin	1.673	3.971	<0.005	<0.005	<0.005	<1	<1	<5	<5	<5	380	<5	<5	<10	<5	<5	<10	<5	<1	52
18/11/2016	MA0171	West Basin	1.799	4.523	<0.005	<0.005	0.009	<1	<1	<5	<5	<5	385	<5	<5	<10	<5	<5	<10	<5	<1	52
04/01/2017	JT0195	West Basin	1.883	4.712	<0.005	<0.005	0.021	<1	<1	<5	<5	<5	417	5	<5	<10	<5	<5	<10	<5	<1	54
12/03/2017	MA0222	West Basin	<10	4.40	<0.5	<0.1	<0.5	<1	<1	2	<1	<1	302	3	2	5	<50	12	<1	<1	<1	33
26/04/2017	JR0259	West Basin	<10	4.02	<0.5	<0.1	<0.5	<1	<1	4	<1	<1	277	2	3	5	<50	3510	28	<1	<1	36
28/06/2017	MA0263	West Basin	<10	4.11	<0.5	<0.1	<0.5	<1	<1	1	<1	<1	280	3	1	4	<50	70	<1	<1	<1	30
05/09/2017	MA0288	West Basin	<10	3.82	<0.5	<0.1	<0.5	<1	<1	1	<1	<1	256	2	<1	4	<50	1730	5	<1	<1	28
08/11/2017	MA0295	West Basin	<10	3.90	<0.5	<0.1	<0.5	<1	<1	1	<1	<1	274	3	<1	5	<50	62	<1	<1	<1	29
23/01/2018	MA0306	West Basin	<10	4.34	<0.5	<0.1	<0.5	<1	<1	<1	<1	<1	302	3	<1	3	<50	68	<1	<1	<1	34
07/03/2018	MA0319	West Basin	2.0	4.50	<0.05	<0.01	<0.05	<5	<1	<1	<1	3	311	<5	<5	<10	11	31		<1	<1	35
08/05/2018	MA0341	West Basin	2.0	4.62	<0.05	<0.01	<0.05	<5	<1	<1	<1	2	310	<5	<5	<10	12	70		<1	<1	33
10/07/2018	MA0364	West Basin	2.2	4.18	<0.05	<0.01	<0.05	<5	<1	<1	<1	<1	279	<5	<5	<10	11	173		<1	<1	31
10/09/2018	MA0378	West Basin	1.7	3.27	<0.05	<0.01	<0.05	<5	<1	<1	<1	<1	231	<5	<5	<10	<10	<10		<1	<1	23

Samples taken by: Martin ankor

Sample ID	Lake Name	Sample Type	Sample Time
MA0021	East Basin	Water	10/06/15 2:36 pm

Sampling depth	0.1m	Coords & QC	-38.326213	143.453522	133.2	16.8

Sampling notes		Water Chemistry	
		pH	
		TDS	
Catchment notes		DO	
		Cond.	
		PSU	
		Temp	

Weather Conditions

Water Condition	Calm		Air Temp & RH	12ºC	Overcast
Water Clarity	Cloudy (0.5-2m visibility)		Wind Speed	Medium (branches moving.	
Clouds			Wind Direction	SSW to NNE	
Weather Notes					

Samples taken by: Martin Ankor

Sample ID	Lake Name	Sample Type	Sample Time
MA0054	East Basin	Water-stable isotopes	5/04/16 10:33 am

Sampling depth	0.2m	Coords & QC	-38.326423	143.453489	110.4	7.8

		Water Chemistry	
Sampling notes		pH	7.68
		TDS	64250ppm
		DO	
Catchment notes		Cond.	128500µS/cm
		PSU	
		Temp	18.54ºC

Weather Conditions

Water Condition	Choppy	18.54ºC	Air Temp & RH	23ºC	25
Water Clarity	Murky (<0.5m visibility)		Wind Speed	Medium (branches moving.	
Clouds			Wind Direction	N to S	
Weather Notes					

Samples taken by: Martin Ankor

Sample ID	Lake Name	Sample Type	Sample Time
MA0111	East Basin	Water - general	2/08/16 10:50 am

Sampling depth	0.2m	Coords & QC	-38.326129	143.453129	97.8	13.0

Sampling notes

Catchment notes

Water Chemistry

pH	8.99
TDS	6320ppm
DO	2.72ppm
Cond.	120600µS/cm
PSU	-
Temp	11.2ºC

Weather Conditions

Water Condition	Choppy	11.2ºC	Air Temp & RH	9.4ºC	81
Water Clarity	Cloudy (0.5-2m visibility)		Wind Speed	Medium (branches moving.	
Clouds	Overcast		Wind Direction	SW to NE	
Weather Notes	Raining lightly				

Samples taken by: Martin Ankor

Sample ID	Lake Name	Sample Type	Sample Time
MA0173	East Basin	Water - bulk	18/11/16 8:39 am

Sampling depth	0.2m	Coords & QC	-38.326309	143.453478	115.9	15.6

		Water Chemistry	
Sampling notes		pH	9.04
		TDS	48650ppm
Catchment notes		DO	2.9ppm
		Cond.	97360µS/cm
		PSU	-
		Temp	19.2ºC

Weather Conditions

Water Condition	Calm	19.2ºC	Air Temp & RH	12.3ºC	97
Water Clarity	Murky (<0.5m visibility)		Wind Speed	Low (calm conditions.	
Clouds	Overcast		Wind Direction	SSW to NNE	
Weather Notes					

Samples taken by: Jonathan Tyler

Sample ID	Lake Name	Sample Type	Sample Time
JT0193	East Basin	Bulk water	4/01/17 10:35 am

Sampling depth	0.3m	Coords & QC	-38.328653	143.456645	137.9	15.6

Sampling notes

Catchment notes

Water Chemistry

pH	8.89
TDS	58640ppm
DO	0.24ppm
Cond.	117300µS/cm
PSU	
Temp	22.32ºC

Weather Conditions

Water Condition	Calm	22.32ºC	Air Temp & RH		
Water Clarity	Murky (<0.5m visibility)		Wind Speed	Low (calm conditions. 1	
Clouds	Sunny		Wind Direction		
Weather Notes					

Samples taken by: Martin Ankor

Sample ID	Lake Name	Sample Type	Sample Time
MA0224	East Basin	Water - bulk	12/03/17 9:39 am

Sampling depth	0.2m	Coords & QC	-38.326051	143.453364	121.3	15.6

Sampling notes

Catchment notes

Water Chemistry

pH	8.96
TDS	52400ppm
DO	0.24ppm
Cond.	104800µS/cm
PSU	-
Temp	21.6ºC

Weather Conditions

Water Condition	Calm	21.6ºC	Air Temp & RH	16ºC	99
Water Clarity	Murky (<0.5m visibility)		Wind Speed	Medium (branches moving.	
Clouds	Partly Cloudy		Wind Direction	ESE to WNW	
Weather Notes					

Samples taken by: Martin Ankor

Sample ID	Lake Name	Sample Type	Sample Time
MA0264	East Basin	Water - stable isotopes and	28/06/17 8:45 am

Sampling depth	0.2m	Coords & QC	-38.326107	143.453188	170.1	33.5

		Water Chemistry	
Sampling notes		pH	9.1
		TDS	51280ppm
Catchment notes		DO	1.57ppm
		Cond.	102500µS/cm
		PSU	-
		Temp	10.1ºC

Weather Conditions

Water Condition	Calm	10.1ºC	Air Temp & RH	7ºC	97
Water Clarity	Murky (<0.5m visibility)		Wind Speed	Low (calm conditions. 1	
Clouds	Partly Cloudy		Wind Direction	NNW to SSE	
Weather Notes					

Samples taken by: Martin Ankor

Sample ID	Lake Name	Sample Type	Sample Time
MA0289	East Basin	Water - stable isotopes and	5/09/17 3:02 pm

Sampling depth	0.3m	Coords & QC	-38.326106	143.453340	115.2	13.0

		Water Chemistry	
Sampling notes		pH	9.14
		TDS	51600ppm
Catchment notes		DO	1.25ppm
		Cond.	103200µS/cm
		PSU	-
		Temp	10.3ºC

Weather Conditions

Water Condition	Choppy	10.3ºC	Air Temp & RH	7.3ºC	100
Water Clarity	Murky (<0.5m visibility)		Wind Speed	High (Windy. 10+ m/s)	
Clouds	Partly Cloudy		Wind Direction	WNW to ESE	
Weather Notes					

Samples taken by: Martin Ankor

Sample ID	Lake Name	Sample Type	Sample Time
MA0296	East Basin	Water - stable isotopes and	8/11/17 12:47 pm

Sampling depth	0.3m	Coords & QC	-38.326070	143.453195	131.8	13.0

Sampling notes

Catchment notes

Water Chemistry

pH	9.1
TDS	52500ppm
DO	2.13ppm
Cond.	104800µS/cm
PSU	
Temp	18.9ºC

Weather Conditions

Water Condition	Calm	18.9ºC	Air Temp & RH	14ºC	71
Water Clarity	Murky (<0.5m visibility)		Wind Speed	Low (calm conditions. 1	
Clouds	Partly Cloudy		Wind Direction	ESE to WNW	
Weather Notes					

Samples taken by: Martin Ankor

Sample ID	Lake Name	Sample Type	Sample Time
MA0307	East Basin	Water - stable isotopes and	23/01/18 10:08 am

Sampling depth	0.3m	Coords & QC	-38.326123	143.453176	114.4	26.0

Sampling notes

Catchment notes

Water Chemistry

pH	9
TDS	52570ppm
DO	0.2ppm
Cond.	105200µS/cm
PSU	-
Temp	25.3ºC

Weather Conditions

Water Condition	Calm	25.3ºC	Air Temp & RH	18ºC	62
Water Clarity	Murky (<0.5m visibility)		Wind Speed	Medium (branches moving.	
Clouds	Sunny		Wind Direction	ESE to WNW	
Weather Notes					

Samples taken by: Martin Ankor

Sample ID	Lake Name	Sample Type	Sample Time
MA0320	East Basin	Water - stable isotopes and	7/03/18 9:11 am

Sampling depth	0.3m	Coords & QC	-38.326231	143.452955	109.8	15.6

Sampling notes

Catchment notes

Water Chemistry

pH	8.91
TDS	62800ppm
DO	8ppm
Cond.	125600µS/cm
PSU	
Temp	20.6ºC

Weather Conditions

Water Condition	Calm	20.6ºC	Air Temp & RH	16ºC	96
Water Clarity	Murky (<0.5m visibility)		Wind Speed	Low (calm conditions. 1	
Clouds	Sunny		Wind Direction	ESE to WNW	
Weather Notes					

Samples taken by: Martin Ankor

Sample ID	Lake Name	Sample Type	Sample Time
MA0342	East Basin	Water - stable isotopes and	8/05/18 9:08 am

Sampling depth	0.3m	Coords & QC	-38.326201	143.453342	117.5	7.8

Sampling notes

Catchment notes

Water Chemistry

pH	8.96
TDS	59650ppm
DO	6.3ppm
Cond.	119200µS/cm
PSU	
Temp	14.4ºC

Weather Conditions

Water Condition	Calm	14.4ºC	Air Temp & RH	97ºC	82
Water Clarity	Murky (<0.5m visibility)		Wind Speed	Low (calm conditions. 1	
Clouds	Sunny		Wind Direction	SE to NW	
Weather Notes					

Samples taken by: Martin Ankor

Sample ID	Lake Name	Sample Type	Sample Time
MA0365	East Basin	Water - stable isotopes and	10/07/18 12:17 pm

Sampling depth	0.2m	Coords & QC	-38.326110	143.453273	129.4	13.0

Sampling notes	
Catchment notes	PSU off chart

Water Chemistry	
pH	8.91
TDS	56960ppm
DO	6.75ppm
Cond.	113800µS/cm
PSU	
Temp	10.5ºC

Weather Conditions

Water Condition	Calm	10.5ºC	Air Temp & RH	8.4ºC	
Water Clarity	Murky (<0.5m visibility)		Wind Speed	Low (calm conditions. 1	
Clouds	Overcast		Wind Direction	NW to SE	
Weather Notes					

Samples taken by: Martin Ankor

Sample ID	Lake Name	Sample Type	Sample Time
MA0379	East Basin	Water - stable isotopes and	10/09/18 11:17 am

Sampling depth	0.2m	Coords & QC	-38.326227	143.453252	99.0	26.0

Sampling notes	
Catchment notes	

Water Chemistry	
pH	8.92
TDS	57670ppm
DO	5.85ppm
Cond.	115300µS/cm
PSU	-
Temp	13.7ºC

Weather Conditions

Water Condition	Calm	13.7ºC	Air Temp & RH	14.2ºC	
Water Clarity	Murky (<0.5m visibility)		Wind Speed	Medium (branches moving.	
Clouds	Partly Cloudy		Wind Direction	NW to SE	
Weather Notes					

Samples taken by: Martin Ankor

Sample ID	Lake Name	Sample Type	Sample Time
MA0012	Lake Bullen Merri	Water	24/05/15 11:17 am

Sampling depth	0.4	Coords & QC	-38.260232	143.095611	138.1	15.6
Sampling notes	End of boat ramp pontoon. Sample capped at depth by hand.					
Catchment notes						

Weather Conditions

Water Condition	Calm		Air Temp & RH	10	
Water Clarity	Clear (>2m visibility)		Wind Speed	Low (calm conditions. 1	
Clouds	Partly Cloudy		Wind Direction	NNE to SSW	
Weather Notes					

Samples taken by: Martin ankor

Sample ID	Lake Name	Sample Type	Sample Time
MA0023	Lake Bullen Merri	Water	10/06/15 5:40 pm

Sampling depth	0.2m	Coords & QC				0.0

Sampling notes	Calcium isotope sample	Water Chemistry	
		pH	
		TDS	
Catchment notes		DO	
		Cond.	
		PSU	
		Temp	

Weather Conditions

Water Condition	Calm		Air Temp & RH		Overcast
Water Clarity	Clear (>2m visibility)		Wind Speed	Low (calm conditions. 1	
Clouds			Wind Direction		
Weather Notes					

Samples taken by: Martin Ankor

Sample ID	Lake Name	Sample Type	Sample Time
MA0031	Lake Bullen Merri	Water	29/08/15 4:22 pm

Sampling depth	0.2m	Coords & QC	-38.260567	143.095482	166.5	13.0

Sampling notes	Lake level 5.413 below tbm sr77m9.	Water Chemistry	
		pH	
		TDS	
Catchment notes		DO	
		Cond.	
		PSU	
		Temp	

Weather Conditions

Water Condition	Calm		Air Temp & RH	9.5°C	
Water Clarity	Clear (>2m visibility)		Wind Speed	Medium (branches moving.	
Clouds	Overcast		Wind Direction	SSW to NNE	
Weather Notes					

Samples taken by: Martin Ankor

Sample ID	Lake Name	Sample Type	Sample Time
MA0032	Lake Bullen Merri	Water	30/08/15 9:57 am

Sampling depth	0.1m	Coords & QC	-38.242986	143.113311	153.5	15.6

Sampling notes		Water Chemistry	
		pH	
		TDS	
Catchment notes		DO	
		Cond.	
		PSU	
		Temp	

Weather Conditions

Water Condition	Calm		Air Temp & RH	9°C	
Water Clarity	Clear (>2m visibility)		Wind Speed	Medium (branches moving.	
Clouds	Overcast		Wind Direction	S to N	
Weather Notes					

Samples taken by: Martin Ankor

Sample ID	Lake Name	Sample Type	Sample Time
MA0062	Lake Bullen Merri	Water-stable isotopes	5/04/16 1:32 pm

Sampling depth	0.2m	Coords & QC	-38.260651	143.095445	134.1	13.0

Sampling notes

Catchment notes

Water Chemistry

pH	8.51
TDS	8343ppm
DO	0.77ppm
Cond.	16660µS/cm
PSU	9.83
Temp	18.52ºC

Weather Conditions

Water Condition	Choppy	18.52ºC	Air Temp & RH	27ºC	24
Water Clarity	Clear (>2m visibility)		Wind Speed	Medium (branches moving.	
Clouds	Partly Cloudy		Wind Direction	N to S	
Weather Notes					

Samples taken by: Martin Ankor

Sample ID	Lake Name	Sample Type	Sample Time
MA0106	Lake Bullen Merri	Water - general	2/08/16 9:26 am

Sampling depth	0.3m	Coords & QC	-38.260269	143.095556	133.5	13.0

Sampling notes	
Catchment notes	

Water Chemistry

pH	9.26
TDS	8193ppm
DO	4.79ppm
Cond.	16270µS/cm
PSU	9.57
Temp	10.59ºC

Weather Conditions

Water Condition	Calm	10.59ºC	Air Temp & RH	8.3ºC	
Water Clarity	Cloudy (0.5-2m visibility)		Wind Speed	Low (calm conditions.	
Clouds	Sunny		Wind Direction	SSW to NNE	
Weather Notes					

Samples taken by: Martin Ankor

Sample ID	Lake Name	Sample Type	Sample Time
MA0180	Lake Bullen Merri	Water - stable isotope	18/11/16 10:59 am

Sampling depth	0.3m	Coords & QC	-38.260245	143.095565	153.4	13.0

Sampling notes

Catchment notes

Water Chemistry	
pH	9.29
TDS	6968ppm
DO	4.7ppm
Cond.	13930µS/cm
PSU	8.11
Temp	15.73ºC

Weather Conditions

Water Condition	Calm	15.73ºC	Air Temp & RH	13ºC	84
Water Clarity	Cloudy (0.5-2m visibility)		Wind Speed	Low (calm conditions. 1	
Clouds	Overcast		Wind Direction	SW to NE	
Weather Notes					

Samples taken by: Jonathan Tyler

Sample ID	Lake Name	Sample Type	Sample Time
JT0201	Lake Bullen Merri	Bulk water	4/01/17 2:29 pm

Sampling depth	0.4m	Coords & QC	-38.260307	143.095667	158.9	18.9

		Water Chemistry	
Sampling notes	4/1/2017	pH	9.22
		TDS	8165ppm
Catchment notes		DO	2ppm
		Cond.	16320µS/cm
		PSU	9.58
		Temp	22.1ºC

Weather Conditions

Water Condition	Calm	22.1ºC	Air Temp & RH		
Water Clarity	Cloudy (0.5-2m visibility)		Wind Speed	Low (calm conditions. 1	
Clouds	Sunny		Wind Direction		
Weather Notes					

Samples taken by: Martin Ankor

Sample ID	Lake Name	Sample Type	Sample Time
MA0233	Lake Bullen Merri	Water - bulk	12/03/17 12:48 pm

Sampling depth	0.3m	Coords & QC	-38.260201	143.095639	142.0	7.8

		Water Chemistry	
Sampling notes		pH	9.3
		TDS	7113ppm
Catchment notes		DO	0.69ppm
		Cond.	14230µS/cm
		PSU	8.27
		Temp	20.9ºC

Weather Conditions

Water Condition	Calm	20.9ºC	Air Temp & RH	20.5ºC	71
Water Clarity	Murky (<0.5m visibility)		Wind Speed	Low (calm conditions. 1	
Clouds	Partly Cloudy		Wind Direction	W to E	
Weather Notes					

Samples taken by: Martin Ankor

Sample ID	Lake Name	Sample Type	Sample Time
MA0268	Lake Bullen Merri	Water - stable isotopes and	28/06/17 12:07 pm

Sampling depth	0.3m	Coords & QC	-38.261045	143.095247	150.9	13.0

Sampling notes

Catchment notes

Water Chemistry

pH	9.4
TDS	7048ppm
DO	2.49ppm
Cond.	14090µS/cm
PSU	8.21
Temp	12.4ºC

Weather Conditions

Water Condition	Choppy	12.4ºC	Air Temp & RH	13.2ºC	77
Water Clarity	Cloudy (0.5-2m visibility)		Wind Speed	Medium (branches moving.	
Clouds	Partly Cloudy		Wind Direction	NNW to SSE	
Weather Notes					

Samples taken by: Martin Ankor

Sample ID	Lake Name	Sample Type	Sample Time
MA0282	Lake Bullen Merri	Water - stable isotopes and	4/09/17 3:39 pm

Sampling depth	0.3m	Coords & QC	-38.260849	143.095191	159.1	16.8

Sampling notes

Catchment notes

Water Chemistry

pH	9.2
TDS	7599ppm
DO	1.9ppm
Cond.	15190µS/cm
PSU	8.9
Temp	10.7ºC

Weather Conditions

Water Condition	Choppy	10.7ºC	Air Temp & RH	7.5ºC	86
Water Clarity	Cloudy (0.5-2m visibility)		Wind Speed	High (Windy. 10+ m/s)	
Clouds	Partly Cloudy		Wind Direction	W to E	
Weather Notes					

Samples taken by: Martin Ankor

Sample ID	Lake Name	Sample Type	Sample Time
MA0302	Lake Bullen Merri	Water - stable isotopes and	8/11/17 6:13 pm

Sampling depth	0.3m	Coords & QC	-38.260200	143.095671	148.0	6.4

Sampling notes

Catchment notes

Water Chemistry

pH	9.28
TDS	7601ppm
DO	3.15ppm
Cond.	15190µS/cm
PSU	8.88
Temp	17.33ºC

Weather Conditions

Water Condition	Calm	17.33ºC	Air Temp & RH	19ºC	57
Water Clarity	Cloudy (0.5-2m visibility)		Wind Speed	Low (calm conditions. 1	
Clouds	Sunny		Wind Direction	ESE to WNW	
Weather Notes					

Samples taken by: Martin Ankor

Sample ID	Lake Name	Sample Type	Sample Time
MA0314	Lake Bullen Merri	Water - stable isotopes and	23/01/18 5:41 pm

Sampling depth	0.3m	Coords & QC	-38.228704	143.099942	111.5	9.4

Sampling notes

Catchment notes

Water Chemistry

pH	9.4
TDS	7260ppm
DO	0.48ppm
Cond.	14520µS/cm
PSU	8.44
Temp	22.7ºC

Weather Conditions

Water Condition	Calm	22.7ºC	Air Temp & RH	23.3ºC	44
Water Clarity	Cloudy (0.5-2m visibility)		Wind Speed	Low (calm conditions. 1	
Clouds	Sunny		Wind Direction	S to N	
Weather Notes					

Samples taken by: Martin Ankor

Sample ID	Lake Name	Sample Type	Sample Time
MA0327	Lake Bullen Merri	Water - stable isotopes and	7/03/18 4:27 pm

Sampling depth	0.3m	Coords & QC	-38.228728	143.099904	99.6	13.0

Sampling notes

Catchment notes

Water Chemistry

pH	9.26
TDS	8406ppm
DO	13ppm
Cond.	16800µS/cm
PSU	9.88
Temp	23ºC

Weather Conditions

Water Condition	Calm	23ºC	Air Temp & RH	30ºC	23
Water Clarity	Murky (<0.5m visibility)		Wind Speed	Low (calm conditions. 1	
Clouds	Sunny		Wind Direction	E to W	
Weather Notes					

Samples taken by: Martin Ankor

Sample ID	Lake Name	Sample Type	Sample Time
MA0352	Lake Bullen Merri	Water - stable isotopes and	8/05/18 5:46 pm

Sampling depth	0.3m	Coords & QC	-38.260322	143.095416	143.8	10.8

Sampling notes

Catchment notes

Water Chemistry

pH	9.3
TDS	7821ppm
DO	10.5ppm
Cond.	15670µS/cm
PSU	9.2
Temp	15.6ºC

Weather Conditions

Water Condition	Calm	15.6ºC	Air Temp & RH	13ºC	60
Water Clarity	Clear (>2m visibility)		Wind Speed	Low (calm conditions. 1	
Clouds	Sunny		Wind Direction	W to E	
Weather Notes					

Samples taken by: Martin Ankor

Sample ID	Lake Name	Sample Type	Sample Time
MA0369	Lake Bullen Merri	Water - stable isotopes and	10/07/18 2:59 pm

Sampling depth	0.2m	Coords & QC	-38.260820	143.095199	192.0	26.0

Sampling notes

Catchment notes

Water Chemistry

pH	9.15
TDS	7701ppm
DO	11.18ppm
Cond.	15400µS/cm
PSU	9.02
Temp	11.13ºC

Weather Conditions

Water Condition	Choppy	11.13ºC	Air Temp & RH	10.3ºC	72
Water Clarity	Cloudy (0.5-2m visibility)		Wind Speed	Medium (branches moving.	
Clouds	Overcast		Wind Direction	WNW to ESE	
Weather Notes					

Samples taken by: Martin Ankor

Sample ID	Lake Name	Sample Type	Sample Time
MA0375	Lake Bullen Merri	Water - stable isotopes and	9/09/18 4:45 pm

Sampling depth	0.2m	Coords & QC	-38.260817	143.095146	173.0	18.9

Sampling notes

Catchment notes

Water Chemistry

pH	9.1
TDS	8065ppm
DO	7.17ppm
Cond.	16110µS/cm
PSU	9.5
Temp	11ºC

Weather Conditions

Water Condition	Calm	11ºC	Air Temp & RH	15.1ºC	70
Water Clarity	Cloudy (0.5-2m visibility)		Wind Speed	Medium (branches moving.	
Clouds	Overcast		Wind Direction	W to E	
Weather Notes					

Samples taken by: Martin Ankor

Sample ID	Lake Name	Sample Type	Sample Time
MA0005	Lake Edward	Water	23/05/15 12:13 pm

Sampling depth	0.2	Coords & QC	-37.626787	140.602945	127.4	26.0
Sampling notes	Lake drying. Water level is -2.15 from top of third permapine post, closest to water, by jetty. Sample taken with 6ft pole, then capped subsurface at shore.					
Catchment notes	Significant soil subsidence and crack formation (to 60cm deep by 30cm across) just back from lake edge (10-30m from water edge). Many dead ferns and wilted plants.					

Weather Conditions

Water Condition	Calm	Air Temp & RH	12
Water Clarity	Clear (>2m visibility)	Wind Speed	Low (calm conditions. 1
Clouds	Partly Cloudy	Wind Direction	NE to SW
Weather Notes			

Samples taken by: Martin Ankor

Sample ID	Lake Name	Sample Type	Sample Time
MA0025	Lake Edward	Water	28/08/15 3:53 pm

Sampling depth	0.2m	Coords & QC	-37.627048	140.603008	98.1	12.8

Sampling notes	Level 1.94 below top of third post closest to water. TPS.
Catchment notes	

Water Chemistry	
pH	
TDS	
DO	
Cond.	
PSU	
Temp	

Weather Conditions

Water Condition	Calm		Air Temp & RH	14ºC	83
Water Clarity	Clear (>2m visibility)		Wind Speed	Low (calm conditions.	
Clouds	Partly Cloudy		Wind Direction	SW to NE	
Weather Notes					

Samples taken by: Martin Ankor

Sample ID	Lake Name	Sample Type	Sample Time
MA0087	Lake Edward	Water-stable isotopes	6/04/16 12:04 pm

Sampling depth	0.1m	Coords & QC	-37.626823	140.603118	89.7	13.0

Sampling notes

Catchment notes

Water Chemistry	
pH	8.77
TDS	3632ppm
DO	0.05ppm
Cond.	7445µS/cm
PSU	4.13
Temp	21.3ºC

Weather Conditions

Water Condition	Calm	21.3ºC	Air Temp & RH	16ºC	50
Water Clarity	Cloudy (0.5-2m visibility)		Wind Speed	Medium (branches moving.	
Clouds	Partly Cloudy		Wind Direction	SW to NE	
Weather Notes					

Samples taken by: Martin Ankor

Sample ID	Lake Name	Sample Type	Sample Time
MA0126	Lake Edward		3/08/16 10:51 am

Sampling depth	0.2m	Coords & QC	-37.626924	140.602970	109.8	16.8

Sampling notes

Catchment notes

Water Chemistry

pH	7
TDS	2947ppm
DO	2.41ppm
Cond.	5900µS/cm
PSU	3.22
Temp	11.02ºC

Weather Conditions

Water Condition	Calm	11.02ºC	Air Temp & RH	11.8ºC	80
Water Clarity	Cloudy (0.5-2m visibility)		Wind Speed	Low (calm conditions.	
Clouds	Partly Cloudy		Wind Direction	SSE to NNW	
Weather Notes					

Samples taken by: Martin Ankor

Sample ID	Lake Name	Sample Type	Sample Time
MA0191	Lake Edward	Water - stable isotope	18/11/16 5:41 pm

Sampling depth	0.2m	Coords & QC	-37.627000	140.602967	94.3	7.8

Sampling notes	
Catchment notes	

Water Chemistry	
pH	6.8
TDS	2237ppm
DO	4.13ppm
Cond.	4477µS/cm
PSU	2.4
Temp	19.9ºC

Weather Conditions

Water Condition	Calm	19.9ºC	Air Temp & RH	16.4ºC	64
Water Clarity	Cloudy (0.5-2m visibility)		Wind Speed	Low (calm conditions. 1	
Clouds	Sunny		Wind Direction	SSW to NNE	
Weather Notes					

Samples taken by: Jonathan Tyler

Sample ID	Lake Name	Sample Type	Sample Time
JT0214	Lake Edward	Bulk water	7/01/17 9:45 am

Sampling depth	0.3m	Coords & QC	-37.627394	140.602905	132.2	26.0

Sampling notes	7/1/20179:45:24 am
Catchment notes	

Water Chemistry	
pH	6.35
TDS	2739ppm
DO	1.46ppm
Cond.	5479µS/cm
PSU	2.95
Temp	24.95ºC

Weather Conditions

Water Condition	Calm	24.95ºC	Air Temp & RH		
Water Clarity	Cloudy (0.5-2m visibility)		Wind Speed	Medium (branches moving.	
Clouds	Partly Cloudy		Wind Direction	N to S	
Weather Notes					

Samples taken by: Martin Ankor

Sample ID	Lake Name	Sample Type	Sample Time
MA0246	Lake Edward	Water - bulk	23/04/17 12:58 pm

Sampling depth	0.3m	Coords & QC	-37.626896	140.602979	111.6	13.0

Sampling notes

Catchment notes

Water Chemistry

pH	
TDS	
DO	
Cond.	
PSU	
Temp	17ºC

Weather Conditions

Water Condition	Calm	17ºC	Air Temp & RH	18.6ºC	81
Water Clarity	Clear (>2m visibility)		Wind Speed	Low (calm conditions. 1	
Clouds	Partly Cloudy		Wind Direction	SE to NW	
Weather Notes					

Samples taken by: Martin Ankor

Sample ID	Lake Name	Sample Type	Sample Time
MA0274	Lake Edward	Water - stable isotopes and	29/06/17 10:49 am

Sampling depth	0.3m	Coords & QC	-37.626840	140.603081	119.3	9.4

Sampling notes	
Catchment notes	

Water Chemistry

pH	6.9
TDS	2450ppm
DO	2.28ppm
Cond.	4898µS/cm
PSU	2.65
Temp	11.1ºC

Weather Conditions

Water Condition	Calm	11.1ºC	Air Temp & RH	13ºC	73
Water Clarity	Clear (>2m visibility)		Wind Speed	Low (calm conditions. 1	
Clouds	Overcast		Wind Direction	WNW to ESE	
Weather Notes					

Samples taken by: Martin Ankor

Sample ID	Lake Name	Sample Type	Sample Time
MA0277	Lake Edward	Water - stable isotopes and	3/09/17 2:07 pm

Sampling depth	0.3m	Coords & QC	-37.626805	140.603015	102.9	9.4

Sampling notes

Catchment notes

Water Chemistry

pH	5.2
TDS	2346ppm
DO	1.59ppm
Cond.	4686µS/cm
PSU	2.52
Temp	13.4ºC

Weather Conditions

Water Condition	Choppy	13.4ºC	Air Temp & RH	10.7ºC	79
Water Clarity	Clear (>2m visibility)		Wind Speed	Medium (branches moving.	
Clouds	Partly Cloudy		Wind Direction	WNW to ESE	
Weather Notes					

Samples taken by: Martin Ankor

Sample ID	Lake Name	Sample Type	Sample Time
MA0292	Lake Edward	Water - stable isotopes and	7/11/17 1:17 pm

Sampling depth	0.3m	Coords & QC	-37.627108	140.603025	108.2	7.8

Sampling notes	Lots of groundwater seepage around catchment
Catchment notes	

Water Chemistry	
pH	4.9
TDS	2291ppm
DO	5.23ppm
Cond.	4582µS/cm
PSU	2.46
Temp	18.05ºC

Weather Conditions

Water Condition	Calm	18.05ºC	Air Temp & RH	16ºC	53
Water Clarity	Cloudy (0.5-2m visibility)		Wind Speed	Medium (branches moving.	
Clouds	Partly Cloudy		Wind Direction	SSE to NNW	
Weather Notes					

Samples taken by: Martin Ankor

Sample ID	Lake Name	Sample Type	Sample Time
MA0304	Lake Edward	Water - stable isotopes and	22/01/18 2:26 pm

Sampling depth	0.3m	Coords & QC	-37.626873	140.603068	100.0	16.8

Sampling notes

Catchment notes

Water Chemistry

pH	6.3
TDS	2305ppm
DO	0.13ppm
Cond.	4626µS/cm
PSU	2.47
Temp	24ºC

Weather Conditions

Water Condition	Calm	24ºC	Air Temp & RH	23ºC	48
Water Clarity	Murky (<0.5m visibility)		Wind Speed	Medium (branches moving.	
Clouds	Sunny		Wind Direction	S to N	
Weather Notes					

Samples taken by: Martin Ankor

Sample ID	Lake Name	Sample Type	Sample Time
MA0317	Lake Edward	Water - stable isotopes and	6/03/18 2:28 pm

Sampling depth	0.3m	Coords & QC	-37.627161	140.602958	147.3	26.0

Sampling notes

Catchment notes

Water Chemistry

pH	7.3
TDS	2794ppm
DO	8.09ppm
Cond.	5585µS/cm
PSU	3.03
Temp	21.7ºC

Weather Conditions

Water Condition	Calm	21.7ºC	Air Temp & RH	24ºC	47
Water Clarity	Cloudy (0.5-2m visibility)		Wind Speed	Medium (branches moving.	
Clouds	Sunny		Wind Direction	SSE to NNW	
Weather Notes					

Samples taken by: Martin Ankor

Sample ID	Lake Name	Sample Type	Sample Time
MA0339	Lake Edward	Water - stable isotopes and	7/05/18 11:51 am

Sampling depth	0.3m	Coords & QC	-37.627338	140.603171	116.6	16.8

Sampling notes

Catchment notes

Water Chemistry

pH	7.3
TDS	2623ppm
DO	9.23ppm
Cond.	5248µS/cm
PSU	2.85
Temp	14.73ºC

Weather Conditions

Water Condition	Choppy	14.73ºC	Air Temp & RH		
Water Clarity	Murky (<0.5m visibility)		Wind Speed	Medium (branches moving.	
Clouds	Overcast		Wind Direction	NNW to SSE	
Weather Notes					

Samples taken by: Martin Ankor

Sample ID	Lake Name	Sample Type	Sample Time
MA0358	Lake Edward	Water - stable isotopes and	9/07/18 12:05 pm

Sampling depth	0.2m	Coords & QC	-37.626997	140.602961	107.3	7.8

		Water Chemistry	
Sampling notes		pH	6
		TDS	2499ppm
Catchment notes		DO	10.14ppm
		Cond.	5000µS/cm
		PSU	2.7
		Temp	10.13ºC

Weather Conditions

Water Condition	Calm	10.13ºC	Air Temp & RH	13ºC	92
Water Clarity	Clear (>2m visibility)		Wind Speed	Low (calm conditions. 1	
Clouds	Overcast		Wind Direction	SW to NE	
Weather Notes					

Samples taken by: Martin Ankor

Sample ID	Lake Name	Sample Type	Sample Time
MA0381	Lake Edward	Water - stable isotopes and	11/09/18 2:19 pm

Sampling depth	0.2m	Coords & QC	-37.626963	140.602952	95.3	26.0

Sampling notes

Catchment notes

Water Chemistry

pH	4.5
TDS	2248ppm
DO	6.58ppm
Cond.	4495µS/cm
PSU	2.42
Temp	14.7ºC

Weather Conditions

Water Condition	Choppy	14.7ºC	Air Temp & RH	21.6ºC	27
Water Clarity	Murky (<0.5m visibility)		Wind Speed	High (Windy. 10+ m/s)	
Clouds	Overcast		Wind Direction	NNW to SSE	
Weather Notes					

Samples taken by: Martin Ankor

Sample ID	Lake Name	Sample Type	Sample Time
MA0010	Lake Elingamite	Water	24/05/15 9:51 am

Sampling depth	0.1	Coords & QC	-38.350112	143.014189	134.7	7.8
Sampling notes	Lake drying. Still easy access at boat ramp. Caution. Wooden boat ramp section is stupidly slippery. Sample taken with 6ft pole, then capped subsurface at shore.					
Catchment notes						

Weather Conditions

Water Condition	Calm		Air Temp & RH	8	
Water Clarity	Murky (<0.5m visibility)		Wind Speed	Low (calm conditions. 1	
Clouds	Partly Cloudy		Wind Direction	NE to SW	
Weather Notes					

Samples taken by: Martin Ankor

Sample ID	Lake Name	Sample Type	Sample Time
MA0030	Lake Elingamite	Water	29/08/15 3:47 pm

Sampling depth	0.2m	Coords & QC	-38.349968	143.014341	122.4	9.4

Sampling notes	Raining. Sample taken by hand from end of pontoon. It's floating!!!	Water Chemistry	
		pH	
		TDS	
Catchment notes		DO	
		Cond.	
		PSU	
		Temp	

Weather Conditions

Water Condition	Choppy		Air Temp & RH	9.5ºC	
Water Clarity	Clear (>2m visibility)		Wind Speed	Medium (branches moving.	
Clouds	Overcast		Wind Direction	SSW to NNE	
Weather Notes					

Samples taken by: Martin Ankor

Sample ID	Lake Name	Sample Type	Sample Time
MA0117	Lake Elingamite	Water - general	2/08/16 2:26 pm

Sampling depth	0.2m	Coords & QC	-38.349952	143.014338	128.9	13.0

Sampling notes	Frog chorus
Catchment notes	

Water Chemistry	
pH	7.01
TDS	2330ppm
DO	2.3ppm
Cond.	4660µS/cm
PSU	2.5
Temp	11.65ºC

Weather Conditions

Water Condition	Choppy	11.65ºC	Air Temp & RH	12.3ºC	83
Water Clarity	Clear (>2m visibility)		Wind Speed	Medium (branches moving.	
Clouds	Partly Cloudy		Wind Direction	SSW to NNE	
Weather Notes					

Samples taken by: Martin Ankor

Sample ID	Lake Name	Sample Type	Sample Time
MA0182	Lake Elingamite	Water - bulk	18/11/16 11:48 am

Sampling depth	0.3m	Coords & QC	-38.349951	143.014194	117.4	49.0

Sampling notes

Catchment notes

Water Chemistry

pH	7.74
TDS	2361ppm
DO	2.06ppm
Cond.	4724µS/cm
PSU	2.54
Temp	18.18ºC

Weather Conditions

Water Condition	Calm	18.18ºC	Air Temp & RH	13.9ºC	84
Water Clarity	Clear (>2m visibility)		Wind Speed	Low (calm conditions. 1	
Clouds	Overcast		Wind Direction	SSW to NNE	
Weather Notes					

Samples taken by: Jonathan Tyler

Sample ID	Lake Name	Sample Type	Sample Time
JT0203	Lake Elimgamite	Bulk water	4/01/17 3:00 pm

Sampling depth	0.3m	Coords & QC	-38.350125	143.014003	126.6	26.0

Sampling notes	4/1/2017
Catchment notes	

Water Chemistry	
pH	7.2
TDS	3323ppm
DO	1.02ppm
Cond.	6649µS/cm
PSU	3.63
Temp	24.18ºC

Weather Conditions

Water Condition	Calm	24.18ºC	Air Temp & RH		
Water Clarity	Clear (>2m visibility)		Wind Speed	Low (calm conditions. 1	
Clouds	Sunny		Wind Direction		
Weather Notes					

Samples taken by: Martin Ankor

Sample ID	Lake Name	Sample Type	Sample Time
MA0235	Lake Elingamite	Water - bulk	12/03/17 1:35 pm

Sampling depth	0.1m	Coords & QC	-38.350176	143.014009	125.7	7.8

Sampling notes

Catchment notes

Water Chemistry

pH	9
TDS	3526ppm
DO	0.86ppm
Cond.	7059µS/cm
PSU	3.87
Temp	26.3ºC

Weather Conditions

Water Condition	Calm	26.3ºC	Air Temp & RH	22ºC	63
Water Clarity	Murky (<0.5m visibility)		Wind Speed	Medium (branches moving.	
Clouds	Partly Cloudy		Wind Direction	W to E	
Weather Notes					

Samples taken by: Martin Ankor

Sample ID	Lake Name	Sample Type	Sample Time
MA0269	Lake Elingamite	Water - stable isotopes and	28/06/17 12:36 pm

Sampling depth	0.15m	Coords & QC	-38.350106	143.014129	130.2	15.6

Sampling notes

Catchment notes

Water Chemistry

pH	8.3
TDS	2997ppm
DO	2.58ppm
Cond.	6000µS/cm
PSU	3.27
Temp	11.2ºC

Weather Conditions

Water Condition	Calm	11.2ºC	Air Temp & RH	13.6ºC	74
Water Clarity	Cloudy (0.5-2m visibility)		Wind Speed	Low (calm conditions. 1	
Clouds	Partly Cloudy		Wind Direction	N to S	
Weather Notes					

Samples taken by: Martin Ankor

Sample ID	Lake Name	Sample Type	Sample Time
MA0286	Lake Elingamite	Water - stable isotopes and	5/09/17 10:23 am

Sampling depth	0.3m	Coords & QC	-38.350035	143.014125	140.8	7.8

Sampling notes

Catchment notes

Water Chemistry

pH	7.9
TDS	2298ppm
DO	2.19ppm
Cond.	4592µS/cm
PSU	2.44
Temp	6.3ºC

Weather Conditions

Water Condition	Choppy	6.3ºC	Air Temp & RH	8.8ºC	78
Water Clarity	Clear (>2m visibility)		Wind Speed	High (Windy. 10+ m/s)	
Clouds	Partly Cloudy		Wind Direction	WNW to ESE	
Weather Notes					

Samples taken by: Martin Ankor

Sample ID	Lake Name	Sample Type	Sample Time
MA0298	Lake Elingamite	Water - stable isotopes and	8/11/17 2:52 pm

Sampling depth	0.3m	Coords & QC	-38.349992	143.014119	161.3	7.8

Sampling notes

Catchment notes

Water Chemistry

pH	7.8
TDS	2362ppm
DO	2.93ppm
Cond.	4739µS/cm
PSU	2.55
Temp	16.14ºC

Weather Conditions

Water Condition		16.14ºC	Air Temp & RH	18ºC	64
Water Clarity	Clear (>2m visibility)		Wind Speed	Low (calm conditions. 1	
Clouds	Partly Cloudy		Wind Direction	SSE to NNW	
Weather Notes	Tannin coloured water				

Samples taken by: Martin Ankor

Sample ID	Lake Name	Sample Type	Sample Time
MA0312	Lake Elingamite	Water - stable isotopes and	23/01/18 3:43 pm

Sampling depth	0.3m	Coords & QC	-38.350124	143.014137	135.0	7.8

		Water Chemistry	
Sampling notes		pH	8.4
		TDS	3111ppm
Catchment notes		DO	0.37ppm
		Cond.	6210µS/cm
		PSU	3.35
		Temp	30ºC

Weather Conditions

Water Condition	Choppy	30ºC	Air Temp & RH	24.6ºC	43
Water Clarity	Murky (<0.5m visibility)		Wind Speed	Medium (branches moving.	
Clouds	Sunny		Wind Direction	SSW to NNE	
Weather Notes					

Samples taken by: Martin Ankor

Sample ID	Lake Name	Sample Type	Sample Time
MA0322	Lake Elingamite	Water - stable isotopes and	7/03/18 11:28 am

Sampling depth	0.2m	Coords & QC	-38.350114	143.014231	131.9	9.4

Sampling notes

Catchment notes

Water Chemistry

pH	7.75
TDS	4030ppm
DO	0.72ppm
Cond.	8154µS/cm
PSU	4.5
Temp	19.6ºC

Weather Conditions

Water Condition	Calm	19.6ºC	Air Temp & RH	22.6ºC	49
Water Clarity	Murky (<0.5m visibility)		Wind Speed	Low (calm conditions. 1	
Clouds			Wind Direction	N to S	
Weather Notes					

Samples taken by: Martin Ankor

Sample ID	Lake Name	Sample Type	Sample Time
MA0344	Lake Elingamite	Water - stable isotopes and	8/05/18 11:12 am

Sampling depth	0.3m	Coords & QC				

Sampling notes	Taken near boat ramp in very shallow water with dark coloured water and sediment
Catchment notes	Catchment Burnt. Lake level low, sample may not be representative as boat ramp was cut off from rest of lake

Water Chemistry	
pH	7.81
TDS	3537ppm
DO	3.87ppm
Cond.	7081µS/cm
PSU	3.93
Temp	14.6ºC

Weather Conditions

Water Condition	Calm	14.6ºC	Air Temp & RH	13.9ºC	57
Water Clarity	Murky (<0.5m visibility)		Wind Speed	Low (calm conditions. 1	
Clouds	Sunny		Wind Direction	WNW to ESE	
Weather Notes					

Samples taken by: Martin Ankor

Sample ID	Lake Name	Sample Type	Sample Time
MA0367	Lake Elingamite	Water - stable isotopes and	10/07/18 1:58 pm

Sampling depth	0.2m	Coords & QC	-38.349938	143.014439	107.4	18.9

Sampling notes

Catchment notes

Water Chemistry

pH	8.03
TDS	2342ppm
DO	12.29ppm
Cond.	4683µS/cm
PSU	2.52
Temp	11.5ºC

Weather Conditions

Water Condition	Choppy	11.5ºC	Air Temp & RH	10.3ºC	69
Water Clarity	Cloudy (0.5-2m visibility)		Wind Speed	Medium (branches moving.	
Clouds	Overcast		Wind Direction	WNW to ESE	
Weather Notes					

Samples taken by: Martin Ankor

Sample ID	Lake Name	Sample Type	Sample Time
MA0373	Lake Elingamite	Water - stable isotopes and	9/09/18 3:40 pm

Sampling depth	0.2m	Coords & QC	-38.350207	143.013932	142.5	9.4

Sampling notes

Catchment notes

Water Chemistry

pH	8.5
TDS	2395ppm
DO	6.83ppm
Cond.	4790µS/cm
PSU	2.59
Temp	13.7ºC

Weather Conditions

Water Condition	Choppy	13.7ºC	Air Temp & RH	14.9ºC	73
Water Clarity	Murky (<0.5m visibility)		Wind Speed	Medium (branches moving.	
Clouds	Overcast		Wind Direction	W to E	
Weather Notes					

Samples taken by: Martin Ankor

Sample ID	Lake Name	Sample Type	Sample Time
MA0013	Lake Gnotuk	Water	24/05/15 11:53 am

Sampling depth	0.2	Coords & QC	-38.227653	143.102393	111.2	18.9
Sampling notes	Access at rocks on east side of golf course. Park in golf course/recreation park car park. Walk to the lake from the flag at hole 10, Camperdown Golf Course. Sample taken with 6ft pole, then capped subsurface at shore.					
Catchment notes	Springs along lake edge on southern side, probably feeding from Lake Bullen Merri.					

Weather Conditions

Water Condition	Calm		Air Temp & RH	12	
Water Clarity	Clear (>2m visibility)		Wind Speed	Low (calm conditions. 1	
Clouds	Partly Cloudy		Wind Direction	NNE to SSW	
Weather Notes					

Samples taken by: Jon Tyler

Sample ID	Lake Name	Sample Type	Sample Time
MA0016	Lake Gnotuk	Water	10/06/15 8:26 am

Sampling depth	0.2m	Coords & QC	-38.227793	143.102237	111.4	15.6

Sampling notes	Calcium isotopes and pH reading. pH taken 3m from shore. Approx 0.2m depth. pH 9.82 DO 1.56ppm Conductivity 104800 ms/cm TDS 52400
Catchment notes	

Water Chemistry	
pH	
TDS	
DO	
Cond.	
PSU	
Temp	

Weather Conditions

Water Condition	Calm		Air Temp & RH	5ºC	Overcast
Water Clarity	Clear (>2m visibility)		Wind Speed	Medium (branches moving.	
Clouds			Wind Direction	WSW to ENE	
Weather Notes					

Samples taken by: Martin Ankor

Sample ID	Lake Name	Sample Type	Sample Time
MA0033	Lake Gnotuk	Water	30/08/15 10:09 am

Sampling depth	0.2m	Coords & QC	-38.227733	143.102438	107.5	49.0

Sampling notes	Lake level 5.839 below tbm sr77m10.	Water Chemistry	
		pH	
		TDS	
Catchment notes		DO	
		Cond.	
		PSU	
		Temp	

Weather Conditions

Water Condition	Calm		Air Temp & RH	9ºC	
Water Clarity	Clear (>2m visibility)		Wind Speed	Medium (branches moving.	
Clouds	Overcast		Wind Direction	S to N	
Weather Notes					

Samples taken by: Martin Ankor

Sample ID	Lake Name	Sample Type	Sample Time
MA0066	Lake Gnotuk	Water-stable isotopes	5/04/16 2:20 pm

Sampling depth	0.2m	Coords & QC	-38.227488	143.102725	90.7	33.5

Sampling notes

Catchment notes

Water Chemistry

pH	8.68
TDS	52870ppm
DO	0.29ppm
Cond.	105700µS/cm
PSU	-
Temp	20.9ºC

Weather Conditions

Water Condition	Choppy	20.9ºC	Air Temp & RH	27ºC	24
Water Clarity	Cloudy (0.5-2m visibility)		Wind Speed	Medium (branches moving.	
Clouds	Partly Cloudy		Wind Direction	NW to SE	
Weather Notes					

Samples taken by: Martin Ankor

Sample ID	Lake Name	Sample Type	Sample Time
MA0103	Lake Gnotuk	Water - general	2/08/16 8:02 am

Sampling depth	0.2m	Coords & QC	-38.227433	143.102343	185.9	49.0

Sampling notes	
Catchment notes	

Water Chemistry	
pH	8.65
TDS	52000ppm
DO	3.36ppm
Cond.	103900µS/cm
PSU	-
Temp	10.29ºC

Weather Conditions

Water Condition	Calm	10.29ºC	Air Temp & RH	5.2ºC	86
Water Clarity	Clear (>2m visibility)		Wind Speed	Low (calm conditions.	
Clouds	Partly Cloudy		Wind Direction	SSW to NNE	
Weather Notes	Rainbow				

Samples taken by: Martin Ankor

Sample ID	Lake Name	Sample Type	Sample Time
MA0177	Lake Gnotuk	Water - bulk	18/11/16 10:23 am

Sampling depth	0.1m	Coords & QC	-38.228764	143.099815	106.0	13.0

Sampling notes	Spring hardly flowing possibly due to rise in lake level Many critters in lake.
Catchment notes	

Water Chemistry	
pH	8.64
TDS	44050ppm
DO	3.5ppm
Cond.	88140µS/cm
PSU	62.6
Temp	18.1ºC

Weather Conditions

Water Condition	Calm	18.1ºC	Air Temp & RH	13.4ºC	94
Water Clarity	Clear (>2m visibility)		Wind Speed	Low (calm conditions. 1	
Clouds	Overcast		Wind Direction	SSW to NNE	
Weather Notes					

Samples taken by: Jonathan Tyler

Sample ID	Lake Name	Sample Type	Sample Time
JT0199	Lake Gnotuk	Bulk water	4/01/17 1:51 pm

Sampling depth	0.2m	Coords & QC	-38.228678	143.099814	104.1	26.0

Sampling notes	4/1/2017
Catchment notes	

Water Chemistry	
pH	8.56
TDS	50840ppm
DO	1.28ppm
Cond.	101600µS/cm
PSU	
Temp	24.14ºC

Weather Conditions

Water Condition	Calm	24.14ºC	Air Temp & RH		
Water Clarity	Clear (>2m visibility)		Wind Speed	Low (calm conditions. 1	
Clouds	Sunny		Wind Direction		
Weather Notes					

Samples taken by: Martin Ankor

Sample ID	Lake Name	Sample Type	Sample Time
MA0231	Lake Gnotuk	Water - bulk	12/03/17 12:21 pm

Sampling depth	0.2m	Coords & QC	-38.228694	143.099890	97.7	9.4

Sampling notes

Catchment notes

Water Chemistry

pH	8.5
TDS	44880ppm
DO	0.44ppm
Cond.	89700µS/cm
PSU	64.08
Temp	23.3ºC

Weather Conditions

Water Condition	Calm	23.3ºC	Air Temp & RH	21.5ºC	69
Water Clarity	Clear (>2m visibility)		Wind Speed	Low (calm conditions. 1	
Clouds	Partly Cloudy		Wind Direction	WNW to ESE	
Weather Notes					

Samples taken by: Martin Ankor

Sample ID	Lake Name	Sample Type	Sample Time
MA0266	Lake Gnotuk	Water - stable isotopes and	28/06/17 11:16 am

Sampling depth	0.2m	Coords & QC	-38.228782	143.099898	104.9	26.0

Sampling notes

Catchment notes

Water Chemistry

pH	8.7
TDS	44040ppm
DO	2.17ppm
Cond.	87980µS/cm
PSU	62.12
Temp	12.7ºC

Weather Conditions

Water Condition	Calm	12.7ºC	Air Temp & RH	12.7ºC	80
Water Clarity	Clear (>2m visibility)		Wind Speed	Low (calm conditions. 1	
Clouds	Sunny		Wind Direction	NW to SE	
Weather Notes					

Samples taken by: Martin Ankor

Sample ID	Lake Name	Sample Type	Sample Time
MA0280	Lake Gnotuk	Water - stable isotopes and	4/09/17 2:10 pm

Sampling depth	0.3m	Coords & QC	-38.228819	143.099830	103.9	16.8

Sampling notes

Catchment notes

Water Chemistry

pH	8.75
TDS	4782ppm
DO	1.21ppm
Cond.	95680µS/cm
PSU	68.66
Temp	13ºC

Weather Conditions

Water Condition	Choppy	13ºC	Air Temp & RH	8.2ºC	74
Water Clarity	Cloudy (0.5-2m visibility)		Wind Speed	Medium (branches moving.	
Clouds	Overcast		Wind Direction	WNW to ESE	
Weather Notes					

Samples taken by: Martin Ankor

Sample ID	Lake Name	Sample Type	Sample Time
MA0301	Lake Gnotuk	Water - stable isotopes and	8/11/17 5:27 pm

Sampling depth	0.3m	Coords & QC	-38.228731	143.099882	91.0	16.8

Sampling notes

Catchment notes

Water Chemistry

pH	8.76
TDS	48140ppm
DO	2.26ppm
Cond.	96280µS/cm
PSU	69.52
Temp	20.66ºC

Weather Conditions

Water Condition	Calm	20.66ºC	Air Temp & RH	19ºC	59
Water Clarity	Clear (>2m visibility)		Wind Speed	Low (calm conditions. 1	
Clouds	Sunny		Wind Direction	SSE to NNW	
Weather Notes					

Samples taken by: Martin Ankor

Sample ID	Lake Name	Sample Type	Sample Time
MA0313	Lake Gnotuk	Water - stable isotopes and	23/01/18 4:42 pm

Sampling depth	0.2m	Coords & QC	-38.228704	143.099942	111.5	9.4

Sampling notes

Catchment notes

Water Chemistry

pH	8.6
TDS	45800ppm
DO	0.32ppm
Cond.	91500µS/cm
PSU	65.4
Temp	24.9ºC

Weather Conditions

Water Condition	Calm	24.9ºC	Air Temp & RH	23.7ºC	44
Water Clarity	Clear (>2m visibility)		Wind Speed	Low (calm conditions. 1	
Clouds	Sunny		Wind Direction	S to N	
Weather Notes					

Samples taken by: Martin Ankor

Sample ID	Lake Name	Sample Type	Sample Time
MA0326	Lake Gnotuk	Water - stable isotopes and	7/03/18 3:40 pm

Sampling depth	0.3m	Coords & QC	-38.228728	143.099904	99.6	13.0

Sampling notes

Catchment notes

Water Chemistry

pH	8.59
TDS	53060ppm
DO	7.48ppm
Cond.	106500µS/cm
PSU	
Temp	26.7ºC

Weather Conditions

Water Condition	Calm	26.7ºC	Air Temp & RH	30ºC	25
Water Clarity	Clear (>2m visibility)		Wind Speed	Low (calm conditions. 1	
Clouds	Sunny		Wind Direction	N to S	
Weather Notes					

Samples taken by: Martin Ankor

Sample ID	Lake Name	Sample Type	Sample Time
MA0351	Lake Gnotuk	Water - stable isotopes and	8/05/18 4:56 pm

Sampling depth	0.2m	Coords & QC	-38.229009	143.099886	91.5	49.0

Sampling notes

Catchment notes

Water Chemistry

pH	8.6
TDS	49950ppm
DO	6.04ppm
Cond.	99930µS/cm
PSU	
Temp	17.6ºC

Weather Conditions

Water Condition	Calm	17.6ºC	Air Temp & RH	14.9ºC	53
Water Clarity	Clear (>2m visibility)		Wind Speed	Low (calm conditions. 1	
Clouds	Sunny		Wind Direction	WNW to ESE	
Weather Notes					

Samples taken by: Martin Ankor

Sample ID	Lake Name	Sample Type	Sample Time
MA0368	Lake Gnotuk	Water - stable isotopes and	10/07/18 2:33 pm

Sampling depth	0.2m	Coords & QC	-38.228725	143.099896	113.5	7.8

Sampling notes	
Catchment notes	PSU off scale

Water Chemistry	
pH	8.5
TDS	49280ppm
DO	8.41ppm
Cond.	98580µS/cm
PSU	
Temp	12.4ºC

Weather Conditions

Water Condition	Calm	12.4ºC	Air Temp & RH	10.3ºC	69
Water Clarity	Clear (>2m visibility)		Wind Speed	Medium (branches moving.	
Clouds	Overcast		Wind Direction	NW to SE	
Weather Notes					

Samples taken by: Martin Ankor

Sample ID	Lake Name	Sample Type	Sample Time
MA0374	Lake Gnotuk	Water - stable isotopes and	9/09/18 4:19 pm

Sampling depth	0.2m	Coords & QC	-38.229040	143.099777	121.7	18.9

Sampling notes

Catchment notes

Water Chemistry

pH	8.5
TDS	51460ppm
DO	5.35ppm
Cond.	102900µS/cm
PSU	-
Temp	13ºC

Weather Conditions

Water Condition	Choppy	13ºC	Air Temp & RH	15.1ºC	73
Water Clarity	Cloudy (0.5-2m visibility)		Wind Speed	Medium (branches moving.	
Clouds	Overcast		Wind Direction	WNW to ESE	
Weather Notes					

Samples taken by: Martin Ankor

Sample ID	Lake Name	Sample Type	Sample Time
MA0074	Lake Keilambete	Water-stable isotopes	5/04/16 4:42 pm

Sampling depth	0.2m	Coords & QC	-38.198161	142.882992	99.0	7.8

Sampling notes

Catchment notes

Water Chemistry

pH	8.64
TDS	74200ppm
DO	0.29ppm
Cond.	148300µS/cm
PSU	
Temp	18.8ºC

Weather Conditions

Water Condition	Choppy	18.8ºC	Air Temp & RH	22ºC	60
Water Clarity	Cloudy (0.5-2m visibility)		Wind Speed	Medium (branches moving.	
Clouds	Overcast		Wind Direction	SW to NE	
Weather Notes					

Samples taken by: Martin Ankor

Sample ID	Lake Name	Sample Type	Sample Time
MA0121	Lake Keilambete	Water - general	2/08/16 4:06 pm

Sampling depth	0.2m	Coords & QC	-38.198027	142.883046	105.8	6.4

		Water Chemistry	
Sampling notes		pH	8.77
		TDS	67180ppm
Catchment notes		DO	1.39ppm
		Cond.	134100µS/cm
		PSU	-
		Temp	12.45ºC

Weather Conditions

Water Condition	Choppy	12.45ºC	Air Temp & RH	11.9ºC	
Water Clarity	Murky (<0.5m visibility)		Wind Speed	Medium (branches moving.	
Clouds	Overcast		Wind Direction	SW to NE	
Weather Notes					

Samples taken by: Martin Ankor

Sample ID	Lake Name	Sample Type	Sample Time
MA0186	Lake Keilambete	Water - bulk	18/11/16 2:02 pm

Sampling depth	0.3m	Coords & QC	-38.212676	142.885122	112.5	6.4

Sampling notes	Sampled from quarry Cool squeaky toy birds
Catchment notes	

Water Chemistry	
pH	8.81
TDS	59600ppm
DO	2.71ppm
Cond.	119100µS/cm
PSU	-
Temp	19.84ºC

Weather Conditions

Water Condition	Calm	19.84ºC	Air Temp & RH	16.1ºC	66
Water Clarity	Murky (<0.5m visibility)		Wind Speed	Medium (branches moving.	
Clouds	Partly Cloudy		Wind Direction	SW to NE	
Weather Notes					

Samples taken by: Jonathan Tyler

Sample ID	Lake Name	Sample Type	Sample Time
JT0207	Lake Keilambete	Bulk water	4/01/17 4:57 pm

Sampling depth	0.3m	Coords & QC	-38.198016	142.882523	109.0	26.0

Sampling notes	4/1/2017	Water Chemistry	
		pH	8.7
		TDS	70560ppm
Catchment notes		DO	0.82ppm
		Cond.	141000µS/cm
		PSU	
		Temp	30.59ºC

Weather Conditions

Water Condition	Choppy	30.59ºC	Air Temp & RH		
Water Clarity	Cloudy (0.5-2m visibility)		Wind Speed	Medium (branches moving.	
Clouds	Sunny		Wind Direction	S to N	
Weather Notes					

Samples taken by: Martin Ankor

Sample ID	Lake Name	Sample Type	Sample Time
MA0239	Lake Keilambete	Water - bulk	12/03/17 3:01 pm

Sampling depth	0.3m	Coords & QC	-38.198203	142.883033	118.7	9.4

Sampling notes

Catchment notes

Water Chemistry

pH	8.7
TDS	62300ppm
DO	0.45ppm
Cond.	124500µS/cm
PSU	-
Temp	23.6ºC

Weather Conditions

Water Condition	Choppy	23.6ºC	Air Temp & RH	22ºC	61
Water Clarity	Murky (<0.5m visibility)		Wind Speed	Medium (branches moving.	
Clouds	Partly Cloudy		Wind Direction	WSW to ENE	
Weather Notes					

Samples taken by: Martin Ankor

Sample ID	Lake Name	Sample Type	Sample Time
MA0271	Lake keilambete	Water	28/06/17 2:14 pm

Sampling depth	0.3m	Coords & QC	-38.198102	142.883042	113.5	5.8

Sampling notes	
Catchment notes	Spring flowing substantial

Water Chemistry	
pH	8.6
TDS	61860ppm
DO	1.58ppm
Cond.	123800µS/cm
PSU	-
Temp	11.3ºC

Weather Conditions

Water Condition	Calm	11.3ºC	Air Temp & RH	13ºC	73
Water Clarity	Cloudy (0.5-2m visibility)		Wind Speed	Medium (branches moving.	
Clouds	Overcast		Wind Direction	WNW to ESE	
Weather Notes					

Samples taken by: Martin Ankor

Sample ID	Lake Name	Sample Type	Sample Time
MA0284	Lake Keilambete	Water - stable isotopes and	4/09/17 5:10 pm

Sampling depth	0.3m	Coords & QC	-38.198194	142.882802	117.3	18.9

Sampling notes

Catchment notes

Water Chemistry

pH	9
TDS	64600ppm
DO	1.28ppm
Cond.	129100µS/cm
PSU	-
Temp	11ºC

Weather Conditions

Water Condition	Choppy	11ºC	Air Temp & RH	3.5ºC	93
Water Clarity	Murky (<0.5m visibility)		Wind Speed	High (Windy. 10+ m/s)	
Clouds	Partly Cloudy		Wind Direction	W to E	
Weather Notes					

Samples taken by: Martin Ankor

Sample ID	Lake Name	Sample Type	Sample Time
MA0300	Lake Keilambete	Water - stable isotopes and	8/11/17 4:38 pm

Sampling depth	0.3m	Coords & QC	-38.198002	142.882424	116.7	26.0

Sampling notes

Catchment notes

Water Chemistry

pH	8.9
TDS	64590ppm
DO	2.27ppm
Cond.	130000µS/cm
PSU	
Temp	19.1ºC

Weather Conditions

Water Condition	Calm	19.1ºC	Air Temp & RH	19ºC	59
Water Clarity	Cloudy (0.5-2m visibility)		Wind Speed	Low (calm conditions. 1	
Clouds	Sunny		Wind Direction	SSE to NNW	
Weather Notes					

Samples taken by: Martin Ankor

Sample ID	Lake Name	Sample Type	Sample Time
MA0310	Lake Keilambete	Water - stable isotopes and	23/01/18 2:15 pm

Sampling depth	0.3m	Coords & QC	-38.198066	142.882943	104.5	13.0

Sampling notes

Catchment notes

Water Chemistry

pH	8.76
TDS	62650ppm
DO	0.2ppm
Cond.	125300µS/cm
PSU	-
Temp	29.6ºC

Weather Conditions

Water Condition	Choppy	29.6ºC	Air Temp & RH	23ºC	42
Water Clarity	Murky (<0.5m visibility)		Wind Speed	Medium (branches moving.	
Clouds	Sunny		Wind Direction	SSW to NNE	
Weather Notes					

Samples taken by: Martin Ankor

Sample ID	Lake Name	Sample Type	Sample Time
MA0324	Lake Keilambete	Water - stable isotopes and	7/03/18 1:16 pm

Sampling depth	0.3m	Coords & QC	-38.198128	142.882960	102.0	9.4

Sampling notes

Catchment notes

Water Chemistry

pH	8.8
TDS	73560ppm
DO	5.88ppm
Cond.	147000µS/cm
PSU	
Temp	22.1ºC

Weather Conditions

Water Condition	Calm	22.1ºC	Air Temp & RH	29ºC	31
Water Clarity	Murky (<0.5m visibility)		Wind Speed	Low (calm conditions. 1	
Clouds	Sunny		Wind Direction	NNW to SSE	
Weather Notes					

Samples taken by: Martin Ankor

Sample ID	Lake Name	Sample Type	Sample Time
MA0347	Lake Keilambete	Water - stable isotopes and	8/05/18 1:10 pm

Sampling depth	0.3m	Coords & QC	-38.198137	142.883024	99.8	6.4

Sampling notes

Catchment notes

Water Chemistry

pH	8.67
TDS	7300ppm
DO	4.48ppm
Cond.	140400µS/cm
PSU	
Temp	15.7ºC

Weather Conditions

Water Condition	Calm	15.7ºC	Air Temp & RH	14.9ºC	49
Water Clarity	Clear (>2m visibility)		Wind Speed	Low (calm conditions. 1	
Clouds	Sunny		Wind Direction	NNW to SSE	
Weather Notes					

Samples taken by: Martin Ankor

Sample ID	Lake Name	Sample Type	Sample Time
MA0361	Lake Keilambete	Water - stable isotopes and	10/07/18 9:14 am

Sampling depth	0.2m	Coords & QC	-38.197883	142.879836	103.4	7.8

Sampling notes	
Catchment notes	PSU off scale

Water Chemistry	
pH	8.62
TDS	68880ppm
DO	6.86ppm
Cond.	137770µS/cm
PSU	
Temp	9.88ºC

Weather Conditions

Water Condition	Calm	9.88ºC	Air Temp & RH	8.4ºC	100
Water Clarity	Cloudy (0.5-2m visibility)		Wind Speed	Low (calm conditions. 1	
Clouds	Overcast		Wind Direction	NW to SE	
Weather Notes					

Samples taken by: Martin Ankor

Sample ID	Lake Name	Sample Type	Sample Time
MA0371	Lake Keilambete	Water - stable isotopes and	9/09/18 2:17 pm

Sampling depth	0.2m	Coords & QC	-38.197791	142.880317	105.6	15.6

Sampling notes

Catchment notes

Water Chemistry

pH	8.7
TDS	69770ppm
DO	3.54ppm
Cond.	139500µS/cm
PSU	-
Temp	13.5ºC

Weather Conditions

Water Condition	Choppy	13.5ºC	Air Temp & RH	14.5ºC	77
Water Clarity	Cloudy (0.5-2m visibility)		Wind Speed	High (Windy. 10+ m/s)	
Clouds	Overcast		Wind Direction	WSW to ENE	
Weather Notes					

Samples taken by: Martin Ankor

Sample ID	Lake Name	Sample Type	Sample Time
MA0004	Lake Leake	Water	23/05/15 11:12 am

Sampling depth	0.1	Coords & QC	-37.611729	140.592388	104.3	26.0
Sampling notes	Lake drying rapidly. Probably ~2m drop since last visit. Water level -6.36 +- 0.2 from top of wall out front of toilets. Sample taken with 6ft pole, then capped subsurface at shore.					
Catchment notes	Lake does visually appear approx 10-20m higher than surrounding landscape. Lake bottom very fine dark grey clay-silt. Pine plantations on southern side of catchment. Quarry and secondary overflow crater to north west side of lake. Farmland with some native vegetation along lake edge.					

Weather Conditions

Water Condition	Calm		Air Temp & RH	12	
Water Clarity	Clear (>2m visibility)		Wind Speed	Low (calm conditions. 1	
Clouds	Partly Cloudy		Wind Direction	NE to SW	
Weather Notes					

Samples taken by: Martin Ankor

Sample ID	Lake Name	Sample Type	Sample Time
MA0024	Lake Leake	Water	28/08/15 3:04 pm

Sampling depth	0.1m	Coords & QC	-37.611960	140.592754	98.9	26.0

Sampling notes	Lake substantially higher than last visit. Water 6.05 below top of retaining wall in front of toilets. TPS.	Water Chemistry	
		pH	
		TDS	
Catchment notes		DO	
		Cond.	
		PSU	
		Temp	

Weather Conditions

Water Condition	Calm		Air Temp & RH	14ºC	83
Water Clarity	Clear (>2m visibility)		Wind Speed	Medium (branches moving.	
Clouds	Partly Cloudy		Wind Direction	SW to NE	
Weather Notes	Cold				

Samples taken by: Martin Ankor

Sample ID	Lake Name	Sample Type	Sample Time
MA0128	Lake Leake	Water - general	3/08/16 11:29 am

Sampling depth	0.2m	Coords & QC	-37.611929	140.592430	98.3	13.0

Sampling notes	Water is tannin coloured
Catchment notes	Suspected ground water seepage from banks along perimeter road.

Water Chemistry	
pH	8.4
TDS	2565ppm
DO	2.36ppm
Cond.	5132µS/cm
PSU	2.78
Temp	12.29ºC

Weather Conditions

Water Condition	Choppy	12.29ºC	Air Temp & RH	10.8ºC	83
Water Clarity	Clear (>2m visibility)		Wind Speed	Medium (branches moving.	
Clouds	Partly Cloudy		Wind Direction	SSE to NNW	
Weather Notes					

Samples taken by: Martin Ankor

Sample ID	Lake Name	Sample Type	Sample Time
MA0193	Lake Leake	Water - bulk	18/11/16 6:16 pm

Sampling depth	0.3m	Coords & QC	-37.611921	140.592759	95.2	9.4

Sampling notes	Possible blue green algae
Catchment notes	

Water Chemistry	
pH	8.61
TDS	1955ppm
DO	4.97ppm
Cond.	3908µS/cm
PSU	2.07
Temp	22.4ºC

Weather Conditions

Water Condition	Calm	22.4ºC	Air Temp & RH	15.8ºC	64
Water Clarity	Clear (>2m visibility)		Wind Speed	Medium (branches moving.	
Clouds	Sunny		Wind Direction	SSW to NNE	
Weather Notes					

Samples taken by: Jonathan Tyler

Sample ID	Lake Name	Sample Type	Sample Time
JT0216	Lake Leake	Bulk water	7/01/17 10:13 am

Sampling depth	0.3m	Coords & QC	-37.611802	140.592548	75.8	26.0

Sampling notes	7/1/201710:13:51 am	Water Chemistry	
		pH	9.18
		TDS	2781ppm
Catchment notes		DO	1.75ppm
		Cond.	5565µS/cm
		PSU	3
		Temp	26.11ºC

Weather Conditions

Water Condition	Calm	26.11ºC	Air Temp & RH		
Water Clarity	Murky (<0.5m visibility)		Wind Speed	Medium (branches moving.	
Clouds	Partly Cloudy		Wind Direction	N to S	
Weather Notes					

Samples taken by: Martin Ankor

Sample ID	Lake Name	Sample Type	Sample Time
MA0243	Lake Leake	Water - bulk	13/03/17 9:19 am

Sampling depth	0.3m	Coords & QC	-37.611935	140.592957	97.0	13.0

Sampling notes	M wants to go kayaking on lake
Catchment notes	

Water Chemistry	
pH	9.1
TDS	3160ppm
DO	0.83ppm
Cond.	6323µS/cm
PSU	3.47
Temp	18.8ºC

Weather Conditions

Water Condition	Calm	18.8ºC	Air Temp & RH	17ºC	89
Water Clarity	Clear (>2m visibility)		Wind Speed	Medium (branches moving.	
Clouds	Overcast		Wind Direction	SSE to NNW	
Weather Notes					

Samples taken by: Martin Ankor

Sample ID	Lake Name	Sample Type	Sample Time
MA0248	Lake Leake	Water - stable isotopes	23/04/17 1:15 pm

Sampling depth	0.3m	Coords & QC	-37.611957	140.592476	86.2	7.8

		Water Chemistry	
Sampling notes		pH	
		TDS	
Catchment notes		DO	
		Cond.	
		PSU	
		Temp	17ºC

Weather Conditions

Water Condition	Calm	17ºC	Air Temp & RH	19.3ºC	79
Water Clarity	Clear (>2m visibility)		Wind Speed	Low (calm conditions. 1	
Clouds	Partly Cloudy		Wind Direction	SE to NW	
Weather Notes					

Samples taken by: Martin Ankor

Sample ID	Lake Name	Sample Type	Sample Time
MA0275	Lake Leake	Water - stable isotopes and	29/06/17 11:13 am

Sampling depth	0.3m	Coords & QC	-37.611892	140.592716	117.1	13.0

		Water Chemistry	
Sampling notes		pH	8.9
		TDS	2933ppm
Catchment notes		DO	2.6ppm
		Cond.	5865µS/cm
		PSU	3.2
		Temp	11.3ºC

Weather Conditions

Water Condition	Choppy	11.3ºC	Air Temp & RH	11ºC	95
Water Clarity	Clear (>2m visibility)		Wind Speed	Medium (branches moving.	
Clouds	Overcast		Wind Direction	NW to SE	
Weather Notes					

Samples taken by: Martin Ankor

Sample ID	Lake Name	Sample Type	Sample Time
MA0276	Lake Leake	Water - stable isotopes and	3/09/17 1:37 pm

Sampling depth	0.3m	Coords & QC	-37.611876	140.592738	88.9	13.0

Sampling notes

Catchment notes

Water Chemistry

pH	8.89
TDS	2378ppm
DO	1.31ppm
Cond.	4753µS/cm
PSU	2.57
Temp	13.6ºC

Weather Conditions

Water Condition	Choppy	13.6ºC	Air Temp & RH	12.9ºC	77
Water Clarity	Cloudy (0.5-2m visibility)		Wind Speed	High (Windy. 10+ m/s)	
Clouds	Partly Cloudy		Wind Direction	NW to SE	
Weather Notes					

Samples taken by: Martin Ankor

Sample ID	Lake Name	Sample Type	Sample Time
MA0291	Lake Leake	Water - stable isotopes and	7/11/17 12:42 pm

Sampling depth	0.3m	Coords & QC	-37.611938	140.592785	99.8	9.4

Sampling notes	
Catchment notes	

Water Chemistry	
pH	9.34
TDS	2239ppm
DO	5.66ppm
Cond.	4478µS/cm
PSU	2.4
Temp	18.66ºC

Weather Conditions

Water Condition	Calm	18.66ºC	Air Temp & RH	16ºC	57
Water Clarity	Clear (>2m visibility)		Wind Speed	Medium (branches moving.	
Clouds	Sunny		Wind Direction	SSE to NNW	
Weather Notes					

Samples taken by: Martin Ankor

Sample ID	Lake Name	Sample Type	Sample Time
MA0303	Lake Leake	Water - stable isotopes and	22/01/18 1:59 pm

Sampling depth	0.3m	Coords & QC	-37.611880	140.592654	100.2	13.0

		Water Chemistry	
Sampling notes		pH	8.81
		TDS	2806ppm
Catchment notes		DO	0.02ppm
		Cond.	5612µS/cm
		PSU	3.03
		Temp	26ºC

Weather Conditions

Water Condition	Choppy	26ºC	Air Temp & RH	22.3ºC	47
Water Clarity	Cloudy (0.5-2m visibility)		Wind Speed	Medium (branches moving.	
Clouds	Sunny		Wind Direction	S to N	
Weather Notes					

Samples taken by: Martin Ankor

Sample ID	Lake Name	Sample Type	Sample Time
MA0316	Lake Leake	Water - stable isotopes and	6/03/18 1:42 pm

Sampling depth	0.3m	Coords & QC	-37.611910	140.592710	96.4	7.8

Sampling notes

Catchment notes

Water Chemistry

pH	8.6
TDS	3887ppm
DO	11.3ppm
Cond.	7774µS/cm
PSU	4.3
Temp	21.9ºC

Weather Conditions

Water Condition	Calm	21.9ºC	Air Temp & RH	24ºC	44
Water Clarity	Cloudy (0.5-2m visibility)		Wind Speed	High (Windy. 10+ m/s)	
Clouds	Sunny		Wind Direction	SSE to NNW	
Weather Notes					

Samples taken by: Martin Ankor

Sample ID	Lake Name	Sample Type	Sample Time
MA0329	Lake Leake		7/05/18 11:51 am

Sampling depth	0.3m	Coords & QC	-37.611870	140.592787	82.3	13.0

Sampling notes

Catchment notes

Water Chemistry

pH	8.55
TDS	3913ppm
DO	7.48ppm
Cond.	7832µS/cm
PSU	4.37
Temp	13.7ºC

Weather Conditions

Water Condition	Choppy	13.7ºC	Air Temp & RH		
Water Clarity	Cloudy (0.5-2m visibility)		Wind Speed	Medium (branches moving.	
Clouds	Overcast		Wind Direction	WNW to ESE	
Weather Notes					

Samples taken by: Martin Ankor

Sample ID	Lake Name	Sample Type	Sample Time
MA0357	Lake Leake	Water - stable isotopes and	9/07/18 11:24 am

Sampling depth	0.2m	Coords & QC	-37.611904	140.592746	103.4	6.4

Sampling notes

Catchment notes

Water Chemistry	
pH	8.35
TDS	3043ppm
DO	8.6ppm
Cond.	6087µS/cm
PSU	3.3
Temp	11.23ºC

Weather Conditions

Water Condition	Calm	11.23ºC	Air Temp & RH	13ºC	92
Water Clarity	Clear (>2m visibility)		Wind Speed	Low (calm conditions. 1	
Clouds	Overcast		Wind Direction	SW to NE	
Weather Notes					

Samples taken by: Martin Ankor

Sample ID	Lake Name	Sample Type	Sample Time
MA0382	Lake Leake	Water - stable isotopes and	11/09/18 2:44 pm

Sampling depth	0.2m	Coords & QC	-37.611877	140.592543	87.4	7.8

Sampling notes

Catchment notes

Water Chemistry

pH	7.97
TDS	2236ppm
DO	7.86ppm
Cond.	4473µS/cm
PSU	2.4
Temp	15.5ºC

Weather Conditions

Water Condition	Choppy	15.5ºC	Air Temp & RH	21ºC	28
Water Clarity	Cloudy (0.5-2m visibility)		Wind Speed	High (Windy. 10+ m/s)	
Clouds	Overcast		Wind Direction	NNW to SSE	
Weather Notes					

Samples taken by: Martin Ankor

Sample ID	Lake Name	Sample Type	Sample Time
MA0029	Lake Mumblin	Water	29/08/15 3:16 pm

Sampling depth	0.2m	Coords & QC	-38.318999	142.913875	130.9	13.0

Sampling notes: Access difficult. Down track to shed, then down to lake. Wear sturdy shoes.
Steep sided little crater. Soil shows water logging and fracturing similar to lake Edward, as high as the pump shed. Watch for holes. Soil near lake fairly robust and

Catchment notes:

Water Chemistry

pH	
TDS	
DO	
Cond.	
PSU	
Temp	

Weather Conditions

Water Condition	Calm		Air Temp & RH	8.5°C	
Water Clarity	Clear (>2m visibility)		Wind Speed	Low (calm conditions.	
Clouds	Overcast		Wind Direction	SSE to NNW	

Weather Notes:

Samples taken by: Martin Ankor

Sample ID	Lake Name	Sample Type	Sample Time
MA0070	Lake Mumblin	Water-stable isotopes	5/04/16 4:00 pm

Sampling depth	0.1m	Coords & QC	-38.318949	142.914024	146.7	18.9

Sampling notes

Catchment notes

Water Chemistry

pH	8.71
TDS	804ppm
DO	0.52ppm
Cond.	1603µS/cm
PSU	0.81
Temp	20.2ºC

Weather Conditions

Water Condition	Calm	20.2ºC	Air Temp & RH	22ºC	60
Water Clarity	Cloudy (0.5-2m visibility)		Wind Speed	Medium (branches moving.	
Clouds	Overcast		Wind Direction	SW to NE	
Weather Notes					

Samples taken by: Martin Ankor

Sample ID	Lake Name	Sample Type	Sample Time
MA0119	Lake Mumblin	Water - general	2/08/16 3:13 pm

Sampling depth	0.2m	Coords & QC	-38.318790	142.914436	165.5	16.8

Sampling notes

Catchment notes

Water Chemistry

pH	8.42
TDS	603ppm
DO	2.81ppm
Cond.	1206µS/cm
PSU	0.61
Temp	11.6ºC

Weather Conditions

Water Condition	Calm	11.6ºC	Air Temp & RH	12ºC	82
Water Clarity	Murky (<0.5m visibility)		Wind Speed	Medium (branches moving.	
Clouds	Partly Cloudy		Wind Direction	SW to NE	
Weather Notes					

Samples taken by: Martin Ankor

Sample ID	Lake Name	Sample Type	Sample Time
MA0184	Lake Mumblin	Water - bulk	18/11/16 12:30 pm

Sampling depth		Coords & QC	-38.318796	142.914561	153.6	9.4

Sampling notes		Water Chemistry	
		pH	
		TDS	
Catchment notes		DO	
		Cond.	
		PSU	
		Temp	

Weather Conditions

Water Condition	Calm		Air Temp & RH	14.9ºC	76
Water Clarity			Wind Speed	Low (calm conditions. 1	
Clouds	Partly Cloudy		Wind Direction	SSW to NNE	
Weather Notes					

Samples taken by: Jonathan Tyler

Sample ID	Lake Name	Sample Type	Sample Time
JT0205	Lake Mumblin	Bulk water	4/01/17 3:47 pm

Sampling depth	0.3m	Coords & QC	-38.318780	142.914288	154.3	49.0

Sampling notes	4/1/20173:47:27 pm
Catchment notes	

Water Chemistry	
pH	9.14
TDS	590ppm
DO	3.62ppm
Cond.	1184µS/cm
PSU	.059
Temp	23.23ºC

Weather Conditions

Water Condition	Calm	23.23ºC	Air Temp & RH		
Water Clarity	Murky (<0.5m visibility)		Wind Speed	Low (calm conditions. 1	
Clouds	Sunny		Wind Direction		
Weather Notes					

Samples taken by: Martin Ankor

Sample ID	Lake Name	Sample Type	Sample Time
MA0237	Lake Mumblin	Water - bulk	12/03/17 2:11 pm

Sampling depth	0.3m	Coords & QC	-38.318711	142.914479	152.0	6.4

		Water Chemistry	
Sampling notes		pH	7.9
		TDS	573ppm
Catchment notes		DO	0.73ppm
		Cond.	1146µS/cm
		PSU	0.57
		Temp	23.7ºC

Weather Conditions

Water Condition		23.7ºC	Air Temp & RH		
Water Clarity			Wind Speed		
Clouds			Wind Direction		
Weather Notes					

Samples taken by: Martin Ankor

Sample ID	Lake Name	Sample Type	Sample Time
MA0270	Lake Mumblin	Water - stable isotopes and	28/06/17 1:11 pm

Sampling depth	0.3m	Coords & QC	-38.318828	142.914380	129.9	18.9

Sampling notes

Catchment notes

Water Chemistry

pH	7.7
TDS	507ppm
DO	2.62ppm
Cond.	1014µS/cm
PSU	0.51
Temp	10.8ºC

Weather Conditions

Water Condition	Calm	10.8ºC	Air Temp & RH	12.8ºC	76
Water Clarity	Cloudy (0.5-2m visibility)		Wind Speed	Low (calm conditions. 1	
Clouds	Overcast		Wind Direction		
Weather Notes					

Samples taken by: Martin Ankor

Sample ID	Lake Name	Sample Type	Sample Time
MA0285	Lake Mumblin	Water - stable isotopes and	5/09/17 9:47 am

Sampling depth	0.3m	Coords & QC	-38.318760	142.914421	148.6	13.0

Sampling notes

Catchment notes

Water Chemistry

pH	7.9
TDS	485ppm
DO	1.69ppm
Cond.	974µS/cm
PSU	0.48
Temp	9.7ºC

Weather Conditions

Water Condition	Choppy	9.7ºC	Air Temp & RH	7.5ºC	85
Water Clarity	Cloudy (0.5-2m visibility)		Wind Speed	Medium (branches moving.	
Clouds	Partly Cloudy		Wind Direction	WNW to ESE	
Weather Notes					

Samples taken by: Martin Ankor

Sample ID	Lake Name	Sample Type	Sample Time
MA0299	Lake Mumblin	Water - stable isotopes and	8/11/17 3:35 pm

Sampling depth	0.3m	Coords & QC	-38.318681	142.914645	157.7	16.8

Sampling notes		Water Chemistry	
		pH	7.2
		TDS	488ppm
Catchment notes		DO	2.7ppm
		Cond.	979µS/cm
		PSU	0.49
		Temp	19.8ºC

Weather Conditions

Water Condition	Calm	19.8ºC	Air Temp & RH	18ºC	61
Water Clarity	Cloudy (0.5-2m visibility)		Wind Speed	Low (calm conditions. 1	
Clouds	Partly Cloudy		Wind Direction	SE to NW	
Weather Notes					

Samples taken by: Martin Ankor

Sample ID	Lake Name	Sample Type	Sample Time
MA0311	Lake Mumblin	Water - stable isotopes and	23/01/18 3:11 pm

Sampling depth	0.3m	Coords & QC	-38.318662	142.914545	160.7	6.4

Sampling notes	Wedge tailed eagle spotted
Catchment notes	

Water Chemistry	
pH	8.2
TDS	510ppm
DO	0.33ppm
Cond.	1024µS/cm
PSU	0.5
Temp	27.4ºC

Weather Conditions

Water Condition	Calm	27.4ºC	Air Temp & RH	25ºC	40
Water Clarity	Cloudy (0.5-2m visibility)		Wind Speed	Medium (branches moving.	
Clouds	Sunny		Wind Direction	SSW to NNE	
Weather Notes					

Samples taken by: Martin Ankor

Sample ID	Lake Name	Sample Type	Sample Time
MA0323	Lake Mumblin	Water - stable isotopes and	7/03/18 12:27 pm

Sampling depth	0.3m	Coords & QC	-38.318835	142.914622	153.7	9.4

Sampling notes

Catchment notes

Water Chemistry

pH	7.8
TDS	634ppm
DO	8.1ppm
Cond.	1268µS/cm
PSU	0.63
Temp	22.1ºC

Weather Conditions

Water Condition	Calm	22.1ºC	Air Temp & RH	26ºC	38
Water Clarity	Murky (<0.5m visibility)		Wind Speed	Low (calm conditions. 1	
Clouds	Sunny		Wind Direction	N to S	
Weather Notes					

Samples taken by: Martin Ankor

Sample ID	Lake Name	Sample Type	Sample Time
MA0346	Lake Mumblin	Water - stable isotopes and	8/05/18 12:13 pm

Sampling depth	0.3m	Coords & QC	-38.318741	142.914274	161.1	15.6

Sampling notes

Catchment notes

Water Chemistry

pH	8
TDS	602ppm
DO	10.8ppm
Cond.	1200µS/cm
PSU	0.6
Temp	14.5ºC

Weather Conditions

Water Condition	Calm	14.5ºC	Air Temp & RH	14.3ºC	55
Water Clarity	Cloudy (0.5-2m visibility)		Wind Speed	Low (calm conditions. 1	
Clouds	Sunny		Wind Direction	W to E	
Weather Notes					

Samples taken by: Martin Ankor

Sample ID	Lake Name	Sample Type	Sample Time
MA0360	Lake Mumblin	Water - stable isotopes and	10/07/18 8:20 am

Sampling depth	0.2m	Coords & QC	-38.318784	142.914725	140.9	33.5

Sampling notes

Catchment notes

Water Chemistry

pH	6.5
TDS	505ppm
DO	9.73ppm
Cond.	1016µS/cm
PSU	0.5
Temp	9.5ºC

Weather Conditions

Water Condition	Calm	9.5ºC	Air Temp & RH	8ºC	100
Water Clarity	Murky (<0.5m visibility)		Wind Speed	Medium (branches moving.	
Clouds	Overcast		Wind Direction	W to E	
Weather Notes					

Samples taken by: Martin Ankor

Sample ID	Lake Name	Sample Type	Sample Time
MA0372	Lake Mumblin	Water - stable isotopes and	9/09/18 3:02 pm

Sampling depth	0.2m	Coords & QC	-38.318833	142.914618	167.4	13.0

Sampling notes		Water Chemistry	
		pH	8
		TDS	500ppm
Catchment notes		DO	6.2ppm
		Cond.	1000µS/cm
		PSU	0.5
		Temp	13.5ºC

Weather Conditions

Water Condition	Calm	13.5ºC	Air Temp & RH	15ºC	78
Water Clarity	Cloudy (0.5-2m visibility)		Wind Speed	Medium (branches moving.	
Clouds	Overcast		Wind Direction	W to E	
Weather Notes					

Samples taken by: Martin Ankor

Sample ID	Lake Name	Sample Type	Sample Time
MA0011	Lake Purrumbete	Water	24/05/15 10:45 am

Sampling depth	0.5	Coords & QC	-38.281240	143.214682	154.1	9.4
Sampling notes	Sample taken at Hoses rocks, good access. Sample taken with 6ft pole, then capped subsurface at shore.					
Catchment notes						

Weather Conditions

Water Condition	Calm		Air Temp & RH	10	
Water Clarity	Clear (>2m visibility)		Wind Speed	Low (calm conditions. 1	
Clouds	Partly Cloudy		Wind Direction	NNE to SSW	
Weather Notes					

Samples taken by: Martin ankor

Sample ID	Lake Name	Sample Type	Sample Time
MA0022	Lake Purrumbete	Water	10/06/15 5:17 pm

Sampling depth	0.2m	Coords & QC	-38.281306	143.214711	149.8	7.8

Sampling notes	Calcium isotope sample	Water Chemistry	
		pH	
		TDS	
Catchment notes		DO	
		Cond.	
		PSU	
		Temp	

Weather Conditions

Water Condition	Calm		Air Temp & RH	11ºC	Overcast
Water Clarity	Clear (>2m visibility)		Wind Speed	Low (calm conditions. 1	
Clouds			Wind Direction		
Weather Notes					

Samples taken by: Martin Ankor

Sample ID	Lake Name	Sample Type	Sample Time
MA0035	Lake Purrumbete	Water	30/08/15 1:03 pm

Sampling depth	0.2m	Coords & QC	-38.293011	143.221279	139.1	7.8

		Water Chemistry	
Sampling notes	Jetty near boat ramp	pH	
		TDS	
Catchment notes		DO	
		Cond.	
		PSU	
		Temp	

Weather Conditions

Water Condition	Calm		Air Temp & RH	11°C	
Water Clarity	Cloudy (0.5-2m visibility)		Wind Speed	Medium (branches moving.	
Clouds	Overcast		Wind Direction	SSW to NNE	
Weather Notes					

Samples taken by: Martin Ankor

Sample ID	Lake Name	Sample Type	Sample Time
MA0058	Lake Purrumbete	Water-stable isotopes	5/04/16 11:51 am

Sampling depth	0.2m	Coords & QC	-38.281340	143.214548	134.9	11.7

Sampling notes	See other db for obs
Catchment notes	

Water Chemistry	
pH	8.43
TDS	424ppm
DO	8.5ppm
Cond.	849µS/cm
PSU	0.42
Temp	18.67ºC

Weather Conditions

Water Condition	Choppy	18.67ºC	Air Temp & RH	25ºC	22
Water Clarity	Clear (>2m visibility)		Wind Speed	High (Windy. 10+ m/s)	
Clouds	Partly Cloudy		Wind Direction	NNW to SSE	
Weather Notes					

Samples taken by: Martin Ankor

Sample ID	Lake Name	Sample Type	Sample Time
MA0113	Lake Purrumbete	Water - general	2/08/16 12:11 pm

Sampling depth		Coords & QC	-38.281230	143.214577	137.0	5.8

Sampling notes

Catchment notes

Water Chemistry

pH	9.19
TDS	423ppm
DO	3.15ppm
Cond.	848µS/cm
PSU	0.42
Temp	10.74ºC

Weather Conditions

Water Condition	Calm	10.74ºC	Air Temp & RH	9.7ºC	83
Water Clarity	Clear (>2m visibility)		Wind Speed	Low (calm conditions.	
Clouds	Overcast		Wind Direction	S to N	
Weather Notes					

Samples taken by: Martin Ankor

Sample ID	Lake Name	Sample Type	Sample Time
MA0175	Lake Purrumbete	Water - stable isotope	18/11/16 9:21 am

Sampling depth	0.3m	Coords & QC	-38.281308	143.214817	165.2	18.9

Sampling notes

Catchment notes

Water Chemistry

pH	9.11
TDS	353ppm
DO	5.44ppm
Cond.	706µS/cm
PSU	0.35
Temp	15.24ºC

Weather Conditions

Water Condition	Calm	15.24ºC	Air Temp & RH	12.9ºC	92
Water Clarity	Clear (>2m visibility)		Wind Speed	Low (calm conditions. 1	
Clouds	Overcast		Wind Direction	S to N	
Weather Notes					

Samples taken by: Jonathan Tyler

Sample ID	Lake Name	Sample Type	Sample Time
JT0197	Lake Purrumbete	Bulk water	4/01/17 12:22 pm

Sampling depth	0.3m	Coords & QC	-38.292429	143.220454	138.5	18.9

		Water Chemistry	
Sampling notes	4/1/2017	pH	9.05
		TDS	
Catchment notes		DO	1.8ppm
		Cond.	815µS/cm
		PSU	.4
		Temp	21.1ºC

Weather Conditions

Water Condition	Calm	21.1ºC	Air Temp & RH		
Water Clarity	Murky (<0.5m visibility)		Wind Speed	Low (calm conditions. 1	
Clouds	Partly Cloudy		Wind Direction		
Weather Notes					

Samples taken by: Martin Ankor

Sample ID	Lake Name	Sample Type	Sample Time
MA0226	Lake Purrumbete	Water - bulk	12/03/17 10:34 am

Sampling depth	0.3m	Coords & QC	-38.281241	143.214616	137.4	13.0

Sampling notes

Catchment notes

Water Chemistry

pH	9.5
TDS	360ppm
DO	0.48ppm
Cond.	720µS/cm
PSU	0.35
Temp	20.6ºC

Weather Conditions

Water Condition	Choppy	20.6ºC	Air Temp & RH	20ºC	72
Water Clarity	Clear (>2m visibility)		Wind Speed	Medium (branches moving.	
Clouds	Partly Cloudy		Wind Direction	NNE to SSW	
Weather Notes					

Samples taken by: Martin Ankor

Sample ID	Lake Name	Sample Type	Sample Time
MA0265	Lake Purrumbete	Water - stable isotopes and	28/06/17 9:52 am

Sampling depth	0.3m	Coords & QC	-38.281259	143.214744	142.9	13.0

Sampling notes

Catchment notes

Water Chemistry

pH	9
TDS	360ppm
DO	2.39ppm
Cond.	723µS/cm
PSU	0.36
Temp	12.3ºC

Weather Conditions

Water Condition	Calm	12.3ºC	Air Temp & RH	8.4ºC	100
Water Clarity	Clear (>2m visibility)		Wind Speed	Low (calm conditions. 1	
Clouds	Partly Cloudy		Wind Direction	N to S	
Weather Notes					

Samples taken by: Martin Ankor

Sample ID	Lake Name	Sample Type	Sample Time
MA0290	Lake Purrumbete	Water - stable isotopes and	5/09/17 4:11 pm

Sampling depth	0.3m	Coords & QC	-38.281239	143.214725	135.6	13.0

Sampling notes

Catchment notes

Water Chemistry

pH	9
TDS	384ppm
DO	2.15ppm
Cond.	767µS/cm
PSU	0.38
Temp	10.6ºC

Weather Conditions

Water Condition	Choppy	10.6ºC	Air Temp & RH	8.2ºC	91
Water Clarity	Cloudy (0.5-2m visibility)		Wind Speed	High (Windy. 10+ m/s)	
Clouds	Overcast		Wind Direction	WNW to ESE	
Weather Notes					

Samples taken by: Martin Ankor

Sample ID	Lake Name	Sample Type	Sample Time
MA0297	Lake Purrumbete	Water - stable isotopes and	8/11/17 1:57 pm

Sampling depth	0.3m	Coords & QC	-38.281239	143.214692	145.4	15.6

Sampling notes

Catchment notes

Water Chemistry

pH	9.3
TDS	388ppm
DO	3.45ppm
Cond.	776µS/cm
PSU	0.38
Temp	17.1ºC

Weather Conditions

Water Condition	Calm	17.1ºC	Air Temp & RH	16ºC	65
Water Clarity	Clear (>2m visibility)		Wind Speed	Low (calm conditions. 1	
Clouds	Partly Cloudy		Wind Direction	SE to NW	
Weather Notes					

Samples taken by: Martin Ankor

Sample ID	Lake Name	Sample Type	Sample Time
MA0308	Lake Purrumbete	Water - stable isotopes and	23/01/18 11:04 am

Sampling depth	0.3m	Coords & QC	-38.281407	143.214703	157.8	13.0

Sampling notes

Catchment notes

Water Chemistry

pH	9.6
TDS	365ppm
DO	0.36ppm
Cond.	732µS/cm
PSU	0.36
Temp	23.3ºC

Weather Conditions

Water Condition	Calm	23.3ºC	Air Temp & RH	20ºC	52
Water Clarity	Clear (>2m visibility)		Wind Speed	Low (calm conditions. 1	
Clouds	Sunny		Wind Direction	SSW to NNE	
Weather Notes					

Samples taken by: Martin Ankor

Sample ID	Lake Name	Sample Type	Sample Time
MA0321	Lake Purrumbete	Water - stable isotopes and	7/03/18 10:12 am

Sampling depth	0.3m	Coords & QC	-38.281278	143.214746	159.7	26.0

Sampling notes

Catchment notes

Water Chemistry

pH	9.34
TDS	422ppm
DO	11.7ppm
Cond.	844µS/cm
PSU	0.42
Temp	20.1ºC

Weather Conditions

Water Condition	Calm	20.1ºC	Air Temp & RH	19ºC	67
Water Clarity	Clear (>2m visibility)		Wind Speed	Low (calm conditions. 1	
Clouds	Sunny		Wind Direction	E to W	
Weather Notes					

Samples taken by: Martin Ankor

Sample ID	Lake Name	Sample Type	Sample Time
MA0343	Lake Purrumbete	Water - stable isotopes and	8/05/18 10:06 am

Sampling depth	0.3m	Coords & QC	-38.281234	143.214307	143.9	33.5

Sampling notes

Catchment notes

Water Chemistry

pH	9
TDS	409ppm
DO	11.37ppm
Cond.	811µS/cm
PSU	0.4
Temp	15.3ºC

Weather Conditions

Water Condition	Calm	15.3ºC	Air Temp & RH	13.4ºC	68
Water Clarity	Clear (>2m visibility)		Wind Speed	Low (calm conditions. 1	
Clouds	Sunny		Wind Direction	W to E	
Weather Notes					

Samples taken by: Martin Ankor

Sample ID	Lake Name	Sample Type	Sample Time
MA0366	Lake Purrumbete	Water - stable isotopes and	10/07/18 1:09 pm

Sampling depth	0.2m	Coords & QC	-38.281237	143.214569	144.4	16.8

Sampling notes

Catchment notes

Water Chemistry	
pH	8.97
TDS	392ppm
DO	13.35ppm
Cond.	784µS/cm
PSU	0.39
Temp	11.23ºC

Weather Conditions

Water Condition	Calm	11.23ºC	Air Temp & RH	8.4ºC	72
Water Clarity	Clear (>2m visibility)		Wind Speed	Low (calm conditions. 1	
Clouds	Overcast		Wind Direction	NW to SE	
Weather Notes					

Samples taken by: Martin Ankor

Sample ID	Lake Name	Sample Type	Sample Time
MA0377	Lake Purrumbete	Water - stable isotopes and	10/09/18 9:30 am

Sampling depth	0.2m	Coords & QC	-38.281237	143.214673	147.2	18.9

Sampling notes

Catchment notes

Water Chemistry

pH	8.67
TDS	408ppm
DO	9.82ppm
Cond.	816µS/cm
PSU	0.4
Temp	10.8ºC

Weather Conditions

Water Condition	Calm	10.8ºC	Air Temp & RH	13ºC	100
Water Clarity	Clear (>2m visibility)		Wind Speed	Low (calm conditions. 1	
Clouds	Overcast		Wind Direction	N to S	
Weather Notes					

Samples taken by: Martin Ankor

Sample ID	Lake Name	Sample Type	Sample Time
MA0006	Lake Surprise	Water	23/05/15 3:44 pm

Sampling depth	0.4	Coords & QC	-38.058909	141.921098	85.0	16.8
Sampling notes	Area sampled in deep afternoon shade. Water level appears to have dropped 0.5 to 1m over last few years. Sample taken with 6ft pole, then capped subsurface at shore.					
Catchment notes						

Weather Conditions

Water Condition	Calm		Air Temp & RH	12	
Water Clarity	Cloudy (0.5-2m visibility)		Wind Speed	Low (calm conditions. 1	
Clouds	Partly Cloudy		Wind Direction		
Weather Notes					

Samples taken by: Martin Ankor

Sample ID	Lake Name	Sample Type	Sample Time
MA0026	Lake Surprise	Water	29/08/15 10:48 am

Sampling depth	0.3m	Coords & QC	-38.058909	141.921098	85.0	

		Water Chemistry	
Sampling notes		pH	
		TDS	
Catchment notes		DO	
		Cond.	
		PSU	
		Temp	

Weather Conditions

Water Condition	Calm		Air Temp & RH	10°C	
Water Clarity	Murky (<0.5m visibility)		Wind Speed	Medium (branches moving.	
Clouds	Partly Cloudy		Wind Direction	SE to NW	
Weather Notes					

Samples taken by: Martin Ankor

Sample ID	Lake Name	Sample Type	Sample Time
MA0081	Lake Surprise	Water-stable isotopes	6/04/16 9:20 am

Sampling depth	0.2m	Coords & QC	-38.059985	141.921366	77.6	26.0

Sampling notes	TBM used on first post on left of lookout
Catchment notes	

Water Chemistry	
pH	8.77
TDS	340ppm
DO	0.75ppm
Cond.	680µS/cm
PSU	0.33
Temp	17.75ºC

Weather Conditions

Water Condition	Calm	17.75ºC	Air Temp & RH	13ºC	90
Water Clarity	Clear (>2m visibility)		Wind Speed	Low (calm conditions. 1	
Clouds	Overcast		Wind Direction	W to E	
Weather Notes					

Samples taken by: Martin Ankor

Sample ID	Lake Name	Sample Type	Sample Time
MA0124	Lake Surprise	Water - general	3/08/16 8:41 am

Sampling depth	0.2m	Coords & QC	-38.059655	141.921271	116.4	49.0

Sampling notes

Catchment notes

Water Chemistry

pH	
TDS	
DO	
Cond.	
PSU	
Temp	

Weather Conditions

Water Condition	Calm		Air Temp & RH	6.4°C	98
Water Clarity	Murky (<0.5m visibility)		Wind Speed	Low (calm conditions.	
Clouds	Partly Cloudy		Wind Direction	SSW to NNE	
Weather Notes					

Samples taken by: Martin Ankor

Sample ID	Lake Name	Sample Type	Sample Time
MA0189	Lake Surprise	Water - bulk	18/11/16 3:54 pm

Sampling depth	0.2m	Coords & QC	-38.059477	141.921227	84.1	18.9

Sampling notes	Blue green algae warning signs up Prickly weeds all along path, painful
Catchment notes	

Water Chemistry	
pH	9.26
TDS	277ppm
DO	5.64ppm
Cond.	553µS/cm
PSU	0.27
Temp	21.45ºC

Weather Conditions

Water Condition	Calm	21.45ºC	Air Temp & RH	18.4ºC	58
Water Clarity	Murky (<0.5m visibility)		Wind Speed	Low (calm conditions. 1	
Clouds	Partly Cloudy		Wind Direction	SSW to NNE	
Weather Notes					

Samples taken by: Jonathan Tyler

Sample ID	Lake Name	Sample Type	Sample Time
JT0212	Lake Surprise	Bulk water	6/01/17 2:50 pm

Sampling depth	0.3m	Coords & QC	-38.059659	141.922081	71.9	18.9

Sampling notes	6/1/2017
Catchment notes	

Water Chemistry	
pH	8.98
TDS	337ppm
DO	1.63ppm
Cond.	676µS/cm
PSU	.33
Temp	25.09ºC

Weather Conditions

Water Condition	Calm	25.09ºC	Air Temp & RH		
Water Clarity	Murky (<0.5m visibility)		Wind Speed	Low (calm conditions. 1	
Clouds	Partly Cloudy		Wind Direction	S to N	
Weather Notes					

Samples taken by: Martin Ankor

Sample ID	Lake Name	Sample Type	Sample Time
MA0241	Lake Surprise	Water - bulk	12/03/17 4:44 pm

Sampling depth	0.3m	Coords & QC	-38.059454	141.921525	89.3	18.9

Sampling notes

Catchment notes

Water Chemistry

pH	9.1
TDS	294ppm
DO	0.92ppm
Cond.	587µS/cm
PSU	0.28
Temp	21.7ºC

Weather Conditions

Water Condition	Calm	21.7ºC	Air Temp & RH	20ºC	62
Water Clarity	Cloudy (0.5-2m visibility)		Wind Speed	Low (calm conditions. 1	
Clouds	Overcast		Wind Direction	WSW to ENE	
Weather Notes					

Samples taken by: Martin Ankor

Sample ID	Lake Name	Sample Type	Sample Time
MA0273	Lake Surprise	Water	29/06/17 8:36 am

Sampling depth	0.3m	Coords & QC	-38.059216	141.921472	63.1	64.8

Sampling notes

Catchment notes

Water Chemistry	
pH	7.7
TDS	298ppm
DO	1.57ppm
Cond.	597µS/cm
PSU	0.29
Temp	10.8ºC

Weather Conditions

Water Condition	Calm	10.8ºC	Air Temp & RH	7.2ºC	99
Water Clarity	Cloudy (0.5-2m visibility)		Wind Speed	Low (calm conditions. 1	
Clouds	Partly Cloudy		Wind Direction	WSW to ENE	
Weather Notes					

Samples taken by: Martin Ankor

Sample ID	Lake Name	Sample Type	Sample Time
MA0278	Lake Surprise	Water - stable isotopes and	3/09/17 4:59 pm

Sampling depth	0.3m	Coords & QC	-38.059506	141.921337	93.9	18.9

Sampling notes

Catchment notes

Water Chemistry

pH	9.2
TDS	303ppm
DO	1.83ppm
Cond.	604µS/cm
PSU	0.3
Temp	12.8ºC

Weather Conditions

Water Condition	Calm	12.8ºC	Air Temp & RH	11.2ºC	68
Water Clarity	Murky (<0.5m visibility)		Wind Speed	Medium (branches moving.	
Clouds	Overcast		Wind Direction	WNW to ESE	
Weather Notes					

Samples taken by: Martin Ankor

Sample ID	Lake Name	Sample Type	Sample Time
MA0293	Lake Surprise	Water - stable isotopes and	7/11/17 4:31 pm

Sampling depth	0.3m	Coords & QC	-38.059507	141.921285	79.1	33.5

Sampling notes

Catchment notes

Water Chemistry

pH	9.26
TDS	292ppm
DO	7.59ppm
Cond.	584µS/cm
PSU	0.28
Temp	18.12ºC

Weather Conditions

Water Condition	Calm	18.12ºC	Air Temp & RH	15ºC	50
Water Clarity	Murky (<0.5m visibility)		Wind Speed	Low (calm conditions. 1	
Clouds	Overcast		Wind Direction	S to N	
Weather Notes					

Samples taken by: Martin Ankor

Sample ID	Lake Name	Sample Type	Sample Time
MA0305	Lake Surprise	Water - stable isotopes and	22/01/18 5:28 pm

Sampling depth	0.3m	Coords & QC	-38.059453	141.921661	123.1	26.0

Sampling notes

Catchment notes

Water Chemistry

pH	8.9
TDS	294ppm
DO	0.28ppm
Cond.	588µS/cm
PSU	0.28
Temp	26ºC

Weather Conditions

Water Condition	Choppy	26ºC	Air Temp & RH	26ºC	40
Water Clarity	Cloudy (0.5-2m visibility)		Wind Speed	Medium (branches moving.	
Clouds	Sunny		Wind Direction	S to N	
Weather Notes					

Samples taken by: Martin Ankor

Sample ID	Lake Name	Sample Type	Sample Time
MA0318	Lake Surprise	Water - stable isotopes and	6/03/18 5:37 pm

Sampling depth	0.3m	Coords & QC	-38.059300	141.921422	100.3	13.0

Sampling notes

Catchment notes

Water Chemistry

pH	8.9
TDS	343ppm
DO	11.76ppm
Cond.	686µS/cm
PSU	0.33
Temp	21.3ºC

Weather Conditions

Water Condition	Calm	21.3ºC	Air Temp & RH	22ºC	48
Water Clarity	Cloudy (0.5-2m visibility)		Wind Speed	Medium (branches moving.	
Clouds	Partly Cloudy		Wind Direction	SE to NW	
Weather Notes					

Samples taken by: Martin Ankor

Sample ID	Lake Name	Sample Type	Sample Time
MA0340	Lake Surprise	Water - stable isotopes and	7/05/18 2:20 pm

Sampling depth	0.3m	Coords & QC	-37.627338	140.603171	116.6	16.8

Sampling notes

Catchment notes

Water Chemistry

pH	8.7
TDS	324ppm
DO	10.8ppm
Cond.	647µS/cm
PSU	0.32
Temp	15ºC

Weather Conditions

Water Condition	Calm	15ºC	Air Temp & RH	16.9ºC	46
Water Clarity	Cloudy (0.5-2m visibility)		Wind Speed	Medium (branches moving.	
Clouds	Overcast		Wind Direction	NNW to SSE	
Weather Notes					

Samples taken by: Martin Ankor

Sample ID	Lake Name	Sample Type	Sample Time
MA0359	Lake Surprise	Water - stable isotopes and	9/07/18 3:32 pm

Sampling depth	0.2m	Coords & QC	-38.059560	141.921178	108.1	26.0

Sampling notes

Catchment notes

Water Chemistry	
pH	7.97
TDS	319ppm
DO	10.46ppm
Cond.	639µS/cm
PSU	.31
Temp	10.44ºC

Weather Conditions

Water Condition		10.44ºC	Air Temp & RH	13ºC	82
Water Clarity	Murky (<0.5m visibility)		Wind Speed	Low (calm conditions. 1	
Clouds	Overcast		Wind Direction	SW to NE	
Weather Notes					

Samples taken by: Martin Ankor

Sample ID	Lake Name	Sample Type	Sample Time
MA0380	Lake Surprise	Water - stable isotopes and	11/09/18 9:21 am

Sampling depth	0.2m	Coords & QC	-38.059389	141.921256	62.2	26.0

Sampling notes

Catchment notes

Water Chemistry

pH	9.28
TDS	330ppm
DO	9.66ppm
Cond.	661µS/cm
PSU	0.32
Temp	12.7ºC

Weather Conditions

Water Condition	Calm	12.7ºC	Air Temp & RH	14.9ºC	65
Water Clarity	Murky (<0.5m visibility)		Wind Speed	Medium (branches moving.	
Clouds	Sunny		Wind Direction	NNE to SSW	
Weather Notes					

Samples taken by: Martin Ankor

Sample ID	Lake Name	Sample Type	Sample Time
MA0014	Lake Tooliorook	Water	24/05/15 2:01 pm

Sampling depth	0.4	Coords & QC	-37.977324	143.283890	155.8	7.8
Sampling notes	Easy access at boat ramp. Lake water clear, sandy bottom. Many aquatic invertebrates swimming around and aquatic vegetation. Really nice lake. :D Sample capped at depth by hand.					
Catchment notes						

Weather Conditions

Water Condition	Calm	Air Temp & RH	14
Water Clarity	Clear (>2m visibility)	Wind Speed	Medium (branches moving.
Clouds	Partly Cloudy	Wind Direction	NNW to SSE
Weather Notes			

Samples taken by: Martin Ankor

Sample ID	Lake Name	Sample Type	Sample Time
MA0036	Lake Toliorook	Water	31/08/15 8:59 am

Sampling depth	0.1m	Coords & QC	-37.977498	143.284477	183.2	26.0

Sampling notes		Water Chemistry	
		pH	
		TDS	
Catchment notes		DO	
		Cond.	
		PSU	
		Temp	

Weather Conditions

Water Condition	Calm		Air Temp & RH	7ºC	
Water Clarity	Clear (>2m visibility)		Wind Speed	Low (calm conditions.	
Clouds	Overcast		Wind Direction	N to S	
Weather Notes					

Samples taken by: Martin Ankor

Sample ID	Lake Name	Sample Type	Sample Time
MA0044	Lake Tooliorook	Water-stable isotopes	5/04/16 7:55 am

Sampling depth	0.2m	Coords & QC	-37.977626	143.284488	164.1	7.8

Sampling notes	Weedy littoral zone.
Catchment notes	

Water Chemistry	
pH	6.66
TDS	6442ppm
DO	
Cond.	12890µS/cm
PSU	7.44
Temp	13.15ºC

Weather Conditions

Water Condition	Choppy	13.15ºC	Air Temp & RH	23ºC	25
Water Clarity	Clear (>2m visibility)		Wind Speed	Medium (branches moving.	
Clouds	Partly Cloudy		Wind Direction	N to S	
Weather Notes					

Samples taken by: Martin Ankor

Sample ID	Lake Name	Sample Type	Sample Time
MA0115	Lake Tooliorook	Water - general	2/08/16 1:20 pm

Sampling depth	0.2m	Coords & QC	-37.977348	143.283745	155.7	7.8

Sampling notes	
Catchment notes	

Water Chemistry

pH	9.18
TDS	5798ppm
DO	2.58ppm
Cond.	11580µS/cm
PSU	6.64
Temp	12.4ºC

Weather Conditions

Water Condition	Choppy	12.4ºC	Air Temp & RH	11.7ºC	85
Water Clarity	Clear (>2m visibility)		Wind Speed	Medium (branches moving.	
Clouds	Partly Cloudy		Wind Direction	SSW to NNE	
Weather Notes	Rained a bit today.				

Samples taken by: Martin Ankor

Sample ID	Lake Name	Sample Type	Sample Time
MA0169	Lake Tooliorook	Water - bulk	17/11/16 6:35 pm

Sampling depth	0.3m	Coords & QC	-37.977567	143.284538	177.5	9.4

Sampling notes	Many wrigglies in shallows
Catchment notes	

Water Chemistry	
pH	7.96
TDS	2379ppm
DO	1.84ppm
Cond.	4762µS/cm
PSU	2.56
Temp	20.3ºC

Weather Conditions

Water Condition	Calm	20.3ºC	Air Temp & RH	26ºC	44
Water Clarity	Clear (>2m visibility)		Wind Speed	Low (calm conditions. 1	
Clouds	Partly Cloudy		Wind Direction	NW to SE	
Weather Notes					

Samples taken by: Jonathan Tyler

Sample ID	Lake Name	Sample Type	Sample Time
JT0209	Lake Tooliorook	Bulk water	6/01/17 11:06 am

Sampling depth	0.3m	Coords & QC	-37.977285	143.283751	158.6	16.8

Sampling notes	Water readings from jetty but sample from ramp due to access
Catchment notes	

Water Chemistry	
pH	8.02
TDS	2995ppm
DO	1.19ppm
Cond.	5990µS/cm
PSU	3.26
Temp	21.39ºC

Weather Conditions

Water Condition	Calm	21.39ºC	Air Temp & RH		
Water Clarity	Cloudy (0.5-2m visibility)		Wind Speed	Low (calm conditions. 1	
Clouds	Sunny		Wind Direction		
Weather Notes					

Samples taken by: Martin Ankor

Sample ID	Lake Name	Sample Type	Sample Time
MA0228	Lake Tooliorook	Water - bulk	12/03/17 11:20 am

Sampling depth	0.3m	Coords & QC	-37.977560	143.284293	149.6	9.4

		Water Chemistry	
Sampling notes		pH	9.02
		TDS	2846ppm
Catchment notes		DO	0.63ppm
		Cond.	5691µS/cm
		PSU	3.09
		Temp	22.8ºC

Weather Conditions

Water Condition	Calm	22.8ºC	Air Temp & RH	21.3ºC	63
Water Clarity	Cloudy (0.5-2m visibility)		Wind Speed	Medium (branches moving.	
Clouds	Partly Cloudy		Wind Direction	WNW to ESE	
Weather Notes					

Samples taken by: Martin Ankor

Sample ID	Lake Name	Sample Type	Sample Time
MA0262	Lake Tooliorook	Water - stable isotopes and	27/06/17 3:30 pm

Sampling depth	0.2m	Coords & QC	-37.977488	143.284562	187.4	6.4

Sampling notes	Conductivity calibration non successful, reading quick cal solution 7100 us/cm
Catchment notes	

Water Chemistry	
pH	9.1
TDS	2700ppm
DO	2.12ppm
Cond.	5406µS/cm
PSU	2.94
Temp	11.6ºC

Weather Conditions

Water Condition	Choppy	11.6ºC	Air Temp & RH	11.7ºC	61
Water Clarity	Murky (<0.5m visibility)		Wind Speed	Medium (branches moving.	
Clouds	Overcast		Wind Direction	N to S	
Weather Notes					

Samples taken by: Martin Ankor

Sample ID	Lake Name	Sample Type	Sample Time
MA0287	Lake Tooliorook	Water - stable isotopes and	5/09/17 11:28 am

Sampling depth	0.3m	Coords & QC	-37.977250	143.284135	160.7	7.8

Sampling notes

Catchment notes

Water Chemistry

pH	8.9
TDS	2842ppm
DO	2.01ppm
Cond.	5682µS/cm
PSU	3.1
Temp	9.6ºC

Weather Conditions

Water Condition	Choppy	9.6ºC	Air Temp & RH	8ºC	83
Water Clarity	Cloudy (0.5-2m visibility)		Wind Speed	High (Windy. 10+ m/s)	
Clouds	Overcast		Wind Direction	WNW to ESE	
Weather Notes					

Samples taken by: Martin Ankor

Sample ID	Lake Name	Sample Type	Sample Time
MA0294	Lake Tooliorook	Water - stable isotopes and	8/11/17 7:53 am

Sampling depth	0.3m	Coords & QC	-37.977529	143.284474	165.2	13.0

Sampling notes

Catchment notes

Water Chemistry

pH	8.17
TDS	2830ppm
DO	7.33ppm
Cond.	5660µS/cm
PSU	3.09
Temp	15.41ºC

Weather Conditions

Water Condition	Calm	15.41ºC	Air Temp & RH	11ºC	79
Water Clarity	Cloudy (0.5-2m visibility)		Wind Speed	Low (calm conditions. 1	
Clouds	Overcast		Wind Direction	E to W	
Weather Notes					

Samples taken by: Martin Ankor

Sample ID	Lake Name	Sample Type	Sample Time
MA0315	Lake Tooliorook	Water - stable isotopes and	24/01/18 7:34 am

Sampling depth	0.3m	Coords & QC	-37.977206	143.283889	151.1	9.4

Sampling notes: Serious algal bloom.
Caution with these results. Sample collected with bucket.

Catchment notes:

Water Chemistry

pH	9
TDS	2890ppm
DO	0.64ppm
Cond.	5775µS/cm
PSU	3.13
Temp	24.6ºC

Weather Conditions

Water Condition	Calm	24.6ºC	Air Temp & RH	9.9ºC	96
Water Clarity	Murky (<0.5m visibility)		Wind Speed	Low (calm conditions. 1	
Clouds	Partly Cloudy		Wind Direction	SSW to NNE	
Weather Notes					

Samples taken by: Martin Ankor

Sample ID	Lake Name	Sample Type	Sample Time
MA0325	Lake Tooliorook	Water - stable isotopes and	7/03/18 2:30 pm

Sampling depth	0.3m	Coords & QC	-37.977460	143.284432	169.7	9.4

Sampling notes

Catchment notes

Water Chemistry

pH	9.36
TDS	3500ppm
DO	19.5ppm
Cond.	7000µS/cm
PSU	3.84
Temp	24.2ºC

Weather Conditions

Water Condition	Calm	24.2ºC	Air Temp & RH	29ºC	31
Water Clarity	Cloudy (0.5-2m visibility)		Wind Speed	Low (calm conditions. 1	
Clouds	Sunny		Wind Direction	NNW to SSE	
Weather Notes					

Samples taken by: Martin Ankor

Sample ID	Lake Name	Sample Type	Sample Time
MA0349	Lake Tooliorook	Water - stable isotopes and	8/05/18 2:15 pm

Sampling depth	0.3m	Coords & QC	-37.977646	143.284523	173.8	13.0

Sampling notes	Blue green algae
Catchment notes	

Water Chemistry	
pH	9.4
TDS	3430ppm
DO	13.8ppm
Cond.	6870µS/cm
PSU	3.8
Temp	16.1ºC

Weather Conditions

Water Condition	Calm	16.1ºC	Air Temp & RH	16ºC	49
Water Clarity	Murky (<0.5m visibility)		Wind Speed	Low (calm conditions. 1	
Clouds	Sunny		Wind Direction	WNW to ESE	
Weather Notes					

Samples taken by: Martin Ankor

Sample ID	Lake Name	Sample Type	Sample Time
MA0363	Lake Tooliorook	Water - stable isotopes and	10/07/18 10:20 am

Sampling depth	0.2m	Coords & QC	-37.977374	143.284247	165.4	13.0

Sampling notes

Catchment notes

Water Chemistry

pH	9.35
TDS	3355ppm
DO	13.7ppm
Cond.	6701µS/cm
PSU	3.69
Temp	9ºC

Weather Conditions

Water Condition	Calm	9ºC	Air Temp & RH	9ºC	92
Water Clarity	Murky (<0.5m visibility)		Wind Speed	Medium (branches moving.	
Clouds	Overcast		Wind Direction	NNW to SSE	
Weather Notes					

Samples taken by: Martin Ankor

Sample ID	Lake Name	Sample Type	Sample Time
MA0370	Lake Tooliorook	Water - stable isotopes and	9/09/18 12:18 pm

Sampling depth	0.2m	Coords & QC	-37.977277	143.284407	136.2	9.4

Sampling notes	Sample E not filtered
Catchment notes	

Water Chemistry	
pH	8.9
TDS	3424ppm
DO	5.56ppm
Cond.	6851µS/cm
PSU	3.8
Temp	12.8ºC

Weather Conditions

Water Condition	Choppy	12.8ºC	Air Temp & RH	14.2ºC	78
Water Clarity	Murky (<0.5m visibility)		Wind Speed	High (Windy. 10+ m/s)	
Clouds	Overcast		Wind Direction	WNW to ESE	
Weather Notes	Horrible				

Samples taken by: Martin Ankor

Sample ID	Lake Name	Sample Type	Sample Time
MA0008	Tower hill	Water	23/05/15 5:39 pm

Sampling depth	0.1	Coords & QC	-38.322950	142.370437	29.4	13.0
Sampling notes	Rather dark :(Decent access to lake using fallen trees. Sample taken with 6ft pole, then capped subsurface at shore.					
Catchment notes						

Weather Conditions

Water Condition	Calm		Air Temp & RH	11	
Water Clarity	Cloudy (0.5-2m visibility)		Wind Speed	Low (calm conditions. 1	
Clouds	Partly Cloudy		Wind Direction	SSE to NNW	
Weather Notes	After sunset.				

Samples taken by: Martin Ankor

Sample ID	Lake Name	Sample Type	Sample Time
MA0027	Tower Hill	Water	29/08/15 1:11 pm

Sampling depth	0.2m	Coords & QC	-38.322783	142.370452	-23.4	18.9

Sampling notes: Tannin coloured water. Watch out for spiky plant.

Catchment notes:

Water Chemistry

pH	
TDS	
DO	
Cond.	
PSU	
Temp	

Weather Conditions

Water Condition	Calm		Air Temp & RH	13ºC	
Water Clarity	Cloudy (0.5-2m visibility)		Wind Speed	Medium (branches moving.	
Clouds	Partly Cloudy		Wind Direction	SSE to NNW	
Weather Notes					

Samples taken by: Jonathan Tyler

Sample ID	Lake Name	Sample Type	Sample Time
JT0211	Tower Hill	Isotope water	6/01/17 1:30 pm

Sampling depth	0.3m	Coords & QC	-38.321284	142.369742	11.3	33.5

Sampling notes	
Catchment notes	

Water Chemistry	
pH	9.25
TDS	3393ppm
DO	1.01ppm
Cond.	6828µS/cm
PSU	3.71
Temp	28.18ºC

Weather Conditions

Water Condition	Calm	28.18ºC	Air Temp & RH		
Water Clarity	Murky (<0.5m visibility)		Wind Speed	Low (calm conditions. 1	
Clouds	Sunny		Wind Direction		
Weather Notes					

Samples taken by: Georgie falster

Sample ID	Lake Name	Sample Type	Sample Time
MA0018	West Basin		10/06/15 12:49 pm

Sampling depth		Coords & QC	-38.321978	143.450497	117.6	18.9

Sampling notes		Water Chemistry	
		pH	
		TDS	
Catchment notes		DO	
		Cond.	
		PSU	
		Temp	

Weather Conditions

Water Condition			Air Temp & RH		
Water Clarity			Wind Speed		
Clouds			Wind Direction		
Weather Notes					

Samples taken by: Georgie falster

Sample ID	Lake Name	Sample Type	Sample Time
MA0019	West Basin	Water	10/06/15 1:00 pm

Sampling depth	0.2m	Coords & QC	-38.324576	143.448410	125.2	18.9

Sampling notes	Calcium isotope samples tds 81720ppm pH 10.37 Conductivity 163400uS/cm DO 0.42ppm
Catchment notes	

Water Chemistry	
pH	
TDS	
DO	
Cond.	
PSU	
Temp	12.86ºC

Weather Conditions

Water Condition	Calm	12.86ºC	Air Temp & RH		Overcast
Water Clarity	Cloudy (0.5-2m visibility)		Wind Speed	Low (calm conditions. 1	
Clouds			Wind Direction	SW to NE	
Weather Notes					

Samples taken by: Martin Ankor

Sample ID	Lake Name	Sample Type	Sample Time
MA0050	West Basin	Water-stable isotopes	5/04/16 9:34 am

Sampling depth	0.2m	Coords & QC	-38.323491	143.448667	92.4	24.5

		Water Chemistry	
Sampling notes		pH	6.87
		TDS	79590ppm
		DO	
Catchment notes	No springs observed on south west side	Cond.	159100µS/cm
		PSU	
		Temp	18.77ºC

Weather Conditions

Water Condition	Choppy	18.77ºC	Air Temp & RH	23ºC	25
Water Clarity	Cloudy (0.5-2m visibility)		Wind Speed	Medium (branches moving.	
Clouds	Partly Cloudy		Wind Direction	N to S	
Weather Notes					

Samples taken by: Martin Ankor

Sample ID	Lake Name	Sample Type	Sample Time
MA0109	West Basin	Water - stable isotopes	2/08/16 10:25 am

Sampling depth	0.2m	Coords & QC	-38.323590	143.448754	119.6	26.0

Sampling notes	
Catchment notes	

Water Chemistry	
pH	8.8
TDS	75250ppm
DO	2.65ppm
Cond.	150300µS/cm
PSU	-
Temp	11ºC

Weather Conditions

Water Condition	Choppy	11ºC	Air Temp & RH	8.3ºC	80
Water Clarity	Murky (<0.5m visibility)		Wind Speed	Medium (branches moving.	
Clouds	Partly Cloudy		Wind Direction	SW to NE	
Weather Notes					

Samples taken by: Martin Ankor

Sample ID	Lake Name	Sample Type	Sample Time
MA0171	West Basin	Water - bulk	18/11/16 8:18 am

Sampling depth	0.3m	Coords & QC	-38.323394	143.449097	104.4	9.4

Sampling notes	Photo opp direction to first
Catchment notes	

Water Chemistry	
pH	8.9
TDS	59930ppm
DO	2.6ppm
Cond.	119800µS/cm
PSU	-
Temp	20.3ºC

Weather Conditions

Water Condition	Calm	20.3ºC	Air Temp & RH	11.8ºC	100
Water Clarity	Murky (<0.5m visibility)		Wind Speed	Low (calm conditions. 1	
Clouds	Overcast		Wind Direction	SSW to NNE	
Weather Notes	Raining gently				

Samples taken by: Jonathan Tyler

Sample ID	Lake Name	Sample Type	Sample Time
JT0195	West Basin	Bulk water	4/01/17 11:20 am

Sampling depth	0.3m	Coords & QC	-38.323452	143.448656	131.7	18.9

Sampling notes

Catchment notes

Water Chemistry

pH	8.8
TDS	72800ppm
DO	0.51ppm
Cond.	145600µS/cm
PSU	
Temp	22.67ºC

Weather Conditions

Water Condition	Calm	22.67ºC	Air Temp & RH		
Water Clarity	Murky (<0.5m visibility)		Wind Speed	Low (calm conditions. 1	
Clouds	Partly Cloudy		Wind Direction		
Weather Notes					

Samples taken by: Martin Ankor

Sample ID	Lake Name	Sample Type	Sample Time
MA0222	West Basin	Water - bulk	12/03/17 9:22 am

Sampling depth	0.3m	Coords & QC	-38.323264	143.449326	108.5	15.6

Sampling notes

Catchment notes

Water Chemistry

pH	8.65
TDS	65750ppm
DO	0.17ppm
Cond.	131500µS/cm
PSU	-
Temp	22.4ºC

Weather Conditions

Water Condition	Calm	22.4ºC	Air Temp & RH	16ºC	99
Water Clarity	Clear (>2m visibility)		Wind Speed	Medium (branches moving.	
Clouds	Partly Cloudy		Wind Direction	ESE to WNW	
Weather Notes					

Samples taken by: Martin Ankor

Sample ID	Lake Name	Sample Type	Sample Time
MA0263	West Basin	Water - stable isotopes and	28/06/17 8:41 am

Sampling depth	0.3m	Coords & QC	-38.323391	143.449151	108.5	15.6

Sampling notes

Catchment notes

Water Chemistry

pH	8.9
TDS	64030ppm
DO	1.44ppm
Cond.	128000µS/cm
PSU	-
Temp	10.3ºC

Weather Conditions

Water Condition	Calm	10.3ºC	Air Temp & RH	6.6ºC	97
Water Clarity	Cloudy (0.5-2m visibility)		Wind Speed	Low (calm conditions. 1	
Clouds	Partly Cloudy		Wind Direction	NNW to SSE	
Weather Notes					

Samples taken by: Martin Ankor

Sample ID	Lake Name	Sample Type	Sample Time
MA0288	West Basin	Water - stable isotopes and	5/09/17 2:48 pm

Sampling depth	0.3m	Coords & QC	-38.323362	143.449087	107.8	13.0

Sampling notes

Catchment notes

Water Chemistry

pH	8.95
TDS	64900ppm
DO	1.1ppm
Cond.	129800µS/cm
PSU	-
Temp	10.3ºC

Weather Conditions

Water Condition	Choppy	10.3ºC	Air Temp & RH	7.3ºC	100
Water Clarity	Murky (<0.5m visibility)		Wind Speed	High (Windy. 10+ m/s)	
Clouds	Overcast		Wind Direction	WNW to ESE	
Weather Notes					

Samples taken by: Martin Ankor

Sample ID	Lake Name	Sample Type	Sample Time
MA0295	West Basin	Water - stable isotopes and	8/11/17 12:17 pm

Sampling depth	0.3m	Coords & QC	-38.323379	143.448978	128.2	7.8

Sampling notes

Catchment notes

Water Chemistry

pH	8.85
TDS	65000ppm
DO	2.11ppm
Cond.	129900µS/cm
PSU	
Temp	17.4ºC

Weather Conditions

Water Condition	Calm	17.4ºC	Air Temp & RH	13ºC	75
Water Clarity	Cloudy (0.5-2m visibility)		Wind Speed	Low (calm conditions. 1	
Clouds	Overcast		Wind Direction	SE to NW	
Weather Notes					

Samples taken by: Martin Ankor

Sample ID	Lake Name	Sample Type	Sample Time
MA0306	West Basin	Water - stable isotopes and	23/01/18 9:54 am

Sampling depth	0.3m	Coords & QC	-38.323392	143.449074	125.8	9.4

		Water Chemistry	
Sampling notes		pH	8.75
		TDS	66260ppm
Catchment notes		DO	0.16ppm
		Cond.	132500µS/cm
		PSU	-
		Temp	25.4ºC

Weather Conditions

Water Condition	Calm	25.4ºC	Air Temp & RH	17ºC	66
Water Clarity	Cloudy (0.5-2m visibility)		Wind Speed	Low (calm conditions. 1	
Clouds	Sunny		Wind Direction	NNE to SSW	
Weather Notes					

Samples taken by: Martin Ankor

Sample ID	Lake Name	Sample Type	Sample Time
MA0319	West Basin	Water - stable isotopes and	7/03/18 8:52 am

Sampling depth	0.3m	Coords & QC	-38.323394	143.449403	93.2	12.8

		Water Chemistry	
Sampling notes		pH	8.62
		TDS	78650ppm
Catchment notes		DO	1.92ppm
		Cond.	157200µS/cm
		PSU	
		Temp	20.6ºC

Weather Conditions

Water Condition	Calm	20.6ºC	Air Temp & RH	16ºC	96
Water Clarity	Cloudy (0.5-2m visibility)		Wind Speed	Low (calm conditions. 1	
Clouds	Sunny		Wind Direction	ESE to WNW	
Weather Notes					

Samples taken by: Martin Ankor

Sample ID	Lake Name	Sample Type	Sample Time
MA0341	West Basin	Water - stable isotopes and	8/05/18 8:42 am

Sampling depth	0.3m	Coords & QC	-38.323460	143.449179	110.9	9.4

Sampling notes

Catchment notes

Water Chemistry

pH	8.65
TDS	74360ppm
DO	6.75ppm
Cond.	148600µS/cm
PSU	
Temp	15.1ºC

Weather Conditions

Water Condition	Calm	15.1ºC	Air Temp & RH	9.7ºC	87
Water Clarity	Murky (<0.5m visibility)		Wind Speed	Low (calm conditions. 1	
Clouds	Sunny		Wind Direction	SE to NW	
Weather Notes					

Samples taken by: Martin Ankor

Sample ID	Lake Name	Sample Type	Sample Time
MA0364	West Basin	Water - stable isotopes and	10/07/18 11:50 am

Sampling depth	0.2m	Coords & QC	-38.323401	143.449245	98.1	12.8

		Water Chemistry	
Sampling notes		pH	8.63
		TDS	71080ppm
Catchment notes	PSU off chart	DO	7.15ppm
		Cond.	142100µS/cm
		PSU	
		Temp	10.6ºC

Weather Conditions

Water Condition	Calm	10.6ºC	Air Temp & RH	8.4ºC	
Water Clarity	Murky (<0.5m visibility)		Wind Speed	Low (calm conditions. 1	
Clouds	Overcast		Wind Direction	NW to SE	
Weather Notes					

Samples taken by: Martin Ankor

Sample ID	Lake Name	Sample Type	Sample Time
MA0378	West Basin	Water - stable isotopes and	10/09/18 10:49 am

Sampling depth	0.2m	Coords & QC	-38.323346	143.449135	124.8	7.8

		Water Chemistry	
Sampling notes		pH	8.74
		TDS	71120ppm
Catchment notes		DO	5.3ppm
		Cond.	142300µS/cm
		PSU	-
		Temp	14ºC

Weather Conditions

Water Condition	Calm	14ºC	Air Temp & RH	13.1ºC	
Water Clarity	Murky (<0.5m visibility)		Wind Speed	Low (calm conditions. 1	
Clouds	Partly Cloudy		Wind Direction	NW to SE	
Weather Notes	Humidity unavailable				

Appendix 2

This appendix comprises some additional information collected for some of the lakes, comprising bathymetric maps for Lake Leake, Lake Edward and Lake Surprise as well as historical lake level reconstructions for Lake Leake and Lake Edward.

Bathymetry surveying of Lake Surprise, Lake Edward and Lake Leake, and historical lake level reconstructions for Lake Edward and Lake Leake

Bathymetric surveys

Lake Surprise 30/09/2019

Lake Surprise sits in a volcanic crater and consists of a main central lagoon around 500 x 200 m, with a smaller, connected lagoon at both the northern and southern ends, joined to the main lagoon by a slightly narrower neck. These smaller lagoons hold the majority of reed beds, as the main lagoon increases in depth rapidly near the shoreline. The northern lagoon was separated from the main lagoon by a reed bed around 5-10 m in thickness. The lake was a reddish brown at the time of survey, with a lake water level of ~78.09 mAHD.

Surveying was performed with a bathymetry kayak (The Bathy-yak). A Native Watercraft Mariner 12.5 kayak, with a pedal driven propeller was used, combined with a Lowrance HDS-5 echo sounder and Leica 1200GG RTK GPS, linked to the Smartnet CORS network. The echo sounder and GPS antenna were mounted in the middle of the kayak, on the port side, with alignment guides to ensure the echo sounder was not tilted. The transducer for the depth sounder was located 0.2 m below the water surface, with the GPS antenna mounted 1.1 m directly above it. Manual sounding was performed with a 30 m tape attached to a 450 gm lead weight.

GPS QA was set to 1 m (combined vertical + height error). Only a few autologged points were discarded during the survey, but it was noted that the full QA tolerance was used on occasion. This was to be expected due to the poor sky visibility in the crater. Individual GPS heights were not used to define the bathymetry. Instead the average height across all 940 autologged points was used. The horizontal quality for ~75% of autologged points is better than 0.1 m, with the remaining 25% of points within 0.5 m.

The bathymetry kayak was unloaded into the northern lagoon and then paddled through the reedbed to the main lake. In the northern lagoon, no cellphone signal was received for the GPS corrections and locations were defined with handheld gps accuracy. This lagoon was very shallow and reedy, and only a few manual sounding depths were taken.

Once through the reeds into the main lagoon, the GPS cellphone connection was established. The initial sounding run along the western shoreline gave poor sounder results. Resetting the sounder to 'freshwater' resolved this issue, with results matching the lead depthing tape to typically within 0.1–0.2 m. Loops were then run around the lake at approximately 20 m spacing. 940 sounding locations were recorded along with 17 manual depth measurements. The sounding line nearest the shoreline was typically in around 1 m of depth, and around 10 m from the shoreline. The presence of fallen trees, boulders and other navigational hazards prevented surveying closer to the shore. The shoreline was unable to be surveyed from land due to the steep rocky bank, and will need to be defined from aerial photography or other means.

The shallower regions of the lakebed seemed to be quite firm, with a well defined "stop" when using the manual sounding line. In the deeper zones near the centre of the lake, the surface sediment seemed to be softer with some sinkage of the sounding weight. There did not appear to be much lake vegetation, with the exception of the reedbeds in the north and south ends of the lagoon, and no vegetation was caught in the propeller or sounder. A large boulder is situated in the centre of the neck to the southern lagoon, with around 2-5 cm exposed above water.

Many ducklings were seen (maybe chestnut teals), as well as some cormorants (black and little pied), sulphur crested cockatoos, chestnut teals, coots, and a peregrine falcon. A tiger snake was observed coiled near the path, and some skinks near the core platform launching area.

Lake Edward 01/10/2019

Lake Edward is a circular maar crater with a lake around 500 m diameter. The shorelines of the lake are generally dense reed beds. Lake Edward is unusually acidic compared to all the other lakes in the monitoring program, with a pH of around 4-5, compared to around 8 for the other lakes.

The bathymetry survey was performed using the same setup as at Lake Surprise. However, unlike at Lake Surprise, connectivity and satellite visibility was always good, and all autologged points have a positional quality better than 0.05 m. 2400 sounder points were recorded. Sounding runs were run around the lake, beginning from ~10 m from the reed beds and working in to the lake centre, with a concentration of soundings taken across regions of unusual bathymetry. Eight manual sounded points were also taken.

Lake Edward has unusual bathymetry with a typical bowl shaped lake bottom with a maximum depth of around 4.5 m in the lake centre, for most of the lake. However there is a depression in the north-east quadrant, with a maximum depth of around 6 m. The depression has well defined edges, with a depth change of 1–1.5 m over only a 10-15 m in position. The floor of the depression also seems to be disturbed in contrast to the smooth bottom of the lake floor away from the depression. A similar degree of disturbance was seen near the jetty on the southern side, though perceived disturbance in this area could also be due to lake vegetation as it is in a shallow, low gradient part of the lake. Such well defined edges suggest that this is not the surface expression of the deeper crater, but instead a more recent subsidence event, possibly due to the presence of acidic water and limestone country rock.

Wildlife spotted during the survey included musk ducks, a pair of swamp harriers, wedgetailed eagle, grey fantails, coots, and a tiger snake swimming across the lake.

Lake Leake 02/10/2019 - 03/10/2019

Lake Leake was surveyed using the same techniques as Edward and Surprise with the exception of the grid method used. Wind speeds over the two days of survey were very high, with gusts up to 25 knots on the first day. To minimise tracking diagonally across the waves, sounding runs were typically run around the sheltered side of the lake, before transects were run across the lake in the direction of the wind.

Water visibility in Lake Leake was excellent. The lake bottom consisted mostly of dense lake vegetation, with occasional regions of sandy bottom. Some floating mats of lake weeds were also observed. The densely vegetated lake bottom presented problems with the sounding, with many sounder readings clearly representing the top of the lake vegetation. In addition, a few areas of lake floor gave persistent double bounce signals (transducer -> bottom -> boat hull-> bottom -> transducer). These zones were associated with particular locations in the lake, typically sandy bottom at a depth of around 1.3-1.5 m.

Connectivity and satellite availability was always good, and all except 12 autologged points have a positional quality better than 0.05 m. ~2800 sounder points were recorded, as well as 19 manual sounding points.

To minimise the effect of the lake vegetation and double bounced echoes a smoothing process was applied to the sounder data as described in the processing section. Lake Leake is a straightforward basin, deepest in the middle, with a maximum depth of around 2m.

Processing

Sounder logs were converted to text files using SonarViewer (Lowrance). For Lake Edward and Lake Surprise, the sounder logged approximately 10 times per second. To minimise random spikes and noise, the average of the 5 preceding readings is used to define the depth used in the bathymetry model. Each depth is linked to the GPS data by time synchronisation.

For Lake Leake additional processing was used to minimise the effects of lake vegetation and double bounced sonar echoes.

In R:

Double bounced returns were halved (if > 2 m) (~15% of sonar data), and 0.15 added (to account for the hull depth).

Invalid surface points were identified and assigned a depth from "Surface Valid", and a weight of 0.1.

A 150 sample rolling average (~15 m at maximum boat speed) was run through the data to remove any spikes. Any points that were greater than 0.3 m from the average were assigned a weight of 0.1 and the average depth.

A 100 sample rolling "lowest points" filter was run through the data to minimise the presence of vegetation. For each sample the lowest point and lowest weight in the surrounding 150 samples was adopted as the depth and weight.

A smoothing spline was run through the lowest points, using the weights and a spar value of 0.15.

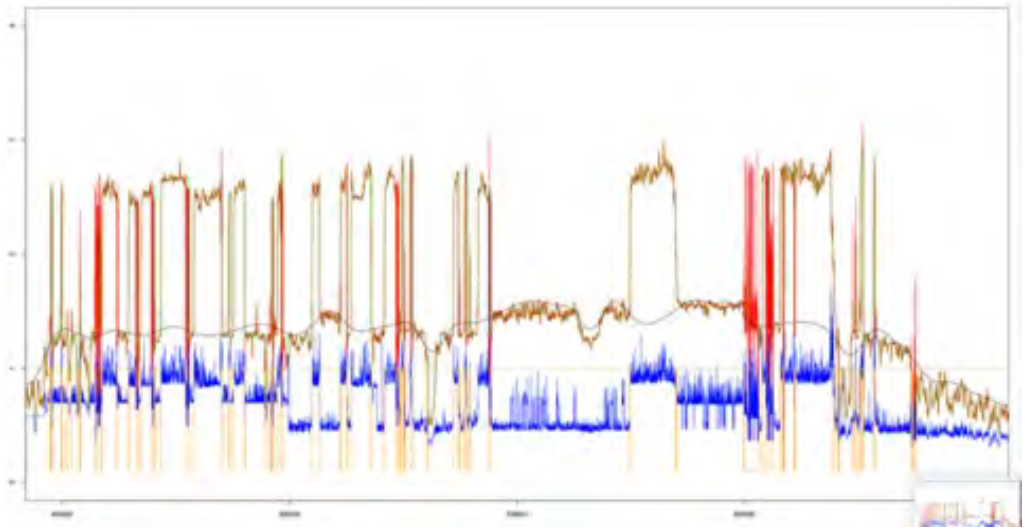

Figure 1: Red is "TopOfBottomValid" (probably deepest echo). Green is logged depth. Blue is "SurfaceValid" (probably shallowest echo). Orange is sample weight. Black is the smoothed, processed depth value. Data shown is from 45000 to 65000 in the log from 02/10/19, representing around 25 minutes of logging.

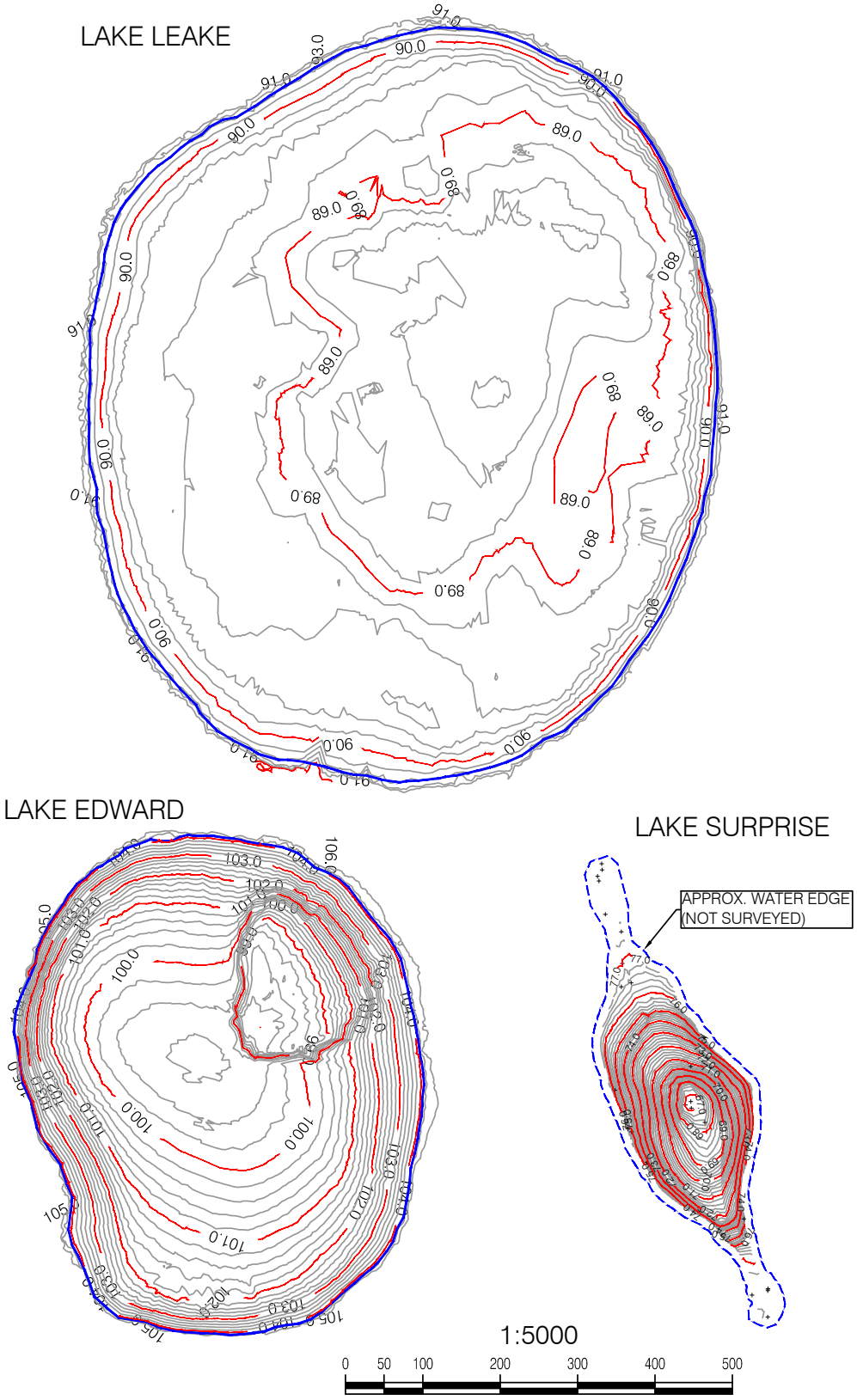

Figure 2: Bathymetry for Lake Leake, Lake Edward, and Lake Surprise. Heights shown are relative to the Australian Height Datum.

Historical lake level reconstructions from aerial photos.

The aerial photographs commonly available for this type of work are single frames from aerial photographic surveys. They are usually not corrected and contain several sources of errors. Only in recent years has orthocorrected imagery become available, typically available as a crop from a mosaic photo product.

The photos used for this project primarily come from the South Australian state government aerial photography archives.

There are three primary errors that need to be accounted for to align aerial photos. The tilt of the camera, topographic effects, and lens distortion. Lens distortion is not something easily accounted for and is not specifically accounted for in this study. It is, however, likely minimal due to the small area being assessed within each photograph. Topographic errors are a complex source of error, affected by the position of the topography within the frame. Topography directly in the centre of the photo frame will be unaffected, but away from the centre of the frame, high points shift away from the centre of the frame, while topographic lows shift towards the centre of the frame. In comparison, tilt is relatively easy to correct for using standard image transformations. The effect of tilt is that the photograph is skewed, and is a relatively simple distortion to correct.

To correct for camera tilt, each aerial photograph is aligned with previous photos using common, identifiable ground reference points. To avoid topographic errors, only ground control points around the lake edge, or at similar elevations to the lake water level were chosen. QGIS was used for georeferencing each image, using the linear-affine transformation.

The most recent photos were already orthorectified, and were used as the base map that older photos were transformed to fit. Working backwards through time, each photo was rectified to the most current set of photos with identifiable ground features common to both the photo being rectified, and previously rectified images. As land use changes have occurred around both lakes, identifiable ground features have also changed over time. Therefore, the 1950 photos may have been rectified using the 1987 image, which was previously rectified using the 2008 mosaic image.

Once all photos were rectified water outlines were traced around each shoreline. These shorelines were then draped onto 2 m LIDAR data (State Government, SA). For each shoreline, an average and standard deviation of the elevations of all the points that defined that shoreline was calculated.

This method provides a useful way to establish historical lake levels for lakes that are poorly documented. Most states have many decades of historical aerial photography, potentially allowing the reconstruction of decades of lake water level change.

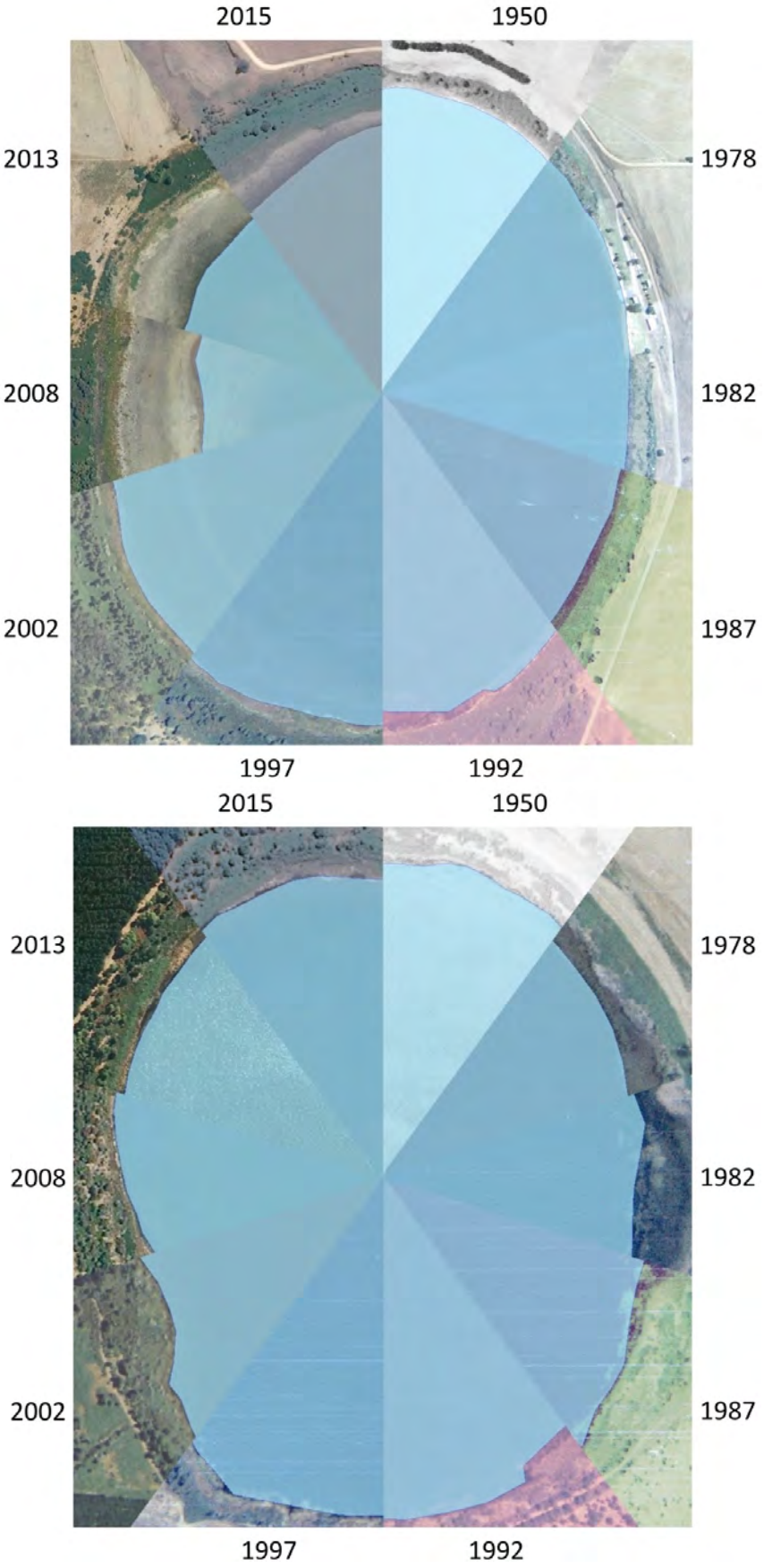

Figure 3: Clock diagrams for Lake Leake (top) and Lake Edward (bottom) showing lake level for selected years, overlaid over the original aerial photographs.

Lake Leake	Elevation	Std Deviation
17 December 1950	90.73	0.31
1 January 1951	90.49	0.52
8 January 1970		
19 February 1978	90.88	0.63
3 March 1982	91.55	0.50
18 February 1987	90.60	0.48
18 February 1988	91.27	0.46
30 January 1992	90.82	0.74
3 January 1997	90.83	0.31
5 February 1997	90.75	0.30
27 January 1998	90.32	0.32
30 November 1999	90.12	0.31
18 January 2002	90.43	0.19
13 February 2002	90.33	0.14
23 January 2003	90.13	0.28
23 January 2003	90.19	0.29
13 October 2003	90.36	0.13
1 November 2005	90.37	0.17
23 January 2008	88.18	1.06
6 February 2010	88.34	0.95
10 December 2012	90.00	0.16
2 March 2013	88.29	0.90
10 January 2014	90.21	0.12
30 January 2014	89.73	0.35
23 May 2015	89.35	0.05
28 August 2015	89.66	0.05
7 November 2015	89.20	0.71
3 December 2015	88.41	1.00
6 April 2016	88.91	0.05
3 August 2016	89.70	0.05

Lake Edward	Elevation	Std Deviation
17 December 1950	104.58	0.52
1 January 1951	104.56	0.50
8 January 1970	104.28	0.37
19 February 1978	104.33	0.35
3 March 1982	104.54	0.44
18 February 1987	104.71	0.47
18 February 1988	105.03	0.25
30 January 1992	104.59	0.39
3 January 1997	104.73	0.28
5 February 1997	104.65	0.31
27 January 1998	104.84	0.24
30 November 1999	104.58	0.27
18 January 2002	104.55	0.31
13 February 2002	104.56	0.35
23 January 2003	104.18	0.25
23 January 2003	104.34	0.22
13 October 2003	104.36	0.35
1 November 2005	104.05	0.23
23 January 2008	103.27	0.46
6 February 2010	103.04	0.55
10 December 2012	103.07	0.54
2 March 2013	102.51	0.61
10 January 2014	103.22	0.57
30 January 2014	102.76	0.67
23 May 2015	103.097	0.05
28 Aug 2015	103.307	0.05
7 November 2015	103.02	0.50
3 December 2015	102.89	0.61
6 Apr 2016	102.653	0.05
3 Aug 2016	103.315	0.05

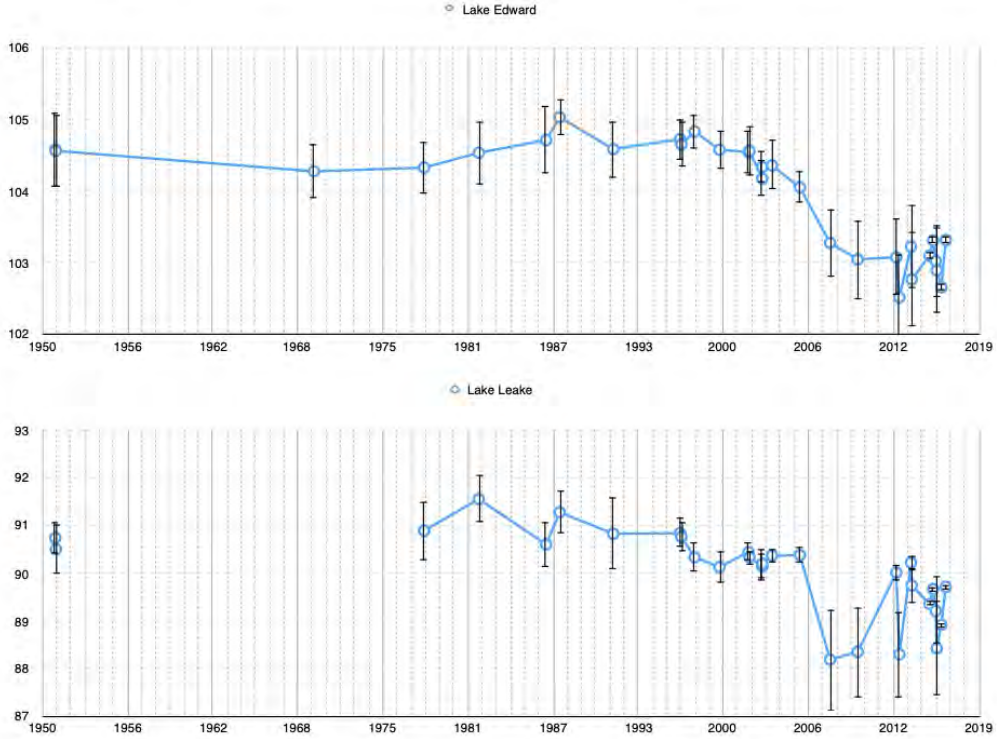

Figure 4: Reconstructed lake levels for Lake Edward and Lake Leake

Appendix 3

This appendix comprises a published journal article, arising from work undertaken for this thesis. The article is identical to Chapter Three, with the exception of some minor formatting changes to match the rest of this thesis.

Journal of Hydrology 575 (2019) 31–41

Contents lists available at ScienceDirect

Journal of Hydrology

journal homepage: www.elsevier.com/locate/jhydrol

Research papers

Development of an autonomous, monthly and daily, rainfall sampler for isotope research

Martin J. Ankor[a,*], Jonathan J. Tyler[a], Catherine E. Hughes[b]

[a] Department of Earth Sciences and Sprigg Geobiology Centre, University of Adelaide, North Terrace Campus, Adelaide 5005, South Australia, Australia
[b] Australian Nuclear Science and Technology Organisation, Locked Bag 2001, Kirrawee DC 2232, New South Wales, Australia

ARTICLE INFO

This manuscript was handled by Marco Borga, Editor-in-Chief, with the assistance of Daniele Penna, Associate Editor

Keywords:
Precipitation
Oxygen isotopes
Hydrogen isotopes
3D printing
Rainfall sampler
Isotopic modelling

ABSTRACT

An autonomous, low cost (< US$750), and open source rainfall sampler has been developed for hydrogen and oxygen isotope research, able to sample daily and monthly for up to 60 days of rainfall, over a three month period. The sampler is designed to use modern fabrication methods such as 3D printing and laser cutting to minimise the need for machined and injection molded components. The sampler can use either paraffin oil or a submerged inlet tube (also known as tube-dip-in samplers) to prevent evaporation, with the use of the inlet tube method facilitated by 3D printed bottle caps. An experiment was performed to identify the most suitable plastic for these caps, with acetone treated ABS (Acrylonitrile Butadiene Styrene) being most suitable, followed by PETG (Polyethylene Terephthalate Glycol), untreated ABS, and PLA (Polylactic acid). In addition, the effectiveness of both paraffin oil and the inlet tube method for preventing evaporation was quantified, with paraffin identified as being the most effective at present. During a 90 day outdoor experiment, the $^{18}O/^{16}O$ vs. $^{2}H/^{1}H$ ratios of some water samples evolved along a local evaporation line, with increased isotopic enrichment of samples correlating to water loss. A coupled hydrologic-isotopic model was applied to these data, and successfully predicted the change in isotope ratios based on the amount of water lost from each sample. This modelling approach, combined with daily and monthly sample collection and quantification of evaporation rates within the sheltered environment of the sampler allows for back calculation of the original volume and isotopic composition of daily and monthly rainfall samples. The rainfall sampler thus facilitates cost -and time- effective remote monitoring of the isotopic composition of precipitation to support an array of Earth system research.

1. Introduction

The natural variation of the oxygen and hydrogen isotopes of water in the hydrological cycle is tied to numerous climatic and meteorological variables (Craig, 1961; Craig and Gordon, 1965; Dansgaard, 1954; Gat, 2010; Gibson et al., 2016; Gibson et al., 2008). This variation forms a key dataset for many branches of research, including climate and meteorological research, water resource management, forensic and ecological source identification and spatial and temporal mapping of changes and fluxes in meteoric water (Bowen and Revenaugh, 2003; Bowen et al., 2005; Gibson and Reid, 2014; Mattey et al., 2008; Steinman et al., 2010; Treble et al., 2005; Tyler et al., 2015; Tyler et al., 2007).

At the centre of the water cycle is precipitation. The Global Network of Isotopes in Precipitation (GNIP) has underpinned knowledge on monthly and annual scale variability in the isotopic composition of precipitation since 1961 (Rozanski et al., 1993), however, several applications demand rainfall sampling at higher spatial and temporal resolution, often from remote locations, placing significant demand upon time and financial resources. In addition, the isotopes of water – $^{3}H/^{2}H/^{1}H$ and $^{18}O/^{17}O/^{16}O$ – fractionate as water molecules undergo phase change and diffusion. In response to evaporation, residual liquid water becomes relatively enriched in the heavy isotopes as a function of both the climate and the evaporative history of the water. Evaporation of collected samples presents a challenge to sampling rainfall, requiring dedicated systems that minimise evaporation and accompanying isotopic alteration. Therefore, there is a need for an adaptable precipitation sampler which preserves the integrity of oxygen and hydrogen isotope ratios ($^{3}H/^{1}H$, $^{2}H/^{1}H$, $^{18}O/^{16}O$ and $^{17}O/^{16}O$).

1.1. Previous designs

There has been no shortage of rainfall sampler designs over the last few decades, with many designs developed for acid rain research in the

* Corresponding author.
E-mail address: martin.ankor@adelaide.edu.au (M.J. Ankor).

https://doi.org/10.1016/j.jhydrol.2019.04.074
Received 25 October 2018; Received in revised form 9 April 2019; Accepted 24 April 2019
Available online 25 April 2019

1970s (Raynor and McNeil, 1978). Laquer (1990) identified over 70 reports of sequential rainfall samplers, focused on recording variations of rainfall over the course of a rainfall event, using a variety of techniques. While some aspects of a sequential rainfall sampler may form a useful design basis for a daily/monthly sampler, many rely on mains power, require manual preparation, are not suited to long term on/off operation, and often segment rainfall by volume rather than time. Few of these older samplers feature designs that are well suited to modern, low cost fabrication techniques. There are, however, some novel innovations as well as commonalities amongst many of these samplers. One of the most robust and simplest sequential sampler designs is the sampler of Kennedy et al. (1979) consisting of a series of interlinked bottles. As each bottle is filled, the overflow is diverted to the next sample bottle. Mixing of samples is prevented by the use of a narrow inlet tube to the base of each sample bottle. Ronneau et al. (1978) developed an entirely mechanical sampler for remote areas driven solely by gravity and using tipping, latching sample containers on a circular platter. A resistance based rainfall detector was used by Asman (1980), whereas Gray et al. (1974) used a loud speaker, which, when struck by a raindrop, would generate an electronic pulse that would trigger the sampler's mechanism. Gatz et al. (1971) developed a sampler able to collect up to 70 samples (500–1000 ml) from 70 mm of rainfall. At 1 × 1 × 2 m and 91 kg, this probably represents the heavyweight class of sequential samplers, closely challenged by the Raynor and McNeil (1978) sampler at 1.5 × 1.5 × 0.64 m, both of which were designed as permanent installations. A more recent sequential sampler design is the 96 vial sampler of Coplen (2010, 2015), that incorporates a novel teflon coated cover to prevent evaporation from inactive sample vials. In terms of commonality between existing sampler designs, many make use of a tipping bucket system to quantify the rainfall amount. As many of these samplers segment rainfall by volume, a tipping bucket sensor provides an effective way to prevent overflows. Circular, rotating platters are also very common, taking advantage of mechanical and electronic simplicity and robustness.

Two more recent designs break with these common design elements. Akkoyunlu et al. (2013) developed a sampler that quantifies rainfall using MATLAB controlled solenoids, located beneath the collector funnel, separated by a tube with a volume of 5 ml. Rainfall was then gravimetrically segmented to 21 individual sample bottles. However, unlike some older systems that rely on sample bottles filling to enable the next bottle in the sequence, the sample bottles were instead capped with solenoids. As each solenoid closed, water was diverted down the inlet tube to the next bottle until all bottles were filled. Hartmann et al. (2018) developed an Arduino based, battery powered field auto-sampler that uses a Cartesian based control system to fill a grid of gas-tight sample vials. Like the design of Akkoyunlu et al. (2013), an inlet tube with a known volume (12 ml) holds the sample prior to storage. A peristaltic pump then transfers the sample via piston flow to the sample vials. A pair of cannulas pierce the vial cap for sample injection and pressure equalisation, and the sealing nature of the rubber vial cap prevents exchange with the atmosphere. This device has been used for sampling of cave waters. The evaporation prevention mechanism is of significant interest to rainfall sampling, however, it is unclear at this stage how this system could be adapted to rainfall collection, as the thin diameters of the auto-sampler cannula will likely face problems with the detritus usually collected in rainfall sampler funnels. In addition to the above, the 3700C Compact and 6712 Fullsize samplers (Teledyne ISCO, USA) represent commercial sampler designs that have been adapted for sequential rainfall sampling (Rücker et al., 2019). These samplers utilise the common design element of a circular array with up to 24 sample bottles, combined with a peristaltic pump for filling samples. There is also ongoing development focused on in-field analysis where mobile labs are established at the site of interest, with analyses of samples undertaken in near real time (Berman et al., 2009; von Freyberg et al., 2017). These systems are typically expensive, require on-site power and regular attendance, making them unsuitable at this stage for use in remote locations with limited infrastructure.

While there are many examples of sequential rainfall samplers in the literature, there are relatively few that are designed for discrete daily/monthly sampling, possibly due to the added complexity required. Unlike sequential samplers, daily/monthly samplers have to prevent evaporation of samples for long time periods, require accurate timekeeping, must be sufficiently robust, and must store sufficient samples to operate for months in the field. Samplers designed for remote sites also need to be small enough to be transported and installed, as well as having the means to maintain power supply for the period of deployment. Of the samplers mentioned above, only the auto-sampler of Hartmann et al. (2018) and the sequential sampler of Coplen (2010) have most of the components required for daily/monthly sampling of rainfall in remote sites. However, in the case of Hartmann et al. (2018), there would be significant modifications required to adapt it for rainfall sampling including attachment of a catchment funnel, rainfall sensor, a water reservoir that the auto-sampler can sample and that can be emptied when rainfall has occurred, and a filter system to deal with the detritus collected in rainfall catchment funnels. The design of Coplen (2010) would require less modification, with the main changes being to the control software, and the inclusion of an evaporation prevention system for the main reservoir, where water is stored prior to being transferred to the sample vials. The design of Akkoyunlu et al. (2013) has potential as a monthly sampling system, as control of ~14 solenoids is manageable with low power electronics such as the open source Arduino platform.

1.2. Fabrication methods and materials

Design and construction of bespoke equipment such as precipitation samplers can be challenging due to the absence of off-the-shelf components that can be easily incorporated. Even parts as simple as a UV stabilised funnel of a suitable size can prove difficult, for example Asman (1980) made use of a square funnel, due to the difficulty of fabricating a large cylindrical funnel. Injection moulding, complex machining and custom electronics are not feasible manufacturing techniques for low volume production as they typically have high initial costs. Fortunately, in the last decade, several developments in manufacturing have emerged that enable low volume, complex designs to be manufactured at low cost (Berman, 2012; Rayna and Striukova, 2016). Two in particular are heavily used in our sampler. 3D Printing, or fused filament fabrication, enables the fabrication of complicated plastic components, though typically of fairly small size. When combined with computer numerical control (CNC) laser cutting, larger designs of considerable complexity can be manufactured. More importantly, once a design is complete, it can easily be fabricated by anyone else with a 3D printer, laser cutting or CNC milling capability. Low cost, extensible, microprocessor based electronics such as the Arduino system provide accurate timing, motor control, data logging and support for multiple sensors, e.g., Hund et al. (2016). In the same way that the manufacturing designs can be published and fabricated, the program that controls the Arduino can be shared.

1.3. Methods of preventing evaporation

With respect to evaporation prevention, two methods have demonstrated effectiveness: paraffin oil, or the submerged inlet tube system of Gröning et al. (2012) (Michelsen et al., 2018; Terzer et al., 2016). The oil method prevents evaporation by the addition of a ~5 mm layer of paraffin oil to the sample, which forms a barrier between the sample and the air. The inlet tube system uses a narrow (typically ~4 mm diameter) inlet tube that passes to the bottom of the sample container. Once the first portion of rainfall enters the sample container, the base of the inlet tube is submerged, and evaporation can only occur through the small surface area exposed in the inlet tube. Pressure is equalised through a second tube that vents the container,

but is sufficiently long and thin to minimise diffusion with the exterior atmosphere. The sample container and vent tube are then protected from sunlight to minimise heating and corresponding pressure changes within the sample container. Given the simplicity and effectiveness of the paraffin oil technique, it might be expected to be the preferred collection method. However, as analysis of the samples is often complicated by the presence of oil in the sample (IAEA, 2014), in many situations the inlet tube method is preferred.

The choice of sampling bottle must also be considered as isotopes may exchange or permeate through the sample bottle material. Spangenberg (2012) investigated multiple plastics for their suitability for storing waters for stable isotope analysis, namely: High and low density polyethylene (HDPE, LDPE), polypropylene, polycarbonate, polyethylene terephthalate (PET), perfluoroalkoxy-Teflon and glass over a timeframe of 659 days. Significant variations of +5‰ for δ^2H and +2‰ for $\delta^{18}O$ were observed for polycarbonate and PET. The recommended materials for use in sample bottles used for stable isotope investigations are glass, HDPE or teflon, with a preference for thicker walled containers. Unfortunately, there is little overlap between the common laboratory plastics tested by (Spangenberg, 2012) and the plastics commonly used in 3D printing: acrylonitrile butadiene styrene (ABS), polylactic acid (PLA) and polyethylene terephthalate-glycol modified (PETG).

1.4. Objectives

There is a clear need for an autonomous rainfall isotope sampler that can be deployed for long time periods in remote locations. Given that no design has thus far been able to prevent losses and fractionation due to evaporation, there is also need to be able to evaluate, and potentially correct for the effects of evaporation on samples. This paper presents the development of a low cost (< US$750), autonomous, battery powered sampler using novel construction methods and open source electronics. Design files are available from https://github.com/Mjankor/MARS-Rainfall-Sampler. Aspects of the design of the sampler are considered, with tests quantifying the amount of water lost due to surface wetting along the flow-path, and the ability of the sampler to divide the flow accurately between daily and monthly samples. In addition to discussing the design of the rainfall sampler, we also present results investigating the effectiveness of 3D printing bottle caps using ABS (Acrylonitrile Butadiene Styrene), PETG (Polyethylene Terephthalate Glycol), PLA (Polylactic acid), and acetone treated ABS, for preserving the integrity of stable isotope ratios in water samples. A coupled hydrologic-isotopic model was applied to the bottle caps experiment data, to predict the change in the isotopic composition of the water based on the water lost from each sample. Based on the results from the isotopic modelling, we describe how a hydrologic-isotopic model, taking advantage of the differing rates of evaporation from daily and monthly samples, can be used to back calculate the original volume and isotopic composition of rainfall samples.

2. Design principles

The many varied designs of rainfall sampler from the last few decades show a few commonalities, but no de facto design standard. Therefore, rather than rework an existing design, we established several design principles that were used as the basis for development.

Usage: The sampler should be easily deployed in remote environments. As major cities often have GNIP stations, and generally have personnel available for event or daily sampling, there is little benefit in designing a sampler that is reliant upon significant infrastructure.
Cost: Samplers will be deployed in remote or uncontrolled environments where there is potential for vandalism, weather damage, and other mishaps. Minimising costs means that the loss of a sampler is less of a burden on research budgets, or that more samplers can be deployed for better spatial resolution and redundancy.
Outer casing: Needs to be weatherproof and robust over the timeframe of years. It should also prevent wildlife from occupying the sampler, and should protect the electronics and interior components from sunlight and excessive heat. In addition, the sampler should be entirely self-contained without any external components such as batteries or cables which can be easily damaged.
Battery powered: The sampler must operate without an external power source for a long period of time. When combined with solar panels, a sampler should be able to operate indefinitely.
Easy to construct: As the intent is to provide a design for others to replicate, it is beneficial that the construction of the sampler is straightforward. This is also an important feature for a field sampler, where repairs and maintenance may need to be carried out at remote locations with minimal equipment.
Sampling capabilities: Capturing both daily and monthly precipitation provides some redundancy in case of failure of some components, and allows for quality control by comparing the mass balance of daily and monthly samples.
Flexibility: The sampler must be suitable for differing rainfall conditions. This is rarely a challenging problem with rainfall samplers as the collection funnel can be changed to increase or reduce the amount of rainfall collected. However, funnels with specific diameters are sometimes difficult to purchase. Therefore the design process included the development of multiple funnel options. In addition, regions with very variable rainfall should be considered, requiring a method to prevent overflow from large events.
The ability to quantify rainfall: Quantifying the amount of rain is important, partly, as an explanatory variable for the isotopic composition of rainfall, and more importantly, to prevent overflows during heavy events and to avoid changing sample bottles on days of no rain.
Preservation of isotope ratios: The rainfall sampler is designed to accommodate both the paraffin oil and inlet tube methods to prevent evaporation, though it is noted that the inlet tube method has analytical and operational benefits. Oil is an option regardless of the sampler design, however the inlet tube method requires significant space to store the vent tubes, and attaching both the inlet tube and vent tube to sample bottles can be complicated or expensive.

2.1. Design

Based on the above criteria, a low cost, automated rainfall sampler was designed for remote field deployment, which for simplicity is named MARS. The choice of outer casing was an early priority in the design process. The sampler needed to be large enough to contain multiple sample bottles, as well as the sampling mechanism, electronics, battery, and a rainfall collection funnel. Fortunately, a cheap, common, off the shelf solution was identified; 200 L plastic drums, typically used for transporting food and chemicals are extremely common, and recycled ones can be purchased for very low cost. These drums are typically blue HDPE plastic around 4 mm thick and are UV resistant. They have a diameter of ~58 cm and a height of ~93 cm, and are typically completely sealed with just two inlet ports for filling and emptying. The entire drum is not used for the sampler. The top half of the drum is used as a lid that can be easily removed to provide access to the daily sample bottle area. The lower third of the drum is used to provide a protected enclosure below the main sampler where monthly sample bottles are placed. It should be noted that the lower shell is not designed to be water proof and it is expected that some water will make its way into that space as the seal between upper and lower shells is not watertight. There is a drain in the lower shell to prevent water building up in that space. The outer shell has had its height reduced as much as possible to minimise the wind effect on rainfall sampling (Bureau of Meteorology, 2007), to reduce the chance of it being blown over, and to make it easy to transport.

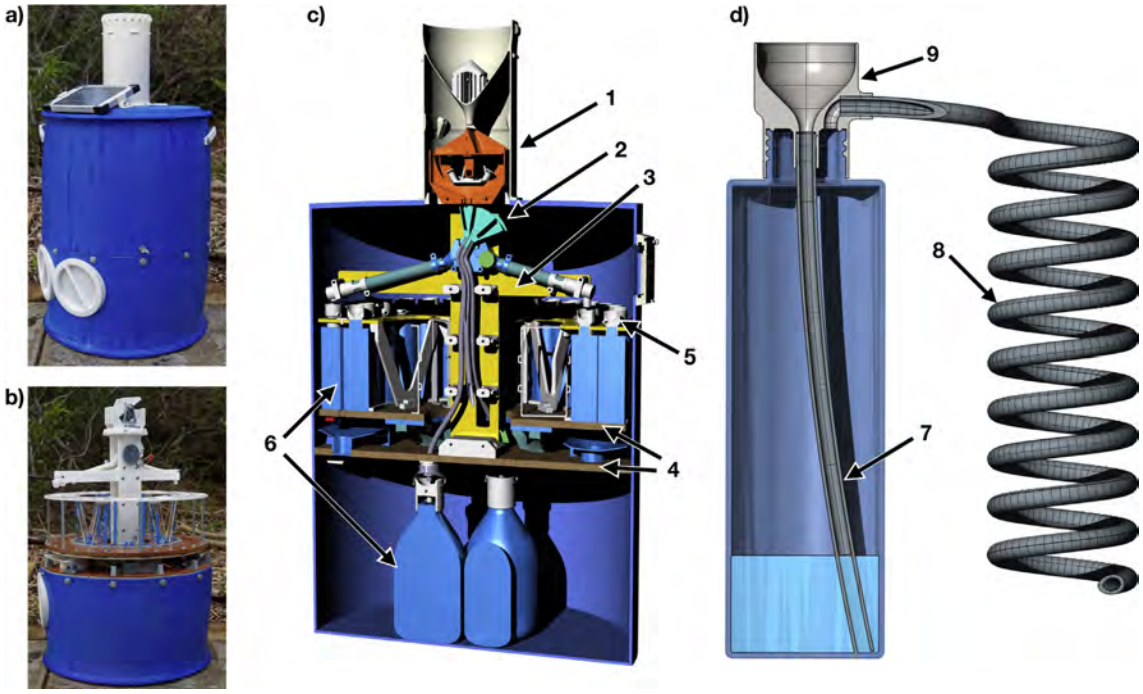

Fig. 1. (a) Photo of sampler, with lid in place. (b) Photo of the sampler with the lid removed. (c) Cutaway view of the MARS rainfall sampler showing tipping bucket (1, orange), water switch (2, cyan), laser cut platter and tower components (3, yellow), baseplate and platter (4, wood texture), bottlecaps (5, grey) and bottles (6, blue). (d) Cutaway view of the inlet tube method, showing inlet tube (7), vent tube (8) and 3D printed bottle cap (9). (For interpretation of the references to colour in this figure legend, the reader is referred to the web version of this article.)

At the centre of the MARS sampler, forming the top of the lower shell, is a 12 mm plywood baseplate. This baseplate holds the electronics, battery, and provides a firm fixing point for the mechanical system (Fig. 1). Positioned about 6 cm above the main baseplate is a rotating platter of 12 mm plywood, sitting on a 30 cm turntable bearing. This platter has a support frame on it designed to hold 60 × 225 ml HDPE bottles (48.4 mm diameter × 161 mm) in two rings of 33 and 27 bottles. A central plastic tower sits at the centre of the baseplate, and holds the tipping bucket mechanism, and a 'water switch' that can divert water from the tipping bucket outflows to either the inner or outer ring of daily sample bottles, and between first, second or third of the monthly samples. One benefit to using a rotating platter is that there is a 'dead spot' in the centre, which provides an ideal location to place the vent tubes used for the inlet tube evaporation prevention method. The platter's rotation is controlled by a ring gear driven by a stepper motor.

Three 8 mm silicone tubes run from the water switch, down the central tower and through the baseplate to 3 monthly sampling bottles (2 L, HDPE). These bottles also use the inlet tube method, with the vent tubes stored inside the lower compartment.

On the baseplate are a cabinet for the electronics, the motor for rotating the main platter, a small 12 V, 2.1 Ah sealed lead acid battery and the support for the platter bearing. In addition are two drains in case of overflow of the daily bottles, and guides with encapsulated nuts around the outer rim, used to guide and secure both top and bottom shells in place. The drains are a holdover from an earlier design and should rarely be needed in the current design.

The electronics are controlled by an Arduino Nano 3.x (Duinotech Nano V3.0) on a breakout board. The breakout board keeps the need for soldering to a minimum, with jumper cables used to connect most of the components. Two stepping motors are used, one driving the platter, and the other controlling the water switch on the tower. A reed sensor determines when the tipping bucket is activated and a microswitch on the tower is used to reset the water switch. The position of the main platter is not reset electronically as it is much quicker to disengage the motor and rotate the platter by hand to the starting position. A real time clock and an SD Card reader keep time and a log for each sample changeover date. The Arduino platform also means that MARS can be easily reprogrammed for different roles, such as time or volume based sequential sampling of rainfall events.

Attached to the outer shell is a 3D printed funnel positioned ~30 cm above the top of the sampler. While it could be positioned closer to the outer shell, 30 cm was chosen to prevent splashes from the casing bouncing into the funnel. The top half of this funnel is designed to be easily replaced so that different sized funnels can be used. There are vents situated around the exterior of the funnel. When combined with the drains in the lower shell, these vent warm air from the sampler, replenished with cooler air from near ground level, thus preventing greenhouse style warming in the sampler. All vents and drains are designed so that mesh can be applied to exclude insects.

The tipping bucket design is unique due to the way that it separates the flow-path for monthly and daily sample collection (Fig. 2). Tipping buckets have been used before to divide rainfall into multiple samples, with alternating tips of the bucket passing water through different flow-paths e.g. Gatz et al. (1971). While such a design is ideal for volumetric based segmentation in a rainfall event, it introduces potential systematic uncertainties. Any difference in tipping volume between the buckets would result in a bias towards either daily or monthly samples. In addition, most tipping buckets are designed to tip for each 0.2 mm of rainfall. If a series of small rainfall events occurs, then on a day with rainfall of 0.2 mm all of the rain may go into the daily sample, and none into the monthly. On a day of 1.4 mm of rainfall, 0.8 mm may go to daily, and 0.6 mm into the monthly. To avoid this issue, and taking advantage of the ability to fabricate complex structures with 3D printing, our tipping bucket splits the flow for each bucket, with half the water from each bucket tip going to daily, and half going to monthly samples. The tipping bucket is designed to tip with a volume of 4 ml, resulting in a tip every 0.2 mm of rainfall with a 159.6 mm diameter funnel. The success of this mechanism to divide water equally is

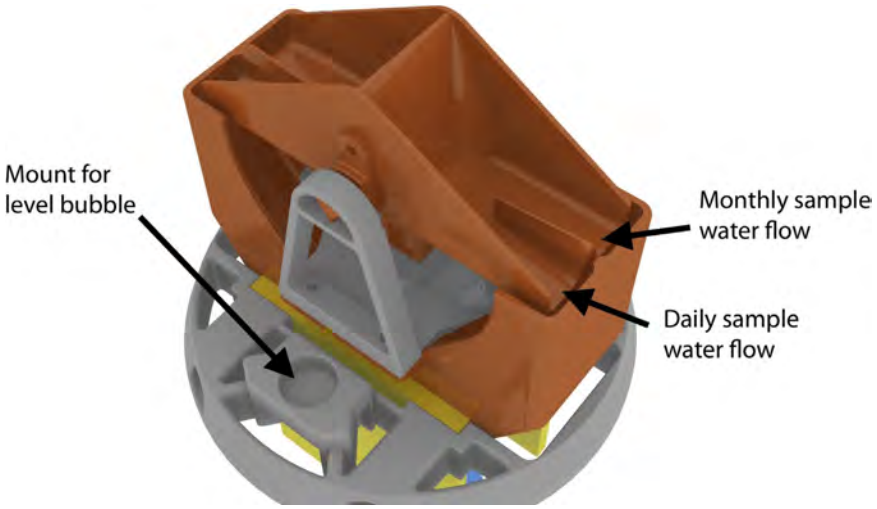

Fig. 2. The tipping bucket, showing the flow splitting divider. A level bubble is incorporated into the design to ensure that the tipping bucket is vertically aligned.

dependent on the rainfall sampler being vertically aligned, thus a level bubble is built into the design of the tipping bucket.

Fabrication is achieved predominantly using 3D printed components, while some of the bottle support structure, ring gear and central tower uses laser cut 6 mm acrylic plastic. To build the design requires a few basic tools (jigsaw, drill, screwdriver, soldering iron) as well as a 3D printer able to print ABS with a build volume of 200 × 200 × 180. All 3D printed parts were printed using a Wanhao i3 Plus 3D printer. Components that form the water flowpath were printed with 0.2 mm layer thickness, and sanded with 1500 grit sandpaper to smooth the layered structure of the printed surface.

3D printing was able to resolve a significant problem in the design of the bottle caps. Modifying existing bottle caps to include an inlet tube and a vent tube is complicated, and space on and above a platter of daily sample bottles is limited. Using 3D printing we were able to fabricate lids featuring a small funnel to capture incoming water, an inlet tube holder that clamped the outside of the inlet tube and a curved vent pipe attachment so that vent tube could be routed horizontally towards the centre of the platter (Fig. 3). By clamping the outside of the inlet tube, the smallest diameter along the water flow-path was the 4 mm diameter of the inlet tube thereby minimising the chance of blockages.

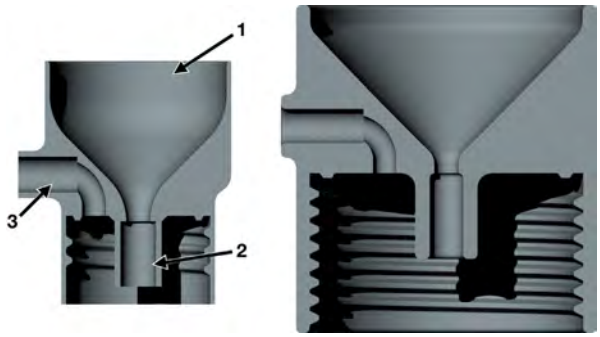

Fig. 3. Cutaway view of the 3D printed bottle caps, with funnel (1), offset formed vent tube holder (2) and central inlet tube holder (3) (Left, cap for 225 ml bottles, right cap for 2 L bottle).

3. Design and material tests: experimental methods

3.1. Quantification of water loss from surface wetting

In order to quantify the amount of water lost through wetting of surfaces along the flow-path, various quantities (12, 20, 40, 60, 100 ml) of water were dripped into the sampler at a rate of ~1 ml/s wetting the entire funnel and top surface of the filter, representing rainfall events from 0.6 to 5 mm of rainfall. The amount of water collected in the bottles were subsequently weighed. This experiment was repeated 3 times.

3.2. Quantification of water loss through bottle caps

The use of 3D printed plastics along the water flow-path was not considered problematic with regard to preservation of water isotope ratio integrity, as water would only be in contact with those plastics briefly. However, the use of 3D printed plastics for bottle closures was a concern. To test which plastics were most effective at preserving the initial water isotope ratio, bottle caps were fabricated using three different types of plastic. The plastics used were blue PLA, grey ABS and white PETG from 3DFillies (https://3dfillies.com/). In addition, grey ABS modified with acetone treatment was also tested, where acetone is used to partially dissolve and smooth the ABS plastic surface, potentially improving the sealing between printed layers (Garg et al., 2016; Singh et al., 2017). Acetone treated parts were placed in a 4 L tin lined with acetone soaked paper towels for 30 min at 20 °C, then allowed to dry overnight.

In order to test the effectiveness of different plastic caps, and to validate the use of the inlet tube system, an experiment was conducted using 33 × 225 ml HDPE bottles, each with ~40 ml of recent rainfall (equivalent to 4 mm of rain, using a 159.6 mm diameter funnel divided between monthly and daily samples). For each plastic, sealed bottle caps were fabricated using the same design as used in the sampler, but with the inlet and outlet holes sealed. Unsealed bottle caps of the same design were also fabricated in all 4 plastics and combined with the inlet tube and vent tube to replicate the system used in the sampler. The inlet and vent tube consisted of ~4 mm Ø (internal) LDPE tubing with a ~1 mm wall thickness. Triplicates of each design were fabricated for each plastic giving a total of 24 bottle-caps (Table 1). Triplicate bottles using the oil method of evaporation prevention were also prepared, with 5 mm of paraffin oil sealing each ~40 ml water sample. As a control, 6 bottles were prepared, sealed with wadded polypropylene caps.

Table 1
Data for each bottle cap showing plastic and evaporation prevention method, water loss and observed and modelled isotopic results. PLA, PETG, ABS in sample names refer to plastic type. ACET refers to acetone treated ABS. PARA refers to paraffin oil samples, and HDPE (highlighted in grey) are the control samples with wadded caps. Columns $\delta 1^8O$ σ and δ^2H σ are the reported instrumental precision.

Sample Description		Mass Change					Observed δ				Modelled δ	
Sample ID/Plastic type	Seal type	Lid weight (or paraffin oil weight) (g)	Initial water weight (g)	Final water weight (g)	Water loss (g)	Water loss (%)	$\delta^{18}O$ (‰)	δ^2H (‰)	$\delta^{18}O$ σ (‰)	δ^2H σ (‰)	$\delta^{18}O$ (‰)	δ^2H (‰)
HPDE01	Wadded PP cap	2.16	39.32	39.32	0	0	-4.6	-18.1	0.02	0.32	-4.57	-18
HPDE02	Wadded PP cap	2.15	39.5	39.5	0	0	-4.55	-17.7	0.01	0.11	-4.57	-18
HPDE03	Wadded PP cap	2.15	38.2	38.2	0	0	-4.56	-17.6	0.02	0.15	-4.57	-18
HPDE04	Wadded PP cap	2.14	39.42	39.3	0.11	0.3	-4.56	-18.1	0.05	0.23	-4.46	-17.7
HPDE05	Wadded PP cap	2.16	39.53	39.44	0.09	0.2	-4.52	-18	0.03	0.29	-4.5	-17.8
HPDE06	Wadded PP cap	2.15	39.36	39.25	0.1	0.3	-4.62	-19.1	0.01	0.11	-4.46	-17.7
PLA01	Inlet Tube	9.23	38.37	35.05	3.33	8.7	-1.45	-10.2	0.06	0.33	-1.43	-10.3
PLA02	Inlet Tube	9.27	39.02	36.22	2.8	7.2	-2.14	-12	0.09	0.25	-1.98	-11.7
PLA03	Inlet Tube	9.28	39.49	36.83	2.67	6.7	-2.23	-12.2	0.04	0.21	-2.16	-12.1
PLA04	Sealed inlet/outlet ports	9.88	39.32	38.66	0.66	1.7	-4.03	-16.7	0.04	0.21	-3.96	-16.5
PLA05	Sealed inlet/outlet ports	9.9	39.89	38.01	1.88	4.7	-2.92	-14.1	0.06	0.41	-2.89	-13.9
PLA06	Sealed inlet/outlet ports	9.87	39.99	38.06	1.94	4.8	-2.76	-13.6	0.06	0.25	-2.85	-13.8
PETG01	Inlet Tube	9.47	39.05	37.72	1.33	3.4	-3.43	-15.3	0.01	0.21	-3.35	-15
PETG02	Inlet Tube	9.49	39.51	38.03	1.48	3.7	-3.29	-14.9	0.03	0.31	-3.25	-14.8
PETG03	Inlet Tube	9.36	40.1	38.72	1.38	3.5	-3.37	-15.1	0.04	0.21	-3.32	-15
PETG04	Sealed inlet/outlet ports	10.01	39.24	38.52	0.72	1.8	-4.02	-17.5	0.08	0.36	-3.93	-16.4
PETG05	Sealed inlet/outlet ports	10.01	39.63	39.01	0.62	1.6	-4.19	-17.3	0.16	0.44	-4	-16.6
PETG06	Sealed inlet/outlet ports	10.03	39.59	39.08	0.51	1.3	-4.12	-16.7	0.06	0.44	-4.11	-16.9
ABS01	Inlet Tube	7.84	39.65	38.05	1.6	4	-3.27	-14.8	0.11	0.59	-3.14	-14.5
ABS02	Inlet Tube	7.84	39.26	37.78	1.49	3.8	-3.29	-14.7	0.06	0.39	-3.21	-14.7
ABS03	Inlet Tube	7.83	39.28	37.69	1.59	4.1	-3.24	-14.8	0.01	0.32	-3.1	-14.4
ABS04	Sealed inlet/outlet ports	8.29	39.59	38.4	1.19	3	-3.5	-15.3	0.03	0.17	-3.5	-15.4
ABS05	Sealed inlet/outlet ports	8.28	38.86	37.65	1.22	3.1	-3.4	-15.1	0.03	0.41	-3.46	-15.3
ABS06	Sealed inlet/outlet ports	8.29	39.27	37.51	1.76	4.5	-3.05	-14.1	0.04	0.48	-2.96	-14.1
ACET01	Inlet Tube	7.95	39.18	37.89	1.29	3.3	-3.49	-15.4	0.04	0.19	-3.39	-15.1
ACET02	Inlet Tube	7.97	38.29	37.25	1.04	2.7	-3.67	-16.6	0.05	0.4	-3.61	-15.7
ACET03	Inlet Tube	7.96	39.76	38.43	1.34	3.4	-3.46	-15.7	0.03	0.14	-3.35	-15
ACET04	Sealed inlet/outlet ports	8.41	40.08	39.7	0.38	1	-4.26	-17.4	0.02	0.11	-4.21	-17.1
ACET05	Sealed inlet/outlet ports	8.41	39.46	39.02	0.45	1.1	-4.22	-17.2	0.05	0.31	-4.18	-17
ACET06	Sealed inlet/outlet ports	8.36	39.18	38.76	0.42	1.1	-4.23	-17.4	0.04	0.37	-4.18	-17
PARA01	Light paraffin oil	12.15	39.26	38.9	0.37	0.9	-4.4	-17.4	0.03	0.18	-4.25	-17.2
PARA02	Light paraffin oil	11.8	39.56	39.2	0.36	0.9	-4.43	-17.6	0.04	0.24	-4.25	-17.2
PARA03	Light paraffin oil	13.56	38.97	38.66	0.31	0.8	-4.46	-17.5	0.04	0.22	-4.29	-17.3

Each bottle was weighed when empty, then again once the ~40 ml of sample was added, using an Ohaus Adventurer AR3130, three decimal point balance. Each lid was also weighed to assess whether any water had been absorbed or condensed onto the lid over the course of the experiment. For the oil bottles each empty bottle was weighed, then weighed again with oil, and then again once the sample was added. Each bottle and lid was then weighed again at the end of the 3 months to determine any loss of water.

Each water sample was filtered through a 0.2 µm polyethersulfone syinge filter directly into 2 ml vials for analysis. Paraffin oil samples were left undisturbed for several hours, then a syringe needle was pushed through the side of the bottle well below the paraffin/water interface to extract the sample. Oxygen and hydrogen isotope analyses were conducted with an L2130-i Picarro Cavity Ring-Down Spectrometer (Picarro, Inc., Santa Clara, CA, USA) with a precision against an in-house QA standard of ± 0.05‰ for $\delta^{18}O$, and ± 0.4‰ for δ^2H. Each batch of 10 samples was preceded by calibration with 2 in-house standards, and a quality check against a 3rd in-house standard, with a final quality check at the end of the sample run. Each sample and standard were injected 7 times, with the first 3 injections discarded to prevent memory effects, and the remaining 4 injection results assessed for any residual trend. Chemcorrect (Picarro Inc.) was used to validate that samples had not been contaminated. Isotopic results are reported using the delta notation as per mil (‰) deviations from Vienna Standard Mean Ocean Water (VSMOW2) where:

$$\delta_x = 1000\left(\frac{R_x}{R_{VSMOW2}} - 1\right)$$

R is $^{18}O/^{16}O$, or $^2H/^1H$ and x is the sample in question.

Water from 3 of the control bottles (HDPE01, HDPE02 & HDPE 03) were analysed for $^{18}O/^{16}O$ and $^2H/^1H$ at the start of the experiment, with average values of −4.57‰ $\delta^{18}O$ (σ of 0.03‰), and δ −17.8‰ δ^2H (σ of 0.2‰). The remaining 30 bottles – 12 sealed plastics, 12 inlet tube plastics, 3 paraffin oil, and 3 sealed control bottles – were stored in a box outside, under shelter, for ~ 3 months (from 31/10/17 to 28/1/18), approximating conditions found in the sampler. Humidity and temperature were monitored with an Arduino data logger, measured every 15 min with an Aosong DHT22 sensor (factory calibrated, accuracy RH ± 2%, Temperature ± 0.5 °C). Sporadic problems with the SD card of the logger resulted in some gaps in the data. However, sufficient data (38 complete days) was collected to correlate local conditions with temperature and humidity data from two nearby weather stations (Australian Bureau of Meteorology site 023,090 - Kent Town, Adelaide and site 023,000 - West Terrace, Adelaide), using 'Patched Point' data from the SILO database (Jeffrey et al., 2001).

3.3. Isotopic modelling

Each sample can be modelled as a slowly desiccating pond, with a slow loss of water from the initial sample volume. A numerical simulation using the Craig & Gordon (1965) model of isotope fractionation (Eq. (1)) during evaporation was applied to the data to investigate

whether a modelling approach could predict the change in $\delta^{18}O$ and $\delta^{2}H$ for a particular amount of evaporative water loss.

$$\delta_E = \frac{\alpha^*\delta_w - h_n\delta_A - \varepsilon_{eq} - \varepsilon_{kin}}{1 - h_n + 0.001\varepsilon_{kin}} \quad (1)$$

where α^* is the reciprocal of the equilibrium fractionation factor, calculated using the equations derived by Horita and Wesolowski (1994). δ_W and δ_A are the isotopic composition of the water and atmosphere respectively. h_n refers to the relative humidity (RH). In studies of natural waters, this value is usually normalized to the temperature of the water. However, in our modelling, due to the small sample size it was assumed that air and sample water had a similar temperature, and the atmospheric RH was used. The per mil equilibrium isotopic separation (ε_{eq}) is calculated by:

$$\varepsilon_{eq} = 1000(1 - \alpha^*) \quad (2)$$

and the kinetic isotopic separation (ε_{kin}) by:

$$\varepsilon_{kin} = (1 - h_n)\theta n C_k \quad (3)$$

C_k is an experimentally derived constant determined by Merlivat (1978) as 28.5‰ for $\delta^{18}O$, and 25.1‰ for $\delta^{2}H$. θ is a parameter describing the transport resistance of the diffusion layer, typically assumed to be 1 for small water bodies, and n is a value relating isotopic separation to wind conditions, ranging from 0.5 for fully turbulent condition, to 1 for stagnant conditions (Gat, 2010). Alternative values of ~14.2‰ for $\delta^{18}O$ and ~12.5‰ for $\delta^{2}H$ are often used for studies of natural waters, combined with a similar equation to eq. (3) without the n term (e.g., Araguás-Araguás et al., 2000; Gibson et al., 2016; Skrzypek et al., 2015; Steinman et al., 2010).

δ_E is the isotopic composition of evaporated flux, and is combined with a simple numerical model to predict the isotopic composition of the remaining sample water (Eq. (4) & (5)).

$$V^t = V^{t-1} - E^{t-1} \quad (4)$$

$$\delta_W^t = \frac{\delta_W^{t-1}V^{t-1} - \delta_E^{t-1}E^{t-1}}{V^t} \quad (5)$$

where t is the timestep (daily). V is the volume of the sample, E is the volume of evaporative flux, and the subscript denotes sample water (W) or evaporative flux (E). Average meteorological conditions and a θ value of 1 (for a fully developed diffusion layer) were applied as model parameters. δ_A was initially assumed to be in equilibrium with precipitation (δ_P) and the original sample. The model was then calibrated to the observed local evaporation line using the technique of Bennett et al. (2008) by shifting δ_A by 14% from equilibrium with (δ_P) (Eq. (6)).

$$\delta_A = \alpha^*\delta_P - 1.14\varepsilon_{eq} \quad (6)$$

4. Results

4.1. Meteorology

Local meteorological conditions correlated well with the observations from both Kent Town and West Terrace weather stations. To fill in the missing data, a linear regression was derived for average daily temperature ($N = 38$, $R^2 = 0.94$) and relative humidity ($N = 37$, $R^2 = 0.88$) based on the correlation with Kent Town (being nearest) (Fig. 4). One outlier was removed from the correlation (Ave RH, 21/11/2017) as it seemed to be a local effect at the Kent Town station, and was not representative of local conditions or those at the West Terrace station. The daily average temperature over the course of the experiment was 25.3 °C, with a range from 16.0 °C to 37 °C. Relative humidity ranged from 15% to 81% with an average of 41.7%. Interpolated pan evaporation estimates for both weather stations were an average of 7.7 mm/day for a total of 695 mm over the timeframe of the experiment (Fig. 4).

4.2. Quantification of water loss from surface wetting

The average loss of water due to surface wetting was 1.9 ml ± 0.53 σ, split fairly evenly between the 159.6 mm diameter funnel (~0.6 ml), tipping bucket and chute (~0.6 ml), and the water switch and pipework (~0.7 ml). This means that for a single event, assuming no re-evaporation of raindrops from the sampler surfaces during the event, ~90% of rainfall for a 1 mm event is collected, rising to ~98% for a 5 mm event. There is also the potential for up to ~4 ml of rainfall (0.2 mm of rainfall with a 159.6 mm diameter funnel) to sit within the tipping bucket if insufficient rain falls to tip the bucket. The ratio for daily vs monthly rainfall captured was evenly split (336.3 ml for daily, 338.1 ml for monthly), demonstrating that the tipping bucket is able to divide the flow accurately with < 1% variation.

4.3. Volumetric variation in samples

Significant differences in water loss were observed between the different techniques and plastics (Fig. 5, Table 1). The HDPE control bottles with wadded caps only lost 0.3% (0.1 ml) of their water over the three months, followed by the paraffin oil bottles with a loss of 0.9% (0.35 ml). With the exception of the sealed ABS and PLA capped bottles, both sealed and unsealed bottles demonstrated consistent differences between plastic types, with the inlet tube bottles typically losing ~2% (0.8 ml) of mass relative to the sealed plastics. Sealed PETG and acetone treated ABS lost 1.6% (0.6 ml) and 1.1% (0.4 ml) respectively, while their corresponding inlet tube variants lost 3.5% (1.4 ml) and 3.1% (1.2 ml). The sealed ABS exhibited an average water loss of 3.5% while the ABS inlet tube bottles lost 4% (1.6 ml) of water. The PLA sealed bottles lost 3.7% (1.5 ml) via the sealed lids, and 7.5% (2.9 ml) for the inlet tube lids. Compared to most of the alternative plastics, the paraffin oil and the control, all of which had a standard deviation of < 0.35%, the sealed ABS lids exhibited a standard deviation of 0.8% and PLA had standard deviations of 1.8% for the sealed and 1% for the inlet tube lids. These results suggest that either the fabrication method did not produce PLA or ABS caps of consistent quality, or the caps did not seal the bottles adequately. As the inlet tube method is identical for all samples, then it would be expected to contribute a similar amount to the water loss for each sample. For both triplicates of PLA, two samples were similar, with the third varying by a significant amount. Assessing just the two similar samples for each set gives a 7% (2.73 ml) loss for the inlet tube method and 4.8% (1.9 ml) loss for the sealed cap, approximately matching the 2% difference between inlet tube and sealed caps observed in the other plastics. Likewise, the sealed ABS appears to be indicative of variation in bottle cap fabrication, or the sealing between the caps and the bottles.

4.4. Isotopic variation in samples

Changes in the $\delta^{18}O$ and $\delta^{2}H$ of the water samples correlated strongly with the water loss for each sample and a linear regression between $\delta^{18}O$ vs $\delta^{2}H$ exhibited a local evaporation line with a slope of 2.5 (Fig. 5). Three potential outliers were noted (PETG04, ACET02 and HDPE06) with $\delta^{2}H$ values falling approximately –0.75‰ below the evaporation line. These outliers are suspected to have occurred due to an analytical error and are excluded from subsequent modelling and analysis. Unfortunately, these samples were not able to be re-analysed. Excluding these outliers, enrichment relative to the average original water composition ranged from an average of 0.14‰ $\delta^{18}O$, and 0.3‰ $\delta^{2}H$ for the paraffin oil samples, up to 2.63‰ $\delta^{18}O$, and 6.3‰ $\delta^{2}H$ for the PLA inlet tube bottles. Of the three remaining plastics, the inlet tube samples were enriched by an average of 1.21‰ $\delta^{18}O$ and 2.7‰ $\delta^{2}H$ for PETG, 1.30‰ $\delta^{18}O$ and 3.1‰ $\delta^{2}H$ for ABS, and 1.10‰ $\delta^{18}O$ and 2.3‰ $\delta^{2}H$ for acetone treated ABS. Sealed caps underwent less enrichment, ranging from an average of 0.33‰ $\delta^{18}O$ and 0.44‰ $\delta^{2}H$ for the acetone treated lids to 0.41‰ $\delta^{18}O$ and 0.8‰ $\delta^{2}H$ for PETG. The sealed,

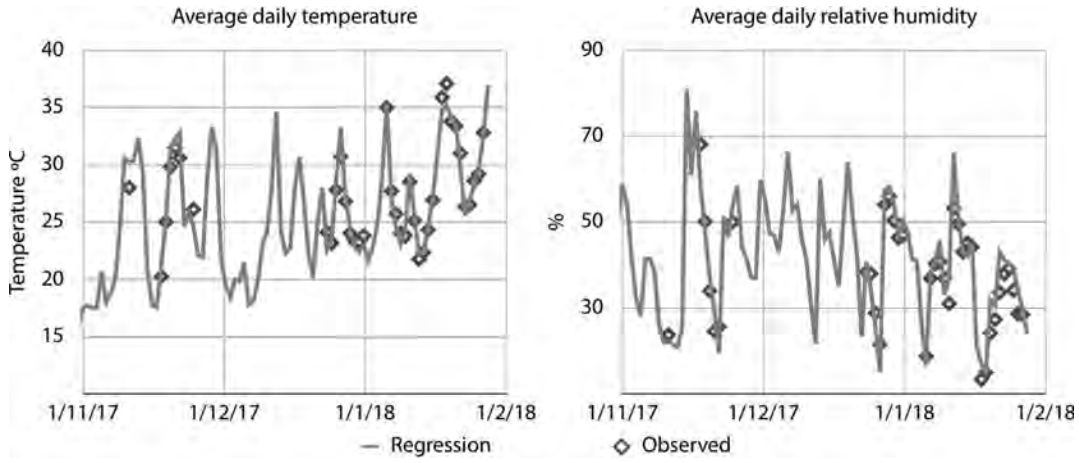

Fig. 4. Predicted vs observed daily average temperature (N = 38, R^2 = 0.94) and relative humidity (N = 37, R^2 = 0.88) based on linear regressions.

untreated ABS lids suffered greater enrichment in line with their large and variable water loss.

4.5. Isotope modelling

Calibration of the modelled to observed isotope values was achieved through adjustment of the δ_A value as described in section 3.3. The modelled evaporation line was aligned to the observed evaporation line by applying a 14% increase in equilibrium isotopic separation (ε_{eq}) between δ_A and δ_P. Differences between modelled and observed $\delta^{18}O$ for all samples except the three potential outliers ranged from 0.19 to −0.09‰ $\delta^{18}O$ with an average of 0.06 and a σ of 0.07‰ $\delta^{18}O$. Differences between modelled and observed δ^2H ranged from 0.7 to −0.5‰ δ^2H with an average of 0.12 and a σ of 0.27‰ δ^2H. For the 3 outliers the differences in $\delta^{18}O$ ranged from 0.06 to 0.16‰ $\delta^{18}O$, and 0.9 to 1.3‰ δ^2H (Fig. 5).

5. Discussion

5.1. General usage notes

Experiments designed to test the validity of the MARS rainfall sampler indicate that the device has the potential to perform remote, automated sampling of rainfall with retention of the primary isotope signature of daily and monthly rainfall. As is the case for manually operated rainfall samplers, the MARS sampler has limits with respect to the minimum amount of rainfall that can be reliably collected, both due to water loss due to wetting of surfaces along the flow-path and due to evaporative loss through the bottle lids. As a result, we recommend that the sampler is suitable for daily rainfall collections greater than 10 ml (equivalent to 1 mm of rainfall with a 159.6 mm funnel diameter, or 0.25 mm of rainfall with a 319.2 mm wide funnel).

5.2. Evaporation and isotope fractionation

The oxygen and hydrogen isotope enrichment along a well-defined local evaporation line (Fig. 5) suggests that the primary method of water loss is evaporation, with a small amount occurring through the paraffin oil, a larger amount through the plastic lids (dependent upon plastic type, degree of sealing, and fabrication consistency), and an additional ~2% through the tubing (most likely through the inlet tube, with its ~14 cm distance from water surface to atmosphere, instead of the 150 cm long vent tube). A very small amount of water is also lost either across the plastic walls, or through the wadded caps in the control bottles. An important result is that there appears to be no fractionation effect that is unique to only one of the isotopologues. With the use of untested plastics, there was a concern that one of the plastics could preferentially exchange with either deuterium or oxygen (e.g. Spangenberg (2012)) however our results suggest that this is not the case. Modelling of the isotopic fractionation of the samples based on the amount of water loss can simulate this evaporative isotopic enrichment in $\delta^{18}O$ and δ^2H to a precision of 0.07‰ $\delta^{18}O$ and 0.27‰ δ^2H (σ^1).

Both the inlet tube and paraffin oil method of preventing evaporation were able to significantly decrease evaporation. For the 40 ml samples used in the experiment, average evaporation occurred at approximately 0.02% of the pan evaporation rate. However, both methods still result in some water loss and isotopic enrichment of samples. This is especially true for small sample volumes. All plastics were substantially less effective than the paraffin oil method at preventing water loss. The inlet tube method, subtracting estimated losses through the plastics, typically resulted in ~0.8 ml loss over the 3 months, compared to 0.35 ml for the paraffin oil samples. This is in contrast to the results from Gröning et al. (2012) who observed that their sampler outperformed a paraffin oil based sampler over the course of a year. The differences between our observations and those of Gröning et al. (2012) likely arise predominantly as a result of differences in the size and shape of the sampling bottles used. The effectiveness of paraffin oil to prevent evaporation depends on the ratio of surface area to volume of the sample and quantification of the rate of water loss through paraffin oil requires consideration of the bottle shape. In contrast, the primary water loss from the inlet tube method is determined by the diameter and length of the inlet and vent tubes. Therefore, under conditions where the paraffin oil surface area is small, then paraffin may outperform the inlet tube method. However, if the bottle diameter was doubled, the surface area of the paraffin oil would be increased fourfold and paraffin may then be outperformed by the inlet tube method. As noted in Section 1.3, the method of sample analysis must be considered before deployment as paraffin oil contamination can compromise laser spectroscopy based stable isotope analysis (IAEA, 2014).

Acetone treated ABS was the most effective plastic at preventing evaporation, followed closely by PETG. Three of the plastics used (inlet tube and sealed PLA and sealed ABS) had greater variation of water loss than the other plastics, raising concerns about the degree of sealing and the fabrication consistency. All the lids had very consistent weights, with a typical range of < 0.05 g. A visual inspection also revealed no significant defects, such as delaminated layers or holes, in any of the lids. However, the nature of 3D printed components – many layers of plastic fused together – means that there is potential for tortuous pathways through the plastic layers, resulting in incomplete sealing (McCullough and Yadavalli, 2013). Leakage through 3D printed

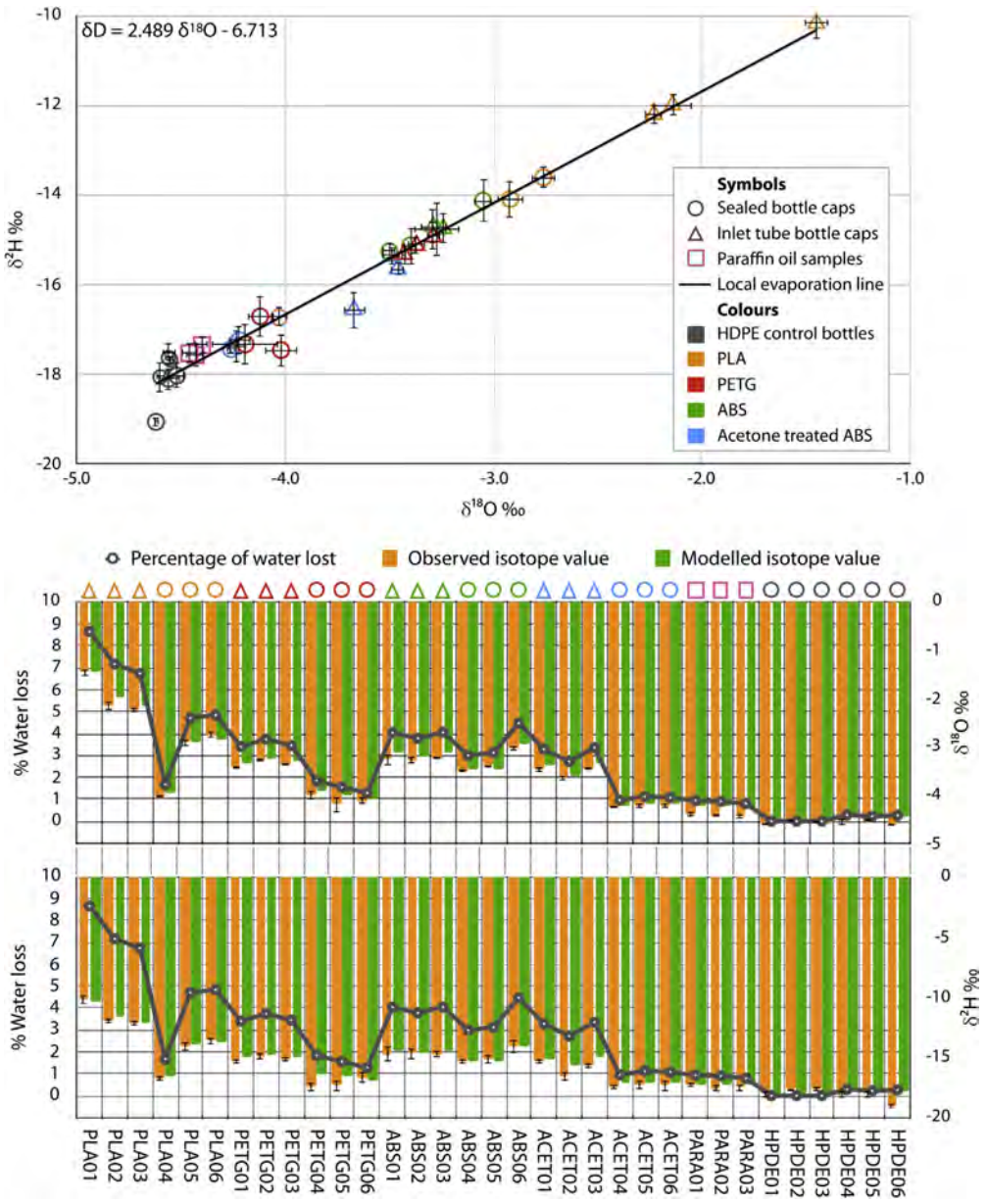

Fig. 5. (a) Graph showing the sample evaporation line derived from the isotopic values for each sample after ~ 3 months storage. (b) Observed and modelled $\delta^{18}O$ results (right axis) and percentage of water loss (left axis) for each sample. (c) As per b, but for $\delta^{2}H$. Error bars show the reported instrumental precision.

components can be prevented through configuration of printer settings, or through post processing of prints. Applying a slight over-extrusion during printing can fill any minor voids and pathways, while decreasing dimensional accuracy. Post processing with acetone treatment to the prints can dissolve filament across and between the layers and improve sealing (McCullough and Yadavalli, 2013). Another potential source of leakage is the seal of the lid against the bottle. The lids do not include a rubber washer or similar seal, instead relying on compression and deformation of the rim of the bottle against the plastic cap to seal. One option is to include a sealing washer or wadding in each cap. Washer seals were not tested here as the sampler requires perfectly fitted washers to be effective. Placing delicate seals may be an option for a single experiment, but is not practical when changing out 60 sample bottles in the field. A potentially better solution, that will be tested in the future, is the printing of seals using TPU (thermoplastic polyurethane) or a similar flexible filament. Using this technique means that the seals can be designed specifically for the caps, with suitable cutouts for the inlet tube and vent tube. With the ongoing development of multi-material 3D printers, the entire cap could be printed in a single process. In the short term, our results indicate that acetone treated ABS is the most appropriate material for bottle lids. More importantly, as there is a lot of variability in 3D printers and the software used to prepare prints, we recommend that each lid be tested to ensure consistent evaporation. A variation of the methodology employed in this paper – mass loss over time – can be used to ensure lid fabrication consistency.

5.3. Potential of mass balance closure modelling

A distinct advantage of the MARS sampler is that both daily and

monthly rainfall are captured at the same time. This potentially allows for the calculation of the original isotopic composition using a modelling approach based on the difference in evaporation rates of monthly and daily rainfall. Assuming the volume of rainfall collected by the sampler is split evenly between daily and monthly samples (Eq. (7)).

$$V_i^{Monthly} = \sum_{n=1}^{m} V_{i,n}^{Daily} \tag{7}$$

where V is the volume of the sample. The superscript represents the sample type – either a daily or monthly sample, m is the total number of daily samples collected. The subscript describes initial (i) or final (f) volume, and sample number (n). Each sample may then undergo some minor evaporation while awaiting collection from the sampler. The initial sample volume for a daily sample (S) is therefore related to the final volume by Eq. (8).

$$V_{i,n}^{Daily} = V_{f,n}^{Daily} + \sum_{d=1}^{t} E_{d,n}^{Daily} \tag{8}$$

E is the daily volumetric loss from evaporation for each sample type, d is the day, and t is the total number of days a sample is exposed to evaporation. The combined volume of all daily samples (n) is therefore:

$$\sum_{n=1}^{m} V_{i,n}^{Daily} = \sum_{n=1}^{m} \left(V_{f,n}^{Daily} + \sum_{d=1}^{t} E_{d,n}^{Daily} \right) = \sum_{n=1}^{m} V_{f,n}^{Daily} + \sum_{n=1}^{m} \sum_{d=1}^{t} E_{d,n}^{Daily} \tag{9}$$

and the integrated monthly sample is related to the initial monthly sample by Eq. (10).

$$V_i^{Monthly} = V_f^{Monthly} + \sum_{d=1}^{t} E_d^{Monthly} \tag{10}$$

From Eq. (7) to (10), it can be seen that:

$$V_f^{Monthly} + \sum_{d=1}^{t} E_d^{Monthly} = \sum_{n=1}^{m} V_{f,n}^{Daily} + \sum_{n=1}^{m} \sum_{d=1}^{t} E_{d,n}^{Daily} \tag{11}$$

We relate daily evaporation rates outside the sampler to evaporation rates within the sampler using a coefficient (similar to relating PET to class-A pan evaporation) such that:

$$E_{d,n}^{Daily} = E_{d,n}^{external} k^{daily} \tag{12}$$

$$E_d^{Monthly} = E_d^{external} k^{monthly} \tag{13}$$

where $E^{external}$ is an evaporative measure (either from meteorological records or calculated using the Penman equation (Penman, 1948) or similar) and k is a coefficient defining a proportional evaporation rate for each sample type. There should be two values of k, one representing the evaporation rate of the daily bottles (k^{daily}), and a second for the monthly bottles ($k^{monthly}$). These coefficients are expected to be similar, but not necessarily identical due to the differences between monthly and daily sample bottles. Rearranging Eq. (11) and substituting Eq. (12) and (13) gives Eq. (14).

$$V_f^{Monthly} - \sum_{n=1}^{m} V_{f,n}^{Daily} = \sum_{n=1}^{m} \sum_{d=1}^{t} E_{d,n}^{external} k^{daily} - \sum_{d=1}^{t} E_d^{external} k^{monthly} \tag{14}$$

For each of Eq. (7)–(14), a parallel series of equations can be written for the isotopic mass balance, resulting in Eq. (15).

$$\delta_f^{Monthly} V_f^{Monthly} - \sum_{n=1}^{m} \delta_{f,n}^{Daily} V_{f,n}^{Daily} = \sum_{n=1}^{m} \sum_{d=1}^{t} \delta_{e,d,n}^{Daily} E_{d,n}^{external} k^{daily} - \sum_{d=1}^{t} \delta_{e,d}^{Monthly} E_d^{external} k^{monthly} \tag{15}$$

where δ describes the isotopic composition of the sample or evaporative flux. The isotopic composition of evaporative fluxes are defined by the 'e' subscript and are calculated using the model of Craig and Gordon (1965). From Eqs. (14) and (15), k^{daily} and $k^{monthly}$ can be solved. As the isotopic fractionation of evaporation is partly determined by the isotopic composition of the sample, a numerical solution should be used with isotopic fractionation calculated at daily (or shorter) timesteps. The original volume and isotopic composition for the integrated monthly sample can then be derived from the initial volume and isotopic composition of the daily samples.

One benefit of applying this modelling technique is that it lowers the ideal sampling requirement from "elimination of evaporation from the sample bottle", to "minimisation and quantification of evaporation from the sample bottle". This latter objective is substantially easier to achieve, with both paraffin oil and inlet tube methods fulfilling that requirement. Even under relatively intense evaporation conditions during an Australian summer, with water losses of up to 9%, modelling of the isotopic change due to evaporation was able to achieve a precision of 0.07‰ $\delta^{18}O$ and 0.27‰ $\delta^{2}H$ (σ^{1}).

6. Conclusion

We have developed an autonomous, daily and monthly rainfall sampler (MARS), able to be deployed and left unattended for up to 3 months between visits, capable of collecting and storing up to 60 daily rainfall samples as well as integrated monthly samples. The sampler can also be reprogrammed for sequential sampling of rainfall events, either on a time or amount basis. This sampler makes significant use of modern fabrication techniques and open source technology to minimise costs and complexity. We have quantified the effectiveness of various plastics commonly used in 3D printing (PETG, PLA, ABS and acetone treated ABS) at preventing evaporation, with acetone treated ABS being most suitable, and PLA being least suitable. The inlet tube method of preventing evaporation from the sample bottles was compared with the use of paraffin oil, and it was noted that the type of sampling bottle, the amount of water and environmental conditions are significant factors in the relative effectiveness of these methods. In our experiments, paraffin oil outperformed the inlet tube method, in contrast to previous research (Gröning et al., 2012). As neither technique can fully prevent evaporation, a modelling approach was developed which takes advantage of the combined monthly and daily sample collection. Our automated rainfall sampler, augmented by a mass balance modelling approach to quantify minor evaporation effects, provides a low cost (< US$750) and effective means of sampling precipitation for isotope analysis with potential applications that span a range of Earth system sciences.

Declaration of interest

None.

Acknowledgements

Martin Ankor received financial support via an Australian Government Research Training Program (RTP) scholarship, and an Australian Institute of Nuclear Science and Engineering (AINSE) postgraduate scholarship (PGRA). We would also like to thank Flinders Analytical for their help in analysing samples, and Fab Lab Adelaide for their workspace and equipment. Discussions with Mark Peterson and Alan Griffiths of ANSTO were invaluable in considering the relative importance of diffusion pathways.

Appendix A. Supplementary data

Supplementary data to this article can be found online at https://doi.org/10.1016/j.jhydrol.2019.04.074.

References

Akkoyunlu, B.O., Dogruel, M., Tayanc, M., Oruc, I., 2013. Design and Construction of a computer controlled automatic sequential rain sampler. Biotechnol. Biotechnol.

Equip. 27 (3), 3890–3895.
Araguás-Araguás, L., Froehlich, K., Rozanski, K., 2000. Deuterium and oxygen-18 isotope composition of precipitation and atmospheric moisture. Hydrol. Process. 14 (8), 1341–1355.
Asman, W.A.H., 1980. Draft, construction and operation of a sequential rain sampler. Water Air Soil Pollut. 13 (2), 235–245. https://doi.org/10.1007/bf02279550.
Bennett, K., Gibson, J., McEachern, P., 2008. Water-yield estimates for critical loadings assessment: comparisons of gauging methods versus an isotopic approach. Can. J. Fish. Aquat. Sci. 65 (1), 83–99.
Berman, B., 2012. 3-D printing: the new industrial revolution. Bus. Horiz. 55 (2), 155–162. https://doi.org/10.1016/j.bushor.2011.11.003.
Berman, E.S., Gupta, M., Gabrielli, C., Garland, T., McDonnell, J.J., 2009. High-frequency field-deployable isotope analyzer for hydrological applications. Water Resour. Res. 45 (10).
Bowen, G.J., Revenaugh, J., 2003. Interpolating the isotopic composition of modern meteoric precipitation. Water Resour. Res. 39 (10), 1–13. https://doi.org/10.1029/2003WR002086.
Bowen, G.J., Wassenaar, L.I., Hobson, K.A., 2005. Global application of stable hydrogen and oxygen isotopes to wildlife forensics. Oecologia 143 (3), 337–348. https://doi.org/10.1007/s00442-004-1813-y.
Bureau of Meteorology, A.G., 2007. Observation of rainfall. Commonwealth of Australia, Bureau of Meteorology.
Coplen, T.B., Neiman, P.J., White, A.B., Ralph, F.M., 2015. Categorisation of northern California rainfall for periods with and without a radar brightband using stable isotopes and a novel automated precipitation collector. Tellus B: Chem. Phys. Meteorol. 67 (1), 28574. https://doi.org/10.3402/tellusb.v67.28574.
Coplen, T.B., 2010. Sequential, time-integrated collector of precipitation, ground water, and surface water for analysis of isotopes: US Patent No. 7,687,028.
Craig, H., 1961. Isotopic variations in meteoric waters. Science 133 (3465), 1702–1703.
Craig, H., Gordon, L.I., 1965. Deuterium and oxygen 18 variations in the ocean and the marine atmosphere. In: Schink, D.R., Corless, J.T. (Eds.), Marine Geochemistry. University, Rhode Island, University, Rhode Island, pp. 277–374.
Dansgaard, W., 1954. The O18-abundance in fresh water. Geochim. Cosmochim. Acta 6 (5–6), 241–260.
Garg, A., Bhattacharya, A., Batish, A., 2016. On surface finish and dimensional accuracy of FDM parts after cold vapor treatment. Mater. Manuf. Processes 31 (4), 522–529. https://doi.org/10.1080/10426914.2015.1070425.
Gat, J., 2010. Isotope Hydrology a Study of the Water Cycle. Imperial College Press, London, London.
Gatz, D.F., Selman, R.F., Langs, R.K., Holtzman, R.B., 1971. An automatic sequential rain sampler. J. Appl. Meteorol. 10 (2), 341–344.
Gibson, J.J., Birks, S.J., Edwards, T.W.D., 2008. Global prediction of δA and δ2H- δ18O evaporation slopes for lakes and soil water accounting for seasonality. Global Biogeochem. Cycles 22 (2), 1–12. https://doi.org/10.1029/2007GB002997.
Gibson, J., Reid, R., 2014. Water balance along a chain of tundra lakes: a 20-year isotopic perspective. J. Hydrol. 519, 2148–2164.
Gibson, J., Birks, S., Yi, Y., 2016. Stable isotope mass balance of lakes: a contemporary perspective. Quat. Sci. Rev. 131, 316–328.
Gray, J., Hage, K.D., Mary, H.W., 1974. An automatic sequential rainfall sampler. Rev. Sci. Instrum. 45 (12), 1517–1519. https://doi.org/10.1063/1.1686550.
Gröning, M., et al., 2012. A simple rain collector preventing water re-evaporation dedicated for δ18O and δ2H analysis of cumulative precipitation samples. J. Hydrol. 448–449, 195–200. https://doi.org/10.1016/j.jhydrol.2012.04.041.
Hartmann, A., et al., 2018. Technical note: GUARD – a automated fluid sampler preventing sample alteration by contamination, evaporation and gas exchange, suitable for remote areas and harsh conditions. Hydrol. Earth Syst. Sci. Discuss. 2018, 1–19. https://doi.org/10.5194/hess-2017-697.
Horita, J., Wesolowski, D.J., 1994. Liquid-vapor fractionation of oxygen and hydrogen isotopes of water from the freezing to the critical temperature. Geochim. Cosmochim. Acta 58 (16), 3425–3437.
Hund, S.V., Johnson, M.S., Keddie, T., 2016. Developing a hydrologic monitoring network in data-scarce regions using open-source arduino dataloggers. Agric. Environ. Lett. 1 (1).
IAEA, 2014. IAEA/GNIP Precipitation Sampling Guide. International Atomic Energy Agency.
Jeffrey, S.J., Carter, J.O., Moodie, K.B., Beswick, A.R., 2001. Using spatial interpolation to construct a comprehensive archive of Australian climate data. Environ. Modell. Software 16 (4), 309–330.
Kennedy, V.C., Zellweger, G.W., Avanzino, R.J., 1979. Variation of rain chemistry during storms at two sites in northern California. Water Resour. Res. 15 (3), 687–702.
Laquer, F.C., 1990. Sequential precipitation samplers: a literature review. Atmos. Environ. Part A 24 (9), 2289–2297.
Mattey, D., et al., 2008. A 53 year seasonally resolved oxygen and carbon isotope record from a modern Gibraltar speleothem: Reconstructed drip water and relationship to local precipitation. Earth Planet. Sci. Lett. 269 (1), 80–95. https://doi.org/10.1016/j.epsl.2008.01.051.
McCullough, E.J., Yadavalli, V.K., 2013. Surface modification of fused deposition modeling ABS to enable rapid prototyping of biomedical microdevices. J. Mater. Process. Technol. 213 (6), 947–954. https://doi.org/10.1016/j.jmatprotec.2012.12.015.
Merlivat, L., 1978. Molecular diffusivities of H 2 16 O, HD 16 O, and H 2 18 O in gases. J. Chem. Phys. 69 (6), 2864–2871.
Michelsen, N., et al., 2018. Comparison of precipitation collectors used in isotope hydrology. Chem. Geol. 488, 171–179. https://doi.org/10.1016/j.chemgeo.2018.04.032.
Penman, H.L., 1948. Natural evaporation from open water, bare soil and grass. Proc. R. Soc. London. Ser. A, Math. Phys. Sci. 193 (1032), 120–145.
Rayna, T., Striukova, L., 2016. From rapid prototyping to home fabrication: How 3D printing is changing business model innovation. Technol. Forecast. Soc. Change. 102, 214–224. https://doi.org/10.1016/j.techfore.2015.07.023.
Raynor, G.S., McNeil, J.P., 1978. Brookhaven Automatic Sequential Precipitation Sampler. BNL-50818 United States 10.2172/7090407 Dep. NTIS, PC A03/MF A01. BNL English; Brookhaven National Lab., Upton, NY (USA).
Ronneau, C., Cara, J., Navarre, J., Priest, P., 1978. An automatic sequential rain sampler. Water Air Soil Pollut. 9 (2), 171–176.
Rozanski, K., Araguás-Araguás, L., Gonfiantini, R., 1993. Isotopic patterns in modern global precipitation. In: Climate Change in Continental Isotopic Records, pp. 1–36.
Rücker, A., Zappa, M., Boss, S., von Freyberg, J., 2019. An optimized snowmelt lysimeter system for monitoring melt rates and collecting samples for stable water isotope analysis. J. Hydrol. Hydromech. 67 (1), 20–31.
Singh, J., Singh, R., Singh, H., 2017. Investigations for improving the surface finish of FDM based ABS replicas by chemical vapor smoothing process: a case study. Assembly Autom. 37 (1), 13–21.
Skrzypek, G., et al., 2015. Estimation of evaporative loss based on the stable isotope composition of water using Hydrocalculator. J. Hydrol. 523, 781–789.
Spangenberg, J.E., 2012. Caution on the storage of waters and aqueous solutions in plastic containers for hydrogen and oxygen stable isotope analysis. Rapid Commun. Mass Spectrom. 26 (22), 2627–2636.
Steinman, B.A., Rosenmeier, M.F., Abbott, M.B., Bain, D.J., 2010. The isotopic and hydrologic response of small, closed-basin lakes to climate forcing from predictive models: application to paleoclimate studies in the upper Columbia River basin. Limnol. Oceanogr. 55 (6), 2231–2245.
Terzer, S., Wassenaar, L.I., Douence, C., Araguas-Araguas, L., 2016. An assessment of the isotopic (2H/18O) integrity of water samples collected and stored by unattended precipitation totalizers. In: EGU General Assembly Conference Abstracts, pp. 15992.
Treble, P.C., Chappell, J., Gagan, M.K., McKeegan, K.D., Harrison, T.M., 2005. In situ measurement of seasonal δ18O variations and analysis of isotopic trends in a modern speleothem from southwest Australia. Earth Planet. Sci. Lett. 233 (1), 17–32. https://doi.org/10.1016/j.epsl.2005.02.013.
Tyler, J.J., Leng, M.J., Arrowsmith, C., 2007. Seasonality and the isotope hydrology of Lochnagar, a Scottish mountain lake: implications for palaeoclimate research. Holocene 17 (6), 717–727. https://doi.org/10.1177/0959683607080513.
Tyler, J.J., Jones, M., Arrowsmith, C., Allott, T., Leng, M.J., 2015. Spatial patterns in the oxygen isotope composition of daily rainfall in the British Isles. Clim. Dyn. (January 2016). https://doi.org/10.1007/s00382-015-2945-y.
von Freyberg, J., Studer, B., Kirchner, J.W., 2017. A lab in the field: high-frequency analysis of water quality and stable isotopes in stream water and precipitation. Hydrol. Earth Syst. Sci. 21, 1721–1739.

Appendix 4

This appendix comprises a published journal article, arising from work undertaken for this thesis. The article is identical to Chapter Four, with the exception of some minor formatting changes to match the rest of this thesis.

Hydrogeology Journal (2019) 27:1865–1878
https://doi.org/10.1007/s10040-019-01996-z

TECHNICAL NOTE

Development of a spreadsheet-based model for transient groundwater modelling

Martin J. Ankor[1] · Jonathan J. Tyler[1]

Received: 8 August 2018 / Accepted: 1 June 2019 / Published online: 24 June 2019

Abstract
Understanding and modelling the passage of groundwater is important for a wide range of environmental and earth science disciplines. The science of groundwater modelling is mature, and advanced modelling algorithms are routinely implemented, for example via the widely used MODFLOW software. However, for the non-specialist scientist or student, the fundamentals of such software can be difficult to comprehend, whilst the algorithms are arguably too complex to be easily applied for many applications which require integration of a groundwater model with climate, surface-water, soil or ecological data. In this context, a spreadsheet-based groundwater model (A2016), capable of solving transient groundwater behaviour in multiple spatial dimensions, was developed. Inter-comparison tests investigating nine transient groundwater scenarios were performed between MODFLOW, A2016 and the Time-dependent Groundwater Modeling using Spreadsheet Simulation (TGMSS) model. Results demonstrated that A2016 is directly comparable to MODFLOW, with identical hydraulic heads in all model experiments. TGMSS was not able to accurately simulate hydraulic heads for any of the model experiments. A groundwater–lake interaction scenario was identified for which MODFLOW will produce unrealistic results, due to the way conductance beneath lakes is determined. Applying a specified saturated thickness approximation for the region beneath the lake resulted in improved lake–groundwater interactions. A2016 is potentially useful for educational purposes and as a tool for groundwater experiments by non-specialists, as it is modular in nature and incorporates MODFLOW terminology and techniques.

Keywords Spreadsheets · General hydrogeology · Transient · Numerical modelling · Education

Introduction

Ongoing development of groundwater modelling software relies upon an understanding of the underlying theory and mathematics describing groundwater behaviour. Of the many groundwater modelling codes available, MODFLOW is considered the de facto standard (Neville and Tonkin 2001; McDonald and Harbaugh 2003; Elemer et al. 2010). Spreadsheet programs provide an excellent introduction to the finite difference technique used in MODFLOW and similar groundwater modelling programs (Olsthoorn 1985; Ousey 1986; Mahmud 1996; Anderson and Bair 2001; Akhter et al. 2006; Anderson et al. 2015). Spreadsheets are commonly used to demonstrate steady-state, two-dimensional finite difference techniques and the accompanying groundwater flow behaviour described by the Laplace and Poisson equations (Anderson and Bair 2001; Bair and Lahm 2006; Anderson et al. 2015). However, there are few examples in the literature of more complex spreadsheet models able to model multidimensional transient behaviour (Olsthoorn 1985; Karahan and Ayvaz 2005a). The most recent published spreadsheet model identified that meets these criteria is the TGMSS model of Karahan and Ayvaz (2005a, b). This gap between simple spreadsheet models and more complex groundwater modelling software is understandable given the maturity and capabilities of software such as MODFLOW. The existence of sophisticated groundwater software could imply that the development of spreadsheet solutions is no longer relevant. However, ongoing development serves two purposes. From a pedagogical perspective, a spreadsheet model capable of demonstrating the transient and three-dimensional behaviour of

Electronic supplementary material The online version of this article (https://doi.org/10.1007/s10040-019-01996-z) contains supplementary material, which is available to authorized users.

✉ Martin J. Ankor
martin.ankor@adelaide.edu.au

[1] School of Earth & Environmental Sciences and Sprigg Geobiology Centre, The University of Adelaide, Adelaide 5005, Australia

groundwater and explaining the theoretical basis of MODFLOW may be a valuable educational tool. In addition, increased reliance on modelling in other scientific fields means there is still a need for new groundwater modelling code, e.g. coupling optimised groundwater models to spatial data systems (Almeida et al. 2014), to isotopic, limnological and palaeoclimate models (Jones et al. 2001; Smerdon et al. 2007; Stets et al. 2010; Ohlendorf et al. 2013), or to resolve engineering problems such as those encountered in tunnel construction (Huang et al. 2013). Developing such models in spreadsheets is an effective way to prototype and to test the model's structure prior to developing dedicated software.

This paper introduces a new spreadsheet-based technique (A2016) able to solve two-dimensional (i.e. one-layer) transient groundwater problems for both confined and unconfined aquifers. A2016 was developed as a precursor to coupling a groundwater model to a hydrological-isotopic lake model for palaeoclimate applications. A2016 is then compared with MODFLOW and the equivalent spreadsheet model (TGMSS) developed by Karahan and Ayvaz (2005a). Model experiments incorporating external sources and sinks, Cauchy (head-dependent), Dirichlet (fixed head) and Neumann (no-flow) boundary conditions, and heterogeneous hydraulic conductivity and storage were performed for both unconfined and confined aquifers. All models are available in the Electronic Supplementary Material (ESM) data sets.

As A2016 is based on the governing groundwater equation and block-centred flow structure used by MODFLOW, it is also ideal for pedagogical purposes. The groundwater equation is simplified into components and uses the same terminology as MODFLOW, thus linking the underlying mathematics to MODFLOW's structure and to groundwater behaviour.

Software and data availability

The models developed for this project run in either Microsoft Excel (v15.27) or MODFLOW 2005 (Harbaugh 2005). MODFLOW models were developed and run using ModelMuse (Winston 2009). All Excel model files are available from the corresponding author's data repository (Ankor 2018), and ModelMuse/MODFLOW files are available from the corresponding author upon request. All models and software will run on recent versions of Microsoft Windows.

Background

Derived from the principles of conservation of mass and Darcy's law, the general governing equation for groundwater flow through a representative elementary volume of heterogeneous and anisotropic material is:

$$\frac{\partial}{\partial x}\left(K_x\frac{\partial h}{\partial x}\right)+\frac{\partial}{\partial y}\left(K_y\frac{\partial h}{\partial y}\right)+\frac{\partial}{\partial z}\left(K_z\frac{\partial h}{\partial z}\right)=S_s\frac{\partial h}{\partial t}-W^* \quad (1)$$

This represents flow in a confined aquifer, where h is the potentiometric hydraulic head and K defines hydraulic conductivity, with the subscripts allowing for anisotropic conditions in the x, y and z directions. S_s refers to the specific storage of the aquifer, and W^* represents sources or sinks, such as wells, recharge and seepage. For a full derivation of this equation, see Anderson et al. (2015).

Numerical models are widely used in groundwater modelling research. By using an approximate form of the groundwater equation, calculated at numerous locations across the region of interest, a numerical model can resolve groundwater flow behaviour in multiple spatial dimensions and time. Numerical models are ideal for solving scenarios with anisotropic and heterogeneous hydraulic properties, and complex initial and boundary conditions (Anderson et al. 2015).

The majority of numerical groundwater models use either the grid-based finite difference technique or the more complex finite element technique, which can solve irregularly shaped triangular networks (Holzbecher and Sorek 2005; Anderson et al. 2015). The finite difference technique is the most well known due to its simplicity and ease of implementation. Finite difference models are further divided into two categories, mesh-centred and block-centred models, based on where the flux boundaries are located. In a mesh-centred model, the flux boundaries are located at each node, whereas in a block-centred model they are located at the edge of each block (Anderson et al. 2015). This means that the two model types treat boundaries differently but nevertheless share many similarities in model structure. Block-centred models are slightly easier to implement and are more commonplace. MODFLOW uses the block-centred finite difference technique.

Anderson and Bair (2001) note that the lack of a common programming language taught in science courses today presents a challenge to teaching students numerical modelling methods. In the past, Fortran was used to demonstrate such techniques. Spreadsheet software has been used to fill this gap and provides an ideal environment for demonstrating the finite difference technique, as the gridded nature of the finite difference model is easily re-created in the grid of spreadsheet cells. Unfortunately, without macros or scripts – aspects not regularly taught in classes – spreadsheets lack the looping function found in general programming languages. Loops are essential for modelling multidimensional transient groundwater behaviour, where the solution for the current time step is used as the starting point for the next calculation. The result is that, although students are introduced to two-dimensional steady-state models or one-dimensional transient models, they rarely have the opportunity to experiment with the full two- or three-

dimensional, transient, finite difference technique that is used in MODFLOW. A spreadsheet model that is capable of modelling multidimensional transient conditions would be a useful educational tool that could provide insight into how programs such as MODFLOW are structured.

There have been several efforts to develop spreadsheet models able to perform multidimensional transient modelling. For example, Olsthoorn (1985) developed a robust set of examples demonstrating methods to solve the Laplace equation, sinks and sources (Poisson equation), heterogeneous aquifers, linked aquifers, unconfined aquifers, three-dimensional flow, transient flow and refinement of the gridded network. Also included was a discussion on the use of over-relaxation as a method to speed up the iteration process. While terminology in the paper reflects earlier practices, the techniques are still applicable today. The lack of macro and scripting capabilities in the spreadsheet software of the time posed difficulties for transient modelling, resolved through manual copying and pasting of the model cells from the current to previous time steps. This requirement for manual data manipulation limits the use of this spreadsheet model for more complex scenarios.

With respect to the requirement for macros in transient modelling, advances were made with the TGMSS models by Karahan and Ayvaz (2005a, b). These two papers present very similar models, with the main difference being the use of the arithmetic mean for determining hydraulic conductivity (K) between cells in Karahan and Ayvaz (2005b) and the harmonic mean in Karahan and Ayvaz (2005a). These papers introduced a single-stage solution algorithm that links the time-stepping process to the iteration process for solving transient problems. However, these models exhibit inconsistencies with MODFLOW, which, as will be described below, is due to the way they handle iteration and the characterisation of the aquifer.

Anderson and Bair (2001) demonstrated spreadsheet models to solve the Laplace and Poisson equations, with examples of both mesh- and block-centred models, implicit and explicit one-dimensional transient models and two-dimensional steady-state models. In addition, mass balance techniques were introduced along with some of the terminology used in MODFLOW, e.g. conductance. Anderson and Bair (2001) also suggested that the block-centred flow structure of MODFLOW could be replicated through linked spreadsheets.

Of the models reviewed here, those described in Olsthoorn (1985) are the most complete from a mathematical perspective, but lack the programming required for automated transient modelling. Karahan and Ayvaz (2005a, b) describe a novel technique for transient modelling; however, results from these models are inconsistent with MODFLOW. There is a need for an up-to-date spreadsheet-based groundwater model, based on current terminology, and capable of transient modelling in multiple spatial dimensions.

Theoretical basis

The governing equation for groundwater (Eq. 1) is applicable to a representative elementary volume (REV), a cube of material representing a portion of the aquifer. By integrating over the thickness (b) of the aquifer, transmissivity (T) and storativity (S) are defined, and the source term W^* is converted to a flux (R) representing flow from external sources.

$$T = Kb \tag{2}$$

$$S = S_s b \tag{3}$$

$$R = W^* b \tag{4}$$

When further simplified to 2D horizontal flow as per the Dupuit-Forchheimer approximation, Eq. 1 becomes:

$$\frac{\partial}{\partial x}\left(T_x \frac{\partial h}{\partial x}\right) + \frac{\partial}{\partial y}\left(T_y \frac{\partial h}{\partial y}\right) = S\frac{\partial h}{\partial t} - R \tag{5}$$

The simplification to 2D is applicable to 3D groundwater modelling, as the determination of vertical conductance between layers requires a slightly different method from that used for horizontal transmissivity (Harbaugh 2005). MODFLOW can be considered a series of 2D layers, linked via vertical flow terms. The 2D structure is also easily represented in a spreadsheet.

Equation 5 determines the behaviour of a singular point location in the aquifer. Adapting this equation to a finite difference model requires an approximation by converting derivatives to differences, defined by the x and y dimensions of each cell (Fig. 1). Therefore, for a model with regular cell dimensions, the equation for a cell with coordinates i,j in the grid becomes:

$$\begin{aligned} T_{i,j-\frac{1}{2}}\left(\frac{h_{i,j-1}-h_{i,j}}{\Delta x^2}\right) + T_{i,j+\frac{1}{2}}\left(\frac{h_{i,j+1}-h_{i,j}}{\Delta x^2}\right) + T_{i-\frac{1}{2},j}\left(\frac{h_{i-1,j}-h_{i,j}}{\Delta y^2}\right) \\ + T_{i+\frac{1}{2},j}\left(\frac{h_{i+1,j}-h_{i,j}}{\Delta y^2}\right) + R_{i,j} = S_{i,j}\frac{dh}{dt} \end{aligned} \tag{6}$$

In the models described in this paper, transmissivity is the harmonic mean (MODFLOW default) between cells (defined by subscripts), taken at the block face between each node. Integrating from the approximated point equation to the full cell dimensions by multiplying both sides of the equation by the x and y dimensions of each cell results in:

$$\begin{aligned} T_{i,j-\frac{1}{2}}\Delta y\left(\frac{h_{i,j-1}-h_{i,j}}{\Delta x}\right) + T_{i,j+\frac{1}{2}}\Delta y\left(\frac{h_{i,j+1}-h_{i,j}}{\Delta x}\right) \\ + T_{i-\frac{1}{2},j,}\Delta x\left(\frac{h_{i-1,j}-h_{i,j}}{\Delta y}\right) + T_{i+\frac{1}{2},j,}\Delta x\left(\frac{h_{i+1,j}-h_{i,j}}{\Delta y}\right) \\ + Q_{S,i,j} = S_{i,j}\Delta x\Delta y\frac{dh}{dt} \end{aligned} \tag{7}$$

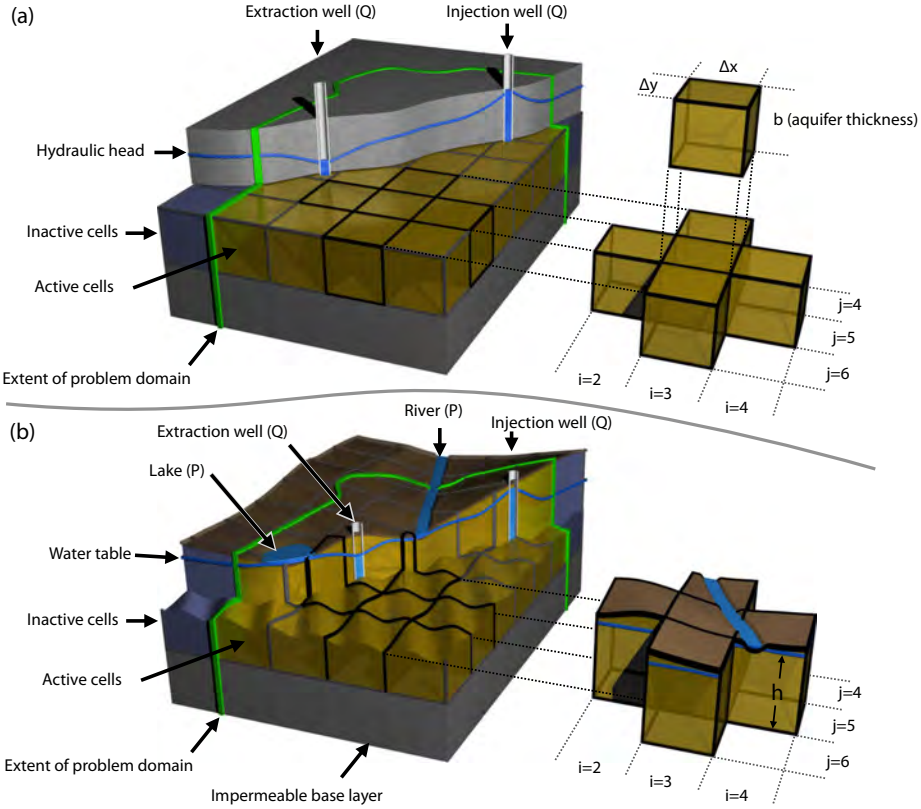

Fig. 1 Cutaway view of a single-layer (2D) finite difference model for (**a**) a confined aquifer and (**b**) an unconfined aquifer. Shown are the various external sources, both head-dependent flows (*P*) which vary depending upon groundwater condition (Cauchy boundary condition), and flows that are independent of the groundwater condition (*Q*). Inactive cells lie outside the problem domain and play no part in the finite difference model. Active cells along the edge of the problem domain are typically defined with a no-flow (Neumann) boundary condition

Q_S is now the volumetric flow into or out of the cell from external sources, and each portion of the left-hand side of the equation represents the volumetric flow from the neighbouring cells, recognisable as Darcy's Law. This is the basis of the governing equation behind MODFLOW, where the change in hydraulic head of a cell is a result of the specific storage and cell volume and the sum of all flows into and out of the cell over a period of time. Flow rate to the cell consists of flows to and from the four surrounding cells and external flows (Q_S) such as recharge or wells.

External flows (Q_S) can be further divided into two categories: fluxes that occur independently of the groundwater condition, such as wells and recharge, and head-dependent fluxes that vary depending on the groundwater head, such as evapotranspiration and river/lake seepage. Both types of flows can be represented by the expression:

$$Q_{S,i,j} = P_{i,j}h_{i,j} + Q_{i,j} \tag{8}$$

where Q_S is the total external flow to the cell, P represents head-dependent flows and Q represents fluxes that are independent of the groundwater head (Fig. 1). For a full derivation of the external flow term, please see Harbaugh (2005).

MODFLOW simplifies Eq. 7 through the introduction of a conductance term (C) that combines transmissivity and the cell dimensions into a single value.

$$T_{i,j+\frac{1}{2}}\Delta y\frac{1}{\Delta x} = C_{i,j+\frac{1}{2}} \tag{9}$$

$$T_{i,j-\frac{1}{2}}\Delta y\frac{1}{\Delta x} = C_{i,j-\frac{1}{2}} \tag{10}$$

$$T_{i+\frac{1}{2},j}\Delta x\frac{1}{\Delta y} = C_{i+\frac{1}{2},j} \tag{11}$$

$$T_{i-\frac{1}{2},j}\Delta x\frac{1}{\Delta y} = C_{i-\frac{1}{2},j} \tag{12}$$

This results in the simplified form of Eq. 7:

$$\begin{aligned} &C_{i,j+\frac{1}{2}}\left(h_{i,j+1}-h_{i,j}\right) + C_{i,j-\frac{1}{2}}\left(h_{i,j-1}-h_{i,j}\right) \\ &+ C_{i+\frac{1}{2},j}\left(h_{i+1,j}-h_{i,j}\right) + C_{i-\frac{1}{2},j}\left(h_{i-1,j}-h_{i,j}\right) \\ &+P_{i,j}h_{i,j} + Q_{i,j} = S_{i,j}\Delta x\Delta y\frac{dh}{dt} \end{aligned} \tag{13}$$

To account for transient behaviour, the time differential is also approximated with a backward difference from the current time (t^m) to the previous time (t^{m-1}), using the hydraulic head for the current time step (h^m), for which the spatial differences are being determined, and the previous time step (h^{m-1}), thereby giving a fully implicit numerical solution.

$$C_{i,j+\frac{1}{2}}\left(h^m_{i,j+1}-h^m_{h_{i,j}}\right)+C_{i,j-\frac{1}{2}}\left(h^m_{i,j-1}-h^m_{h_{i,j}}\right)+C_{i+\frac{1}{2},j}\left(h^m_{i+1,j}-h^m_{h_{i,j}}\right)+C_{i-\frac{1}{2},j}\left(h^m_{i-1,j}-h^m_{h_{i,j}}\right)+P^m_{i,j}h^m_{i,j}+Q^m_{i,j}=S_{i,j}\Delta x\Delta y\frac{h^m_{h_{i,j}}-h^{m-1}_{h_{i,j}}}{t^m-t^{m-1}} \quad (14)$$

Expanding and rearranging Eq. 13 forms a 2D finite difference equation (Eq. 14), similar to that of MODFLOW, and suitable to be rewritten in matrix form for use with matrix solution methods.

$$C_{i,j+\frac{1}{2}}h^m_{i,j+1}+C_{i,j-\frac{1}{2}}h^m_{i,j-1}+C_{i+\frac{1}{2},j}h^m_{i+1,j}+C_{i-\frac{1}{2},j}h^m_{i-1,j}+h^m\left(-C_{i,j+\frac{1}{2}}-C_{i,j-\frac{1}{2}}-C_{i+\frac{1}{2},j}-C_{i-\frac{1}{2},j}+\mathrm{HCOF}_{i,j}\right)=\mathrm{RHS}_{i,j} \quad (15)$$

where HCOF represents all the coefficients of h^{m} that do not include conductance or storage, and RHS represents the remaining right-hand-side components.:

$$\mathrm{HCOF}_{i,j}=P^m_{i,j}-S_{i,j}\Delta x\Delta y\frac{1}{t^m-t^{m-1}} \quad (16)$$

$$\mathrm{RHS}_{i,j}=-S_{i,j}\Delta x\Delta y\frac{h^{m-1}}{t^m-t^{m-1}}-Q^m_{i,j} \quad (17)$$

Equation 15 has one major difference compared to the complete MODFLOW equation, as the vertical flow terms are not included (Harbaugh 2005). These are straightforward to add if required, but were not considered necessary for the purpose of this project.

A spreadsheet often cannot use matrix solvers, instead relying on Gauss-Seidel iteration at each point of the grid until a convergence value has been achieved (Wang and Anderson 1982; Ousey 1986). Rewriting Eq. 15 gives the equation (Eq. 18) for use where point-by-point iteration is required.

$$h_{i,j}=\frac{\mathrm{RHS}_{i,j}-\left(C_{i,j+\frac{1}{2}}h^m_{i,j+1}+C_{i,j-\frac{1}{2}}h^m_{i,j-1}+C_{i+\frac{1}{2},j}h^m_{i+1,j}+C_{i-\frac{1}{2},j}h^m_{i-1,j}\right)}{\left(-C_{i,j+\frac{1}{2}}-C_{i,j-\frac{1}{2}}-C_{i+\frac{1}{2},j}-C_{i-\frac{1}{2},j}+\mathrm{HCOF}_{i,j}\right)} \quad (18)$$

The above equations define groundwater behaviour for a confined aquifer. For an unconfined aquifer, modifications are required. Storativity must be changed from $S_S b$ (specific storage integrated over the aquifer thickness) to S_Y (specific yield), as the water released from storage is no longer determined primarily by rearrangement of the solid matrix and, to a lesser degree, the expansion of water, but instead by the drainable porosity of the cell (Anderson et al. 2015). The RHS and HCOF terms then become:

$$\mathrm{RHS}_{i,j}=-S_{Yi,j}\Delta x\Delta y\frac{h^{m-1}}{t^m-t^{m-1}}-Q^m_{i,j} \quad (19)$$

$$\mathrm{HCOF}_{i,j}=P^m_{i,j}-S_{Yi,j}\Delta x\Delta y\frac{1}{t^m-t^{m-1}} \quad (20)$$

In addition, references in the equations (2, 3, 4) to aquifer thickness (b) must be modified to incorporate the hydraulic head (h), as the thickness of the aquifer is now defined by the modelled water table (Fig. 1). The equation for an unconfined aquifer spreadsheet is therefore:

$$h_{i,j}=\frac{\mathrm{RHS}_{i,j}-\left(h^m_{i,j+\frac{1}{2}}K^m_{i,j+\frac{1}{2}}\Delta y\frac{1}{\Delta x}h^m_{i,j+1}+h^m_{i,j-\frac{1}{2}}K^m_{i,j-\frac{1}{2}}\Delta y\frac{1}{\Delta x}h^m_{i,j-1}+h^m_{i+\frac{1}{2},j}K^m_{i+\frac{1}{2},j}\Delta x\frac{1}{\Delta y}h^m_{i+1,j}+h^m_{i-\frac{1}{2},j}K^m_{i-\frac{1}{2},j}\Delta x\frac{1}{\Delta y}h^m_{i-1,j}\right)}{\left(-h^m_{i,j+\frac{1}{2}}K^m_{i,j+\frac{1}{2}}\Delta y\frac{1}{\Delta x}-h^m_{i,j-\frac{1}{2}}K^m_{i,j-\frac{1}{2}}\Delta y\frac{1}{\Delta x}-h^m_{i+\frac{1}{2},j}K^m_{i+\frac{1}{2},j}\Delta x\frac{1}{\Delta y}-h^m_{i-\frac{1}{2},j}K^m_{i-\frac{1}{2},j}\Delta x\frac{1}{\Delta y}+\mathrm{HCOF}_{i,j}\right)}. \quad (21)$$

While Eq. 21 appears long-winded, the structure and simplified conductance terms applied in the confined aquifer equation can still be used within an unconfined aquifer spreadsheet model by linking the aquifer thickness value to the current hydraulic head for each cell.

Methodology

Model structure

The spreadsheet model (A2016) separates Eqs. 18 and 21 into components, with RHS, HCOF, conductance and the $C_{i,j+\frac{1}{2}}h^m_{i,j+1}+C_{i,j-\frac{1}{2}}h^m_{i,j-1}+C_{i+\frac{1}{2},j}h^m_{i+1,j}+C_{i-\frac{1}{2},j}h^m_{i-1,j}$ section computed in separate sheets. This reduces the likelihood of errors in the spreadsheet formulas and makes it straightforward to update and replace components, for example, replacing the averaging method used to determine inter-cell conductance. Additional sheets were used to define hydrogeological parameters such as specific storage, conductivity, wells, recharge and aquifer thickness, as well as the head values (h^{m-1}) for the previous time step.

Transient modelling requires the head values from the end of the previous time step as initial values for the current time step. A macro was developed that manages the time-step loop and transfers the calculated head values to the previous values

sheet at the beginning of each iteration cycle. Additional macros were developed to allow the user to step through individual time steps or reset the model.

Conductance was determined in separate sheets for each cardinal direction. Instead of starting the model in the first row and column of the spreadsheet, a border of blank cells was left, surrounding the grid representing the model region. This border then forms part of the conductance calculations and means that conductance along the edge of each model boundary is 0, thereby representing the commonly used no-flow boundary condition. It should be noted that this technique is only suitable for the spreadsheet model. Developing a similar model in other software or programming language would typically require the use of edge and corner nodes that do not rely on data from outside the FDM grid. A useful benefit of structuring the spreadsheet in this fashion is that it removes the need for different equations at the edge of the model. The same formula is used throughout the spreadsheet without the need to mirror or remove nodes outside the model boundary, thus simplifying the rebuilding of the model for different shaped regions.

A mass balance was run in parallel with the model, quantifying flows to each cell for each time step, as well as cumulative flows for the simulation run. These values were then compared to the combined inflow and outflow to the model from external sources.

K2005M

K2005M is a modified version of Karahan and Ayvaz's (2005a) TGMSS model. K2005M was developed to investigate the cause of the discrepancies observed between MODFLOW and TGMSS. In K2005M, an aquifer thickness variable has been included and used in place of hydraulic heads in the source term (W), and an initial head value has been defined for the storage term ($CC(H_{i,j})$) (Karahan and Ayvaz 2005a).

Experiments

Nine model experiments were run (Table 1), loosely based on the first example of Karahan and Ayvaz (2005a). Four experiments (#1–4) compared MODFLOW 2005 and the spreadsheet models of A2016, TGMSS and the modified version of TGMSS (K2005M). The model runs simulated the transient behaviour of groundwater in a confined aquifer, consisting of homogenous or heterogeneous hydraulic conductivity and storage conditions, with one central pumping well, two nearby injection wells and areal recharge over the modelled region. Aquifer thickness was set to 20 m.

Four further experiments (#5–8) compared MODFLOW with the unconfined aquifer variant of A2016, simulating the transient behaviour of groundwater in an unconfined aquifer under conditions similar to the confined aquifer experiments.

Experiment 9a compared the unconfined aquifer variant of A2016 with MODFLOW in a simulation incorporating topography, two head-dependent boundary conditions, no-flow and fixed head perimeter boundaries and recharge. The two head-dependent boundaries consisted of evapotranspiration of 0.002 mm/day over the whole model, with a 0.1-m extinction depth, linked to the topographic surface, and a lake covering the central 49 cells of the model. Parameters for the lake are similar to those required for the RES (reservoir) package in MODFLOW, with a specified lake stage (20 m), bottom sediment thickness (0.5–2.0 m) and sediment hydraulic conductivity (0.01 m/day). Recharge was set at 0.001 mm/day. For complete parameters and topography, please see the Electronic Supplementary Material (ESM).

Experiment 9b expanded upon 9a by testing an alternative method of calculating conductance for the cells beneath the lake, using the specified saturated thickness approximation (Sheets et al. 2015). In Experiment 9a, A2016 featured cell-to-cell conductance for the full model region, determined by the aquifer thickness from base of aquifer to the water table as per an unconfined aquifer (Fig. 2). This represents the standard MODFLOW + RES package and is similar to the scenario demonstrated in the RES package documentation (Fenske et al. 1996) where a reservoir is situated within, and interacting with, an unconfined aquifer. Experiment 9b used a variant of A2016 ($A2016_{STA}$), where cell-to-cell conductance beneath the lake was derived from the specified saturated aquifer thickness between the base of the aquifer and the base of the lake sediments (Fig. 2). Two lake depths were modelled to identify how the different transmissivities might affect the interaction between the lake and groundwater. Parameters were chosen to approximate the water table configuration from Winter (1976; Fig. 12), with a flow-through lake and a steady-state hydraulic head just above lake level, leading to seepage into the lake across the lake floor. As a groundwater model using the Dupuit-Forchheimer cannot simulate three-dimensional flow, a fixed flux across the model was included to approximate seepage from the layer to deeper flow paths.

It should be noted that parameters for these model experiments were not intended to represent real-world conditions. Instead, parameters that result in significant variation in modelled hydraulic heads were selected to emphasise differences between the models.

Results

MODFLOW, A2016 and K2005M showed good agreement in all confined aquifer experiments. In experiment 1, for a confined aquifer with injection and pumping wells, MODFLOW and A2016 showed identical results (Fig. 3a).

Table 1 Table defining hydrogeological conditions and model parameters for each set of model experiments

Exp. #	Model name	Hydraulic conductivity	Specific storage	Simulation time (days)	Boundaries	Grid dimensions
Confined aquifer: wells						
1	TGMSS K2005M A2016 Confined MODFLOW	Homogeneous	Homogeneous	1, 30, 360, 3600	Specified head, specified flow	23 × 23 rows and columns. 100-m grid spacing
Confined aquifer: wells + recharge						
2	TGMSS K2005M A2016 Confined MODFLOW Confined	Homogeneous	Homogenous	1, 30, 360, 3600	Specified head, specified flow	23 × 23 rows and columns. 100-m grid spacing
3	TGMSS K2005M A2016 Confined MODFLOW Confined	Heterogeneous	Homogeneous			
4	TGMSS K2005M A2016 Confined MODFLOW Confined	Homogeneous	Heterogeneous			
Unconfined aquifer: wells						
5	A2016 Unconfined MODFLOW Unconfined	Homogeneous	Homogeneous	1, 30, 360, 3600	Specified head, specified flux	23 × 23 rows and columns. 100-m grid spacing
Unconfined aquifer: wells + recharge						
6	A2016 Unconfined MODFLOW Unconfined	Homogeneous	Homogeneous	1, 30, 360, 3600	Specified head, specified flow	23 × 23 rows and columns. 100-m grid spacing
7	A2016 Unconfined MODFLOW Unconfined	Heterogeneous	Homogeneous			
8	A2016 Unconfined MODFLOW Unconfined	Homogeneous	Heterogeneous			
Lake, recharge, evapotranspiration and head-dependent boundaries						
9a	A2016 Unconfined MODFLOW Unconfined	Homogeneous	Homogeneous	1, 30, 360, 3600	Specified head, specified flow, no flow, head-dependent	23 × 23 rows and columns. 100-m grid spacing
9b	A2016 / MODFLOW $A2016_{STA}$			3600		

Differences for calculated hydraulic heads between the two models were less than 1 mm in all grid cells for all time steps. In contrast, hydraulic head values of Model K2005M differed from MODFLOW and A2016 as the time frame for the model simulation increased. At the central pumping well, K2005M and MODFLOW had identical hydraulic heads for day 1. By day 30, K2005M was 0.008 m higher than MODFLOW, 0.14 m higher at day 360 and 0.16 m higher at day 3600

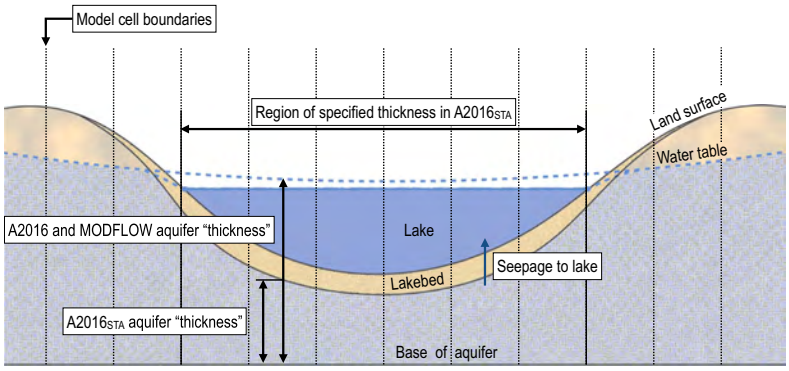

Fig. 2 Differences in aquifer thickness for A2016 and MODFLOW (experiment 9a), and A2016STA, which uses a specified thickness approximation for the region beneath the lake (experiment 9b)

(Table 2). TGMSS displayed very different results to the other models. For day 1 and day 30 at the central well, TGMSS's surface was ~1.6 m lower than the other models, 1.05 m lower at day 360, and 0.16 m lower at day 3600 (Table 2, Fig. 4). MODFLOW, A2016 and K2005M did not achieve steady state within 3600 days. Additional model runs suggest that steady-state groundwater flow for the first simulation would be achieved after ~100,000 days. TGMSS achieved steady state after ~10 days (Fig. 4).

MODFLOW, A2016 and K2005M also produced similar results for experiments 2–4, incorporating recharge and heterogeneous conductivities and specific storage (Figs. 3b–d and 5). At all time steps, MODFLOW and A2016 gave identical results, with hydraulic head differences of less than 1 mm. K2005M diverged from MODFLOW and A2016 as simulation time increased, with a maximum difference observed in the heterogeneous storage experiment, where one of the injection wells had a surface 0.36 m lower than the MODFLOW hydraulic head on day 3600 (Fig. 3d, Table 2). This well was in a region of low specific storage. TGMSS showed significant differences from the other models at all time steps. The maximum difference was on day 30 in the heterogeneous conductivity experiment (experiment 3), where TGMSS simulated a hydraulic head ~7.4 m above the MODFLOW value for one of the injection wells (Table 2).

A2016 was also compared against MODFLOW in a series of unconfined aquifer experiments (Fig. 6). TGMSS and K2005M were not included in this comparison, as they are not designed to model unconfined aquifers. Identical results were achieved in all simulations, for all time steps, with a maximum difference in hydraulic head of less than 1 mm.

Performance in A2016 is slower than MODFLOW, with a time of around 10–15 min for 3600 time steps. In comparison, MODFLOW takes around 1 to 3 min using the preconditioned

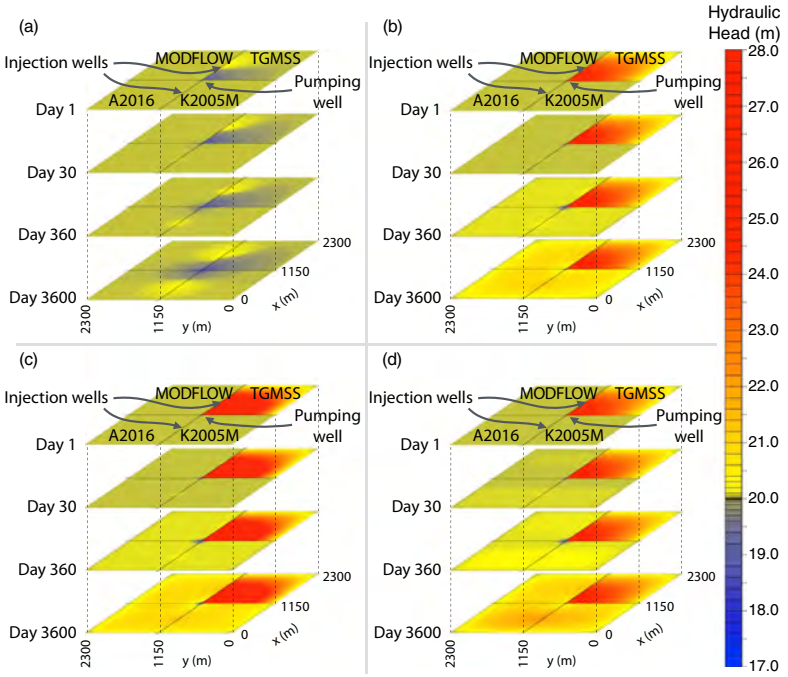

Fig. 3 Hydraulic head (m) maps showing modelled transient groundwater behaviour for model experiments 1–4, for days 1, 30, 360 and 3600. Each quadrant shows results for one of the models examined (MODFLOW, A2016, TGMSS, K2005M). Model experiments shown are: (**a**) Confined aquifer with pumping and injection wells. (**b**) Confined aquifer with wells and recharge. (**c**) Confined aquifer with wells, recharge and heterogeneous conductivity. (**d**) Confined aquifer with wells, recharge and heterogeneous storage

Table 2 Hydraulic heads for each cell containing an injection or pumping well

Exp.#	Time step (days)	MODFLOW			A2016			K2005M			TGMSS		
		LIW	CPW	RIW	LIW	CPW	RIW	LIW	CPW	RIW	LIW	CPW	RIW
1	1	20.002	19.996	20.002	20.002	19.996	20.002	20.002	19.996	20.002	20.621	18.391	20.621
	30	20.059	19.882	20.059	20.059	19.882	20.059	20.055	19.890	20.055	20.549	18.254	20.549
	360	20.355	19.290	20.355	20.355	19.290	20.355	20.286	19.428	20.286	20.546	18.248	20.546
	3600	20.635	18.711	20.635	20.635	18.711	20.635	20.552	18.867	20.552	20.546	18.248	20.546
2	1	20.002	19.996	20.002	20.002	19.996	20.002	20.002	19.996	20.002	24.126	23.560	24.126
	30	20.067	19.889	20.067	20.067	19.889	20.067	20.063	19.897	20.063	24.210	23.700	24.211
	360	20.445	19.380	20.445	20.445	19.380	20.445	20.376	19.518	20.376	24.213	23.704	24.213
	3600	21.493	19.610	21.493	21.493	19.610	21.493	21.335	19.736	21.335	24.213	23.705	24.213
3	1	20.002	19.996	20.002	20.002	19.996	20.002	20.002	19.996	20.002	27.275	25.943	26.184
	30	20.068	19.886	20.069	20.068	19.886	20.069	20.065	19.893	20.066	27.454	26.180	26.298
	360	20.506	19.259	20.545	20.505	19.259	20.545	20.427	19.417	20.460	27.460	26.187	26.302
	3600	21.735	19.188	21.882	21.735	19.188	21.882	21.588	19.403	21.689	27.460	26.188	26.302
4	1	20.009	19.996	20.003	20.009	19.996	20.003	20.009	19.996	20.003	24.162	23.585	24.142
	30	20.217	19.889	20.087	20.217	19.889	20.087	20.188	19.897	20.080	24.212	23.701	24.211
	360	20.887	19.380	20.518	20.887	19.380	20.518	20.780	19.519	20.442	24.213	23.704	24.213
	3600	22.522	19.743	21.723	22.522	19.743	21.723	22.158	19.864	21.523	24.213	23.705	24.213

Locations of wells are shown in Fig. 5

CPW central pumping well, *LIW* left injection well, *RIW* right injection well

conjugate gradient solver. These values are from model runs on different systems (A2016 was run on the Mac version of Excel 2015, whereas MODFLOW was run with the ModelMuse graphical user interface (GUI) on a Windows 7 virtual machine, both on a MacBook Pro 2.8 Ghz i7).

Model experiment 9a incorporates specified head, specified flux, no-flow and head-dependent boundaries. In the initial experiment, cell-to-cell conductance for all cells was determined by the aquifer "thickness" between the base of the aquifer and the water table. MODFLOW and A2016 produced identical results (Fig. 7) for all cells and time steps. Initial seepage to the lake occurred as inflow across the entire lake floor, with the majority of seepage, combined with rapid drawdown of the groundwater head, occurring near the thinner sediments along the lake shore (average 910 m^3/day per cell). At day 30, inflow to the lake occurred at a consistent rate (average 120 m^3/day per cell) across the whole lake floor, with the increased flow through the thicker central sediments occurring due to a high remnant water table hydraulic head in the centre of the lake. By day 360, the water table mound in the centre of the lake had become a depression with a hydraulic head of ~19.8 m, and lake seepage occurred as inflow along the lake edges (average 48 m^3/day per cell) and outflow in the lake centre (average 8 m^3/day per cell). By day 3600, the overall pattern was similar, with an increase in inflow along the lake edges (average 78 m^3/day per cell). Away from the lake, the water table height increased due to recharge until near day 3600, when the water table height intersected the evapotranspiration boundary in areas of lower topography. Once this

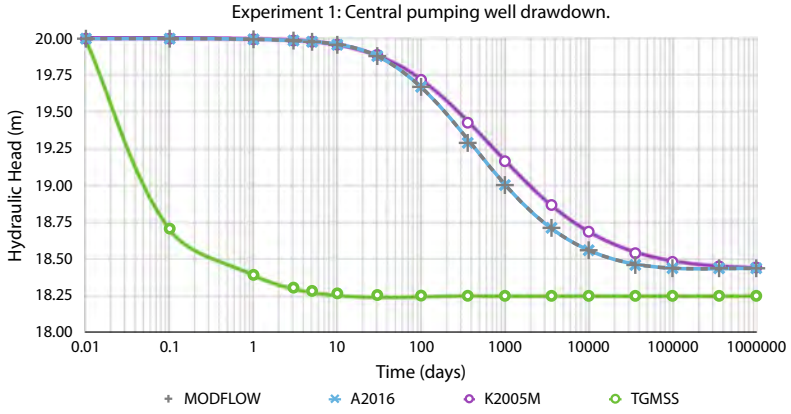

Fig. 4 Modelled hydraulic heads (m) at the central pumping well for each model for model experiment 1, with injection and pumping wells, and homogenous conductivity and storage

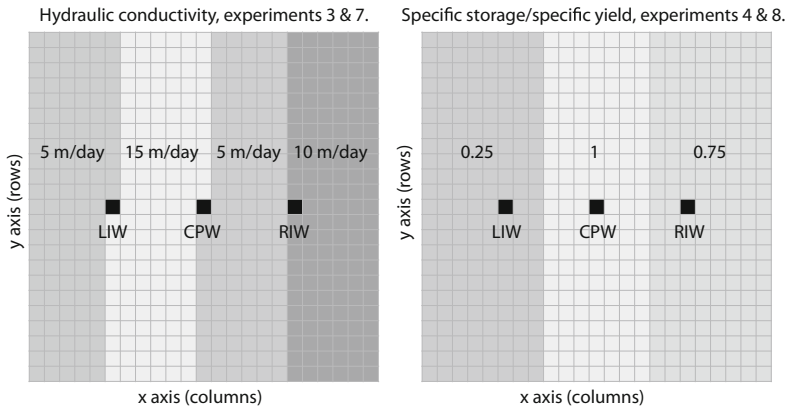

Fig. 5 Map showing left and right injection wells (*LIW* and *RIW*) and the central pumping well (*CPW*). Greyscale is indicative of regions with different hydraulic conductivities and specific storage or specific yield within the model space

occurred, the water table followed the topography as seen in the region around *x*: 2100, *y*: 20 (Fig. 7).

In the second series of simulations (9b), conductance in $A2016_{STA}$ was calculated differently for cells that lay beneath the lake. The thickness of the aquifer in this region was specified as the distance between the base of the aquifer and the base of the lake sediments (Fig. 2), using the specified thickness approximation (Sheets et al. 2015). Initial comparisons between MODFLOW/A2016 and $A2016_{STA}$ using a shallow lake (5.5 m depth) showed small differences (Fig. 8). Hydraulic heads for $A2016_{STA}$ were slightly higher (~25 mm) than MODFLOW/A2016 for the water table mounds, and slightly lower (~70 mm) across the lake, resulting in slightly less seepage into the lake. Seepage into the lake occurred across the entire lake floor in both models, with the largest seepage occurring on the "downstream" side of the lake (columns 13 and 14; Fig. 8).

In contrast, simulations with the deep lake showed no change in the MODFLOW/A2016 simulations, but significant change in the $A2016_{STA}$ simulation (Fig. 8). Hydraulic heads away from the lake were an average of ~170 mm higher, and lake cells were ~440 mm lower, than the MODFLOW/A2016 simulations. In addition, the lake changed from gaining water, to losing water across ~1/3 of the lake floor (Fig. 8).

Discussion

MODFLOW is the de facto standard for groundwater modelling software. The primary objective of this paper was to

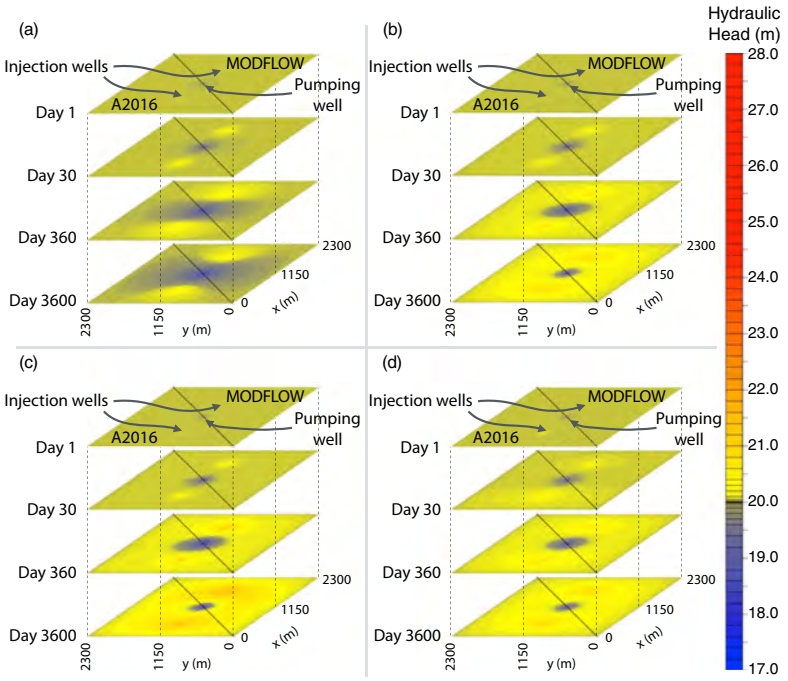

Fig. 6 Hydraulic head (m) maps showing modelled transient groundwater behaviour for experiments 5–8, for days 1, 30, 360 and 3600. Each half shows results for one of the models examined (MODFLOW and A2016). Model experiments shown are: (**a**) Unconfined aquifer with pumping and injection wells. (**b**) Unconfined aquifer with wells and recharge. (**c**) Unconfined aquifer with wells, recharge and heterogeneous conductivity. (**d**) Unconfined aquifer with wells, recharge and heterogeneous storage

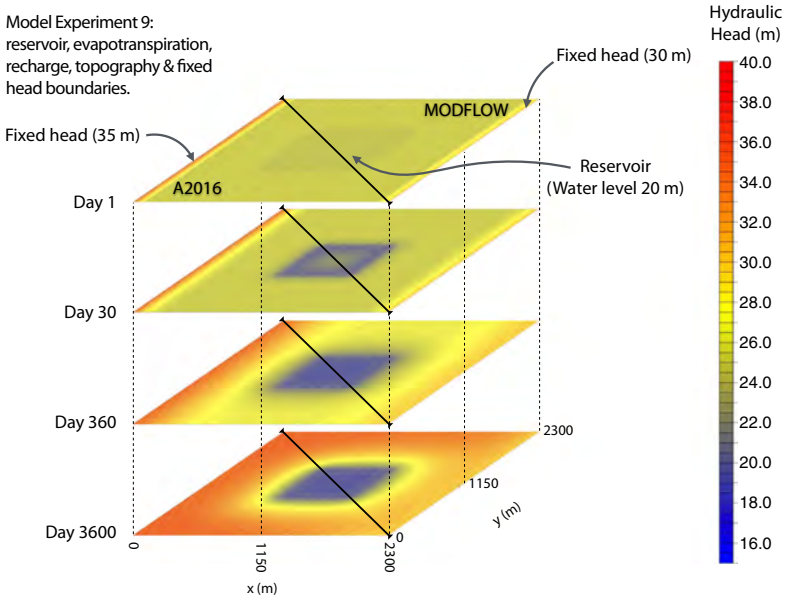

Fig. 7 Hydraulic head (m) map showing modelled transient groundwater behaviour for model experiment 9, for days 1, 30, 360 and 3600. Each half shows results for one of the models examined (MODFLOW and A2016). Model experiment conditions consist of a central reservoir with head-dependent boundaries determining seepage through the lake floor, recharge and evapotranspiration over the model, and no-flow and fixed head perimeter boundaries. Initial hydraulic heads were 25 m, and the reservoir hydraulic head was set at 20 m. Evapotranspiration is linked to the topographic surface with an extinction depth of 0.1 m. The water table in the region centred around $x = 2100$, $y = 200$ is constrained by the evapotranspiration boundary

investigate the development of a comparable spreadsheet model for simple experiments, prototyping and teaching purposes. From the model inter-comparison, it is clear that A2016 is a simple and suitable alternative to MODFLOW for the scenarios investigated in this paper (Table 1). A2016 gave identical results to MODFLOW in all simulations. However, there are two caveats that must be considered: MODFLOW and A2016 differ in the method of iteration, and A2016 does not include the full and extensive range of features of MODFLOW. The difference in iteration method, with A2016 using Gauss-Seidel point-based iteration compared to MODFLOW's matrix solver, is unlikely to lead to significant disparities, though it may occasionally result in situations where the contours do not align perfectly between models; while the difference in hydraulic heads between models may be sub-millimetre, even minuscule variations between models may define a contour. Of the numerous MODFLOW features not included in A2016, two notable omissions include the 3D layer structure and anisotropy of hydraulic conductivity. The relative simplicity of A2016 compared to MODFLOW should

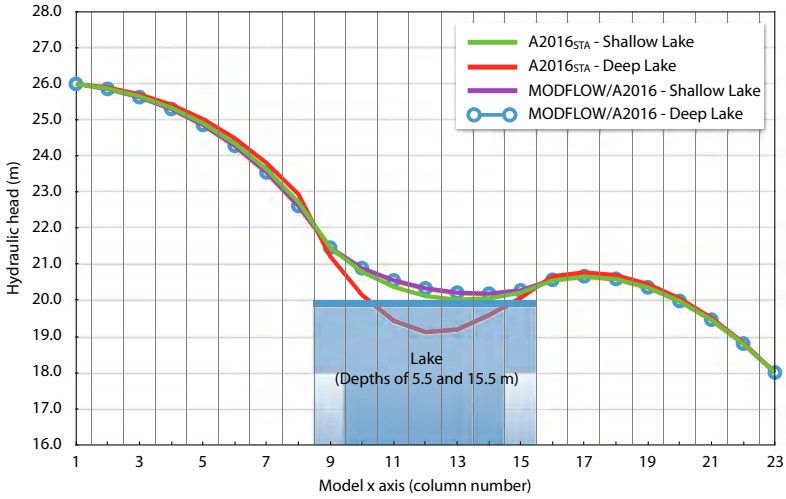

Fig. 8 Hydraulic heads for day 3600 along the middle row of the model, for MODFLOW/A2016 and A2016STA. A2016STA calculates conductance for the region beneath the lake using a specified thickness as described in Fig. 1

not pose significant problems as long as usage is appropriate and the limitations of the single-layer Dupuit-Forchheimer approximation are considered. The structured nature of A2016, with separate, clearly named sheets for the hydrogeological features and model layers, should minimise the use of inappropriate data.

The tendency of K2005M to deviate from MODFLOW and A2016 as simulation time increases before returning to a similar steady flow condition (Fig. 4) is understandable once the model structure for K2005M is examined. The model structure of K2005M is that of a single-layer groundwater model (as per A2016), able to do a single time step. The initial head value is parameterised, and there is no mechanism to update it for incrementing time steps. Therefore, a simulation over 3600 days using K2005M is identical to a simulation in MODFLOW or A2016 over 3600 days, using a single time step of 3600 days. There are no stability concerns in using long time-step lengths in these models, as they all use implicit calculation techniques. However, longer time steps can result in decreased accuracy (Table 2, Fig. 4).

TGMSS was able to approximate the MODFLOW steady-state solution in only one experiment (Fig. 3a), and was unable to model the transient behaviour of groundwater in any of the simulations. This is primarily the result of linking the hydraulic head in the storage term to the iteration process (Eq. 22) instead of using the hydraulic head from the previous time step (Eq. 23). In TGMSS, the hydraulic head value is calculated during each iteration. With each iteration, a new "initial" hydraulic head is introduced to the FDM, which is not likely to be correct (as the iteration cycle is not complete) and which has little relation to the actual initial head value from the start of the time step. In essence, this makes the model "chase its own tail" during each iteration cycle, yielding spurious results.

$$\frac{S_{i,j}\left(h^{m}-h^{\text{iteration}}\right)}{t_m-t_{m-1}} \tag{22}$$

$$\frac{S_{i,j}\left(h^{m}-h^{m-1}\right)}{t_m-t_{m-1}} \tag{23}$$

A further difference between the models that must be considered during use is that the spreadsheet equations used for TGMSS and K2005M do not define the volumetric flows to and from each cell. Instead, these are based on the equation for a representative elementary volume (REV). Therefore, care must be taken to ensure that appropriate integration is carried out to determine actual flow rates. This is not a concern with A2016, as the integration to account for cell size is incorporated into the spreadsheet equations (Eq. 7).

While MODFLOW and the unmodified version of A2016 had identical results in all experiments, the results from experiment 9a and 9b suggest that care must be taken with MODFLOW when used with the RES (reservoir) package. In MODFLOW, by default, conductance between cells beneath the reservoir is calculated without taking into account any confinement of the aquifer or change in aquifer thickness caused by the placement of the reservoir (Fig. 2). As the reservoir takes up a greater proportion of the layer thickness, the discrepancy between MODFLOW's calculated conductance and the actual conductance of groundwater beneath the reservoir increases. In these situations, MODFLOW will calculate greater horizontal flow through the cells beneath the reservoir, potentially resulting in lower hydraulic heads and less groundwater mounding. This is particularly relevant in situations where a lake provides a natural barrier to groundwater flow. Winter (1976; Figures 12 and 18) demonstrated that for many groundwater systems, such as those approximated in experiment 9b, shallow lakes may gain water from surrounding local groundwater systems, whereas deeper lakes in the same setting are likely to lose water. This behaviour is observed in $A2016_{STA}$, where the seepage through the base of the layer, recharge and cell-to-cell conductance combine to form a water table and lake behaviour that is qualitatively similar to the simulations of Winter (1976). In contrast, MODFLOW and A2016 were unaffected by changes in the lake depth and penetration of the aquifer.

The approach taken in $A2016_{STA}$ is based on the specified saturated thickness approximation (Sheets et al. 2015). The specified thickness approximation is commonly used to simplify and linearise the determination of transmissivity through an unconfined aquifer. Specifying the aquifer thickness disconnects the non-linear derivation of transmissivity from saturated thickness. The commonly cited benefit of this approximation is that model run times may be much faster, and stability improved (Sheets et al. 2015). In addition, the specified thickness approximation is an ideal method for limiting the transmissivity of an aquifer that is limited in thickness by an overlying lake.

The RES package and its precursor, the RIV (river) package (Fenske et al. 1996), share similar designs, and both may see some benefit from the application of the specified thickness approximation to define conductance beneath reservoirs, lakes and rivers. However, the approximation is most relevant to the RES package, as reservoirs and lakes are more likely to take up a significant proportion of a layer's thickness, resulting in a much greater difference between the default MODFLOW calculation for conductance and the lower conductance derived from the specified thickness approximation.

Applying the specific thickness approximation only to the region beneath lakes presents a difficulty, as MODFLOW does not allow for specification of the thickness of an unconfined layer. For many groundwater scenarios, the specified

thickness approximation is commonly implemented using a confined layer (Sheets et al. 2015). This method is not suitable for limiting conductance beneath lakes unless the specified thickness approximation is applied across the whole model. The use of a convertible layer with a top surface mirroring the land surface may be applicable, assuming that the water table never rises above the land surface. The modular nature of MODFLOW allows packages to append the HCOF and RHS matrices, but does not include a way for packages to modify layer thickness or type. To make use of the specified thickness approximation on an ad hoc basis over small regions of cells, implementation could be achieved by adding a "layer surface" matrix alongside the HCOF and RHS matrices. Components of the groundwater model would be able to append the HCOF and RHS matrix, as occurs currently in MODFLOW, and modify the "layer surface" matrix as well, to account for regions where the user may want to specify the saturated thickness. In the lake scenario, the layer surface matrix would simply mirror the water table (for unconfined) or top of aquifer (for confined) matrices. In regions where a lake penetrates the aquifer, then the layer surface values for cells beneath the lake would be defined by the bottom lake sediments, rather than the water table/top of the layer.

Conclusion

Groundwater modelling is a complex science, for which comprehensive models such as MODFLOW are required. However, despite the existence of such advanced modelling software, development of simple spreadsheet-based groundwater models is important for both teaching purposes and prototyping new modelling code. A prototype model – A2016 – was developed in preparation for linking a groundwater model to a coupled hydrological-isotopic mass balance lake model. Nine experimental simulations were carried out to test numerous hydrogeological conditions, including sources and sinks, heterogeneous storage and hydraulic conductivity, and specified head, specified flux, head-dependent and no-flow boundary conditions.

In all simulations, A2016 produced identical results to MODFLOW 2005 for both transient and steady-state groundwater conditions, in both confined and unconfined aquifers. In addition, the model inter-comparison from this study demonstrates that modelling transient behaviour of groundwater still requires the use of macros or similar programmatic constructs to control the time-stepping. Previous efforts to develop a spreadsheet that is not reliant on macros (TGMSS; Karahan and Ayvaz 2005a, b) have been shown to be unable to simulate transient groundwater behaviour. In this respect, A2016 provides a clear advancement over existing spreadsheet-based models.

Spreadsheet models also provide the means to examine functions within more complex groundwater models. Experiment 9b highlighted a scenario in which MODFLOW may derive incorrect conductance values for cells beneath a lake in an unconfined aquifer when using the RES package. This is attributed to the use of an aquifer thickness calculated from the water table to the base of the aquifer. A modified version of A2016 was developed that uses the specified thickness approximation (Sheets et al. 2015) and calculates aquifer thickness from the base of the lake sediments to the base of the aquifer.

A2016 provides an excellent framework for teaching by linking the underlying mathematics, MODFLOW concepts and modelled groundwater behaviour in a structured environment, using spreadsheet software that all students are familiar with. While only features deemed necessary to the ongoing project were included and tested in A2016, adding features such as anisotropy or 3D flow modelling should be straightforward and may provide an excellent educational opportunity. Most additions to the model can be achieved through standard spreadsheet manipulation, thereby providing a simple and flexible tool of value for both research and teaching.

Acknowledgements The authors would like to thank Deborah Haynes and Karen Anderson for their comments on an earlier version of this manuscript. Martin Ankor received financial support via an Australian Government Research Training Program (RTP) scholarship and an Australian Institute of Nuclear Science and Engineering (AINSE) postgraduate scholarship (Award – PGRA). All data and model files generated for this project are available as supplementary information.

References

Akhter MG, Ahmad Z, Khan KA (2006) Excel based finite difference modeling of ground water flow. J Himal Earth Sci 39:49–53

Almeida CN, Roehrig J, Wendland E (2014) Development and integration of a groundwater simulation model to an open geographic information system. J Am Water Resour Assoc 50:101–110. https://doi.org/10.1111/jawr.12119

Anderson M, Bair E (2001) The power of spreadsheet models. Proceedings, MODFLOW 2001 and Other Modeling Odysseys Conference, pp 815–822

Anderson MP, Woessner WW, Hunt RJ (2015) Applied groundwater modeling: simulation of flow and advective transport. Academic Press, San Diego

Ankor MJ (2018) Transient groundwater modelling using spreadsheets for education and model prototyping. https://doi.org/10.17632/r6hcbkp53n.4; https://data.mendeley.com/datasets/r6hcbkp53n/4. Accessed 8 Aug 2018

Bair ES, Lahm TD (2006) Practical problems in groundwater hydrology. Prentice Hall, Upper Saddle River

Elemer B, Sz P, Aniko T, Attila K (2010) Complex scientific analysis in geothermal exploration in the Pannonian Basin. Proceedings of the

World Geothermal Congress 2010, Bali, Indonesia, 25–29 April 2010
Fenske JP, Leake S, Prudic DE (1996) Documentation of a computer program (RES1) to simulate leakage from reservoirs using the modular finite-difference ground-water flow model (MODFLOW), US Geological Survey Open-File Report 96-36
Harbaugh AW (2005) MODFLOW-2005, the US Geological Survey modular ground-water model: the ground-water flow process: US Department of the Interior, US Geological Survey Reston, VA, USA
Holzbecher E, Sorek S (2006) Numerical models of groundwater flow and transport. In: Anderson MG, McDonnell JJ (ed) Encyclopedia of Hydrological Sciences. Wiley. https://doi.org/10.1002/0470848944.hsa157
Huang Y, Yu Z, Zhou Z (2013) Simulating groundwater inflow in the underground tunnel with a coupled fracture-matrix model. J Hydrol Eng 18:1557–1561. https://doi.org/10.1061/(ASCE)HE.1943-5584.0000455
Jones RN, McMahon TA, Bowler JM (2001) Modelling historical lake levels and recent climate change at three closed lakes, Western Victoria, Australia (c.1840–1990). J Hydrol 246:159–180
Karahan H, Ayvaz MT (2005a) Time-dependent groundwater modeling using spreadsheet. Comput Appl Eng Educ 13:192–199
Karahan H, Ayvaz MT (2005b) Transient groundwater modeling using spreadsheets. Adv Eng Softw 36:374–384
Mahmud M (1996) Spreadsheet solutions to Laplace's equation: seepage and flow net. J Teknol 25:53–67
McDonald MG, Harbaugh AW (2003) The history of MODFLOW. Groundwater 41:280–283
Neville CJ, Tonkin MJ (2001) Representation of multiaquifer wells in MODFLOW. Proceedings of Modflow 2001 Conference at the International Ground Water Modeling Center, Golden, Colorado, pp 51–59
Ohlendorf C, Fey M, Gebhardt C, Haberzettl T, Lücke A, Mayr C, Schäbitz F, Wille M, Zolitschka B (2013) Mechanisms of lake-level change at Laguna Potrok Aike (Argentina)—insights from hydrological balance calculations. Quat Sci Rev 71:27–45. https://doi.org/10.1016/j.quascirev.2012.10.040
Olsthoorn TN (1985) The power of the electronic worksheet: modeling without special programs. Groundwater 23:381–390
Ousey JR (1986) Modeling steady-state groundwater flow using microcomputer spreadsheets. J Geol Educ 35:305–311
Sheets RA, Hill MC, Haitjema HM, Provost AM, Masterson JP (2015) Simulation of water-table aquifers using specified saturated thickness. Groundwater 53:151–157
Smerdon BD, Mendoza CA, Devito KJ (2007) Simulations of fully coupled lake-groundwater exchange in a subhumid climate with an integrated hydrologic model. Water Resour Res 43:1–13. https://doi.org/10.1029/2006WR005137
Stets EG, Winter TC, Rosenberry DO, Striegl RG (2010) Quantification of surface water and groundwater flows to open- and closed-basin lakes in a headwaters watershed using a descriptive oxygen stable isotope model. Water Resour Res 46:W03515. https://doi.org/10.1029/2009WR007793
Wang HF, Anderson MP (1982) Introduction to groundwater modeling : finite difference and finite element methods. Academic Press, San Francisco
Winston RB (2009) ModelMuse: a graphical user interface for MODFLOW-2005 and PHAST. US Geological Survey, Reston
Winter TC (1976) Numerical simulation analysis of the interaction of lakes and ground water. USGS Professional Paper 1001